The spatial characterisation of contaminant distribution found at industrial sites using combined geophysical / hydrogeological field-studies and laboratory modelling

Rahman Yaccup

Cardiff University

May 2012

Summary

Integrated geophysical, geochemical and hydrogeological modelling techniques have been used in this PhD research study to characterise the ground contamination at four study sites. The primary aim of the research is to study the efficiency of using an integrated approach to study hydrocarbon and heavy metal contamination in the sub-surface soil, geology and groundwater systems. Each of the four sites have different industrial legacies (hence types of contamination) and periods of operation. The sites in increasing age are: Bromsgrove landfill, Cathays Railway Depot, Barry Docks and Weston-Super-Mare gasworks. The geophysical methods used in this study are Electrical Resistivity imaging (IRIS) and multifrequency ground conductivity (Gem-2). These techniques can map the electrical properties of the sub-surface in both 2D and 3D. The electrical properties are then compared with independent professional geochemical sampling programmes for both soil and groundwater.

The results of this project show that the geophysical methods provide a clear indication of the zones of ground contamination (hydrocarbons and heavy metals) in both 2D and 3D. Electrical resistivity/conductivity mapping using both independent techniques show consistent results. The geophysical results also show a good correlation with the geochemical sampling programmes for soil, water and gas. The results are encouraging in that geophysics could be used more widely in professional contaminated land site investigations to supplement conventional invasive techniques and sampling programmes.

The research has also investigated whether geophysical parameters such as electrical conductivity could be used as a groundwater modelling parameter in the Visual Modflow software. The advantage being that geophysics can provide a high intensity of data in 3D and even temporal 4D at a site. The geophysical results can define an accurate spatial distribution of the contaminated area. This can be used to assign a 'concentration recharge' in the modelling compared to the normal practice of using chemical data from a small number of discrete sampling points. However this approach will still require chemical data for validation.

ACKNOWLEDGEMENTS

These acknowledgements could not demonstrate how I'm appreciating those who have helping me during the course of my PhD research here. However I would like to express my gratitude to those people without them this thesis would not been possibly completed.

I must firstly thank to Dr Peter Brabham, Dr Yuesuo Yang and Dr Tim Jones for supervising my thesis with endless patience and enthusiasm. The support and professional advice offered a clear direction every time that I was lost. The attention and encouragement they gave are very much appreciated.

My sincere thanks to those who have provided assistance throughout my time at Cardiff University especially to Dr Alessia Tobaga for helping me much on the fieldwork, Damian Lee, who was helping me a lot in the groundwater modelling. Not forgotten my roommate Dr Hussein Basher and Muhammad Isah who's given valuable ideas in discussions and a great supports for me to complete the project.

I also would like to thanks the Environment Agency whose give the permission to use the Bromsgrove Landfill as one of the research site in this project. I'm also grateful to Enviros Consultant Ltd, Ove Arup Company and Parsons Brinkerhoff Company who's allows me to use some of the materials from their consulting report.

Special thanks to my other Malaysian friends especially Dr Halikul who is my host family in the beginning arrived in Cardiff in 2008, Dr Syafie and family and Izham Saiman. My apologies to anyone who offered assistance during we staying in Cardiff but is not acknowledged. It is purely there are too many kind persons providing their help to be indicated in this page.

I'm very lucky because has been awarded a scholarship to pursue my PhD in the Cardiff University. Thanks to Government of Malaysia under the Public Service Department and the Malaysian Nuclear Agency for the opportunity.

Finally, families are always my solid supporters especially my lovely wife, Sharifah Rogayah Wan Sulong who's give a lot of sacrifice and support, and my three daughters, Nur Fatin Sahirah, Fatin Nur Izzati and Fatin Na`tasha Ellyana. Without encouragement from them, I would not possible completed this long-term study. Not to forget my family at home, my father's Hj. Yaccup Abg Hassim, my mum Hjh.Beknah Uging, my father in-law Hj Wan Sulong Tku Da for their continuous du'a for my success. Thanks you all.

Table of Contents

CHAPTER 11 OVERALL RESULTS AND DISCUSSION

CHAPTER 12 CONCLUSIONS, RECOMMENDATION AND FUTURE WORKS

LIST OF FIGURES

LIST OF PHOTOS

LIST OF TABLES

CHAPTER 1

INTRODUCTION

1.1 Introduction

Today in industrialized countries, land contamination is a major concern, not only to the governmental environmental authorities that are protecting, monitoring and remediating these contamination problems but to the general public as well. In the UK, many thousands of sites have been contaminated by a wide variety of previous industrial uses, often associated with traditional industrial processes which that have now ceased, where their waste products or remaining residues present a major hazard to the general environment. Although these sites may present a hazard to the general environment, but there is also a growing need to reclaim and redevelop these "brownfield" sites for new uses (Environment Agency, 2011b) – **Web 1.1**.

According to the Environment Agency, the term 'land contamination' covers a wide range of situations where land is contaminated in some way. Only in a small number of these situations where certain criteria are met, a site might be officially determined as 'contaminated land' which is has a specific legal definition set out in Part IIA of the Environmental Protection Act (1990) - (Environment Agency, 2011b) – **Web 1.1**.

1.2 Part IIA of the Environmental Protection Act 1990

Part IIA of the Environmental Protection Act 1990 was introduced by the Parliament to help address the problem of historical land contamination and the risks it can pose to people's health and environment including controlled waters (Environment Agency, 2011a) – **Web 1.2**. The Part IIA only came into force on 1 April 2000 in England and on 1 September 2001 in Wales. This requires local authorities to identify contaminated land and ensure that wherever possible its significant risks are addressed.

One of the key features of Part IIA is a statutory definition of "contaminated land" - defined as: *"any land which appears to the local authority in whose area it is situated to be in such a condition, by reason of substances in, on or under the land, that:*
(a) significant harm is being caused or there is a significant possibility of such harm being caused; or
(b) pollution of controlled waters is being, or is likely to be caused".

1.3 Recent scenario of the contamination land in the UK

Various estimates have been made of the extent of the problem. In the report „*Contaminated Land'*, published in 1993, the Parliamentary Office of Science and Technology referred to expert estimates of between 50,000 and 100,000 potentially contaminated sites across the UK, with estimates of the extent of land ranging between 100,000 and 200,000 hectares. The report did comment, however, on international experience, which suggests that only a small proportion of potentially contaminated sites posed an immediate threat to human health and the environment. More recently, the Environment Agency has estimated that there may be some 300,000 hectares of land in the UK affected to some extent by industrial or natural contamination (EUGRIS, 2011) – **Web 1.3**.

According to the same website, as of May 2005, the number of sites formally determined as Contaminated Land under Part IIA of the Environmental Protection Act 1990 in England stands at 305, and can be broken down as shown in Table 1.1.

The Environment Agency reported, in the end of March 2007, about 781 sites had been determined as contaminated land under Part IIA of the Environmental Protection Act 1990 across England and Wales (information provided by 91 per cent of local authorities). Out of these, 35 had been designated as special sites and 149 out of 781 determined sites had completed remediation by end of March 2007 (Environment Agency, 2011b) – **Web 1.1**.

Generally, land that is contaminated contains substances at surface or in the sub-surface that are actually or potentially hazardous to health or the environment. In Britain which has a long history of industrial processes since the 1750s, there are numerous sites where land has become contaminated by human activities such as mining, industry, chemical and hydrocarbon spills and unregulated waste disposal. Contamination can also occur naturally as result of the natural geology of the area, or through intensive agricultural use (Environmental Protection UK, 2011)– **Web 1.4**.

Table 1.1: The overview of contaminated sites in England in 2005

Part IIA regulatory Activity - England						
	LA Determinations	Special Sites	Remediation Statements	Remediation Notices	Remediation declarations	Special Site Inspections
2000/01	13	2	0	0	0	**7**
2001/02	21	11	9	2	0	**22**
2002/03	39	2	13 (9 special)	1	0	**28**
2003/04	9	5	2	1	0	**42**
2004/05	221	1	17 (3 special)	0	1	**26**
2005/06	2	1	0	0	0	**0**
Totals	305	22	41 (12 special)	4 (0 special)	1 (0 special)	**125**

Source: EUGRIS, Portal of Soil and Water Management in Europe – **Web 1.3**

In certain circumstances, the presence of contamination in the ground does not necessarily mean that there is a problem. In many cases there will be minimal risk from living or working on contaminated ground. Indeed many contaminated sites have been successfully and safely redeveloped to provide high quality housing, retailing park and new working environments. Only in a few cases are some sites so contaminated that they present an unacceptable risk to human health or the environment. Human exposure to contaminants can be through inhalation of dust or gases, contact with soil, or through food grown on the land. Leachates (pollutants draining from the site in liquid form) can pollute groundwater and rivers or ponds. Some contaminants may be corrosive, and some can pose a risk of explosive fires.

Once a contaminant is present in the soil, it may naturally break down or be neutralised; be washed out by rain, evaporate or it may remain in the soil building up to higher concentrations. The enrichment of the contaminants in the site is dependent on the balance between the rate of input and the rate of removal of the contaminant where its

properties are influenced by the rate or amount of the rainfall and the organic activities in the soil.

1.4 Current issues and research challenges

The contaminated land issues including soil and groundwater contamination are arising more frequently due to the heightened public concerns on the importance of a hygienic and sustainable living environment. The public are aware of the issues of ground and groundwater pollution as they are regularly discussed in dialogs with various governmental authority bodies, in newspapers, television and on the internet. At a research level, contaminated land issues are debated in many journals by scientists and also in Government Reports. This shows us that pollution issues are not just discussed amongst the small group of researchers or academics but it is a global environmental issue.

So, this Ph.D. research project is designed (aim) to study the efficiency of the integration of geophysical techniques and hydrogeological approaches to study heavy metal and hydrocarbon contamination in the soil and groundwater systems. By knowing the efficiency of these techniques for contamination site investigation, possibly it will help to optimise the cost of the investigation by reducing period of investigation, reduce the amount of boreholes and trial pits which can lessen the overall monitoring costs.

Four research sites have been chosen, with each of them having different activities in the past (historical), operation periods, contamination sources and geological condition. The choice of sites was opportunistic arising from industrial links particularly with sponsored MSc projects in Applied Environmental Geology at Cardiff University. For logistical ease, all the sites used are within 2 hours drive of Cardiff. The youngest site is Bromsgrove Landfill near Birmingham followed by the Cathays Railway Depot Cardiff, Barry Docks and the former Weston Super-Mare town gasworks station. A summary of information from all four sites are shown in Table 1.2.

One of the essential things that have to be done before starting any quantitative site investigation project is equipment calibration. The resistivity imaging technique has to be calibrated to better define the accuracy and the precision of the technique to identify the dimension and location of the materials in the sub-surface. Calibration testing is also

required to calculate the most appropriate electrode array that has to be used for the particular site investigation. The GEM-2 equipment had been sent to the manufacturer to be repaired and calibrated before the project period started.

Generally, the use of geophysical techniques or specifically the Resistivity Imaging Technique and Ground Conductivity Surveys (GEM-2) in this research is to obtain the geophysical parameters of the ground or groundwater which will be compared with the chemical properties of the soil and water samples (perched water and groundwater) at each study site. However, at Weston Super-Mare gasworks station, the geophysical data are compared only with the selected gases distributions which are obtained from an independent Soil Vapour Survey. That means, in this research the geophysical results will be compared with the chemical contents from three different phases of materials i.e. solid (soil), liquid (groundwater and perched water) and gas (soil vapour).

Overall, the research is expected to provide accurate geophysical data that can be linked well to the distributions of the chemical content of the groundwater. This will allow the combination of geophysical and chemical parameters to be effectively used for the groundwater modelling. Geophysical investigation will provide both the vertical and horizontal contamination boundaries of the rocks and contaminant plume. Whereas, the chemical parameters will be use especially in fate and transport modelling. The possibility of the geophysical data such as electrical conductivity and resistivity of the material can be used in the groundwater modelling also will be evaluated in this research project and a further discussion regarding this will be done in the Chapter 10.

1.5 Research methodologies

Defining a research methodology is usually the best way to systematically overcome research problems. It may be understood as a science of how research is done scientifically (Kumar, 2008). Included in the research methodology is the study of various steps generally designed by a researcher to solve the research problems and understand the logic behind them. The research methods are usually a set of techniques or tools such as geophysical techniques, soil sampling, water sampling or other related techniques which are best suited to deploy to achieve the research objectives.

Table 1.2: The summary of the research sites information

Site	Duration	Past activities	Source of Contamination	Pathways	Receptors
Bromsgrove Landfill	1958 – 1993 (Yew Tree Farm)	Industrial and municipal waste landfill	Both heavy metals and hydrocarbon from leachate and gas	Fractured in rock, boreholes release the gas (inhale)	Groundwater, farmer, trespasser, animals
Cathays Railway Depot	1964 – 2005	Diesel Multiple Unit (DMU) Locomotive workshops	Both heavy metals and hydrocarbon	Evaporation, soil layer (fractures) and surface runoff (rain water)	Residents and workers
Barry Docks	1940's – 2000	International Coal port, Docks, HC storage tank, landfill and locomotive scrap yard	Both heavy metals and hydrocarbon	Evaporation, soil layer (fractures) and surface runoff (rain water)	Residents, workers and groundwater. Probably the sea and docks habitats
Weston Super-Mare	1856 – 1989	Town gasworks station and high intensity of the railways	Both heavy metals and hydrocarbon	Evaporation, soil layer (fractures) and surface runoff (rain water)	Residents and workers

Normally a research methodology starts with formulating the research problems, which is then followed by understanding the problem deeply using a literature review or desk study. Gaining enough information will allow a researcher develop a research hypothesis. It will lead to creation of a research design which is followed by data collection and analysis. Normally in a pure research there is a step which a researcher needs to test a research hypothesis before the interpretation of the research outputs can be made. The last step of research methodology is report writing or presenting the results.

The general views of the approaches that will be used in this research are shown in Figure 1.1.

1.6 Thesis structure

This thesis has twelve chapters which can be divided into four sections.

The first section includes the Introduction (Chapter 1), Literature Review / Research Methodology (Chapter 2) and Research Objectives / Site Information in Chapter 3. The second section includes Chapter 4 which discusses the Calibration and Proof Testing of the IRIS Syscal Jr. Resistivity System (72 Switch) and Chapter 5 discusses the Data Acquisition and Laboratory testing.

The third section of the thesis represents the data analysis, results and interpretation of the data from every research site. Each research site has its own chapter and makes this section contribute four chapters in the thesis. Chapter 6 will discusses the Cathays Railway Depot, Chapter 7 (Weston Super-Mare Gasworks Station), Chapter 8 (Barry Docks) and Chapter 9 (Bromsgrove Landfill). In addition Chapter 10 discusses the detailed Groundwater Modelling performed at the Bromsgrove Landfill Sites.

The last section of the thesis is Chapter 11 and Chapter 12 talks about the Overall Discussion (Chapter 11) and the Conclusions, Recommendations and future research directions in Chapter 12.

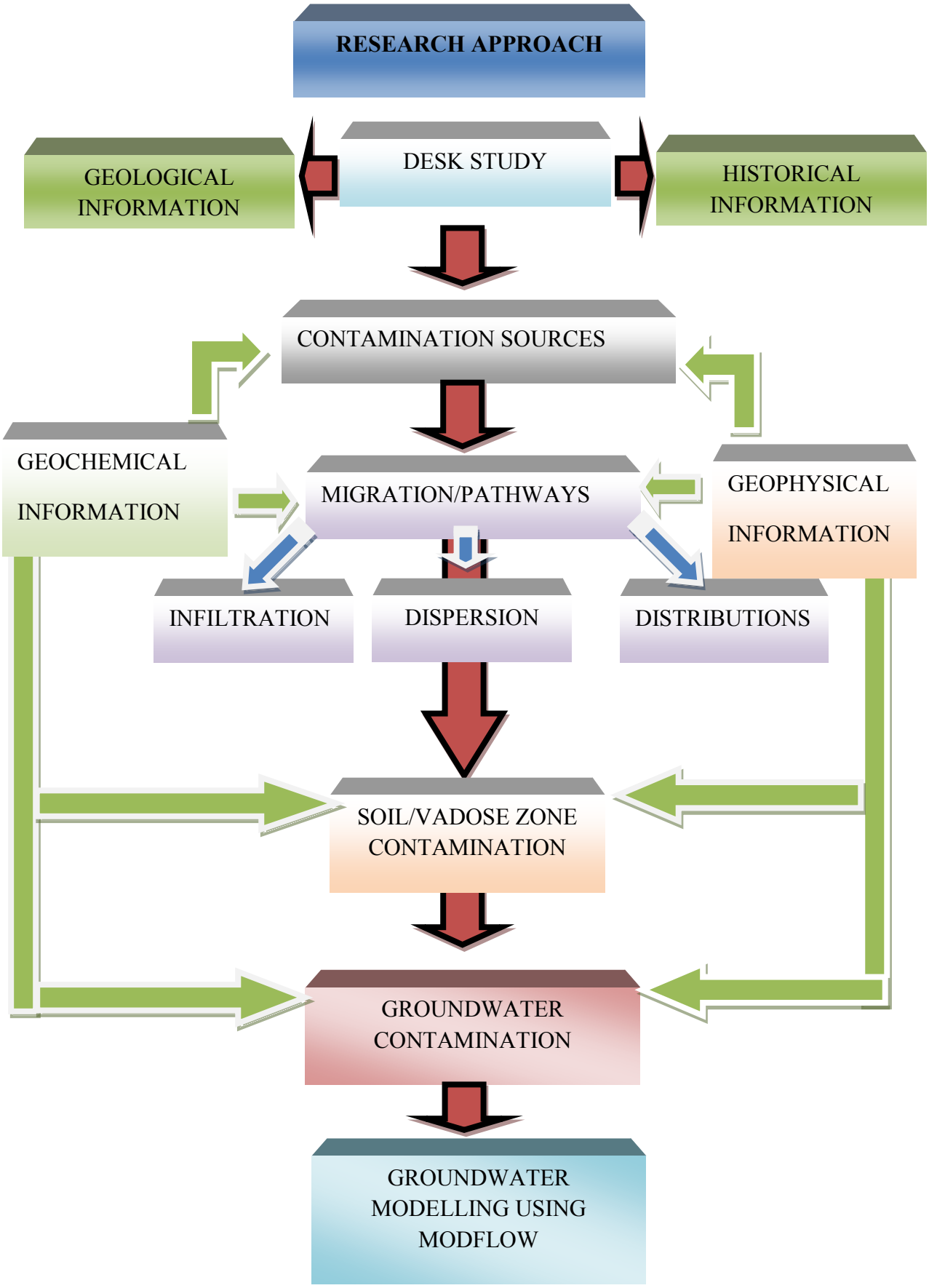

Figure 1.1: The general views of research approaches

CHAPTER 2
LITERATURE REVIEW AND RESEARCH APPROACHES

2.1 Introduction

The aim of this research project is to appraise the use of a number of geophysical techniques to monitor land and groundwater contamination as a result of industrial contamination and waste disposal. In the professional analysis of derelict brown-field industrial sites contaminated by heavy metal or hydrocarbon pollution, a three dimensional understanding of the sub-surface pollution is required in order to design an efficient site clean-up methodology.

This chapter will review a number of relevant scientific principles covering related topics; hydrology, groundwater contamination, hydrogeology, hydrochemistry and the application of geophysical surveying to groundwater contamination and groundwater modelling. Finally, the chapter will discuss present gaps in our research knowledge of these related topics.

2.2 Hydrology in general

Hydrology is concerned with the transport of water through the air, over the ground surface and through the strata of the earth (Ward and Trimble, 2004). Knowledge of hydrological principles is very important in practically all problems that involve the natural use of water. Hydrology is important not only in agriculture, but in engineering, forestry, oil and gas industries and many other branches of the environmental sciences. It is important to understand the hydrological cycle which defines pathways of water travelling through the global system from several processes. The visible components of these processes are any process that takes place on the Earth's surface such as precipitation, runoff and springs, while invisible components including condensation, evaporation, transpiration, infiltration, interception and underground flow. These all work together to create a complete Hydrological Cycle as shown in Figure 2.1.

2.2.1 Surface Water

Surface water can be defined as water collecting on the Earth's surface or in a stream, river, lake, wetland or ocean. Surface water is naturally replenished by precipitation and lost through discharge by evaporation, and sub-surface seepage into the ground.

2.2.2 Groundwater

Groundwater is commonly understood to mean water occupying all the voids within the geologic stratum (Todd and Mays, 2005). This layer is called the saturated zone and is distinguished from the base of the unsaturated zone because all the voids or pore spaces are totally filled with water. A unit of rock or an unconsolidated deposit is normally called an aquifer when it can store and subsequently yield a usable quantity of water. The important parameter in any groundwater investigation is the water table which is defined as where an atmospheric pressure is equal to zero. Above it is capillary fringe which is also fully saturated but the pressure is negative (Kelussa, 2012). Groundwater is recharged from, and eventually flows to, the surface naturally. Natural discharge often occurs at springs and seeps, and can form oases or wetlands. Water is also often withdrawn for agricultural, municipal and industrial use by constructing and operating extraction wells.

Detailed explanation of where the Earth's water resources exist has been given in Figure 2.2. Of the world's total water supply of about 332.5 million cubic miles of water, over 96 percent is saline, 4% freshwater. Of the total freshwater component, over 68 percent is locked up in ice and glaciers and another 30 percent of freshwater is in the ground. Fresh surface-water sources, such as rivers and lakes, only constitute about 22,300 cubic miles (93,100 cubic kilometers), which is about $1/150^{th}$ of one percent of total water. Yet, rivers and lakes are the sources of most of the freshwater people use everyday.

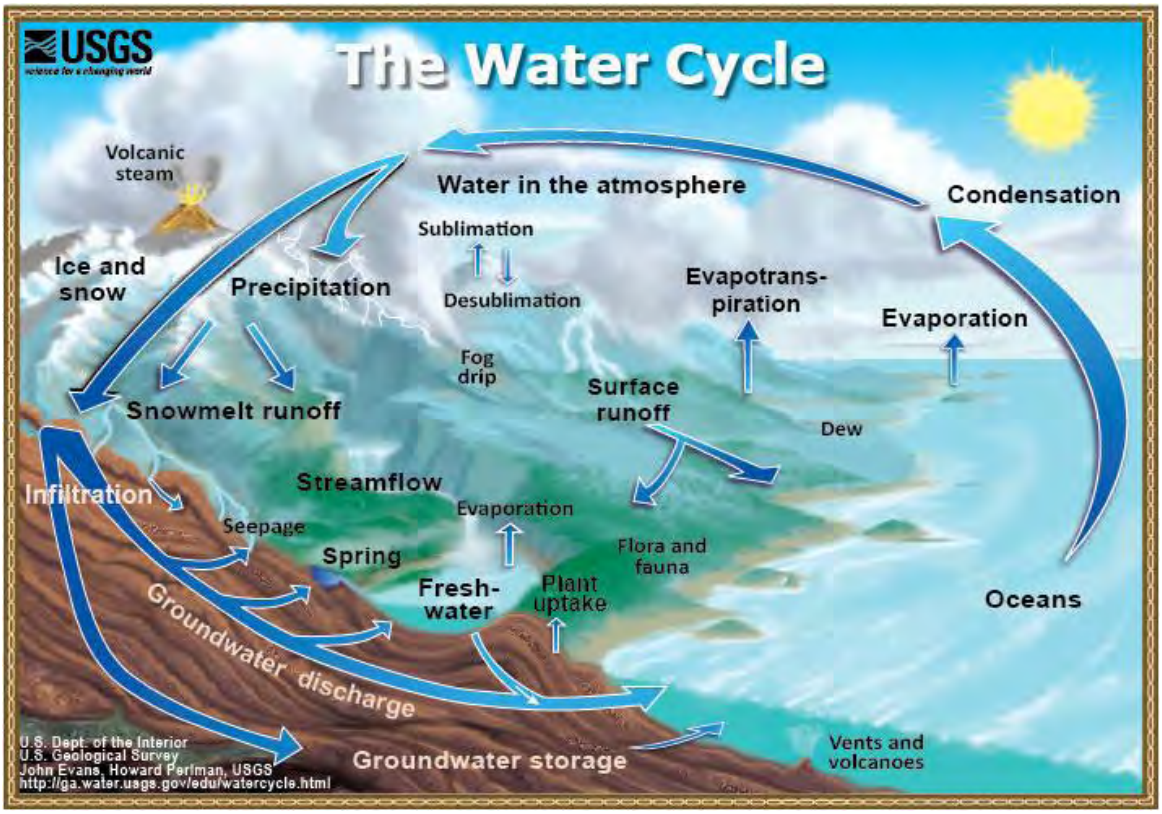

Figure 2.1: The movement of water around, over, and through the Earth is called the Hydrological Cycle (USGS, 2010)– **Web 2.1.**

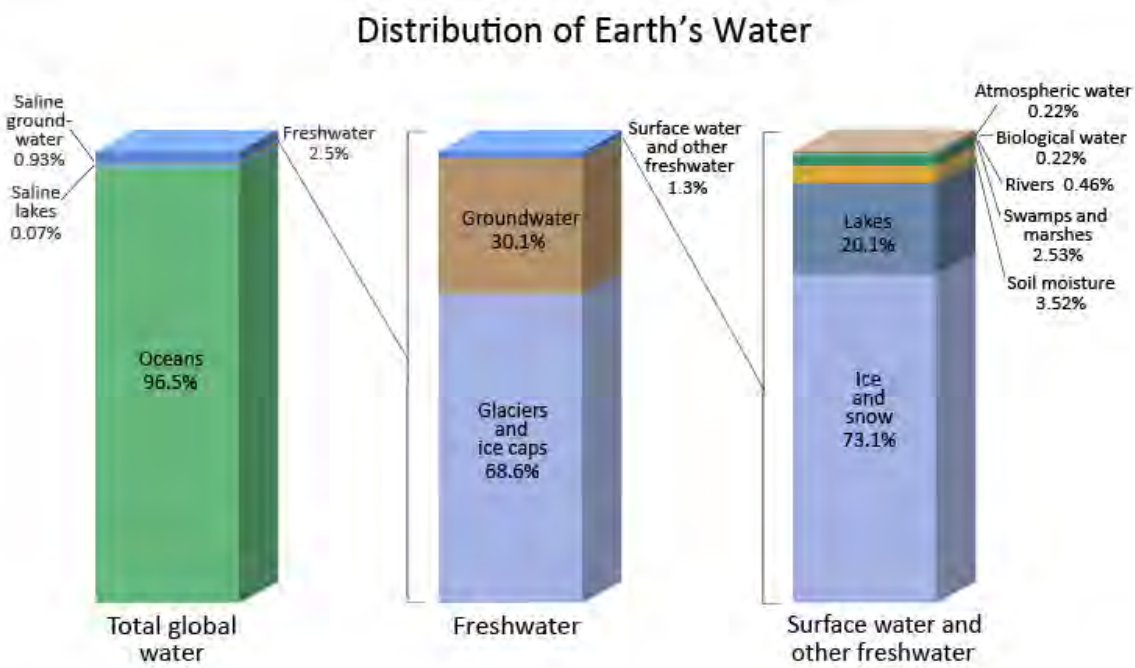

Figure 2.2: Global water distribution (USGS, 2010) – **Web 2.1)**

2.2.3 Hydrogeology

Hydrogeology (like most Earth Sciences) is an interdisciplinary subject; it can be difficult to account fully for the chemical, physical, biological and even legal interactions between soil, water, nature and society. Understanding the character, occurrence and movement of groundwater in the subsurface and its interaction with surface water is the study of hydrogeology (Weight, 2008). Todd and Mays (2005) stated that hydrogeology (Geohydrology) is similar to groundwater hydrology, which has an identical connotation, but hydrogeology differs only by its greater emphasis on geology. The study of the interaction between groundwater movement and geology can be complex because groundwater does not always flow on surface topography but generally follows the groundwater pressure gradients (flows from high to the lower pressure gradient) often through fractures and conduits by circuitous paths.

2.3 What is groundwater and how can it be contaminated?

Groundwater is water that comes from the ground or water existing in the sub-surface. Many people drink and use groundwater but don't even know where it comes from. In the United States almost half of the population use groundwater for their everyday consumption (The Groundwater Foundation, 2009) – **Web 2.2**. Groundwater is also widely used for crop irrigation in many countries in the world.

Sources of groundwater are normally rain, snow, sleet, and hail that soak into the ground by passing between particles of soil, sand, gravel, or rock until it reaches a depth where the ground is filled, or saturated, with water due to gravitational forces. Groundwater may exist very near to the ground's surface or it may be found hundreds of meters below ground level.

Groundwater is stored in the ground in natural materials like gravel or sand. It's kind of like the Earth is a big sponge holding all that water. It can also move through rock formations like sandstone or through cracks in rocks to create a saturated zone called hard rock aquifer.

One estimate of global water distribution:				
Water source	**Water volume, in cubic miles**	**Water volume, in cubic kilometers**	**Percent of freshwater**	**Percent of total water**
Oceans, Seas, & Bays	321,000,000	1,338,000,000	--	96.5
Ice caps, Glaciers, & Permanent Snow	5,773,000	24,064,000	68.7	1.74
Groundwater	5,614,000	23,400,000	--	1.7
Fresh	2,526,000	10,530,000	30.1	0.76
Saline	3,088,000	12,870,000	--	0.94
Soil Moisture	3,959	16,500	0.05	0.001
Ground Ice & Permafrost	71,970	300,000	0.86	0.022
Lakes	42,320	176,400	--	0.013
Fresh	21,830	91,000	0.26	0.007
Saline	20,490	85,400	--	0.006
Atmosphere	3,095	12,900	0.04	0.001
Swamp Water	2,752	11,470	0.03	0.0008
Rivers	509	2,120	0.006	0.0002
Biological Water	269	1,120	0.003	0.0001
Total	332,500,000	1,386,000,000	-	100

Figure 2.3: Water resources. In Encyclopedia of Climate and Weather (USGS, 2010) – **Web 2.1**

Most groundwater is clean, but groundwater can easily become polluted or contaminated. As described by Domenico and Schwartz (1990), a contaminant is any dissolved solute or nonaqueous liquid that enters groundwater as a consequence of human activities. Pollution can originate from leaky underground tanks that store liquid products, leaky landfills or from land run off when people apply too much fertilizer or pesticides onto their fields or lawns. When pollutants leak, spill, or are carelessly dumped on the ground they can move through the soil and are generally difficult and expensive to clean up, especially when it involves deep groundwater pollution.

Three important attributes distinguish sources of groundwater contamination: 1) their degree of localization, 2) their loading history, and 3) the kinds of contaminants emanating from them (Domenico and Schwartz, 1990). They also divided the non-aqueous phase liquid (NAPL) into 5 subgroups of contaminants.

1) Radioactive contaminants (radionuclides)
2) Trace Metals
3) Nutrients
4) Other inorganic Species
5) Organic Contaminants

Radioactive contaminants are generated by the nuclear industry from the nuclear fuel cycle; mining uranium, uranium enrichment and fuel fabrication, power plant operation, fuel reprocessing and waste disposal (Domenico and Schwartz, 1990). Trace metals or heavy metals are the greatest contributors to the groundwater contaminants. Pollution sources come either from effluents from mining operations, industrial waste water, runoff, solid wastes or waste water from urban areas, agricultural wastes / fertilizers and also from fossil fuels.

For nutrient contaminants, most of the pollution sources come from the organic compounds containing either nitrogen or phosphorus. They always exist in groundwater due to agricultural activities that use these nutrients as their fertiliser. The examples of typical nutrients are nitrate (NO^{-3}) and ammonium (NH^{+4}). Other inorganic species which commonly contaminate the groundwater originate from metals present in nontrace quantities such as Ca, Mg and Na, plus nonmetals such as ions containing Carbon and Sulphur (HCO^{-3}, HS^{-}, $CO2^{-3}$, SO_2^{-4} and H_2CO_3). These sources originate from saline water that is polluted with oil, leachate from mine tailings, mine spoil or sanitary landfills. Many other sources also came from industrial waste water that often has large concentrations of common ions in addition to heavy metals or organic compounds. The organic contaminants are the most serious issues debated by hydrogeologists because the pollution sources are complex. The sources originate in different phases, it can be from gas, liquid or solid.

Fetter (1999), divided the sources of groundwater contaminant into six groups including synthetic organic chemicals, hydrocarbons, inorganic cations, inorganic anions, pathogens and radionuclides (Fetter, 1999). Most of these materials will dissolve in water to varying degrees. Some of the organic compounds are only slightly soluble and will exist in both a dissolved form and as an insoluble nonaqueous phase, which can also migrate through the ground.

2.4 Recent Scenario of groundwater uses and pollution

Groundwater is the most important source of drinking water for almost all nations especially in developed countries such as USA, UK, EU countries and Japan (Food and Agriculture Organisation of The Union Nation, 2003) – **Web 2.3**. In fact it was reported, the total water resources in the World are estimated in the order of 43,750km^3/year. America has the largest share of the world's total freshwater resources with 45%, followed by Asia with about 28%, Europe with 15.5% and the Africa Continent with 9%. In term of resources per inhabitant in each continent, America has 24,000m^3/year, Europe 9,300m^3/year, Africa 5,000m^3/year and Asia 3,400m^3/year. At the country level, there is a huge variation of water resources per inhabitant with the lowest water resources being Kuwait with about 10m^3/year and the highest is in Canada, Gabon, Suriname and Iceland with more than 100,000m^3/year. According to same report, the poorest ten countries based on water resources per inhabitant are: Bahrain, Jordan, Kuwait, Libyan Arab Jamahirya, Maldives, Malta, Qatar, Saudi Arabia, United Arab Emirates and Yemen.

Water related disease remains one of the major health concerns in the World especially in the countries having very limited water resources and especially where the water does not go through a proper treatment procedure. Diarrhoeal diseases, which are largely derived from poor water and sanitation, accounted for 1.8 million deaths in 2002 and contributed around 62 million Disability Adjusted Life Years per annum (WHO, 2009b) – **Web 2.4** On a global scale, this places diarrhoeal disease as the sixth highest cause of mortality and third in the list of morbidity. It is estimated that 3.7 per cent of the global disease burden is derived from poor water, sanitation and hygiene (Organisation for Economic Co-operation and Development, 2006) – **Web 2.5**). This health burden is primarily borne by the populations of developing countries and mainly by children.

At 2002 estimates, roughly one-sixth of humanity (1.1 billion people) lack access to any form of improved water supply within 1 kilometre of their home, and approximately 40 per cent of humanity (2.6 billion people) lack access to some form of improved excreta disposal (UNICEF and WHO, 2004) – **Web 2.6**. If the quality of water or sanitation were taken into account, the number of people without access to water supplies and sanitation would increase even further.

Endemic and epidemic disease derived from poor water supply affects all nations. Outbreaks of waterborne disease continue to occur in both the developed and developing Worlds. The improvement of water quality control strategies, in conjunction with improvements in excreta disposal and personal hygiene can be expected to deliver substantial health benefits to the population.

Information on strategies for the protection of groundwater sources used for drinking-water as a component of an integrated approach to drinking water safety management can be found in the WHO report on the Global Water Supply and Sanitation Assessment 2000 (WHO, 2000) – **Web 2.7**. Groundwater safety management and safety of drinking water has been discussed in detail in the WHO report on Protecting Groundwater for Health: Managing the Quality of Drinking Water Sources (WHO, 2006) – **Web 2.8.** The importance of source protection as the first stage of managing water quality has been an important component in both national and international efforts. The World Health Organization's Guidelines for Drinking-water Quality (WHO, 2009a) – **Web 2.9**), emphasizes the need for effective source protection for future generation.

2.5 Types of groundwater pollution

Groundwater pollution can be divided into two types, which relate to human activities and natural activities. Pollution caused by human activities can be divided into two other sub-categories: point-source pollution and non point-source (diffuse) pollution.

Point-source pollution by human activities refers to contamination originating from a single tank, disposal site, or industrial facility**.** Waste disposal sites, accidental spills, leaking gasoline storage tanks, and dumps or landfills are examples of point sources.

Whereas the chemicals used in agriculture activities such as fertilizers, pesticides, and herbicides are examples of non point-source (diffuse) pollution, because they are spread out across wide areas and they collectively can have a larger impact on the general quality of water in an aquifer than point sources. It can often happen particularly when these chemicals are used in land areas that overlie aquifers that are vulnerable to pollution. If impacts from many individual pollution sources such as septic system drain fields occur over large enough areas, they are often collectively treated as a non point source of pollution.

Some groundwater pollution occurs naturally. The toxic metal arsenic, for instance, is commonly found in the natural geological sediments and can be naturally present in groundwater at concentrations that exceed safe levels for drinking water.

Radon gas is a radioactive product of the decay of naturally occurring Uranium in the Earth's crust. Groundwater entering a house through a home water-supply system might release radon indoors where it could be breathed in and may cause radioactive related lung diseases.

2.5.1 Pollution by petroleum-based fuels

One of the most common and best known types of groundwater contamination includes petroleum-based fuels such as gasoline and diesel. Gasoline consists of a mixture of various hydrocarbons (chemicals made up of carbon and hydrogen atoms) it evaporates easily, dissolves to some extent in water, and is toxic. Benzene, a common component of gasoline, is considered to cause cancer in humans, whereas other gasoline components, such as toluene, ethylbenzene, and xylene, are not believed to cause cancer in humans, but may be toxic in other ways such as irritation of sensory and skin problem and Central Nervous System problem like tiredness, dizziness, headache and loss of coordination (Bureau of Environmental Health, 2009) – **Web 2.10**. One property of gasoline is that it is less dense than water, so it tends to float on top of the water table.

Aquifers in industrialized areas are at significant risk of being contaminated by chemicals and petroleum products. In most developed countries, various laws attempt to prevent land and water pollution, and are enforced to clean up contaminated areas when they

occur. Developing countries and countries in economic distress are less likely than developed nations to assess the risk of groundwater contamination by land-use activities.

2.5.2 Chlorinated solvents

Another common class of groundwater contaminants includes chemicals known as chlorinated solvents. Chlorinated solvents are defined as methylene chloride (chloromethane family), perchloroethylene and trichloroethylene (both in the chloroethane family). One example of a chlorinated solvent is dry-cleaning fluid, also known as perchloroethylene (European Chlorinated Solvents Association, 2011) – **Web 2.11**). These chemicals are similar to petroleum hydrocarbons in that they are made up of Carbon and Hydrogen atoms, but the molecules also have Chlorine atoms in their structure.

As a general rule, the Chlorine present in chlorinated solvents makes this class of compounds more toxic than fuels. Unlike petroleum-based fuels, these solvents are usually heavier than water, and thus tend to sink to the bottom of aquifers. This makes solvent-contaminated aquifers much more difficult to clean up than those contaminated by fuels.

2.5.3 Heavy metal pollution

Waste disposal by landfill is very common in many countries and the ever increasing demand for larger space for domestic and industrial wastes from urban areas makes them a necessary part of the human activities. Designated landfill sites commonly use the space available in disused quarries or special-purpose-built structures, but unauthorised disposal in moats (defence ditches around ancient city walls) and dry rivers channels can also be found near some urban areas in the UK. Historical landfill sites in the UK were unlined, relying only on the natural geology, which may or may not be impermeable, thus working on a „dilute and disperse' principle (Meju, 2000). Modern landfills are now lined with a thick HDPE plastic liner or built on impermeable clays to avoid off site migration of polluted water. These large waste contamination facilities are often polluted, hence the need for stringent statutory controls. The contamination produced from historical landfills introduces heavy metals into the local groundwater system or aquifer.

Our interest in landfill sites may lie in assessing the pollution threat they pose since they may contain hazardous substances. In standard landfill site investigations, the usual objectives are to determine the geometrical characteristics (size and shape), its physical properties and the chemical compositions of the fill material. Geophysical surveys have an important although difficult role to play in fulfilling parts of these requirements. However, because geophysical methods respond to changes in the physico-chemical conditions in subsurface, it makes this technique potentially one the best non-invasive tools to remotely investigate groundwater pollution by heavy metals.

A variety of types of non-invasive geophysical methods are used in landfill investigations, however electrical and electromagnetic methods are the most popular due to their natural ability to remotely detect changes of soil and groundwater properties in subsurface (Whiteley and Jewell, 1992). Since the presence of saline fluids in the groundwater enhances its ability to conduct electrical current, it is potentially possible to locate a sub-surface contaminant plume in 3D view by remotely measuring the resistivity distribution of the subsurface. The most useful resistivity measurement for groundwater contamination studies are direct current (DC) resistivity methods e.g. (Barker, 1990), (Ross *et al*., 1990), (Meju, 1993), (Meju, 1995), (Rahman *et al*., 2004a) and transient electromagnetic (TEM) methods e.g. (Buselli et al., 1988), (Buselli et al., 1992), (Meju, 1993), (Meju, 1995), (Rahman *et al*., 2004b). Note that several geophysical methods have been successfully applied to landfill characterization but all techniques require borehole information to validate the geophysical results.

The decomposition of landfill wastes by long term physico-chemical (notably hydrolysis, hydration, carbonation, oxidation and solution) and biological degradation (mostly microbial) processes cause the dissolution or deterioration of landfill materials, gas generation and production of leachate. Landfill sites provide ideal environments for bacterial colonies to grow and most bacteria flourish in the aerobic condition above the groundwater table (Fang, 1995). Initially, the microbial activities are under aerobic conditions and as the oxygen becomes depleted by the microbial activity, anaerobic conditions rapidly set in the biodegradation of organic materials which becomes anaerobic and generates methane gas from the abundant organic materials (Meju, 2000).

Water infiltration from rainwater, groundwater or others liquids disposed of within the landfill will dissolve some soluble mineral constituents of the landfill waste, once the absorbent capacity of the fill is exceeded free drainage of water can then occur. This leaching process may remove common mineral elements such as calcium, magnesium, potassium, nitrogen and phosphorus or remove the bonding materials such as clay, thus resulting in changes in the matrix cement or the ion concentration within the landfill pore water system. This process will also change the physical properties of the fill materials.

In general, the pore fluids produced from landfill are mostly acidic, but will vary in composition depending on the countries where the landfill located, materials produced by different communities and different weather conditions. As an example, on average, leachate composition collected in various landfill sites in England contained Mg^{2+} in the range 12 – 480 mg/l, compared to 250 – 600 mg/l in Germany (Meju, 2000).

Considering stable isotopes in groundwater studies, generally nitrogen, hydrogen, oxygen, carbon and sulphur are the common stable isotopes used. Measuring the isotopic ratio present in the groundwater by using IRMS (Isotope Ratio Mass Spectrometry) and GCMS (Gas Chromatography Mass Spectrometry) are recognised as the best approach to study contaminated groundwater. By understanding the ratio of oxygen and hydrogen isotopes will help understand the mixing processes and the origin of groundwater.

The most abundant isotope in the environment (atmosphere) is Nitrogen (Berner and Berner, 1987) which contributes about 78%, followed by Oxygen, 21% and one per cent for others gases (hydrogen, carbon dioxide, argon, helium etc). Gaseous nitrogen can be found in many forms, the major ones consisting of N_2, N_2O, NO, NO_2, NH_3 (Haller et al., 2011) – **Web 2.12**. The two most important compounds that result from the reaction of these gases and rainwater are nitrate (NO^{3-}, an anion) and ammonium (NH^{4+}, a cation). These ions can become part of the soil layer composition, or even enter into a groundwater solution.

Small amounts of nitrate are normal, but excess amounts can pollute supplies of groundwater. Common sources of nitrogen in the soil are fertilizers, livestock waste, and septic systems. Excess nitrate in the soil is most often found in rural and agricultural areas. Nitrate travels easily through the soil, carried by rain or irrigation water into

groundwater supplies. Wells that tap groundwater may be affected. Shallow wells in sandy soil or wells that are improperly constructed or maintained are more likely to have nitrate contamination. High concentrations of nitrate in water supply can cause methemoglobinemia (oxygen deficiency in blood), and have also been cited as a risk factor in developing gastric an intestinal cancer (Vigil *et.al*., 1965).

2.6 Hydrocarbon contamination in groundwater

Groundwater contamination by hydrocarbons has been increasingly recognised as a serious environmental problem due to the increased use of hydrocarbon products in industrial activities especially where the waste is not managed properly. Hydrocarbon are introduced into the environment by uncontrolled drainage system (spills), leaking storage and disposal facilities, weakness in the isolation of pipelines, sewers and purge chambers. The sources of the contamination may be produced by petroleum fuels, solvents, coal-tars and other mobile hydrocarbons which pose serious groundwater, surface water, soils and public health problems throughout the industrial and developing world (Cassidy, 2007).

2.6.1 What is a hydrocarbon?

Hydrocarbon is any organic compound composed solely of carbon and hydrogen. In organic chemistry the hydrocarbon compound is divided into two classes. The aromatic compounds containing benzene rings or similar rings of atoms, and the aliphatic compounds which do not containing aromatic rings. Hydrocarbons include aliphatic compounds, in which the carbon atoms form a chain, and aromatic compounds, in which the carbon atoms form stable rings. The aliphatic group is divided into alkanes (e.g., methane and propane), alkenes, and alkynes (e.g., acetylene), depending on whether the molecules of the compounds contain, respectively, only single bonds, one or more carbon-carbon double bonds, or one or more carbon-carbon triple bonds. Petroleum distillation yields useful fractions that are hydrocarbon mixtures, e.g., natural gas, gasoline, kerosene, home heating oil, lubricating oils, paraffin, and asphalt. Coal tar is also a source of hydrocarbons. Hydrocarbon derivatives contain additional elements, e.g., oxygen, and include alcohols, aldehydes, ketones, carboxylic acids, and halocarbons (Vollhardt and Schore, 2006).

2.6.2 Aliphatic compounds

Generally, in aliphatic compounds, carbon atoms can be joined together in straight chains, branched chains, or non-aromatic rings (in which case they are called alicyclic). They can be joined by single bonds (alkanes), double bonds (alkenes), or triple bonds (alkynes). Besides hydrogen, other elements can be bound to the carbon chain, the most common being oxygen, nitrogen, sulfur, and chlorine (Vollhardt and Schore, 2006). The simplest aliphatic compound is methane (CH_4).

Most aliphatic compounds are flammable, allowing the use of hydrocarbons as fuel, such as methane, Liquified Natural Gas (LNG), and acetylene used in metallic welding.

2.6.3 Aromatic compounds

Benzene and its derivatives were originally called aromatic hydrocarbon compounds because many of them give off a strong aroma (Vollhardt and Schore, 2006). Some other hydrocarbons may also contain traces of impurities which cause other distinctive scents, resulting in chemists to also call these compounds “aromatic hydrocarbons.” In fact, not all aromatic hydrocarbons produce the aromatic smell and it was thought to be linked to the benzene ring, but it is actually caused by minor impurities.

A benzene ring is a molecular structure which is created when six carbon atoms connect with each other in a linked ring. Each carbon atom has four electrons; two electrons link up with neighbouring carbon atoms, while one goes to a hydrogen atom. The fourth is what is known as a delocalized electron, meaning that it is not directly involved with a specific atom. Benzene rings are often drawn as hexagonal shapes with a circle in the middle to represent these delocalized electrons. Benzene happens to be a particularly toxic form of aromatic hydrocarbon.

When benzene rings link up, they can form a range of aromatic hydrocarbons, including so-called polycyclic aromatic hydrocarbons (PAHs), or polyaromatic hydrocarbons. These aromatic hydrocarbons are created through incomplete combustion, which is why they are so widely distributed in the natural environment. Most manufacturing facilities, for example, utilize combustion in their operations, potentially generating large amounts of PAHs. Some PAHs are extremely toxic, which can lead to serious problems when they have been deposited in large amounts as a result of human activity.

2.6.4 Types of hydrocarbon in groundwater contamination

Typically, there are two types of hydrocarbon which normally contribute to the groundwater contamination and had been classified based on their density compared to water. Non-Aqueous Phase Liquids (NAPLs) are the main contributor to the groundwater hydrocarbon contamination and it is sparingly soluble in water as they do not mix with water and form a separate phase. For example, oil is a NAPL because it does not mix with water, oil and water poured into a glass will separate into two separate phases. NAPLs can be lighter than water (USGS, 2008b) – **Web 2.13** or denser than water (USGS, 2008a) – **Web 2.14**. Hydrocarbons, such as oil and gasoline, and chlorinated solvents, such as trichloroethylene, are examples of NAPLs (USGS, 2008c) **– Web 2.15.**

LNAPLs stands for Light Non-Aqueous Phase Liquids and they normally emerge on the groundwater surface (on the groundwater level) while the DNAPLs, stand for Dense Non-Aqueous Phase Liquids which are more dense and the most difficult to deal with. With a density relatively higher than water they can infiltrate beneath the groundwater table and as a result may potentially contaminate the full thickness of the aquifer system. Indeed, they can migrate many meters vertically in soils within hours or days, they pool at horizontal porosity and permeability boundaries, their migration is little affected by groundwater flow or gradients and there is no in situ practical method currently available to study and quantify DNAPLs saturation (Stewart and North, 2006).

According to Olhoeft (1992) the organic chemical that mostly contribute to groundwater contaminations are Trichloroethene (TCE), Dichloromethane, Tetrachloroethene (PCE), Toluene, 1,1-Dichloroethane, Bis(2-ethylhexyl) phthalate, Benzene, Tran-1,2-Dichloroethene, 1,1,1-Trichloroethene and Chloroform. In terms of density, only Toluene (0.87 g/cm^3) and Benzene (0.879 g/cm^3) can be classified as LNAPLs and Bis(2-ethylhexyl) phthalate (0.98g/cm^3) has density nearly equal to water. Whereas, other solutions have density ranges between 1.17 – 1.62 g/cm^3. The most obvious contaminations are those which are either insoluble in water or which chemically react with clay minerals.

Hydrocarbons can be introduced into groundwater from many industrial processes. The sources may be from crude oil, gasoline, liquefied petroleum gas and natural liquids gas mainly due to fractures in the isolation of pipelines, sewers and purge chambers. These

leakage or spills will then disperse and infiltrate to the surrounding materials, reach the water table and can then move from one aquifer to another. To overcome these problems, the 3D distribution of the contaminant plume must be detected first before any remediation options can be applied. Then, it is also necessary to know the properties and the characteristics of the materials at the surrounding area as well as the properties of the water/soil contaminated by hydrocarbon, because by understanding all of these properties the migration of contamination plumes can be modelled and predicted using software.

2.7 Typical geophysical properties of the contaminated land/groundwater

The best tools available to remotely detect hydrocarbon plumes in the sub-surface are a variety of geophysical techniques. Over the past decade, many researchers have investigated the problems of groundwater contaminated by hydrocarbon using geophysical techniques. Electrical Resistivity Imaging, Ground Penetration Radar (GPR), Transient Electromagnetic (TEM) and Ground Conductivity Survey (GEM) are all geophysical techniques typically used for groundwater contamination studies. Generally, the direct current (DC) resistivity methods are favoured for such applications especially on DNAPLs as the leachate produced by hydrocarbons are slightly higher in resistivity thus decrease conductivity of the solution compared to fresh water (Sauck et.al. 2008). For the LNAPLs, which are lighter than DNAPLs, they are always found on the top of water table, the GPR technique is the best geophysical techniques to detect and monitor their changes, and probably the migration paths of the LNAPLs plumes in subsurface based on GPR signal attenuation e.g. Sauck et al. (1998), Sauck (2000), Atekwana *et al*. (2000) and Cassidy, 2007).

The resistivity value of a hydrocarbon is always higher than that of freshwater. This is a useful physical property used to monitor and map the distribution and migration paths below the ground surface e.g. Martinho *et al.* (2006), Sauck (2000) and Olivar *et al*. (1995). A clear resistivity profile for the hydrocarbon contamination also had been reported by Buselli and Lu (2001), Olheoft (1992) and Endres and Greenhouse (1996).

However, different results have been reported by Sauck *et al*. (1998) and Atekwana et al. (2000), they show that a volume impacted by a hydrocarbon spills in a natural environment changes from electrically resistive to more electrically conductive

behaviour with time, due to variety of biogeochemical processes. This temporal change in the resistive behaviour of hydrocarbon contaminated zones has not been adequately exploited in geophysical models of contamination sites, although it has been suggested that many hydrocarbons and organic chemical contaminant plumes change with time due to variety of active processes e.g. (Olheoft, 1992, Benson and Stubben, 1995 and Benson, 1995). The increasing electrical conductivity also could be be result of enhanced mineral weathering due to acids produced during the biodegradation of organic molecules (Sauck, 2000).

The use of time domain induced polarization for hydrocarbon contaminant was performed by Martinho et al. (2006) in laboratory experiments for selected organic contaminated (gasoline, isopentane, toluene and benzene) and uncontaminated clayey soils samples to define the Induced Polarization (IP) effects on the materials.

The combination of TEM-MT and resistivity techniques has been used for groundwater contamination by heavy metals and related to the closed landfills Meju, (1993, 1995 and 2000) and the most useful resistivity measurement for groundwater contamination studies are direct current (DC) resistivity methods e.g. Ross *et al*. (1990), Meju (1993 and 1995) and transient electromagnetic (TEM) methods e.g. Buselli *et al.* (1988, 1992) and Meju (1993 and 1995). Note that several geophysical methods have been successfully applied to landfill characterization but the results still need borehole data for validation.

Ground Penetration Radar is one of the most important tools to image and to monitor the Light Non-Aqueous Phase Liquids according to Cassidy (2007). The properties of signal such as the decreasing of signal strength (amplitude) are used to determine the properties of the material underneath. Many reports have been produced by researchers on the use of GPR for groundwater contamination such as Pettersson and Nobes (2003), Cassidy (2007), Lopes de Castro *et al*. (2003), Sneddon *et al*. (2000), Olheoft (1992), Ajo-Franklin *et al*. (2006) and Jordan *et al*. (2004).

Integration of various geophysical methods will be deployed in this study and the output from such study will be used to evaluate the probability or the potential of the contaminant to reach the aquifer and also to determine if there any possibility for a contaminant conduit to another aquifers

2.8 Typical hydrogeological properties of the contaminated groundwater

Hydrogeological investigation is the best approach to study groundwater contaminantion by hydrocarbons. This type of contamination is also known as organic compounds contamination and are normally a consequence of breakdown and leaching of natural occurring organic material such as soil and organic matter associated with other geological strata. It also can appear from human activities such as domestic agricultural activities, commercial and industrial activities. Natural organic matter comprises water-soluble compounds of rather complex nature having broad range of chemical and physical properties. Natural organic matter in groundwater is composed of humic substances and non-humic material such as proteins, carbohydrates and hydrocarbons (USGS, 2008c) – **Web 2.15**. Natural organic matter is complex and heterogeneous but it can be characterised according to its size, structure, functionality and reactivity of the organic compounds (UNICEF and WHO, 2004) – **Web 2.6**. Natural organic compounds can originate from terrestrial sources and algal and bacterial sources within the water. Dissolved organic carbon (DOC) is considered as a most suitable parameter for quantifying organic matter present in groundwater. However, DOC is a bulk quality parameter and does not provide specific identification data and also incorporates organic compounds arising from human activity. The occurrence of organic compounds in groundwater is controlled not only by their intensity and release potential, but also by their physical and chemical properties which influence subsurface transport and attenuation (Drewes *et.al*., 2006) – **Web 2.16**.

Developing the correct conceptual model to understanding behaviour of organic compounds as well as hydrocarbons is the most important device for assessing the subsurface migration of contaminants. The important key to understand is the recognition that hydrocarbons have various different affinities for water, ranging from hydrocarbons that „love water' (hydrophilic) to these that „fear water' (hydrophobic). Such concepts are used to develop appropriate contamination conceptual models.

Understanding water and the hydrocarbon (HC) characteristics is essential before any further studies can be carried out. Water is a highly polar solvent which has a hydrogen bonded structure which will easily dissolve and solvate ionic species. Most hydrocarbons or other organic compounds are covalent molecule bonded rather than ionic species

bonded. It also has a limited tendency to partition or dissolve into water. The degree of dissolution decreases with the weight or size of the molecule. The bigger the molecule, the harder it is for it to dissolve into water. The small molecule is easier to dissolve into water because it has a polar structure and may hydrogen-bond with water, they normally have a few carbon atoms and often contain oxygen. Examples are methanol (single carbon atom, ethanol (double carbon atoms), propanol (three carbon atoms). Most hydrocarbons are relatively hydrophobic as they are comparatively larger molecules of limited polarity and with low hydrogen-bonding potential compared to small molecule structures.

2.9 Water in vadose zone

Historically, hydrogeologists have focused their attention on the phreatic (saturated) zone without paying much attention to water moving through the vadose (unsaturated) zone. The vadose zone cannot be ignored in the study of contaminant hydrogeology because it may be a significant reservoir for the capture, storage and release of contaminants. Unsaturated fluid flow is complicated by matric and osmotic energy potentials. Although the term „unsaturated zone' is often used loosely to refer to the vadose zone, part or all of the entire zone may be intermittently saturated and may contain several important subdivisions (Boulding and Ginn, 2004).

2.9.1 Soil water energy concepts

The movement of water in the vadose zone is influenced by the three major forces (water energy potential) which include the Matrics Potential, Osmotic Potential (Po) and the Gravitational Potential. Water can potentially move from the higher to the lower free energy level with the critical factor being the differences in energy level from one contiguous site to another.

2.9.1.1 Matrics potential

The matrics potential takes place due to the attraction of water to solids in the subsurface and it arises from both adsorption of water onto solids and capillary action in soil pores. The force causing of this energy potential reduce the free energy of water and are often

called as matric suction. Generally, the smaller the particle and pore size, the greater the matric potential.

2.9.1.2 Osmotic potential (Po)

Osmotic Potential results from dissolved constituents in subsurface water. The attraction of solute ions to water molecules reduces the free energy of water. Consequently, pure water will move across a semi permeable membrane to the side with the higher solute concentration. This is sometime called osmotic suction. The higher the solute concentration differential across a membrane the greater it generates osmotic suction.

2.9.1.3 Gravitational potential (Pg)

Gravitational Potential is the attraction of the force of gravity toward the Earth's centre. Pg = Gh, where the G is the acceleration of gravity and h is the height above a reference elevation (usually chosen below the lowest point at which this potential will be measured so that the gravitational potential will always be positive).

Total soil water potential is the sum of the contributions of the various forces acting on soil water.

$$Pt = Pg + Pm + Po + ... \qquad \text{Eq (2.1)}$$

Where the gravitational, matric and osmotic potentials are as defined above and other less significant potentials are indicated by ellipses. Since gravity is always a positive potential and matric and osmotic potentials are negative, water will only move through the soil profile if Pg > Pm + Po (Todd and Mays, 2005).

Generally, the vadose zone has subdivisions which can divide it into three layers. The upper layer called soil water zone or root zone where it lies between the ground surface and the maximum depth to roots penetration. Its major characteristics cause large fluctuations in quality and quantity of the moisture response due to the transpiration and evaporation of the water through the plants. The second layer is called Intermediate Vadose which contains residual moisture determined by the matric potential. Typically

the coarse-grained size material (sand and gravel) has a lower matric compared to the small-grained size of material (Silt and clay) but the amount of water held may be higher. The pores also contain a significant amount of air space, which makes the gravitational water penetrate slower into the saturated layer.

The deeper layer called a Capillary Fringe or capillary zone extends from the water table up to the limit of capillary rise of water (Todd and Mays, 2005). If the pore space can be idealized to represent a capillary tube, the capillary rise h_c, can be derived from the equilibrium between surface tension of water and the weight of the water rose which is represent by the equation below (Figure 2.4).

$$h_c = \frac{2\tau}{r\gamma}\cos\lambda \qquad \text{Eq (2.2)}$$

Where, h_c = height of capillary water

τ = surface tension,

r = radius of the capillary tube,

γ = specific weight of water

λ = the angle of contact between the meniscus and the tube wall

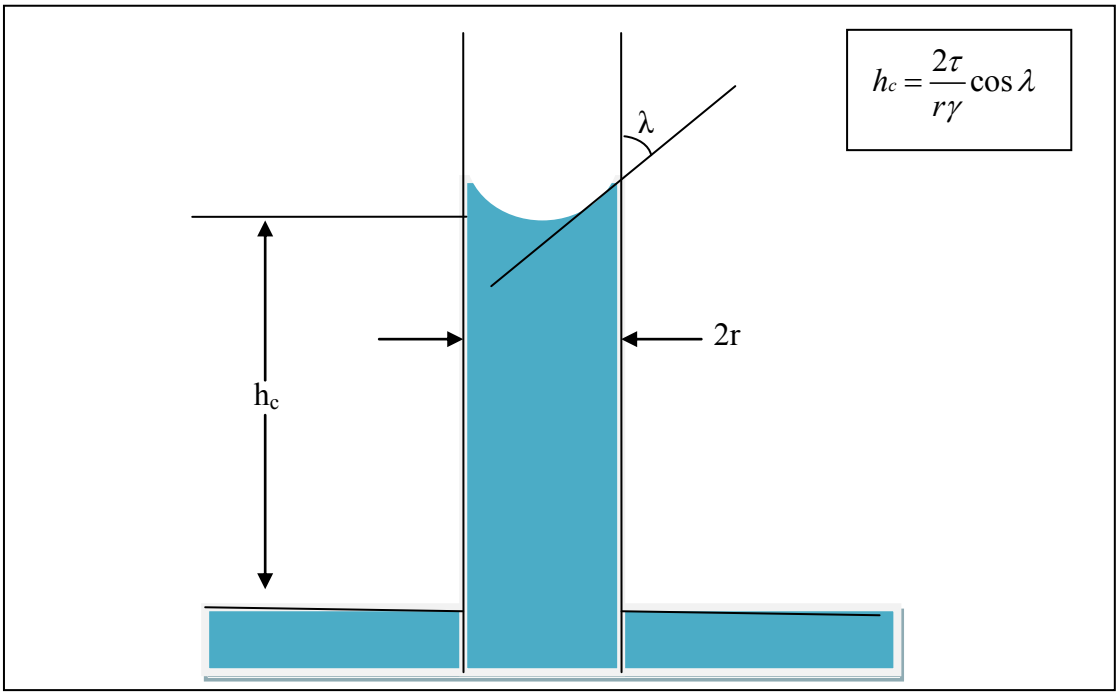

Figure 2.4: The rise of water in a capillary tube, the calculation of the height

However, for pure water in a clean glass, λ=0 and at 20°C, τ = 0.074gm/cm, γ = 1.0gm/cm^3, so the capillary rise is approximately given following the equation below (Boulding and Ginn, 2003, Todd and Mays, 2005).

$$hc = \frac{0.15}{r} \qquad \text{Eq (2.3)}$$

Where, h_c = height of capillary water

r = radius of the capillary tube

These two equations are true for the consolidated material but for unconsolidated material it bears out from the relationship (Todd and Mays, 2005).

Understanding the characteristics of water flowing in the saturated and unsaturated layer is of great importance to study the migration of pollution in any contamination site. A saturated flow can occur in the vadose zone when sufficient water has filled into the pore space in a soil. Typically it is in a temporary state and will be changing to unsaturated when the water stops flowing into the ground. Normally the gravitational water will flow quickly in the larger pore space and take one to three days flowing in the soil layer (Boulding and Ginn, 2004).

2.9.2 Challenges to understanding geophysical and hydrological properties of the vadose zone

The hydrologic characterisation of the vadose zone is technically challenging, particularly when the investigation extends deeper than a couple of metres below ground (Deiana et al., 2008). Direct measurements always involve invasive techniques such as drilling and sample collection. Successful repetition of these measurements is problematic due to inconsistency of material properties particularly in the volumetric water content as a result of previous sampling. In other words, a measurement cannot be repeated over time on similar soil samples. Thus, data provide only a single snapshot of volumetric water contents without providing an opportunity to monitor any changing properties against time. In fact, some limitation may also have to be considered because the volume of invasive measurements are small and localised, while the soil water content has a large spatial variation and predictive models usually can represent reality only at a much larger scale. This situation leads to the increasing use of non-invasive geophysical techniques for the investigation. Particularly for the investigation of water content in the vadose zone, Annan (ISO 9000:2005) used a GPR on his study, ERT by Binley and Kemna (2005), Binley e*t al*. (2002), Alumbaugh *et al*. (2002.) and Cassiani *et al*. (2004).

The important soil properties used in investigation are dielectric constant and electrical resistivity, but the direct relationship between these physical properties and the hydrological parameter such as hydraulic conductivity and unsaturated flow rate is generally not available. More reliable links can be established between geophysical parameters and the water chemical content and solute concentration. The classical empirical and semi empirical relationships had been established by Archie in 1942 (Robert, 2011) – **Web 2.17**.

2.10 Literature review on research techniques and tools

This research project was designed to integrate geophysical techniques, geochemical and hydrogeological approaches to study the contamination of land and groundwater. Geophysics will help in the mapping of the contamination zones and the chemical investigations will provide the data which can be linked with the geophysical anomalies. The information from both investigations will later be used as a guide line to run a

groundwater model on selected sites. In the following sub-sections, details of the main techniques used in this research are discussed.

2.10.1 Geophysical techniques

„Geophysics is the application of the principles of physics to the study of the Earth' (Parasnis, 1986). According to Telford et al. (2000), geophysics has to do with the physics of the Earth and the surrounding atmosphere. But recently, the definition of geophysics is more conclusive where it is described as a study of the Earth using physical principles where it is used for varieties of objectives which include (personal communication with Brabham, 2011):

1) Academic studies of deep Earth structures and geology

2) Resource exploration (e.g. Mineral/hydrocarbon)

3) Hydrogeological investigation for groundwater exploration in sedimentary and in the hard rock geology

4) Geo-Environmental studies which encompasses contaminated land, soil and groundwater pollution

5) Hazard analysis, especially for landslides and slope failures

6) Archaeological investigations to locate ancient buried structures (foundations, tombs etc.)

7) Glaciology investigation to understanding of the response of the world's ice masses to past, present, and future climatic change, as well as to address related scientific problems of anthropogenic impact

Selected geophysical techniques can be used on land (terrestrial), at sea (marine), in the air (airborne) and even down boreholes. Geophysical methods can be divided into two families:

a) **Passive Geophysics** where the geophysical data that is obtained simply measures natural Earth fields which include Gravity (macro and micro survey),

Magnetic Fields, Self Potential, Magneto telluric and the seismic information from natural Earthquakes.

b) **Active Geophysics** is where the investigation of the Earth properties needs the geophysicist to provide the energy or source into the Earth. Receivers are used to record the result of the energies passage though the Earth. The outputs are the response given by the signal (introduced energy sources) in their passage through the sub-surface which has to be analyzed. The techniques included in this active geophysics group are Seismic (refraction, reflection, and SASW), Resistivity (Vertical Electrical Sounding, Resistivity imaging, Cross Hole Resistivity Tomography), Induced Polarization Survey (Binley *et al*., 2002), Transient Electromagnetic Survey, Ground Penetration Radar and Electric Conductivity Survey.

Contaminated land usually has anomalous physical characteristics in term of electrical resistivity. Normally the resistivity values present in the contaminated land are lower (less resistive or more conductive) compared to uncontaminated land. The presence of contaminated elements such as heavy metals will reduce the resistivity. But with hydrocarbon contamination, the resistivity values are expected to be higher due to the hydrocarbon characteristic that it is an electrical insulator. The resistivity value in areas of fresh hydrocarbon contamination area is high, in some cases the values then decreases with time as the biodegradation processes by organisms takes place.

i) Resistivity Imaging Technique

Electrical DC resistivity techniques, usually referred to as electrical resistivity imaging or vertical electric sounding, measures earth resistivity values by injecting a direct current (DC) signal into the ground and measuring the resulting potentials (voltages) created. From that data the electrical properties of the Earth (the geoelectrical section) can be derived and thereby the geological properties inferred.

Common applications of the DC resistivity method include delineation of aggregate deposits for quarry operations, measuring earth impedance or resistance for electrical grounding circuits protection, estimating depth to bedrock, to measure the water table, or to other geoelectrical boundaries, and mapping and/or detecting other geologic features. In the last two decades, resistivity techniques have frequently been used for

environmental studies which involve soil or land contamination i.e. Porsani *et al*. (2004) and Aristodemou and Thomas-Betts (2000), groundwater contamination by landfill (Meju, 1993, 1995 and 2000), hydrocarbon contamination i.e. Cassidy (2007) and Atekwana *et.al*. (2000) and slope movement (slope failure and landslide study) i.e. Loke (2000).– **Web 2.18**) Recently, this technique was used for slope failure investigations including rock avalanche deposits and rockslides (Heincke *et al.*, 2010). The techniques have been applied commercially for underground pipe leakage (water and petroleum), seepage at dams (Sjodahl *et al*., 2008), archaeological exploration i.e. Jordan (2009), Keay *et al*. (2009), Clarks (1986), Hesse *et al*. (1986), Scollar *et al*. (1986) and Kampke (1999) and foundation investigation at construction sites for nuclear waste (Rucker *et al*., 2009). It was also used in the search of high permeability zones beneath dams by integrated with a seismic refraction technique Osazuwa and Chinedu (2008).

A schematic diagram in Figure 2.5 shows the basic principle of DC resistivity measurements. Two short stainless steel rods (electrodes) are driven about 15cm – 30cm into the Earth though which current is applied into the ground. Two additional electrodes are used to measure the Earth Voltage (or electrical potential) generated by the current. The depth of investigation is a function of the electrode spacing used. The greater the spacing between the outer current electrodes, the deeper the electrical currents will flow in the Earth, hence the greater the depth of exploration.

Instrument readings (current and voltage) are generally reduced to "apparent resistivity" values. The apparent resistivity is the resistivity of the homogeneous half-space which would produce the observed instrument response for a given electrode spacing. Apparent resistivity is a weighted average of soil resistivities over the full depth of investigation. The end product from a DC resistivity survey is generally 2D “geoelectric" cross section (model) showing thicknesses and resistivities of all the geoelectric units or layers. If borehole data is available, then a geological interpretation can be made from the geoelectric results. A three-dimensional geoelectric section can be made up of a series of parallel two -dimensional soundings joined together to form a three-dimensional block model which can be plotted with available software (Loke and Barker, 1996). Theoretical details of this method had been reported by Loke (2004) – **Web 2.19**. The end product from a DC resistivity modeling exercise is a "geoelectric" cross section (model) showing thicknesses and resistivities of all the geoelectric units or layers to a maximum depth

limit. There are many electrode arrays which have been developed for the resistivity imaging surveys such as Wenner array (Figure 2.6), Schlumberger (Figure 2.7), Wenner-Schlumberger, Dipole-dipole, Pole-dipole etc. An example the process of obtaining the field data is shown in Figure 2.8.

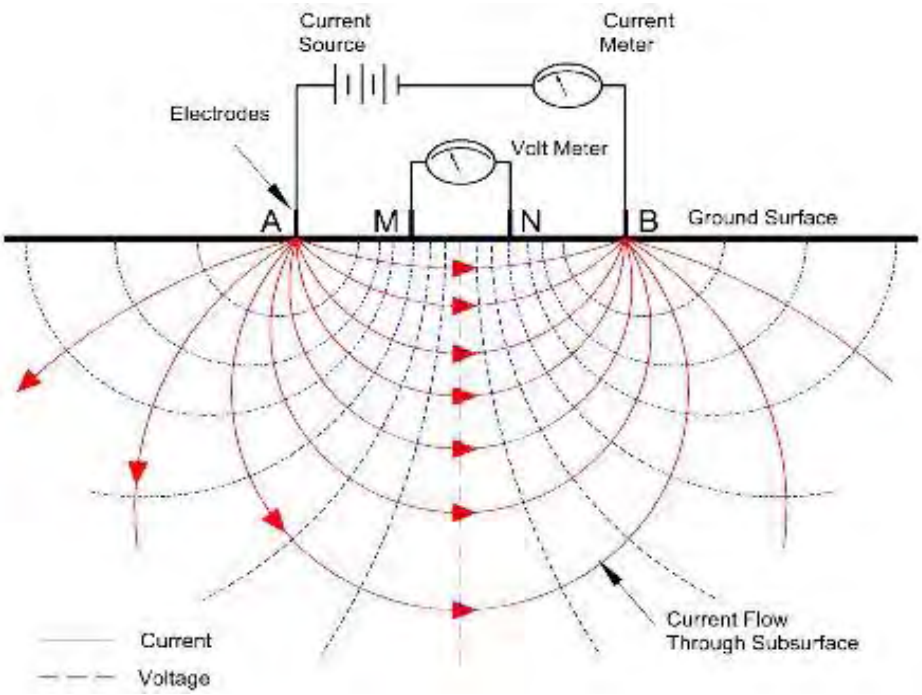

Figure 2.5: Schematic diagram showing basic principle of DC resistivity measurements (adaptation from Loke, 2004 – **Web 2.19**)

Electrical Properties of Earth Materials

Normally, electric current flows in the Earth at shallow depths by two main methods, which are electronic conduction and electrolytic conduction (Loke, 2000). In the electronic conduction, current flow is via free electrons such as in metal and in electrolytic conduction the current flow through the movement of ions in the groundwater or the moisture in the soil/ground. The electrolytic condition is important for environmental and engineering investigation, whereas the electronic conduction normally has been used for mineral exploration or when conductive minerals are present.

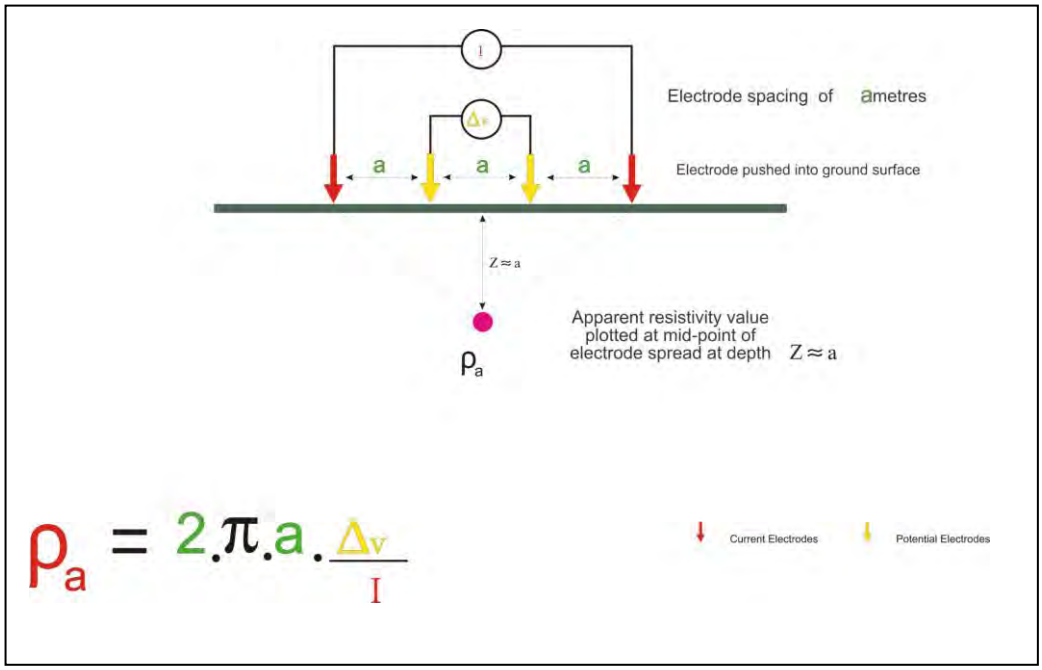

Figure 2.6: The electrode array for Wenner Configuration

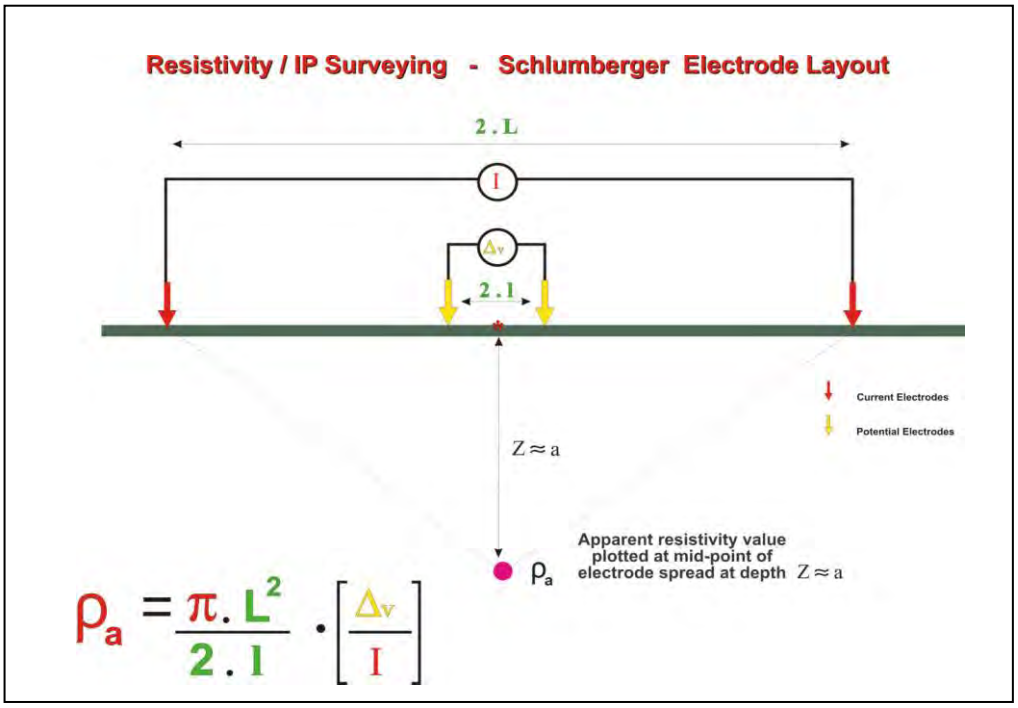

Figure 2.7: The electrode array for Wenner Sclumberger Configuration

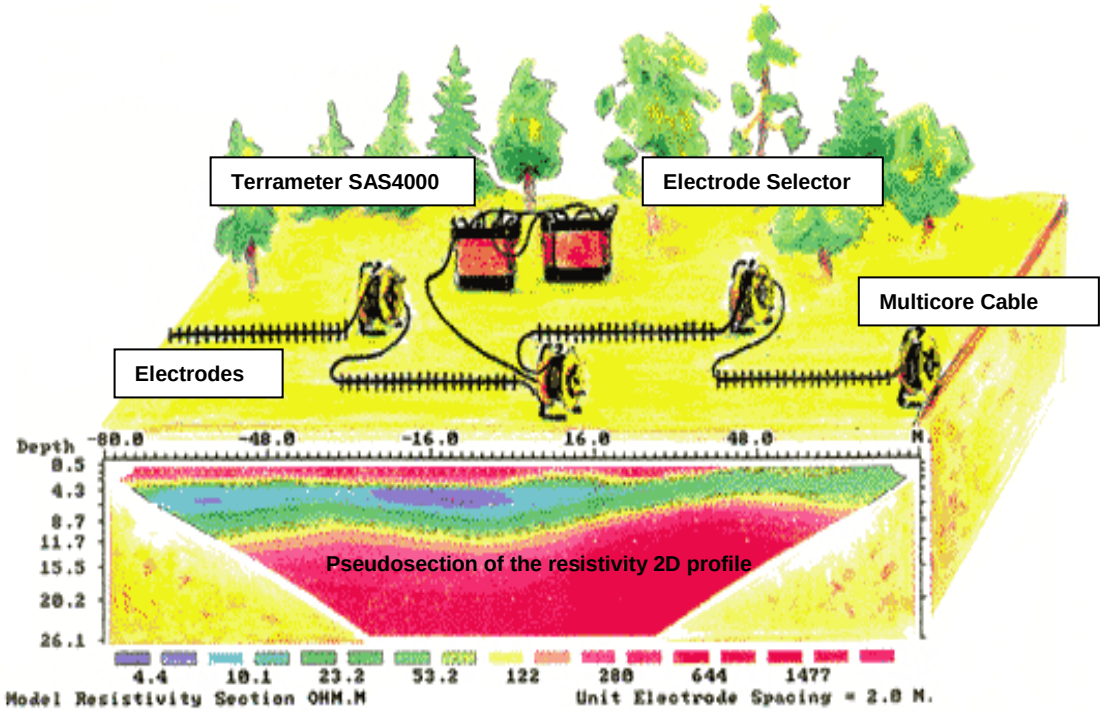

Figure 2.8: Resistivity imaging showing the general setup and the resulting image processed by 2D inversion (ABEM Instrument AB, 2009) – **Web 2.20**

For rocks composed of non-conducting matrix minerals and saturated with water**,** an empirical relationship known as Archie's Law is useful in analysis of electrical properties. Archie's Law is commonly written

$$\rho_{ROCK} = \rho_{FLUID} \; A \; \phi^{-m} \qquad \text{Eq ----------(2.4)}$$

where ρ_{FLUID} equals the electrical properties of the fluid in the pores, ϕ is the porosity (ratio of void volume/total volume), and A and m are constants that depend on the geometry of the pores. For many rocks, A = ***about*** 1 and m = ***about*** 2. See Keller, G.V. (1986 for a broader discussion. Papers discussing various A and m values for specific rocks (shale sands, clean sandstones, etc.) have been published in the journal Geophysics (Stierman, 2005) – **Web 2.21**.

> Note: there are several versions of Archie's Law that attempt to include the effects of partial saturation (water-gas or water-oil) or mixed fluids in the pores, or, the air water mixes in the vadose zone. Archie's Law is not valid for rocks containing a significant percentage of clay**.** Clay provides for conductive matrix, rendering a

fundamental assumption invalid. Graphite, native metals, and minerals with metallic lustre's are also electrical conductors, but these are far scarcer than clays (Stierman, 2005) – **Web 2.21**.

Generally another explanation for the resistivity of common rocks and minerals are presented in Figure 2.9, (summaries from Keller and Frischknecht (1966) and Telford et al. (1990)) and typically is controlled by the porosity of the rocks and the salinity of the fluid flowing contained in the rock mass. Igneous and metamorphic rocks usually display high resistivity values and the resistivity of the rocks is greatly dependent on the presence of the discontinuities or fractures in the rock mass. These types of rock typically display resistivity values from 1000 Ωm to 1,000,000 Ωm depending on whether they are wet or dry (Loke, 2004). Porosity is one of the most important parameters for determining whether the rock is suitable for engineering proposes or for groundwater supply.

Also according to Loke (2000), sedimentary rocks commonly display a resistivity range from 10 to 10 000 Ωm, typically averaging around 1000 Ωm. Again the resistivity values are largely dependent on the porosity of the rocks, and the salinity of the pore water.

Groundwater can display resistivity values from 10 up to 100 Ωm depending on how much total dissolved solid is present in the water. Sea water for example has a resistivity value as low as 0.2 Ωm due to the Na^{2+} and Cl^{-} dissolved in it. Unconsolidated sediments generally have a lower resistivity value compared to sedimentary rocks. The resistivity values are typically about 10 to 1000 Ωm and are again dependent on porosity and water content.

The resistivity values of several industrial contaminants are also given in Figure 2.9. Metals, such as iron, have extremely low resistivity values. Chemicals that are strong electrolytes, such as potassium chloride and sodium chloride, can also greatly reduce the resistivity of ground water to less than 1 Ωm even at fairly low concentrations. The effect of weak electrolytes, such as acetic acid, is comparatively smaller. Hydrocarbons, such as xylene (6.998×10^{16} Ωm), have very high resistivity values. However, in practice the percentage of hydrocarbons present in a rock or soil is usually quite small, and thus might not have a significant effect on the bulk resistivity. As an example, oil sands in Figure 2.9 have the same range of resistivity values as alluvium.

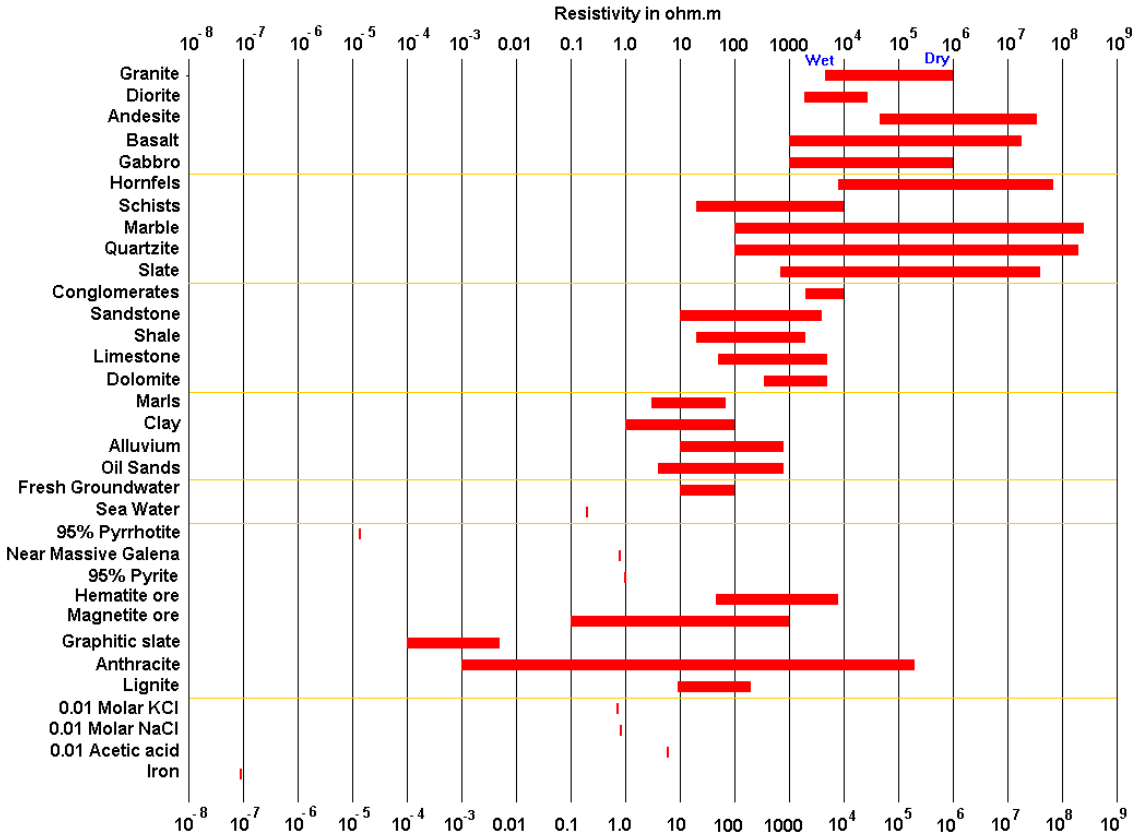

Figure 2.9: The resistivity of rocks, soils and minerals (source, Loke, 2000)

ii) **Electromagnetic / Ground Conductivity Survey (GEM-2)**

This is an active method that uses an electromagnetic (EM) signal to detect variations in subsurface electrical conductivity. These currents result in a secondary electromagnetic field that is measured together with the original transmitted signal, using a receiver coil on the EM instrument (Figure 2.10). The secondary field is then separated into two orthogonal components, the real and imaginary (quadrature) components, representing respectively the vector components of the field in-phase and 90 degrees out of phase with the primary (Terraplus, 2011) – **Web 2.22**. The quadrature component provides a measure of the apparent ground conductivity whilst the real (in-phase) component is responsive to buried metallic objects (Geo-Service International (UK) Limited, 2009) – **Web 2.23**.

The depth of penetration attained by the method is dependent on a number of factors including the ground conductivity, the loop spacing and the orientation of the primary

field (dipole orientation). A large number of different EM instruments are available which cover a depth of investigation range of less than 0.5m to over 30m. Typically „metal detectors' used by treasure seekers have a detection depth of less than 1m, whereas for surveys of geo-environmental interest, the typical depth of investigation is usually in the order of 10m or more. The use of three or more loop spacing in both dipole orientations enables quantitative modelling of the depth to individual conductive layers. This is commonly known as EM depth sounding. In principle, this technique uses the secondary electromagnetic field generated from the conductive layer (material) beneath the surface and transforms the signal into conductivity (mS/m). This parameter will be used to determine the ground and subsurface conditions.

Terrestrial electromagnetic has many applications including: archaeological, buried weapon detection and also for numerous environmental issues described by Won *et.al.* (1996 and 2004), Won and Huang (2004), Huang (2005), Huang and Won (2000, 2003 and 2004) and Witten *et.al.* (2000 and 2003). Airborne electromagnetic is used for large scale mineral and regional hydrogeological investigations and is outside the scope of this research project.

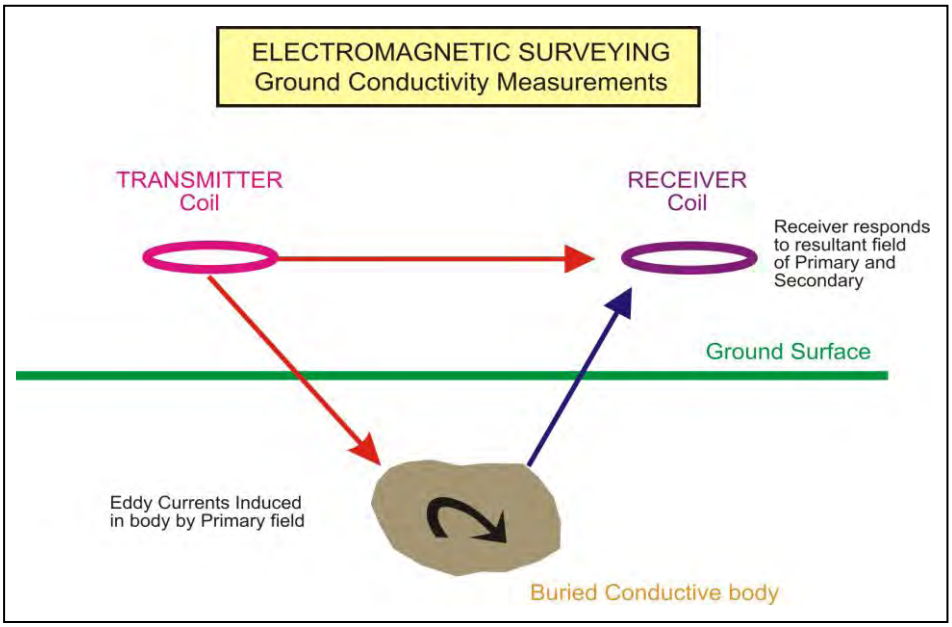

Figure 2.10: The schematic diagram showing the principle of the EM technique for site investigation

2.10.2 Resistivity measurement theory

As previously discussed, ground resistivity surveys involve the measurement of resistance by introducing an electrical current across a pair of grounded metal electrodes (AB) and measuring the voltage potential between an adjacent electrode-pair (MN). This concept is illustrated in Figure 2.11.

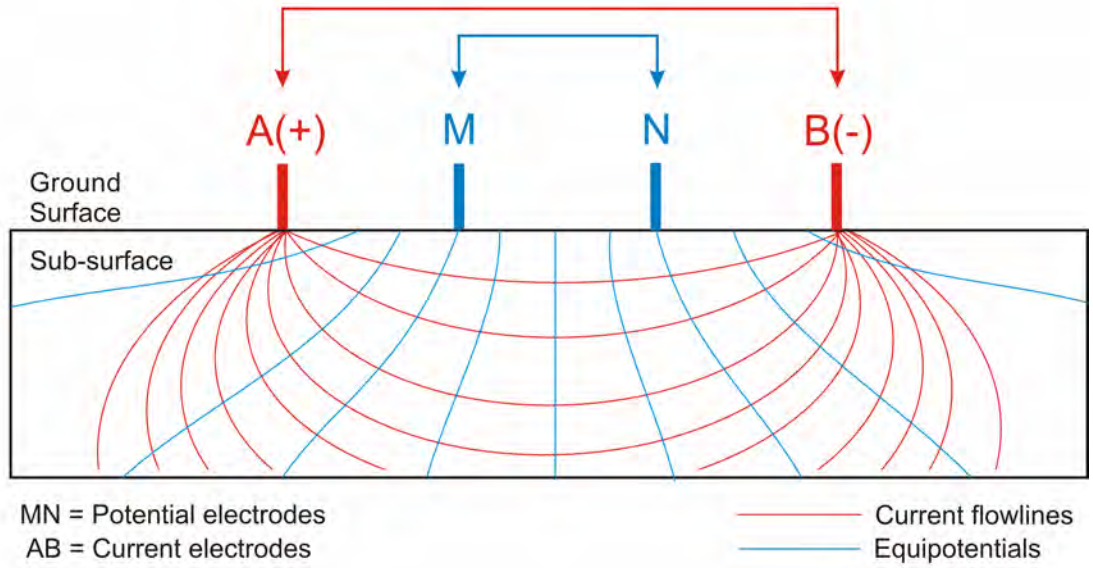

Figure 2.11: A diagram illustrating the basic theory of ground resistivity measurement by introducing electrical current and measuring voltage potential

An equation for the potential distribution due to a point current source $\boldsymbol{I_s}$ located at point $\mathbf{x_s}$ can be derived from:

Ohm's law:

$$j\,(x) = \sigma\,(x)\,e\,(x) \tag{2.5}$$

and the *divergence condition:*

$$\Delta \cdot j\,(x) = I_s\,\delta\,(x - x_s) \tag{2.6}$$

where **e** is the electric field (in V/m), **j** is the current density (in A/m^2), **σ** is the conductivity of the medium (in S/m) and **x** = (x, y, z) (Keller and Frischknecht, 1970).

The time independent form of the first Maxwell equation, $\mathbf{\Delta} \times \mathbf{e} = 0$, implies the existence of a scalar electric potential:

$$e(x) = -\Delta \Phi(x) \tag{2.7}$$

which may be combined with Eq. (2.6) and Eq. (2.7) to give:

$$\Delta \sigma(x) \cdot \Delta \Phi(x) + \sigma(x) \Delta^2 \Phi(x) = I_s \, \delta(x - x_s) \tag{2.8}$$

Assuming a homogenous half-space Earth model, the first term on the left hand side of equation (2.8) is not used and the potential caused by a current source located at
x = (0, 0, 0) is given by:

$$\Phi(x) = \rho \, I_s \, 1 / 2\pi \, [x] \tag{2.9}$$

where $\rho = 1 / \sigma$ is the resistivity and [x] is the distance from the origin. So, the boundary conditions $\Phi = 0$ for $[x] \rightarrow \infty$ and $\Phi \rightarrow \infty$ for x = (0, 0, 0) are applied.

Since potential functions can be added arithmetically, the total potential at one observation point may be calculated by adding the potential contributions from each source. The potential difference between two potential electrodes (MN) induced by a pair of current electrodes (AB) is then given by:

$$\Phi_M - \Phi_N = \Delta \Phi = \rho \, I_s / 2\pi \, (1/AM - 1/BM - 1/AN - 1/BN) \tag{2.10}$$

where *AM* denotes the distance between current electrode A and potential electrode M. So, the minus sign for two of the distance terms arise since one of the current electrodes in a normal two-electrode current must have a negative sense of current flow compared to the other.

When σ is allowed to vary over a full 2D or 3D half-space Earth model the first term in Eq. (2.7) does not vanish. Integrating over volume *V* and applying Green's theorem:

$$\iint_s \sigma(x)\,[\partial\,\Phi(x) / \partial n]\,dS = I(x) \tag{2.11}$$

where **n** is the unit vector normal to the surface.

Using the finite-difference discretisation of Dey and Morrison (1979) this leads to a matrix equation of the form:

$$\mathbf{G}\,\Phi = \mathrm{I} \tag{2.12}$$

where **G** is the conductance matrix consisting of the discretised conductivities and Φ are the discretised potentials. The generally sparse conductance matrix **G** can be inverted using a sparse matrix solver to give the potentials over the whole 2D or 3D model grid.

During DC resistivity surveys, the quantity that is actually measured is *potential difference* between the two potential electrodes (MN). For a homogeneous Earth, Eq. (2.10) can then be used to calculate the *resistivity* (***ρ***), so the terms can be rearranged to obtain:

$$\rho = \mathrm{K}\,(\Delta\,\Phi / I) \tag{2.13}$$

where ***K*** is called the *geometric factor* combining the effect of electrode separation distances (Keller and Frishknecht, 1966).

If the sub-surface is non-uniform, the so called *apparent resistivity* (**ρ_a**) is determined from Eq. (2.13).

2.10.3 Electrode array geometries

Resistivity ground surveys were primarily developed using the four-electrode system comprising two current and two potential electrodes. However, modern ERT acquisition systems utilise multi-electrode arrays, whereby it is possible to use between 18 and 72 electrodes connected along a single traverse with multi-core cables. Multi-electrode acquisition systems were developed to minimise the time spent during field data acquisition and to enable resistivity variations to be determined over significant distances and depths. A four-electrode configuration can be applied to a multi-electrode survey

traverse by a range of different geometries. The most widely used electrode array geometries, the *Wenner*, the *Wenner-Schlumberger*, and the *Double-Dipole*, are described and illustrated in Figure 2.12.

In the Wenner array geometry, current is applied to the outer electrodes with potential difference being measured across the inner pair. When this geometry is applied to a multi-electrode array, greater depths and distances are progressed by increasing the spacing between electrodes, whereby the spacing increase is always a multiple of the minimum spacing (*a* in Figure 2.12). If the Wenner array geometry is used during field data acquisition, the number of readings is relatively small; therefore this array configuration can minimise the time taken to run a survey. However, the resolution is only suitable for analysing vertical layered changes and small scale lateral heterogeneities often remain unresolved.

In the Double-Dipole geometry, two „dipoles' are established comprising the current pair (AB) on one side of the array and the potential pair (MN) on the other side. When this array geometry is applied to a multi-electrode traverse, the spacing (a) of the dipoles remains constant and always equal or less than the spacing between the dipoles (na). Data acquisition is progressed vertically and horizontally by increasing the spacing between the dipoles (na). The Double-Dipole configuration results in a larger number of measurements than the Wenner array and horizontal resolution is good, however this is at the compromise of decreased depth penetration.

In the Wenner-Schlumberger array geometry, current is applied to the outer electrode pair whilst potential difference is measured across the inner pair. The difference between this and the standard Wenner array is that the midpoint spacing between the potential electrodes (a) is kept constant and the spacings between AM and NB are increased logarithmically. This results in an enhanced data resolution and with a slightly increased number of spacings, but not as many as the Double Dipole array.

2.10.4 ERT instrumentation and field data acquisition

Equipment utilised during ERT surveys is relatively inexpensive, portable and commercially available. Hardware consists of a resistivity meter integrating a multi-

channel switching unit and data logger, a 12 Volt DC power supply, a set of stainless steel electrodes, multi-core cables, electrode connectors, and multi-channel cable link nodes. A commercially available resistivity instrument (Figures 2.13, 2.14) would normally be supplied with interface software enabling the operator to compile and upload electrode sequence address configurations and to download raw data for processing.

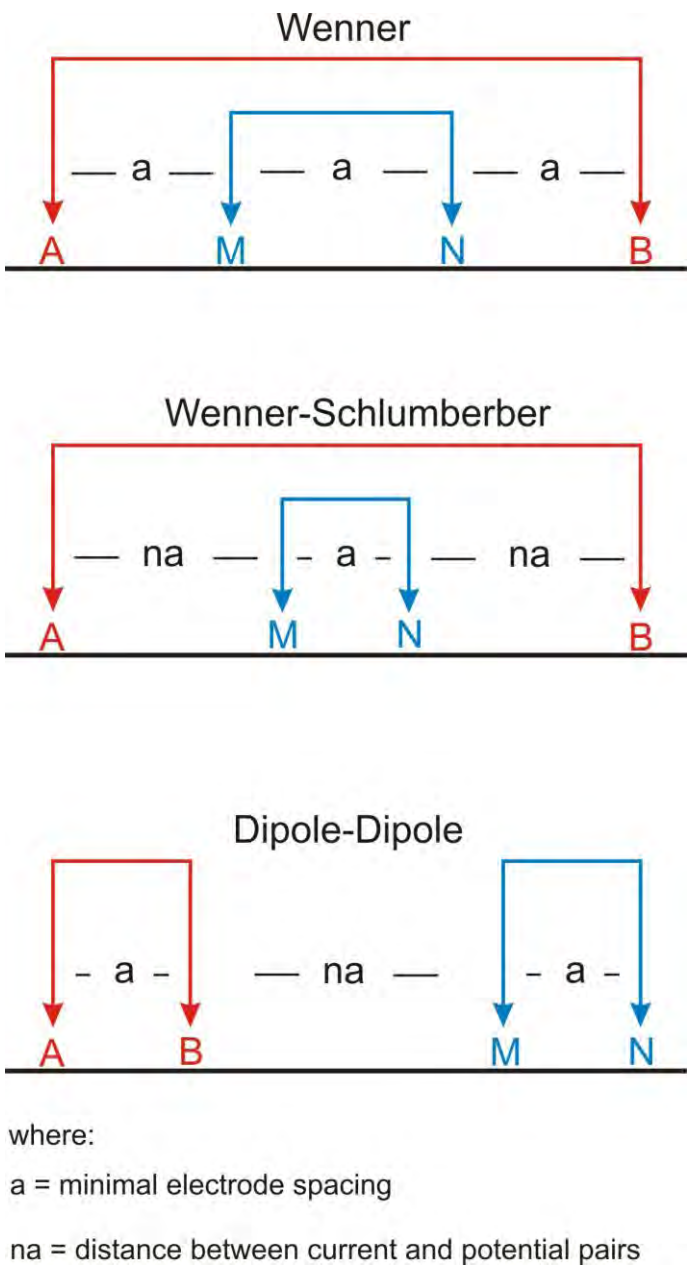

Figure 2.12: Schematic representations of the commonly used Wenner, Wenner-Schlumberger, and Double-Dipole electrode array geometries.

Figure 2.13 illustrates a modern commercial resistivity meter and external 12 Volt DC supply. In this photograph, the IRIS Instruments® SYSCAL 72-Switch is illustrated and was used during this research programme. Figure 2.14 illustrates an ERT survey traverse in operation during a geophysical site characterisation.

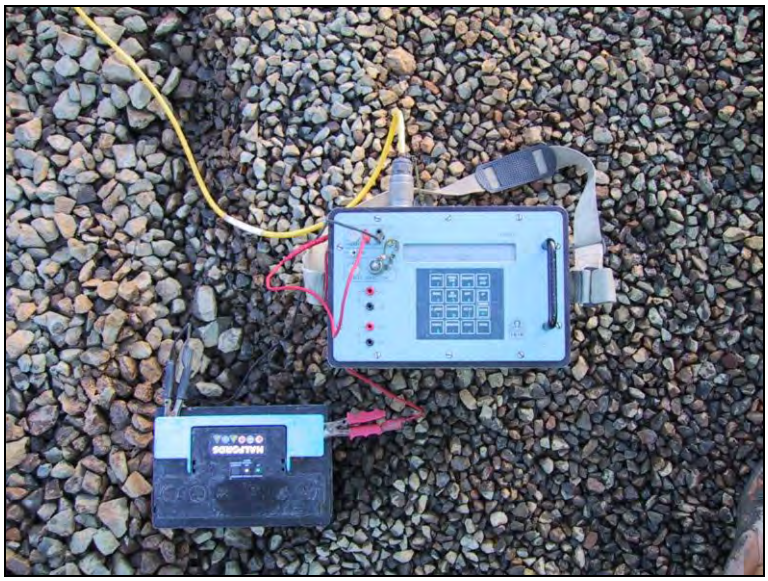

Figure 2.13: A photograph illustrating a modern commercial resistivity meter and external 12 Volt DC supply (George, 2006).

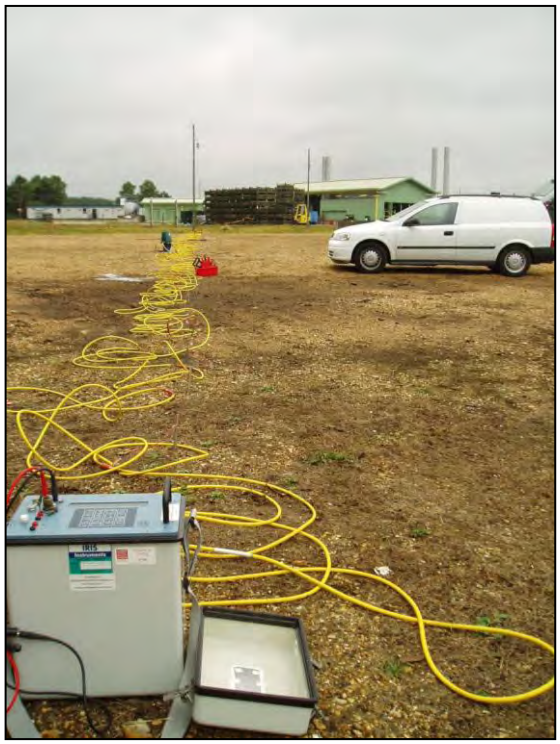

Figure 2.14: A photograph illustrating ERT data acquisition during a geophysical site characterisation (George, 2006).

An ERT survey is usually planned by collaboration between the geophysical contractor and client according to information relating to sub-surface targets or possible anomalies obtained from desk study research. A survey plan of the site will show ERT profile traverse positions, the start and end electrode locations, and electrode spacing.

ERT traverses are established by inserting stainless steel electrodes into the ground surface along a pre-determined traverse, whilst ensuring that the probes are well-grounded. Electrodes are connected to multi-core cable, which in turn is linked to the resistivity meter (Figure 2.14). A fixed electrode spacing must be used throughout each survey line and will be prescribed according to the resolution and/or depth required. It is generally accepted that the geophysicist must use a wide electrode spacing to obtain greater depths of investigation, but at the compromise of vertical and horizontal resolution, which is greater using smaller electrode spacings.

Prior to an ERT survey, an electrode sequence address file is uploaded from PC onto the resistivity meter. A sequence address file contains a list of configurations instructing the instrument to apply electrical current and measure potential difference according to the electrode array geometry used for a given number of electrodes.

Poorly grounded electrodes and/or very dry soil conditions will undoubtedly result in a low signal to noise ratio and inaccurate readings of resistance and apparent resistivity. Therefore, care must be taken prior to data acquisition to ensure all electrodes are well-grounded and to perform a contact resistance test. Modern resistivity meters have an in-built function to test the contact resistance between electrode pairs and the ground surface prior to a survey. High contact resistances (>4 kΩ) can be rectified by improving the ground contact. In cases where high contact resistances persist, a suitable contact can be obtained by application of saline water to the ground immediately around the electrode. It is widely accepted that contact resistances should be less than 4kΩ across all electrodes in a traverse in order to optimise the signal to noise ratio and obtain accurate readings of apparent resistivity.

On completion of data acquisition the readings are downloaded to PC using interface software, which will enable the operator to assess the quality of the raw data in the field, remove erroneous data points, and export the results in a format suitable for inversion.

2.10.5 Tomographic inversion – RES2DINV®

Following the acquisition of resistance and/or apparent resistivity data points from the sub-surface during an ERT survey, an inversion routine must be performed to produce a two-dimensional image tomogram, which is a model of the difference between measured and calculated apparent resistivity values.

Apparent resistivity raw data acquired from all field test sites during this research was subject to inversion using the RES2DINV® software (Loke, 2004). This software incorporates a forward modelling sub-routine to calculate the apparent resistivity values and a non-linear least-squares optimisation technique for the inversion routine (Loke and Barker, 1996).

The smoothness-constrained least-squares inversion method used by RES2DINV® is based on the following equation (Loke, 2004):

$$(J^T J + uF)d = J^T g \qquad (2.14)$$

where $F = f_x f_x^T + f_z f_z^T$

f_x = horizontal flatness filter

f_z = vertical flatness filter

J = matrix of partial derivatives

u = damping factor

d = model perturbation vector

g = discrepancy vector

As described in Loke (2004), RES2DINV® incorporates a new implementation of the least-squares method based on a quasi-Newton optimisation technique (Loke and Barker, 1996). This technique is more than 10 times faster for large datasets than the conventional least-squares method and requires less processing memory. A further advantage of this method is that the damping factor and flatness filters can be adjusted to suit different types of data.

RES2DINV® uses a two-dimensional model to divide the sub-surface into a number of rectangular blocks, the purpose of which is to determine the resistivity of the blocks that will produce an apparent resistivity pseudosection that agrees with the actual measurements. An optimisation method used by the program attempts to reduce the difference between the calculated and measured apparent resistivity values by adjusting the resistivity of the model blocks. A measure of this difference is given by the root-mean-squared (RMS) error. It is important to note that the inversion model with the lowest RMS error can sometimes show large and unrealistic variations in the model resistivity values and may not always be the best model from a geological perspective. In general, the most prudent approach is to choose the model at the iteration after which the RMS error does not change significantly - usually between the 3rd and 5th iterations.

The effectiveness of resistivity data inversion and the quality of tomographic interpretation is highly dependent on accuracy, resolution and equivalence, a description of which is provided in Hauck (2001). In order to estimate the quality of the inversion results, the model *resolution* and *accuracy* must be analysed. Both quantities are strongly influenced by the number of model parameters; that is the number of model blocks in a tomographic inversion. If many model parameters are selected the accuracy of these parameters may be low, whereas the resolution of the inversion result is high. If only a few model parameters are selected the accuracy is high but the resolution is low. In effect, there is a compromise between accuracy and resolution in choosing the number of model parameters for a given data set.

Non-invasive ERT is restricted to acquisition of measurements from the ground surface, which usually results in a decrease of the sensitivity of the model parameters to the data with increasing depth. One possibility is to increase the model block size with depth leading to fewer model parameters and higher accuracy at larger depths. At shallow depth, where the sensitivity is usually largest, a higher resolution is often achievable.

A further problem of uncertainty sometimes arises from the principle of *equivalence*, which implies that two highly resistive anomalies with slightly different resistivities and dimensions may show the same response if the product of their thickness and resistivity values ($z\ \rho$) is the same. Furthermore, two highly conductive bodies will give the same response if the ratio between their thickness and resistivity values ($z\ /\ \rho$) is the same.

It is essential that non-invasive ERT results must not be relied upon solely and should be calibrated by comparison to results from conventional site investigation information, such as moisture content and hydrogeochemical analysis obtained from boreholes, trail pits and monitoring wells.

2.10.6 Data presentation and interpretation

Tomographic inversion, using a program such as RES2DINV®, produces a two-dimensional colour-scaled image of resistivity variation with distance and depth beneath the survey electrode profile. Modelled apparent resistivity data can be viewed as a numerical block image, or alternatively data points can be contoured, and in both cases a scale of resistivity in ohm.meter (Ωm) from low to high is provided.

Interpretation of modelled apparent resistivity may be qualitative, which involves visual inspection of resistivity variation and anomalous occurrences. It is advisable to compare the resistivity image produced with a geological or conceptual model of the perceived ground characteristics. For example, a landfill site would be expected to contain leachate within the waste-mass and possible migration into the background geological deposits and as these liquids are electrically conductive, zones of low resistivity may be inferred to be characteristic of leachate. This approach may be adequate for initial reconnaissance ground investigations, but must be calibrated by comparison to observation well data, geological logs and intrusive sampling.

Occasionally, resistivity surveys are repeated in a temporal sense by acquiring raw data along a fixed array of electrodes on an hourly, daily, or monthly basis. On this basis, the acquisition of multiple data sets from the same electrode profile will permit qualitative interpretation involving timelapse inversion. This can be performed using the RES2DINV® program. Several apparent resistivity data sets can be inverted simultaneously to produce an ERT image of the first data set acquired, followed by subsequent images of resistivity variation between specified time intervals. A timelapse processing approach is particularly useful for analysing resistivity changes within bulk background resistivity values, whereby variations may be caused by increased saturation, desaturation, or the migration of conductive saline groundwater or contaminated plumes.

2.11.1 Background to electromagnetic induction methods

A transmitter coil with an alternating current placed above the ground generates a primary electromagnetic field that propagates both above and below the ground surface. According to EM induction laws, the time-varying magnetic field generated by the alternating current of the transmitter induces eddy currents in any conductor in the subsurface, which in turn generate a secondary time-varying magnetic field. A receiver coil placed above the surface can detect the resultant of the primary and secondary magnetic fields. The differences in phase and intensity between received and transmitted fields can provide information on the electrical properties, geometry and location of the conductor Figure 2.15.

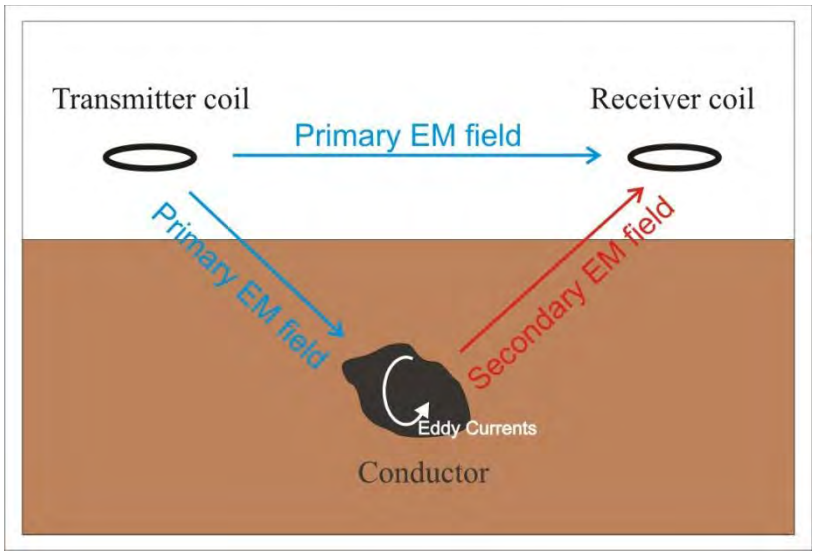

Figure 2.15: Schematic diagram illustrating the principle behind electromagnetic induction methods (Tobaga, 2011)

<u>In-phase and quadrature</u>

The primary electromagnetic field generated by the transmitter travels above the ground maintaining its original phase and with only a very limited decrease in amplitude due to geometrical spreading. The alternating voltage induced in the conductor in the ground has the same frequency of the primary field but has a phase lag of $\pi/2$. The properties of the conductor cause an additional phase lag Φ equal to:

$$\Phi = \tan^{-1}\left(\frac{2\pi fL}{r}\right) \qquad 2.15$$

where f is the frequency of the electromagnetic field, L and r are the inductance and the resistance of the conductor respectively.

Therefore, the secondary field is $\pi/2+\Phi$ phase lag behind the primary field. For very good conductors the phase of the secondary field is almost π behind the primary filed (as r tend to 0 and Φ to $\pi/2$), whereas for very poor conductors is $\pi/2$ behind the primary field (as r tend to ∞ and Φ to 0).

The relationship between primary (P), secondary (S) and resultant (R) fields measured by the receiver can be illustrated through a vector diagram (Figure 2.16). The horizontal projection of the secondary field (on the primary field) is equal to $S\sin\Phi$, is at π phase from the primary and is known as the in-phase or real component of the secondary field. The vertical projection of the secondary field is equal to $S\cos\Phi$, is at $\pi/2$ phase from the primary and is known as the out-of-phase, quadrature or imaginary component of the secondary field (Kearey et al, 2002).

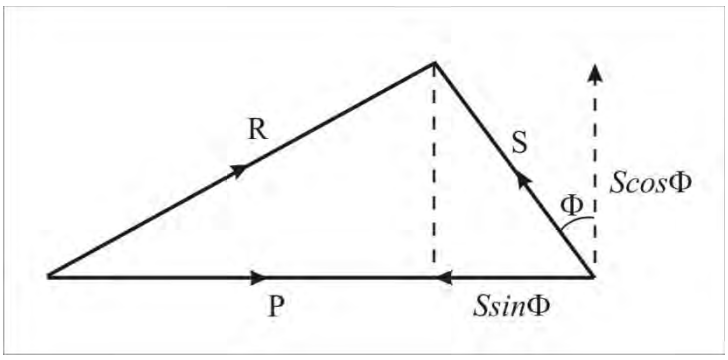

Figure 2.16: Vector diagram illustrating the amplitude and phase relationships between primary (P), secondary (S) and resultant (R) electromagnetic fields (Kearey et al., 2002)

<u>Applications and usual targets</u>

Electromagnetic induction (EMI) instruments have been widely used for site characterisation in environmental and engineering studies as they offer a rapid and cost-effective means to map electrical conductivity variations. Compared to conventional galvanic resistivity techniques, the electromagnetic induction method does not require contact with the ground, leading to surveys that can be carried out more rapidly and with less manpower (therefore less expensive), and providing measurements that are not affected by potential resistivite inhomogeneities located in the near-surface close to the electrodes (McNeill, 1980).

The differences in electrical conductivity mapped by EMI instruments can be associated to changes in rock/soil type, fracturing degree, porosity, clay content, water saturation degree, and electrical properties of water/fluid in the soil (i.e. contaminants such as dissolved salts or acid mine drainage) (McNeill, 1980). Typical values of conductivity (or resistivity) for geological materials found in sedimentary or igneous/methamorphic environments are reported in Figures 2.17 and 2.18.

Moreover, as metals can cause strong anomalies, EMI methods have been often used to locate buried metallic containers/pipes or unexploded ordnance (UXO) in combination with the magnetic technique (mostly if some of the targets are expected to be non-ferrous).

In general, a wide range of electromagnetic methods and instruments is available to the geophysicist. Descriptions of several instruments and methods together with detailed EM mathematical background can be found in many geophysical text books (Kearey et al. 2002 and McNeill 1980). The following section focuses on the instrument GEM-2 (Geophex), which was used for this project.

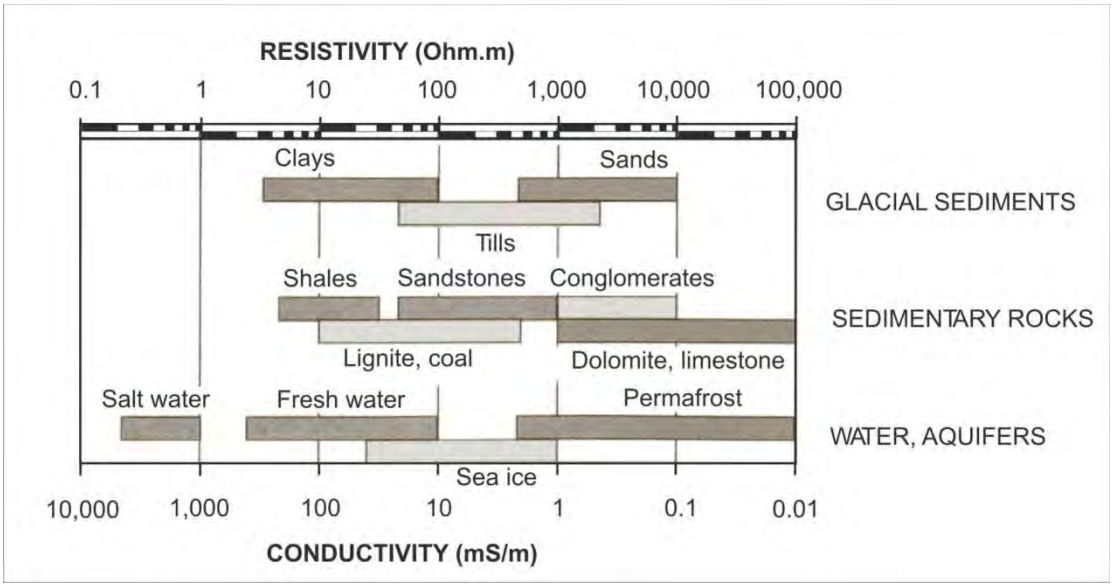

Figure 2.17 Conductivity (or resistivity) values for geological materials found in sedimentary environments (Tobaga, 2011)

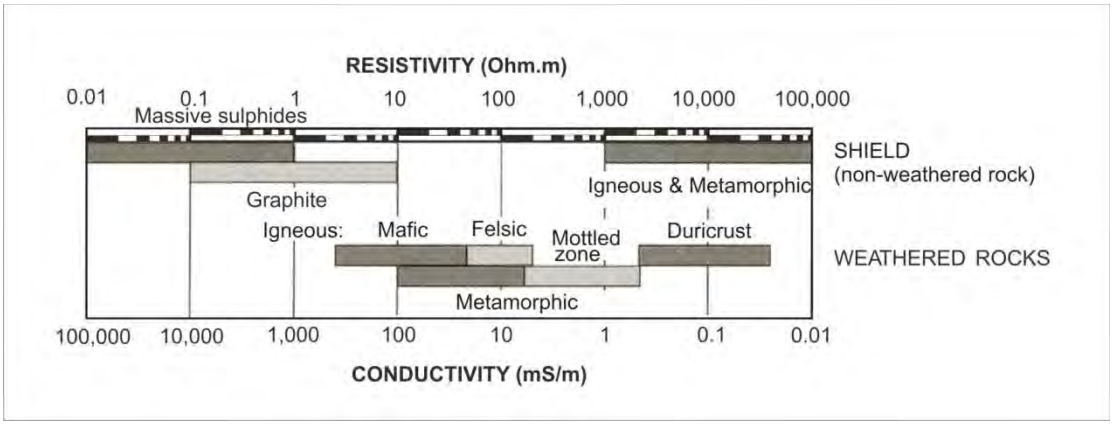

Figure 2.18 Conductivity (or resistivity) values for geological materials found in igneous or methamorphic environments (Tobaga, 2011)

2.11.2 The broadband multi-frequency instrument GEM-2 (Geophex)

GEM-2 is a broadband, hand-held, digital, multi-frequency EM sensor developed by Geophex since the beginning of 1995. The instrument consists of a light and portable board ("ski") containing three coils: a transmitter and a receiver, at a fixed spacing of 1.66 m, and a third coil, which has the function of cancelling ("bucking") the primary field from the receiver coil. A small removable console used to control the instrument and store data is attached to the board (Figure 2.19).

Figure 2.19 GEM-2 instrument used in horizontal coplanar configuration (Tobaga, 2011)

The instrument owned by Cardiff University can operate in a frequency range between 330 Hz and 47970 Hz and with up to 15 simultaneous frequencies. However, as the transmitter energy is sheared between the selected frequencies, only up to 3 to 5 frequencies should be used simultaneously during a survey (GEM-2 Manual).

The frequencies selected by the operator are converted into a digital "bit-stream", which is used to construct a transmitter waveform for the survey, with a technique called pulse-modulation. For UK (and all Europe) a base period of 1/25th of a second for the bit-stream must be selected to minimise noise from the power supply operating at 50 Hz (Won, 1996).

Signal is recorded and then digitised at both bucking and receiver coils. These time-series are successively convolved with sets of sin and cos series to obtain the values of in-phase and quadrature in part-per-million, which are the raw data stored by the instrument (ppm; Won, 1996):

$$ppm = 10^6 \frac{\textit{secondary magnetic field at receiver coil}}{\textit{primary magnetic field at receiver coil}} \qquad 2.16$$

These values in ppm are sensor specific and therefore do not have scientific significance. However, they can be converted to values of apparent conductivity (values of conductivity for a ground below the sensor assumed to be a homogeneous and isotropic half-space). For example, for a horizontal coplanar configuration, the secondary field normalized against the primary at the receiver coil (or mutual coupling ratio, Q) is (Won, 1996):

$$Q = \frac{H_S}{H_P} - 1 = -r^3 \int_0^\infty \lambda^2 R(\lambda) J_0(\lambda r) e^{-2\lambda h} d\lambda \qquad 2.17$$

where R is the kernel function for a uniform half-space:

$$R(\lambda) = \frac{\lambda - \sqrt{\lambda^2 + i2\pi f\mu\sigma}}{\lambda + \sqrt{\lambda^2 + i2\pi f\mu\sigma}} \qquad 2.18$$

H_S and H_P are the secondary and primary field at the receiver coil, r is the coil spacing, h is the height of the sensor above the ground, J_0 is the zeroth-order Bessel function, f is the transmitter frequency (in Hz), μ is the magnetic permeability and σ is the earth conductivity.

Equations 2.17 and 2.18 differ only for a factor of 10^6. Therefore, knowing coil separation, instrument height and operating frequency, the observed ppm values can be converted to apparent conductivity (Won, 1996). Huang and Won (2000) provide more details on this process of conversion to apparent conductivity.

<u>Advantages of frequency sounding and definition of skin depth</u>

In general, the depth of a target can be determined in two ways with EMI methods (Figure 4.6; Witten et al., 1997; Won, 1996; 2003):

- By geometrical sounding: using an instrument operating at a fixed frequency and taking measurements at a range of different coil separations;
- By frequency or broadband sounding: using an instrument with a fixed coil separation but taking measurements at a range of different frequencies (such as GEM-2).

The instruments relying on geometrical sounding (i.e. EM34-3 of Geonics) have the disadvantage of requiring more than one operator, being more time-consuming and suffering for the difficulty of maintaining an accurate coil separation. By contrast, the instrument GEM-2 is extremely portable, light (4 kg weight) and can be operated by one person, rendering it an attractive solution in areas of difficult site conditions such as landslides.

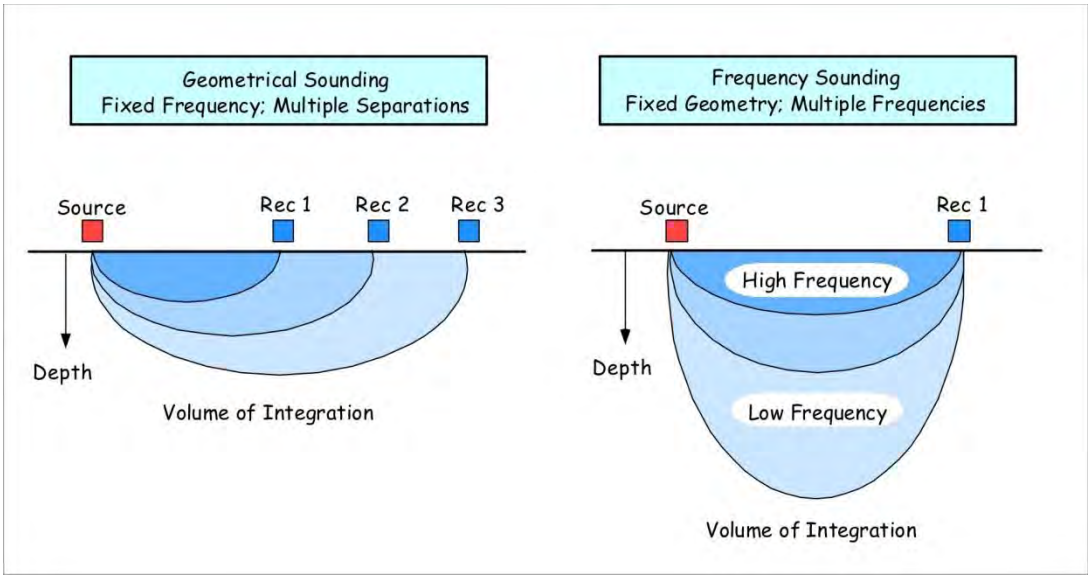

Figure 2.20 Schematic diagram illustrating geometrical and frequency sounding with EMI methods

While propagating through the ground, the amplitude of electromagnetic waves decreases exponentially with depth (Kearey et al., 2002). For a homogeneous medium, the depth at which the amplitude of a plane wave is reduced to 1/e (or to 37%) of its original value is called skin depth (δ) and is equal to (Huang, 2005):

$$\delta = \sqrt{\frac{2}{\sigma\mu\omega}} \qquad 2.19$$

where σ and μ are the conductivity and the magnetic permeability of the medium respectively and ω is the angular frequency of the plane wave. The value of skin depth can be calculated also as $503.8/\sqrt{(\sigma f)}$, with conductivity in S/m and frequency in Hz (Kearey et al, 2002).

From equation 2.20 it is evident that skin depth depends on the frequency of the source and on the conductivity of the ground. Figure 2.21 shows a simple diagram that can be used for a rapid evaluation of skin depth (Won, 1980). More in particular, the skin depth is inversely proportional to frequency, meaning that in a conductive earth low frequencies travel deeper into the ground than high frequencies, leading to the possibility of using broadband instruments for depth sounding (Won, 1980; 1996).

Therefore, for example, in order to locate a conductive target at depth *z*, three frequencies could be used (Witten et al., 1997):

- a high frequency, for which the primary electromagnetic field decays to negligible value much before reaching depth z so that no anomaly is detected by the receiver coil;
- an intermediate frequency, for which the primary field reaches the target causing eddy currents so that a measurable anomaly is detected by the receiver coil;
- a very low frequency, for which the primary field decays at a depth much greater than z so that only a weak anomaly is detected by the receiver coil. The weakness of this anomaly is due to the fact that the receiver measures a response that is a depth-integrated function of the conductivity inversely weighted for the depth and the target occupies only a small portion of such depth.

Theoretical studies conducted by Won (1980) showed that, for a target in a conductive half-space, peak amplitude of response occurs at the frequency with the corresponding skin depth slightly greater than the depth of the target.

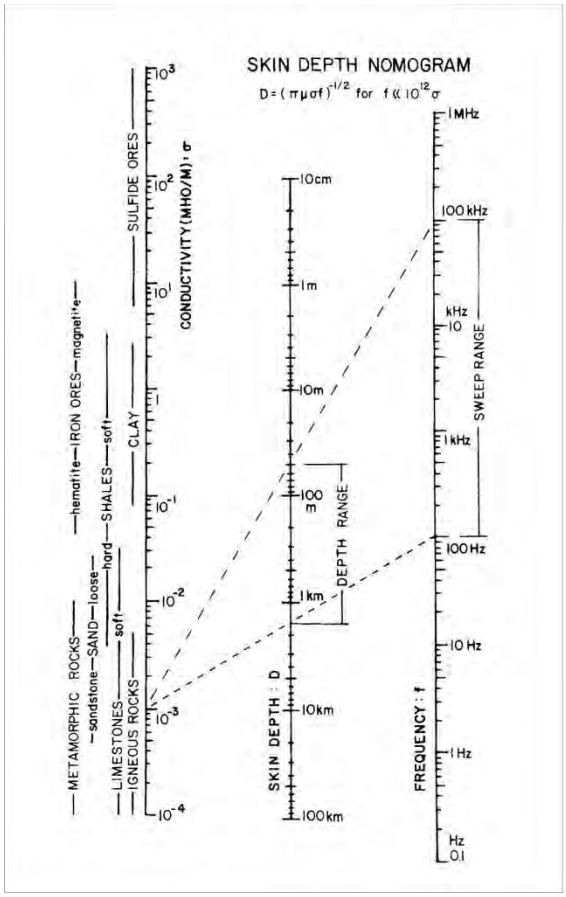

Figure 2.21 Diagram illustrating the relationship between instrument frequency, ground conductivity and skin depth. For example, in an area of igneous rocks, if the source sweeps between 100 Hz and 100 KHz, the skin depth is 40-1500 m (from Won, 1980)

<u>Investigation depth</u>

Investigation depth is defined as the maximum practical depth for which a given target in a given host material can be detected by a sensor (Huang, 2005).

Although skin depth is often considered by authors a synonymous of investigation depth, the two terms are different. Investigation depth is empirical and depends on many factors, such as type of sensor, data processing and interpretation methods, properties of target and host material, and site noise (Huang, 2005)

Mathematical empirical equations for the determination of investigation depth for the instrument GEM-2 at a specific detection threshold have been proposed and discussed by Huang (2005). For the simplified case of a half-space below a single layer, the investigation depth (DI) can be calculated following these 5 steps:

1- Set a value of detection threshold (*T*, in percentage). The target is detected when the ratio between the amplitude of the anomaly and the amplitude of the background (or ratio between conductivity of the target and conductivity of the background) is greater than 1+T or smaller than 1-T. In ideal circumstances (i.e. a conductive target in area of low noise) T can be considered 5-10%, whereas for resistive targets, noisy urban areas or areas with low conductivity (<50 mS/m) should be increased to 20-30%;
2- Calculate the equation:

$$\varphi(T) = 3.10 - 0.61\ln(T) \qquad 2.20$$

3- Calculate the equation:

$$\Psi(r) = 0.84 + 0.10r - 0.0015r^2 \qquad 2.21$$

where *r* is the coil spacing (equal to 1.66 m for GEM-2);
4- Calculate the skin depth of the upper layer (δ_1) from equation 4.5 (using conductivity of the first layer and operating frequency);
5- Determine the approximate depth of investigation (*DI*) from the equation:

$$DI \approx \sqrt{\delta_1}\varphi(T)\Psi(r) \qquad 2.22$$

The concept of cumulative conductance can be applied for the detection of a half-space at a depth *z* below multiple layers. The multiple layers above the half-space can be substituted by an equivalent single layer of effective conductivity σ_e up to a depth *z* and the two-layer procedure described in the above five steps can be followed.
The cumulative conductance of the multiple layers down to depth *z* is given by (Huang, 2005):

$$S(z) = \int_0^z \sigma(z)dz \qquad 2.23$$

where $\sigma(z)$ is conductivity as a function of depth, and the effective conductivity σ_e is equal to:

$$\sigma_e(z) = \frac{S(z)}{z} \qquad 2.24$$

Imaging algorithms and inversion techniques to layered models for broadband data acquired with Geophex instruments such as GEM-2 are still matter of research (i.e. in Witten et al., 1997; Huang, 2005) and not commonly applied. Generally GEM-2 data (as in-phase and quadrature ppm or apparent conductivity and magnetic susceptibility) are simply plotted as a series of contour maps, one for each frequency. It can be observed that targets are more or only evident for a particular frequency band. The target depth is simply estimated by visual comparison between the maps.

Technical explanations on the reasons behind the reliability of the instrument GEM-2 for depth sounding regardless of its small coil separation are discussed in Won, 2003.

Examples on the use of GEM-2 to locate abandoned wells, buried pipes, trenches of waste disposal, underground structures and archeological features can be found in the literature (Witten et al., 1997; Witten et al., 2003; Won, 1996). Moreover, Won and Huang (2004) have shown that at sufficiently low frequencies (within the resistive limit) the instrument can function as an "active magnetometer", because it responds only to magnetic susceptibility, but only for shallow investigations and with the advantage of producing reduced-to-pole anomalies when compared to a magnetometer.

2.12.1 Geochemistry techniques

Many issues related to a successful environmental clean-up need a multidisciplinary approach to understand these issues more efficiently. Less cost and time taken to produce an accurate and conclusive output will impress the decision makers and the authority bodies. There is no doubt that a geochemical approach is the best option which can be used to understand environmental contamination, as this provides solid scientific data on the chemicals present and at what levels on the site.

According to Goldschmidt (1954), geochemistry has been described as: „The primary purpose of geochemistry is on the one hand to determine quantitatively the composition of the earth and its parts, and to discover the laws which control the distribution of the individual elements'. To solve these problems the geochemist requires a comprehensive collection of analytical data on terrestrial material, such as rocks, water, and the atmosphere; and geophysical data on the nature of the Earth's interior. Much valuable information has also been derived from the laboratory synthesis of minerals and the investigation of their mode of formation and their stability condition.

Mason (1966) described geochemistry as „a science concerned with the chemistry of the Earth as a whole and of its component parts. At one and the same time it is more restricted and also more extensive in scope than geology'. Geochemistry deals with the distribution and migration of the chemical elements within the earth in space and in time. The American Heritage® Science Dictionary (2005) – **Web 2.24,** described geochemistry as the scientific study of the chemical composition of the Earth or other celestial body of the reactions that control the distribution of chemical elements in its minerals, rocks, soil, waters and atmosphere.

Dealing with contaminated land and groundwater issue requires a geochemical approach to analyse the groundwater and soil chemical properties. It's also essential to support the geophysical data in order to get a clear, solid and conclusive research output. The geochemical techniques used in this research can be divided into two components which include field sampling/measurements and subsequent laboratory analysis. The information regarding field and laboratory works are discussed in more detail in Chapter 5.

2.10.2 Typical chemical contain in contaminated land

Referring to DEFRA (Department of Environment, Food and Rural Affairs) 2006, the contaminated land regime in Part 2A of the Environmental Protection Act 1990 (Part 2A) was introduced specifically to address the historical legacy of land contamination (Department of Environment Foods and Rural Affairs, 2006) – **Web 2.25**. One of the key features of Part 2A is a statutory definition of "contaminated land" - defined as: *"any land*

which appears to the local authority in whose area it is situated to be in such a condition, by reason of substances in, on or under the land, that:
(a) significant harm is being caused or there is a significant possibility of such harm being caused; or
(b) pollution of controlled waters is being, or is likely to be caused".

Following this definition, the investigation of the Cathays Railway Depot had been proposed to define any significant soil contamination issues. There are two main sets of guidelines currently used in the UK on contamination land and these are:-

a) ICRCL 59/83 (The Interdepartmental Committee on the Redevelopment of Contaminated Land) - **Web 2.26**

b) The Dutch List (initially known as the "A B C List" but now modified to the New Dutch List) - **Web 2.27**

The former is based on the most appropriate use of the site (in the UK), whilst the second is based on multifunctionality (Dutch).

Beside the above, the GLC (The Greater London Council) carried out an investigation into former gasworks sites and produced another set of guidelines - known as the Kelly Indices (**Web 2.28**)- named after the officer who instigated and oversaw the work (**Web 2.29**).

Table 2.1: The three Soil Guideline Values currently used in the UK

Parameter	Kelly Indices mg/kg	ICRCL 59/83 (Threshold) Domestic/parks mg/kg	**Dutchlist (mg/kg)**	
			Soil mg/kg	GW **mg/l**
pH (acid)	**4-5**	**<5**		
pH (Alkaline)	**9-10**			
Antimony	**50-100**		**3**	
Aluminium				
Arsenics	**50-100**	**10/40**	**29**	10
Boron	**5-50**	**3**		
Barium	**1000-2000**		**200**	50
Beryllium	**10-20**			
Cadmium	**3-10**	**3/15**	**0.8**	0.4
Chromium	**200-500**	**600/1000**	**100**	1
Cooper	**200-500**	**130**	**36**	15
Cyanide (free)	**5-50**	**25/100**		
Cyanide	**25-250**	**250/250**		
Ferricyanide	**500-1000**			
Lead	**1000-2000**	**500/2000**	**85**	15
Lead (Available)	**500-1000**		**85**	15
Mercury	**3-10**	**1/20**	**0.3**	0.05
Magnesium	**1000-2000**			
Nickel	**50-200**	**70**	**35**	15
PAHs (Coal Tar)	**1000-2000**	**50/1000**	**1**	
Manganese	**1000-2000**			

Parameter	**Kelly Indices mg/kg**	**ICRCL 59/83 (Threshold) Domestic/parks mg/kg**	Dutchlist (mg/kg)	
			Soil mg/kg	**GW mg/l**
Phenol	**5-50**	**5/5**	**0.05**	0.2
Selenium	**3-10**	**3/6**		
Sulphate	**5000-1%**	**2000/2000**		
Sulphur	**500-1000**	**5000**		
Sulphide	**20-100**	**250**		
Tin				
Tiocyanate	**50-100**	**50**	**0**	20
Toluene Extract	**1-5%**		**0**	0.2
Vanadium	**200-500**			
Zink Available	**500-1000**	**300**	**140**	65
Zink Equivalent	500-2000		140	65

2.11 Conclusions

Groundwater and soil contamination are a big problem to the environment. For the past two decades many researchers have been involved with the study of these issues. It is really important in order to provide the appropriate control mechanisms and remediation to avoid worse impact to the environment and human health. Many techniques had been suggested to be employed to understand this problem including: drilling, remote sensing, geophysical, hydrogeological and groundwater modelling. By integrating the geophysical, geochemical and hydrogeological in this research, hopefully it can provide a more solid conclusion regarding the use of a multi-diciplinary approach. Indeed, the use of these three separate techniques for site investigation especially to understanding the migration of pollution in the vadose zone is quite new. A vadose zone is an unsaturated layer where the pressure head is less than atmospheric pressure, and is retained by a combination of adhesion (funiculary groundwater), and capillary action (capillary groundwater), Boulding and Ginn, 2004. The migration of the pollution in this layer is less known and by using the integrated of those techniques, an appropriate understanding

and characteristics of the fluid movement can be determine. This will allow a proper groundwater model can be developed.

Another factor of interest is further knowledge of the significant impact of biodegradation process on the hydrocarbon contamination and how this affects the electrical properties of the material over a period of time. In this study four research sites which have historically had hydrocarbon contamination all with a different ages are been studied in detail.

CHAPTER 3
RESEARCH OBJECTIVES & SITE INFORMATION

3.1 Introduction

Today, soil and groundwater contamination is increasingly recognised as being a serious environmental problem. This is due in the main to drastically increased use of hydrocarbon products and other metallic material in industrial activities, especially where the waste is not managed properly. UK residential areas also contribute a large amount of domestic waste which also greatly increases the number of sources of land and groundwater contamination. While, hydrocarbons are usually introduced into the environment by uncontrolled discharges into drains, drainage system fractures, and accidental spills, leaking storage tanks, fractures in pipelines, sewers and purge chambers.

3.2 Objectives of the study

This research project was designed to study the efficiency of the integration of geophysical techniques and hydrogeological approaches to study heavy metal and hydrocarbon contamination in the soil and the groundwater systems. This information then will be used to evaluate and to predict the seriousness of the contamination by running a groundwater modelling software program – MODFLOW in the selected site. To achieve these aims, listed below are the objectives of the study:

1. To map the geometrical dimension of the contamination area and the geological properties using geophysical techniques. By understanding the background physical properties of the study site in this first stage of research will allow the detection of changing properties within the period of study.
2. To map the 3D soil or groundwater contamination plumes by integrated geophysical surveys and hydrochemical analysis. By constructing several geophysical surveys lines (resistivity imaging technique and electromagnetic GEM) at the study site, the 3D geometry of the contamination layers (soil or groundwater) can be mapped precisely. This map can be integrated with a hydrochemical approach to produce appropriate data to map the distribution of the contaminants.

3. To obtain the hydrogeological properties of the study area including the major anions and cations, hydrocarbon solutions and other contaminant solvents present in groundwater. This is the most important approach to monitor the plume properties over the period of time. The data from the analysis will be use in the groundwater modelling using Visual MODFLOW as well as a parameter to evaluate the degree of the groundwater pollution in the study area.
4. To model the groundwater system and it properties using MODFLOW in selected research site.

These are the objectives of the research, where, the information gained in this research will be published and distributed to the appropriate government bodies or other organisations to help people overcome this groundwater pollution problem in the future.

3.2.1 Research scopes / limitations

This research will be divided into three major parts which consist of geophysical investigations, geochemical investigations and the groundwater modelling. The geophysical techniques will envisage having three major applications in connection with ground and groundwater contamination around the study site:

a) obtaining the information about the geological and geophysical properties of the study area
b) mapping for identification and delineation of contaminations
c) identify the boundary of the research area for the hydrogeological modelling

In most cases regarding the soil and groundwater contamination, typical geophysical techniques used are electrical resistivity imaging techniques and ground conductivity surveys. Both techniques are commonly used to measure the electrical properties of the material in subsurface. The DNAPLs as example has a property which can infiltrate into the groundwater system as its density is higher than water. Generally higher resistivity values observed under the water table are probably due to the resistivity of the

hydrocarbon is higher than water. This will make the resistivity imaging technique particularly interesting in mapping the plumes of the contamination in groundwater systems (Meju, 2000).

The chemical investigations will involve a water sampling programme which is planned to be collected from the boreholes, rivers, rainwater or the existing ponds if necessary. The water samples then will be analysed to get a chemical fingerprint and the hydrocarbon concentrations in it. These data later will correlate with the geophysical data to provide conclusive information about the scenario of the groundwater contamination at the study areas.

Both the geophysical and geochemical techniques provide the input parameters for the groundwater modelling using Visual Modflow Professional. Modelling is used to better define the present scenario and future rates of pollution migration. In this study not all research sites are used in the groundwater modelling because of the limited amount of hydrogeological data or due to the fact that a particular site does not overly principal aquifers (as classified by the Environment Agency and British Geological Survey). In this research study, only the Bromsgrove site is used for detailed groundwater modelling, the other two sites, Western Super-Mare Gasworks Station and the Cathays Railway Depot are situated above Secondary B and Secondary A aquifers respectively and much less information is known regarding the hydrogeological properties at these sites. While at Barry Docks, the chemical variation of the groundwater samples taken from the boreholes make this site suitable for detailed groundwater modelling. However, due to time limitations, the research scope for this site is restricted to the characterisation of the contamination by using integrated geophysical and hydrochemical investigations only. A comparison then will be done to find out any significant relationship between the geophysical and geochemical parameters. The last stage in this research project is to evaluate the current situation of groundwater contamination, looking at the efficiency of the geophysical techniques as a supporting tool in the groundwater modelling and define the various options for remediation works if necessary.

3.2.2 Research work plan

The research will be divided into five stages which include literature reviews and site selection, site investigation and monitoring, laboratory and data analysis, data visualisation / groundwater modelling and report writing.

3.3 Site information and desk studies

Four sites have been used in this research study which all has different source types of contamination. Cathay Railway Depot in Cardiff has been used as an initial testing site to determine the efficiency of the techniques as tools for site investigation. The Barry Island Dock site was previously a major shipping dock and historically a storage site for hydrocarbons and many other industrial materials. The Western Super-Mare site is related to a historical abandoned town gasworks and the final site at Bromsgrove was previously a landfill site for domestic and industrial wastes particularly from the car manufacturing industry.

3.3.1 Cathays Railway Depot

The Cathays Railway Depot is located along Maindy Road in Cathays, Cardiff and it has been long established as a railway depot. It is approximately 1 km north of Cardiff City Centre, at a National Grid Reference of ST 177 779 (Figure 3.1).

The site is roughly rectangular in shape alongside the still operational Cardiff – Pontypridd railway line, the site narrows to a point towards the north- west and occupies an area of about 3.1 hectares. The boundaries of the site are defined by Maindy Road to the north-east, the railway line to the south-west, and in the north-west by the Cambrian Point Student accommodation. To the south-east is a new Cardiff University Optometry Building (Figure 3.1, Figure 3.2 and Figure 3.3). The site is almost flat and is less than 20m Above Ordnance Datum (AoD) in topography.

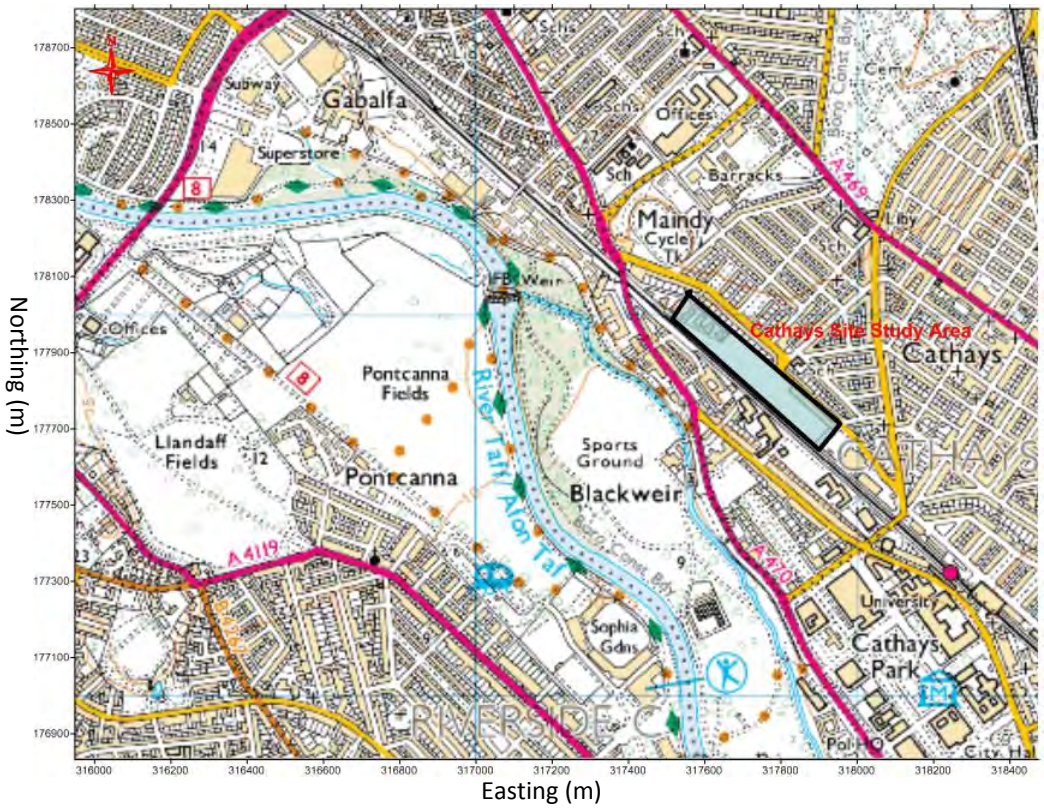

Figure 3.1: Cathays Depot Location (Source, Edina Digimap, 2011)

Figure 3.2: Cathays Depot Location (Source, Google Earth, Feb 2011)

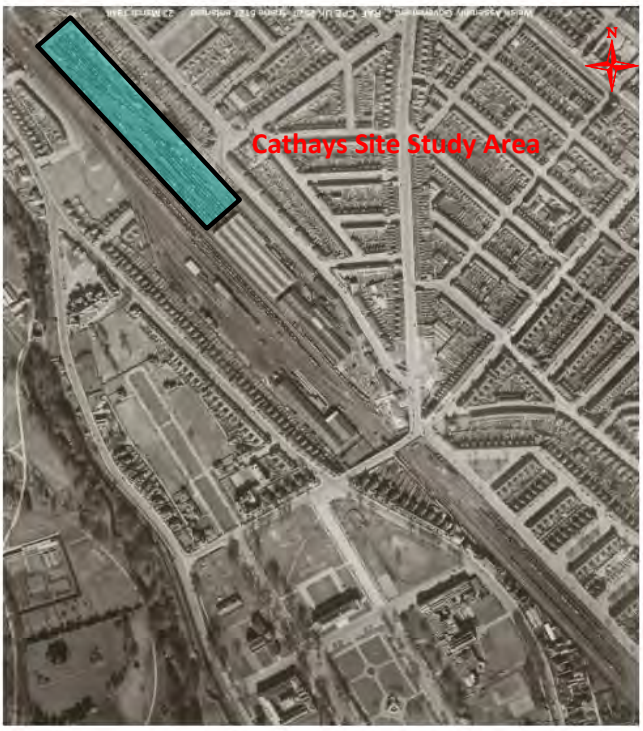

Figure 3.3: Cathays Depot Location (Aerial photograph 23 March 1948, source Welsh Assembly Government)

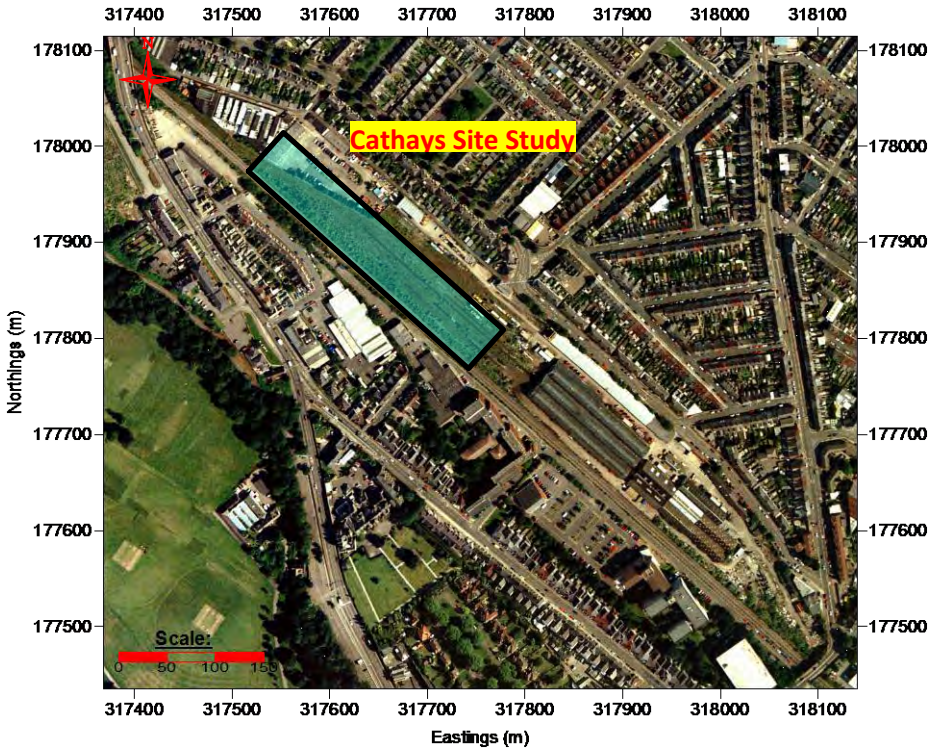

Figure 3.4: Cathays Depot Location (Aerial photograph year 2000, Google Earth)

3.3.1.1 Site history

The Taff Vale Railway Company was incorporated on 21 June 1836 to construct a railway from Merthyr Tydfil to the docks at Cardiff (Waters, 1995). Freight services were always an important part of railway operation in Cardiff especially traffic of coal, iron ore and others commodities to the docks. At the turn of the 19th century the Taff Vale Railway was operating 250 general goods, minerals and empty wagons trains each day in order to cope with the large amounts of coal and other goods. A number of large marshalling yards and wagon storage sidings were opened in the Cardiff area (Waters, 1995).

Locomotive Sheds and Depots

The first locomotive depot was built in Cardiff by the Taff Vale Railway at the West Yard in Butetown 1845. This shed remained in use until 1884, when the company opened a very much larger depot at Cathays (Waters, 1995) – Figure 3.5 to Figure 3.8.

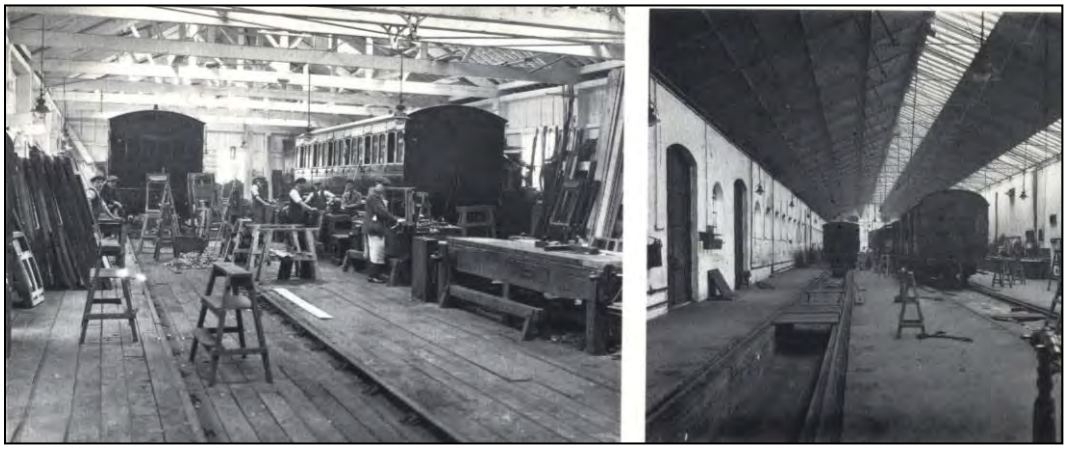

Figure 3.5: Picture taken on the 22 April 1926 shows the main carriage shop at Cathays. (Source: Waters, 1995)

Figure 3.6: In 1958 main shed building at Cathays was converted into a servicing depot. (Source: Waters, 1995)

Figure 3.7: A view of Cathays depot Cardiff taken on 4 September 1955. (Source: Waters, 1995)

Figure 3.8: A view of Cathays depot on 8 August 1924. (Source: Waters, 1995)

This new Taff Vale depot at Cathays contained 10 roads and was the largest in the Taff Vale system. Civil Engineering repair facilities were added in 1892. After the Grouping the works were modernised by the Great Western, and in 1929 several of the old repair shops were demolished and replaced by a new larger building. The new wagon repair shop was opened in August 1931. It was the GWR's intention to concentrate all carriage and wagon repairs at Cathays. Following the introduction of Diesel Multiple Units (DMU) onto valley services in October 1957 the main building was converted into a DMU depot and in July 1958 the shed was officially closed to steam. Since 1964 the Cathays site was used as a wagon repair facility until 2005 when it was put up for sale. The southern end of the site was purchased by Lidl who constructed a supermarket. The rest of the site was purchased by Cardiff University which has built a new Optometry building and demolished many of the railway buildings. A large percentage of the site remained derelict until summer 2011 when new Cardiff University buildings are starting to be built.

3.3.1.2 Geological properties of the site

The solid geology of Cardiff city centre comprises of Triassic strata of the Mercia Mudstone Group formerly known as the Keuper Marl (Figure 3.9). The sequence is dominated by mudstones but includes a wide range of lithologies from stiff clays with lithological variations over small vertical and horizontal distances (Gordon et. al, 2004). Superficial deposits overly the solid geology over most of the site. These comprise of fluvioglacial terrace sands and gravels representing outwash deposits from the Devensian ice age when the glacial limit lay around 4 miles to the north of the site (Anderson, 1958).

Given the recent industrial history of the site, made ground must also overly the superficial glacial deposits. The site lies in an area where Cardiff City Council Buildings Regulation Department states basic protective measures are required for new buildings. (Anderson, 1958)

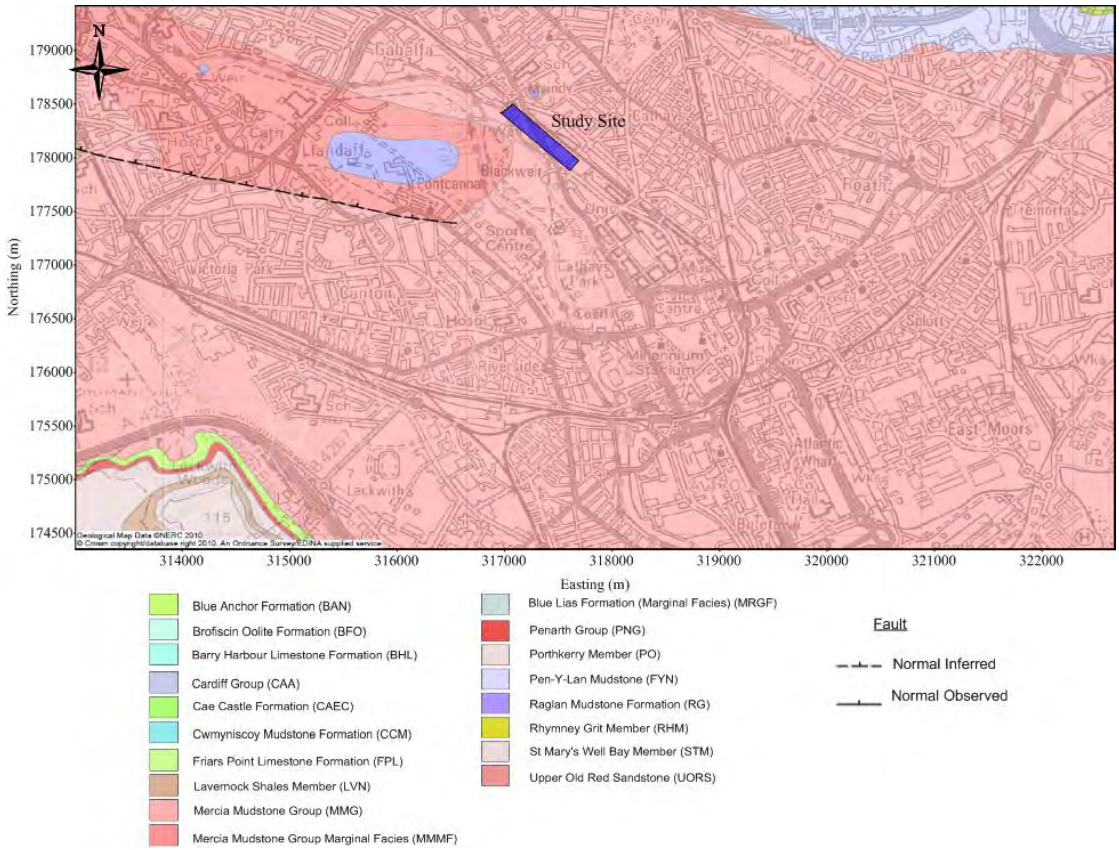

Figure 3.9: Geological map of the study area (Source, Edina 2011)

3.3.1.3 Hydrogeological properties of the site

According to the Environment Agency the formations beneath the Maindy Road (Former Railway Shed, Cathays) site are a **Secondary A aquifer** - permeable layers capable of supporting water supplies at a local rather than strategic scale, and in some cases forming an important source of base flow to rivers. These are generally aquifers formerly classified as minor aquifers. These formations rarely produce enough water for abstraction purposes, but can be important for local supplies and in providing base flow for rivers (Environment Agency, 2011a) – **Web 3.4.**

The soil shows a high leaching potential. This soil has little ability to attenuate diffuse source pollutants and non-absorbed disperse source pollutants and liquid discharges have the potential to move rapidly to underlying strata or to shallow groundwater.

3.3.1.4 Geophysical properties of the site

The geophysical properties of the material in the former train depot in Cathays are largely influenced by the historical site activity. The surface materials (structural foundations) and type of contamination itself may also be able to give significant geophysical signals. In this study area, there are no deep soils and groundwater samples are collected due to the university didn't have any facilities to perform a sampling works on this site. But based on the literature as shown in Table 3.1, most of contamination is historically related to the railway activities and are from hydrocarbons and metals. It is expected that lower resistivity values will be observed if the major contamination present are from metals. It also can be lower if the site contaminated by the hydrocarbon which is highly depending upon the ages of the hydrocarbons that have been dumped into the site.

3.3.1.5 Contamination Issues on the Site

The contaminants on any industrial site will largely depend on the history of the site and on the range of materials produced there. Potential contaminants and the probable distribution on the site of the main groups of contaminants are shown in Table 3.1. It is most unlikely that any one site will contain all of the contaminants listed. It is recommended that an appropriate site investigation be carried out to determine the exact nature of the contaminants associated with individual sites (Environment Agency, 1995) – **Web 3.5**.

Typically on railway sites, in some areas, ash ballast (possibly containing metals, phenols, sulphates, and polycyclic aromatic hydrocarbons (PAHs)), may be found in siding complexes. Ash ballast may also be buried below modern ballast layers (**Web 3. 5**).

There are various factors affecting contamination in railway land. Fuel oils, lubricating oils and greases may cause localised contamination of ballast and of areas where locomotives and multiples units have stood for significant periods of time, for example at terminal stations and in sidings. There may also be localised contamination due to the use of antifreeze liquids such as ethylene glycol (**Web 3. 5**).

Table 3.1: Potential contaminants in terms of activity, material process and hazards (Source, EA, 1995 (**Web 3. 5**)).

Potential Contaminants		
Activity	*Material Process*	*Contamination/Hazards*
Railway/Sidings	Rail tracks, Sheds	Metals, PAH's, Hydrocarbons
Storage/repair sheds	Fuel, oils, storage and use of various materials	Diesel, oil spillages, asbestos, grease, solvents, coolants, paint, glue, varnish, creosote, toluene, acetylene, propane and hydraulic fluids
Gasometer and associated buildings/land	Residual waste from old gas works	Hydrocarbons, phenols, PAH's, asbestos

Tracks and the immediate trackside margins may be subject to the accumulation of herbicides. Contamination is possible through spillages and leaks of materials stored or used at infrastructure engineering workshops, e.g. fuel oil, lubricating oils, solvents. There may be contaminations in sidings resulting from spillages of the cargoes; the nature of contaminations would depend on the types of cargoes handled at sidings. Asbestos may have been used as roofing or engine cladding or lagging to pipe work and may have caused contamination during the dismantling of buildings or dismantling of engines. Lead-based paint may have been dumped if the site contained a repair facility. General contamination of a site may also occur through the wind dispersal of airborne contaminants e.g. coal dust from open wagons in transit and from steam locomotive tenders, metal particulates and asbestos fibres (**Web 3. 5**).

3.3.2 Gasworks Station Weston Super-Mare

This site was formerly the town gasworks, typical of all towns and cities in the UK. It is geographically located right in the middle of Weston Super-Mare town in the South-West of England (Figure 3.10 and Figure 3.11). The site has undergone many re-building episodes since its Victorian origin. Today part of the site remains a gas storage facility and part is available for re-development.

The structures related to the earlier gasworks processes still remain in the site including two redundant gasholders and a mono Ethylene Glycol plant, four operational bullet tanks, a governor building and a site office. Generally, the site is almost flat in topography and about 6m AoD and is surrounded by residential housing on the south west, a school at the south and main road at the west, north and east.

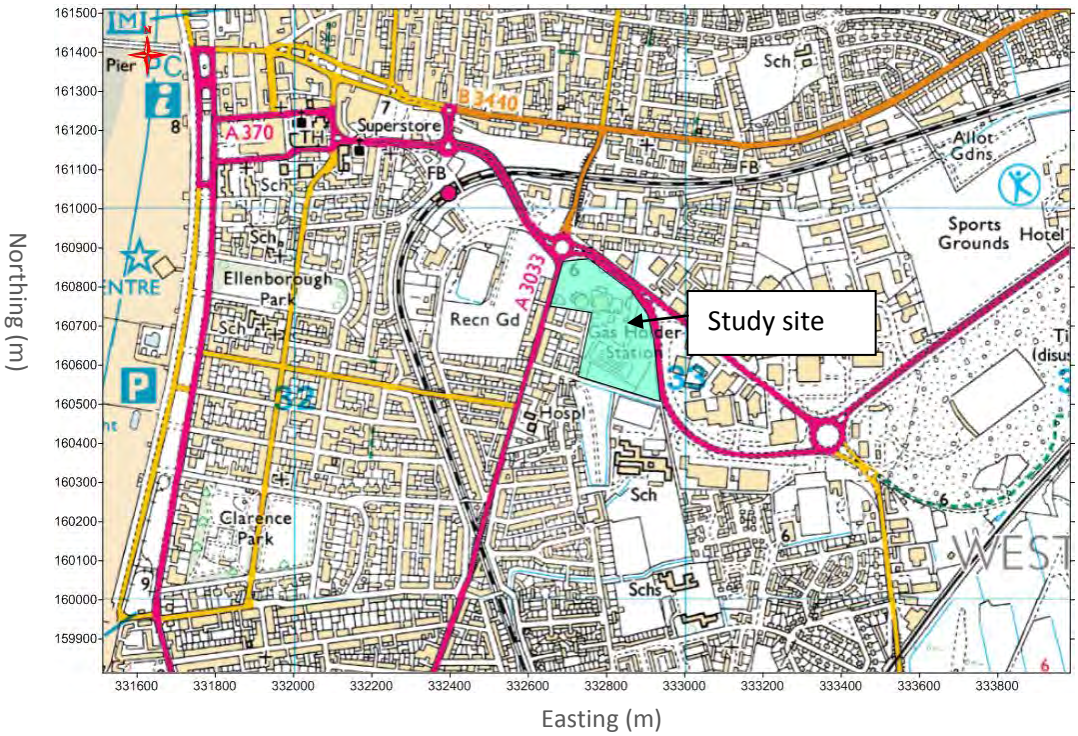

Figure 3.10: Ordnance Survey map of the study area (Source, Edina Digimap)

An intensive investigation concentrated at the south east of the site, near to the trial pits number 10 (TP110) as shown in Figure 3:12 where the previous investigation found tar in the ground. It is expected to come from a leaking historical wooden tank buried in the shallow sub-surface.

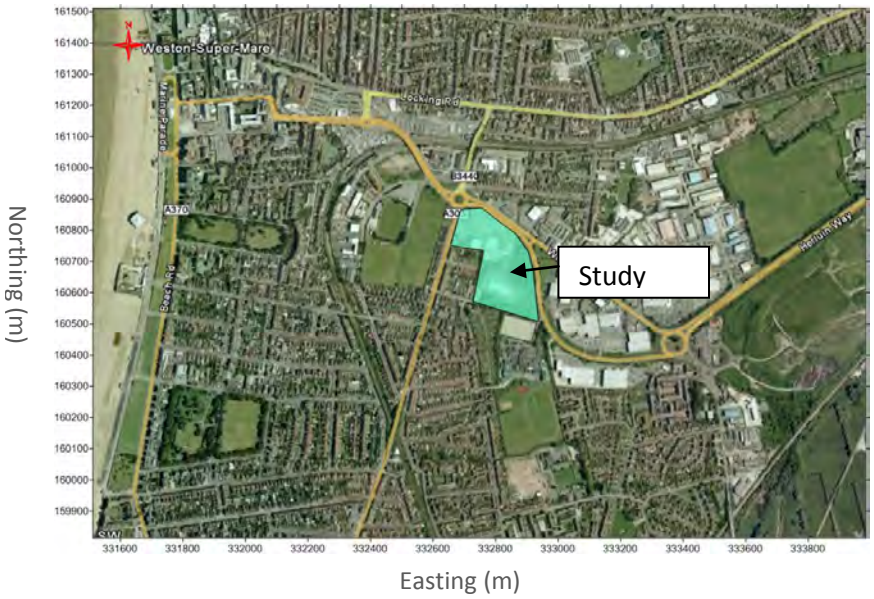

Figure 3.11: Study site location from Google earth

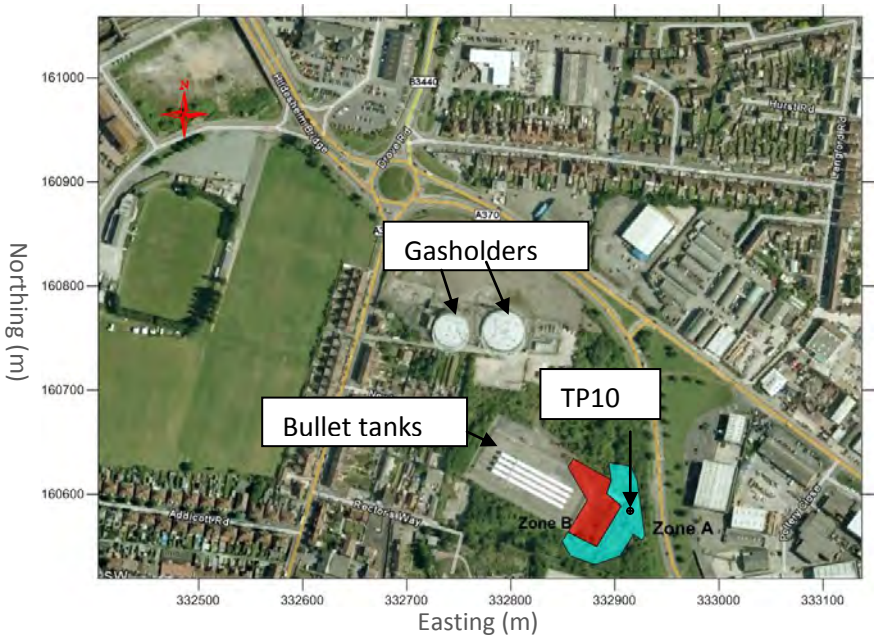

Figure 3.12: Showing the study site divided into two zones and the old structures that still remained

3.3.2.1 Site history

The gasworks station was first recorded in the middle of 19th century around 1856. It was developed at a new location to replace the old town gas works (Gledhill, 2003). Walk-

over observations at the site and a Google map image shows that some of the structures still remain on site.

The historical map from the 1880s shows three storage tanks had been built on the site. After that, the site was progressively developed until 1950's and sequences of construction are shown in Figure 3:13 to Figure 3:17. By 1989, many of the historical gasworks structures were demolished.

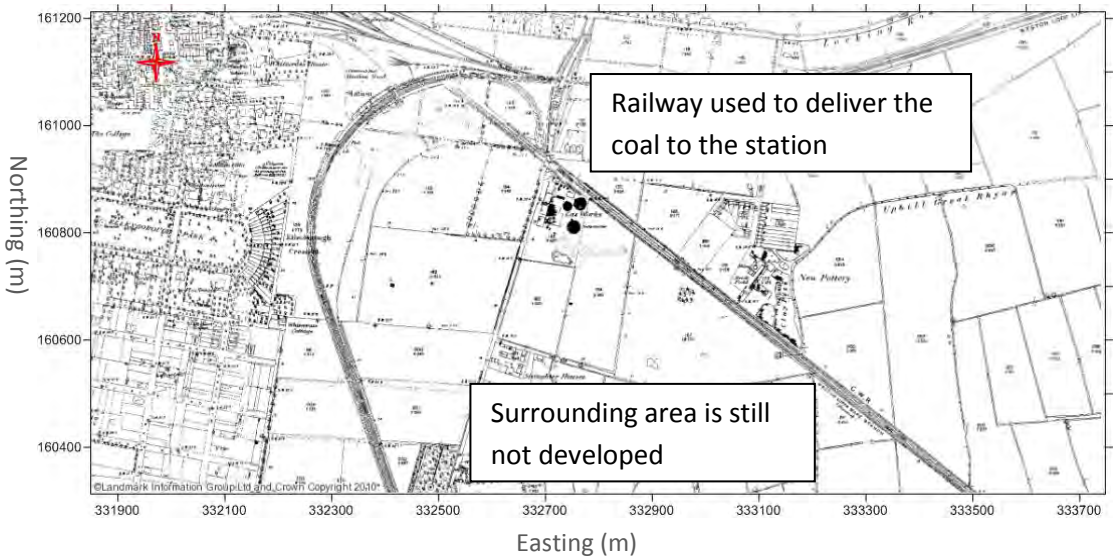

Figure 3: 13. Historical map 1880's, showing a few structures had been built for the gasworks operation (Ordnance Survey, 2011)

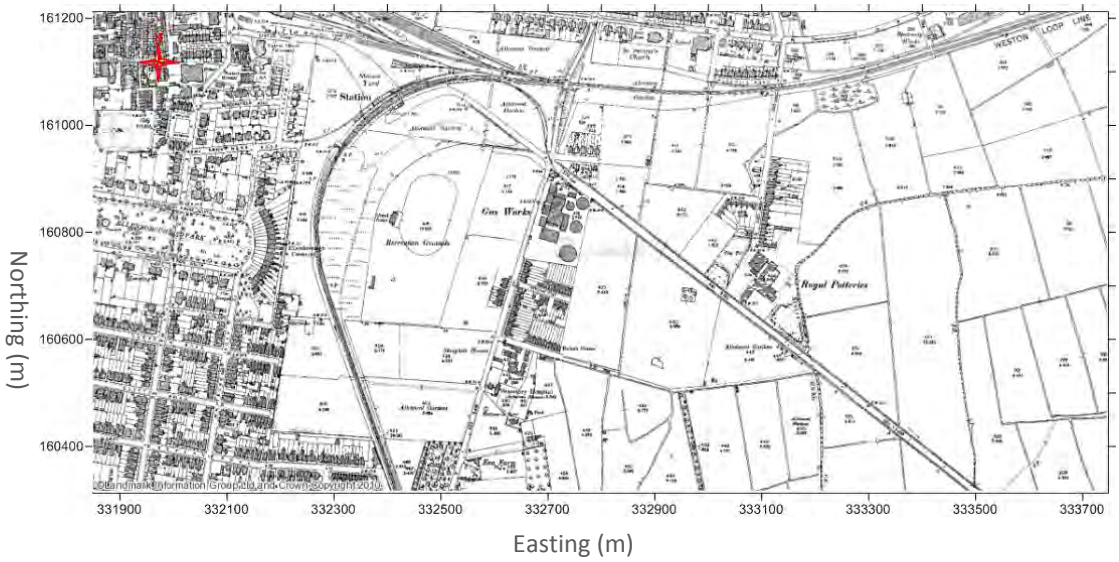

Figure 3:14: Historical map 1890's showing an extension of the gasworks area, the residential start to built (Ordnance Survey, 2011)

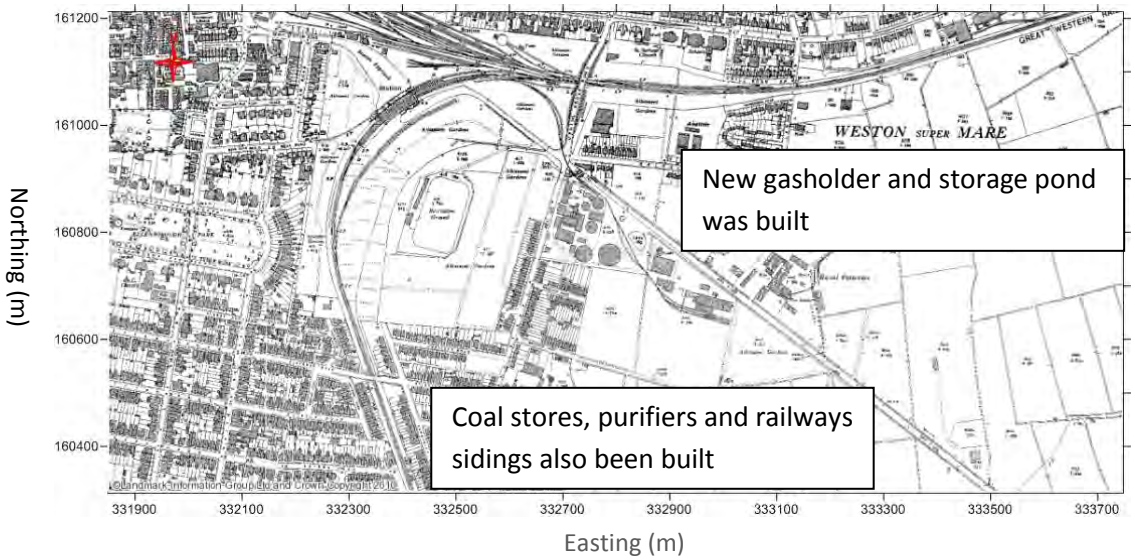

Figure 3:15: Historical map 1930's (Ordnance Survey, 2011), showing the expansion continue

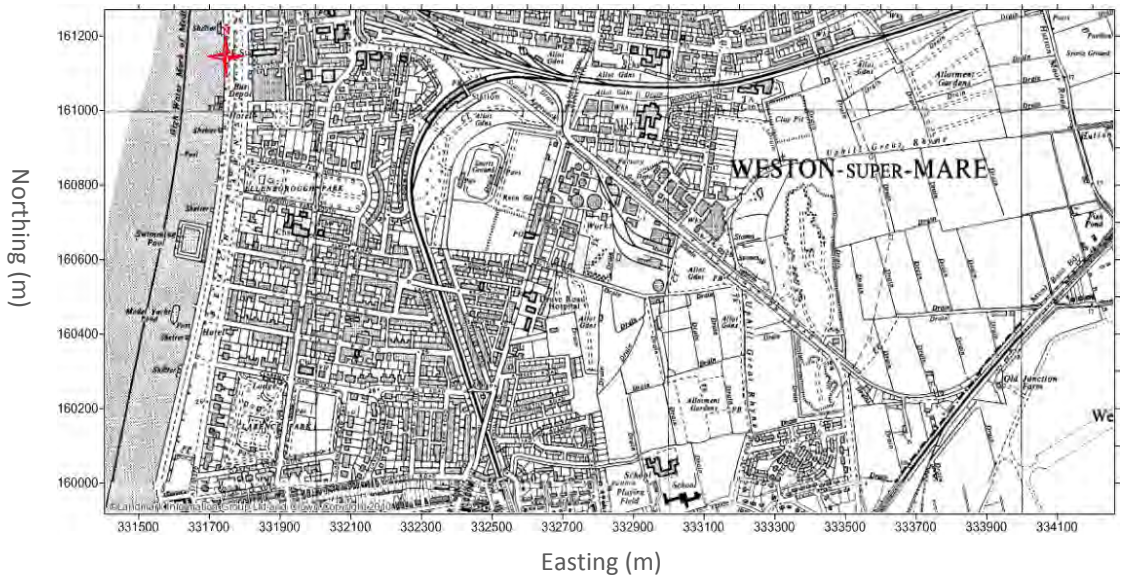

Figure 3:16: Historical map 1960's (Ordnance Survey, 2011), the site extended at the peak of the gasworks operation and the residential area was drastically developed

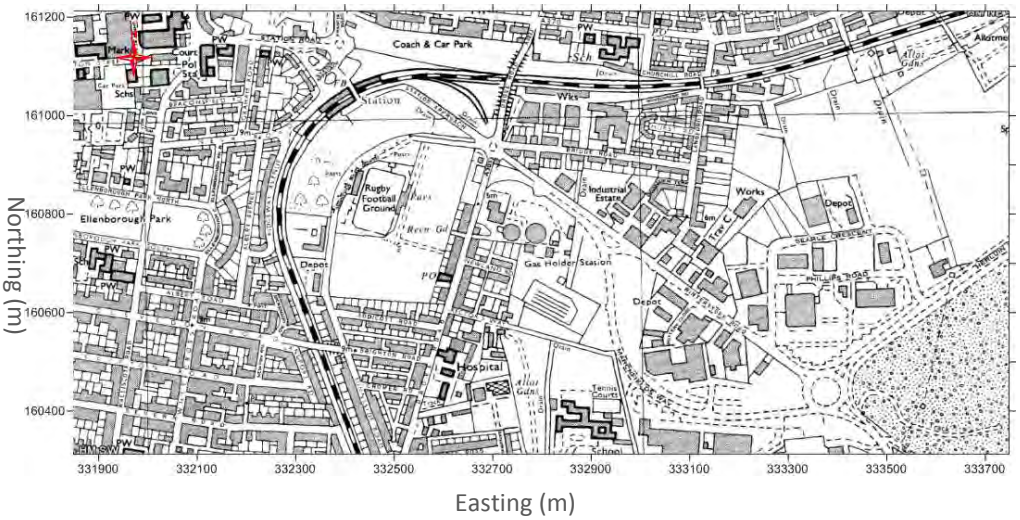

Figure 3:17: Historical map 1980's showing many of the gasworks structures were demolished (Ordnance Survey, 2011).

3.3.2.2 Geological properties of the site

The study site at Weston Super-Mare is on the Mercia Mudstone Group which has an age between Mid Triassic (Anisian) to late Triassic (Rhaetian) (Howard et al., 2008) – Figure 3.18. The Mercia Mudstone Group is composed mainly of red and, less commonly, green and grey mudstones and siltstones (Howard et.al. 2008). On top of the bedrock are superficial deposits from blown sand (BSA) as it's near to the beach and tidal flat deposits (TFD) are found further inland – Figure 3.19.

A study by Persons Brinckerhoff Ltd. in 2010 divided the superficial deposits at the research site into three different classifications which are; a thin ground cover, made ground and natural ground. The ground cover across the site consists of the gravel scalping and vegetation, mostly scrub bushes and small trees. While the made ground comprises a brown gravely sand which is present all over the site and up to 2.7m thick. This layer also comprises of bricks, piping materials, sheet materials, fabric and clinker, which can be found in several trial pits in the study area. The natural ground, which is made from the light blue sandy clay, is found as a deeper layer in the superficial deposits. It is an alluvial deposit and contains occasional peat, silt and sand horizons. It has a strong peaty smell indicating that the depositional environment is anoxic (Parsons Brinckerhofff, 2010).

3.3.2.3 Hydrogeological properties of the site

The Mercia Mudstone Group, (formerly the Keuper Marl), has traditionally been regarded as weakly permeable and a poor aquifer. Despite the fact that as an effectively a non-aquifer in many areas, limited quantities of groundwater are still suitable for domestic or small-scale agricultural use (Cheney, 2004) – **Web 3.6**. The Environment Agency, 2010 has classified the aquifer at this site as a **Secondary B** - predominantly lower permeability layers which may store and yield limited amounts of groundwater due to localised features such as fissures, thin permeable horizons and weathering. These are generally the water-bearing parts of the former non-aquifers (**Web 3.7**).

3.3.2.4 Geophysical properties of the site

Tidal flat deposits would be expected to have low resistivity values (or higher electrical conductivity). However, some of the areas where the gravel is present near to the surface and associated with a building material, this can make the ground resistivity higher than expected, especially in dry conditions. Resistivity of the hydrocarbons would be theoretically high, up to $10^{16}\Omega$m (Xylene) (Loke, 2000), but will possibly decrease when the biodegradation processes have taken place. So, the investigation using a resistivity and conductivity of the hydrocarbon contamination should have to consider these factors. The research site was established more than a century ago as a town gasworks station and will thus be expected to produce a lower resistivity or higher ground conductivity.

3.3.2.5 Contamination issues on the site

As the site previously was a town gasworks, the contamination is expected from the materials being used for the gasworks operations, waste, storages and transportation. According to Persons and Brinckerhoff Ltd. (2010), a location in the south east of the site , has a significant contamination issue where free phase coal tar had been found in the trial pits TP110 at 0.8 – 1.5m bgl depth and at TP 111 between 0.8 – 1.9m bgl depth (Zone A). Tar pools have also been found on surface at the Zone B area as shown in the Photo 3.1 and Photo 3.2. According to PB, based on visual and olfactory evidence of contamination, the source of contamination is possibly from a broken wooden tank at the location TP110.

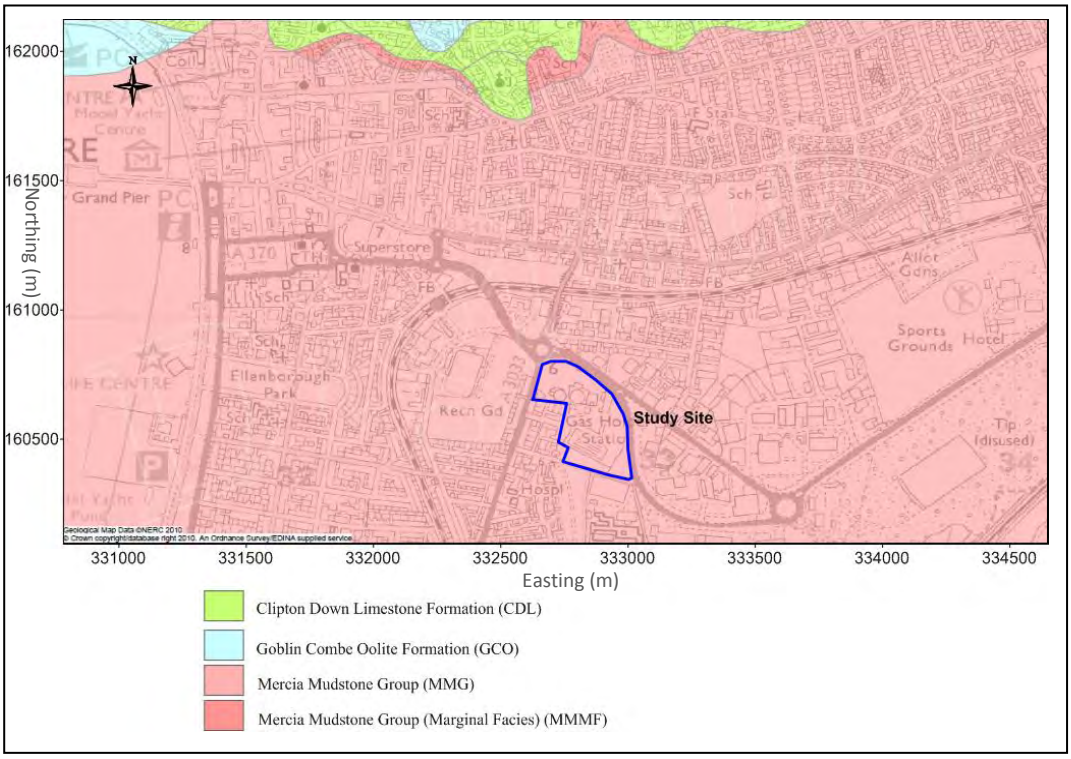

Figure 3.18: Geological map (bedrock) of the study site showing it lies on the Mercia Mudstone Group (MMG) – source Edina Digimap, March 2011

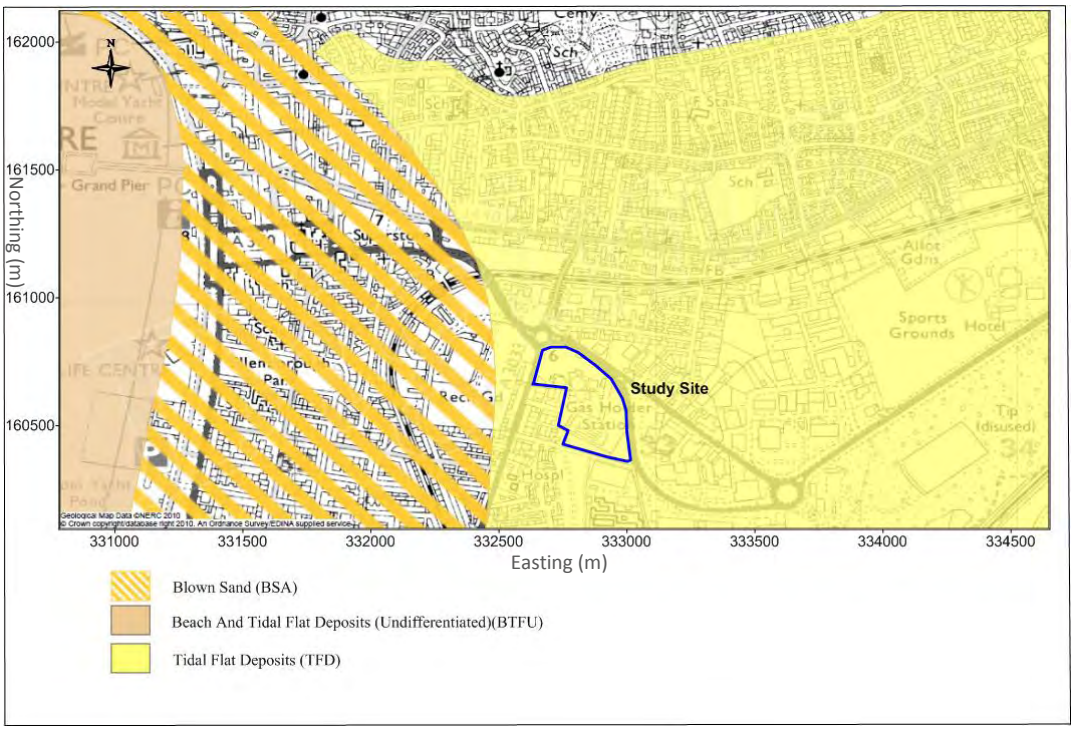

Figure 3.19: Superficial deposits map showing the site lies on the Tidal Flat Deposits (TFD)

Photo 3.1: Showing the tar on the surface

Photo 3.2: Tar is associated with the soil and rock aggregates

3.3.3 Barry Docks

Barry Docks is located between Barry Island and the mainland (Barry Town) on the southern coast of Wales (Figure 3.20). The site was originally the tidal river estuary of the River Cadoxton flowing into the Bristol Channel. This site was developed in the late 1800s into a major docks complex. The site itself has had a considerable industrial history

due to the intensive industrial and docks activities from the past. It was famous as a major coal exporting port by the end of the 19th century.

Generally, the Barry Docks can be divided into four zones based upon the historical activities and land use which include: the South Quay, West Pond, Mole and the Tanks Farm between the dock and the West Pond as shown in Figure 3.21. This research study only concentrates on the western end of the No.1 dock at the West Pond and Tank Farm zones.

Figure 3.20: Barry Docks at the South Wales Map (Source, Edina Digimap, 2011)

Topographically, the site is generally almost flat with less than 10m in elevation above Ordnance Datum (AoD) (Figure 3.22). The highest point is in the West Pond zone where the embankment of soil from backfill materials has been dumped.

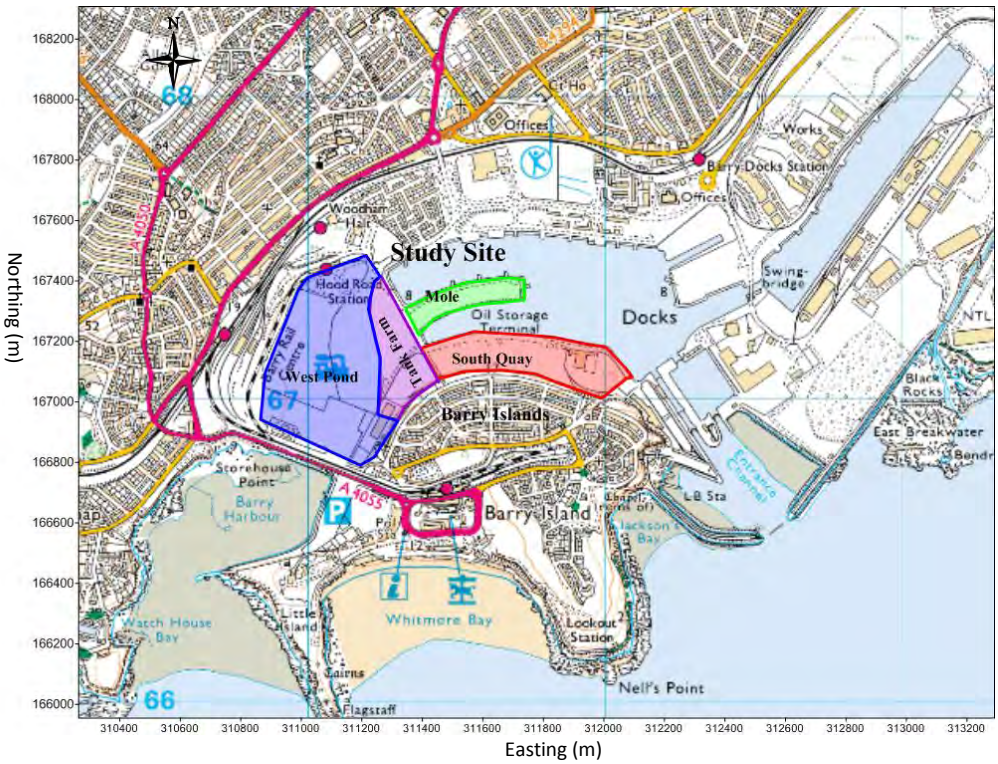

Figure 3.21: Barry Docks showing the zones but only Tank Farm and West Pond area are included in this research

3.3.3.1 Site history

The rapid development of the Barry Docks was a result of the booming coal industry in Wales at the end of 19th century. The dock was built in 1884-1889 between Barry Island and Barry (mainland) by damming the River Cadoxton. A causeway was also built between Barry Town and the Island to provide a rail link and develop the island for tourism. The area between the dock and the causeway became a large pond known as West Pond. The historical O.S. map drawn before the docks were built is shown in Figure 3.23.

The research site lies on the West Pond site, as seen in the historical map of the 1890s (Figure 3.24). The oil storage tanks were believed to be built in the 1940's as part of the World War II effort storing material for USA troops supplies, as shown in Figure 3.26. For security reasons the tanks are not shown on historical OS maps of this period.

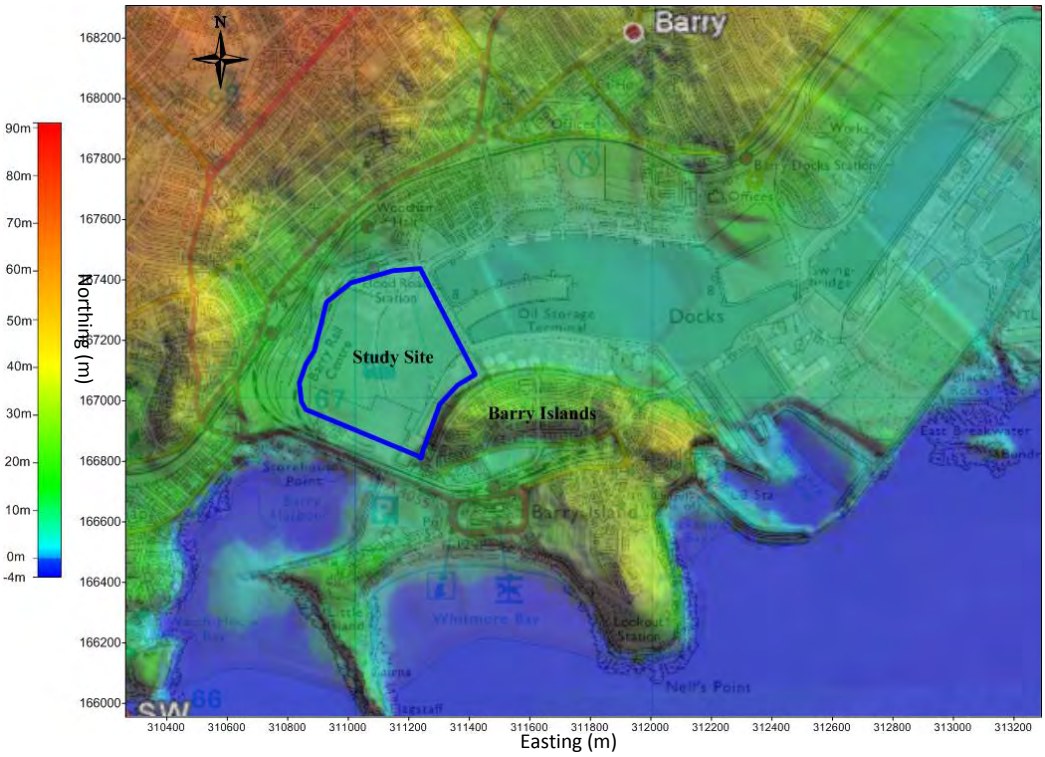

Figure 3.22: The study site is laid on the flat (<10m) area but surrounded by the high elevation of Barry Town on the North-West and Barry Island on the South-East

The West Pond was used as a landfill site in the mid 1950s by progressively dumping steelworks slag from progressively moving railway sidings. This left a large area of derelict land that was later occupied by the cutting area of Woodham's train scrap yard (Figure 3.27 and Figure 3.28). The famous train scrap yard lasted until 1990 when the final steam locomotives had been moved off site for preservation (Figure 3.29).

Aerial photographs (Photo 3.3 to Photo 3.6) and Photo 3.7, shows a historical sequence and changing site conditions since the 1941 until it's nearly all totally demolished in 2010.

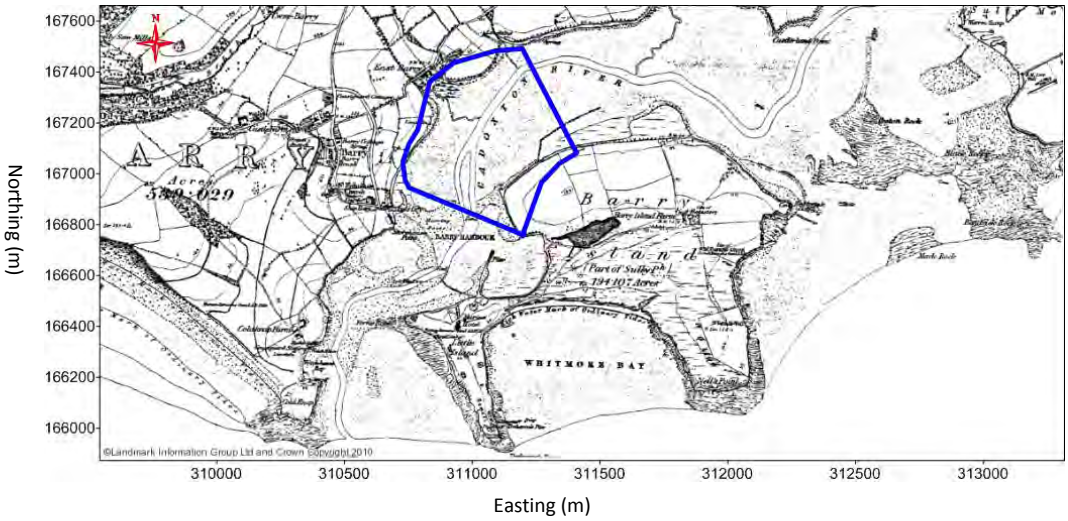

Figure 3.23: Historical map 1880's showing the Cadoxton River flowing into the Bristol Channel between Barry Island and Barry mainland before it was dammed to build the docks which created a West Pond (Source Edina, 2011)

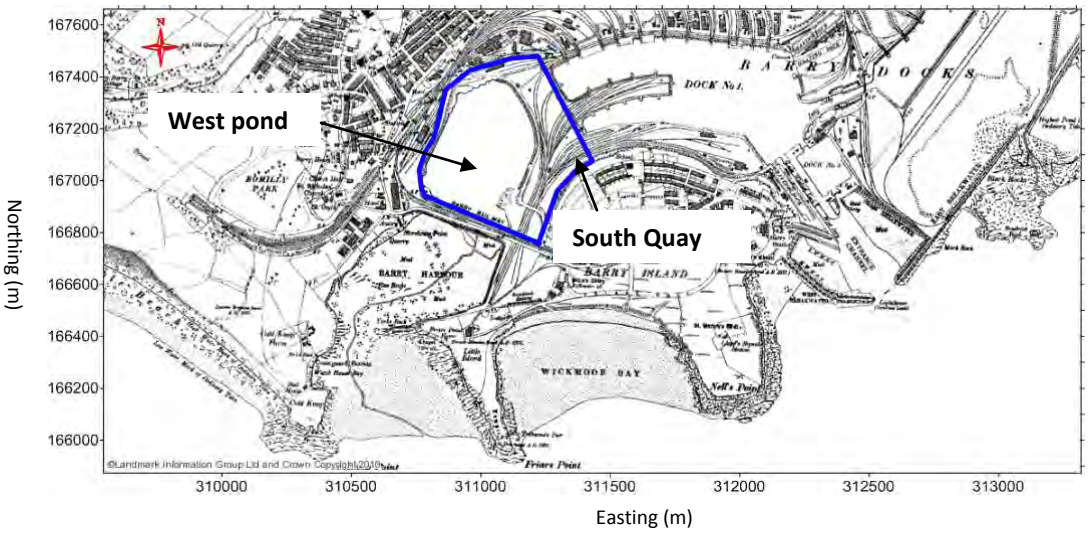

Figure 3.24: Historical map 1890's, showing that the Cadoxton River has been dammed to build the docks. The railway tracks also were built at the South Quay to facilitate ships loading the coal (Source Edina, 2011)

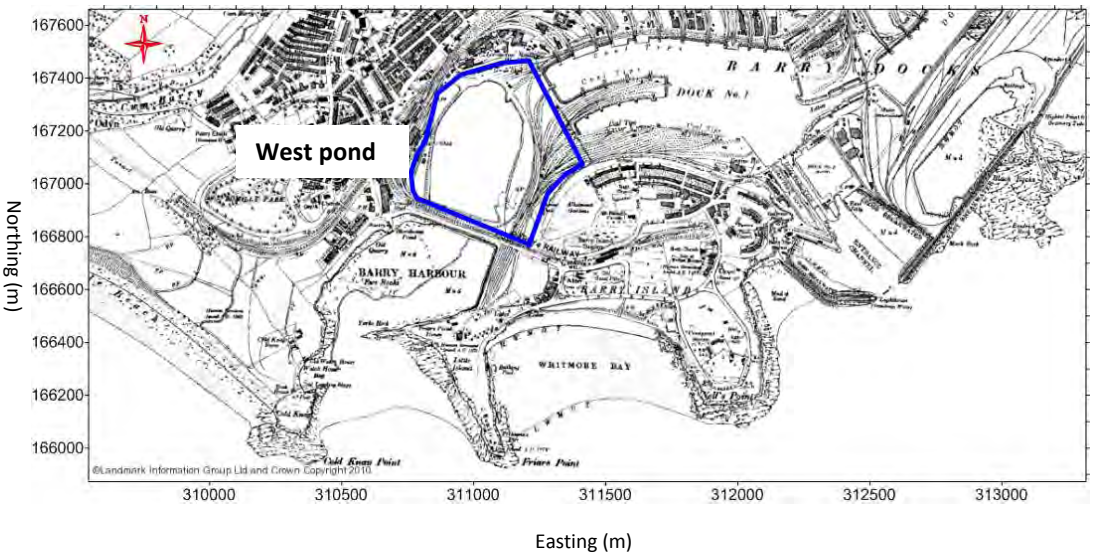

Figure 3.25: Historical map 1920's showing the study site has continued to be developed but the West Pond remains (Source Edina, 2011)

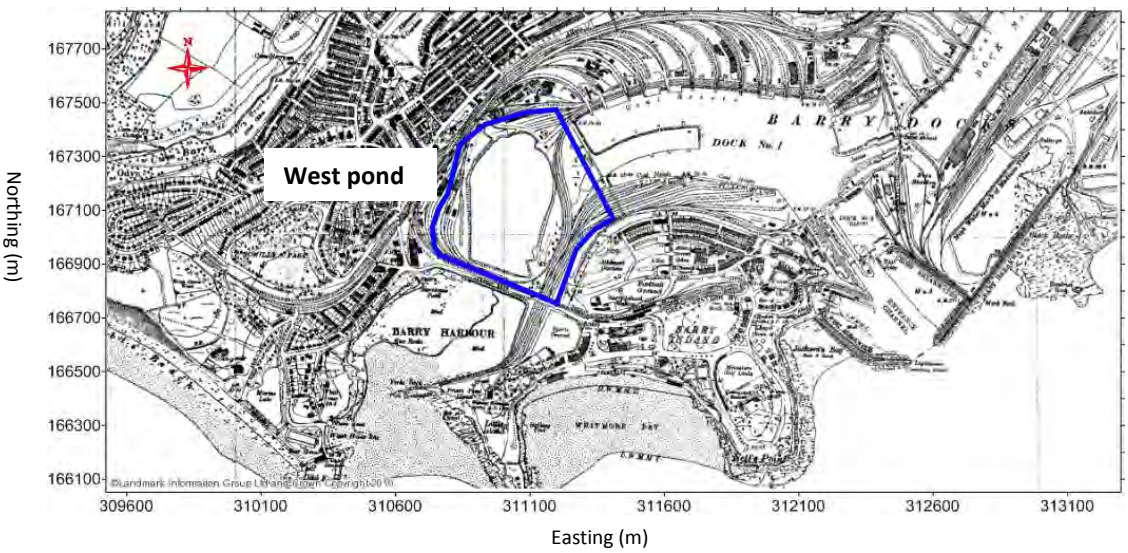

Figure 3.26: Historical map 1940's, showing that the storage tanks have started to be built at the South Quay (Source Edina, 2011)

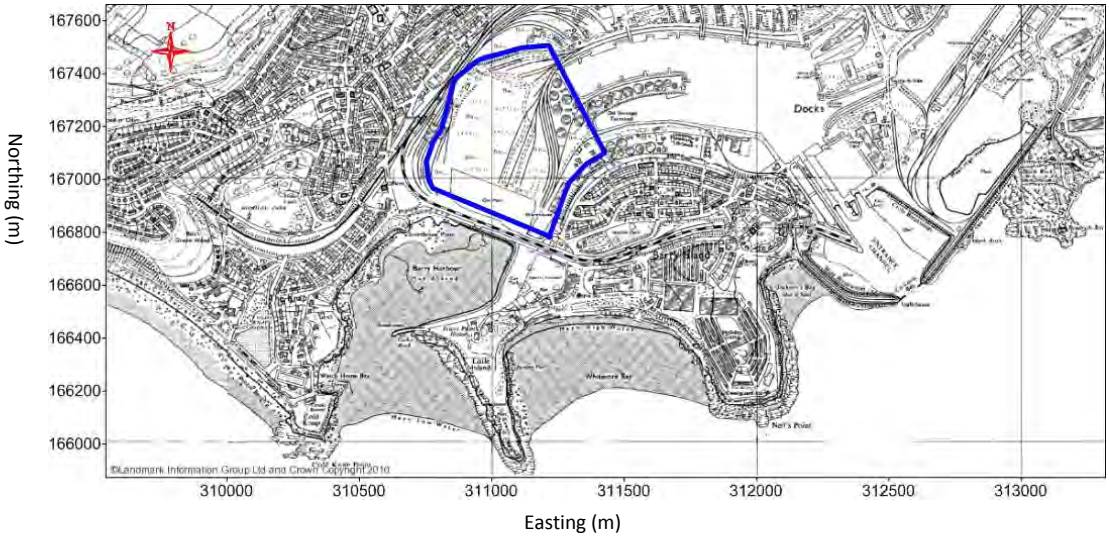

Figure 3.27: Historical map 1960's (Source Edina, 2011), showing the West Pond now has been completely backfilled and the additional railway sidings laid on its eastern edge

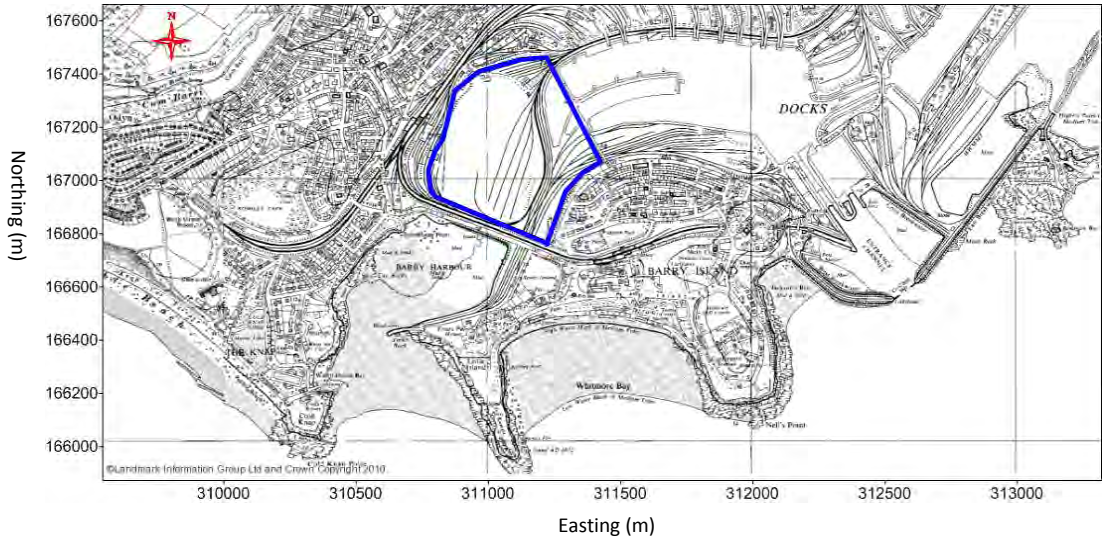

Figure 3.28: Historical map 1970's (Source Edina, 2011) showing continued development of the West Pond purposely to restore the abundance of locomotives and carriers after the end of coal locomotive era, railway tracks at the South Quay and Mole were removed but the storage tanks remain

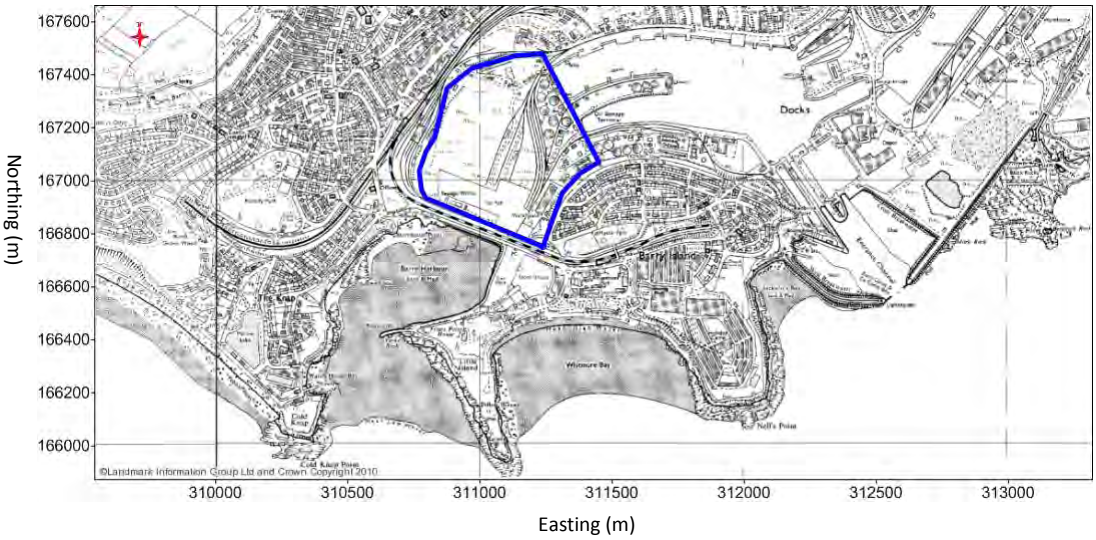

Figure 3.29: Historical map 1990's (Source Edina, 2011), showing that some tanks are demolished from the Mole and South Quay

Photo 3.3: Aerial photo late 1941 showing the Barry Dock No. 1 and the oil tank farm (Source, Welsh Assembly Government)

Photo 3.4: Aerial photo of Barry Docks in July 1971 showing the oil tanks farm and railway sidings with over 200 obsolete steam locomotives and wagon cutting areas (source South Glamorgan Council).

Photo 3.5: Aerial photo of the Barry Dock sometime in 1979 (Source, Ordnance Survey).

Photo 3.6: Aerial photo Barry Docks in 2000 showing that most of the storage tanks are demolished and areas are available for redevelopment (source : Google Earth, 2011).

Photo 3.7: Two images of Woodham's locomotive scrap yard and a tank farm located at the South at Dock 1 (Source: Peter Brabham, 2010)

2.3.3.2 Geological properties of the site

Barry Island is famous for the exposed unconformity between horizontal Permo-Triassic beds and the dipping underlying Carboniferous formations. The Permo-Triassic deposits consist of the Penarth Group (PNG; grey to black mudstones with subordinate limestones and sandstones), (Figure 3.30). Superficial deposits of tidal flat deposits overly the bedrock in the study area especially along the former Cadoxton River (Figure 3.31)

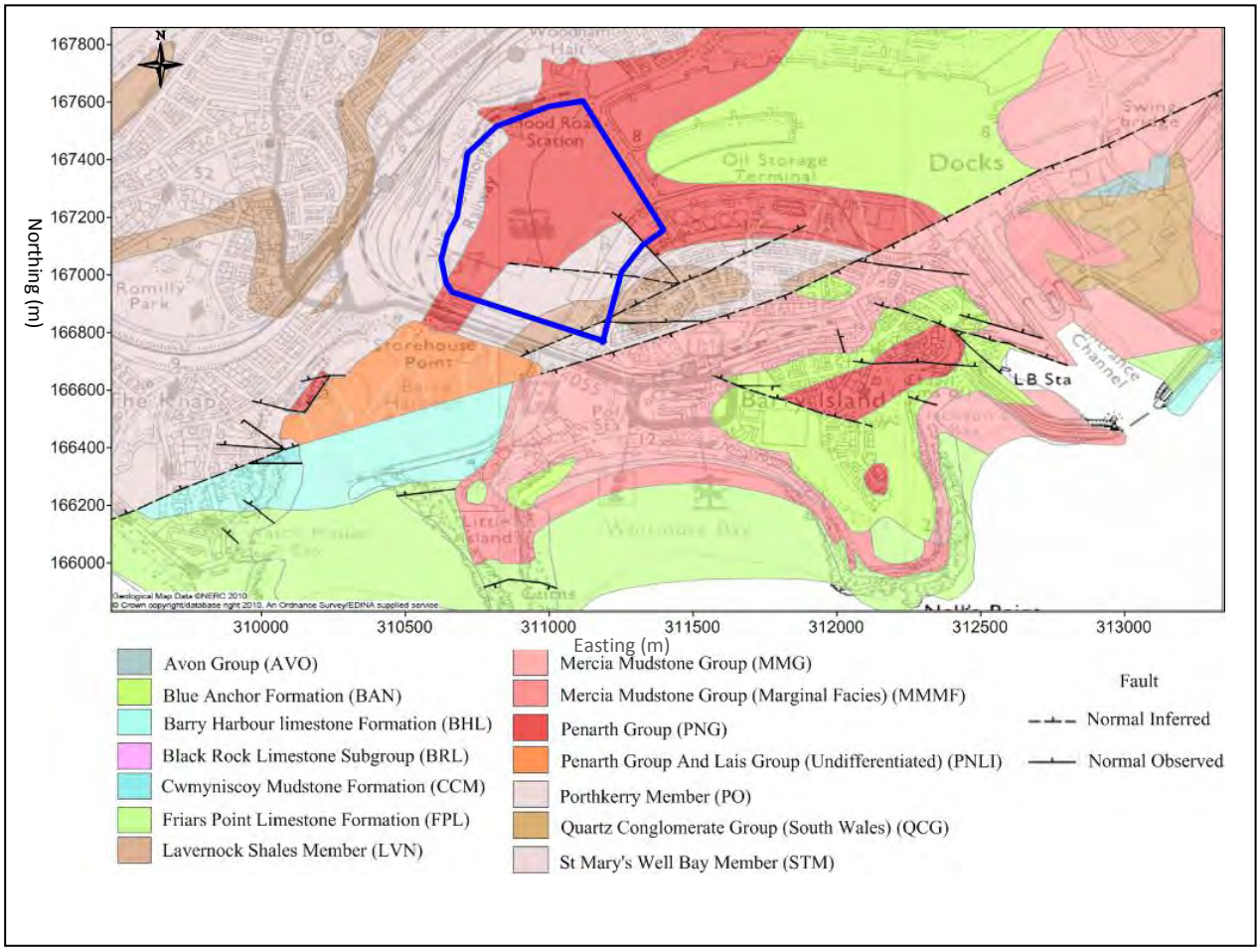

Figure 3.30: The geological map of the Barry and Barry Islands, the study site is shown by the blue polygon (Source, Edina Digimap, 2011)

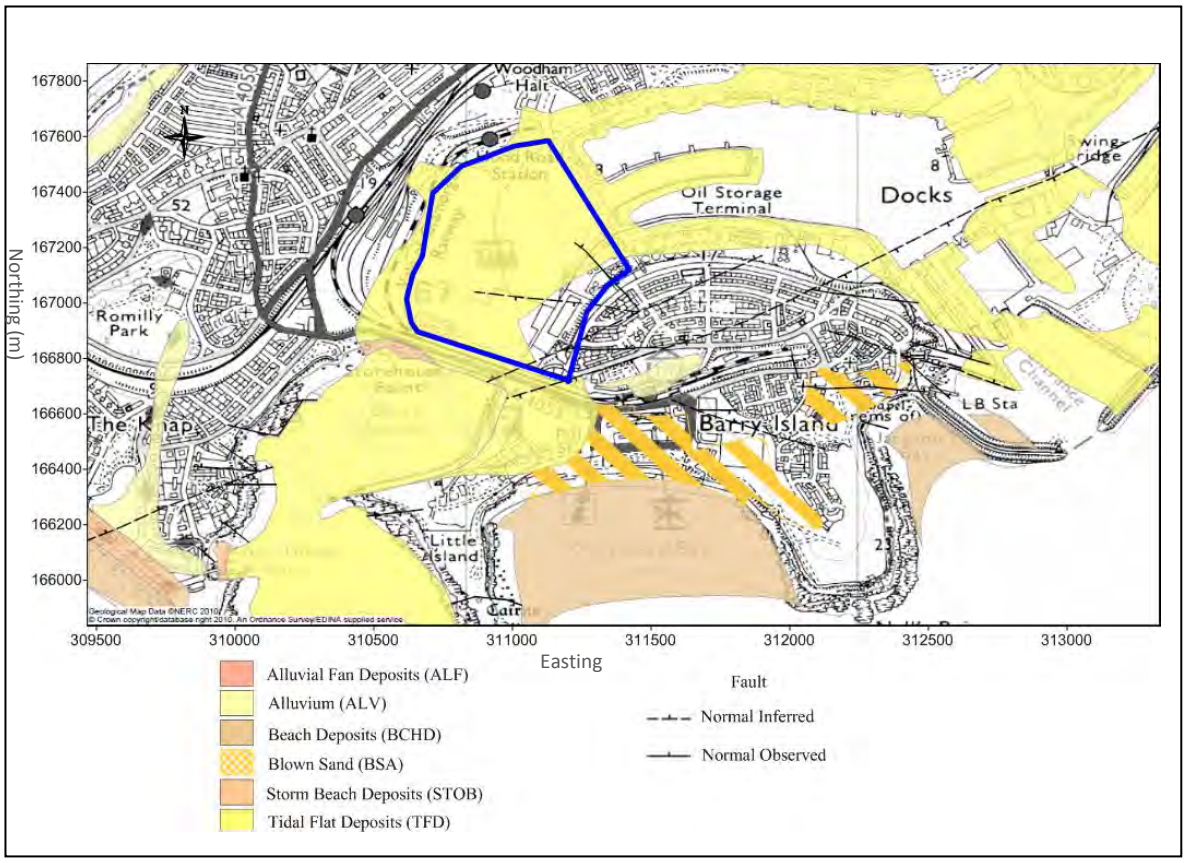

Figure 3.31: The superficial deposits map showing most of the study site is covered by the Tidal Flat Deposits (TFD) (Source Edina Digimap, 2011)

3.3.3.3 Hydrogeological properties of the site

Although the site is near to the sea, the Environment Agency declared the groundwater to the North-East of the study area as Groundwater Protection Zone which is in the SPZ-3 zone (Environment Agency, 2011b) – **Web 3.8**. They defined the zone as 'the area around a source within which all groundwater recharge is presumed to be discharged at the source. In confined aquifers, the source catchment may be displaced some distance from the source. For heavily exploited aquifers, the final Source Catchment Protection Zone can be defined as the whole aquifer recharge area where the ratio of groundwater abstraction to aquifer recharge (average recharge multiplied by outcrop area) is >0.75. There is still the need to define individual source protection areas to assist operators in catchment management', (Environment Agency, 2011d) – **Web 3.9**.

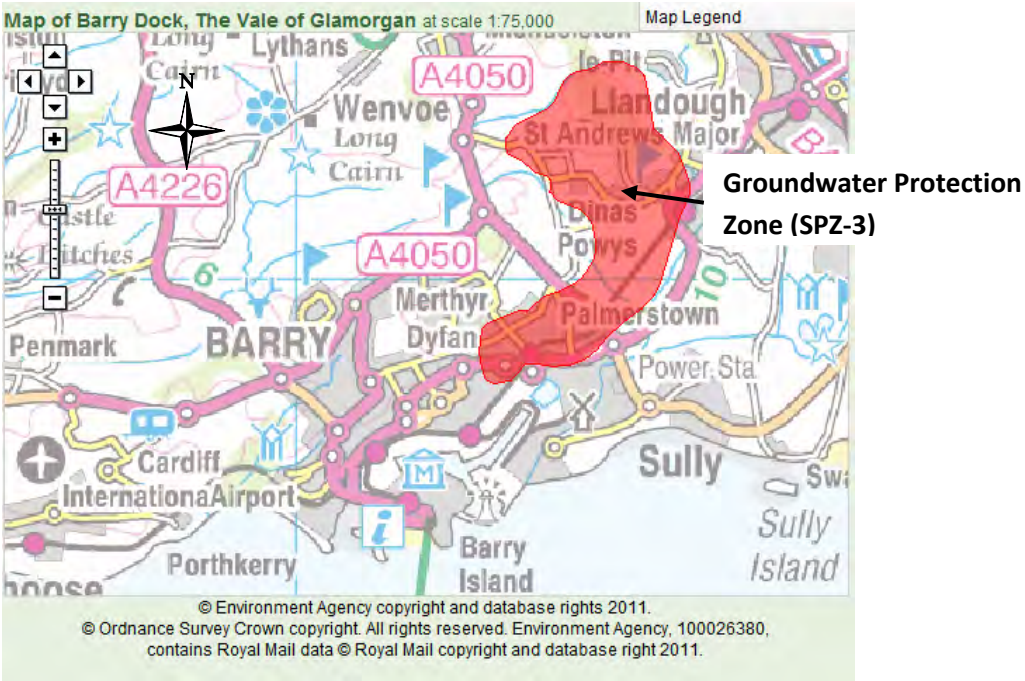

Figure 3.32: SPZ-3 (red colour) near the study site but there is no other groundwater protection zone in the 10km radius from the Barry Docks (Source, Environment Agency)

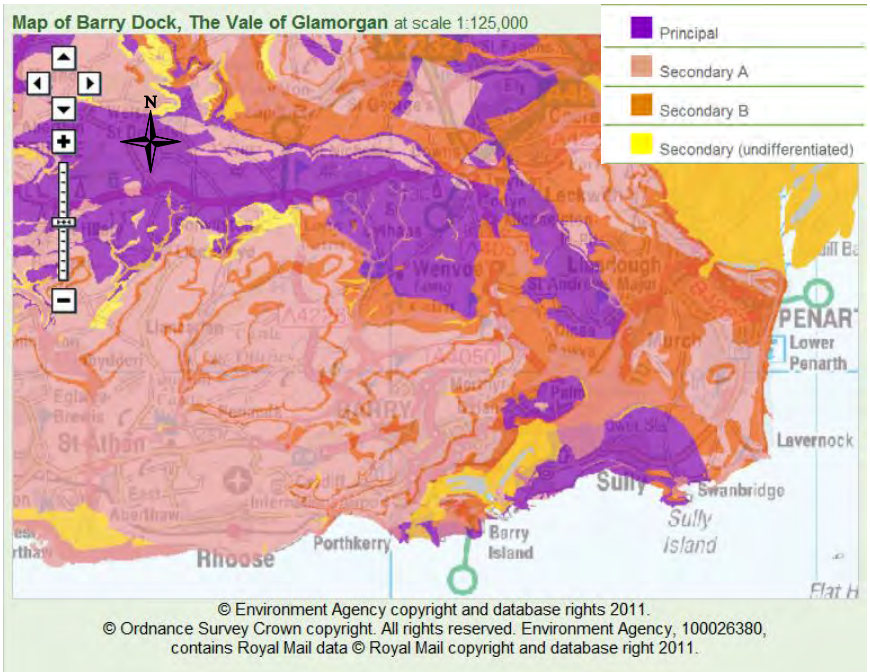

Figure 3.33: Map of superficial deposits and bedrock aquifer. The yellow colour represents the Secondary undifferentiated aquifer at the study site (Source, Environment Agency)

The superficial deposits of the site which are mostly formed from the Tidal Flat Deposits are classified as secondary undifferentiated aquifer by the Environment Agency (Figure 3.33) and the south of Barry Island is a Secondary B Aquifer.

3.3.3.4 Geophysical properties of the site

In terms of a geophysical view the site, it can be classified as a difficult site to deal with due to it complex geological setting, near to the sea, with abundant docks activities over the past 100 years. The complex geological setting with at least three types of rock formations observed at the site could give rise to many different geophysical properties. The clay rich bedrock material will be expected to exhibit a lower resistivity value compared to those rich in sand material. The superficial deposits, along the old Cadoxton River channel and the West Pond area are likely to exhibit a much lower resistivity. This is in contrast to the higher resistivity of the other bedrock such as Portkerry Member (PO) and Quartz Conglomerate Group (South Wales) (QCG). A higher resistivity also may be generated by the old concrete tank foundations and the bricks found on the site but it's expected to only influence the very thin top most layers.

Electrical geophysical properties can also be controlled by saltwater intrusion, because the site is very near to the Bristol Channel. But the groundwater hydraulic gradient will likely limit the amount of the intrusion of the sea water inland because the docks are at a higher groundwater level compared to the sea which has a high tidal range. The salt water will produce a very low resistivity (higher conductivity) of the ground since it is an electrolyte. Interpretation of the GEM and Resistivity Imaging data expected will be difficult because of the complex layering of geology, groundwater and types of contamination found on this docks site.

3.3.3.5 Contamination issues on the site

The historical activities are a major concern to site re-development, this is why the geophysical investigation has been carried out at this site. This activity including the docks, oil storage tanks and a locomotive scrap yard make a site potentially contaminated by heavy metals and hydrocarbons. In terms of expected geophysical results, the heavy metal will generate a lower resistivity and higher conductivity due to it being conductive.

The hydrocarbons will generally give a high resistivity, however after considering the biodegradation processes and the 60 year period of the hydrocarbons being dumped on the site, the resistivity of contaminated zone may be lower.

3.3.4 Bromsgrove Landfill

This study site is located at Bromsgrove in the south-west of Birmingham adjacent to the M5 motorway (Figure 3.34). It lies within Worcestershire County, Bromsgrove District Council. The Bromsgrove Landfill comprises of the Madeley Heath Landfill (MH) to the north and the Yew Tree Farm Landfill (YTF) to the south, and was originally sand and gravel quarry pits (Figure 3.35). The national grid references for the centres of these sites are 396000, 277150 and 396050, 276900 respectively.

According to Enviros (2009), the MH landfill was operated over the period 1966 to 1986 (20 years) and the amount of waste dumped into the site was estimated at about 684,000 m^3 and forms a waste layer up to 19m thick. Most the waste was from the municipal residential area around the landfill. While the YTF landfill commenced operation in 1958 an run until 1993 and the waste sources were from industrial activities (44%), municipal waste (25%), household waste (29%) and others (1%). The waste amount was estimated at about 456 000 m^3 and the maximum thickness of the waste layer is up to 20m. Both of the landfills followed the “dilute and disperse “principle in use at the time and were not constructed using a modern engineering liner and as a consequence will likely contribute to the groundwater pollution in that region (Enviros, 2009).

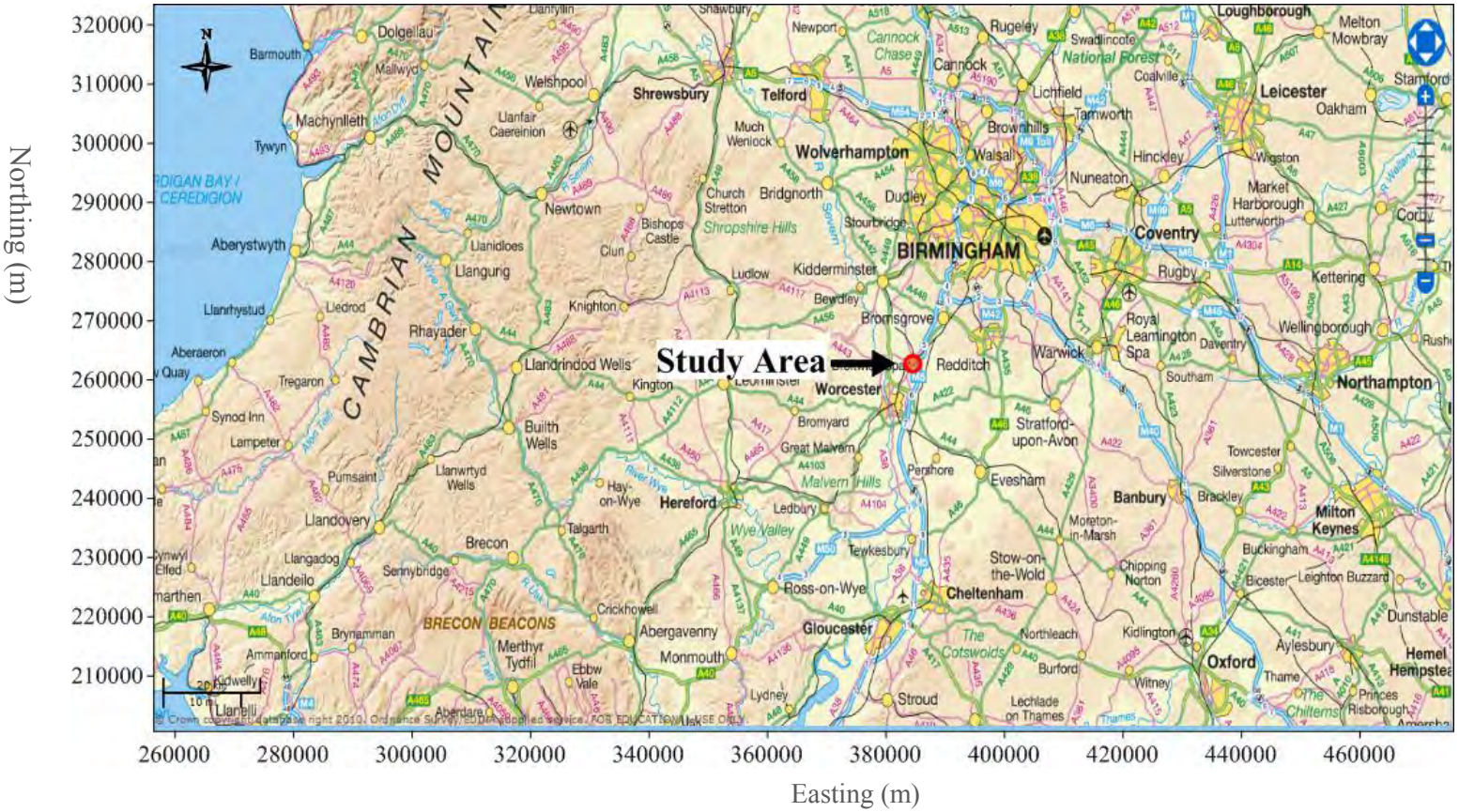

Figure 3.34: The location of the Bromsgrove Landfill (Study Site)

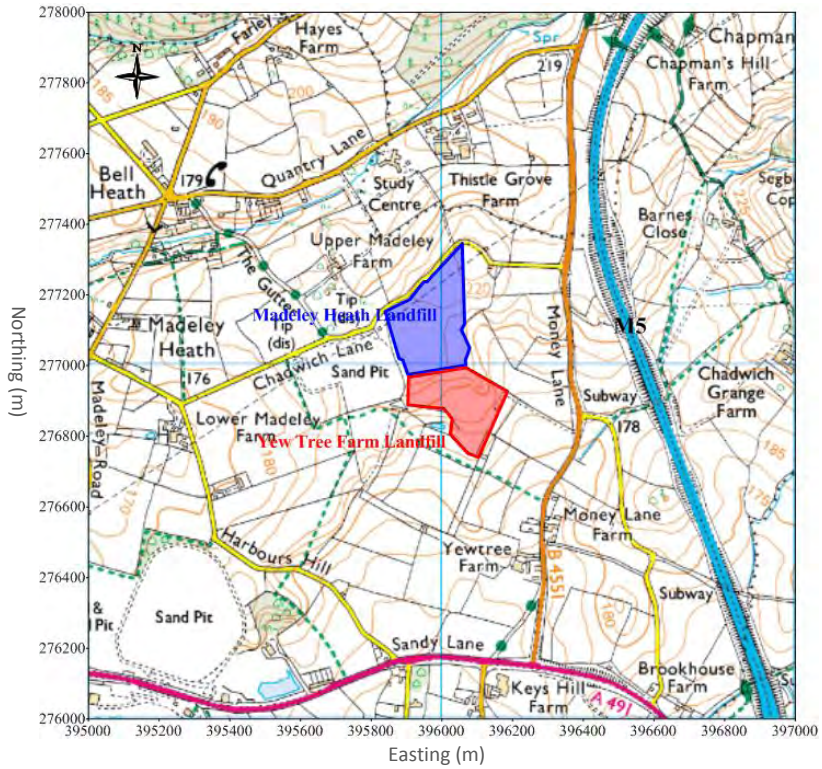

Figure 3.35: The map showing the boundary of Madeley Heath and Yew Tree Farm landfill

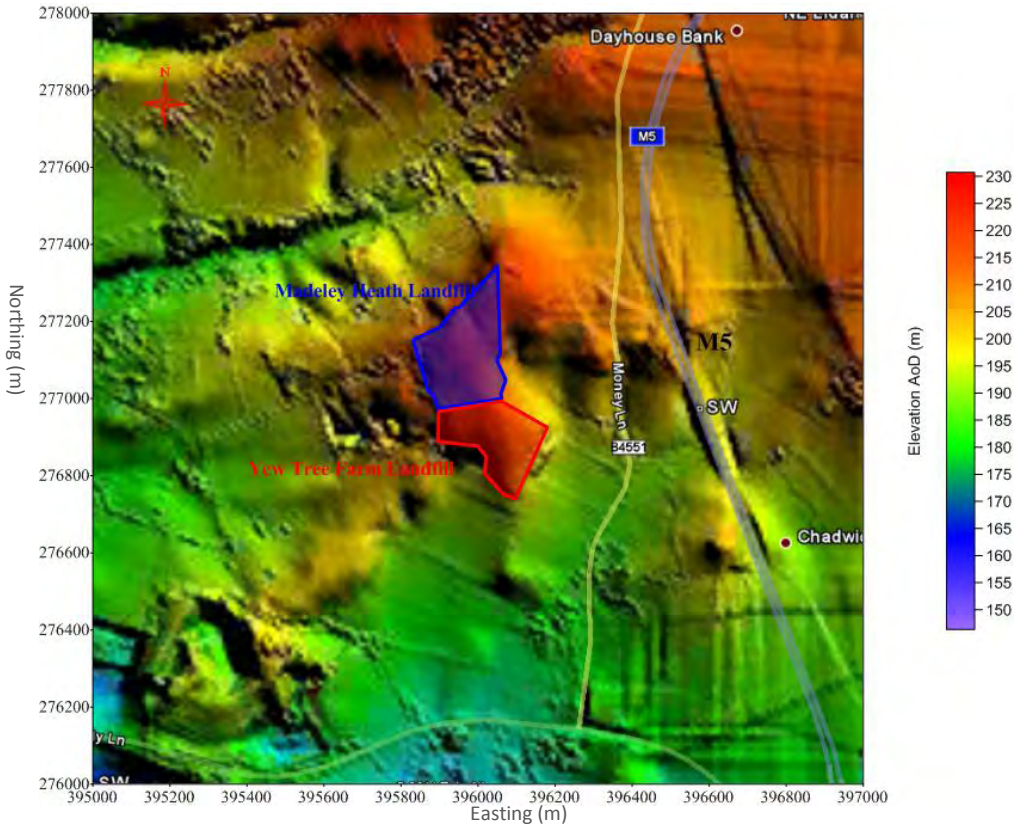

Figure 3.36: The topography map of the study area (LIDAR Data)

The topography of the study area is influenced by the hardness of rocks within the Permo-Triassic sandstone, combined with sand and gravel extraction and land filling within the landfills generated a varied topography. The harder Kidderminster Sandstone Formation forms a steep scrap slope immediately to the north from 217m AoD dropped to 185m AoD to the valley floor (Enviros, 2009). The MH landfill has an almost flat topography (AoD) with the highest elevation recorded to the north (227m AoD) and slightly declined to the south to about 217m AoD. However, the YTF landfill elevation is declining rapidly toward the south of the landfill (Figure 3.36) from the highest elevation 220m on the north to the lowest level 185m (AoD).

3.3.4.1 Site history

Historically, the YTF landfill site is thought to have first been land filled around 1958, following its excavation for sand and gravel resources. Filling of the site however may have possibly commenced slightly earlier. Its formerly had been used by British Leyland to dispose of various different waste types from their Longbridge car plant site, including solid wastes (incinerator ash, paper, wood, rexine and tins) and liquid wastes (cutting oils, solvents, and zinc hydroxides). Environment Agency records indicate that the site was used from 1958 to 1972 for tipping ‘chemical and oily waste’. These wastes are thought to have been deposited in two lagoons; a northern and a southern lagoon (Dutton, 2008). Disposal of household waste was across the entire site in three main ‘cells’.

The Madeley Heath site was originally used in 1964 as gravel borrow pit for the construction of the M5. The site was operated by Herefordshire and Worcestershire County Council from the late 1960s until the late 1980s or early 1990s. In 1978, the site was licensed under the Control of Pollution Act to accept both domestic and commercial non-hazardous waste and was restored in 1992 with a minimum of 1m of mixed clay soil capping (Enviros, 2009 and Dutton, 2008).

The sequences of the land use history are shown in Figure 3.37 to Figure 3.45

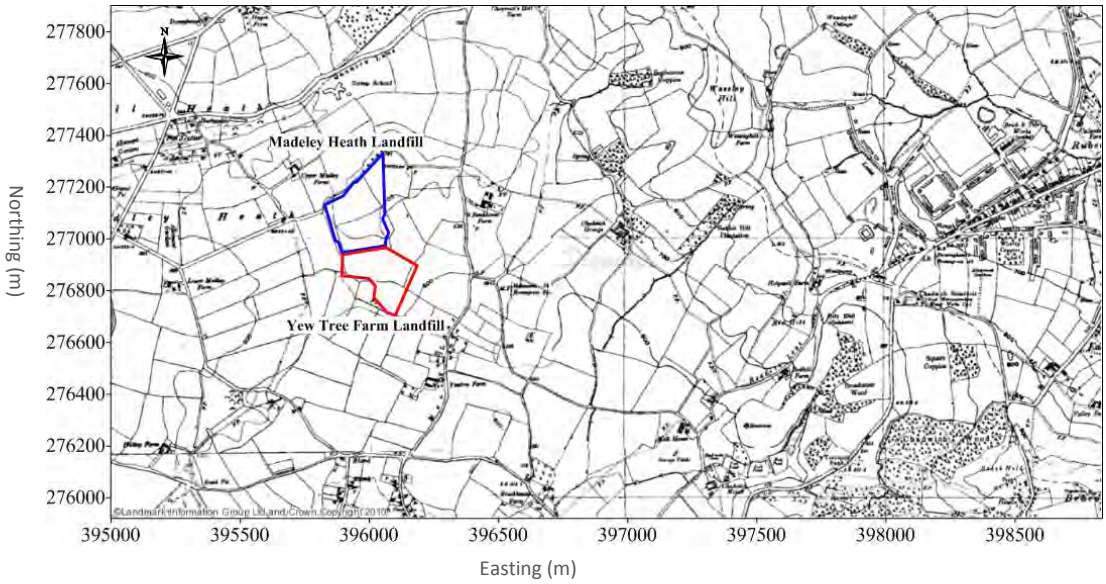

Figure 3.37: The historical map of the study area in 1940's (Source, Edina Digimap, 2011) showing it was agricultural land

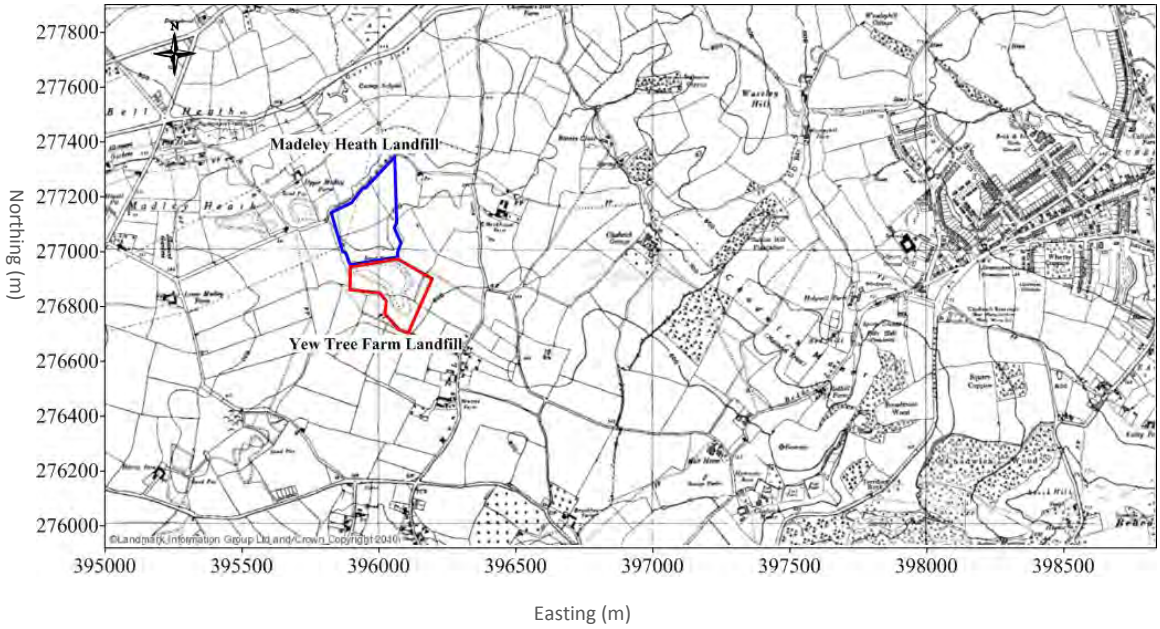

Figure 3.38: The historical map 1950's (Source, Edina Digimap, 2011) showing that the YTF occupied by the sand pit quarries.

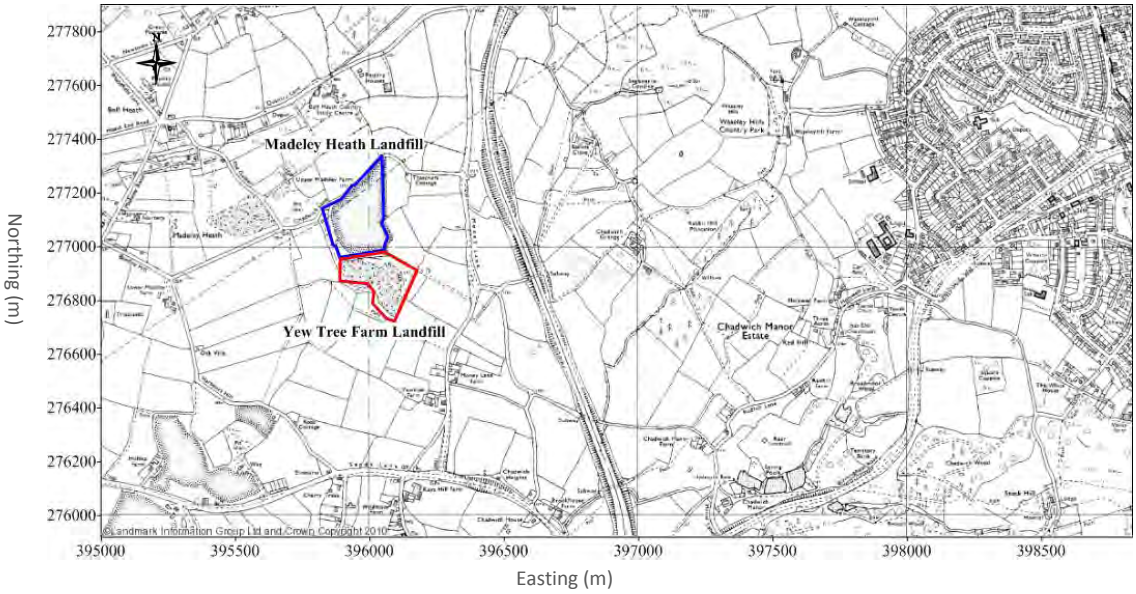

Figure 3.39: The Historical map 1960's (Source, Edina Digimap, 2011) showing almost all of YTF and half of MH have been excavated

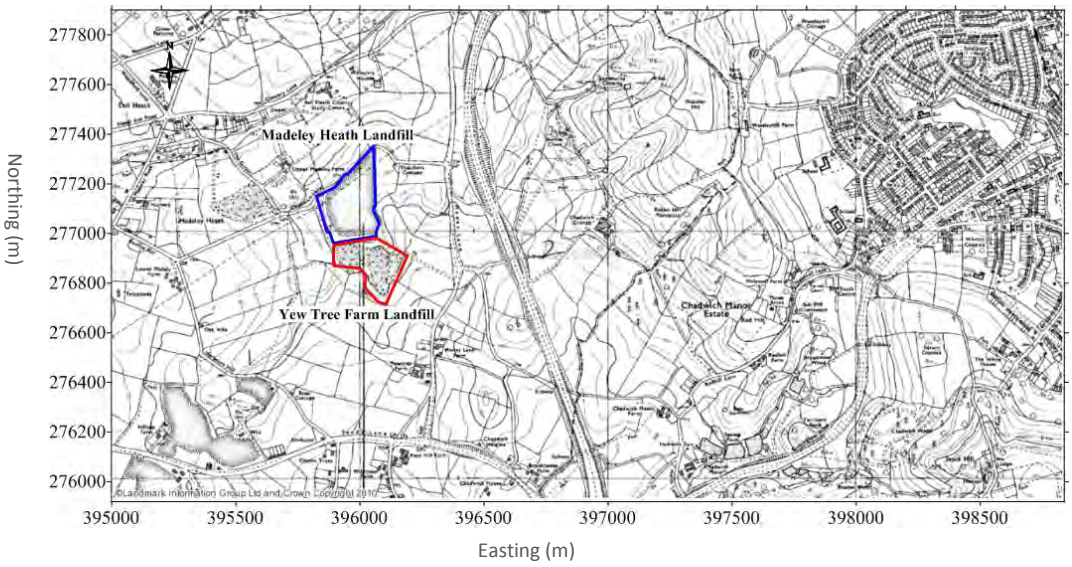

Figure 3.40: Historical map 1970's (Source, Edina Digimap, 2011) showing the YTF still active which is believed through the landfill activities

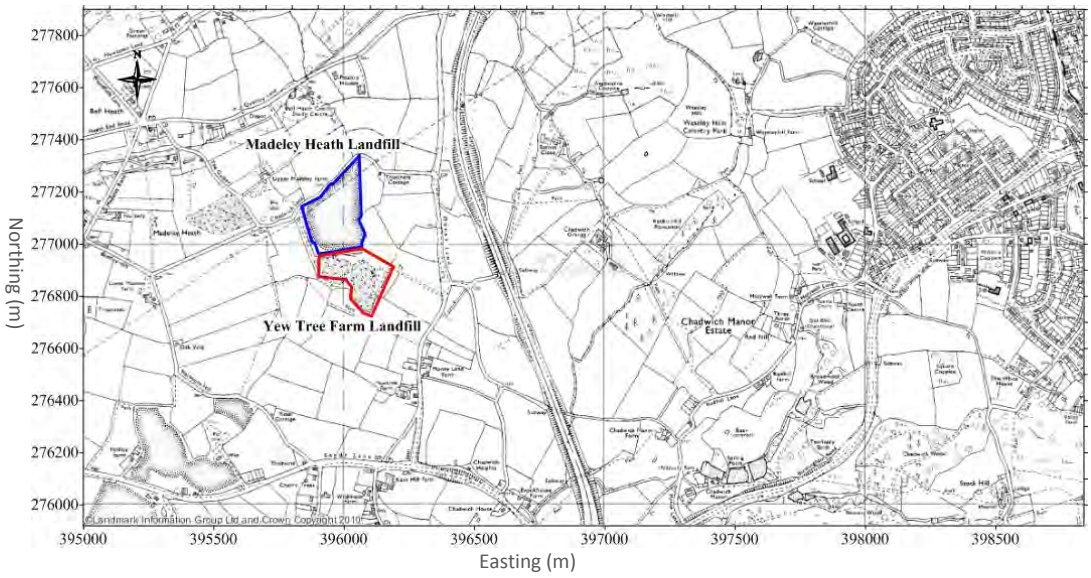

Figure 3.41: The historical map 1980's (Source, Edina Digimap, 2011) showing no significant change on both sites but have ongoing landfill activities based on the Enviros Report 2009

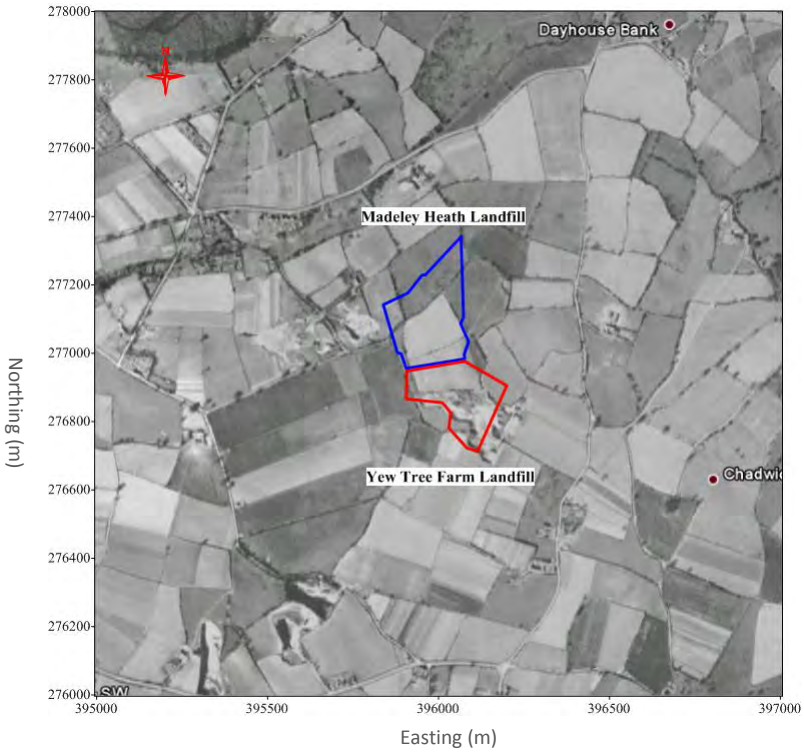

Figure 3.42: Sand pits excavation the south of the YTF through the Google Earth Image 12/ 1945 (Source, Google Earth, 2011)

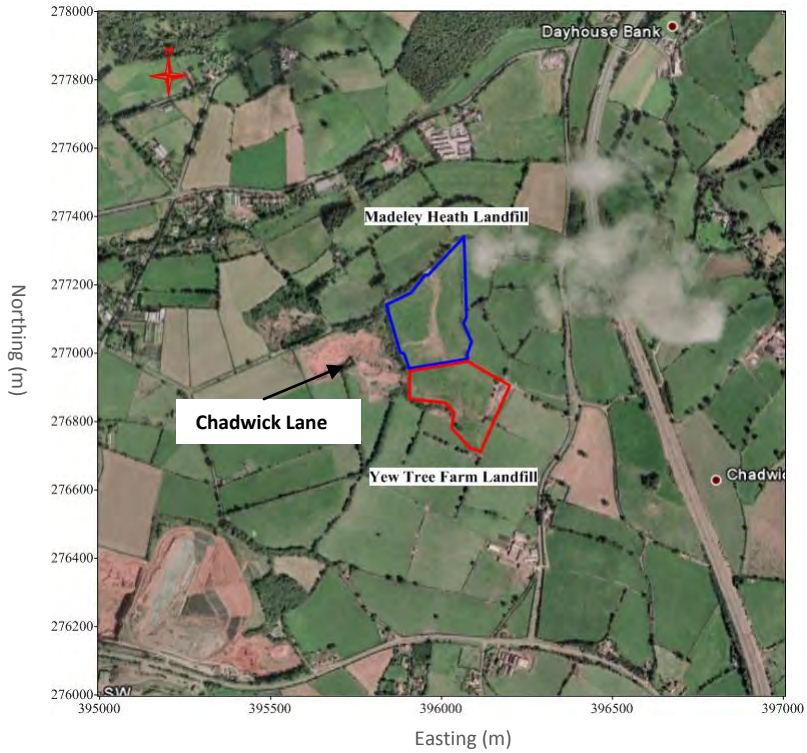

Figure 3.43: The Google Earth Image 12/ 2001 (Source, Google Earth, 2011) showing both YTF and MH now covered but a Chadwick Lane sand pits is still operating to the west of the landfills

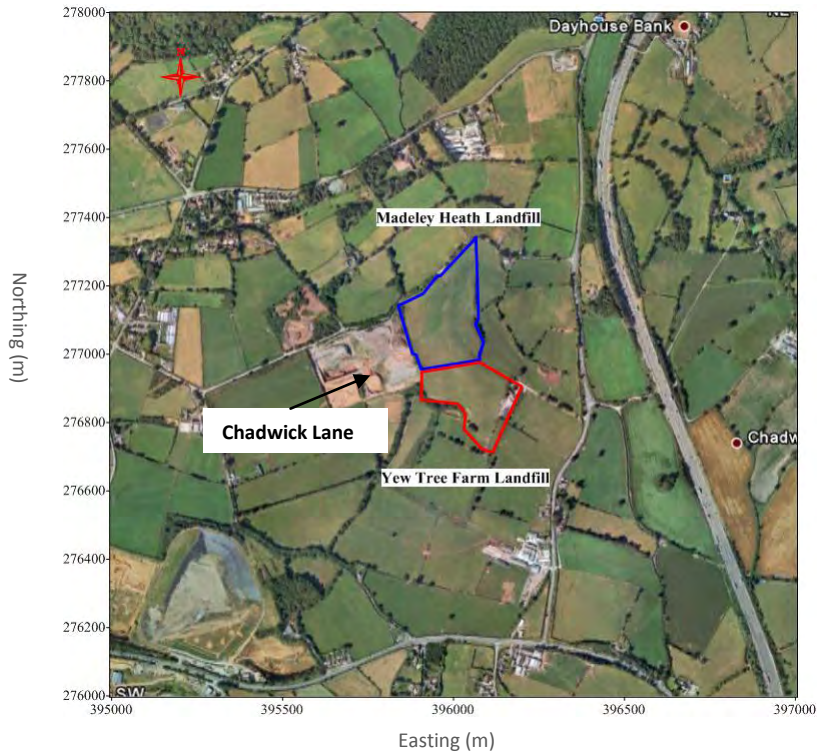

Figure 3.44: The Google Earth Image 12/2005 (Source, Google Earth, 2011) showing YTF and MH hasn't had a significant changes but the Chadwick Lane site is more active

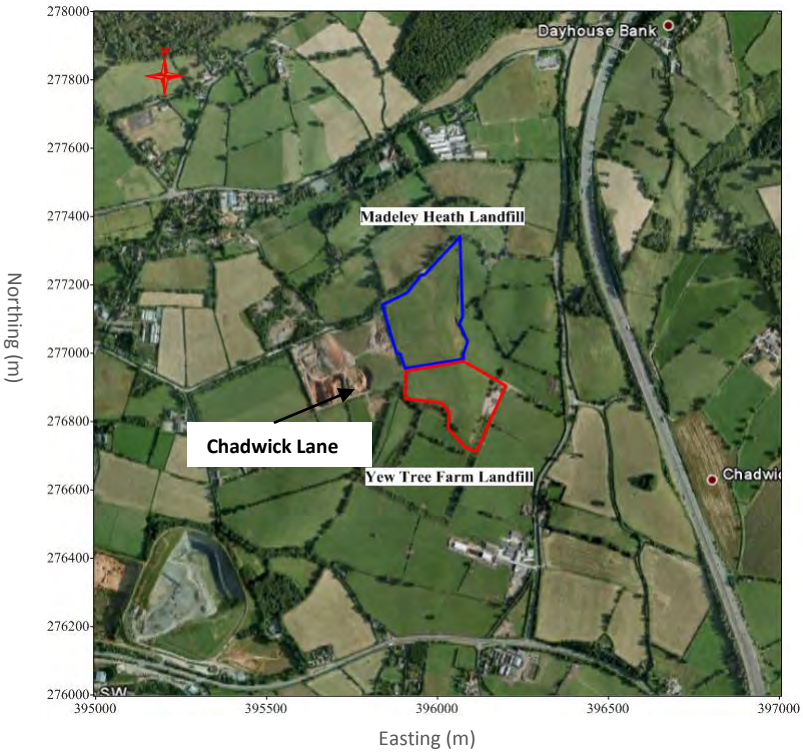

Figure 3.45: The Google Earth Image 12/2007 (Source, Google Earth, 2011) showing YTF and MH hasn't significantly changed but the Chadwick Lane is getting less active

3.3.4.2 Geological properties of the site

Generally the regional geology of the study area can be divided into three types, which include solid geology, made ground and superficial deposits.

The solid geology at the study area is formed of the West Midlands Triassic Sandstone which comprises of three main lithologies (from youngest to oldest) the Bromsgrove Sandstone, Wildmoor Sandstone (WSF) and the Kidderminster Formation (KDM) with the base of the Kidderminster Formation underlain by the Quartzite Breccia. The Breccia is composed of Palaeozoic Lickey Quartzite of local origin and is evident at the base of the Wildmoor public water supply borehole. The Breccia passes conformably into the sandstone sequence above (Dutton, 2008).

The KDM has an approximate 90m thickness and is formed of a pebbles layer comprised of quartzite pebble (65%), vein quartz (25%) and lesser quantity of quartz tourmaline rock and sandstone. The Wildmoor Sandstone Formation (WSF), it only present at the south-west of the YTF landfill and separated from the KDM by the Blackwell fault. The

made ground layer was made by the waste and backfilled material which form s a top layer of the landfills. The thickness of the made ground is estimated to be about 12 – 19m in the MH landfill and about 4 – 20m in the YTF landfill. While the superficial deposits were formed by periglacial flood gravel, boulder clay, glacial sand and gravel beneath the man made ground layer with an average two metre thickness (low permeability layer) (Enviros, 2009).

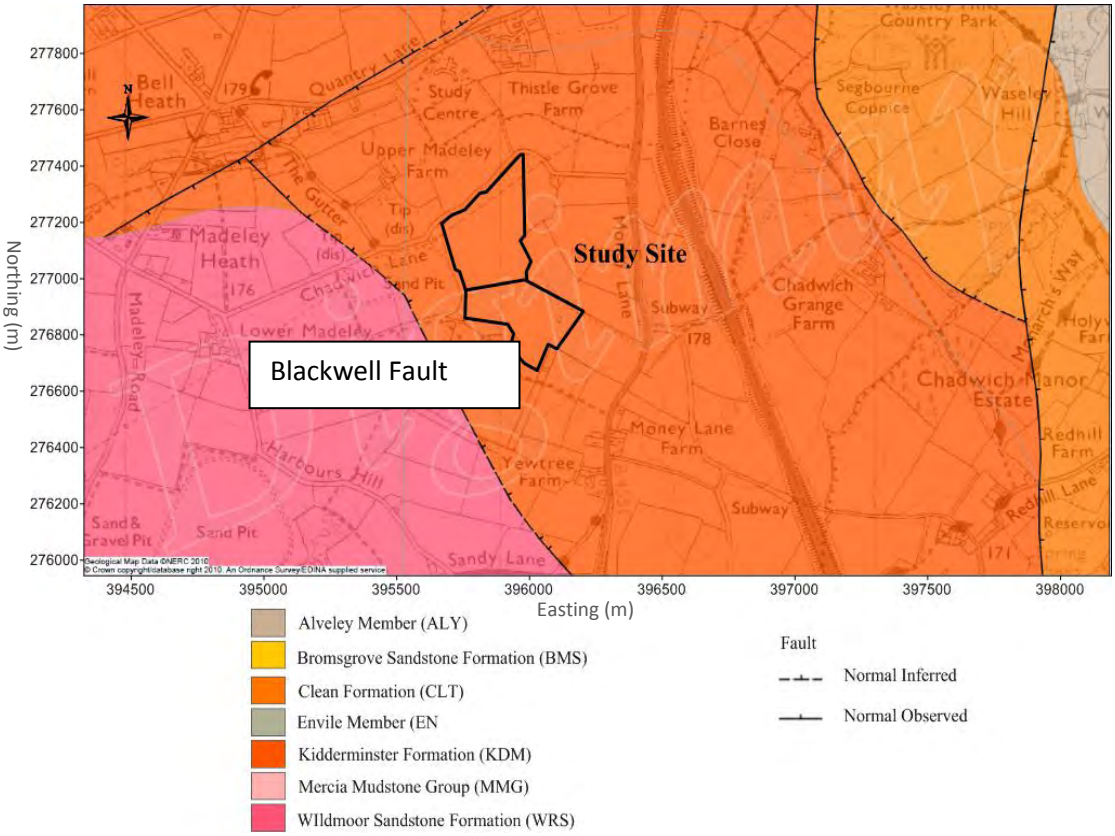

Figure 3.46: Solid geology map of the study area (Source, Edina Digimap 2011)

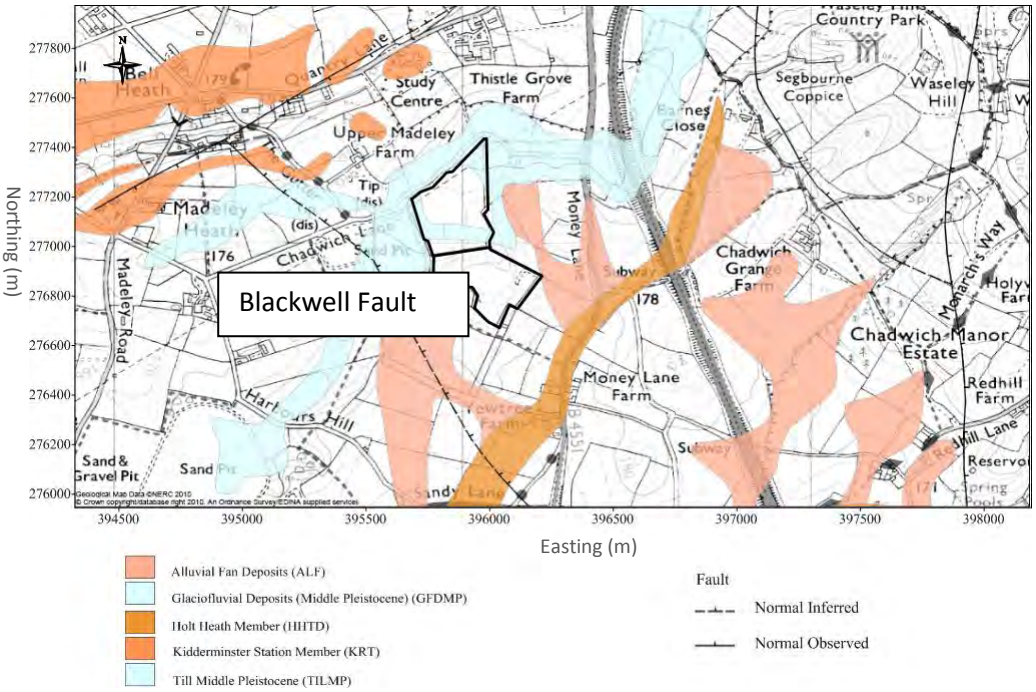

Figure 3.47: Superficial deposits map of the study area (Source, Edina Digimap 2011) and the made ground mostly found in the landfills

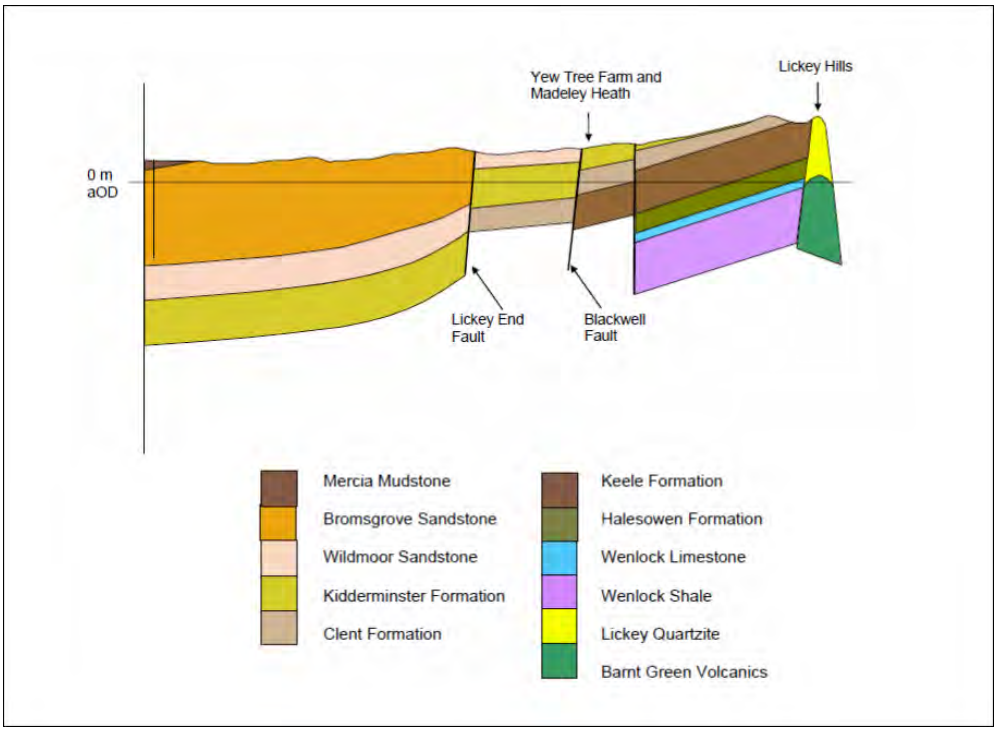

Figure 3.48: Cross section showing the faults near to the landfills which are suspected to change the groundwater level over the study area (Source Environment Agency, modified from Dutton, 2009)

3.3.4.3 Hydrogeological properties of the site

The study area is classified as a total catchment area which is important as a major resource for the groundwater recharge in the study area (Figure 3.49). The Kidderminster Formation (KDM) and the Wildmoor Sandstone Formation which are the major bedrock in that area are classified as a principal aquifer (Figure 3.50) or formerly known as major aquifer by the Environment Agency. Observation from several deep boreholes surrounding the study area shows that the depth of the groundwater is between 145m to 158m AoD. The highest groundwater table observed at the BH 1B and BH 5B on the north and north-east of the study area with about 158m AoD. While, the lowest groundwater level was observed in the BH10B at the south west of the study area which recorded at about 145m AoD. It generally shows that the regional groundwater gradient is flowing toward the south west of the study area.

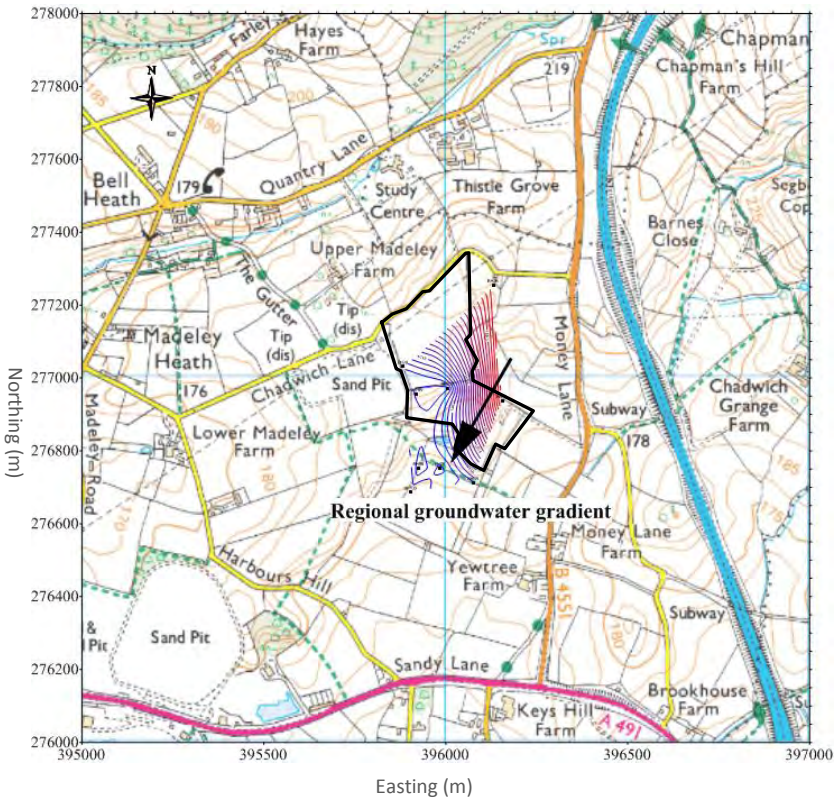

Figure 3.49: Showing the regional *groundwater* gradient toward south-west of the study area

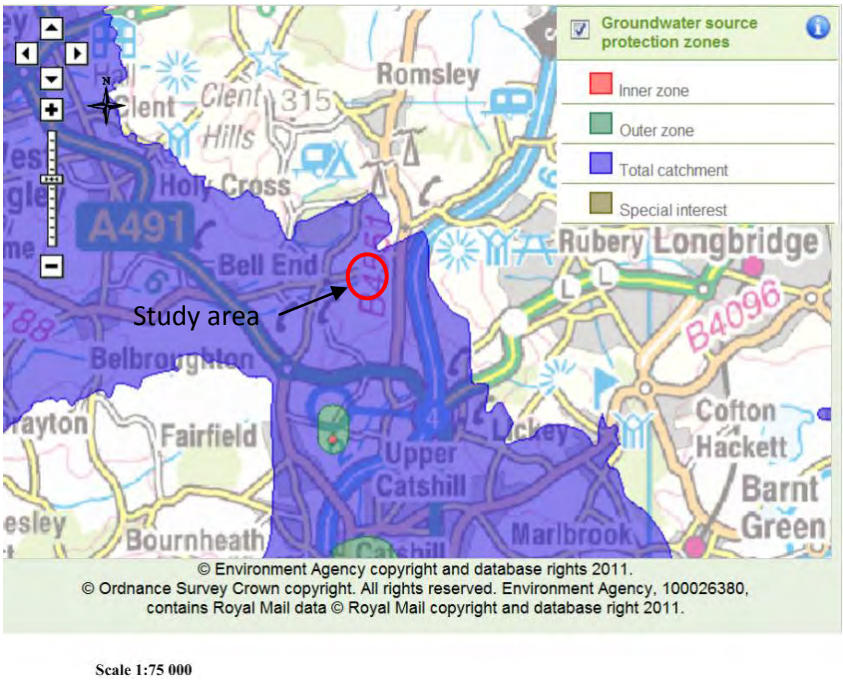

Figure 3.50: The study area is located at the important catchment area for the groundwater resources (Environment Agency, 2011c) – **Web 3.10**

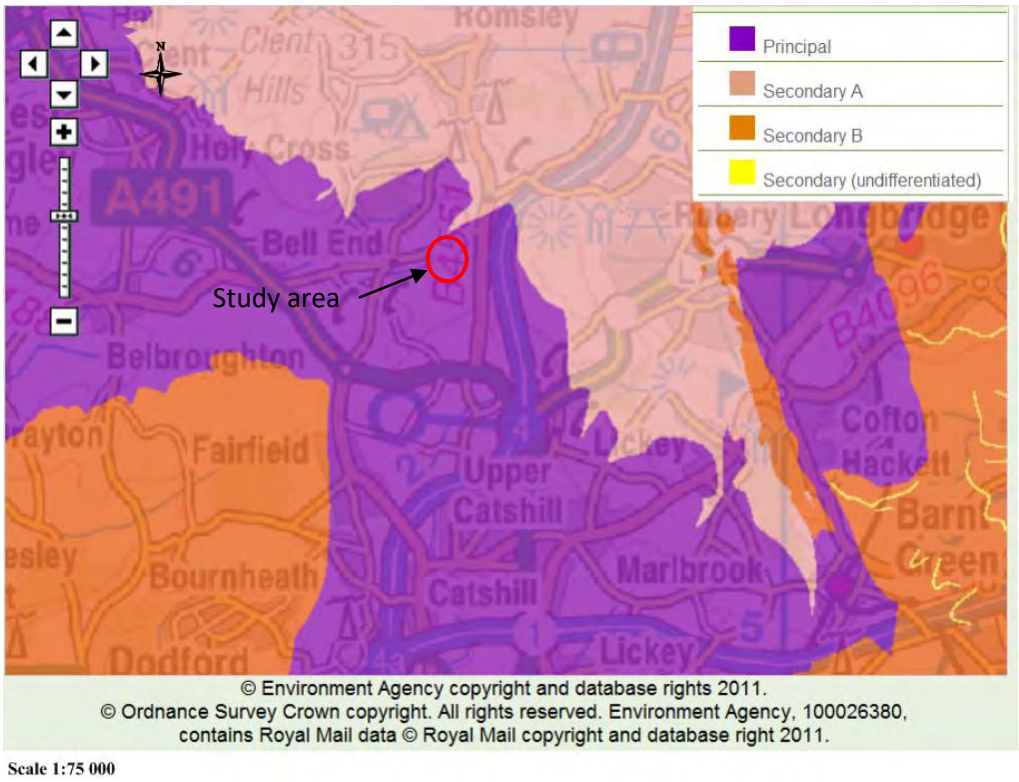

Figure 3.51: The study area is classified as a principal aquifer by the Environment Agency 2010 (Environment Agency, 2011e) – **Web 3.11**

3.3.4.4 Geophysical properties of the site

Geophysical properties of the materials at the landfill area are influenced by the type of waste materials and how long they have been dumped on the site. Generally, domestic wastes normally exhibit a lower resistivity or higher conductivity compared to the surrounding materials. But in certain cases where the basement rock has a very low permeability like clay or clayey silt the interpretation can be difficult since the resistivity properties of the surrounding material with the waste are similar. Luckily, the Bromsgrove Landfill is located at a higher elevation and lies on the Kidderminster Formation which is expected to have a very high resistivity or lower conductivity due to its lithology and the thickness of the vadose zone in that area. The unsaturated zone can be up to 50-60m in thickness.

Generally, the geophysical scenario of the study area can be divided into three categories which include a higher resistivity (lower conductivity) of the landfill area and a metres top surface of capping materials, integrated lower and higher resistivity in the landfill zone up to the bottom of the landfill and the last is a lower resistivity or higher conductivity beneath the bottom of the landfill (expected pollution leakage). Within the landfill zone itself, there is possibility to have a variation of resistivity and electrical conductivity value due to the heterogeneous distribution of the waste material in the landfill. MH landfill is expected to give a lower resistivity in the landfill zone but might be slightly different in geophysical properties to the YTF landfill due to the documented disposal of HC and industrial wastes.

3.3.4.5 Contamination Issues on the Site

There are three major issues that have to be highlighted to understand landfill contamination scenarios at this complicated study site. Firstly the location of the landfills boundaries, since there are two landfills which are adjacent to each other. Madeley Heath (MH) landfill on the north was purposely built to receive domestic waste from surrounding area. It is expected to contribute to the heavy metal contamination on the site from north. Meanwhile, the Yew Tree Farm (YTF) landfill to the south was for industrial waste dumping site and has been expected to release both heavy metal and a large amount of hydrocarbon contaminants. When considering the regional groundwater patterns of the

area, contaminants are potentially flowing toward the south-west following the groundwater gradient which produces a zone of mixing.

The second issue to be understood is the thickness of the vadose zone and unsaturated zone in the study area. Records from boreholes show thickness of the vadose and unsaturated zone can be up to 60m from the surface on the top of the landfill and about 40m at the ground valley (on the south of YTF). This gives a good background contrast to the geophysical survey since the vadose and unsaturated zones are expected to exhibit a higher resistivity or lower conductivity compared to the contamination zones.

Thirdly is regarding decomposing landfill materials, the perched water (leachate) in the bottom of the landfill and potentially some leakages through the vadose / unsaturated zone into the groundwater. These generate a huge bulk of lower resistivity liquids that might be difficult to differentiate in the resistivity profiles. So, the understanding of approximate locations of the lower resistivity materials from the boreholes data would be really helpful for precise interpretation.

3.4 Conclusions

Four different research sites, each with a different chemical / physical characterisation, site history and a variety of likely contamination sources make this research project interesting. A variety of points such as chemical characteristics of the contamination sites, contaminant transport, and links with the hydrogeological properties of the contamination site can be explored. However, this research concentrates more on the efficiency of the geophysical techniques as a tool to characterise the contamination of each site in 3D with supporting data from the geochemical and hydrogeological studies.

In the Cathays Railway Depot, contamination is expected only to be in the soil layer, because the site as classified as a Secondary-A aquifer (minor aquifer) by the Environment Agency (2010). So there are no deeper groundwater contamination issues at the site. The 3D characterisation will be generated by the information from the geophysical data and the chemical properties of soil only.

In Barry Docks, the interrelation between sea water, dock water and the groundwater make the groundwater properties in this site very complex. Contamination issues can be both present in the soil and groundwater due to the extremely varied industrial activities of the past and the situation where groundwater table is near to the ground surface. The 2D and 3D characterisation of the site can be established using both geochemical borehole/ soil sampling and geophysical data.

The town gasworks at Weston Super-Mare, off-site groundwater contamination issues are probably not occurring at this site because most of the area is covered by the tidal superficial clay deposits. The only issue is a contamination from the gasworks activities in past into the soil as a shallow contamination. A buried wooden tank is suspected to contribute to the contamination on the site, which is part of the buried building structure and waste from activity in the past. So, a 2D or 3D image of the contamination can be established using only geophysical data.

At the Bromsgrove landfill which comprises the adjacent Madeley Heath and Yew Tree Farm Landfills, the conceptual model of the contamination is complex involving different type of wastes, non barrier landfill, a complex rock and soil strata, and the deep groundwater level. Although, the site setting and contamination scenario is complex, a contrast of the geophysical properties of the contamination zones against the geophysical properties of the background materials is an advantage to the geophysical interpretation.

CHAPTER 4
CALIBRATION AND PROOF TESTING OF THE IRIS SYSCAL RESISTIVITY SYSTEM

4.1 Introduction

It is essential before any geophysical survey is performed that the instrument being used is correctly measuring and recording data with a high precision and accuracy. This can only be ensured by careful laboratory calibration of the instrument against known values. Calibration tests have been applied to the resistivity meter (IRIS SYSCAL SYSTEM) to ensure accuracy in measuring against the known resistivity of material in laboratory scale and in-situ field experiments. Although all resistivity meters are designed for rugged field use, they need regular calibration tests.

The IRIS Syscal Jr. Resistivity System consists of an internal switching board for connecting 72 (Switch-72) electrodes and an internal 12V, (100 W) power source. The output current is automatically adjusted (automatic ranging) to optimize the input voltage values to ensure quality measurements. The system is designed to measure the material's resistance using pre-defined electrode arrays. Only four electrodes are chosen at any time by the switch-72 for every measurement, all the rest of the electrodes will be connected successively for subsequent measurements. Two sets of cables, each with 36 electrode take-outs are connected to sockets on the back of the resistivity meter (Cardiff's IRIS SYSCAL Jr. System). These cables are made up of heavy duty material and are constructed with fixed electrode spacing. The electrode spacing can be adjusted to any distance to measure the resistivity of earth materials. The exact electrode spacing that is used for any survey depends on the target depth.

Therefore regular calibration tests are mandatory before any new resistivity mapping project is carried out either in the laboratory or using a field test site. Issues of calibration were first brought to light when the Cardiff University Iris system was used in conjunction with two identical systems owned by Terradat UK Ltd at a local test site. It was noted that although all three systems gave relatively similar mapping results, the absolute resistivity values showed some variation. This suggested that all three instruments had slightly different calibrations.

4.2 Why is equipment calibration important?

It is essential for any survey that the operator is confident that the instrument is making accurate measurements. Figure 4.1 and Figure 4.2; show the steps taken for the calibration processes. For a perfectly calibrated instrument, the readings for a series of tests would fall on a line as shown in Figure 4.1, labelled as "Ideal Results". If however data from a calibration test fall on another line labelled as "Actual result", these actual data are considered as being in error because they are different from the ideal result. Even though the test data are considered as being in error, they are in error by a constant based on its linear curve/line shape.

Figure 4.2 shows how a correctly performed calibration test can improve instrument performance. Based on the calibration curves, the difference between „Actual' and „Ideal' results are calculated and used in the correction of data obtained from subsequent field surveys or laboratory experiments. In this case, the equipment setting is not changed and by measuring different readings for similar materials against other calibrated equipment. This calibration factor is used in the correction of any non-calibrated equipment.

Another way of calibrating equipment is by determining the difference between "Actual results" (measured data) and a standard value (Ideal value). The "Actual Results" will converge to the "Ideal Results" by tuning some equipment parameter towards a calibrated value (normally using a buffer, reagent and procedures established by equipment manufacturer).

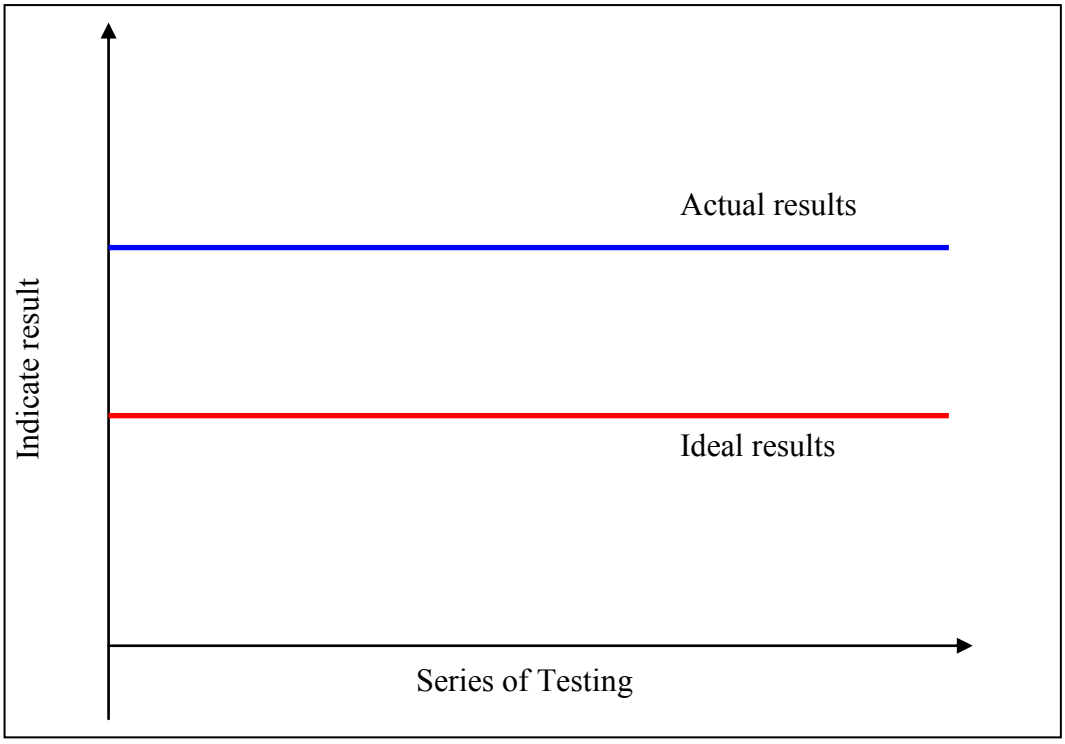

Figure 4.1: Data curves produced from equipment calibration tests

Calibrating the instrument can improve this situation significantly. The procedures are shown in Figure 4.2. Known calibrators are used for the instrument to predict what result it should get. This process eliminates the errors at these two points, which in actual fact is considered as moving the Actual Results curve closer to the Ideal Results curve. The „Error At any Point' is reduced to zero at the calibration points, and the residual error at any other point within the operating range (exaggerated by the curve) is within the manufacturer's published linearity or accuracy specification (British Standards Institution).

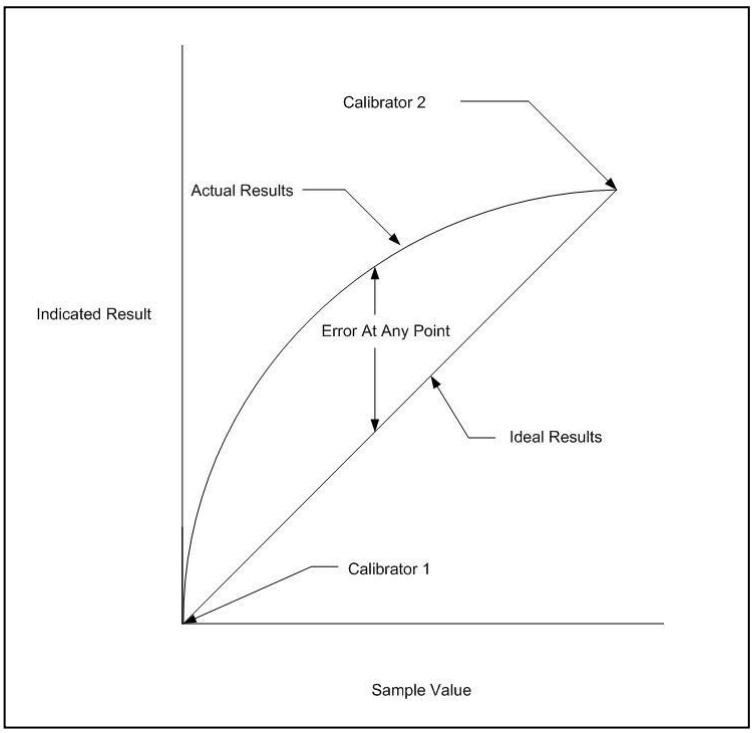

Figure 4.2: Calibrating the equipment by tuning the equipment to reach the Ideal Results (Advance Instruments, 2010) – **Web 4.1**.

Normally in the UK, test monitoring equipment is specified as an essential element of any quality assurance for standard calibration in accordance to the ISO 9000:2005 (2005) – (**Web 4.2)** series of standards. Any test equipment monitoring must assure that all instruments used for assuring product quality measures "correctly".

In order to ensure the instrument makes correct measurements, test equipment must be calibrated on a regular basis, and this must be retraceable to national standards. The measured values of the calibration tests must be documented. Retracing of calibration results to national standards is confirmed for the user by means of a "factory certificate".

For the IRIS SYSCAL Resistivity System, there is no specific standard for calibration given by the system manufacturers, the user will normally send the equipment back to the manufacturer for calibration. This is time consuming as well as being costly. A simple experiment for the calibration was designed and successfully performed in the laboratory. The calibration factor is determined by calculating the difference of measured resistivity values against the calibrated laboratory conductivities (NORFOLKS and Hydroponics Centre Ltd, 2010) – **Web 4.3**) and the IRIS SYSCAL Resistivity System (**Web 4.4** and **Web 4.5**).

The Resistivity Imaging Technique is commonly used to investigate aggregate deposits, measuring earth impedance or resistance for electrical grounding circuits protection, archaeological surveys, estimating depth to bedrock in ground engineering and to measure the water table for hydrogeology. However in this research project, the technique is to be used to study groundwater and soil contamination at industrial sites. The appropriate electrode arrays and degree of detectability of the system has to be established before carrying out any intensive field survey programme.

4.3 Objective of the calibration and a proof test

As stated above, both calibration and proof testing are important in this study for accurate data and confident interpretation of the field results. Highlighted here are detailed objectives of both tests.

4.3.1 Calibration

The calibration tests were performed for detecting any difference in resistivity values acquired by IRIS System and Calibrated Laboratory Hanna Combo Conductivity meter. It is also carried out to calculate the percentage of difference reading between both equipments which can be used as comparison for future resistivity investigation

4.3.2 Proof test

This test is performed in order to justify whether the technique used for this research is appropriate for subsurface investigations especially in terms of:

a) Identifying the best electrode array for resistivity survey
b) Defining the accuracy of the equipment in detecting the existence of different resistivity materials in the sub-surface.
c) Determining the efficiency of the equipment in imaging the sub-surface.

4.4 Methodologies

The calibration tests were carried out in laboratory using a 35x25x25cm size plastic container with water used as the medium for current conduction. The plastic tank is a perfect insulator and may influence the results by producing a high resistivity edge effect to the testing system. The container was half filled with fresh water (approximately 12cm depth). Specially designed cables with a total of 36 mini-electrodes were used. The 2cm gold coated electrodes were equally spaced at 1cm and fixed in a Perspex ruler (Photo 4.1). All electrodes are connected to a multi-switch box which is in turn connected to IRIS system (Photo 4.2). With this electrode configuration, the maximum predicted depth of penetration for Wenner array is approximately 5.8 cm and 6.4cm for the Wenner-Schlumberger array (Electrode II software – **Web 4. 4** and **Web 4.5**). In a complete data acquisition programme, 195 measurements will be made using the Wenner array and 215 measurements using the Wenner-Schlumberger array.

The resistivity of the water was measured using a laboratory Hanna Combo Conductivity meter which was pre-calibrated with a standard reagent (1413µS/cm). An average conductivity value was calculated by taking several measurements at different locations and depths with tap water in the tank. The Resistivity of water can be calculated using the equation below (resistivity is the reciprocal of conductivity (***C***)):-

r (Ohm- metre) = ***1/C*** **----------*Eq. 4.1*** (Zerelli, 2011) **– Web 4.6**

Two calibration tests were carried out using both Wenner and Wenner-Schlumberger electrode arrays. For each test, the resistivity of selected models was measured using either fresh tap water or fresh tap water mixed with deionised water. The electrodes are plugging on the Perspex rule and floating on the water (Photo 4.3 and 4.4). Theoretically, a slight different is expected in the resistivity values measured with different electrode depths in the water and also with different distance of electrode from the tank walls. Consequently, the measured apparent resistivity of the water will be slightly higher at electrodes located closer to the tank wall and closer to the base of the tank or at deeper data points (due to the edge effect of the insulating plastic). Therefore, the average resistivity values measured from each calibration test will be used to calculate the calibration factor applied to future data correction. In this research, tap water is used as a

conductive medium in defining the effect of small resistivity values less than 50 Ωm, while mixed tap and deionised water is used for estimating materials of slightly higher resistivity with values greater than 200 Ωm.

4.4.1 First experiment

In the first experiment, the electrode spacing used was 1cm and the average conductivity (10 readings) of the water measured from Hanna Pro Combo conductivity meter was 293±0.1μS/cm (34.21Ωm). The water depth in the tank was approximately 12 cm. The current voltage used in the IRIS setup was 50mV with a relay time of 1000ms. The experiment started with a Wenner array electrode configuration. The second electrode array used was a Wenner Schlumberger array, all other parameters remained unchanged. Data from these arrays are then used for comparison.

4.4.2 Second experiment

The second experiment was carried out by increasing a water level from 12cm to 18cm. The conductivity of water was also made less conductive, with an average value of 49±0.1μS/cm (resistivity 204 Ωm) by adding deionised water into the tap water. The experiment started with Wenner array which was then followed by a Wenner-Schlumberger array.

As for the proof test, data acquisition started with the most commonly used electrode array which was Wenner and followed by Wenner-Schlumberger array. This experiment or test was carried out to characterise the best array to be used for the tank experiment and hence the most suitable array for any subsurface investigation. The tank model experiment also has a great advantage in comparing several electrode arrays and hence deciding on the best array to use for certain ground conditions. In this experiment, several shapes of physical models were used as targets as shown in Table 4.1. Clean fine to medium grain homogenous and non-adhesive sand (Photo 4.5) was used as the host medium. This type of sand was easy to handle especially when replacing the tested physical model. A hollow *Polyvinyl Chloride* (PVC – Photo 4.6) pipe closed at both ends was used to simulate a high resistivity material buried in water-saturated sand. In characterising this model, maximum data depths as well as the image resolution will be

defined for Wenner, Wenner-Schlumberger and Dipole-Dipole arrays. Experiment no. 1 to 6 as shown in Table 4.1, were carried out for determining background information and served as controls for the experiments. Dry sand, followed by half saturated and then fully saturated sand were used as medium for the model tests.

In order to characterise the detection capability of the electrode arrays, a 1.0 cm diameter and 15 cm length of PVC hollow pipe (closed at both ends) was kept horizontally in the sand medium at several depths beginning from 2cm to 8cm. In this test, performance of Wenner-Schlumberger and Dipole-Dipole arrays in detecting the object in terms of its resolutions were compared. The experiment setup of the physical models are described in Table 4.2

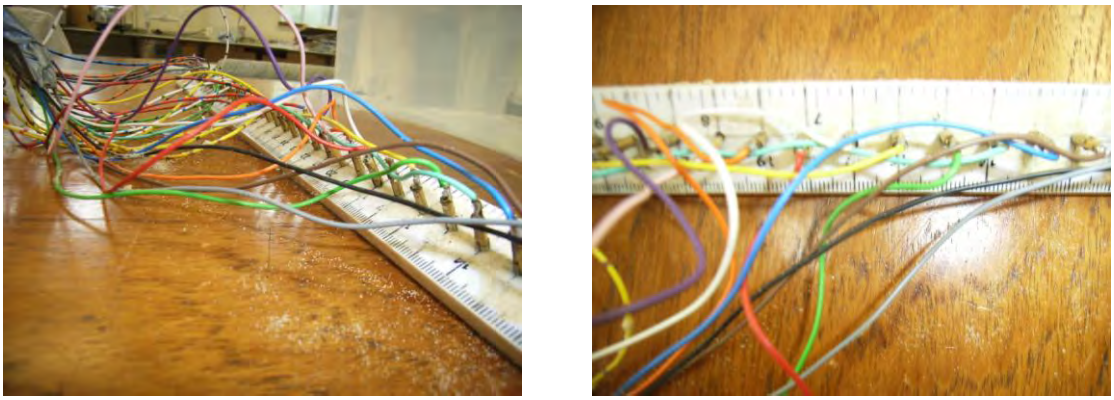

Photo 4.1: The connection between wires and the electrodes which are plugged in through the Perspex ruler

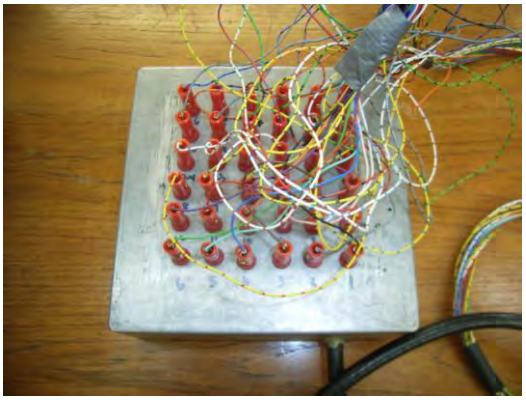

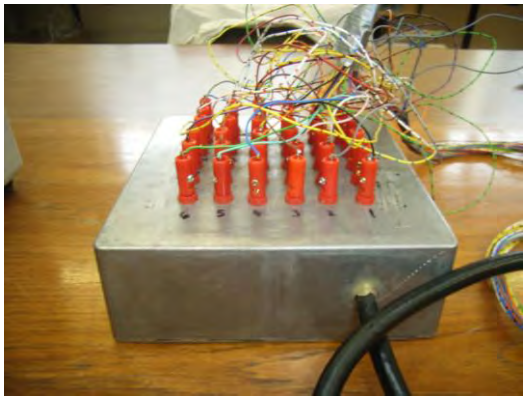

Photo 4.2: The interface box connecting the electrode wires to the IRIS System

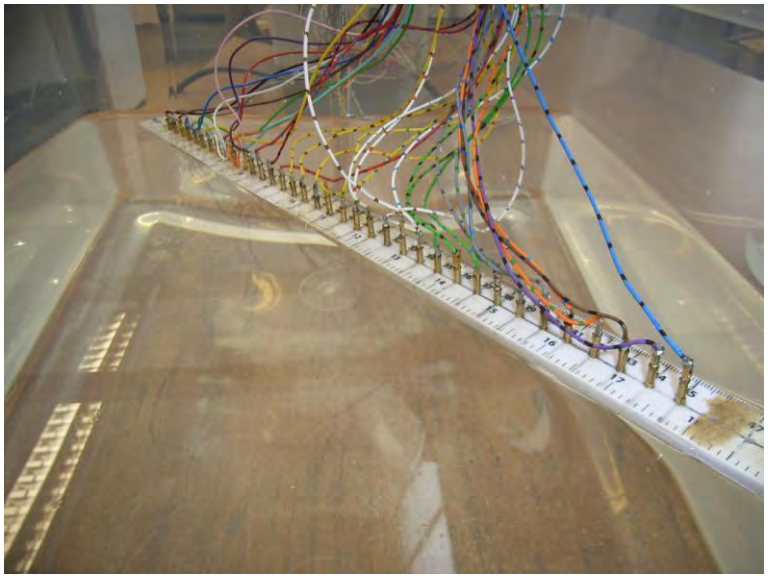

Photo 4.3: Electrodes hanging near to the water surface by plugging into the Perspex ruler

Photo 4.4: This photo taken from the side of the plastic tank, showing slightly different depths of the electrodes in the water which may have a minor effect on the quality of data collection.

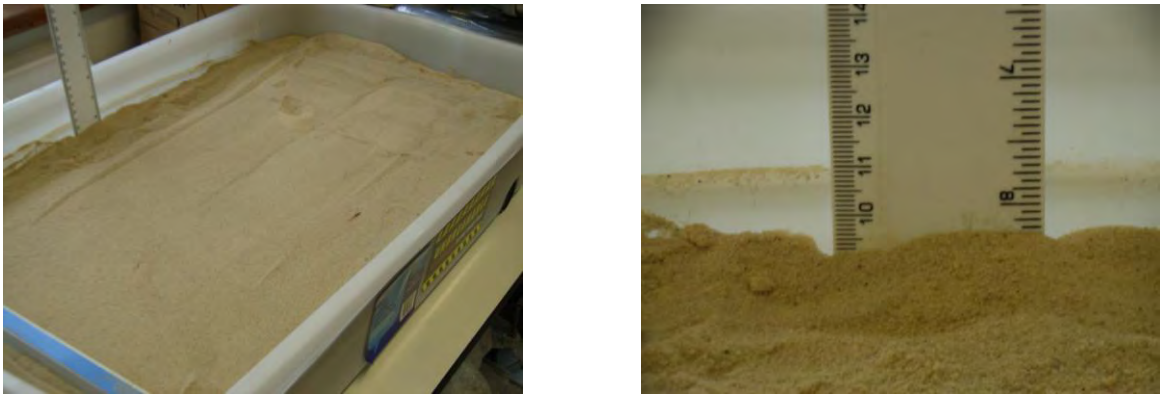

Photo 4.5: The proof test sand tank model with a clean fine to medium size sand and it thickness (9cm). The testing material are buried into the sand up to 8cm depth

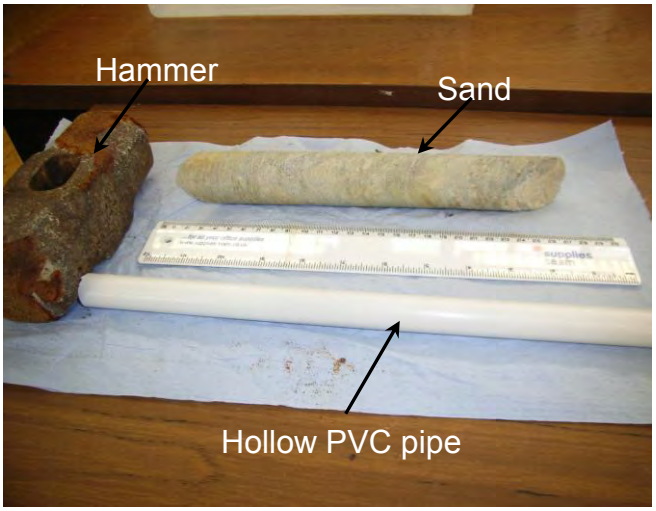

Photo 4.6: Testing materials for the proof test

Table 4.1: Details of physical models used in the proof tests between Wenner and Wenner-Schlumberger array

Experiment No	Electrode Array	Medium	Model description	Note
1	Wenner	Dry sand	Pure sand	Dry surface
2	Wenner-Schlumberger	Dry sand	Pure sand	Dry surface
3	Wenner	Half saturated	Pure sand + tap water	Dry surface
4	Wenner-Schlumberger	Half Saturated sand	Pure sand + tap water	Dry surface
5	Wenner	Saturated sand	Pure sand + tap water	Wet surface
6	Wenner-Schlumberger	Saturated Sand	Pure sand + tap water	Wet surface
7	Wenner-Schlumberger	Saturated Sand	Pure sand + tap water	A hollow PVC pipe buried into the sand with the depth about 8cm approximately
8	Wenner	Saturated sand	Pure sand + tap water	A hollow PVC pipe buried into the sand with the depth about 6cm approximately
9	Wenner-Schlumberger	Saturated Sand	Pure sand + tap water	A hollow PVC pipe buried into the sand with the depth about 6cm approximately
10	Wenner	Saturated sand	Pure sand + tap water	A hollow PVC pipe buried into the sand with the depth about 2cm approximately
11	Wenner-Schlumberger	Saturated Sand	Pure sand + tap water	A hollow PVC pipe buried into the sand with the depth about 2cm approximately

Table 4.2: The information of physical model that been used in the proof test for Wenner-Schlumberger and Dipole-Dipole array

Experiment No	Electrode Array	Medium	Model description	Note
1	Wenner-Schlumberger	Saturated Sand	Pure sand + tap water	Two hollow PVC pipes with diameter about 1cm buried into the sand for a depth of about 2cm (electrode No 29 – No.32) and 5cm (electrode No.9 – No.10). The line built perpendicularly crossing the pipe and crossing point was at the middle of the line
2	Dipole-Dipole	Saturated Sand	Pure sand + tap water	Two hollow PVC pipes with diameter about 1cm buried into the sand for a depth of about 2cm (electrode No 29 – No.32) and 5cm (electrode No.9 – No.10). The line built perpendicularly crossing the pipe and crossing point was at the middle of the line
3	Wenner-Schlumberger	Saturated Sand	Pure sand + tap water	Two different material limestone core and iron hammer buried into the sand at depth of about 2cm. The limestone core buried under electrode numbers 6 to 11, while the iron hammer is at electrode number 26 – 31.
4	Dipole-Dipole	Saturated Sand	Pure sand + tap water	Two different material limestone core and iron hammer buried into the sand at depth of about 2cm. The limestone core buried under electrode numbers 6 to 11, while the iron hammer is at electrode number 26 – 31.

4.5 Results and discussion

Two different calibration and proof tests studies were carried out and are discussed in this chapter.

4.5.1 Calibration works

The discussion will be divided into two parts following the type of experiments to get a clear view of the relationship between these two equipments.

4.5.1.1 First experiment results

In the first experiment, the calibrated conductivity meter measures an average reading of water conductivity of 293μS/cm (resistivity 34.21Ωm). Raw data measured by the IRIS are plotted and the plotted curves shown Figure 4.3 to Figure 4.6 with the actual measured values by conductivity meter and the average value for the first four layers of data points. The deeper data were not used in this calibration because these data are suspected to be influenced by the plastic tank base. Data from the first four layers produced resistivity measurements with an average value of 65.87 Ωm for the Wenner array and 65.43 Ωm for the Wenner-Schlumberger array. This is much higher than the actual value (34.21 Ωm). The calibration factor was calculated as being **1.9255** for Wenner array and **1.9126** for Wenner-Schlumberger array.

4.5.1.2 Second experiment results

The second experiment was conducted by changing the tap water with a mixture of deionised water and tap water. The mixture produced a higher resistivity solution. The model depth was increased from 12 cm to 18cm to avoid the effect of plastic tank wall on the measurement. The average conductivity (ten readings) of the solution used in the tank was 49±0.1 μS/cm or (resistivity 204 Ωm). The results are as shown in Figure 4.7 to Figure 4.10. The average resistivity value measured in the survey was 368 Ωm for Wenner array and 363 Ωm for Wenner-Schlumberger array. Again, it shows a calibration factor of **1.8039** and **1.7794** higher than the actual value (204Ωm). The average calibration factor measured in all these experiments was **1.8554**. As a result of these

calibration tests, all subsequent field data must be corrected by dividing the measured resistivity data by average factor (**1.8554**) prior to the use of RES2DINV modelling software.

4.5.2 Proof test results

The main objective of the proof test was to verify whether the technique is suitable to be used for this research project in the subsurface imaging of contamination plumes. The proof test was run with three different background resistivity values representing 3 types of materials. Referring to the information given in Table 4.1, experiments no. 1 to no. 6 were designed to estimate the background resistivity of the models. In experiment 1 and 2, both utilizing dry sand as the host medium as well as experiment 3 and 4 (semi saturated sand), no resistivity value was recorded by the equipment because of the perfect insulating effect of dry quartzite sand. Even after improving the electrode connections no reliable data could be made so in these four tests, no resistivity profiles could be obtained.

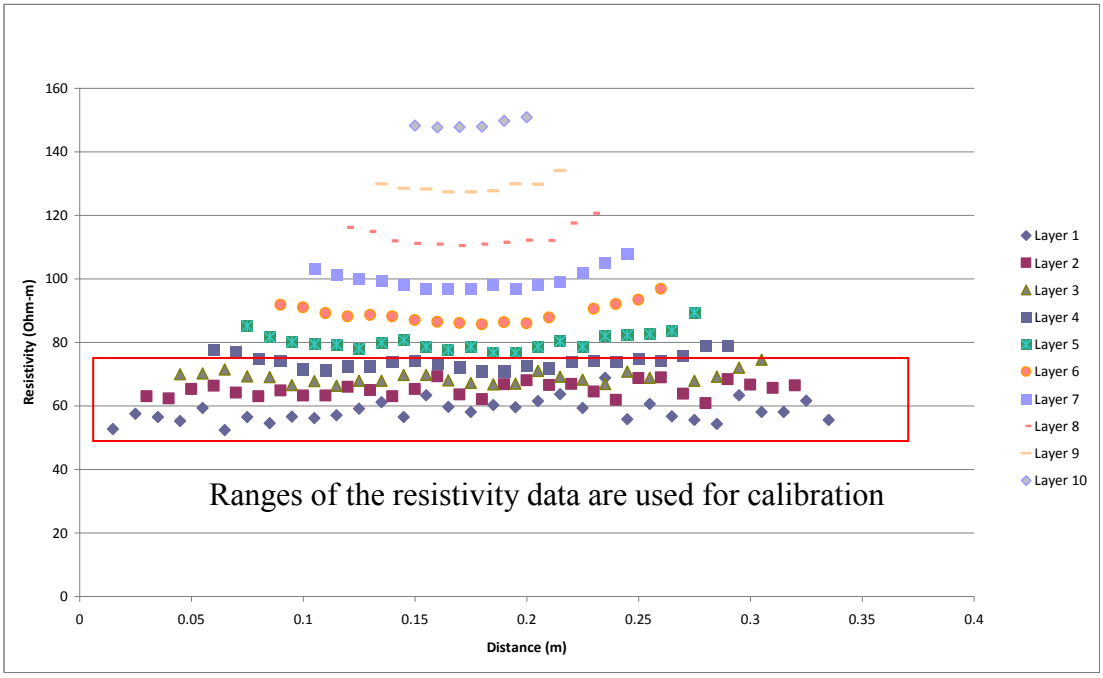

Figure 4.3: The resistivity of tap water obtained using Wenner array

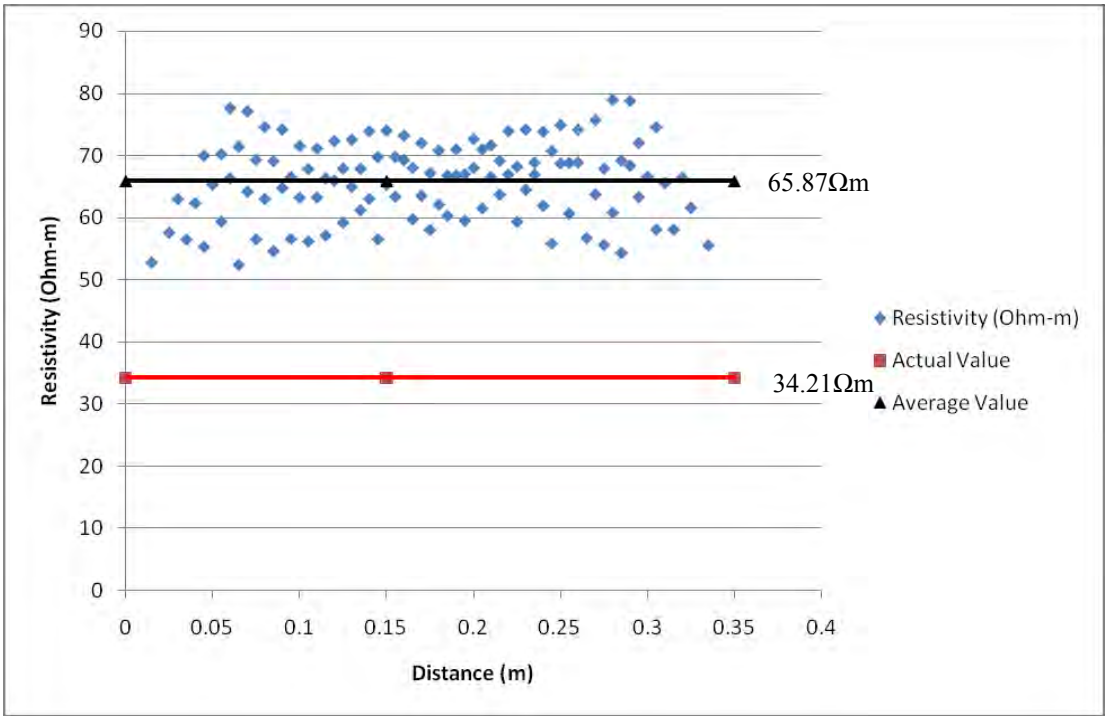

Figure 4.4: The resistivity of tap water obtained using Wenner array for first four layers

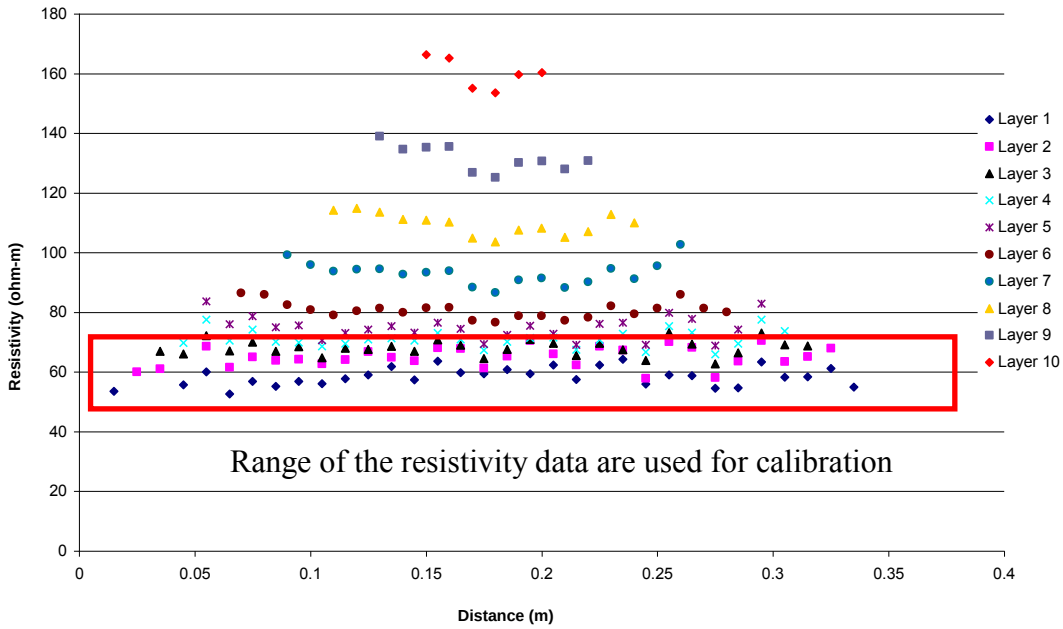

Figure 4.5: The resistivity of tap water obtained using Wenner-Schlumberger array

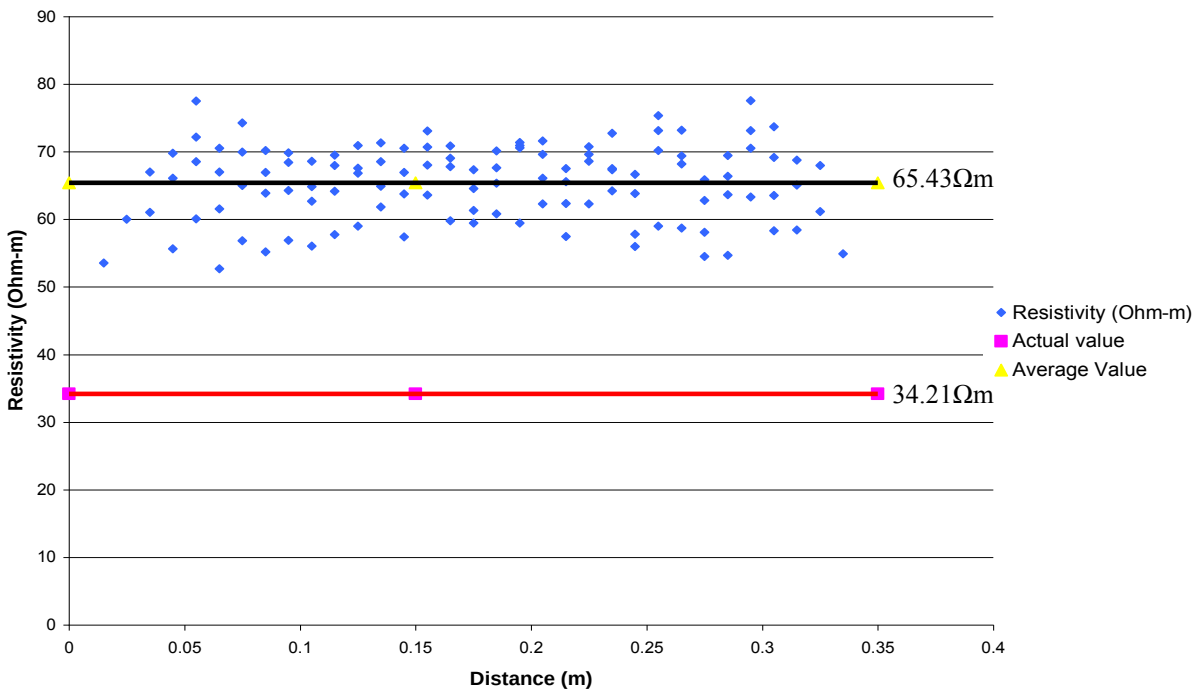

Figure 4.6: The resistivity of tap water obtained using Wenner - Schlumberger array for first four layers

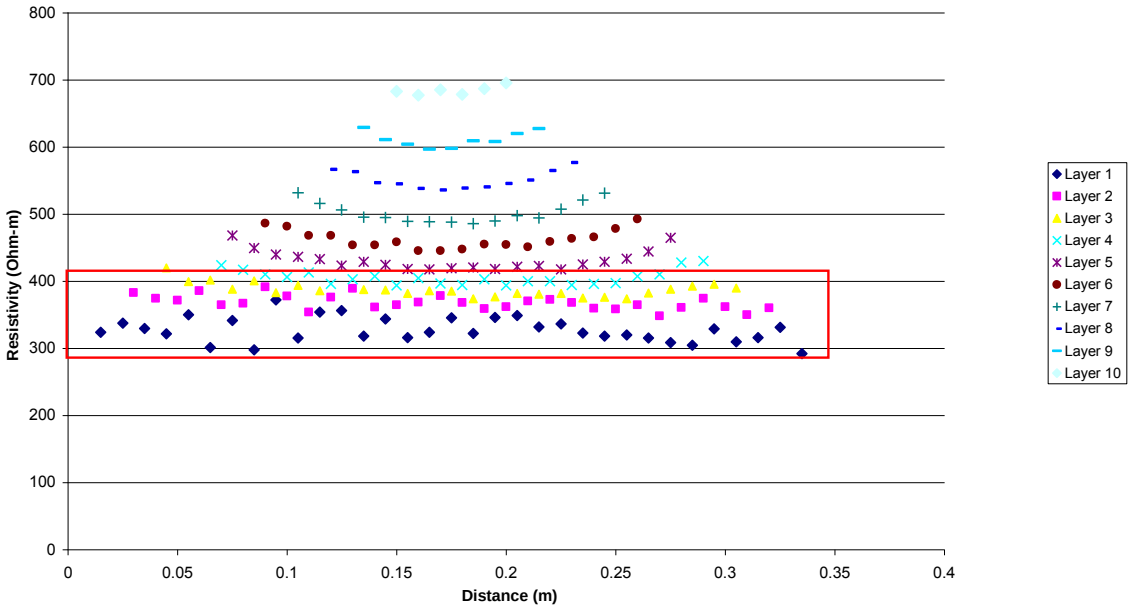

Figure 4.7: The resistivity of mixed tap and deionised water obtained using Wenner array

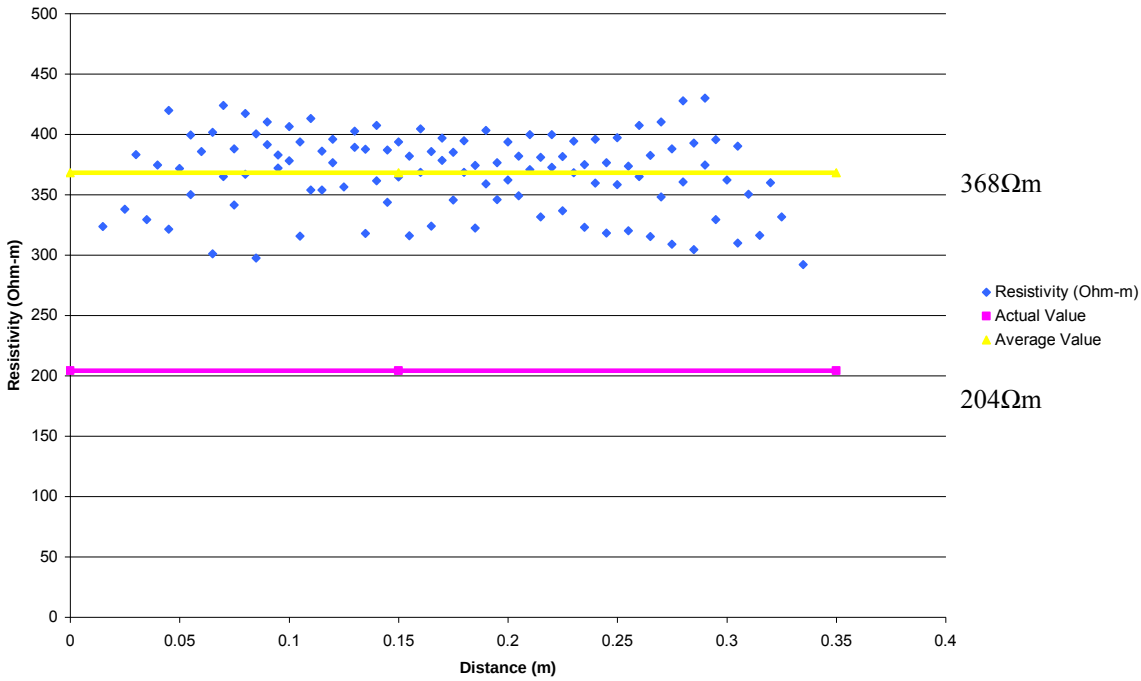

Figure 4.8: The resistivity of mixed tap and deionised water obtained using Wenner array for first four layers

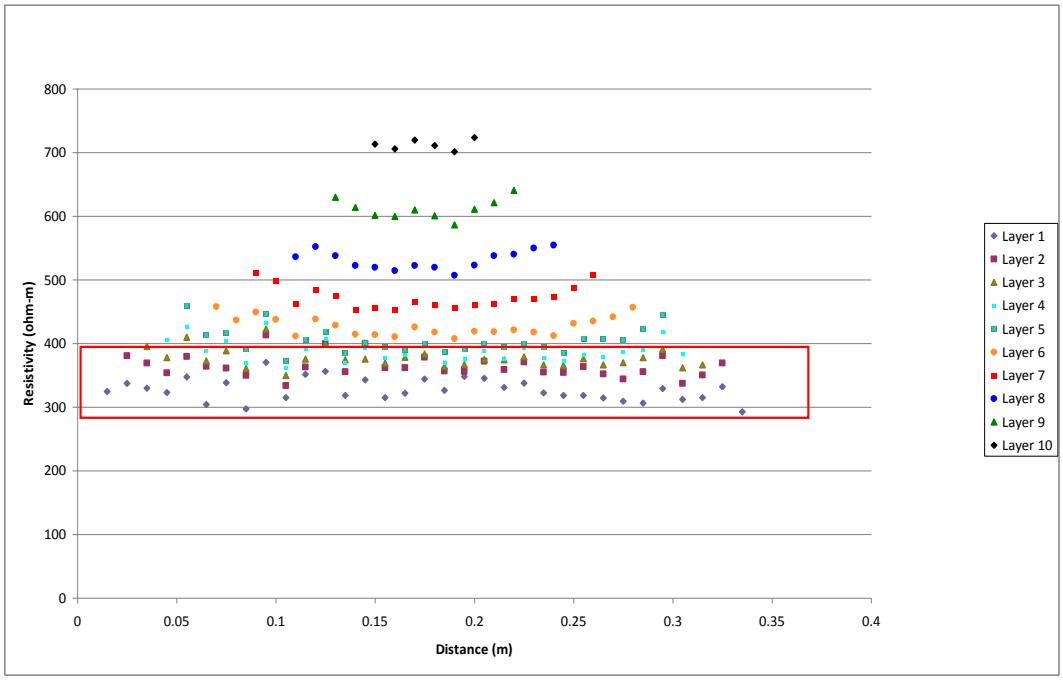

Figure 4.9: The resistivity of mixed tap and deionised water obtained using Wenner-Schlumberger Array

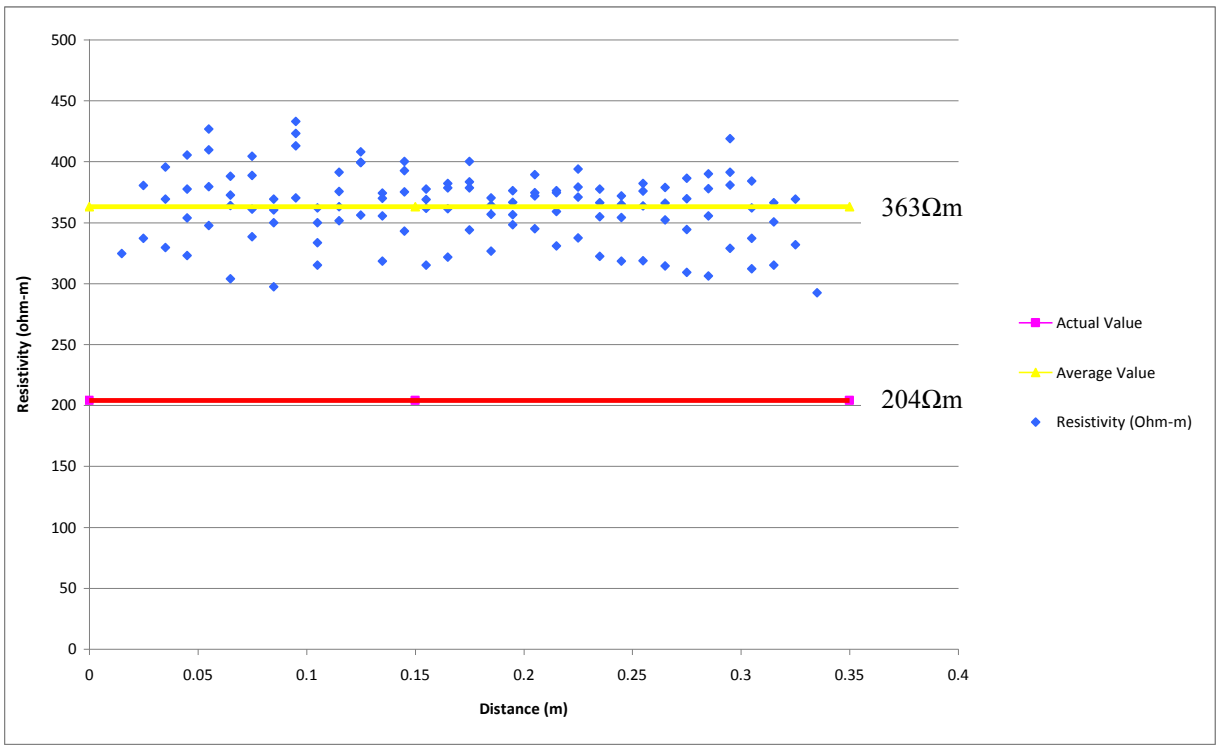

Figure 4.10: The resistivity of mixed tap and deionised water obtained using Wenner - Schlumberger Array for first four layers

In case of a sand model fully saturated with water, as in the experiment No. 5 and No.6, good quality data with smooth resistivity profiles were obtained from both experiments using Wenner (Figure 4.11) and Wenner-Schlumberger (Figure 4.12) arrays.

In conclusion, both arrays give good results for saturated sand and the resistivity values of the sand ranged between 100 - 400 Ωm and display a homogenous resistivity distribution. As for the Wenner array, the deepest resistivity profile showed some depression in the resistivity values at the middle of the profile instead of an expected horizontal profile. This effect will be explained at the end of the chapter.

Experiments number 7 to 9 were designed purposely to determine the maximum depth that can be measured using each array type. A hollow PVC pipe buried into the saturated sand was as used as a test model and it is expected to create a high resistivity anomaly detectable by the equipment. The test commenced with the hollow PVC pipe buried at 8cm depth and used both Wenner and Wenner-Schlumberger electrode arrays. The experiment was repeated by changing the depth of the model to 6cm below surface. Results of the tests showed unpromising results where both arrays failed to detect the hollow PVC pipe at all depth positions (Figure 4.13 to Figure 4.15). According to the Electrode II software, maximum depth of data points of Wenner and Wenner Schlumberger array was 5.8cm and 6.4cm respectively. The shallow depths could possibly be due to less data points at deeper layers where the distribution of data are wider compared to the diameter of the PVC pipe. Therefore the difficulties in detecting the presence of the pipe were due to the wide data spacing compared to the diameter of the PVC pipe. This is an important parameter to be considered in any subsequent actual site investigation especially in locating a buried pipe or canal as well as in archaeological site investigations. With the diameter of pipe equal to one electrode spacing (1 cm), depths of penetration from both arrays are shallower than 6cm or less than 20% of its length (< 6cm/35cm). A drop in resistivity values were still observed in the middle of the Wenner profiles (Figure 4.13 and Figure 4:14).

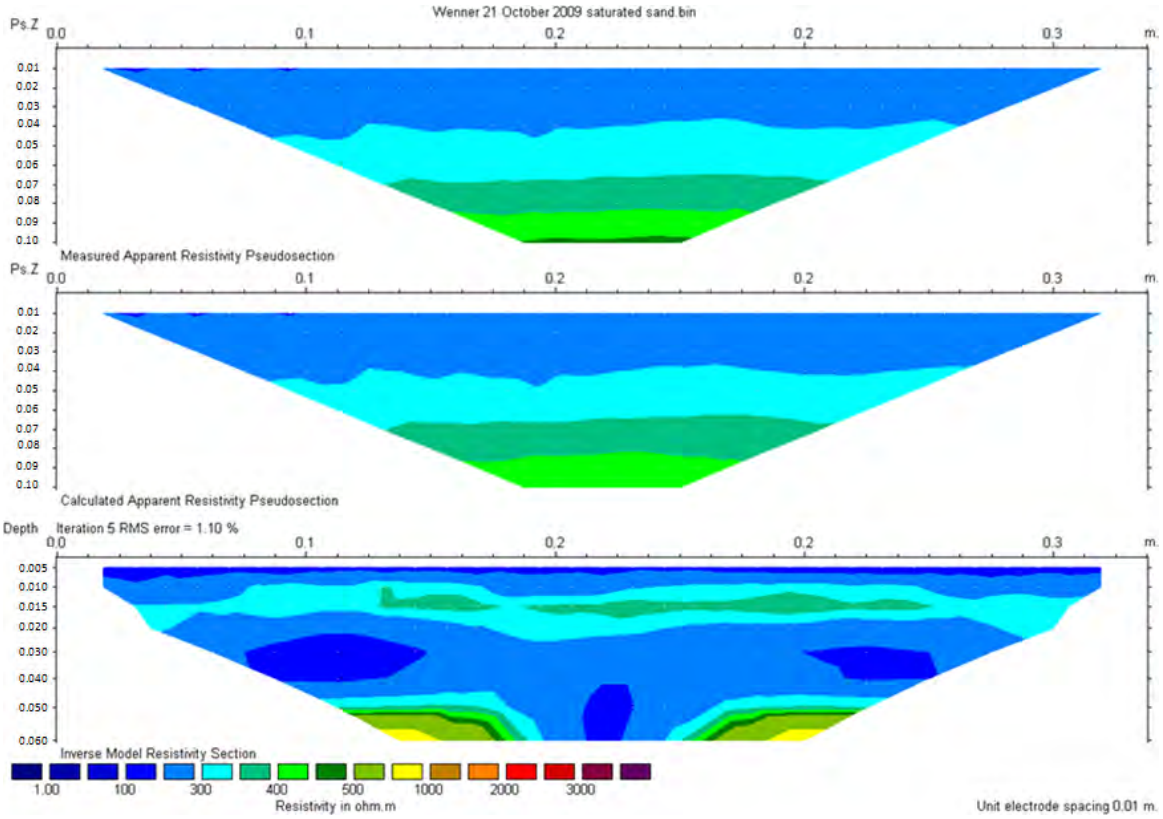

Figure 4.11: The resistivity profile from the Wenner array survey using saturated sand

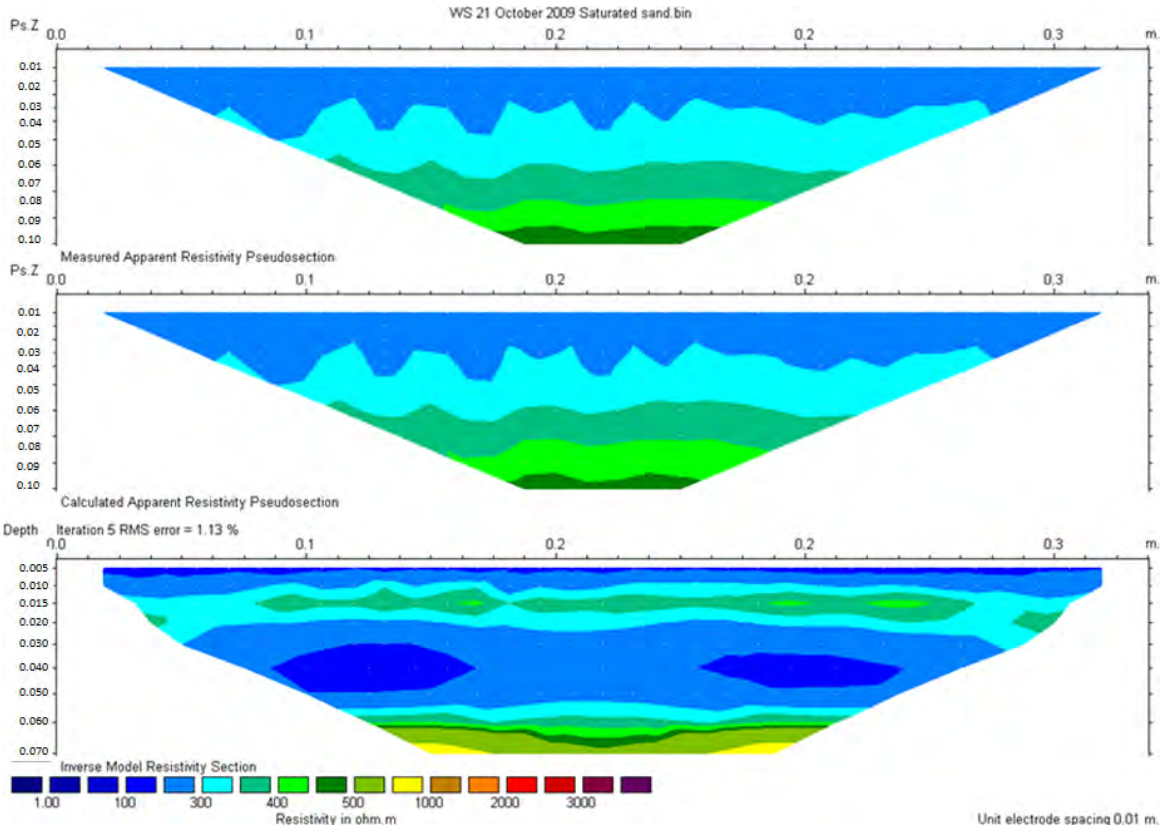

Figure 4.12: The resistivity profile from the Wenner-Schlumberger array survey using saturated sand

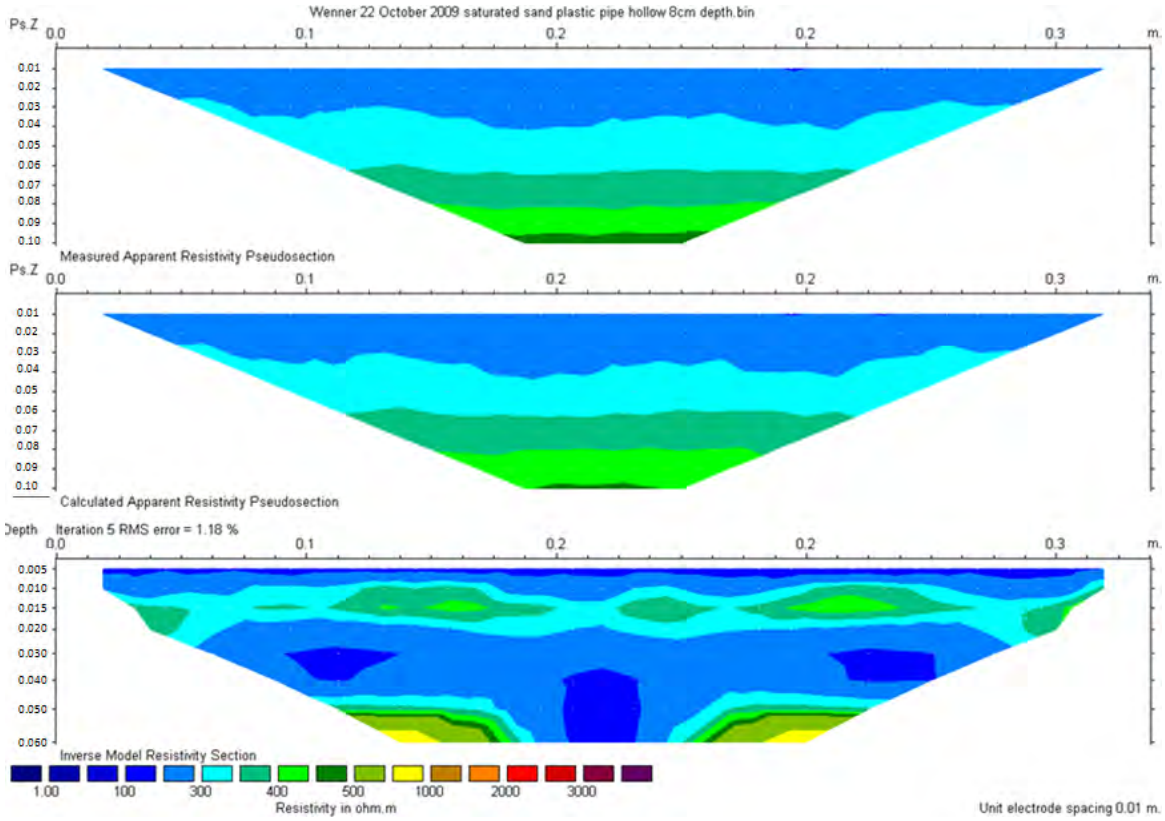

Figure 4.13: The Wenner resistivity profile showing undetectable hollow plastic pipe at 8cm depth

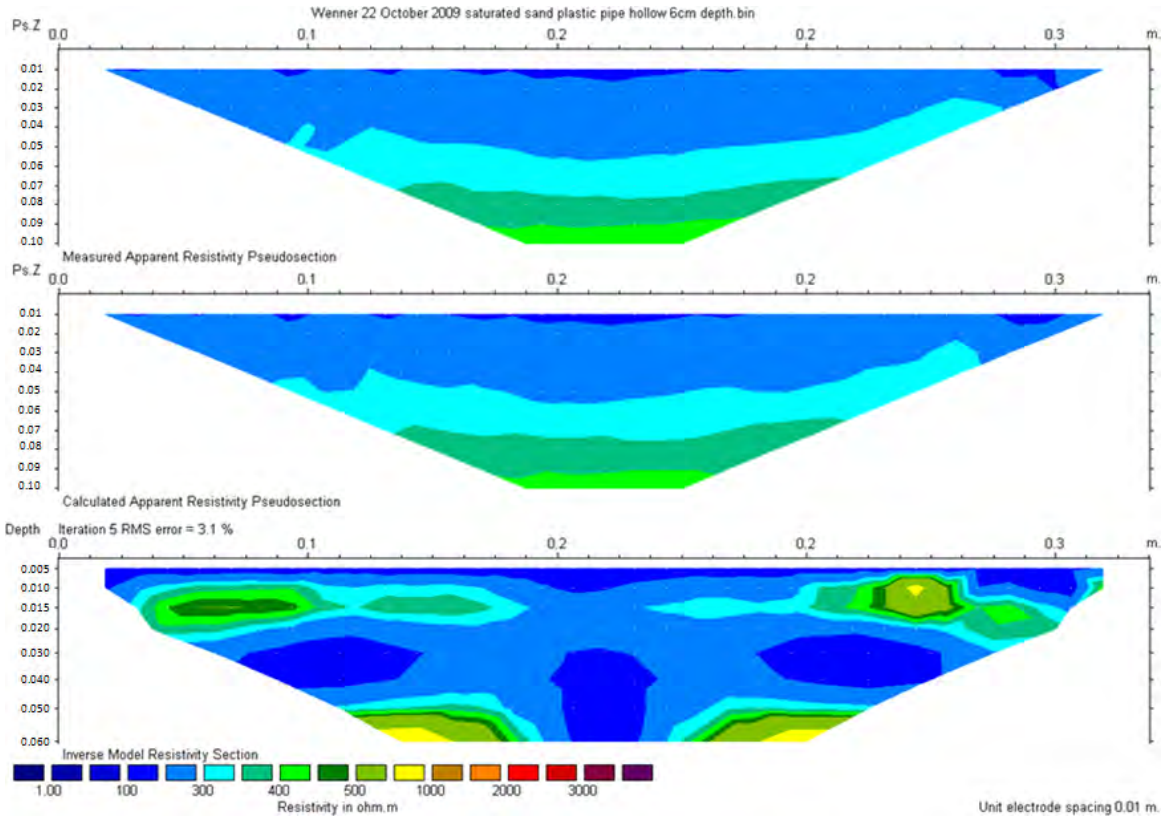

Figure 4.14: The Wenner resistivity profile showing undetectable hollow plastic pipe at 6cm depth

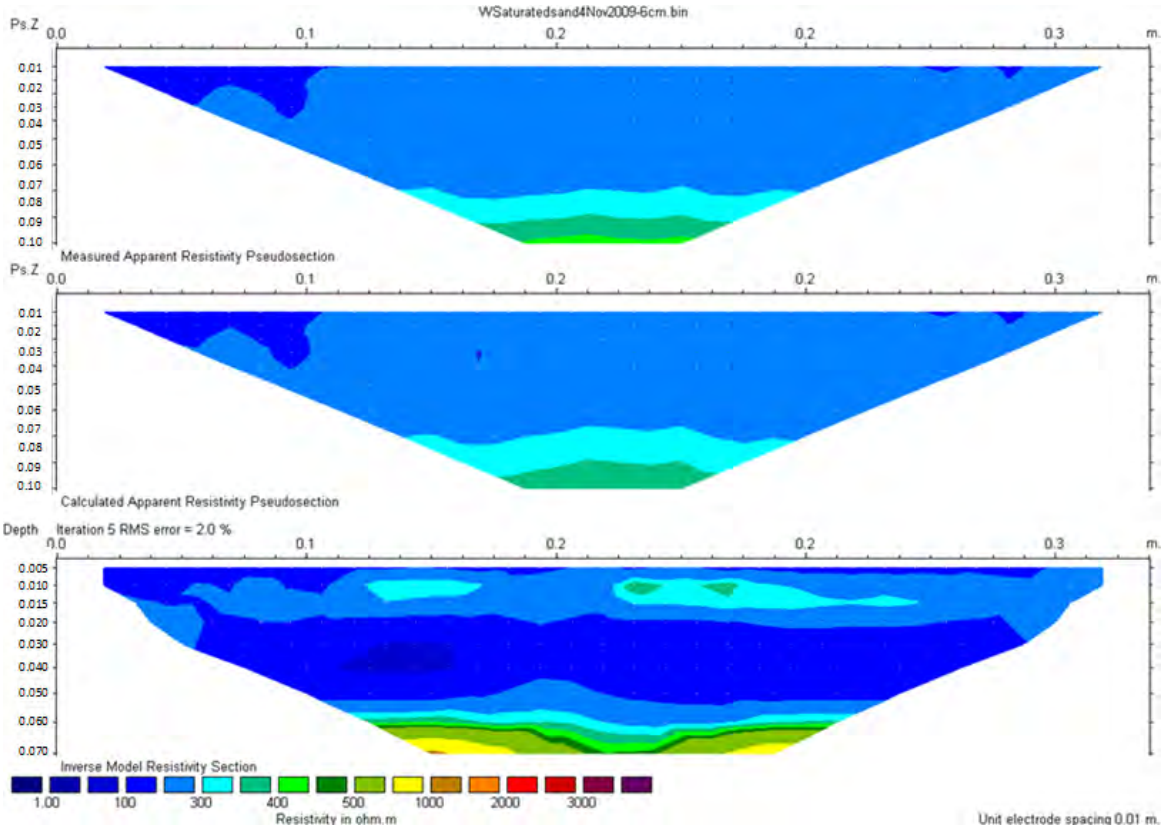

Figure 4.15: The Wenner-Schlumberger resistivity profile showing undetectable hollow plastic pipe buried at 6cm depth

In the experiments No.10 and No. 11, the hollow PVC pipe was buried at 2cm depth and the test was carried out using Wenner and Wenner-Schlumberger array. Results from both tests are shown in Figure 4.16 and Figure 4.17. Generally, high resistivity anomaly was observed in both tests and the pipe location is marked as black circle in the profiles. In these tests, the inverse models reveal several interesting points that should be discussed further regarding the performance of the arrays used. Firstly, the degree of sharpness of the anomaly was found to be clearer using the Wenner-Schlumberger array compared to the Wenner array. Secondly, the precision and the accuracy of the equipment were very good where the hollow plastic pipe model was detected as a high resistivity anomaly between electrodes 28 and 30 (27 – 29cm) and this anomaly was shown in both profiles at similar location at a depth of 2cm. The third point to be highlighted is related to the drop in resistivity values observed using the Wenner array at the middle of the bottom layer. Since there is no possible explanation related to modelling parameters, the only possible reason is that it is an artefact produced in the inversion processing software using the Wenner electrode configuration.

In general, based on resolution and degree of detection of the embedded target, Wenner-Schlumberger array is found to be a relatively better tool for subsurface imaging. Although this array is less sensitive to deeper targets (similar with Wenner array), it was proven to give a significant and better resistivity image for shallow investigation compared to Wenner array.

Wenner-Schlumberger and Dipole-Dipole electrode arrays were also tested using resistivity tank modelling. The experiment setups for these tests are given in Table 4.2. In the first test, two empty PVC pipes were used as targets simulating high resistivity anomalies buried in a low resistivity medium. Both of the pipes were buried horizontally at 2cm and 5cm below the surface. Resistivity profiling using Wenner-Schlumberger array was carried out in a line perpendicular to the PVC pipes. Consequently, the test was repeated by using the Dipole-Dipole electrode array and the test results are shown in Figure 4.18 and Figure 4.19. Both Wenner-Schlumberger and Dipole-Dipole arrays give high resistivity anomalies coinciding exactly with the location of the PVC hollow pipes. The results show clearer imaging of the shallow pipe compared to the deeper pipe. The reason for the good response or detection of shallower pipe is possibly due to higher distribution of near surface data compared to the deeper pipe.

The anomaly image corresponding to the pipe border is poorly defined in these tests. Its shape is observed in the inverse model but its apparent size is slightly larger than its true size. Indeed, the anomaly image of the deeper pipe is slightly shifted from its original position to electrode No.10 – No.12 instead of No.9 – No.10 as shown in the Dipole-Dipole array inverse model. The location of the pipe as high resistivity value was shown in the inverse model. Using the Wenner-Schlumberger array the results show a similar location of the pipe in the tank model but the apparent size of anomaly in the profile is much larger than the true pipe.

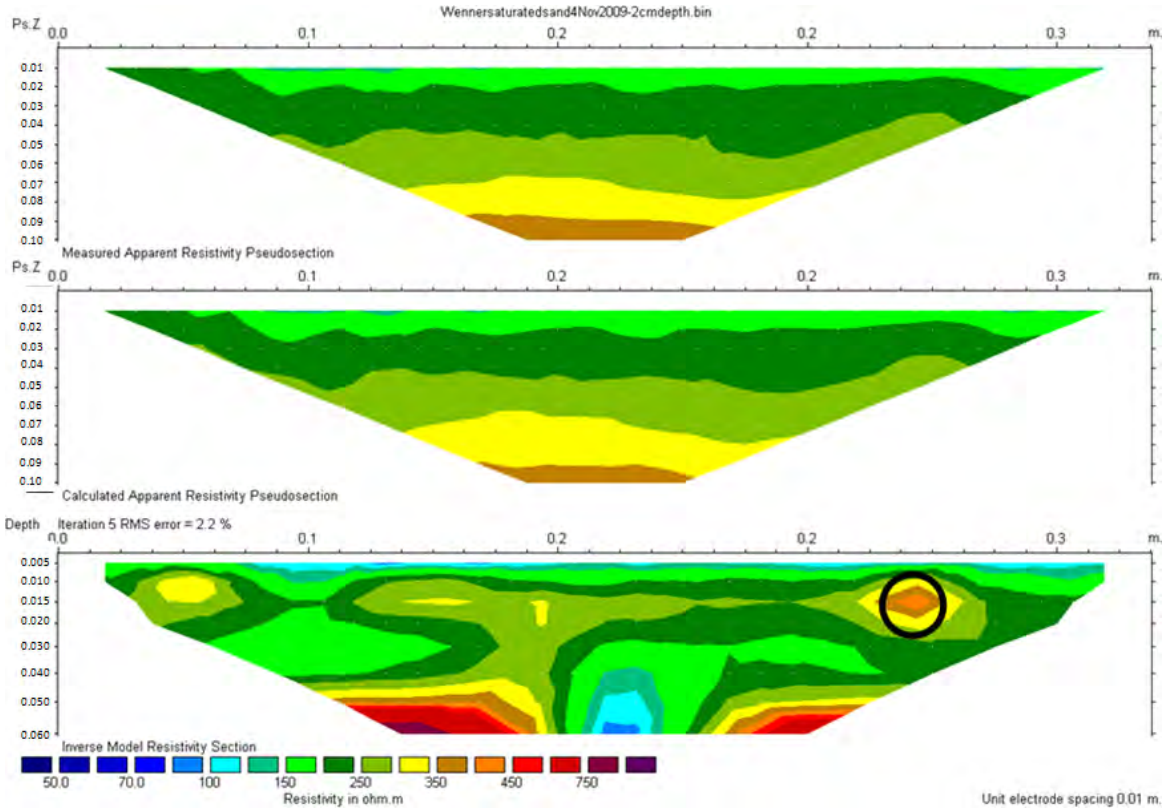

Figure 4.16: A Resistivity profile obtained from Wenner array showing a strong anomaly produced by a hollow pipe at 2cm depth

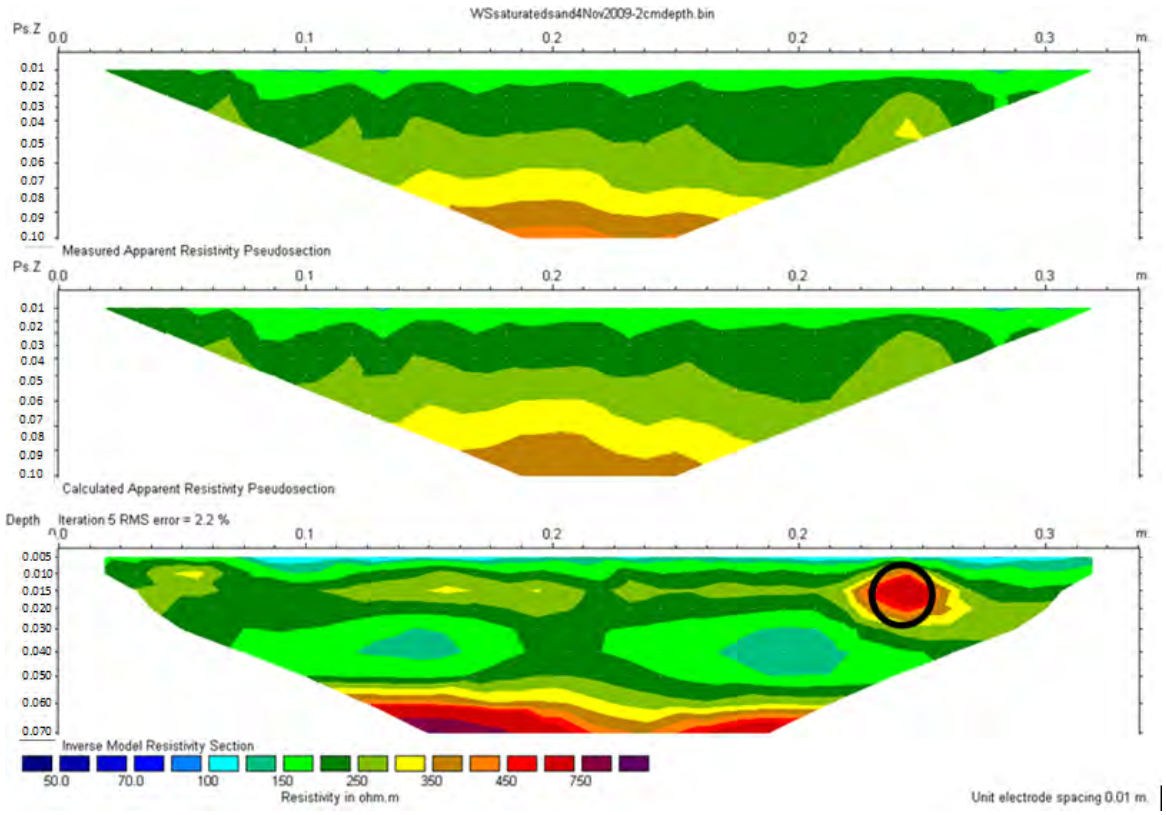

Figure 4.17: A Resistivity profile from the Wenner-Schlumberger array showing a stronger and sharper anomaly produced by a hollow pipe at 2cm depth

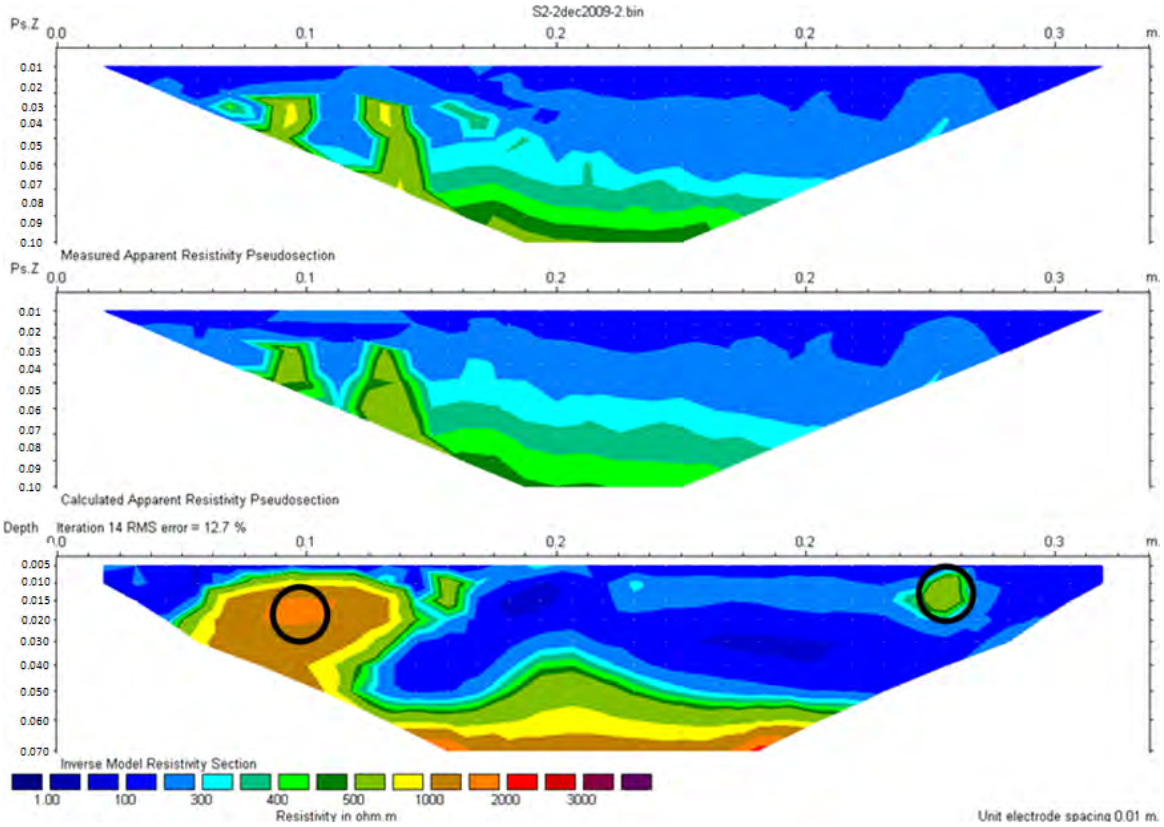

Figure 4.18: A resistivity profile produced by a Wenner-Schlumberger array detecting 2cm and 5cm depth of hollow pipes

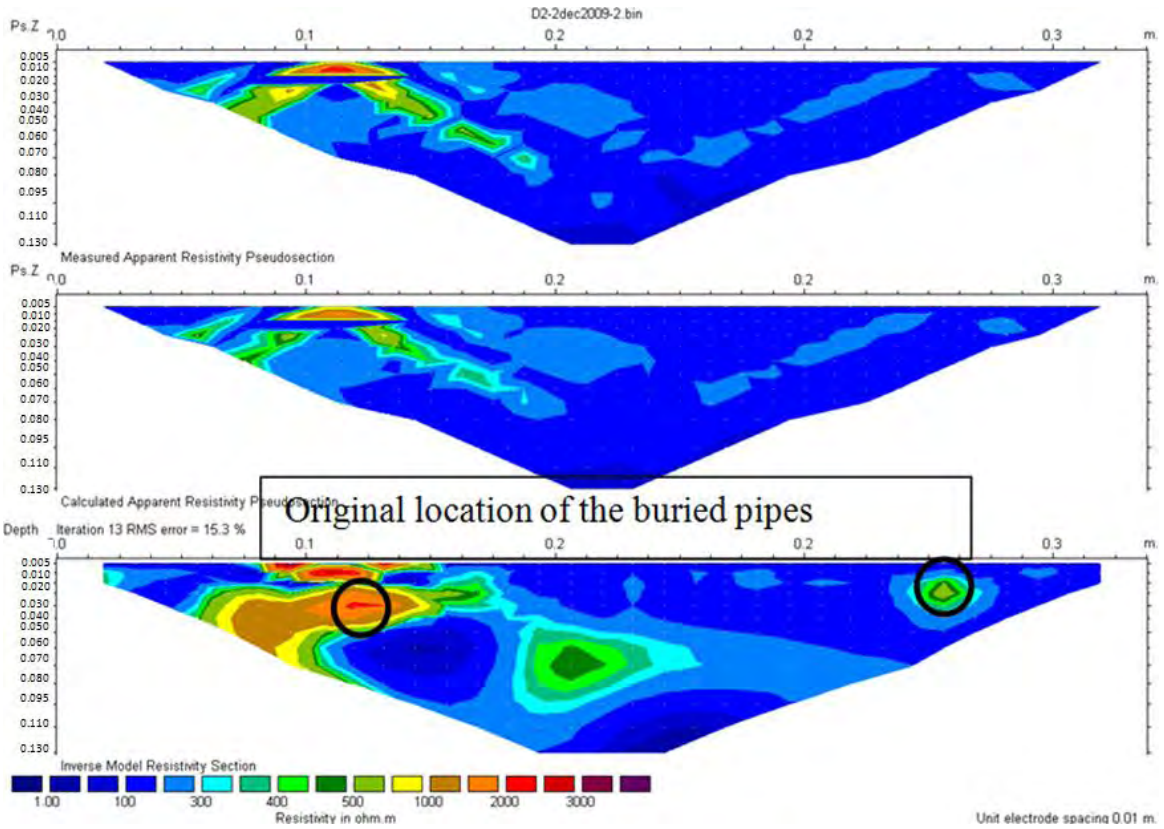

Figure 4.19: A resistivity profile produced by a Dipole-Dipole array detecting 2cm and 5cm depth of hollow pipes

In support of the previous results, other physical models such as a steel hammer head and sand cylindrical core were also used as models in tests. These models are immersed in saturated sand at depth of 2 cm. Electrical anomalies representing both models are shown in the inverse models (Figure 4:20 and Figure 4:21). As in the previous tests, the Wenner-Schlumberger array produced much better image resolution in terms of detecting the correct positions of the models as compared to Dipole-Dipole array.

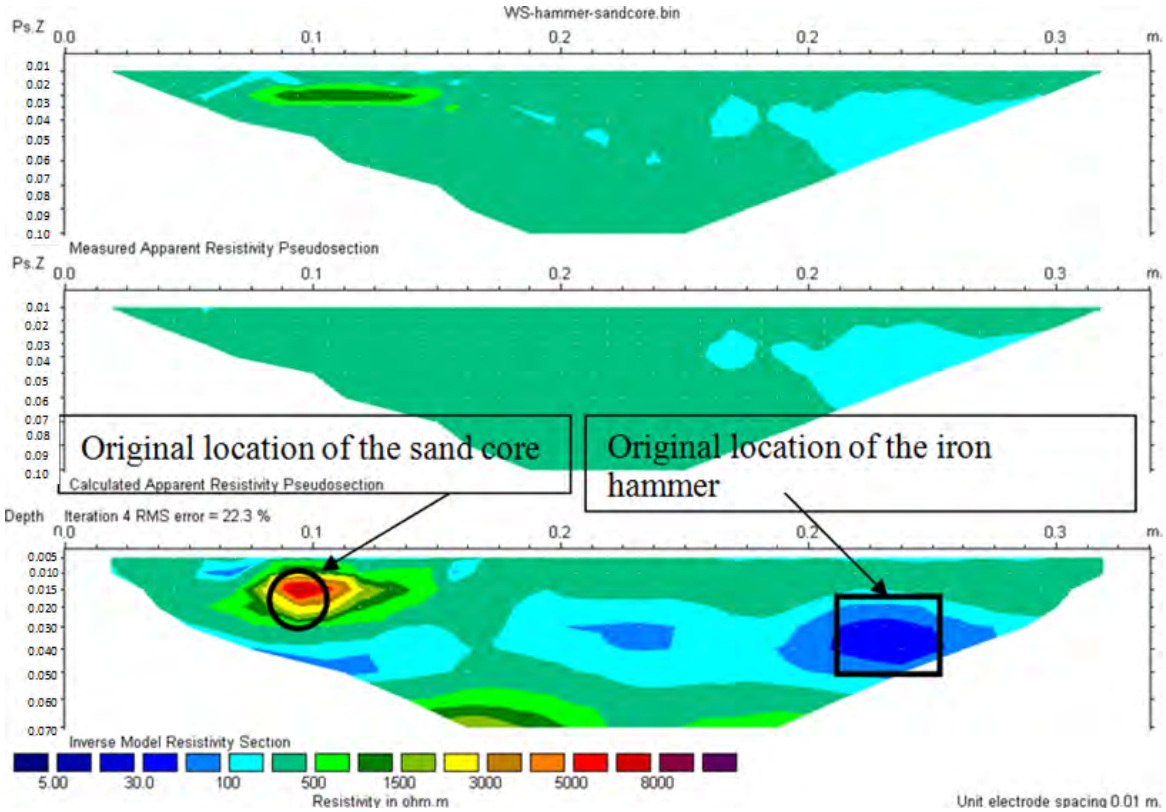

Figure 4.20: A resistivity profile showing the anomalies of the iron hammer and a sand core by using a Wenner-Schlumberger array

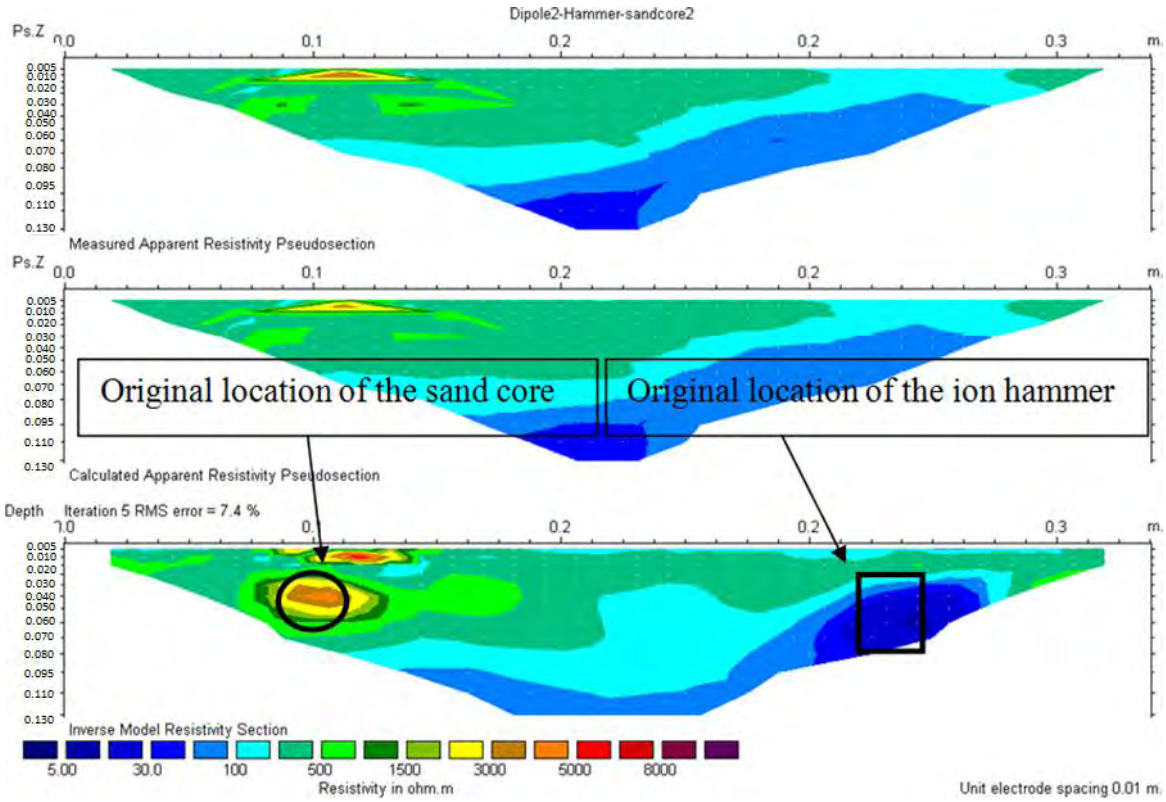

Figure 4.21: A resistivity profile showing the anomalies of iron hammer and a sand core by using a Dipole-Dipole array

4.6 Conclusions and recommendations

Two test programs were carried out involving the calibration of IRIS SYSCAL Resistivity system and proof testing to determine the equipment performance as a sub-surface imaging technique using several electrode arrays and different physical models.

Results from calibration tests show that the absolute resistivity values obtained using the IRIS SYSCAL system were inaccurate and required calibration. The measurement error is calculated as **1.8554** times greater than the true values measured using a calibrated conductivity meter (Hanna Combo Conductivity meter). Consequently, in any future use, resistivity values have to be corrected using a calibration factor (**1.8554**) prior to any modelling with RES2DINV software.

In the proof testing experiments, the maximum depth of penetration and the most appropriate resistivity array for underground detection were successfully determined. The maximum depth of data penetration as well as the exact position of the iron head hammer and the sand cylindrical core is based on the electrode spacing and the array was built into

the Electrode II software. In these experiments, Wenner and Wenner- Schlumberger arrays showed a greater depth of investigation, with a maximum depth of about one fifth of the survey length.

These experiments and the proof tests also proved that the accuracy of a resistivity survey used for sub-surface imaging is very much influenced by the choice of electrode arrays. The best electrode array for resistivity imaging is the Wenner-Schlumberger, based on its high accuracy in detecting embedded models in terms of giving a sharp anomaly image shown in the inverse model.

It is recommended that all resistivity systems are regularly tested for calibration and that the manufacturer's certificates are not taken for granted. Further laboratory tank tests are recommended in determining the equipment capability of detecting buried objects of a variety of different sizes and buried at different depths. Using the results of these numerous experiments, empirical relationships between the resistivity images of these objects and the equipment geometry can be better established.

CHAPTER 5
DATA ACQUISITION AND LABORATORY WORKS

5.1 Introduction

An initial site investigation does not necessarily need extensive field surveys or the integration of many techniques. It's also doesn't need repeated surveys, because this will be costly and time consuming. Generally, a field survey has to be efficiently planned by focussing on the survey objectives, time taken, the reliability of the data acquired and most importantly the cost. Most conventional techniques like drilling will normally involve a high cost and is also invasive and time consuming. In fact, data provided by this technique only produces single point information and several boreholes have to be used in order to get a good correlation on the variable soil/rock and groundwater conditions. Using geophysical techniques is an alternative approach helping to overcome this problem. It not only provides continual ground information but also saves a lot of cost by reducing the time for data collection. Indeed, it also helps by reducing the number of boreholes required in any site investigation. However, geophysicists still require borehole information for sub-surface geological validation.

In this thesis, geophysics has been used as the primary ground investigation technique and it is supported by a soil and groundwater sampling and geo-chemical analysis. This chapter will provide information on the field survey approaches made at each research site.

5.2 Field survey and soil/water sampling

As mentioned previously in Chapter 3, four sites with different contamination issues and sources are involved in this research study. The field surveys employed also need to be appropriate to the site conditions, geological setting, hydrogeological properties and the ground contamination that is found at each site. The geophysical techniques deployed at every site include Electrical Resistivity Imaging Technique (ERT) and the Ground Conductivity Survey using GEM-2 device. The decision to choose resistivity imaging technique and Ground Conductivity Surveys (GEM-2) as the primary techniques in this study are due to the reasons developed in the following discussion.

i) The resistivity imaging technique and ground conductivity techniques maps the physical property of material (electrical conductivity) in their survey. Easy correlation can be made between the data provided by each method.

ii) Resistivity results are in the form of a 2D profile where the X-axis is a length on the ground surface and Y-axis represent the depth of the profile. While a contour within the profile maps a resistivity value of the material underneath the ground surface. Generally the resistivity profile represents a vertical slice of the resistivity value of the ground material. The plan view of resistivity value also can be presented by using integrated parallel several resistivity lines whether using SURFER or using RES3Dinv interpretation software.

iii) In Ground Conductivity surveys, the final outcome is a plan view of the ground conductivity distribution in mS/m unit at five different acquisition frequencies which correspond to different depths of investigation. The relative depths of each layer are determined based upon the frequency of the electromagnetic wave which is used in the survey. The higher frequency will represent a contribution of a smaller volume of ground and the lower frequency a larger volumetric contribution, although the exact calculation of the volumetric contribution of the ground to the apparent measured conductivity is complex.

iv) The density of data provided by these two techniques is very good. The GEM-2 survey as an example can provide about 20-30 thousand data points in a one hour survey. While the resistivity can give about 600 to 700 data points in an hour. Compared to other conventional techniques such as drilling and augering, the geophysical technique provides a high density data coverage in a short time.

v) By using parallel resistivity lines / EM mapping in tandem and by integrating the results of both techniques, a 3D visualising of the ground can be developed.

The soil and groundwater sampling was carried out at selected sites depending upon the site access and the type of contamination encountered. Detailed information regarding the field survey and sampling approach taken at each site is discussed in the following sub chapters.

5.2.1 Cathays Railway Depot

At Cathays Railway Depot, the main pollution problem is believed to occur in the soil because the aquifer in the area is classified as a secondary-A. Therefore, only field studies involving the use of combined geophysical methods and soil sampling can obtain the chemical properties of the soil at the site.

5.2.1.1 Soil sampling approach by Gridding System

The study area is located on flat topography but still has a lot of aggregates present due to past activities and partially demolished buildings. The aggregates are from old buildings and manmade materials dumped on the surface and make it difficult to collect the soil samples at regular spatial intervals and at the appropriate depth. So in this study only surface soil samples were collected from 24 sampling locations (Figure 5.1). The sampling strategy designed was based on a gridding system with four straight lines parallel with each other. Each line is separated by 15m and the sampling points spacing is 10m spacing. Every sample line has six sampling points making the total length of the sampling line 50m. Soil samples were collected by manual augering (0.3 – 0.5m depth) and the soil samples stored in the plastic container at about one kilogram weight. Before the analysis can be done, the soil samples have to go through a chemical leachate process. The end products must be prepared as a water sample before it's sent for IC and ICP-MS analysis.

5.2.1.2 Geophysical survey using Resistivity and Gem-2

Seven resistivity survey lines were laid out on the Cathays Rail Depot site each of 67m length. Resistivity data were collected with Wenner – Schlumberger electrode array. The lines were parallel with each other at 10m line spacing. Resistivity line Res 1 and Res 3, overlaid directly with the soil samples grid line C7 – C12 and C19 – C24 respectively (Figure 5.1 and Figure 5.2). For data acquisition, IRIS Syscal Junior 72-Switch been used with a one meter electrode spacing and the model data was displayed up to 12m depth.

The GEM-2 is a complex digital electromagnetic sensor but logistically it is straight forward to use. For this survey, five frequencies of electromagnetic wave been chosen to obtain the information at variable depths (975Hz, 5125Hz, 15025Hz, 30025Hz and 47025Hz). The higher frequency is for shallow information and the lower for the greater depth penetration. The console stores data for about two hours (50,000 data points) before the memory becomes full and it requires downloading. The location of each sample point was determined by using an integrated differential GPS to sub-metre accuracy. The survey lines are shown in Figure 5.3.

Figure 5.1: The geochemical soil sample locations

Figure 5.2: Seven parallel resistivity survey lines with the 10m line interval

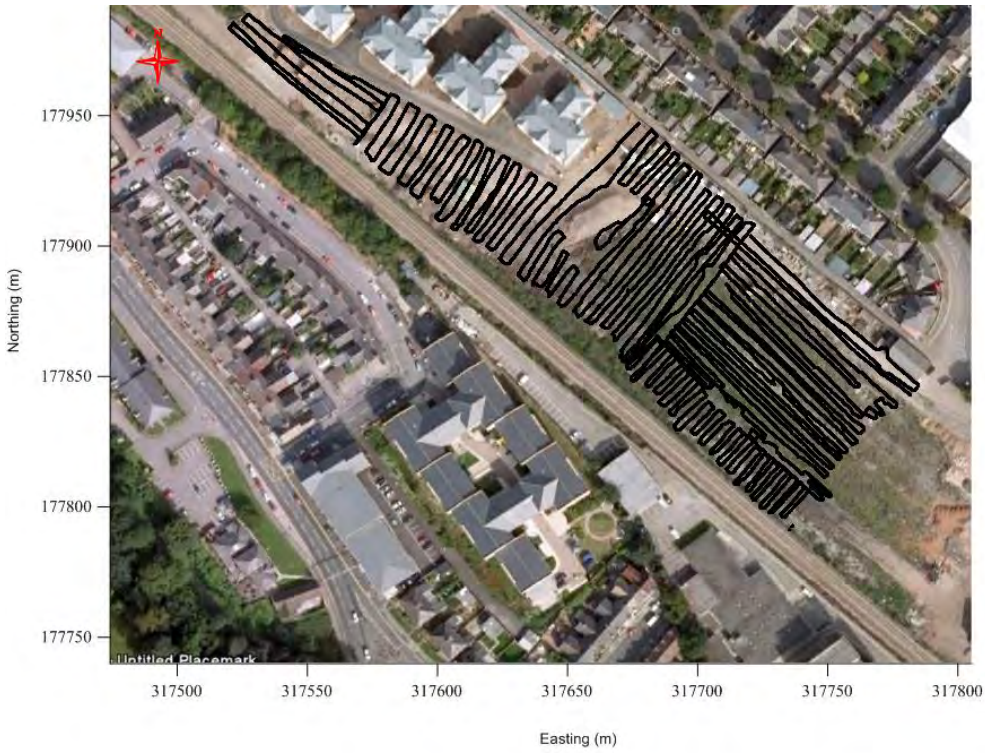

Figure 5.3: GEM-2 survey track

5.2.2 Weston Super Mare Gasworks Station

The geophysical survey at this site was concentrated at a location where the expected leaking wooden tank was reported from an initial previous investigation which is near to the TP110 area (Zone A). The available site survey area was irregular and constrained by metal fences and dense vegetation. The study area extended toward the west up to the bullet tanks (Zone B) (Figure 5.7). Similarly like the Cathays Railway Depot, this site also has been classified as a secondary aquifer or poor aquifer by the Environment Agency (2011) – **Web 3.7**. Therefore, only the geophysical approaches and in situ gases analyser had been performed at this site.

5.2.2.1 In situ gases measurement (Soil Vapour Survey)

The survey was carried out by Jim Whiteley as part of a Cardiff University MSc project using an Ecoprobe 5 (Figure 5.4), which was manufactured by the RS Dynamics. In the Zone A the gridding sampling procedure had been deployed by using a grid dimension of 2m x 2m, and a random sampling where access permitted in Zone B (Figure 5.6). Each station was positioned using a Topcon Electronic Distance Meter (EDM) (Figure 5.5) to an accuracy of ±3mm (Whiteley, 2010). In this survey, 128 stations (G1 – G128) were sampled in the whole survey area. Prior to the investigation, utility plans were consulted in order to ascertain the presence of any services; no services were seen to be present in the survey area.

Ecoprobe 5 Methodology

The initial survey design specified sampling from hand augured holes at a constant depth of 0.5mbgl, however, the presence of coarse granular material as well as the presence of brick, concrete pads and other large debris in the made ground significantly impeded the effectiveness of the hand auger. In order to excavate sufficiently deep and consistent sampling holes a large electrical drill and portable generator had to be used.

The sampling probe was inserted into the hole and left to allow ground conditions to equilibrate for approximately 1 minute. Prior to each reading, the Ecoprobe unit was reset, nulling the gas analyser to background atmospheric conditions. The Ecoprobe unit was then connected to the sampling probe, and the gas sampled for a period of 20 seconds

at a pumping rate of 1.5 l/min. Maximal and average data from the PID, IR analyser and paramagnetic sensor were collected every 0.1 seconds in the sampling cycle. The unit is highly sensitive to the presence of water in the ground, however, as trial pit logs had shown a perched water to exist below 1.5mbgl, water was not considered an issue, or encountered when sampling to 0.5mbgl.

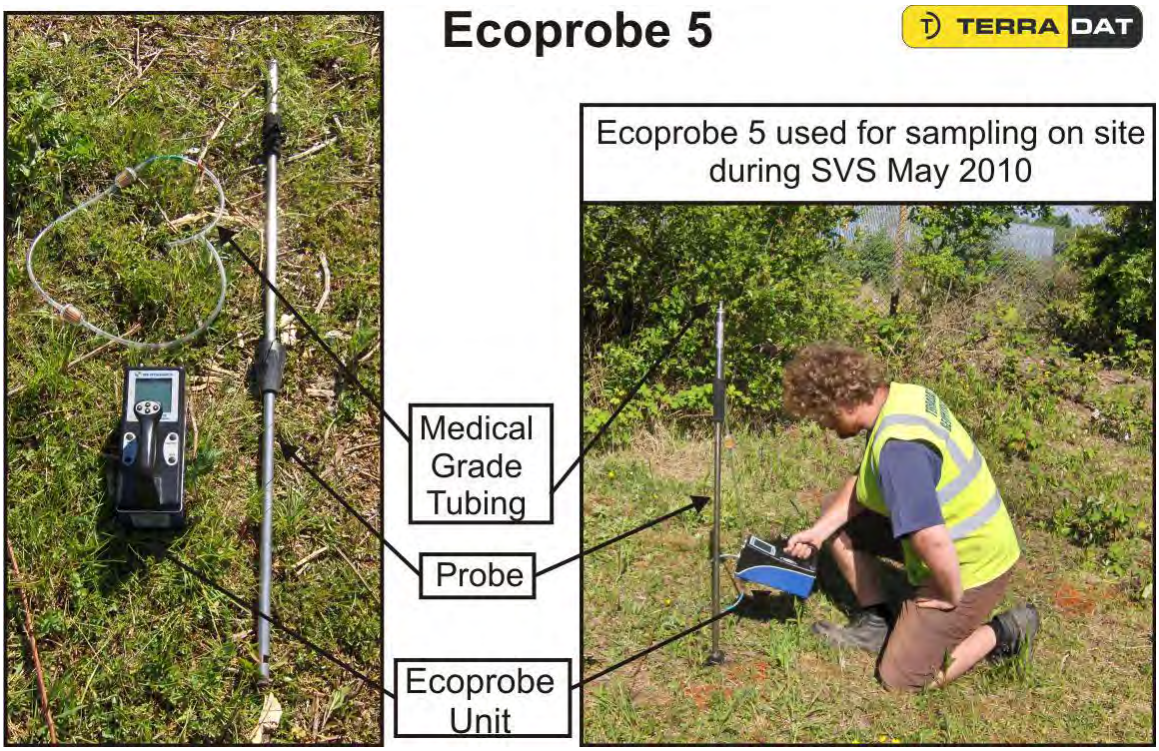

Figure 5.4: Ecoprobe 5, the equipment for in situ gas measurement (source, Whiteley, J. 2010)

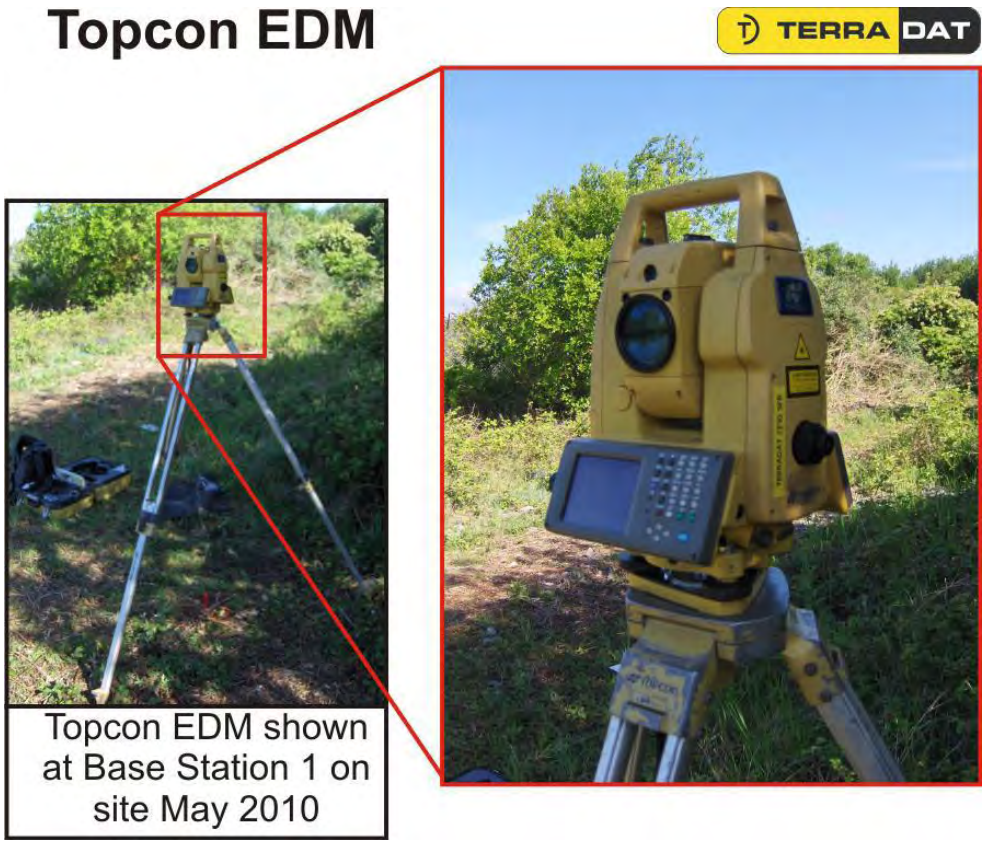

Figure 5.5: EDM used for surveying SVS stations and referencing the local grid to site plans (source, Whiteley J, 2010)

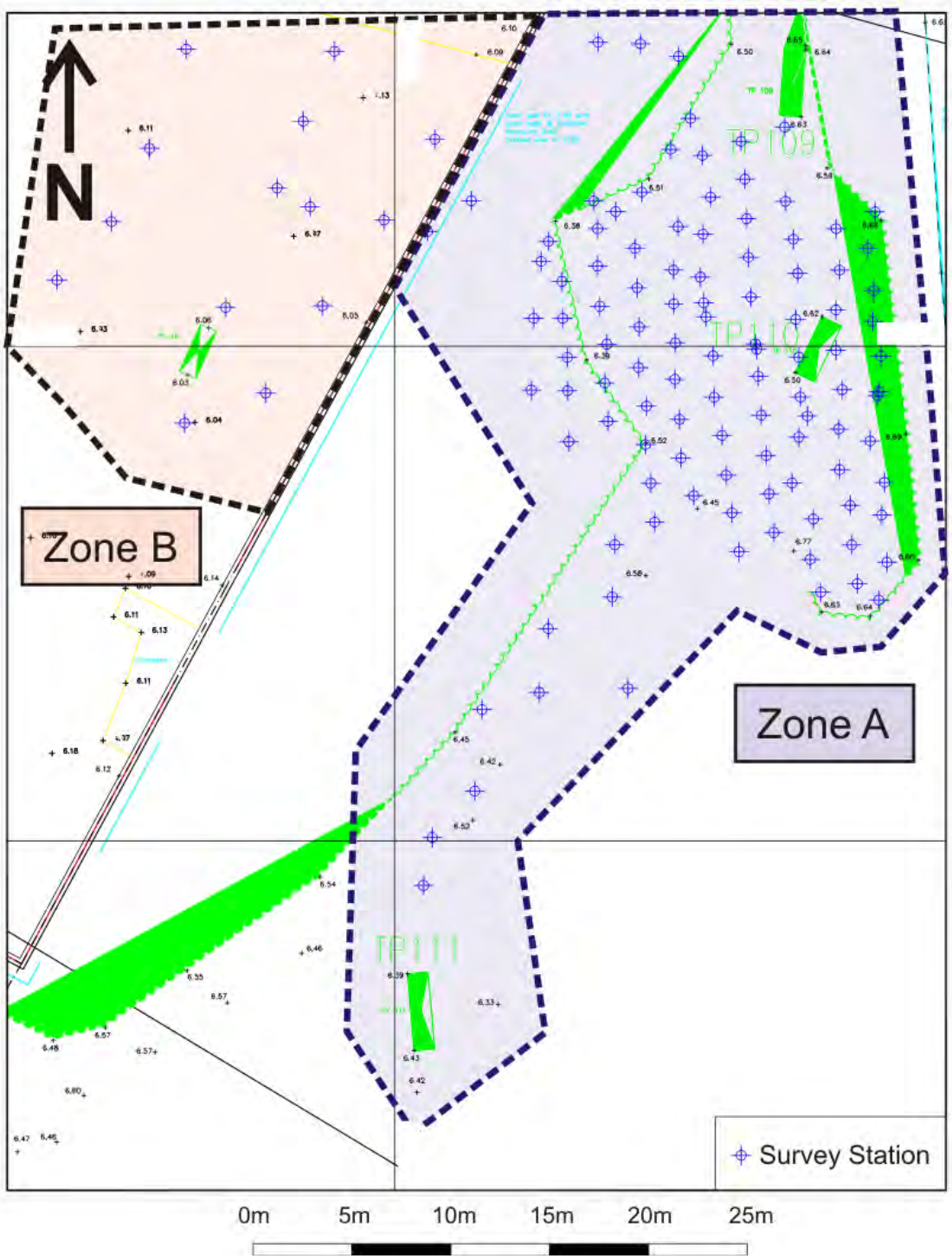

Figure 5.6: Location of in situ gas measurement stations (source, Whiteley J, 2010)

5.2.2.2 Geophysical Survey using Gem-2 and Resistivity

Some of the areas in Zone A are comprised of dense bushes and shrubs and this constrains the GEM-2 surveying area. As a result, the survey only covered the area which has a clear pathway. However, in Zone B a better survey line had been created because of the clear and flat topography site as shown in Figure 5.7. The frequencies of electromagnetic wave been chosen in this survey are 825Hz, 7075Hz, 16075Hz, 31025Hz and 47025Hz which is representing different depths of soil layer investigation.

Figure 5.7: Showing the GEM-2 survey tracks. A proper survey tracks is in the Zone B compared to the limited tracks in the Zone A (Weston Super-Mare)

For the resistivity surveys, five lines had been carried out, Res 1, Res 2 and Res 4 have a 53m length (one metre electrode spacing) and 35m for two other lines (Res 3 and Res5). The Res 1 and Res 2 were constructed almost crossing the TP110 as shown in Figure 5.8 to get a clear view of any significant change of the resistivity values near to the TP110. While three other lines specifically designed to get the information of any migration of the pollutants within the area.

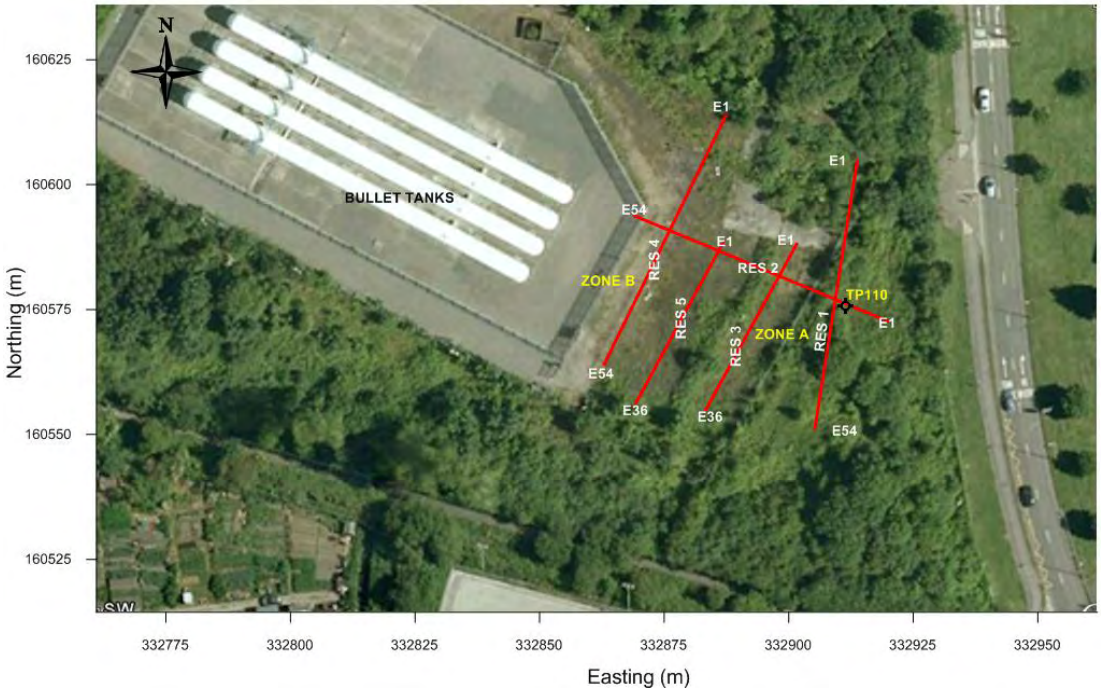

Figure 5.8: Five resistivity lines were constructed in this study (Weston Super-Mare)

5.2.3 Barry Docks Site

The investigation of the ground pollutants at Barry Dock was concentrated at the tank farm and the West Pond area located at the western end of Dock No.1. Geophysical surveys had been carried out at the old tank farm area and also a small 3D survey area located at the south east near to the cliff (where small storage tanks were located). At the time when the survey has been carried out, all the small tanks in small area had been totally demolished. While the water and soil samples were collected over the whole area at the tank farm and the West Pond site.

5.2.3.1 Soil and water sampling approaches

Water and soil sampling works had been previously done by the Ove Arup & Partners Ltd. In this research, the chemical content of the soil samples from the trial pits and the groundwater from the boreholes mostly taken from the Ove ARUP and Partners reports (2008). The soil samples and the boreholes location used are shown Figure 5.9 and Figure 5.10. Twenty nine boreholes and about a hundred trial pits data were included in the analysis. Each of them will represent the information of groundwater and soil condition respectively. In this project the chemical data were re-plotted and re-analysed to define the contaminants distribution and it relation to the geophysical parameters.

Figure 5.9: Showing the location of the boreholes where the groundwater has been collected for analysis (Barry Docks)

The survey area was decided upon based on the footprint of the previous tank farm and at the area where the tar was found on the site (in the south east; Figure 5.11). It was believed that this would be the area of highest contamination, and if migration of the pollutants were taking place, it would be more easily followed from its source. The electromagnetic survey was done using five different electromagnetic wave frequencies (825Hz, 7075Hz, 16075Hz, 31025Hz and 40075Hz) to obtain conductivity information at different depths simultaneously. The depth of penetration depends on the individual frequencies being used, with lower frequencies (longer wavelengths) is penetrated deeper compared to higher frequencies. It is also depending on the material type which has a different electrical conductivity values. The GEM-2 survey tracks are shown in Figure 5.11.

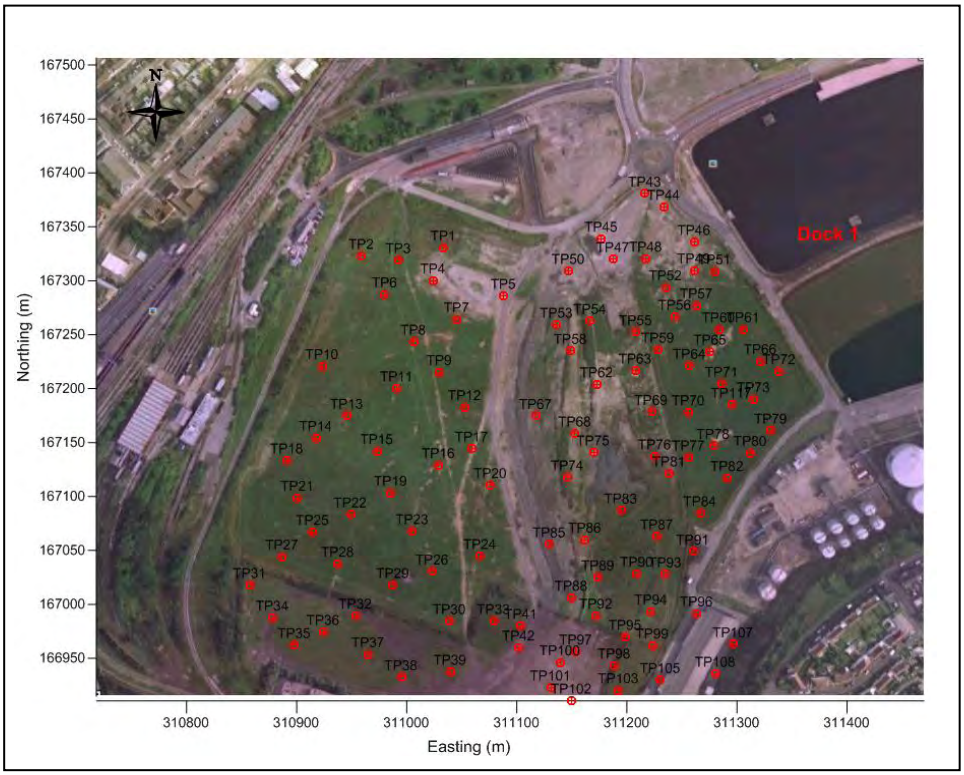

Figure 5.10: The location of the trial pits where the soil samples were collected

5.2.3.2 Geophysical Survey Gem-2 and Resistivity

For the resistivity survey, the locations of the resistivity lines based upon historical site information and data taken from previous site investigations and through a practical observation of the site. Two long resistivity surveys were completed, with RES-1 crossing in a northwest- southeast direction, and RES-2 from a northeast to southwest direction. The locations of these can be seen in Figure 5.12. The survey lines were designed in that particular way to map the location of the buried river channel of the Cadoxton River a part of it main objective to map any contamination layer along the traverse.

Previous site investigations reported by Ove ARUP and Partners (2008), show that the area to the east of RES-1 had the highest contaminant and tar is still present on the ground surface. Laboratory analyses show that the main contamination is PAH which has levels over 650 mg/kg in soil (Ove ARUP and Partners, 2008). It was hoped that the presence of

the contamination would also show up in the resistivity survey, and that the method could then be utilised as a useful, non-invasive tool in delineating the extent of the contamination.

RES-2 was placed perpendicular to RES-1, in a northeast –southwest direction, as can be seen in Figure 5.12 This extended from the edge of Powell Duffryn Way, to the car park area in the south west. It was hoped that this would identify any continuity that might be present in the geological layers underlying the site. Also, as this line was passing through known areas of both high and low contamination, it was envisaged that comparisons could be made between the two, and that the location of contaminant plumes could be further delineated.

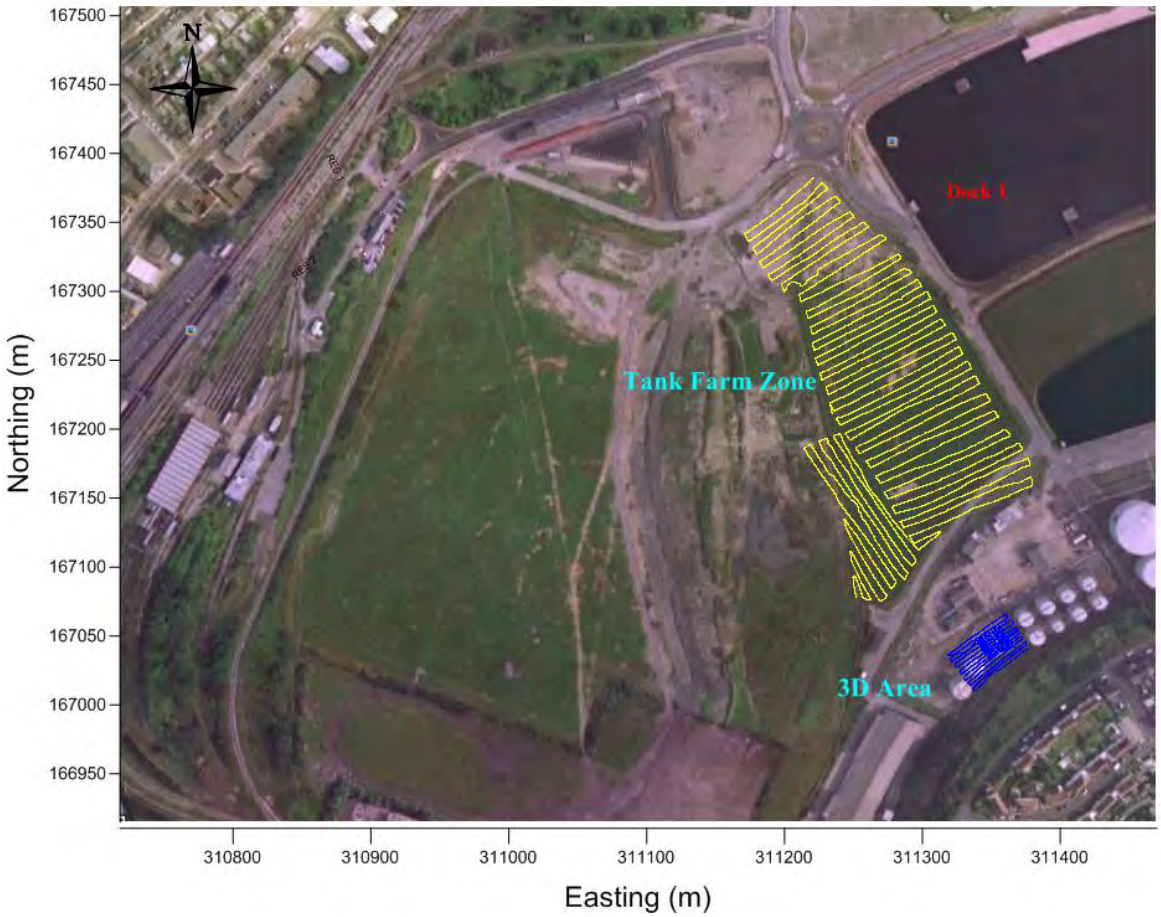

Figure 5.11: Map showing the GEM-2 survey tracks. The yellow colour was carried out on the old tank farm and the blue tracks line on the area of tar present on the surface

At the small area where the tar pools exist on the site, six parallel resistivity lines have been carried out. Each line uses 36 electrodes with 1m electrode spacing and is separated by 5m (Figure 5.13).

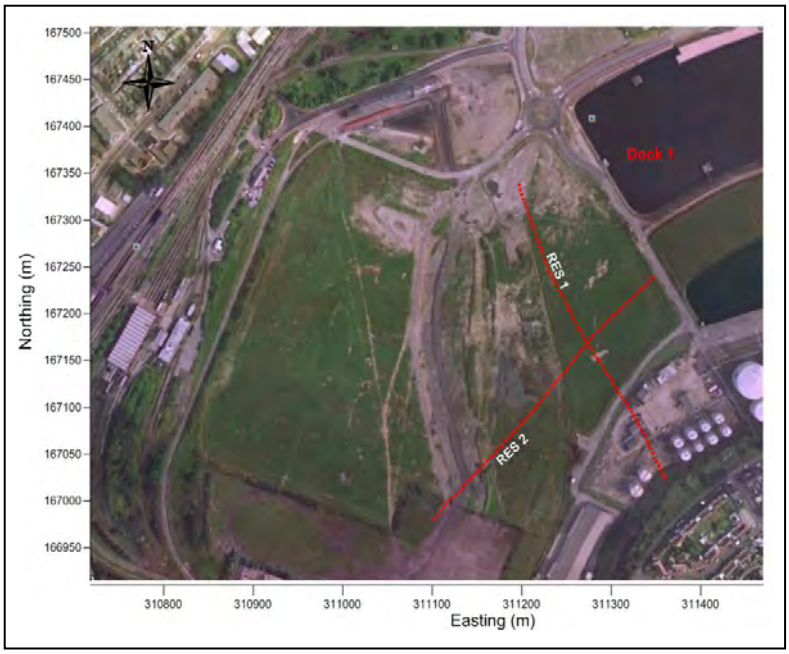

Figure 5.12: The RES-1 and RES-2 layout, crossing is about perpendicular to each other

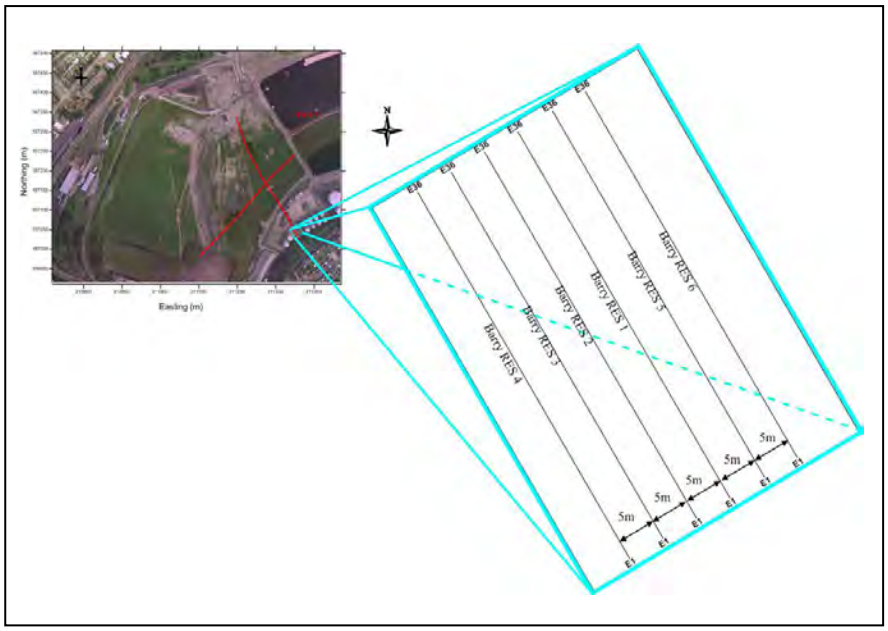

Figure 5.13: Zoom in small area where the tar is found on site. Six resistivity lines were built parallel with each other and separated by 5m line spacing

5.2.4 Bromsgrove Landfill

Similarly like the previous two sites, the investigation approach taken at the Bromsgrove Landfill site uses data from a previous study, due to the limited time available for monitoring and the huge study area. Site access was difficult as this is a working farm and cows had to be moved out of the fields for surveying to take place. The EA has an agreement for sampling for one day at monthly intervals and this research project had to fit into this schedule. Most of old data used in this site investigation are taken from the ENVIROS Consulting Limited and from the EA sponsored studies by two Cardiff University MSc students.

5.2.4.1 Soil and water sampling approaches

Water samples were collected from the old series of boreholes installed by the DoE when they carried out an initial investigation of this site between the 1970s and 1990s. The majority of the water samples were collected from the BHB (deep borehole) and W (perch water/leachate) series boreholes made by the ENVIROS investigation in 2008/9 (Figure 5.14). Water retrieval was carried out using bailers which were rinsed between boreholes to avoid cross contamination.

Water samples from each borehole were separated into two portions, each of them is used for field water testing and for the laboratory analysis. Water testing in the field involved a Hanna multi-parameter water quality meter which took measurements of the pH, Eh, temperature, conductivity and dissolved oxygen content (DO) of the water bailed from the boreholes. A Hach alkalinity titrator also had been used to measure the carbonate and bicarbonate content in a water sample. While the laboratory water samples were stored in a bottle at a low temperature in an ice box to prevent any chemical reactions due to changing ambient temperature.

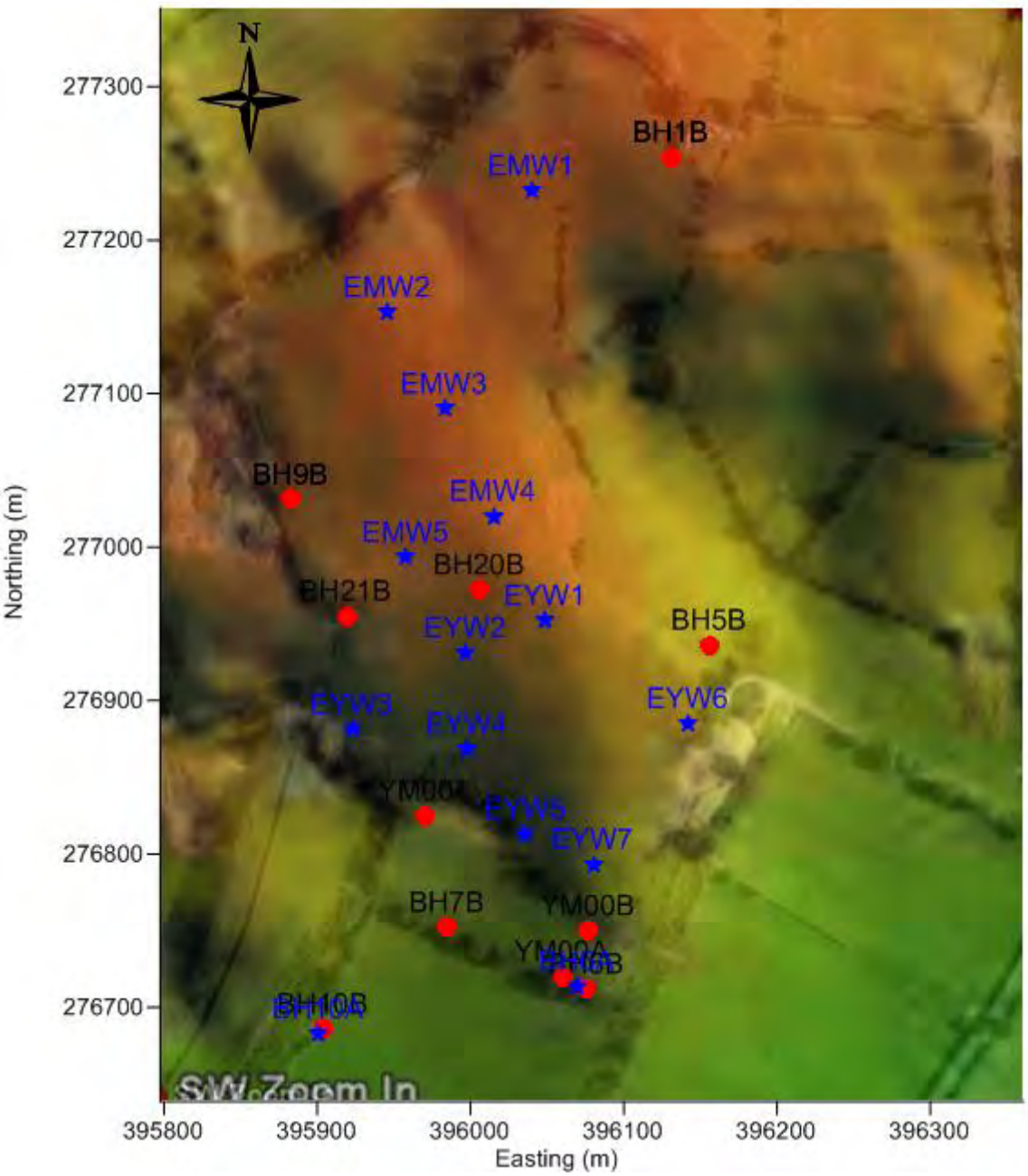

Figure 5.14: Showing the water sample locations. The BH series are for the deep groundwater sample, W series for the perched water sample (leachate) and YM series are the old DoE's boreholes

5.2.4.2 Geophysical Survey Gem-2 and Resistivity

Two series of resistivity imaging and GEM -2 surveys have been carried out on the site. The first GEM-2 survey was conducted on August 2009 in the Yew Tree Farm landfill and it is represented by the dark blue colour track in a Figure 5.15. A second GEM survey was carried out in May 2010 and it is shown in the red, yellow and light blue tracks in

GEM-2 map (Figure 5.15). Five different electromagnetic waves had been used in these surveys (975Hz, 7075Hz, 16075Hz, 30025Hz and 40075Hz).

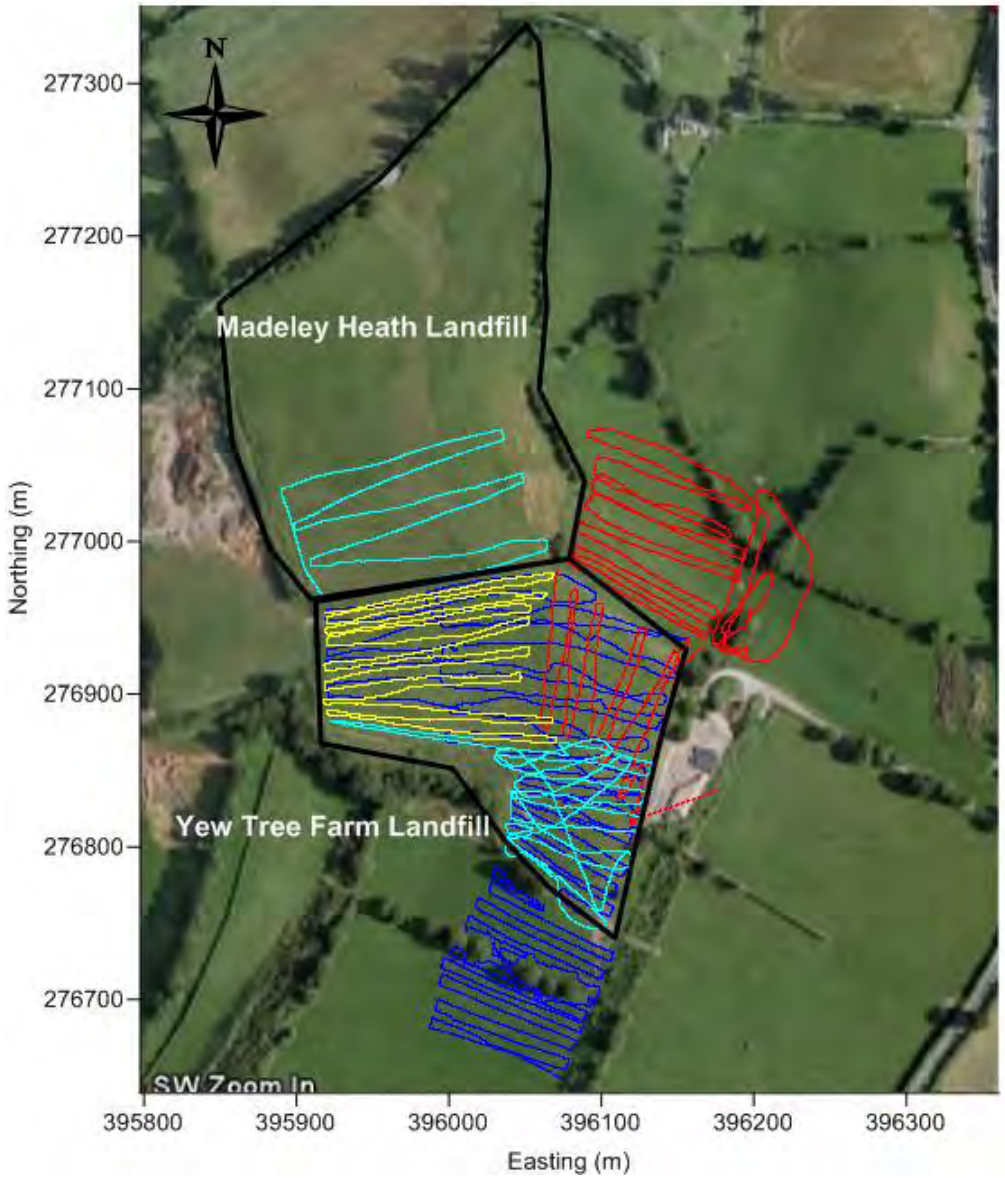

Figure 5.15: This map shows a GEM-2 survey lines where the dark blue line was carried out on August 2009 and other lines in May 2010

The first resistivity survey was carried out in 2009 (RES1 KD and RES2 KD; Figure 5.16). These resistivity lines were part of a previous dataset that had been used by an MSc student (Dutton, 2009). The raw data has subsequently been re-processed as a supporting data to a new data set. A second survey was carried out in May 2010 as shown in yellow lines in Figure 5.16. Each line is 355m in length and crossed the YTF landfill at differences angles. These have been designed with the aim to define any changing landfill structures (boundaries), plumes movements and orientation of possible groundwater flow.

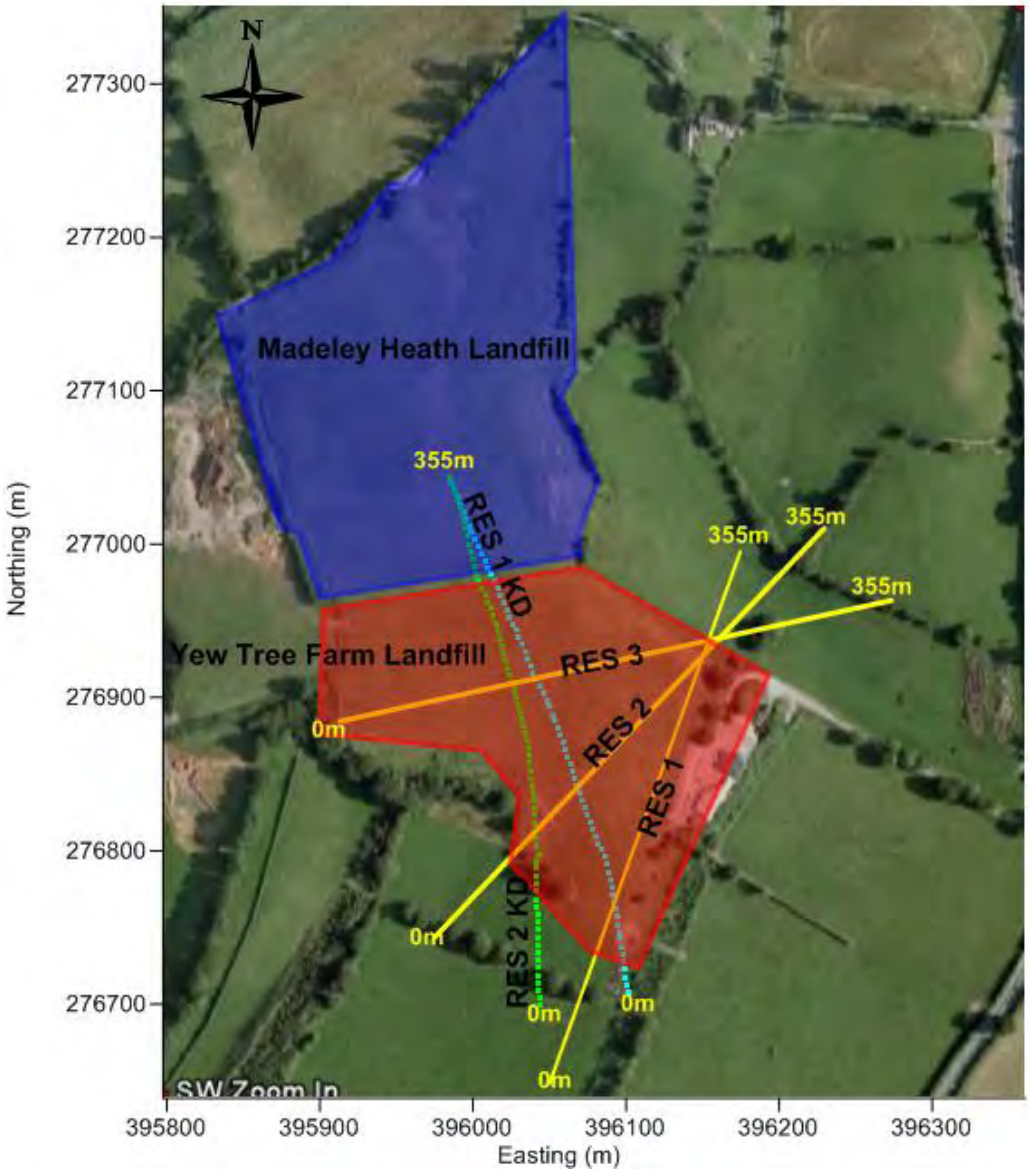

Figure 5.16: The resistivity lines layout on the top of the YTF landfill. The RES 1KD and RES 2KD are the lines carried out by Dutton, 2009 and three yellow lines carried out in May 2010

5.3 Geophysical data processing and analysis

Raw resistivity data from IRIS Instrument was transferred from a BIN file to an ASCII file format by using PROSYS II (Resistivity data management software) and then was converted into RES2DINV format for modelling. Only in this format can the input data be processed with the RES2DINV software. The final output from the analysis is 2D resistivity profile which shows the surface distance, depth of the profile and the colour contour scale representing the resistivity values in ohm-m (Ωm). Topographic data for the electrodes acquired by a separate EDM survey is also input at this point.

In order to understand the three dimensional (3D) distributions of resistivity values over the study area, all data from survey lines have been combined using Surfer 9. Seven resistivity survey lines have been used in Cathays Railways Depot and six short lines for the Barry Docks (Small Area). These allow different depths of resistivity distribution plan views to be plotted. The 2D plan views are created by using the final resistivity inversion data from the resistivity profiles. The ASCII format file has the resistivity values of every calculated point and as well the depth of a layer. It is also provides the X and Y location on the surface. Using this information a set of data including the X and Y location and the resistivity values of every line in a similar depth can be compiled.

Data from the GEM-2 console are downloaded using WinGEM software and the position of each data points can be located from GPS data in Trimble GPS. Data is downloaded as an excel spreadsheet and the GPS latitude/longitude values converted to the UK national grid using the Ordnance Survey GridInqest software. The data can be contoured and spatially mapped using Surfer V9 software. Five different 2D plan views representing five different frequencies are produced in this survey, each of them represent a different depth of ground investigation.

5.4 Geochemical approaches

The geochemical sampling procedures include both field measurements and laboratory analysis.

5.4.1 Field sampling and measurement

The field samples include a soil sample (Cathays Railway depot), surface water and groundwater sampling (Barry Docks and Bromsgrove landfill) to measure at least six chemical parameters of in-situ water sample which including pH, Redox Potential (Eh), Dissolve Oxygen (DO), Conductivity, Temperature and Total dissolve Solid (TDS). A water sample has also been collected for laboratory analysis by the analytical facilites at the School of Earth & Ocean Sciences Cardiff University.

5.4.2 Laboratory analysis

In the laboratory, the soil samples are normally taken through a generating leachate process which follows the British Standard BS 12547-2 (2002) guide line. Generally, the processes includes drying the soil samples in the oven at 50°C for 3 days, sieving the soil with 4mm sieve size and take about 100gm soil samples, add water (deionised water), mixed them in washed bottled (washed with 10% HNO3 acid – let the bottle fully filled with acid for about one day and washed the bottle with deionised water). With the ratio liquid to solid 10litres/1kg or 1litre/100gram the leaching liquid are ready for shaking process for about 24 hours to ensure the solid is completely mixed in the water. Usually to separate solid from water, the water sample has to settle down for a few days (not included in the BS 12547-2 standard but essential with many samples) until it is ready for filtering process with 0.45 µm filter to have an about 50ml clear water sample. Then the water sample can proceed for the Anion (IC) and Cation (IC-PMS) analysis (Figure 5.17).

5.5 The ICP- MS and IC analysis

Inductively Coupled Plasma Mass Spectrometry (ICP-MS) was developed in the early 1980's to combine the easy sample introduction and quick analysis of ICP technology with the accurate and low detection limits of mass spectrometry. The resulting device is capable of trace multi element analysis precise at part per trillion levels. Ion Chromatography (IC) also does a similar analysis as ICP-MS but it's more specialised on the anions analysis. Both ICP-MS and IC are applicable to determine the ions contained in the water samples especially in the field of drinking water quality, wastewater, natural water systems (hydrogeology), geology and soil science, mining/metallurgy, food science and medicine.

In the ICP-MS analysis, the water sample will be through four main processes including preparation of the sample and aerosol generation, ionization by argon plasma source, mass discrimination and detection system. The schematic diagram in Figure 2.3 and Figure 2.4 illustrates those processes.

The ICP-MS samples preparation need 10ml water samples for each specimen which will be added with 1ml 10% HNO3. The device has to be calibrated with the standard reagents first before running the analysis. ICP-MS has been set to repeat the analysis four times for every sample and the efficiency of the device worked will be recorded as a guideline in data interpretation. The ICP-MS will measure the amount of cations or the elements in the water sample and for this analysis 26 cations had been detected with the precision up to part per billion (ppb).

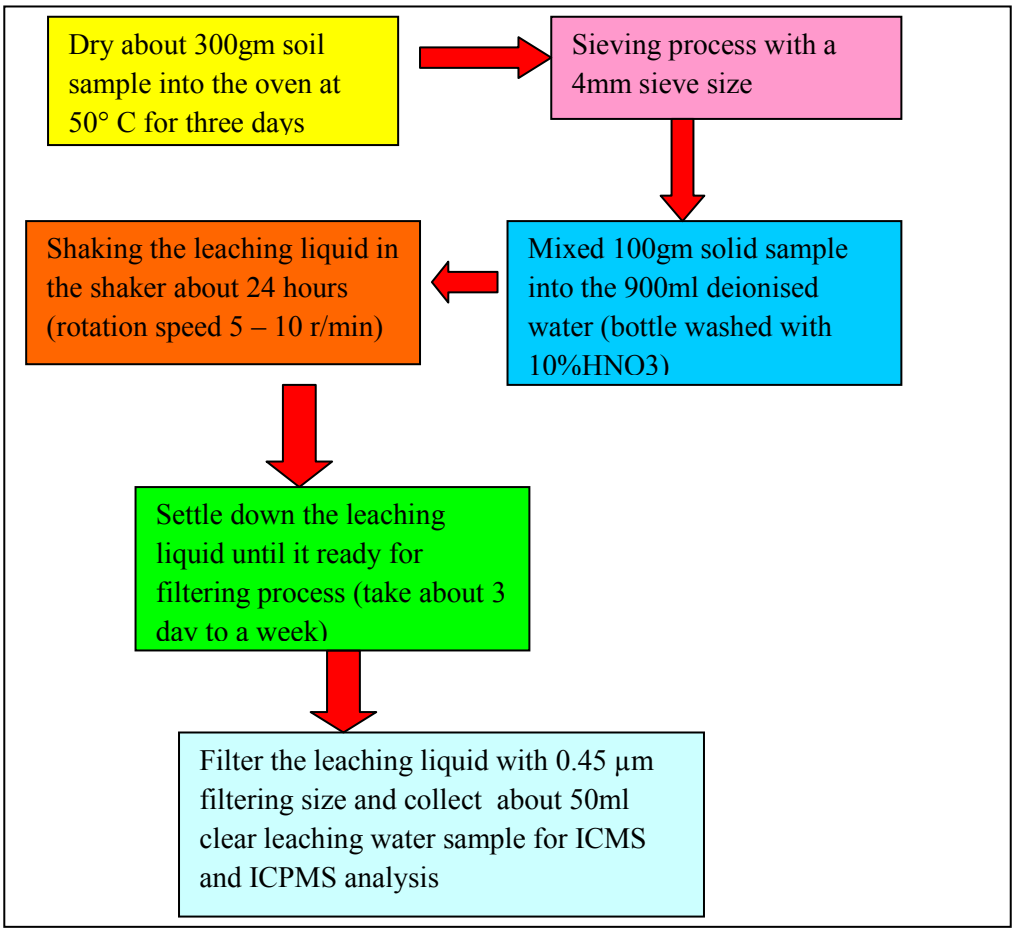

Figure 5.17: The major processes for generating leachate from soil sample

The IC water sample preparation is simple compared to the ICP-MS analysis. The water sample is filled into a small plastic bottle (specialized for IC analysis) and covered with a cap. The device has a sample racks which is used to hold the samples when sample analyzing in progress. Each rack has six slots and the first slot will be allocate for standard (deionised water) and followed with five bottles of water sample. The sequence will continue until the last sample and then end with another standard.

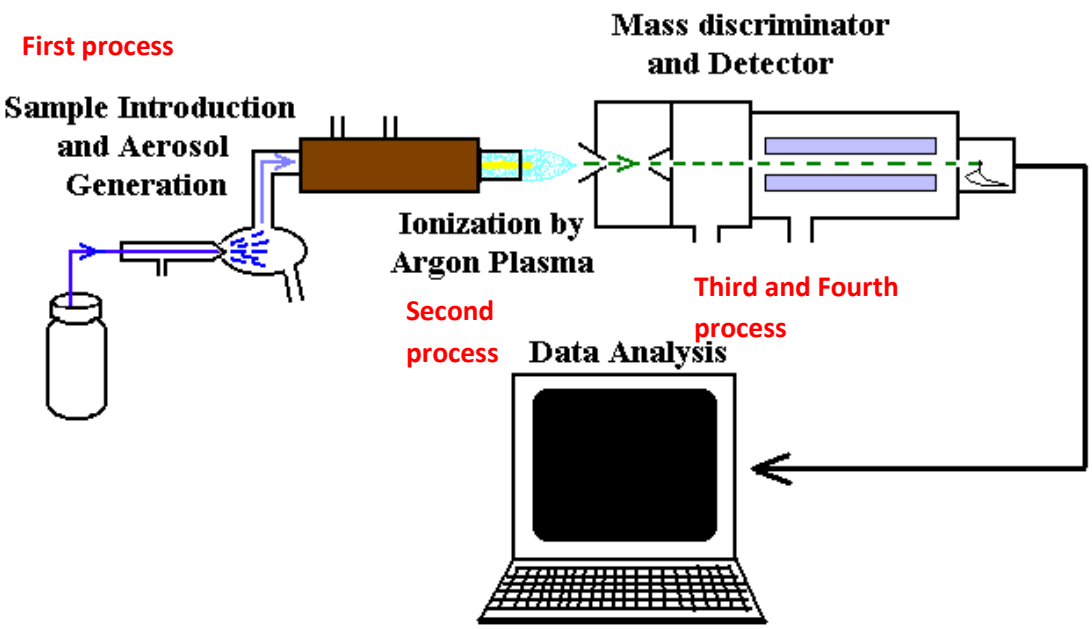

Figure 5.18: The schematic diagram of the ICP-MS processes (Worley and Kvech, 2009) – **Web 5.1**

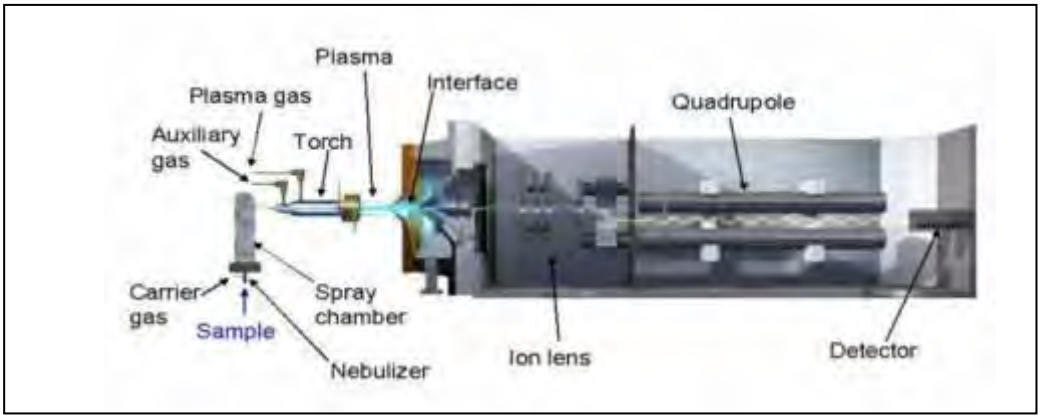

Figure 5.19: The cross section of the ICP-MS (University of California, 2009) – **Web 5.2**

5.6 Conclusions

Four geographical sites of different types of ground contamination are used in this research study. Geophysical surveys have been deployed to obtain both a 2D and 3D view of the current contamination scenario found at each site. Borehole data mostly exist for the sites from previous professional investigations. These data give information regarding the lithological strata and the expected depth of the groundwater table. Existing boreholes also provide an access for groundwater sample collection. The degree of contamination on site is determined by the geochemical analysis of the soil and water samples, whether from the previous or current investigations.

CHAPTER 6
RESULTS AND INTERPRETATION
CASE STUDY I: CATHAYS RAILWAY DEPOT

6.1 Introduction

In this chapter, the results and the interpretation of the investigations that has been performed at the Cathays Railway Depot are discussed. Originally, this site was used for instrument calibration and for training to use the equipment before going into the other contaminant sites. However, the encouraging site results have meant that the site is included in its own right into this PhD project.

Results and interpretation will be discussed in three parts which include geochemical, geophysical analyses and in combination. Geochemical results include the analysis of anions and cations (metal) in the soil and its distribution at the site based upon the chemical contains obtained from the soil samples. The results are displayed in 2D plan view using Surfer 9 software. Whereas the geophysical data comprise of Resistivity and GEM-2 results and will be represented by 2D profiling and also in 2D plan view. Then, those results will be combined to show any possible correlation or relationship between them. However, this correlation only involve the near surface soil samples (up to 1m depth).

6.2 Geochemical results

Results obtained from the analysis are presented in two parts which include the anions and the cations elements. Each of the elements is plotted using Surfer-9 software in order to define the spatial distribution of each major element. Besides that, the overall distributions of anions and cations also were plotted in percentage by calculating the amount of total percentage of all anions and cations at the study site.

Electrical resistivity possibly has a special relationship with the ions contained in the soil samples. Ions are good conductor, and they will allow the electric current to flow easily and reduce the electrical resistivity. The high concentration of ions in certain area will be expected to generate low resistivity values. In order to define the relative relationship, the

total amount of the cations and anions had been calculated based on percentage approach. Results of the cations concentration in ppm and ppb are shown in Appendix A. Two types of analysis have been done to get the percentage of ion in the sample:

a) $$\text{Percentage of ions} = \frac{\text{amount ion in each soil sample}}{\text{total amount of similar ion in 24 samples}} X100\% \quad \text{--- (6.1)}$$

b) $$\text{\% of 26 cations } (\mathbf{x'}) = \frac{x_{n1} + x_{n2} + \ldots\ldots\ldots\ldots\ldots\ldots\ldots x_{n26}}{26} X100\% \text{-------(6.2)}$$

Where n = name of ion
x = percentage (%) of ion 'n' in the soil sample
1,2,3,…….26 = total number of elements (ions)

i) First method is used to determine the percentage of certain elements (ions) in the soil sample. So, the distribution of the ion can be plotted individually.

ii) While in the second method, the percentage of all ions in a soil sample against the total ions in the whole 24 soil samples. The results than are plotting by using Surfer 9 to define the total ions distribution.

Higher percentages represent high concentration of ions whilst the lower percentages are representing lower concentration of ions. By this technique any correlations with resistivity values can be established.

A similar procedure has been repeated to calculate the total distribution of the anions but instead of dividing by 26 for cations, the anions are only divided by seven, which represents the seven anions obtained from the IC analysis.

6.2.1 Major anions contain

In the major anions analysis, the concentrate of seven anions have been measured include Fluoride, Chloride, Nitrite, Nitrate, Bromide, Sulphate and Phosphate. All amounts are in mg/l or ppm units and the results are shown in Table 6.1. Through the IC analysis, every sample was analysed twice and the results shown in the table are the averages. The overall distribution of total anions in ppm or mg/l and percentage are shown in Figure 6.1. It is clear that the distributions of major anions are mostly concentrated on the Northeast of the study site. Generally, the dispersion patterns follow the old railway tracks (Figure 6.2). This pattern can probably be linked with the activities in the past. There are a

various factors affecting contamination in railway land. The workshops and a storage building as an example, produce a huge amount of waste and may can contaminating the site by the fuel lubricants, diesel, oil spillages, asbestos, grease, solvents, coolants, paint, glue, varnish, creosote, toluene, acetylene, propane and hydraulic fluids (Environment Agency, 1995) – **Web 3.5.** Fuel oils, lubricating oils and greases may also cause localised contamination of ballast and of areas where locomotives and multiples units have stood for significant periods of time, for example at terminal stations and in sidings.

6.2.2 Major cations contain

The cations analysed results indicate that all the elements do not exceed the threshold values suggested by ICRCL 59/83 (**Web 2.25**), Dutch List (**Web 2.26**) and Kelly Indices (**Web 2.27**) from (Table 6.2). But in term of distribution of the elements, there are three patterns which were detected in the Surfer plots (Surfer V9 software).

i) The first pattern is showing the concentration of certain cations more toward the Northeast of the study area (sample ID – C12, C13, C14, C22, C23 and C24). This pattern was represented by eleven cations which are including 23Na, 26Mg, 29Si, 31P, 51V, 52Cr, 66Zn, 88Sr, 111Cd, 137Ba and 208Pb (example 23Na and 52Cr in Figure 6.3).

ii) The second pattern follows the old railway tracks which are shown by the distribution of 39K, 57Fe, 59Co, 65Cu, 85Rb, 121Sb and 202Hg (example 39K and 57Fe in Figure 6.4).

iii) The last is a random pattern which does not follow the patterns mentioned above. This random distribution pattern is represented by the 27Al, 44Ca, 60Ni, 75As, 77Se, 133Cs, 182W and 208Pb (example 27Al and 44Ca in Figure 6.5).

All the figures for the cations distribution can be seen in the Appendix B. While, the distribution of total cations is shows in the Figure 6.6 and Figure 6.7, which dominate the overall distribution and follow the location of the old railway tracks, workshops and railway sidings.

Table 6.1: The amount of anions in the water samples (soil leachate)

Sample ID	Amount mg/L Fluoride	Amount mg/L Chloride	Amount mg/L Nitrite	Amount mg/L Bromide	Amount mg/L Nitrate	Amount mg/L Phosphate	Amount mg/L Sulphate
C1	0.198	0.612	0.000	0.000	14.663	0.000	2.737
C2	0.009	0.831	0.066	0.000	12.239	2.926	3.531
C3	0.000	0.655	0.048	0.000	7.759	0.000	2.529
C4	0.045	0.490	0.046	0.000	7.259	0.000	1.420
C5	0.037	2.193	0.000	0.000	10.036	0.229	1.557
C6	0.102	0.684	0.043	0.000	8.369	0.109	2.393
C7	0.000	0.793	0.000	0.000	14.860	0.000	2.370
C8	0.017	0.545	0.000	0.000	7.333	0.000	1.646
C9	0.033	0.563	0.052	0.000	11.600	0.000	2.689
C10	0.047	0.789	0.049	0.000	4.941	0.000	1.812
C11	0.315	0.618	0.000	0.000	5.621	0.000	10.926
C12	0.000	0.761	0.000	0.000	10.576	0.118	3.033
C13	0.054	0.540	0.045	0.000	10.498	0.000	3.396
C14	0.369	1.132	0.040	0.004	5.705	0.000	7.120
C15	0.000	1.153	0.040	0.000	2.982	0.000	1.414
C16	0.000	0.724	0.060	0.000	14.071	0.000	2.573
C17	0.000	0.991	0.063	0.000	7.437	0.000	1.395
C18	0.072	0.418	0.051	0.000	7.845	0.129	2.694
C19	0.017	0.514	0.046	0.000	2.192	0.128	1.973
C20	0.011	0.588	0.042	0.000	6.977	0.000	1.259
C21	0.000	0.548	0.051	0.000	4.985	0.000	1.793
C22	0.048	0.788	0.047	0.000	5.575	0.000	1.298
C23	0.043	1.332	0.043	0.005	3.429	0.000	1.563
C24	0.156	0.714	0.048	0.000	9.051	0.390	3.326

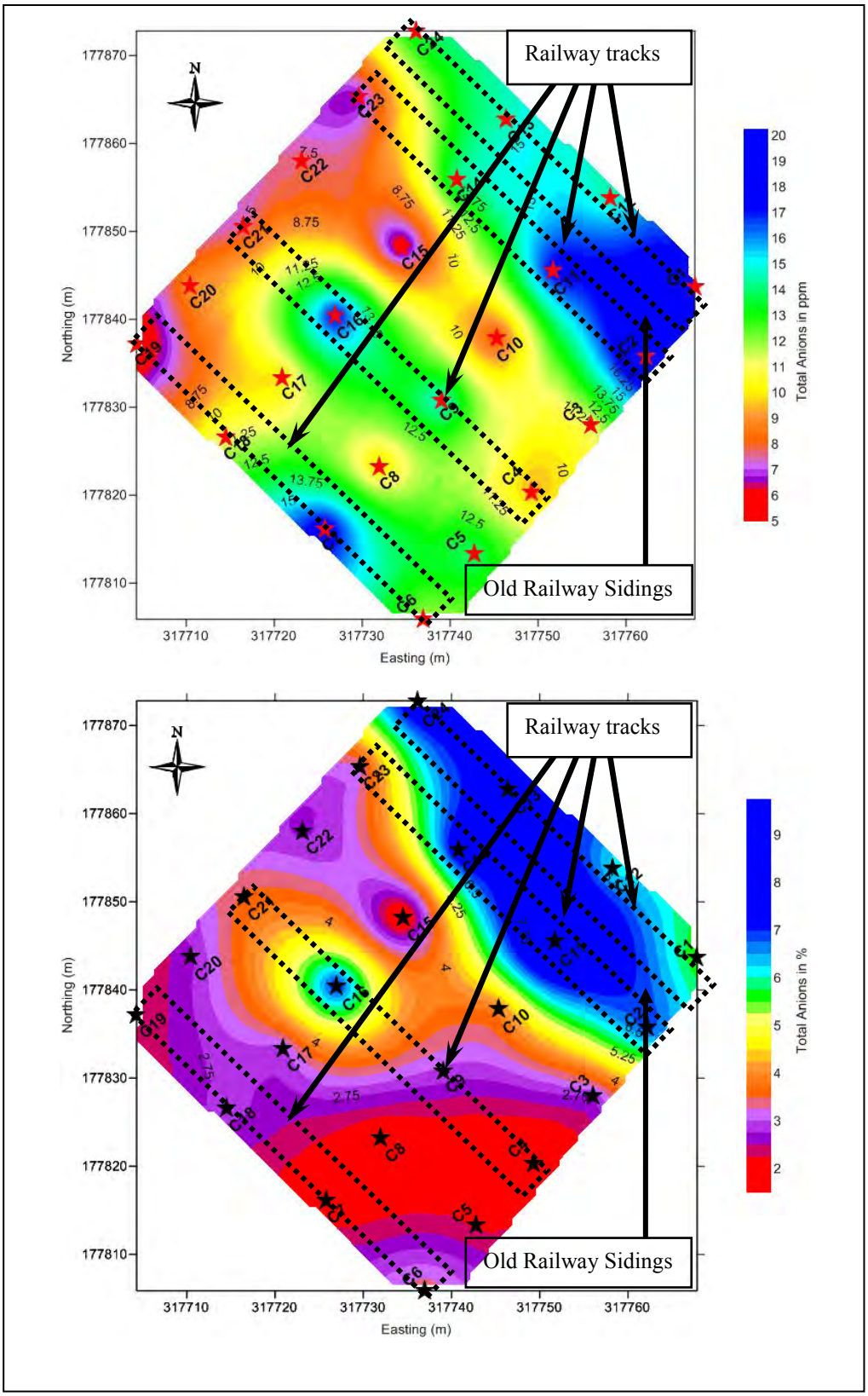

Figure 6.1: The distribution of the total anions in ppm and percentage

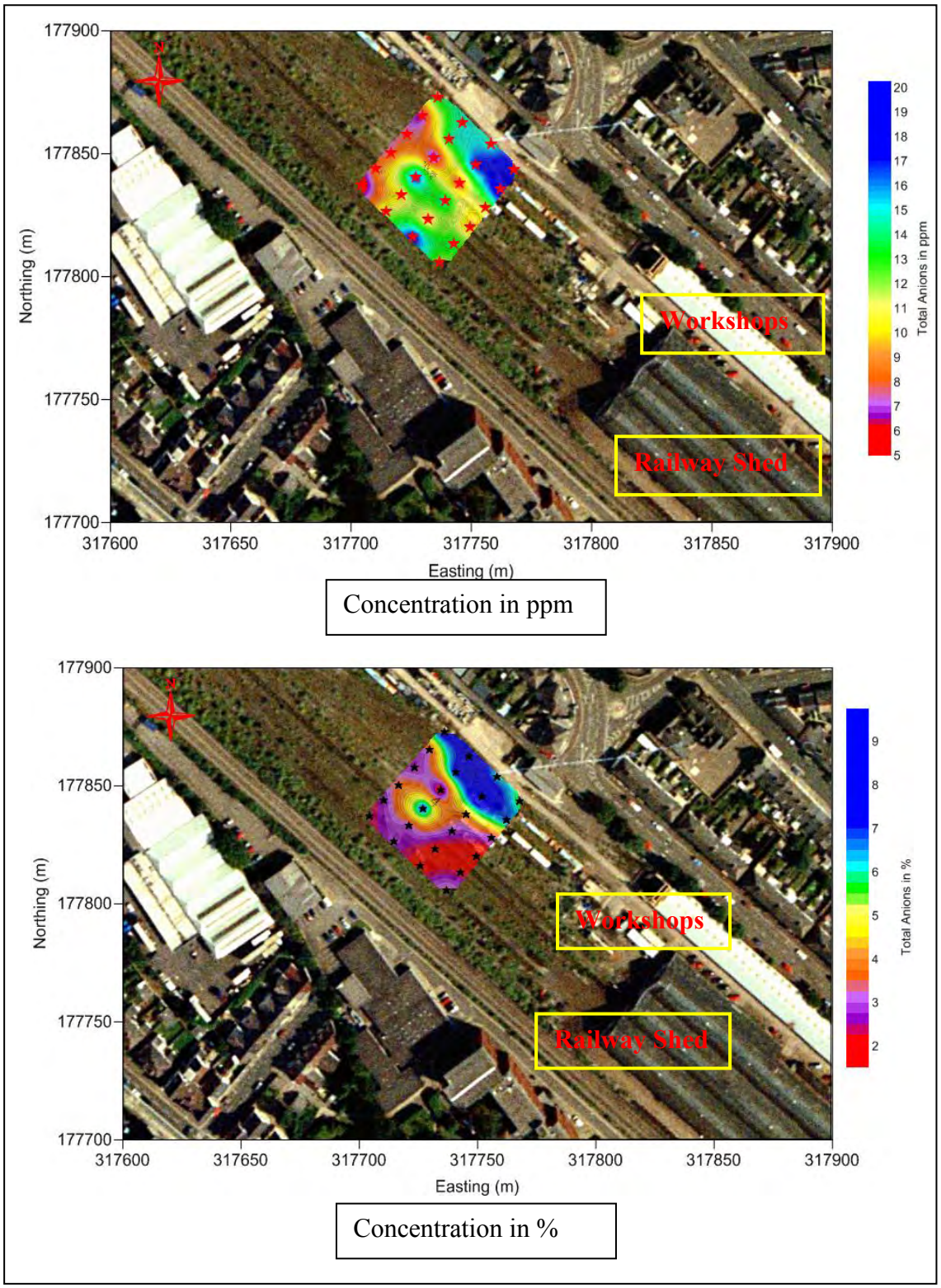

Figure 6.2: Concentration of total anions at study area showing its distribution follows the location of the old railway tracks and sidings

Table 6.2: The comparison amounts of selected anions and cations obtained from this study to the soil guideline value standards

Parameter	Kelly Indices (Contaminate) mg/kg	ICRCL 59/83 (Threshold) Domestic/parks	Dutchlist (mg/kg)		Cathays Site data (unit in ppm or ppb)
			Soil	GW	
pH (acid)	4-5	<5			
pH (Alkaline)	9-10				
Antimony	50-100		3		0.36 – 3.18
Aluminium					0.08 – 0.51
Arsenics	50-100	10/40	29	10	0.45 – 3.9
Boron	5-50	3			
Barium	1000-2000		200	50	38 – 538 ppb
Beryllium	10-20				
Cadmium	3-10	3/15	0.8	0.4	0.01 – 0.13
Chromium	200-500	600/1000	100	1	0.67 – 1.67
Copper	200-500	130	36	15	5.87 – 188.1
Cyanide (free)	5-50	25/100			
Cyanide	25-250	250/250			
Ferricyanide	500-1000				
Lead	1000-2000	500/2000	85	15	1 – 454 ppb
Lead	500-1000		85	15	
Mercury	3-10	1/20	0.3	0.05	0.1 – 0.4 ppb
Magnesium	1000-2000				0.4 – 3.0 ppm
Nickel	50-200	70	35	15	0.7 – 21.0
PAHs (Coal	1000-2000	50/1000	1		
Manganese	1000-2000				1.6 – 67 ppb
Phenol	5-50	5/5	0.05	0.2	
Selenium	3-10	3/6			0.28 – 0.78
Sulphate	5000-1%	2000/2000			1.3 – 11 ppm
Sulphur	500-1000	5000			
Sulphide	20-100	250			
Tin					
Tiocyanate	50-100	50	0	20	
Toluene Extract	1-5%		0	0.2	
Vanadium	200-500				
Zink Available	500-1000	300	140	65	
Zink Equivalent	500-2000		140	65	

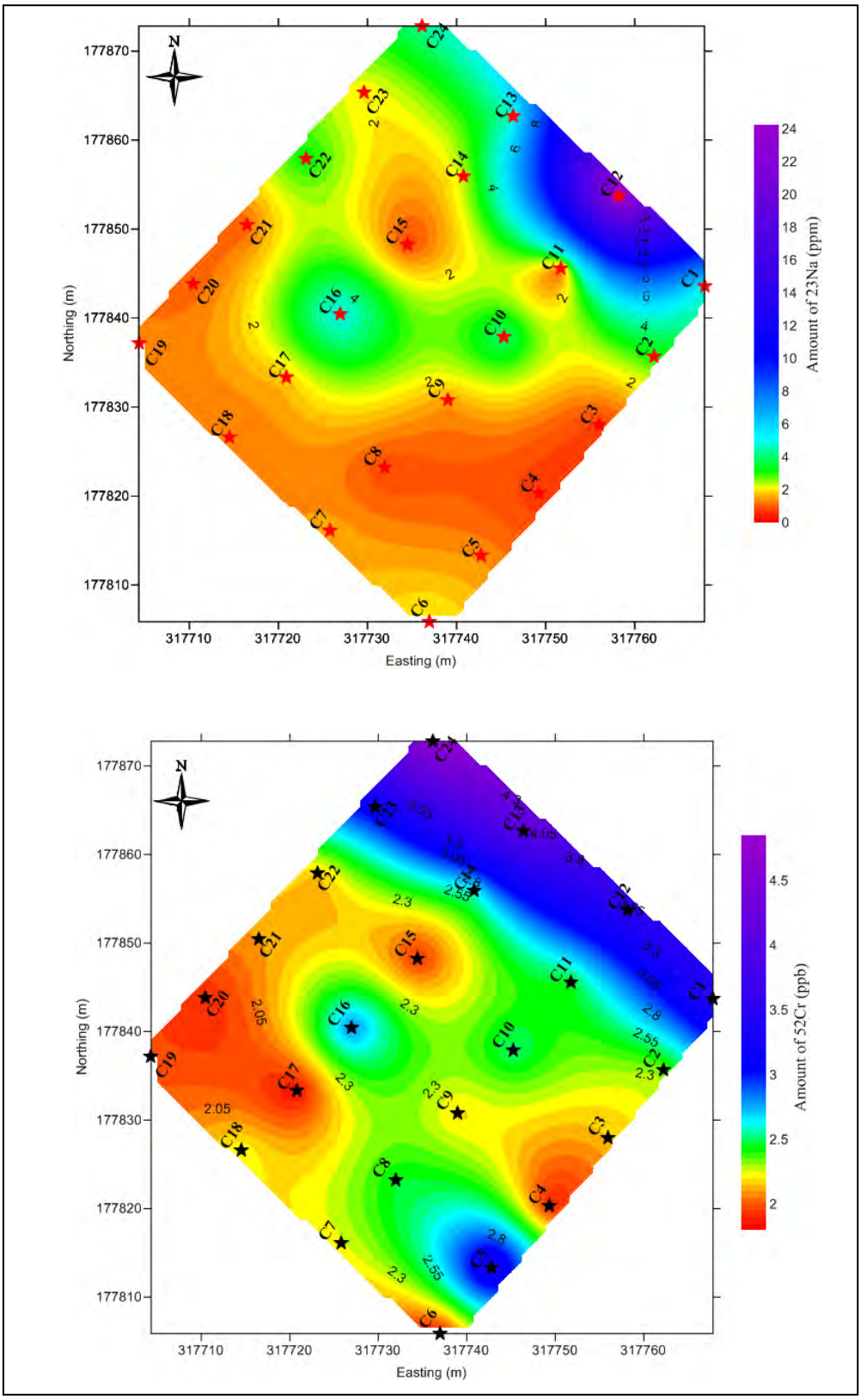

Figure 6.3: The northeast elements distribution pattern

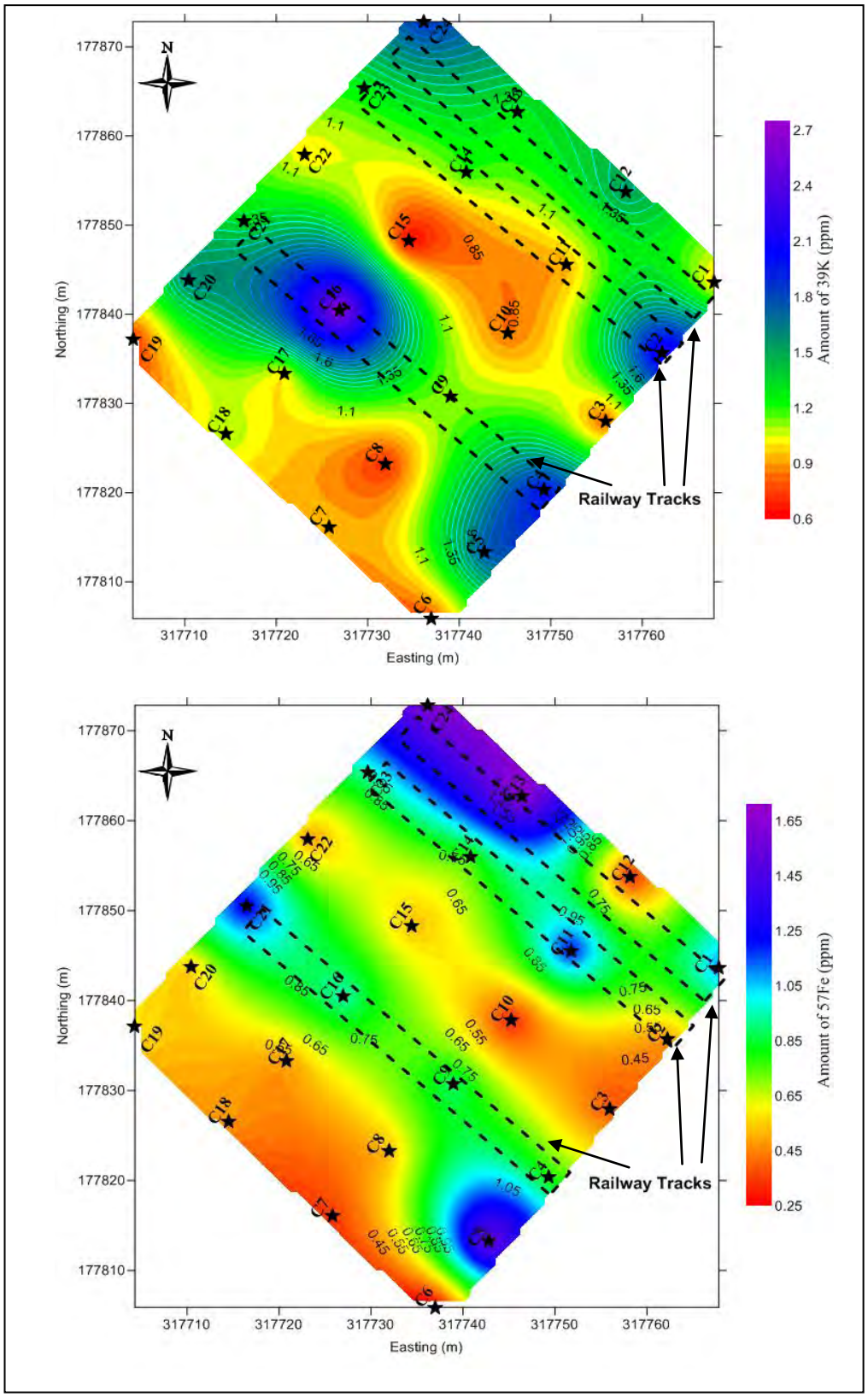

Figure 6.4: Showing the distribution pattern followed the old railway tracks

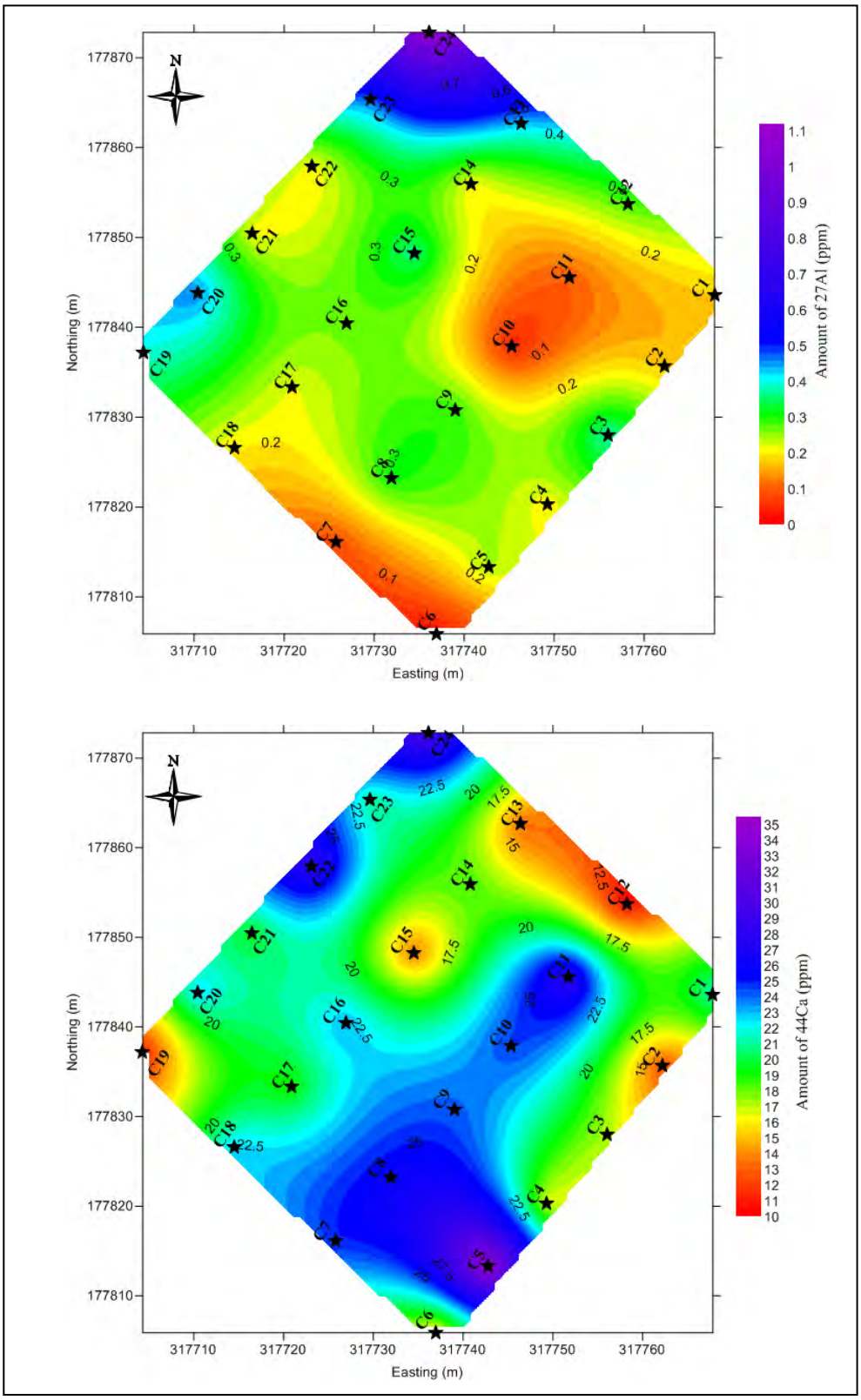

Figure 6.5: Showing a random distribution pattern

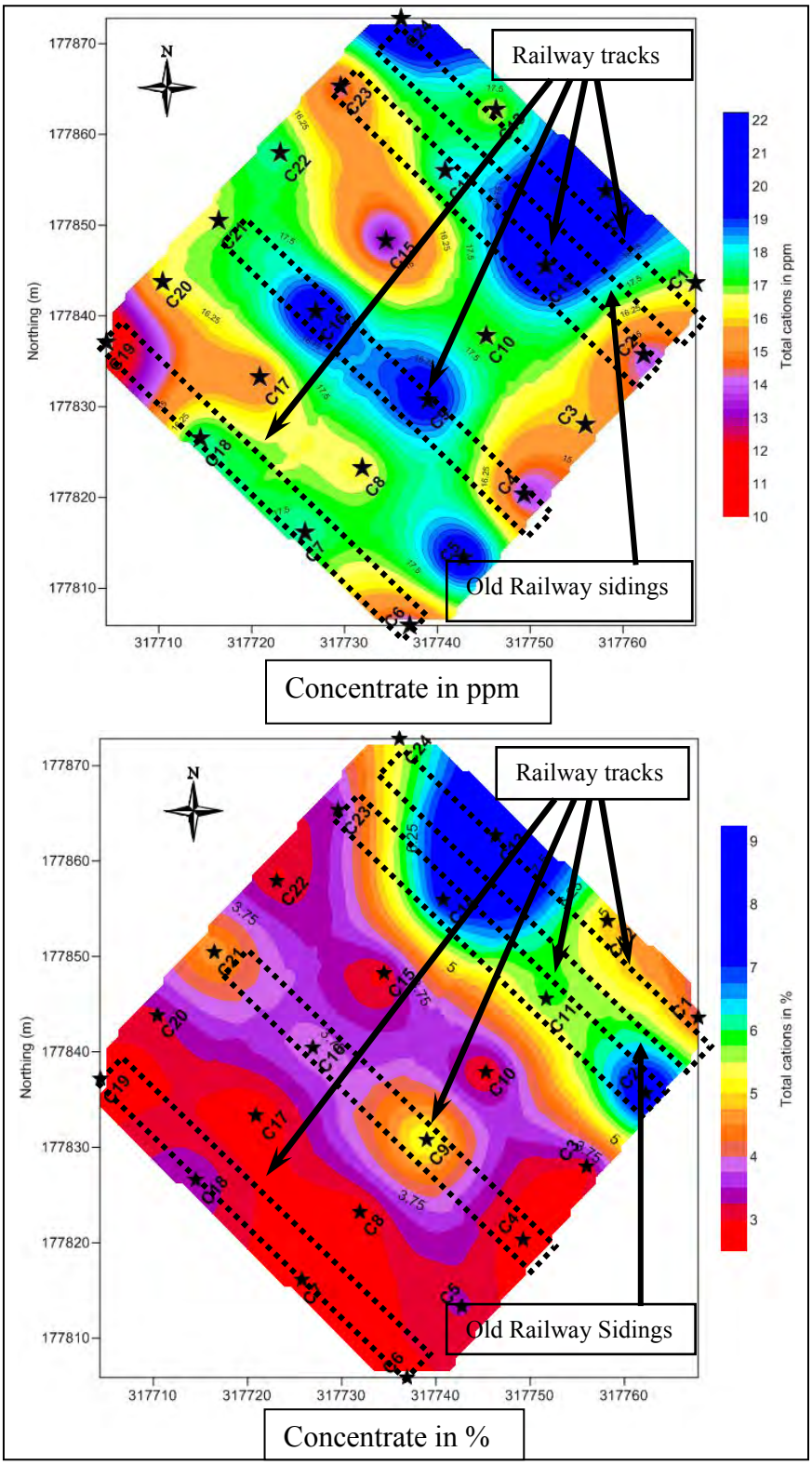

Figure 6.6: Higher amount of metals are concentrated in the northeast and the middle of the study site following the location of the railway tracks/sidings

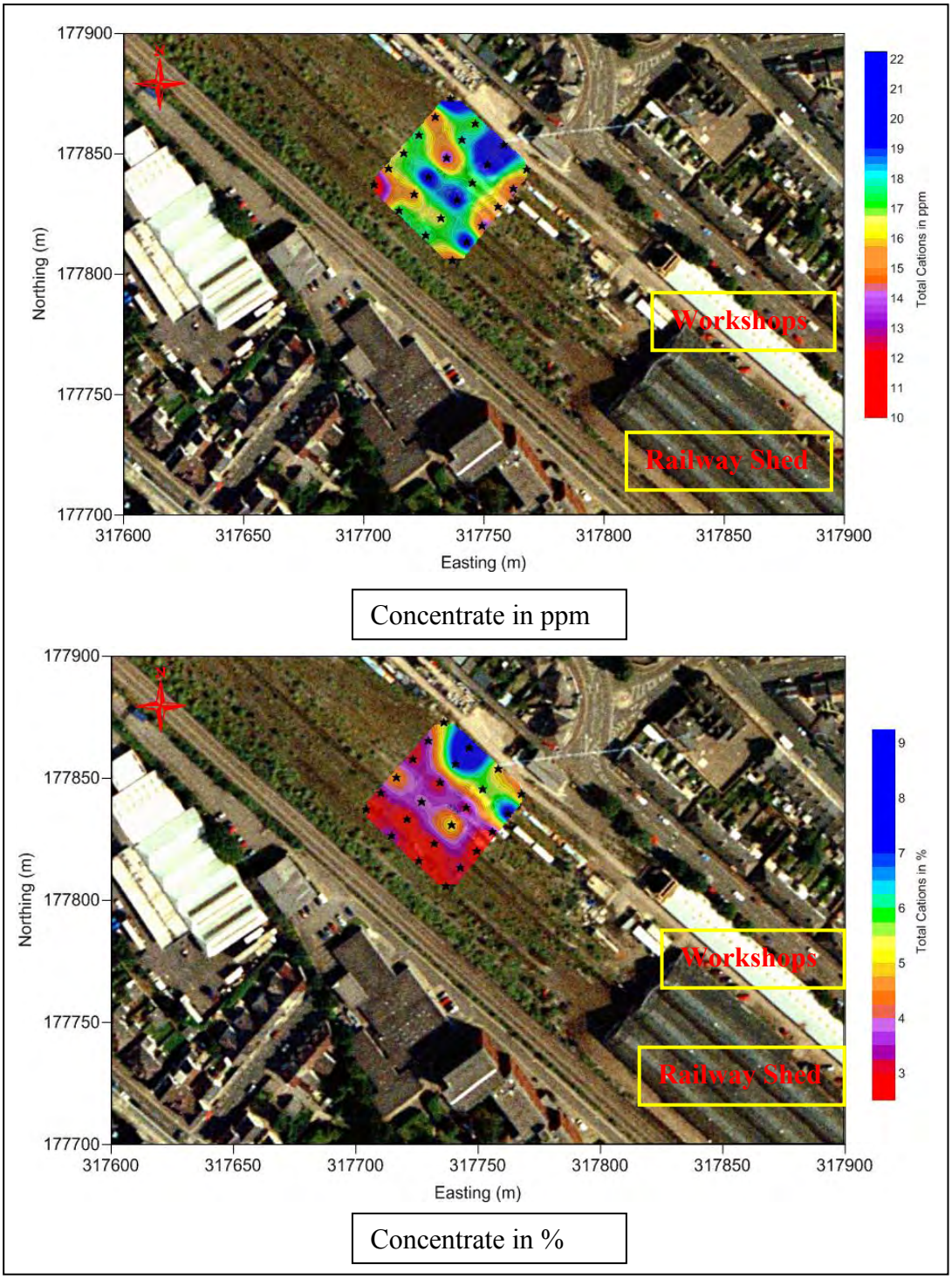

Figure 6.7: Showing the ions/metals distribution on the site

6.2.3 Combination of total anions and cations

The combination total of elements in the site from 24 soil samples had been calculated in order to get an overall view of its distribution in site. It is really important in order to define any significant relationship to the geophysical parameter. Generally, the distributions of the elements mainly follow the location of the old railway tracks, workshops and railway sidings. It can be related with the historical site activities and the distributions are shown in Figure 6.8.

6.3 Resistivity and Gem-2 survey results

This section comprises four subsections which includes the 2D resistivity profile interpretation, 2D plan view of resistivity interpretation, GEM-2 results and interpretation and the combination of all geophysical data. Although the chemical analysis shows the site is not legally contaminated but this only represents the topmost soil layer. The resistivity and the GEM-2 results discussed here are indicative the quality of soil layer near surface soil layer to about 10m depth.

6.3.1 2D Resistivity profiling

Overall, all the seven resistivity profiles display similar results where the resistivity values range between 1 Ωm and up to 10,000 Ωm. An interpretation is made by dividing the values into five ranges which are from 1 – 20 Ωm, between 20 Ωm to 150 Ωm, 150 Ωm to 400 Ωm, 400 Ωm to 2000 Ωm and more than 2000 Ωm.

Based on these five ranges of resistivity values, the lower range, mostly distributed near surface of the resistivity profiles (up to one meter depth) is most likely due to a man made contaminated layer. The site was originally a train depot, therefore, the contamination on site is expected to be from a variety of contaminants especially ash ballast, hydrocarbon oils and other waste material (coal, lime, tar and etc). Other ranges of resistivity representing possible material on the site are shown in Table 6.3.

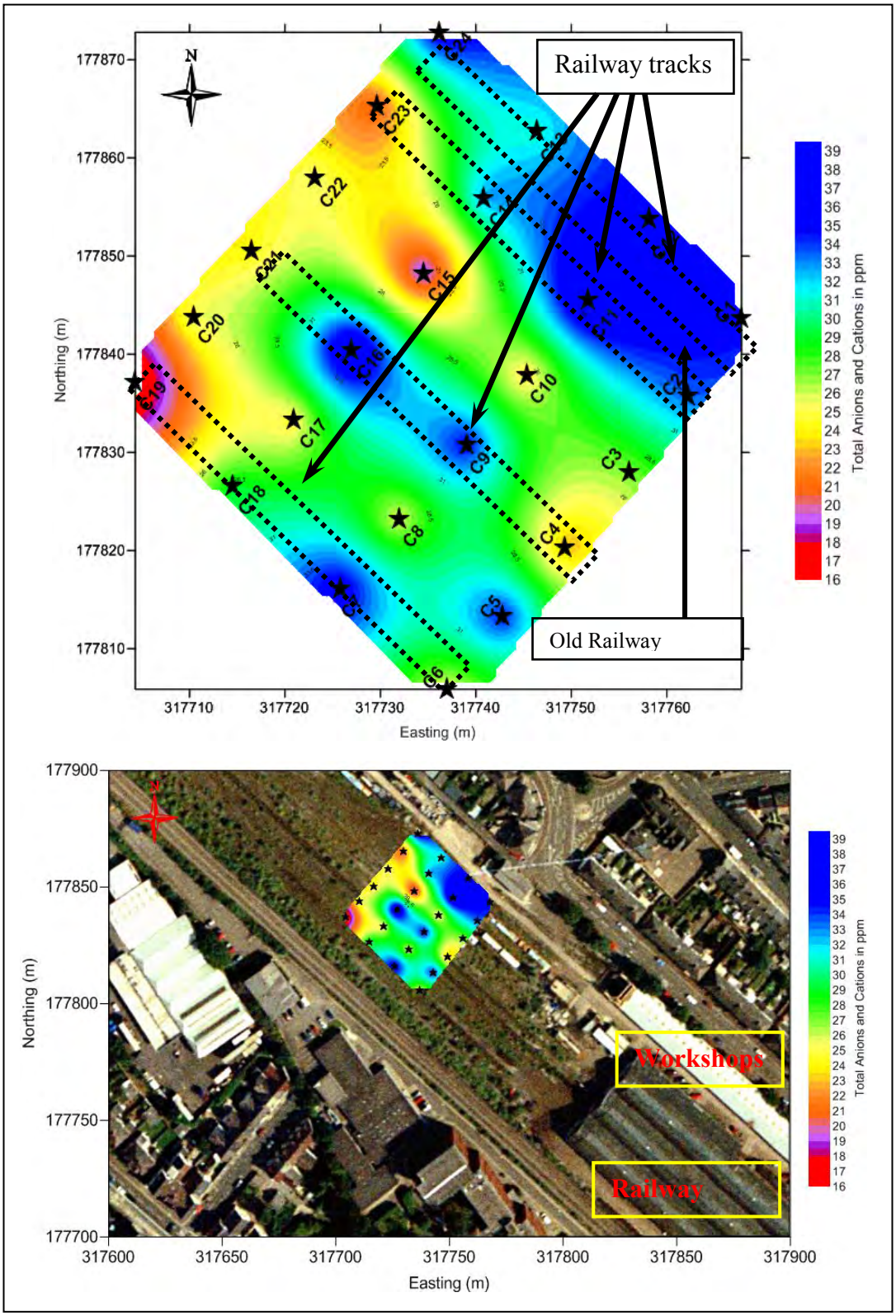

Figure 6.8: A distribution of combination total anions and cations on site showing a pattern which generally follows the location of old railway track, siding and the workshops

But the interesting range is between a 400 to 2000 Ωm (contour colour yellow to orange) because it's represents a potential contamination by hydrocarbons (Atekwana et.al., 1998) The distribution of the zones / layers with those ranges of resistivity values dominate in profiles Resistivity 6, Resistivity 1, Resistivity 2, Resistivity 7 and slightly decrease in the profile Resistivity 4 and Resistivity 5 toward the north of the study area remote from where the old workshops/sidings were located (Figure 6.9 to Figure 6.15). Generally, interpretation of the resistivity data shows a larger distribution of hydrocarbon plumes, most probably started from Resistivity Line 6 toward the middle of the study area (up to Resistivity Line 7).

The most important evidence about likely hydrocarbon contamination shown in the site is from the pattern of the HC plumes. The hydrocarbon contamination layer is sandwiched between low resistivity layers which are interpreted as a contamination soil layer on the top and the groundwater at the bottom. All anomalies of the potential HC contamination are cycled by the thick black lines in the 2D resistivity profiles in the Figure 6.9 to Figure 6.15.

The resistivity data seems to indicate that the hydrocarbons plumes are introduced from the surface, and then infiltrated through the soil particles until reaching the groundwater. A denser part of the HC sinks to the bottom of groundwater level and maybe at the top of bedrock. These situations can be explained by understanding types and the characteristics of the hydrocarbon contamination presence in the environment. With reference to the density of the HC contamination occurring in the environment, it can be divided into two types which a density less than water, called as LNAPLs (Light Non Aqueous Phase Liquids) and the denser than water is DNAPLs (Dense Non Aqueous Phase Liquids). The anomalies showing in the resistivity profiles above the groundwater table can be expected to be the LNAPLs and for below the groundwater table interpreted as DNAPLs.

The correlations between all the resistivity profiles are shown in Figure 6.16. Most of the high resistivity zones which are believed occur due to HC presence is found in the Res 6, Res 1 and Res 7 profiles.

Table 6.3: The ranges of resistivity values representing the probable types of material based on previous researchers

Resistivity Values (Ωm)	Probable Types of Material	References
1 – 20	Contaminated soil/groundwater	Meju.A.2000.
10 – 100	Fresh soil/groundwater	Keller and Frischknecht, 1970
150 – 400	Incompact material (alluvium, clay, sandstone, Shale and limestone)	Loke 2000 (**www 2.18**) and 2004(**www 2.19**)
400 – 2000	Potential Hydrocarbon contamination	Atekwana et.al. 1998
More then 2000	Vadose zone and hard rock or loose fill material.	Atekwana et.al. 1998

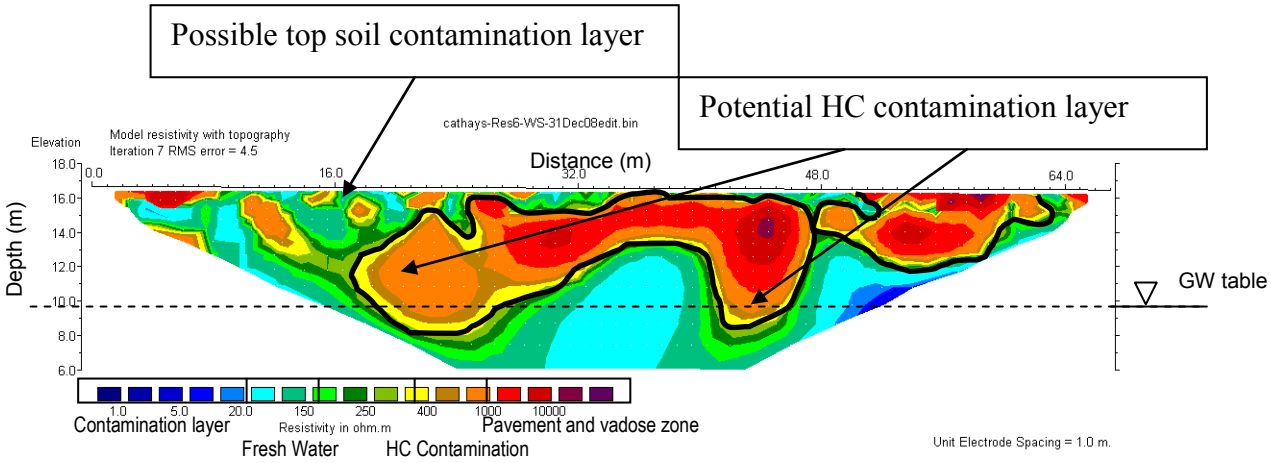

Figure 6.9: 2D Resistivity profile for survey line Resistivity 6

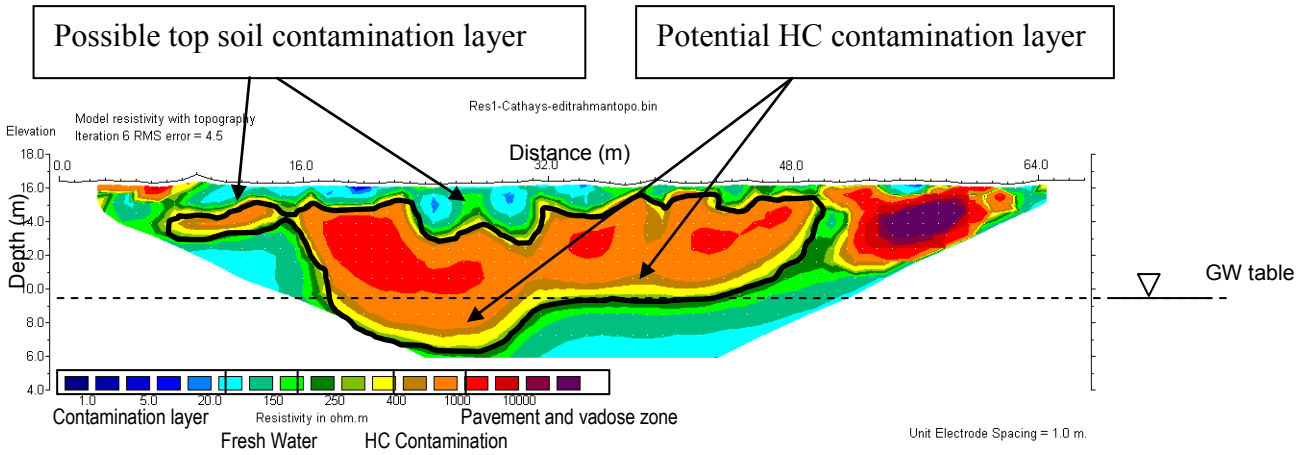

Figure 6.10: 2D Resistivity profile for survey line Resistivity 1

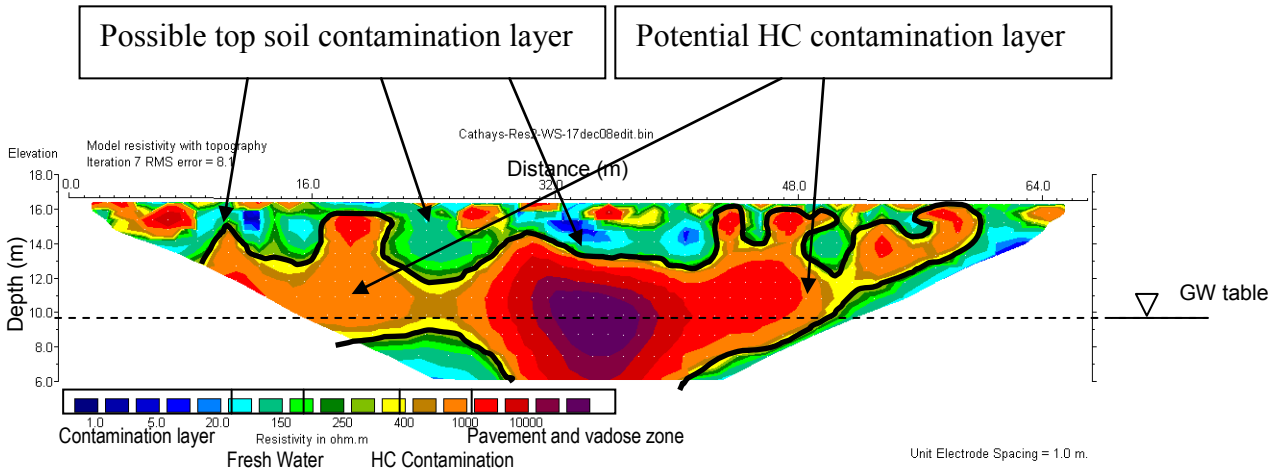

Figure 6.11: 2D Resistivity profile for survey line Resistivity 2

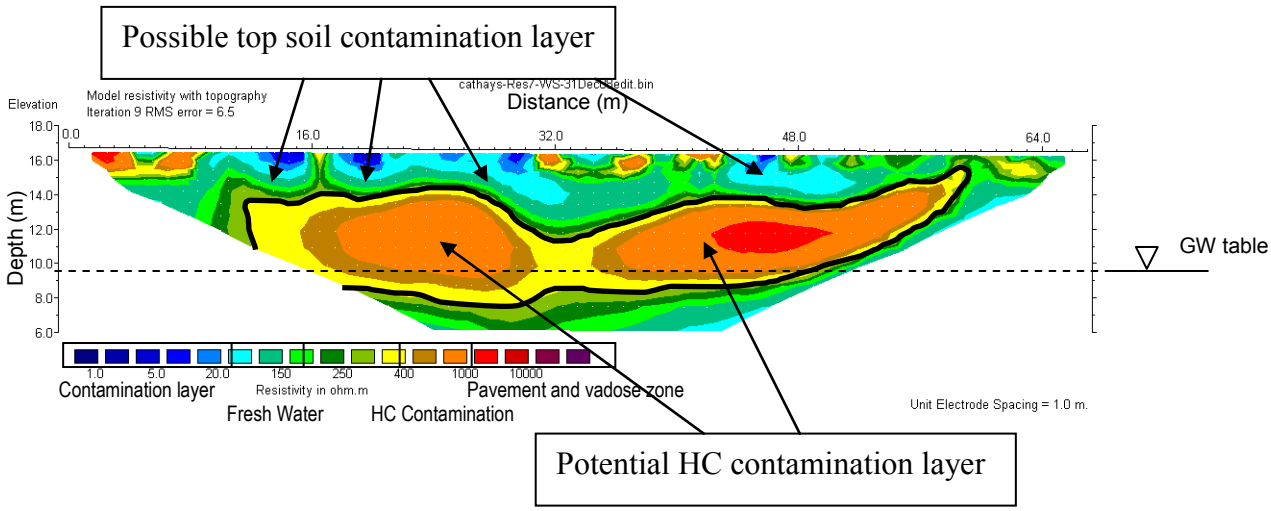

Figure 6.12: 2D Resistivity profile for survey line Resistivity 7

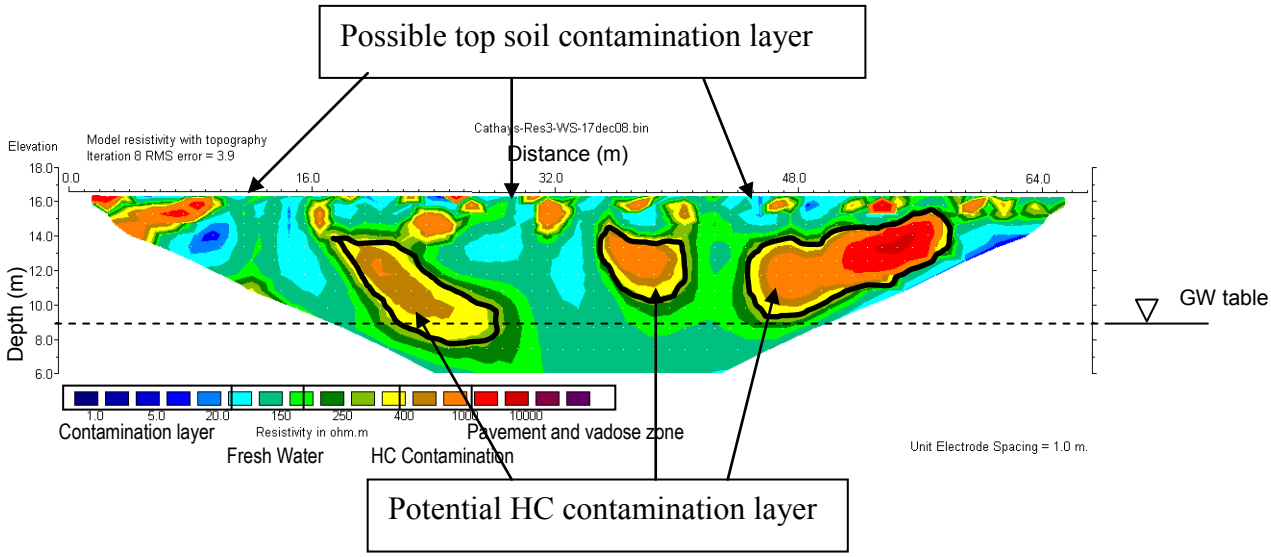

Figure 6.13: 2D Resistivity profile for survey line Resistivity 3

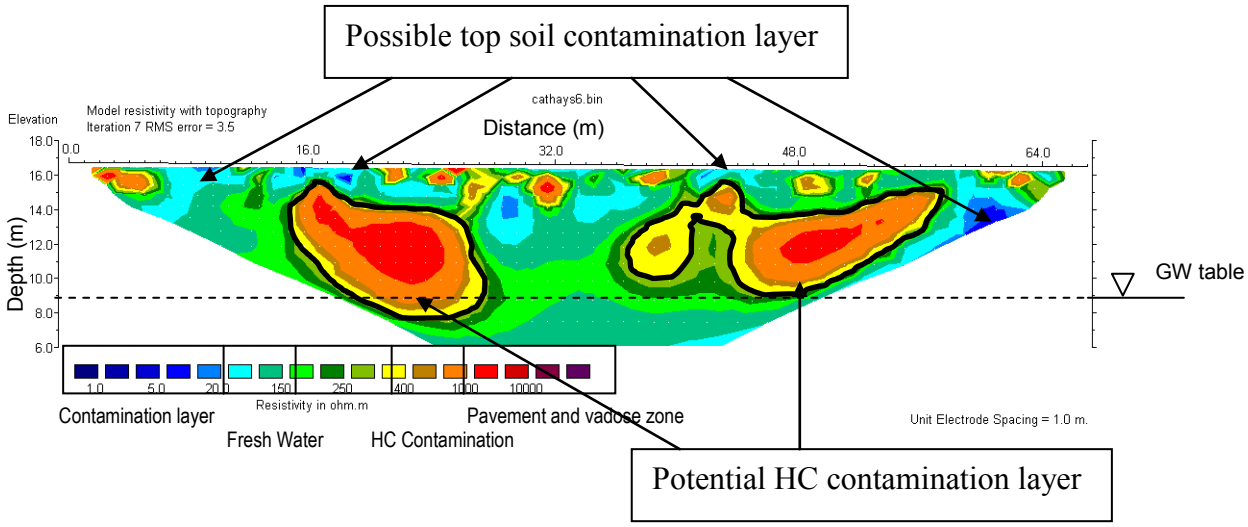

Figure 6.14: 2D Resistivity profile for survey line Resistivity 4

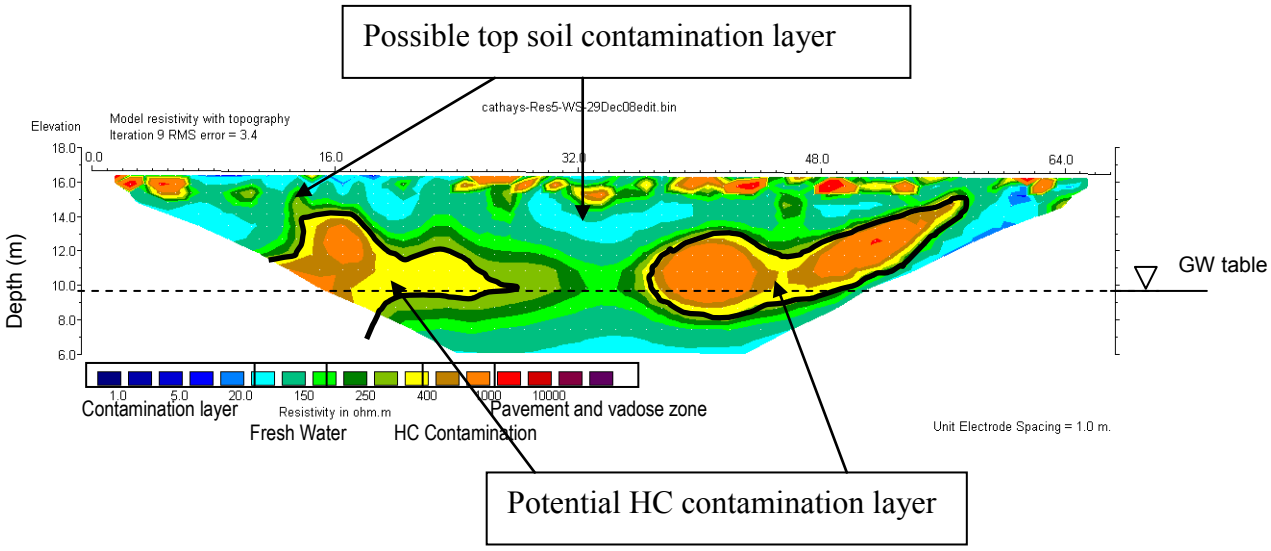

Figure 6.15: 2D Resistivity profile for survey line Resistivity 5

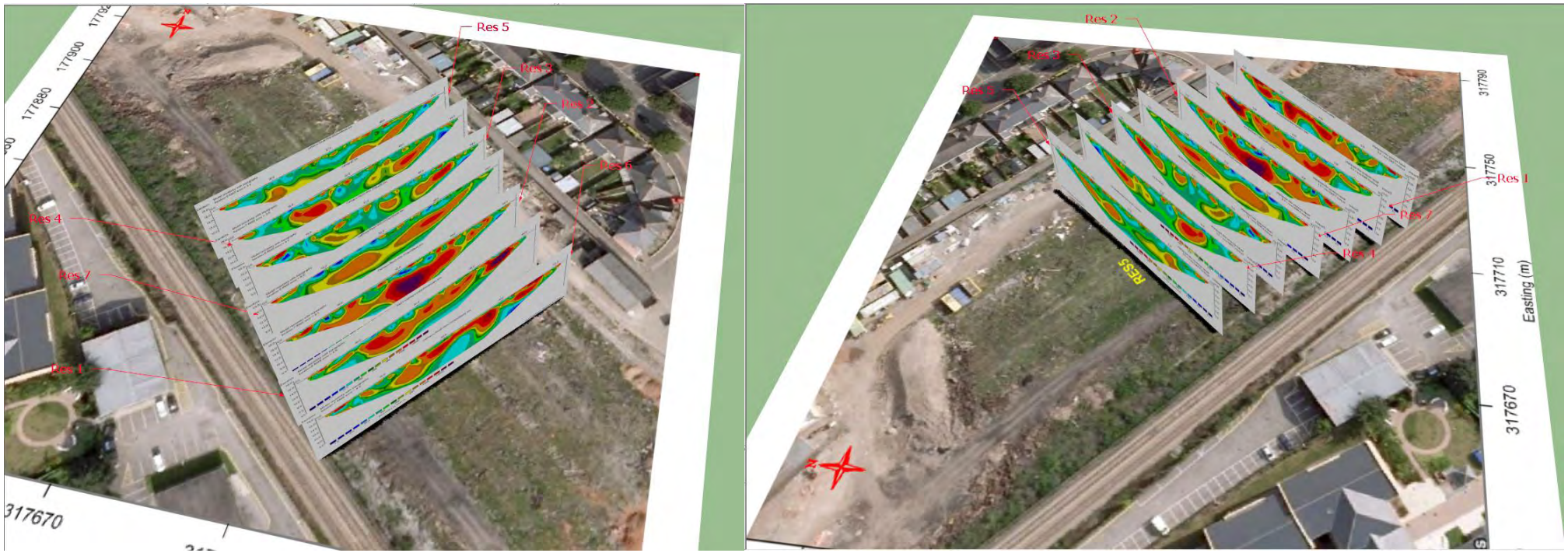

Figure 6.16: The combined resistivity profiles showing most of the high resistivity zones are found in the Res 1, Res 6 and Res 7

6.3.2 2D Resistivity map interpretations

Seven 2D resistivity inversion results were used to plot a 2D resistivity map of the material over the site. The 2D plan view used the inversion data from the same depth in the individual 2D inversion results. The easting and northing direction in the 2D plan view represent the surface distance in metres and the contour showing the resistivity values at the particular depths. There are twelve 2D plan views which represent the distribution of the resistivity values in different depths (Figure 6.17 – Figure 3.29) have been plotted.

From the resistivity results, there are two ranges of values which may be related to the contamination occurring on site.

a) The first range is less than 20 Ωm which related to the existence of anions and cations contamination (heavy metal) and inter related with existing soil moisture and any surface water. It is represented by the dark blue colour in the plan views. The distribution of the low resistivity values at first four layers (0.5m, 1.0m,1.55m and 2.16m) are slightly larger compared to others and it's mainly located at the centre of the study area (Figure 6.17 and Figure 6.20). However, the presence of this zone at the shallower surface most probably due to water log and moisture content because the heavy metal and anions analysed revealed that the surface soil is not contaminated.

b) The second range of resistivity value is between 400 and 2000 Ωm represented by the deeper layers from 2.8m up to 6.2m depth (Figure 6.21 to Figure 6.25). The low resistivity values decreased but the resistivity values range from 400 – 2000 Ωm (yellow to red colors) appearing as dominant. According to Atekwana et.al, (1998), these values are likely to represent hydrocarbon contamination in the soil. By taking these values into consideration it can be concluded that the distribution of hydrocarbon contamination in the soil layers increases in depth toward 6.2m. Referring to the 2D plan views, the hydrocarbon started dispersing from bottom right corner (southeast) in the shallow layers and slightly increasing to covered larger area toward the deeper layers. All the hydrocarbon contamination anomalies located above of the groundwater table and can be conclude occurring due to the presence of LNAPLs.

Overall, the distribution of the hydrocarbon contaminant rapidly seems to decrease when it reaches 7.3m depth (Figure 6.26) which is expected due to an interrelation with groundwater. A similar pattern occurred at the deeper layers as shown in Figure 6.27 and Figure 6.28. The groundwater as expected will lower the resistivity values as it's a good conductive medium. But the presence of the high resistivity values at the centre of the 2D views showing that the hydrocarbon still remains in that particular layers. Indeed, the similar pattern and location of the anomalies can be use as an indicator showing that the DNAPLs contamination is taking place and creating a DNAPLs pool.

The lowest resistivity values in the deeper layers surrounding the higher anomaly resistivity again indicate that the groundwater in the study area is likely to be contaminated.

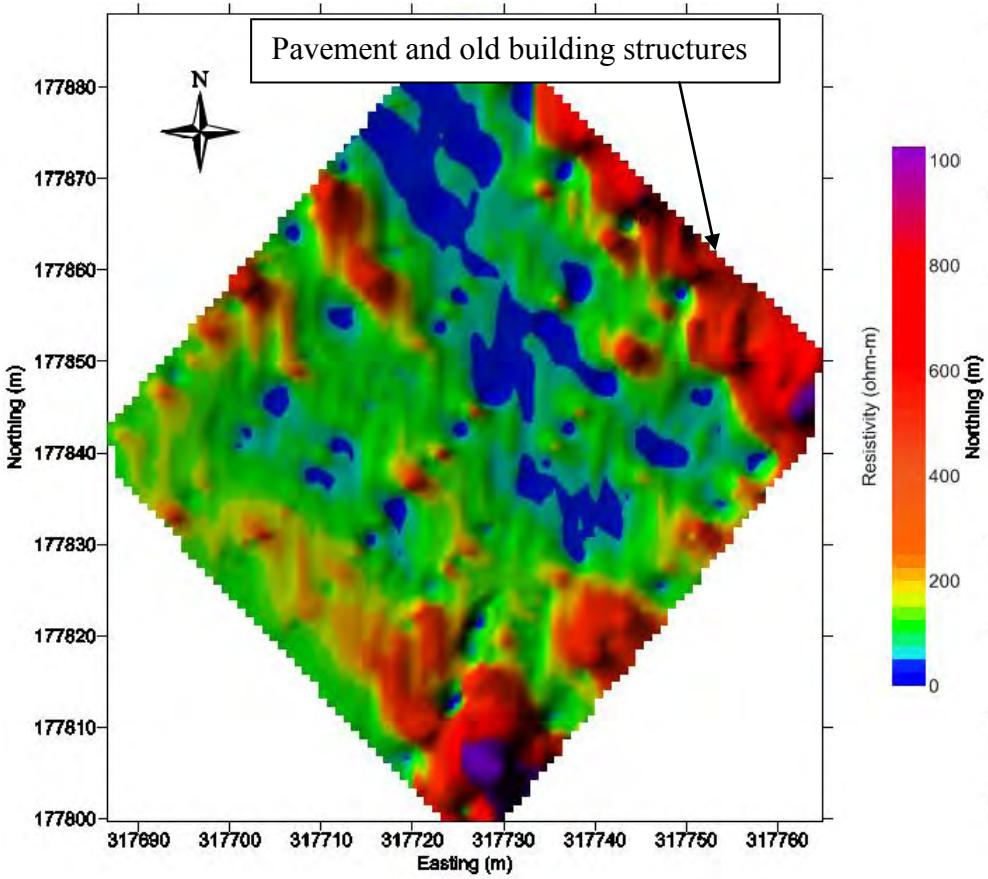

Figure 6.17: The distribution of resistivity at 0.5m depth showing a deviation of resistivity value near to the surface most probably due to the different types of the materials (foundation materials and irregular soil moisture)

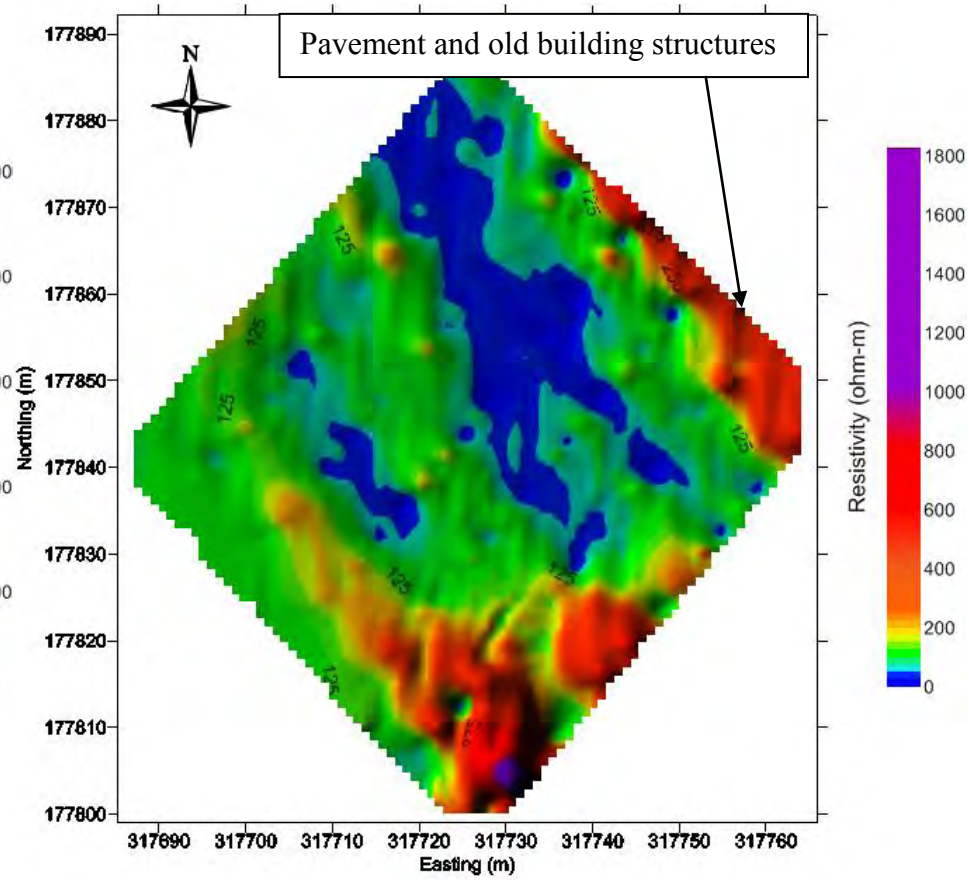

Figure 6.18: At 1.0m depth the distribution of the resistivity shows a similar pattern as 0.5m but reduced high resistivity value area probably less effect by the surface materials

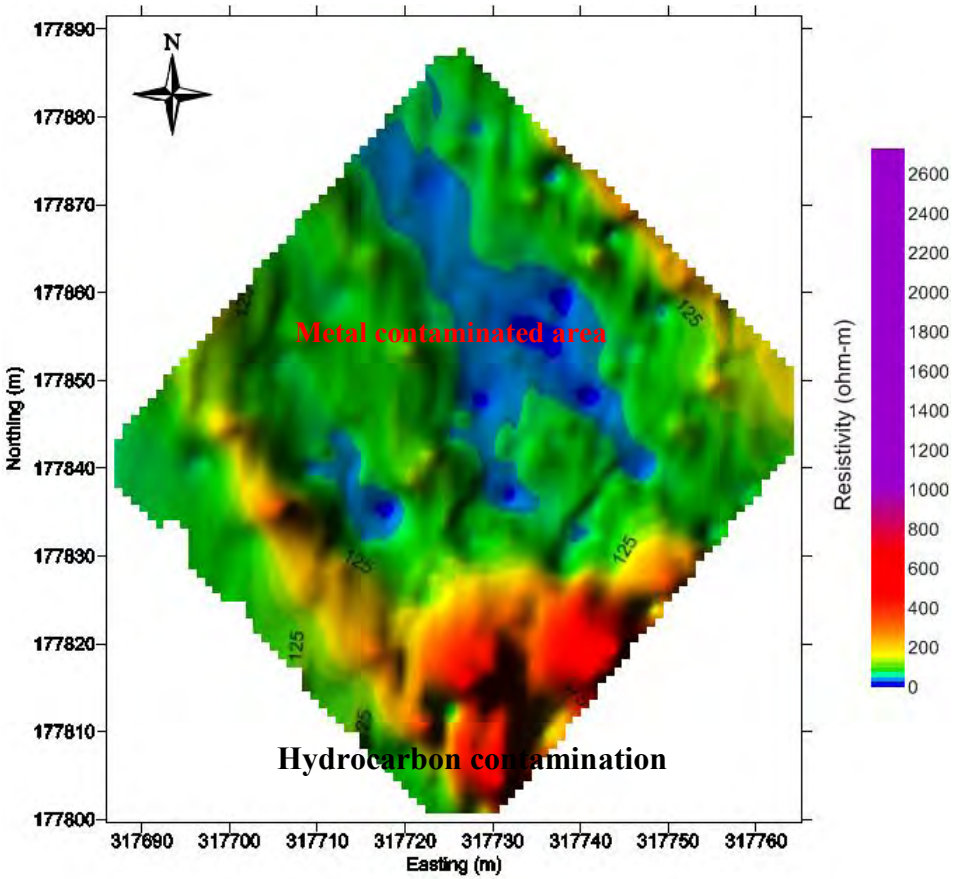

Figure 6.19: At 1.55m depth the high resistivity zone at northeast now disappears most probably due to the foundation material is placed above this layer. However at the south, the zone is getting larger and a clear lower resistivity zone presence at the middle

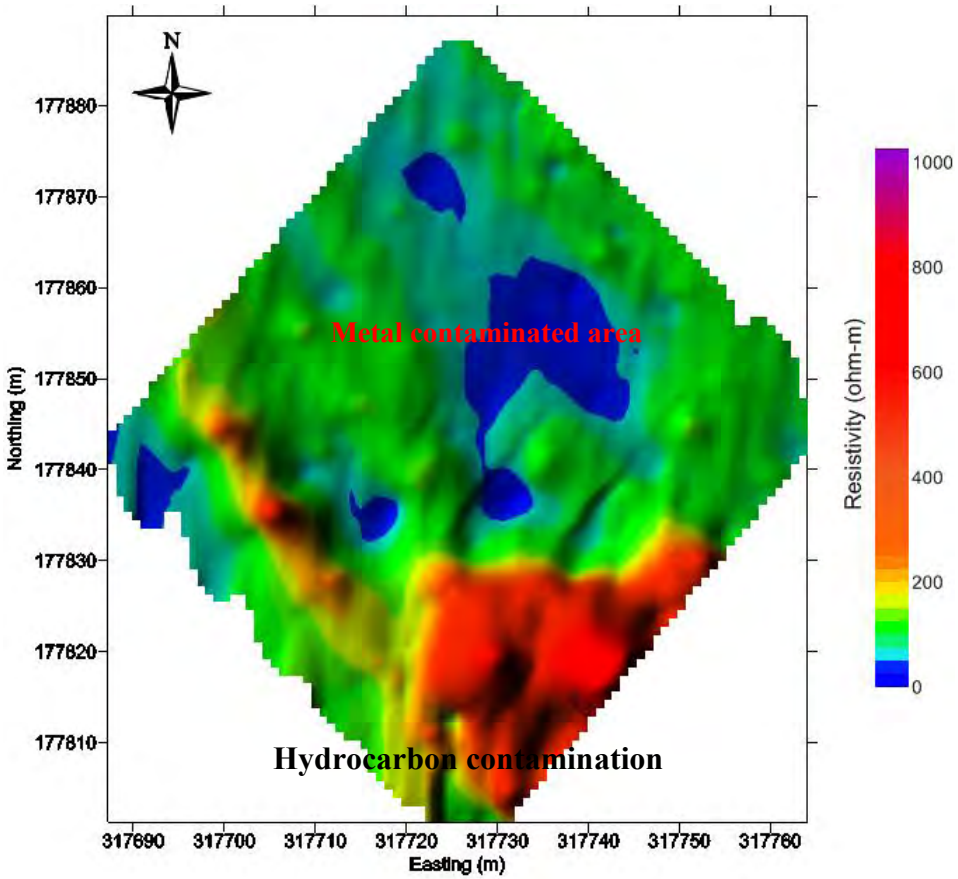

Figure 6.20: At 2.16m depth the high resistivity zone is getting clear showing that a similar material exist at this layer and keep growing up

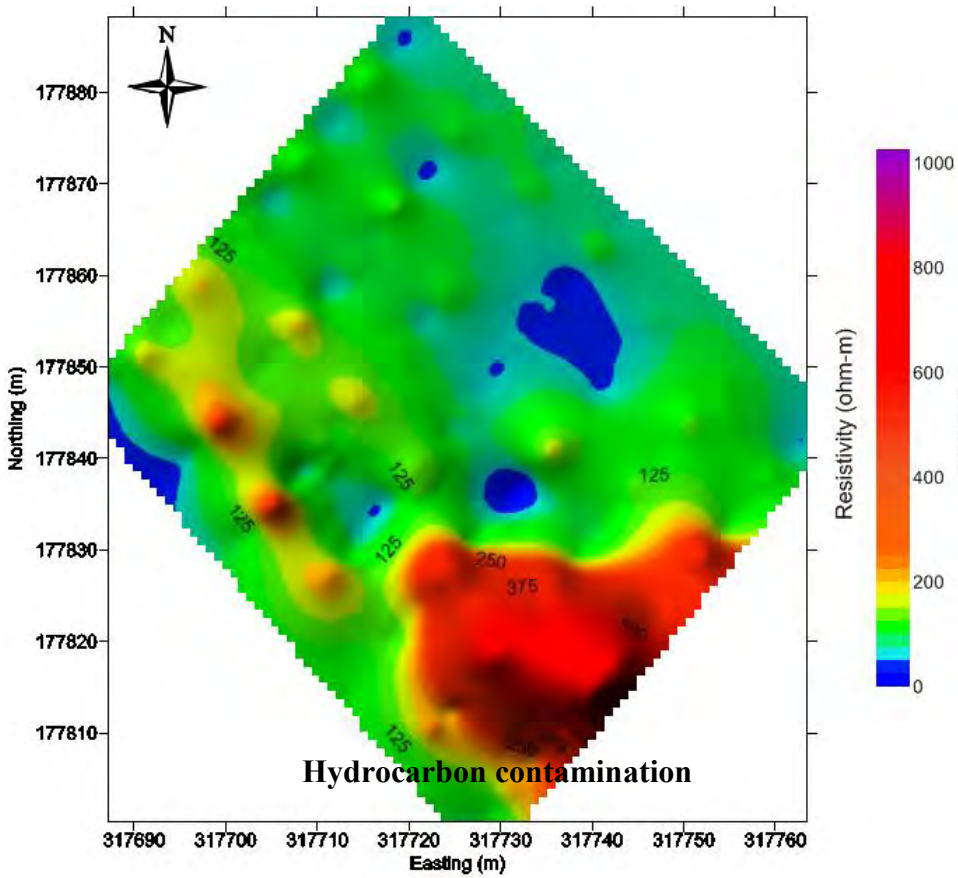

Figure 6.21: At 2.82m depth the high resistivity zone is seem maintain it pattern similarly like the above layer but almost all other area is cover by the lower resistivity between 50 – 200 (Ωm) which is interpret as a un-contamination zone (light blue – green)

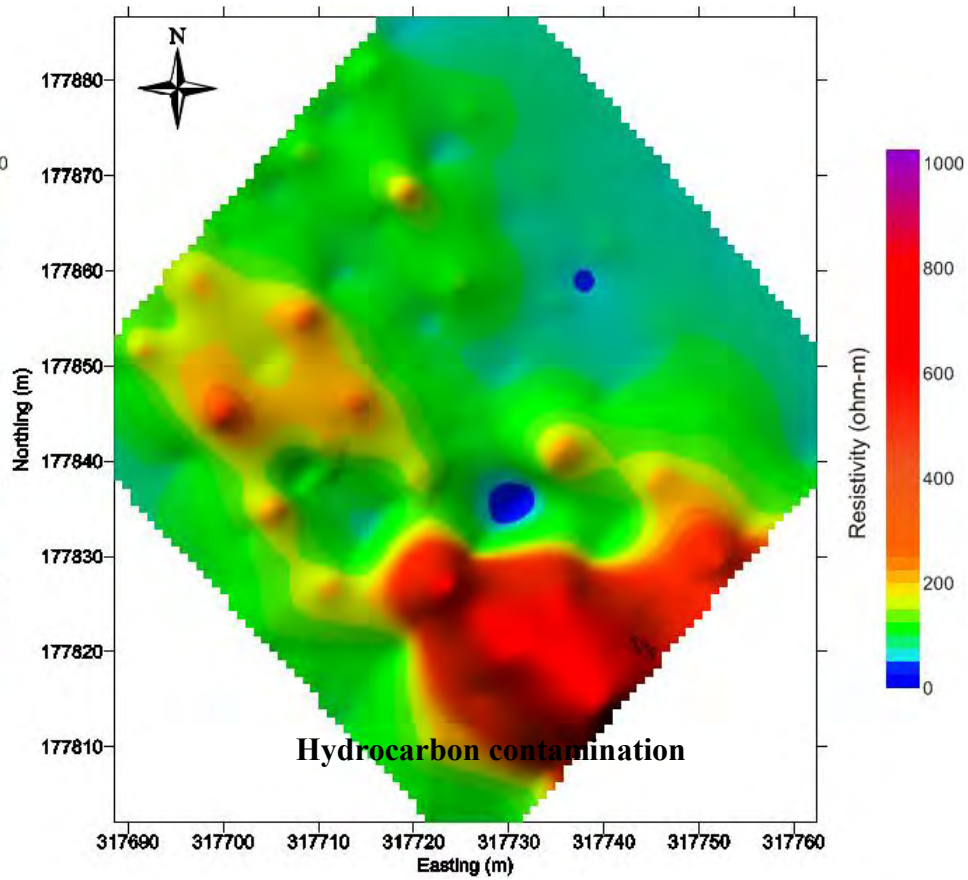

Figure 6.22: At 3.55m depth the high resistivity zone showing a similar pattern like the two above layers but slightly presence a dispersing of higher resistivity value at the northwest (merging of higher resistivity zones)

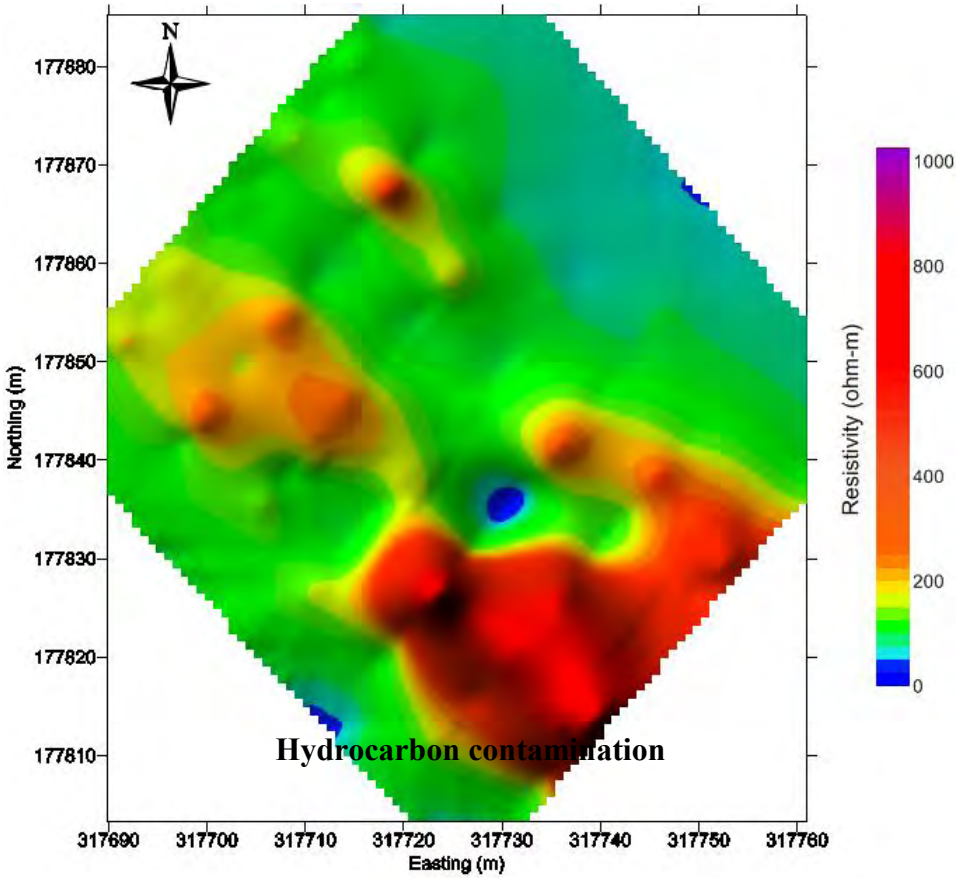

Figure 6.23: At 4.36m depth the high resistivity expending its zone to the northwest showing a merging process is taking part

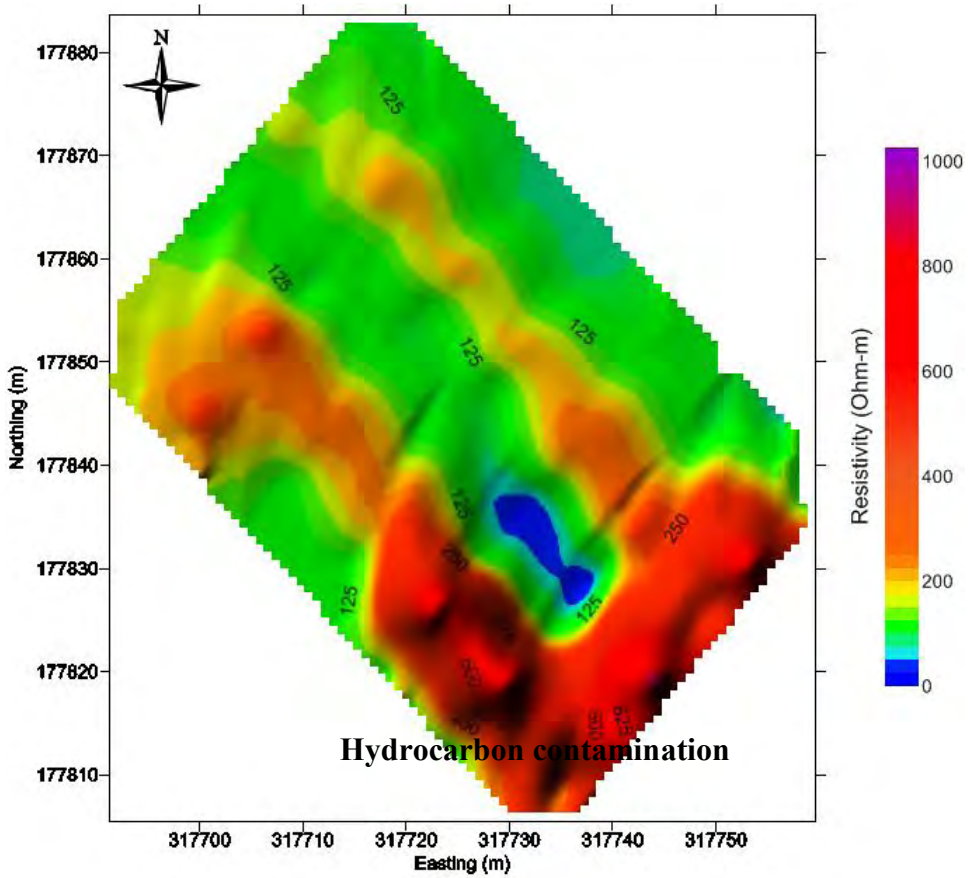

Figure 6.24: At 5.24m depth the high resistivity zone is expending

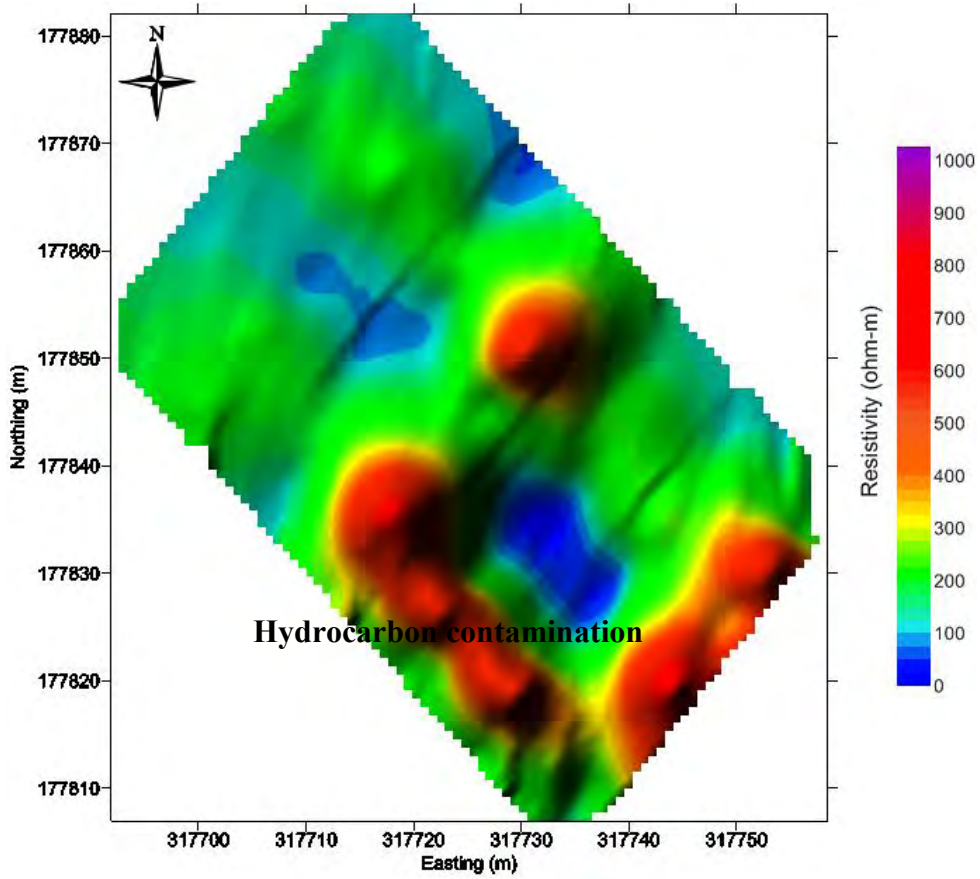

Figure 6.25: At 6.22m depth, most probably the DNAPLs now are precipitated onto the top of the bedrock or a place on the un-permeable layer to start forming a DNAPLs pool at 7.2897m depth

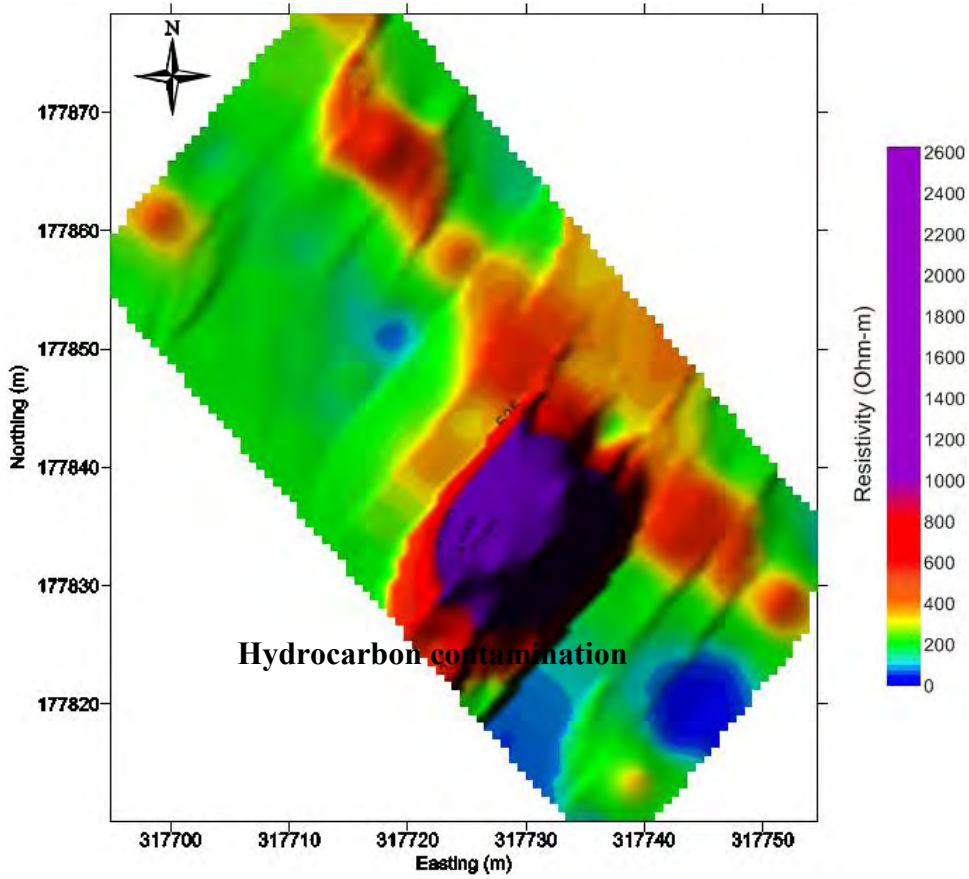

Figure 6.26: This layer (7.29m) is supposed to be under the groundwater table and the high resistivity zone surrounding by the lower resistivity and interpret due to presence of the DNAPLs (it density is higher than water)

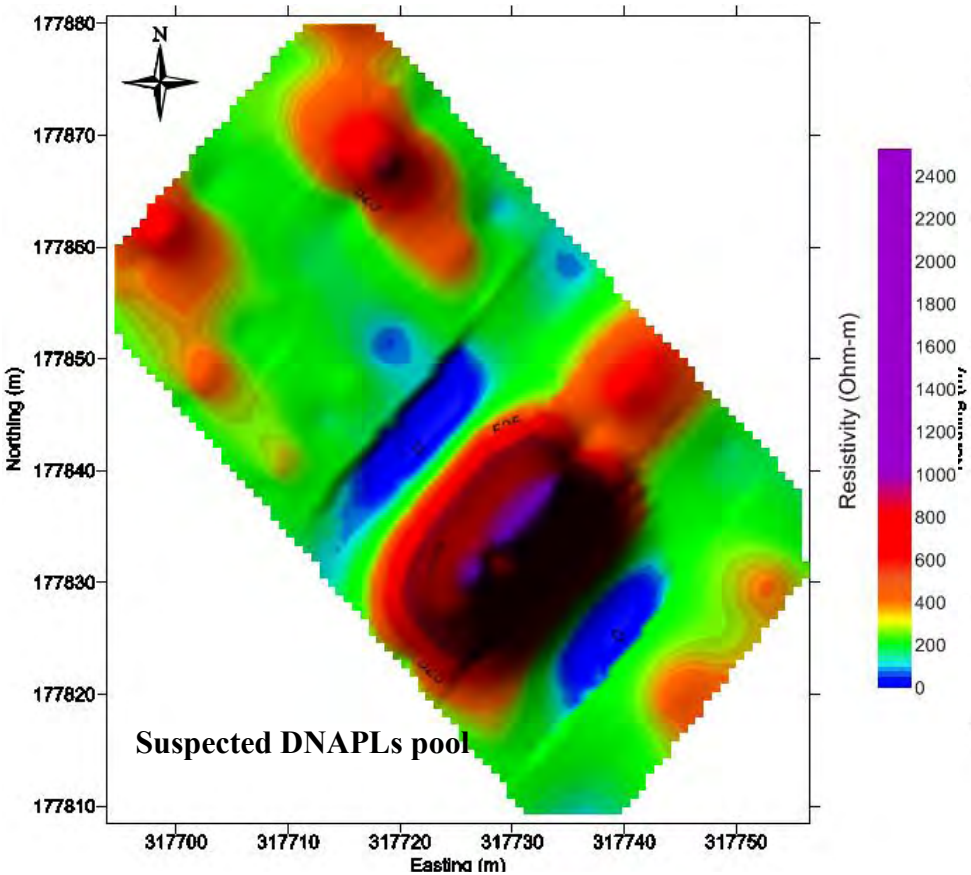

Figure 6.27: At the deeper layer (8.47m) showing a reducing of size the high resistivity zone

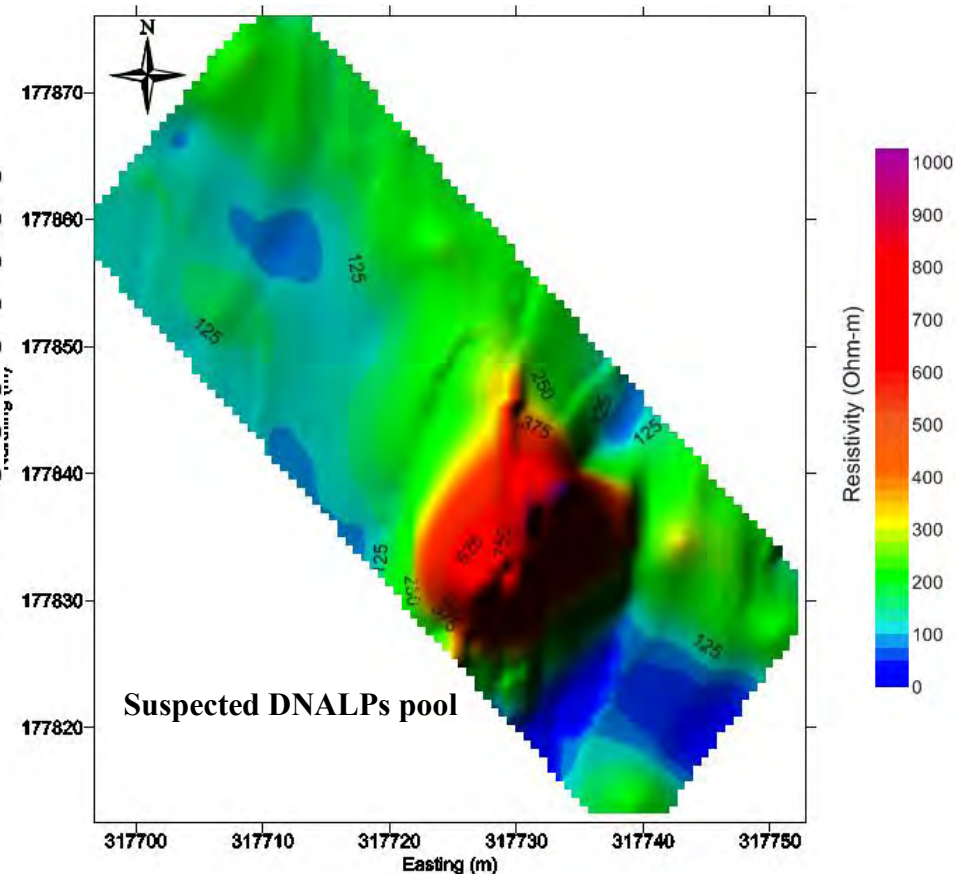

Figure 6.28: The continuously reduction of the high resistivity zone and built an island pattern which is interpret as a DNAPLs pool under the groundwater table and at the top of bedrock or un-permeable layer (9.77m depth)

6.3.3 GEM results

Five electrical conductivity plan view layers have been plotted, representing different electromagnetic wave frequencies used on the site. In this study, the higher frequencies represent the electrical conductivity near to surface which can be correlated with the distribution of the soil chemical composition present on the site.

The distribution of the conductivity is shown in the plan views are presented in log scale unit. For the interpretation the contour ranges can be divided into 5 particular ranges as shown in Table 6.4 below.

Table 6.4: Ranges of the values for the GEM-2 data interpretation

	Log scale	Conductivity (mS/m)	Resistivity (Ωm)	Potential materials
1	Less than -0.3	Less than 0.5	More than 2000	Vadose zone, pavement, building material and bedrock
2	-0.3 to 0.4	0.5 – 2.5	2000 – 400	Potentially has a hydrocarbon contamination
3	0.4 to 1.0	2.5 – 10	400 – 100	Surface materials, uncontaminated and bit dry. It also represents a fresh water / groundwater
4	1.0 to 1.7	10 – 50	100 – 20	Ground is slightly contaminated most probably due to the existing of the metals into the ground
5	More than 1.7	More than 50	20 - 0	Contamination ground or layer

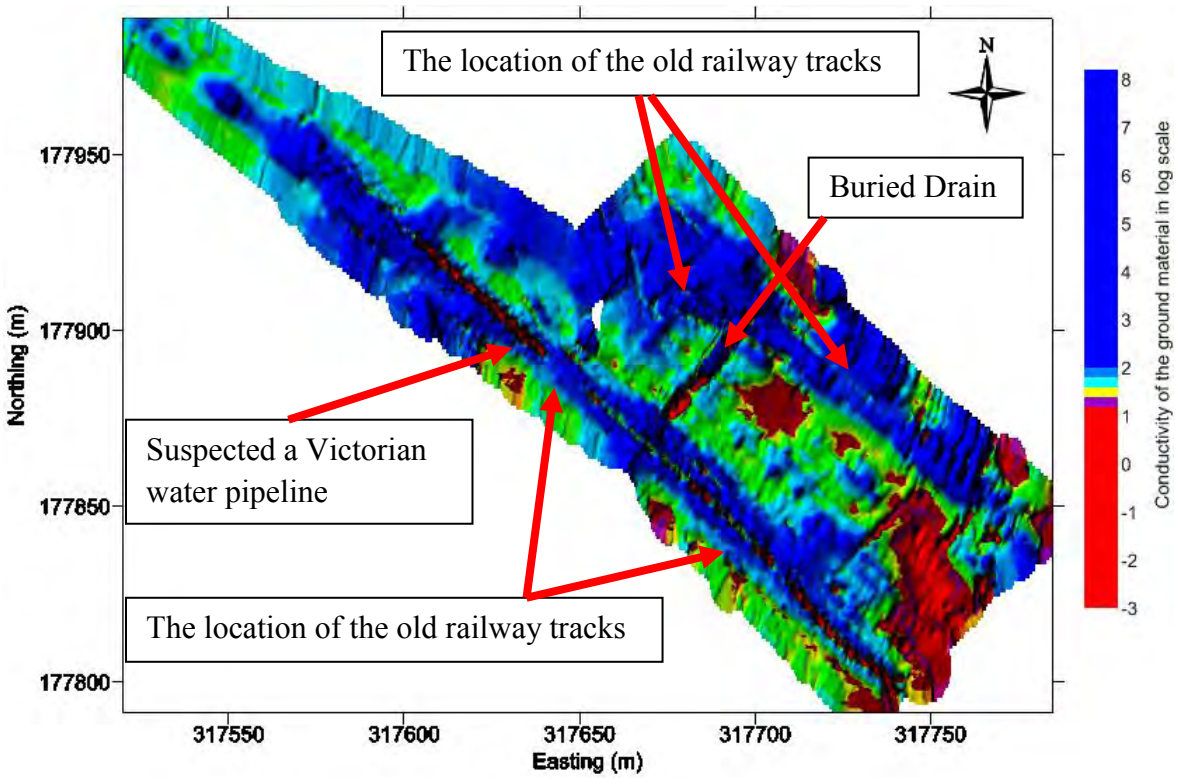

Figure 6.29: The distribution of the electrical conductivity from the 47025Hz electromagnetic frequency survey

The 47025Hz frequency shown in Figure 6.29 is represents the conductivity of the shallower layer. There are four observations can be make using the information from the conductivity map above.

i) Clearly the contaminated areas are plotted by the blue colour which has conductivity more than 50 mS/m or less then 20Ωm converted to resistivity. It generally generates a unique pattern by following an old railway tracks layout as seen in the northeast and southwest of the map.

ii) The figure represents a shallower layer, the higher conductivity which is representing by red colour is likely due to the existing structures, foundation and the drains.

iii) The other colours represent uncontaminated areas where the location is at the middle of the study area. It's expected to be there due to fewer activities in the past and hasn't been built with the railway structures.

iv) A very obvious observation is a long straight line lower conductivity or higher resistivity anomaly suspected to be generated by an old Victorian pipeline as shown in the figure

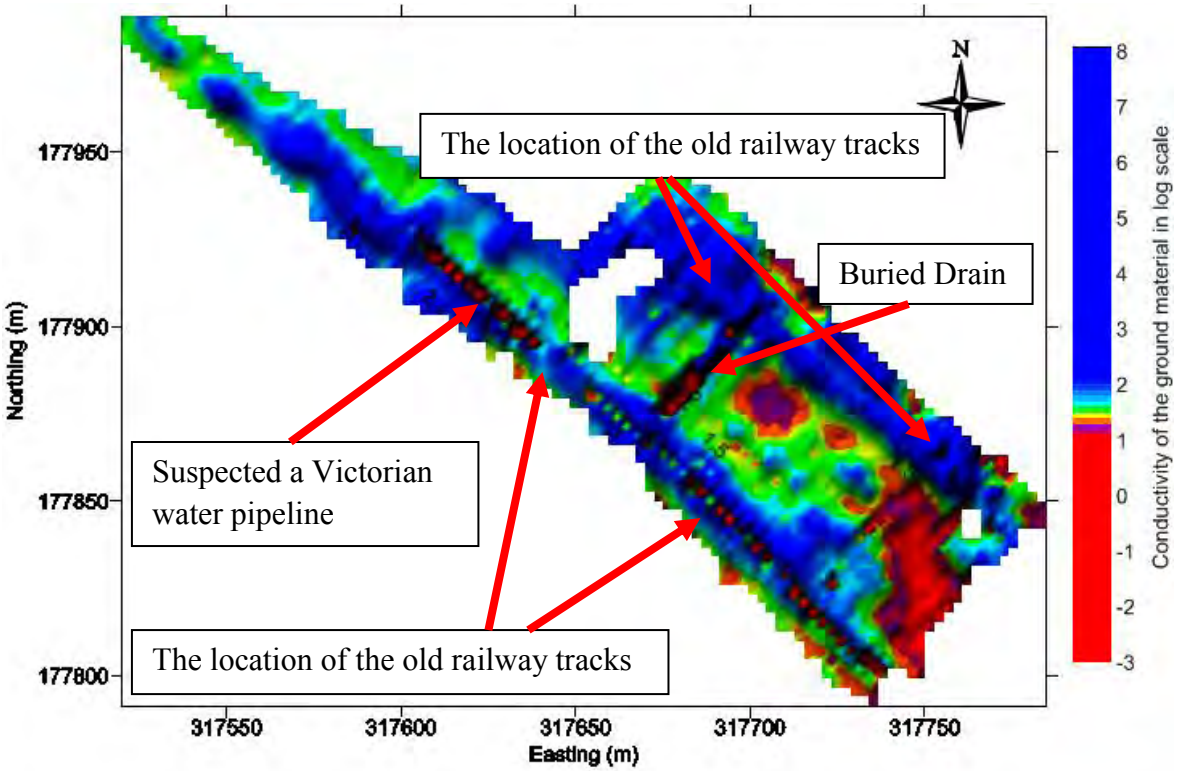

Figure 6.30: Showing conductivity dispersion on the site generated by the 30025Hz electromagnetic frequency GEM-2 survey

The conductivity of material in the deeper layer is showing in Figure 6.30. The distribution pattern is remaining as show in the upper layer (Figure 6.29). Even this is continuing to the deeper layers represented by the lowest GEM-2 electromagnetic frequencies in Figure 6.31 (15025Hz) and Figure 6.32 (5125Hz). However, in the Figure 6.32 the lower conductivity areas are slightly larger which can be interpreted as two possibilities.

a) First possibility is the presence of the bedrock where the study area has about 7m depth of the weathered bedrock which can generates a lower conductivity layer

b) Second possibility is the presence of the HC in the soil layer which also can generates a lower conductivity or higher resistivity

In the deepest layer, represented by the 975Hz electromagnetic wave frequency (Figure 6.33), the output signals are weaker with high noise levels so that data obtained is not discussed.

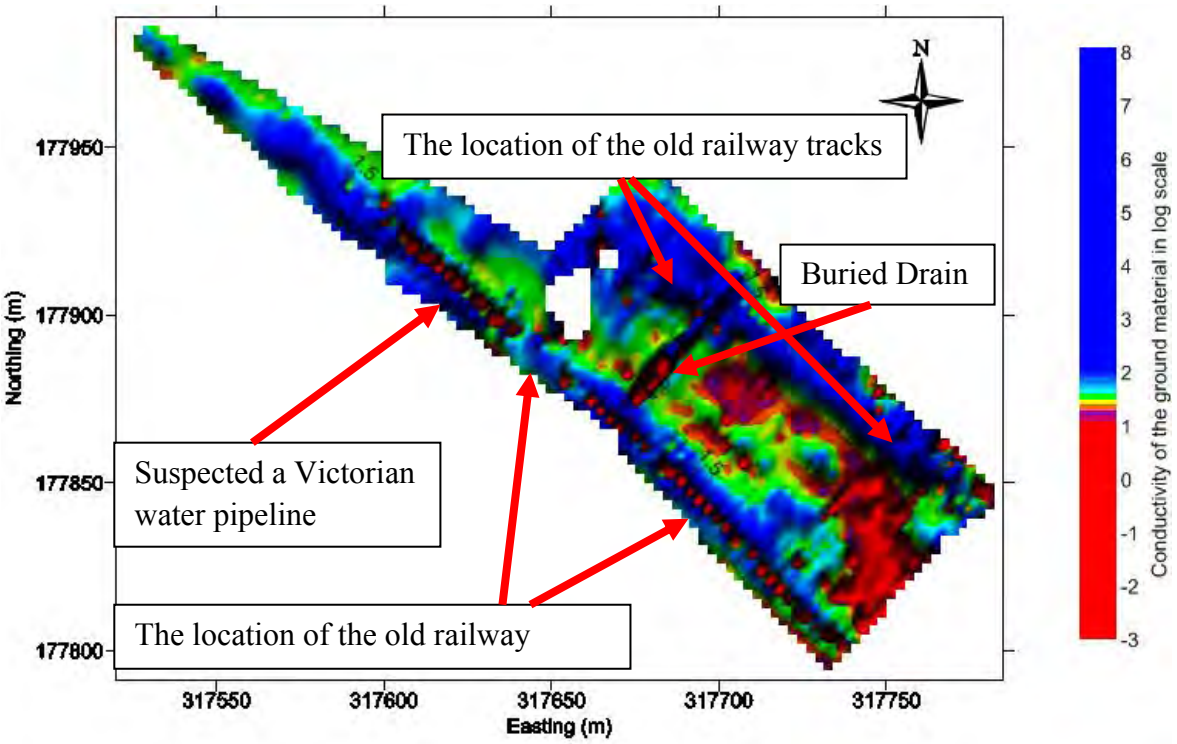

Figure 6.31: The conductivity distribution of the layer generated by the 15025Hz electromagnetic frequency showing the pattern is still remain as the above layers

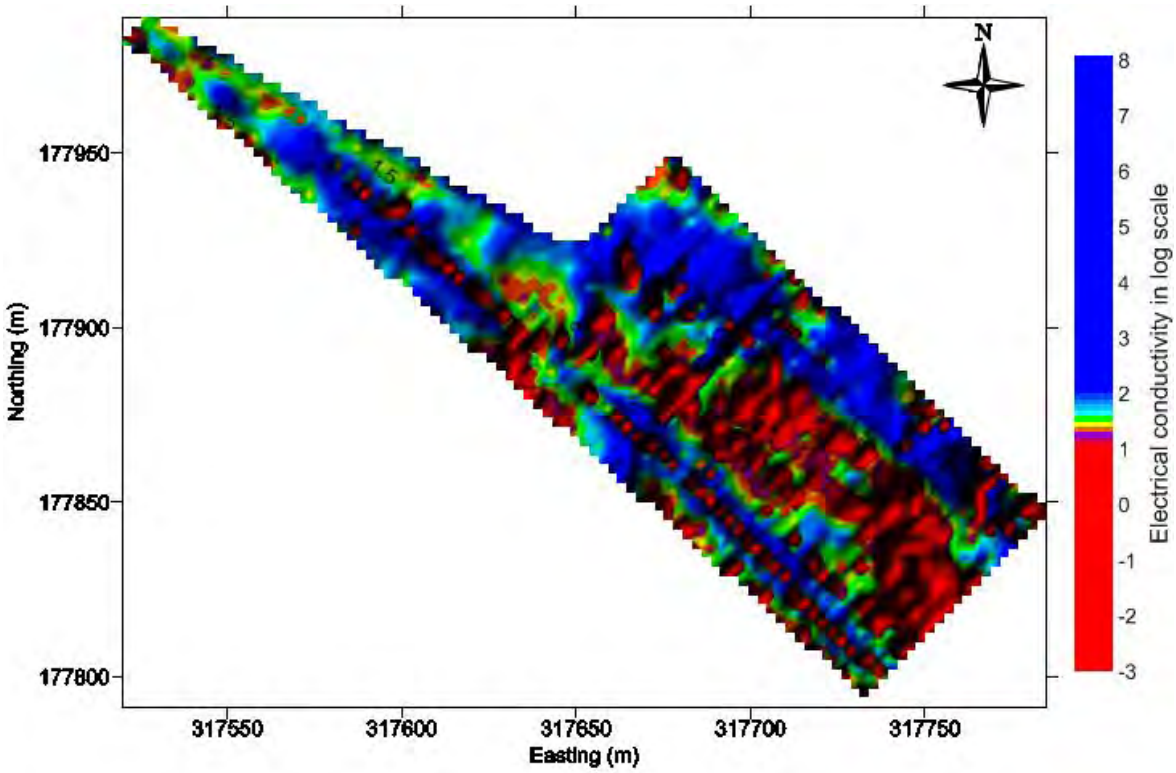

Figure 6.32: The conductivity distribution of the layer generating by the 5125Hz electromagnetic frequency showing the pattern is still remain as the above layers

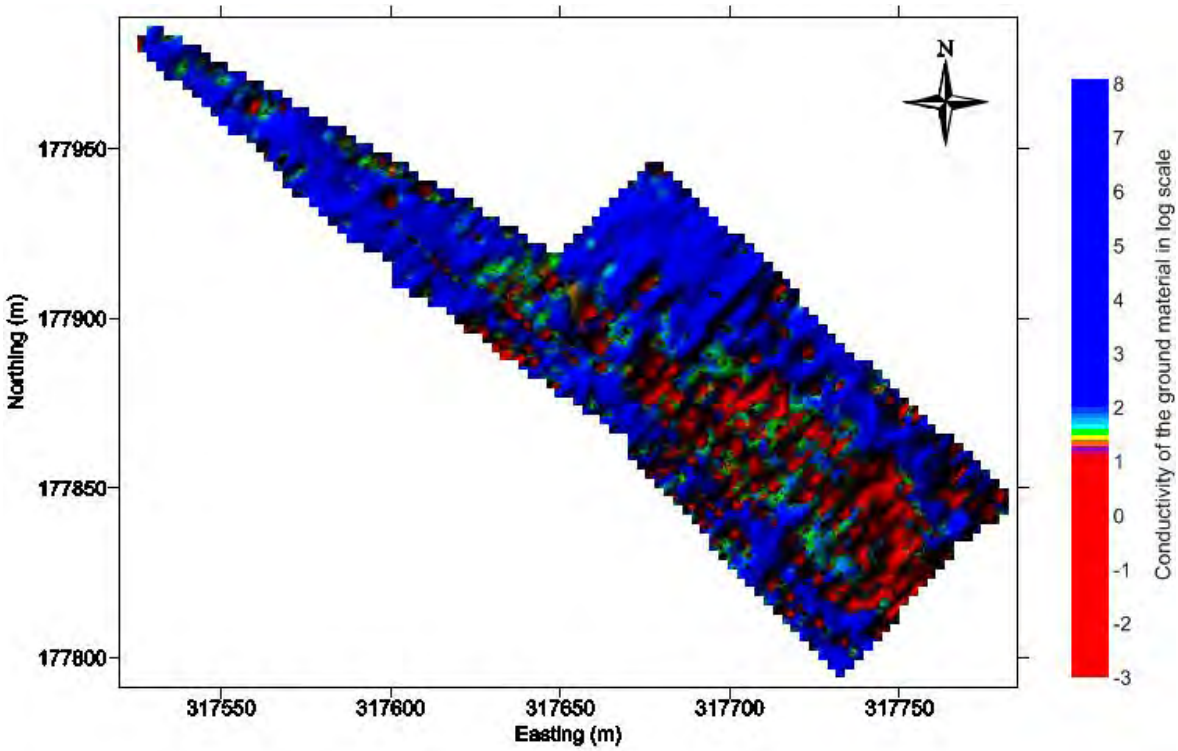

Figure 6.33: The conductivity distribution of the layer generating by the 975Hz electromagnetic frequency showing the signal is noisy and weaker

6.4. Combination of research outputs

This study revealed there are possible qualitative correlations that can be established between geochemical and geophysical results. The correlation had been done for the top soil layer due to limitation of geochemical information which is only provided by the surface soil samples. The resistivity information used for correlation only at 0.5 to 1.0m depths (from the 2D plan view) and the GEM-2 survey were included the electromagnetic wave with a frequency of 47025Hz (given the information for shallower layer).

A total amount of the cations and anions has been used in a comparison with the geophysical results. Generally a good correlation between them has been observed in the shallower layer as shown in Figure 6.34. Listed here are some of the observations:

a) There are three high density zones of the chemical components which have been found, showing by the black circle on the map (Zone 1, Zone 2 and Zone 3)

b) These zones are present as a lower resistivity zones in 2D view resistivity plot which is expected as the chemical elements will decrease the resistivity of the material. However only two zones have a clear correlation with the chemical distributions (Zone 1 and Zone 2). While the Zone 3 doesn't have a good correlation as it showing a medium resistivity value (100 – 200 Ωm) in the higher amount of chemical compound

c) In the 2D resistivity profiles, Res 1 and Res 2 show a good correlation with the chemical dispersion on the site. Considering it only uses the near surface resistivity value, all those three zones can be seen clearly in those two profiles. Regardless, in the Res 6 profile, which has two clear zones of high chemical composition, only Zone 1 can be observed in the resistivity profile.

d) The electromagnetic survey results showing an excellent correlation with the chemical dispersion in the site. All three zones are clearly present on both maps

Similar results also can be seen in the deeper (1.0m depth) resistivity 2D view plot (Figure 6.35). The third zone seems to get clearer in this plot compared to the uppermost layer (0.5m depth).

6.5 Conclusions

Overall, a geochemical approach had been successfully used to plot the distribution of the anions and cations at the study area. Based on soil quality standards from Kelly Indices, ICRCL 59/83, Dutchlist and latest Environmental Agency standard for Soil Guideline Values, the top soil at the study site was not legally contaminated. This study also revealed that the geophysical techniques can be used together with geochemistry as there is a significant relationship and the results obtained from those techniques which have a qualitative correlation.

i) The higher concentration of the chemical composition will produce a lower resistivity zone which can be detected by the Resistivity Imaging technique which can be plotted by 2D profiling and using a modified 2D plan view using Surfer 9.

ii) While the Ground Electromagnetic Survey (GEM-2 survey) also found that a higher amount of chemical composition can be detected by correlation with a higher conductivity zone on a 2D plan view map

However the correlations are subject to the very near surface materials only (up to 1m depth) and cannot be extended into the deeper geological layers as shown in resistivity profiles. In the geophysical investigation, the data interpretation cannot be related to the deeper geological properties in the site in any detail due to the lack of borehole data at the area. The only information for deeper geological layers was obtained from a single borehole which is located 200m from the study site close to the Cardiff University Optometry Building. Further detail investigations should be done to validate the information provided by the geophysical technique against the pre-industrial natural geology

At this site also, unfortunately the hydrocarbon analysis had not been undertaken due to the lack of University facilities and the high cost of commercial analyses.

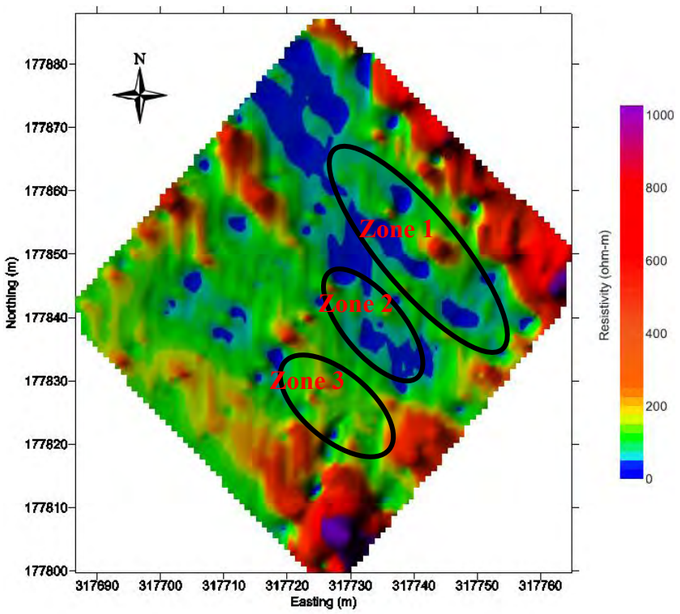

Resistivity 2D plan view at 0.5m depth

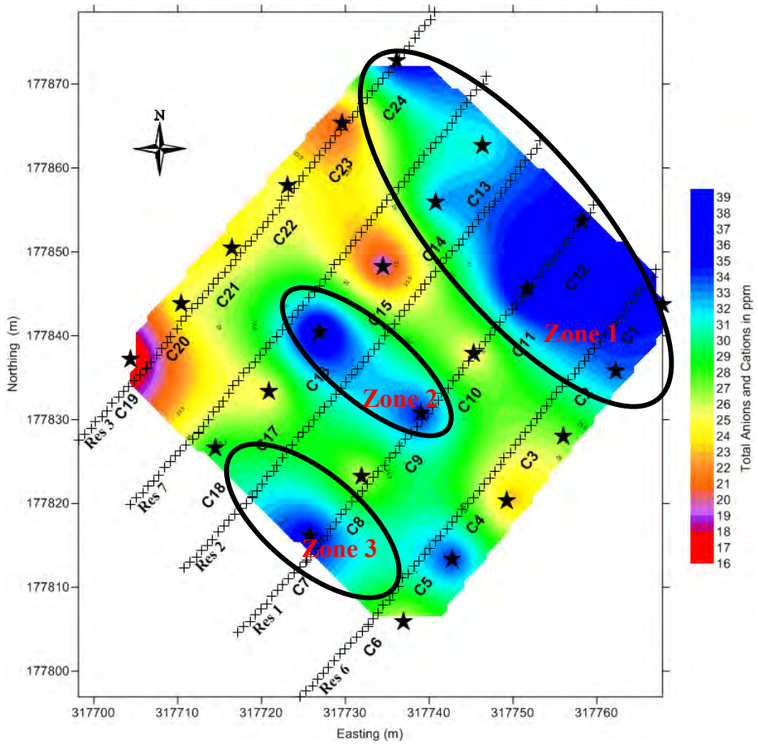

Total anions and cations distribution

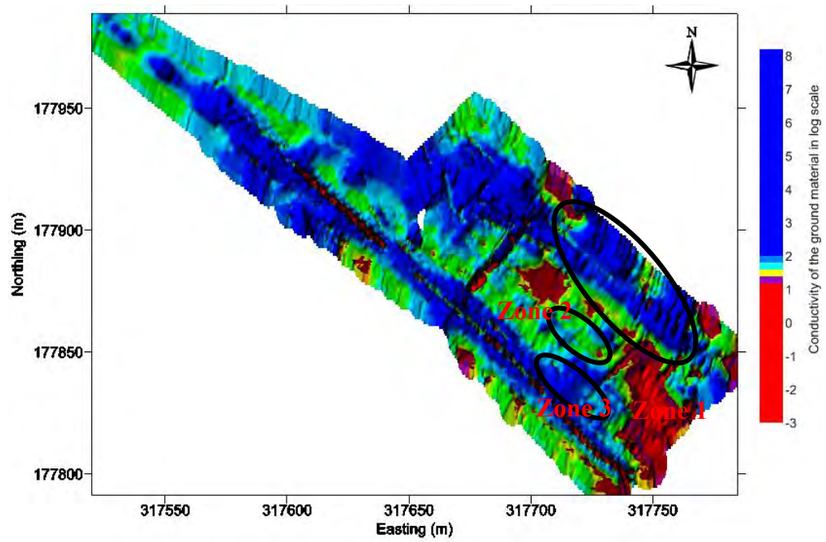

Conductivity of material from the 47025Hz frequency GEM-2 survey

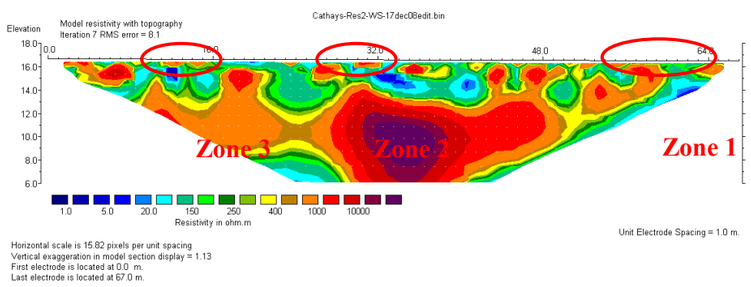

Res 2 line

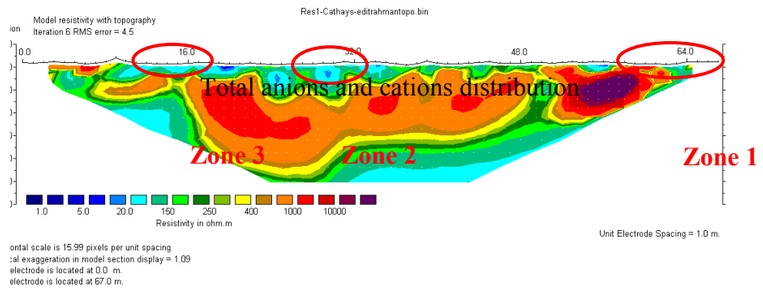

Res 1 line

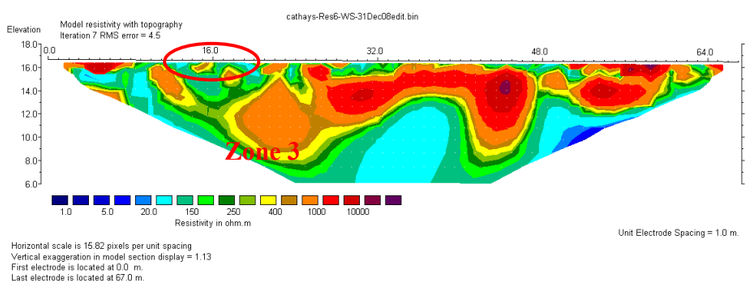

Res 6 line

Figure 6.34: The correlation between the geophysical data and the total elements distributions at 0.5m depth

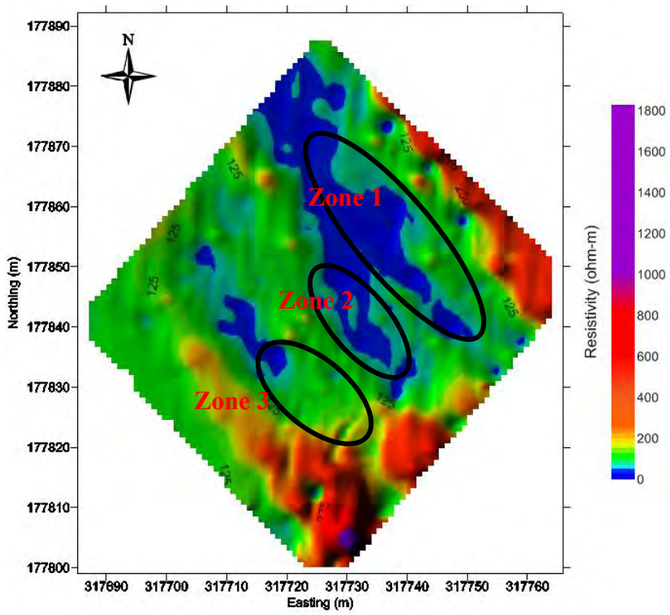

Resistivity 2D plan view plot at 1.0m depth

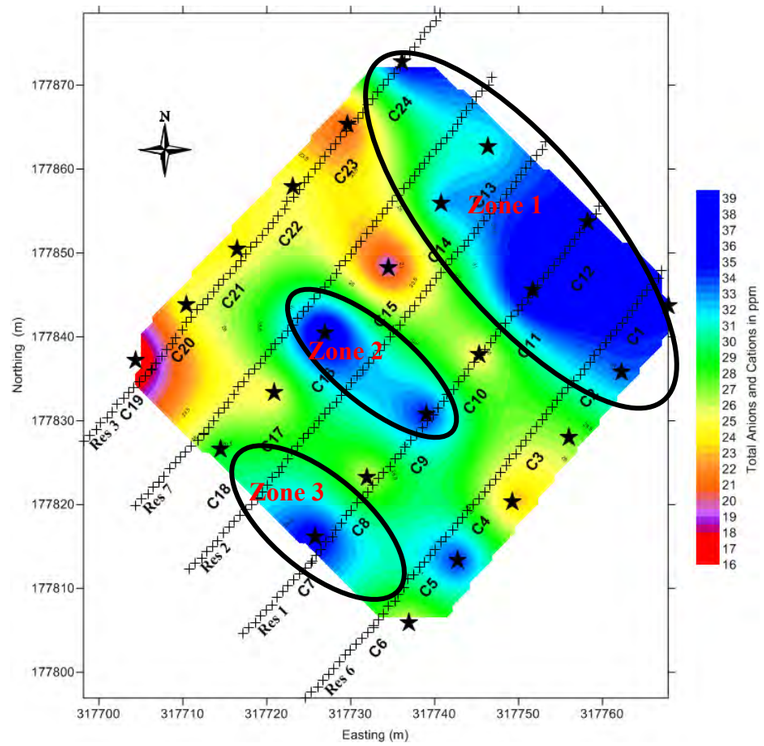

Total anions and cations distribution

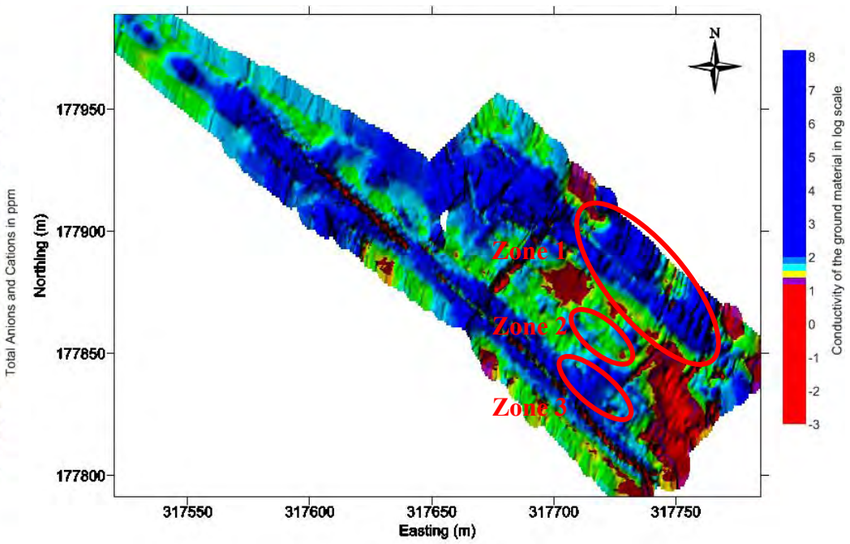

Conductivity of material from the 47025Hz frequency GEM-2 survey

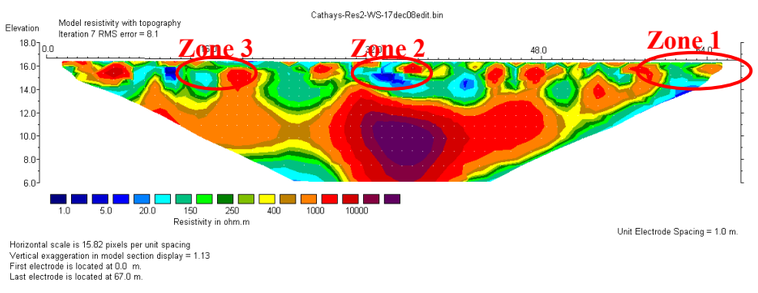

Res 2 line

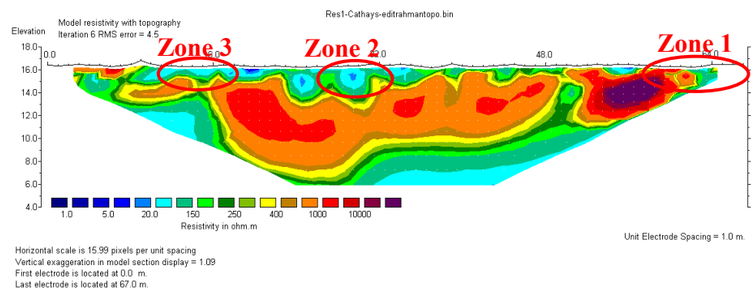

Res 1 line

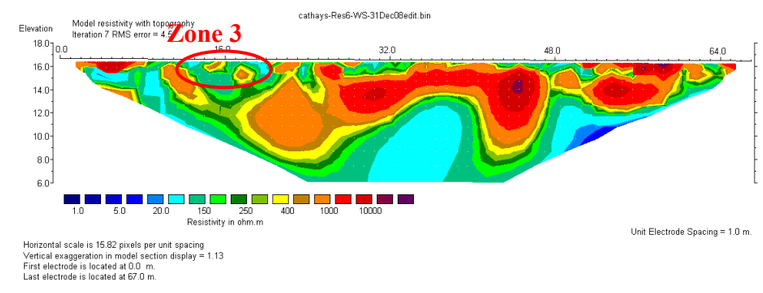

Res 6 line

Figure 6.35: The correlation between the geophysical data and the total elements distributions at 1.0m depth

CHAPTER 7
RESULTS AND INTERPRETATION
CASE STUDY II: WESTON SUPER-MARE GASWORKS STATION

7.1 Introduction

This chapter is a discussion of the investigations and results from the study site at Weston-Super-Mare. As previously stated, the site is the former town gasworks and the on-site contamination are expected to come from the waste produced by its past activities, this includes both heavy metals and hydrocarbons. The results and interpretation will be discussed in three parts; which include the Soil Vapour Survey technique (SVS) which is used to detect hydrocarbons in the soil, the E/M geophysical survey (GEM-2 ground conductivity surveys) and the Resistivity Imaging Technique.

The SVS is used to measure the amounts of Methane, CO2 and TPH gases in the soil layer. The distributions of these gases will indicate the amounts and location of hydrocarbon contamination. The results are displayed in 2D plan view using Surfer 9 software. The geophysical data are used to map the distributions of Electrical Conductivity of the soil layer which can be linked to the distribution of gases from the SVS. Due to the fact that the SVS only measures at less than a metre depth, corresponding shallow depths of EC and resistivity data will be used in correlations. The heavy metals data are not included in this report as this study concentrates on the interrelation between gas released from ground and the measured geophysical properties of the ground materials.

7.2 Aerobic and anaerobic biodegradation

When discussing the biodegradation of hydrocarbons, aerobic and anaerobic activities are the important processes involved. According to the USGS (2011a) - **Web 7.1**, ***Aerobic biodegradation*** is the breakdown of organic contaminants by microorganisms when oxygen is present. In the same web also stated that the aerobic biodegradation also is known as aerobic respiration. In an aerobic biodegradation, micro-organisms convert oxygen to water in the process of transforming other components into simpler products.

Aerobic Respiration - "The process of destroying organic compounds with the aid of O_2 [oxygen] is called aerobic respiration. In aerobic respiration, microbes use O_2 to oxidise part of the carbon in the contaminant to carbon dioxide (CO_2), with the rest of the carbon used to produce new cell mass. In this process the O_2 gets reduced, producing water. Thus, the major by products of aerobic respiration are carbon dioxide, water, and an increased population of micro-organisms." - National Research Council, 1993 (**Web 7.1**)

Anaerobic Biodegradation - "The degradation of compounds by microorganisms in the absence of oxygen". - National Research Council, 1994 (USGS, 2011b) - **Web 7.2**.

Anaerobic Respiration - "In anaerobic respiration, nitrate (NO_3^-), sulfate (SO_4^{2-}), metals such as iron (Fe^{3+}) and manganese (Mn^{4+}), or even CO_2 can play the role of oxygen, accepting electrons from the degraded contaminant. Thus, anaerobic respiration uses inorganic chemicals as electron acceptors. In addition to new cell matter, the by-products of anaerobic respiration may include nitrogen gas (N_2), hydrogen sulfide (H_2S), reduced forms of metals, and methane (CH_4), depending on the electron acceptor." - National Research Council, 1993 (**Web 7.2**)

7.3 Contamination background on the site

Widespread contamination associated with the former gasworks is located across the site, including Zones A and B. Remediation has been undertaken in the northern part of the site, and is now currently used as a hub site for an engineering firm conducting pipe replacement works (Parsons Brinckerhoff, 2010). It is known that some structures associated with the former gasworks process existed outside of the current site boundaries; there is therefore potential for considerable offsite contamination to be present, as it is not known what, if any, remediation work was undertaken in these areas prior to the sites current redevelopment.

Significant contamination is alluded to in the survey area. Figure 7.1 shows photographs from TP110, displaying the presence of free phase coal tar in the trial pit (Parsons Brinckerhoff, 2010). A copy of the borehole log is also shown, indicating the presence of possible hydrocarbon based contamination in the trial pit. In TP110, a black sandy silty ash material is found between 0.8 – 1.5mbgl; similar ground conditions are found between 0.8 – 1.9mbgl in TP111. Both pits have hydrocarbon odour, and TP111 also

contains deposits of spent oxides, and ferrous tar staining (Parsons Brinckerhoff, 2010). Below 1.5mbgl in TP110, made ground comprising of firm black and grey clay is present. Tar pockets are found throughout the material, along with fragments of wood. A strong hydrocarbon odour is present, and free phase tar is found mixed with perched groundwater. The visual and olfactory evidence of contamination, along with the suspicion of a possible wooden tank found in TP110 prompted the subsequent investigations on the site.

All noted contamination and buried structures that may be associated with contamination presence on the site are found within the made ground (Parsons Brinckerhoff, 2010). Table 7.1 shows the types of contamination present in which trial pits, and at the depths found.

Table 7.1: Contamination data synthesised from the Environmental Assessment Supplementary Site Investigation Report (Parsons Brinckerhoff, 2010)

Trial Pit No.	Contaminant (depths present)					Buried Structure
	Spent Oxide	Ash	Tar	Clinker	Hydrocarbon Odour	
TP101	-	-	-	-	-	Buried structure at 1.00mbgl
TP102	0.6 – 0.7 and 0.8 – 1.15mbgl	-	-	-	-	-
TP103	-	0 – 0.55mbgl	-	0 – 0.75mbgl	0 – 0.75mbgl	-
TP104	0.5 – 1.1mbgl	-	0.5 – 1.1mbgl	0.5 – 1.1mbgl	0.5 – 1.1mbgl	-
TP105	-	-	-	-	-	-
TP106	-	-	-	0 – 0.9mbgl	0 – 0.9mbgl	-
TP107	-	-	-	0 – 0.95mbgl	0.7 – 0.95mbgl	-
TP108	-	0.8 – 1.2mbgl	-	0 – 1.2mbgl	-	-
TP109	-	-	-	-	-	Hardstanding at ~0.6mbgl
TP110	-	0.8 – 1.5mbgl	1.5 – 2.4mbgl	0.8 – 1.5mbgl	0.8 – 2.4mbgl	Possible wooden tar tank at 1.6mbgl
TP111	0.8 – 1.9mbgl	-	-	0 – 0.8mbgl	0.8 – 1.9mbgl	-
TP112	-	-	-	-	-	-

Trial Pit 110 (TP110)

As previously mentioned, Trial Pit 110 (TP110) is the location where the free phase tar was found on site (Figure 7.1). The free phase tar was found at a depth between 1.50m and 2.40m and it is believed to originate from an old Victorian age wooden tank buried at that location. It is located within Zone A of the study area. Two resistivity lines (RES 1 and RES 2) were carried out crossing the trial pits (Figure 7.2) and a gas station point number G69 was sampled on the top of it.

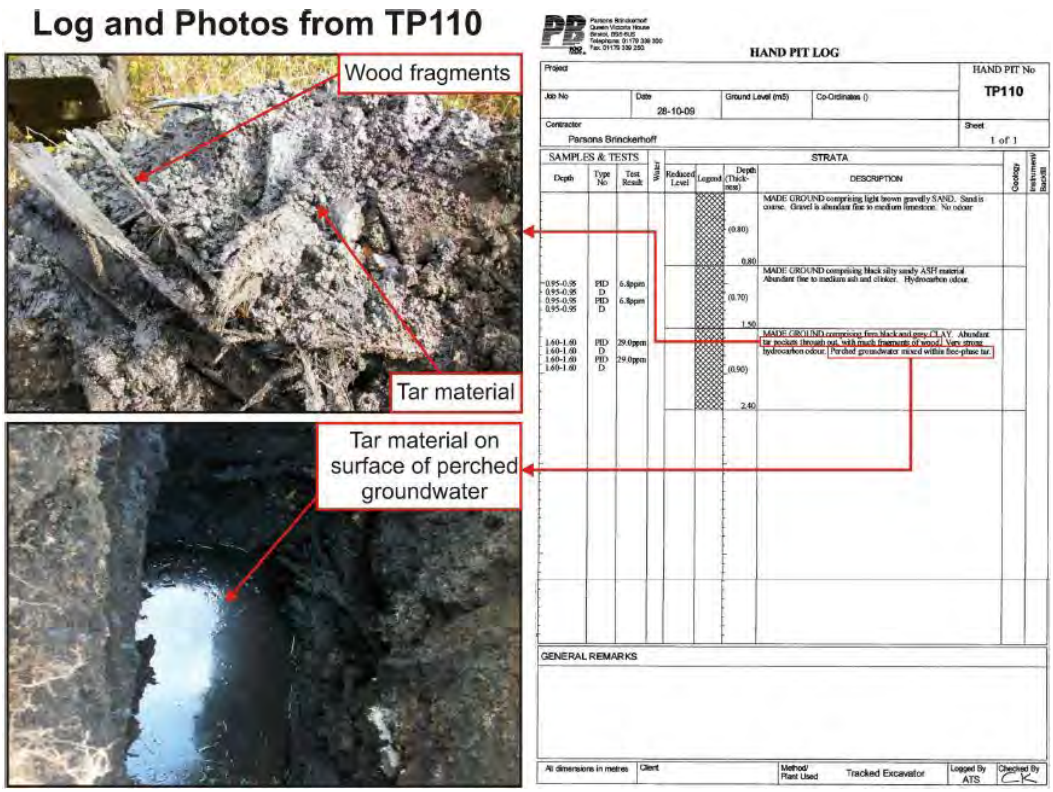

Figure 7.1: The log and a photo of trial pits (TP110) showing the presence of the free phase tar on the perched water surface (Source, Whiteley, 2010)

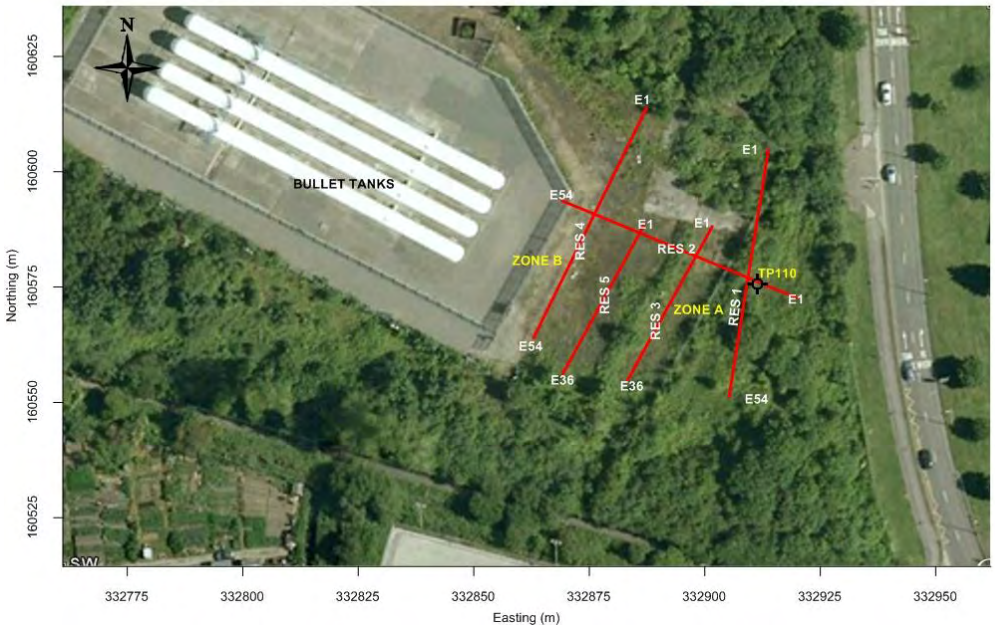

Figure 7.2: The location of trial Pit (TP110)

7.4 Gas analyser results

In the SVS survey, methane, CO_2 and TPH (Total Petroleum Hydrocarbon) are measured. Generally, the amount of Methane and CO_2 are related to the biodegradation activity of the hydrocarbons. The geology is formed of superficial deposits and sandy Tidal Flood Deposits which may give a lower organic compound that will contribute less to the release of the methane and CO_2 from the ground. By assuming the methane and CO_2 are released from the decay of hydrocarbons, (whether from spills or from the leaking of wooden storage tank) the distributions of both in the soil will be correlate with the TPH distribution, which depends on the distribution of petroleum products on the soil. In total 128 gas sampling points were used in the site survey.

7.4.1 Total Petroleum hydrocarbon gases (TPH)

High elevated TPH gases were recorded near to TP110 with a maximum value recorded of 14242 ppm at gas measurement point G69 (on top of TP110). The high distribution of TPH gases were also found at northeast of the site, about 15m southeast of TP110 and

15m. It appears that the high amounts of TPH gases are observed only in Zone A, as seen in Figure 7.3 and 7.4.

7.4.2 Methane (CH_4)

In the area where the hydrocarbon contamination had been reported, monitoring the amount of methane released from the ground is normally the easiest way to determine the distributions of the hydrocarbon across the site. Methane is the most volatile hydrocarbon gas and can easily be released from the ground through soil vapours. Its distribution over the study site is shown in Figure 7.5. This is overlain on the Google Earth Map of the study area and the approximate location of trial pit 110 (TP110) has also been marked (Figure 7.6).

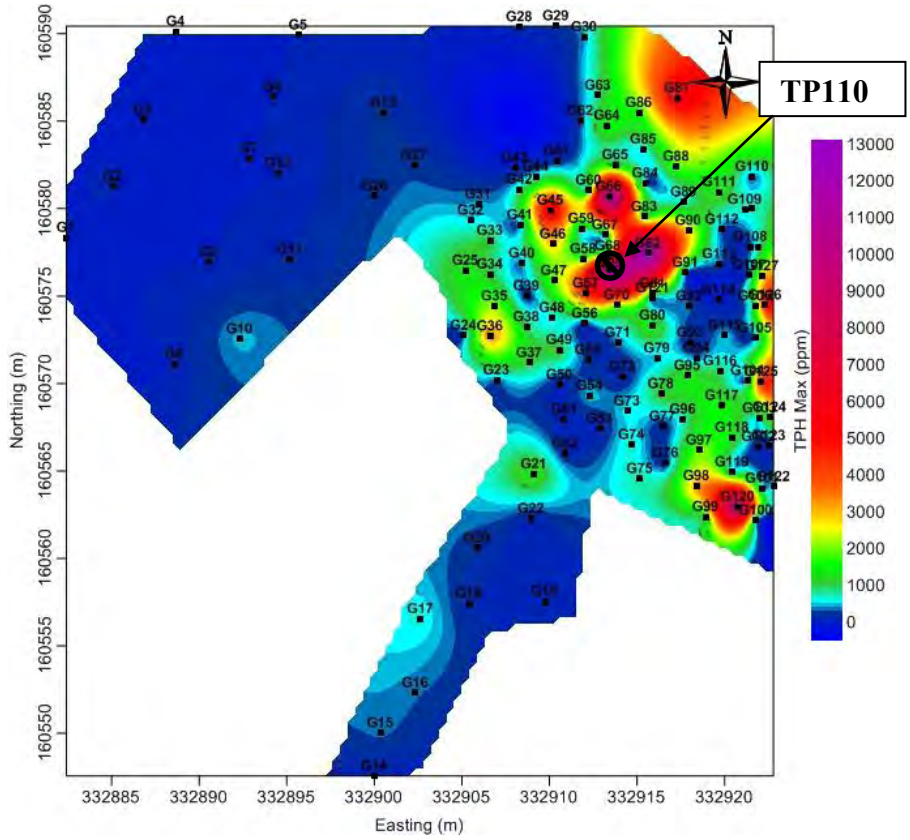

Figure 7.3: Showing the distribution of the TPH gas which the elevated amount at the TP110

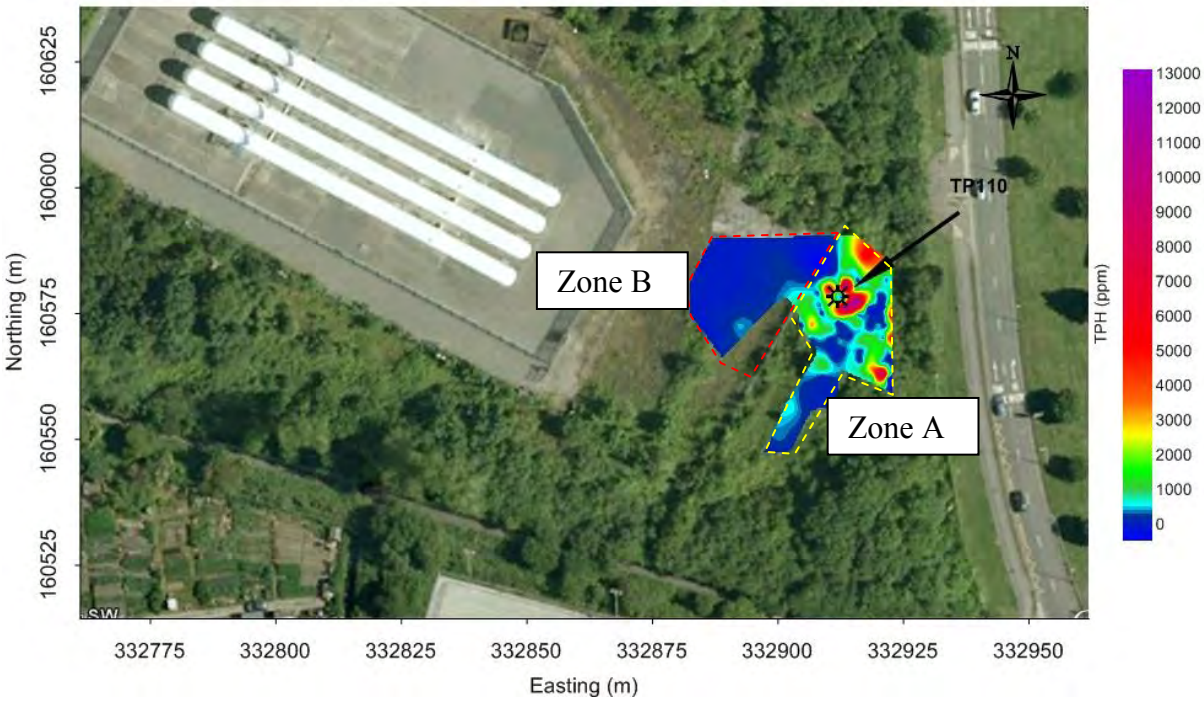

Figure 7.4: The TPH distributions on the map. Low amount of the TPH's observed in Zone B

The distributions of the CH_4 around TP110 are high and it also disperses into the Zone B as well. However, the highest amount isn't recorded exactly at TP110 but at G58 (1063 ppm) near to TP110, to the southeast at station G98 (2028 ppm) and station G21 (1282ppm) to the south of TP110.

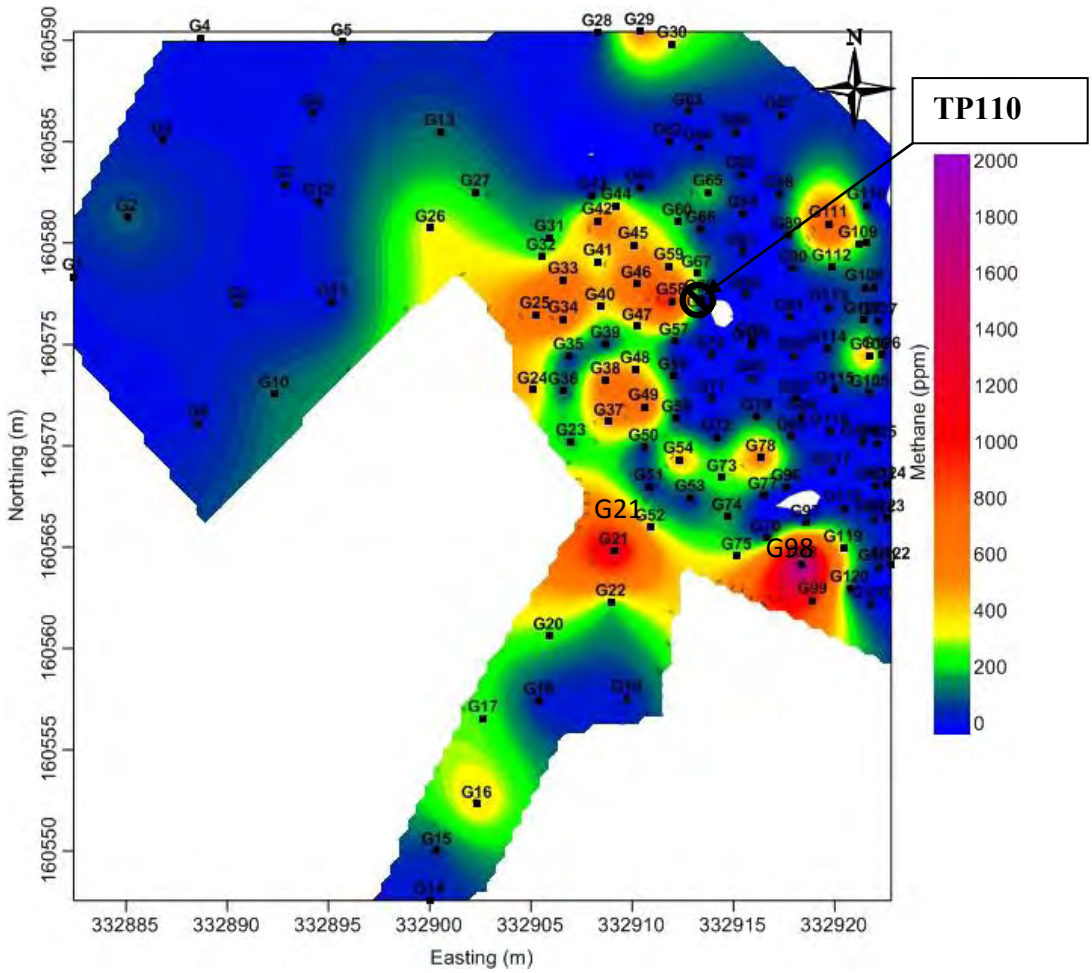

Figure 7.5: Methane distributions across the study site showing high amounts at the middle. The highest amount at the gas measurement point G98 at southeast of TP110

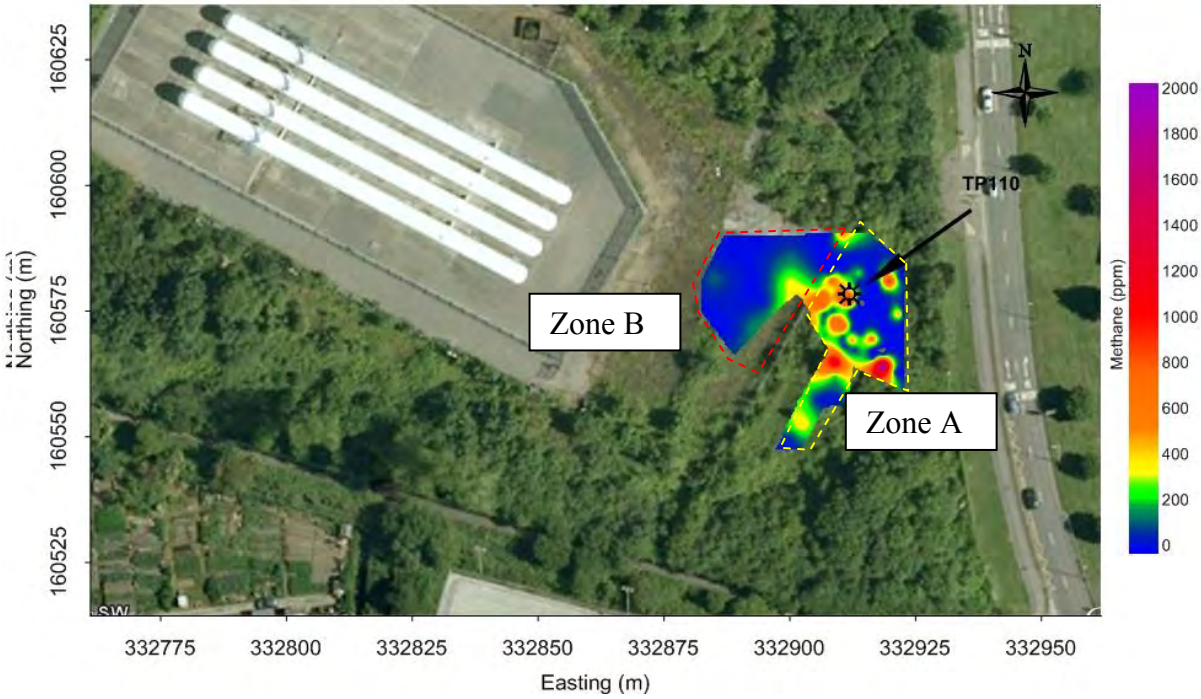

Figure 7.6: Most of the high amounts of CH_4 are found at Zone A where the TP110 is located

7.4.3 Carbon Dioxide (CO_2)

The presence of elevated values of CO2 in the soil is probably due to the breakdown of hydrocarbons in an aerobic environment (USGS – **Web 7.1**). The variable presence of CO_2 in the subsurface may be related to varying ground conditions across the site indicating areas in which aerobic degradation is taking place. Elevated CO_2 is found surrounding TP110 and the highest amounts are recorded at G77 (108000 ppm). Elevated CO_2 levels are also detected in Zone B, G10 (17472 ppm) G11 (23536 ppm) and G12 (24734 ppm) – Figure 7.7 and 7.8. Areas of depleted CO_2 readings across the site tend to coincide with areas of depleted TPH. Therefore, this indicates in which areas aerobic degradation may have broken down the hydrocarbons in the subsurface.

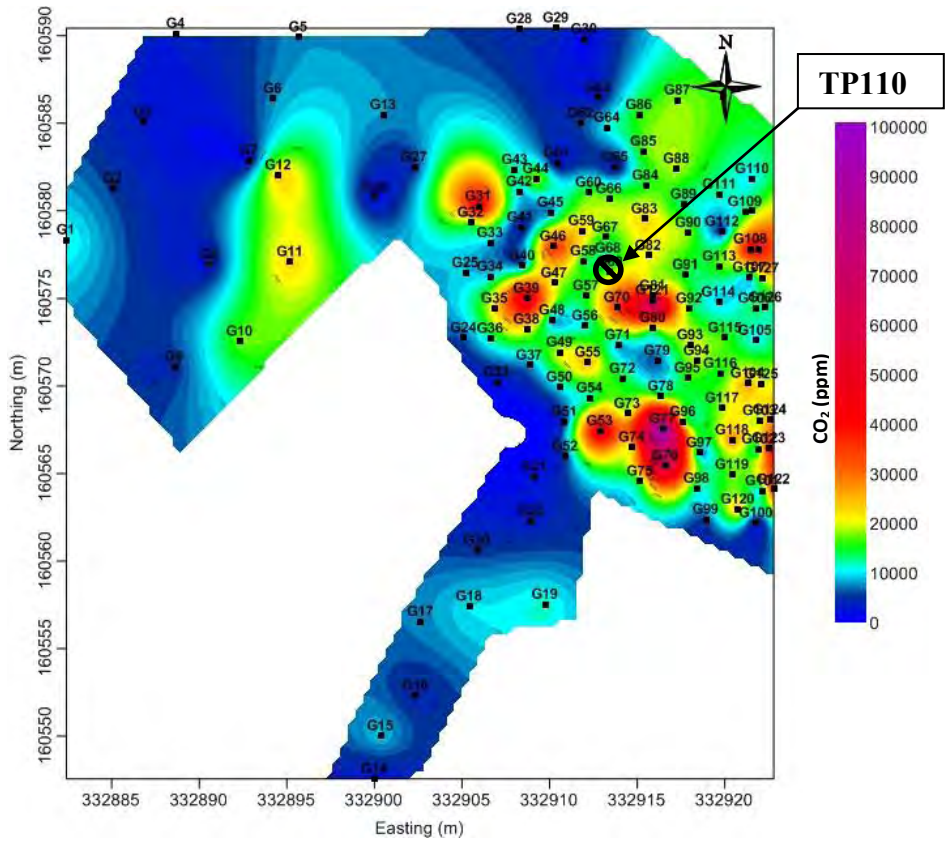

Figure 7.7: Distributions of CO_2 obtained from gas survey showing it has a similar pattern as the TPH distributions.

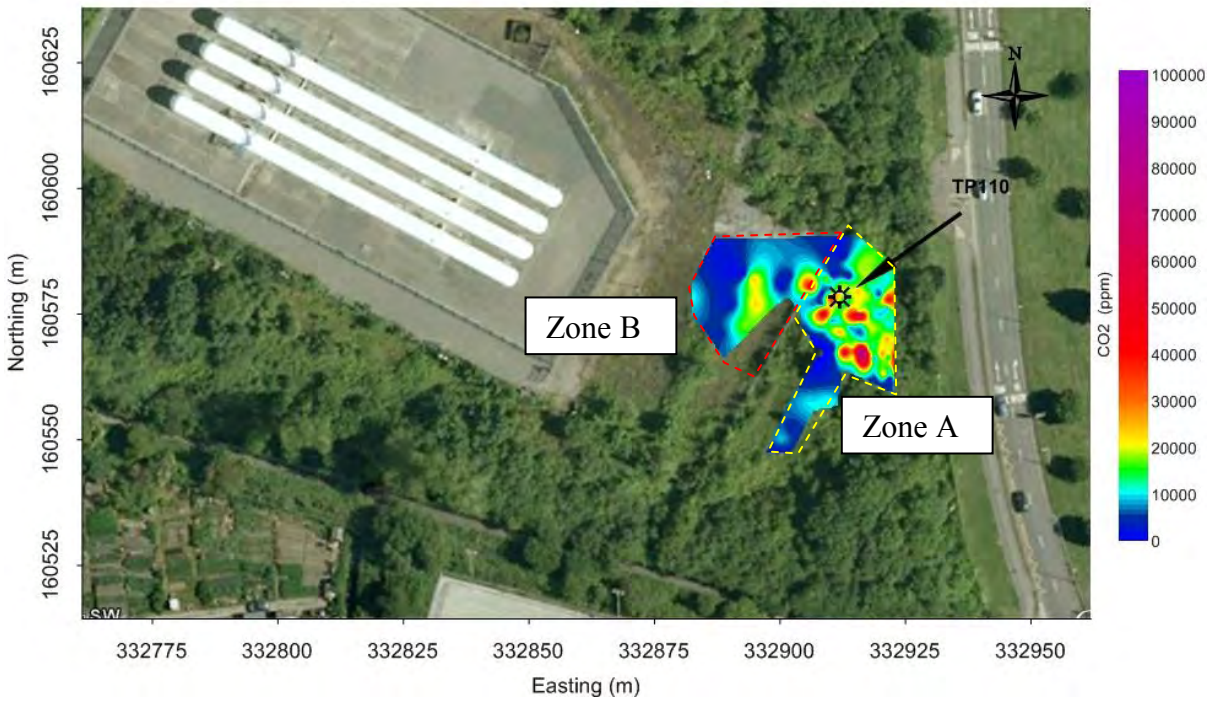

Figure 7.8: The high reading of CO_2 also been found in the Zone B indicate that area has an aerobic biodegradation taking place as well.

7.5 Geophysical results

The Geophysical results have two subsections which discuss the Resistivity Imaging outputs from five resistivity profiles and the Ground Conductivity survey using GEM-2 which have 5 different depth layers. Generally, most chemically contaminated ground has a lower resistivity or higher conductivity, due to the fact that the contaminants are usually good electrical conductors. However, in the area where the hydrocarbon contamination is a major concern, the electrical properties of the contaminants might be significantly different. To begin with, the discussion will start with the electrical properties of materials surrounding area TP110 where the free phase tar was found.

7.5.1 Electrical Properties of the material surrounding Trial Pit 110

TP110 is confirmed as having significant tar contamination by the site consultants Parsons Brinkerhoff (2010). Two resistivity survey lines crossed over TP110 (RES 1 and RES 2) with the aim of delineating the dispersion of the hydrocarbon contamination in the area. The depth of the trial pit is 2.4m; the EC's values are obtained using the 31025Hz frequency of E/M data which represents an equivalent depth layer of 2.5m (from the Skin depth Nomogram). The location of TP110 is marked on the profile RES 1 and RES 2 and shows that the resistivity of the material surrounding the area of TP110 is very low, less than 10Ωm or about 100mS/m. This indicates the area is contaminated (George, 2006). The biodegradation processes by the microorganisms is believed to have changed the chemical properties of the tar from an insulator into an electrical conductor (low resistivity). This process is continuous, probably since the gasworks station started a century ago. The longer the process carries on, the higher the electrical conductivity of the HC will become (Atekwana et al., 2000). The EC data from E/M 31025Hz layer also shows high conductivity values for the material near to TP110 which means the resistivity is lower. When the values are more than 1000 mS/m or less 1 Ωm in resistivity, the area can be classified as contaminated using combined resistivity and electrical conductivity methods.

7.5.2 2D resistivity profiling

For this discussion, the electrical resistivity properties of the materials in the study site can be broadly classified into 3 categories (Table 7.2).

Table 7.2: The ranges of resistivity values representing the probable types of material

Material Type	Resistivity (Ωm)	Colours Contour
Near surface materials (bricks, foundation material, wood, gravel, roots and plants)	> 100	Yellow to Red
Uncontaminated ground - Tidal Flats Deposits (clayey sand/ sandy clay)	Between 10 - 100	Green to Light Blue
Contaminated ground/layer	< 10	Dark Blue

Generally, all the resistivity profiles show that the ground is contaminated (Figure 7.9). The source from TP110 (tar) is possibly only dispersed within the marked area in the profile RES 1 (Figure 7.9). Other low resistivity zones possibly have their own contaminant sources i.e. coal related products that have been used at the gasworks operations.

Resistivity profile RES 3 and RES 5 are shorter and shallower and show that almost all materials under the line are contaminated. These can probably be linked to the low resistivity zone observed in line Res 4 between electrode no. 26 (25m) and electrode no. 54 (53m).

Overall 3D views of the relationships of the low resistivity values in the whole profiles are shown in Figure 7.10.

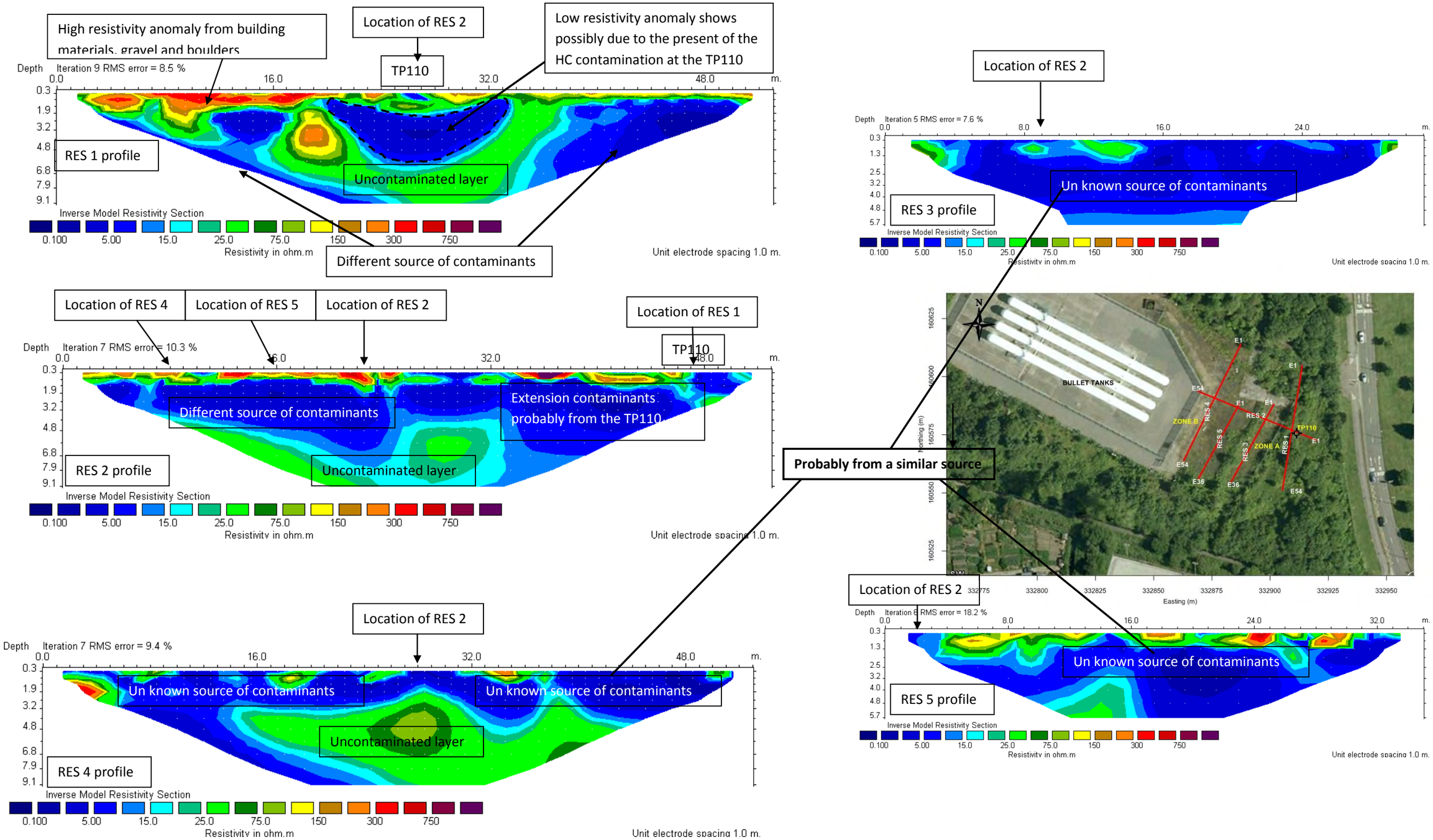

Figure 7.9: All resistivity profiles showing the possible locations of the contamination zones and the interrelations between them

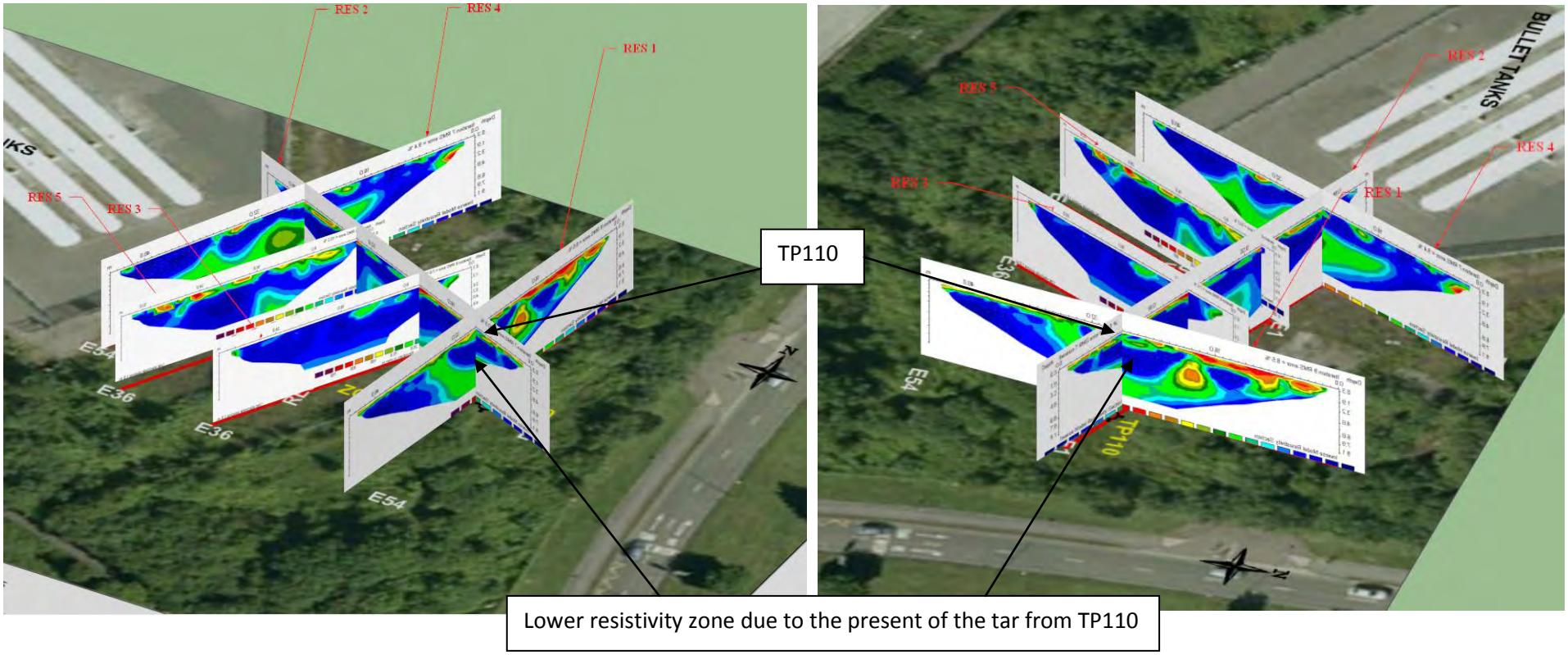

Figure **7.10**: The 3D views provide the resistivity interrelation between the resistivity profiles. Low resistivity zones probably occurred due to the different sources of contamination

7.5.3 GEM-2 survey results

The average ground conductivity obtained using all 432,000 GEM-2 data points is 1707mS/m or 1.707S/m. By using a 'skin depth nomogram', the calculated depth of penetration given by the electromagnetic wave frequencies is shown in Table 7.3

Table 7.3: The effective depth of the electromagnetic wave which penetrates into the ground based on the frequencies employed

Frequency (Hz)	Depth (m)
825	15m
7075	5.0m
16075	3.5m
31025	2.5m
40075	2.0m

A total of five different EC's distribution plots were generated from the GEM-2 data set, each representing a different depth of EC information (Table 7.3). Only the first four layers will be discussed, because data from fifth layer is not reliable due to the fact that the average EC values obtained from that layer are too high. An average EC's value from 108,878 data points from this layer is 8.04×10^6 mS/m (1.2438E-4 Ωm in the resistivity), which is significantly high.

Due to the wide range of EC values, the potential contamination zone is represented by the value >1000mS/m (1Ωm in the resistivity). This is shown by the yellow to the dark blue colour in the EC's layer plots. Possibly, the distribution of the contaminated zone is wider due to the fact that the boundary of EC's value for the contamination material is 100mS/m or 10Ωm (Meju, 2000).

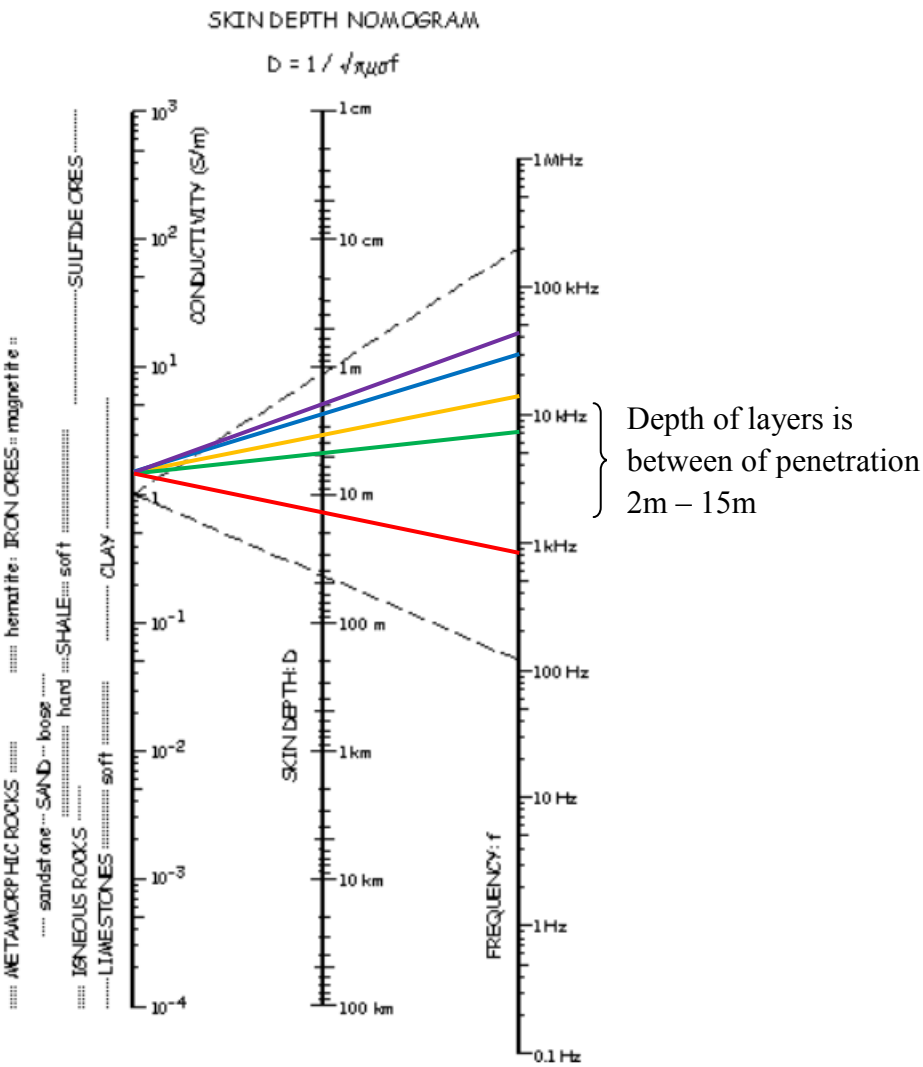

Figure 7.11: Depth of the respective E/M data determine by the 'Skin Depth Nomogram' for the study area. The average conductivity of material is 1.707 S/m which is an average of the 108,000 points GEM-2 data

Table 7.4: The EC values obtained from a different E/M wave frequency from GEM-2 survey

Description	875Hz	7075Hz	16075Hz	31025Hz	40075Hz
Number of point	108, 878	108, 878	108, 878	108, 878	108, 878
Min (mS/m)	1E-5	1.18E-3	1.09E-3	2.78E-3	1.58E-3
Max (mS/m)	1.7E+9	9.88E+6	9.11E+6	1.55E+6	4.2E+6
Average (mS/m)	**8.04E+6**	**1788.66**	**1935.14**	**1990.50**	**1128.26**

Based to the GEM-2 data, the whole of the study area is contaminated due to the fact that the average EC's is >1000mS/m for all layers. This value is equal to 1Ωm in electrical resistivity, which is classified as very contaminated ground by many researchers i.e. Meju (2000) and George (2006). The data displayed will be only used to define the worse contamination area and to identify what is the GEM-2 signal given by the existing tar's contamination area in the TP110. This will help with data interpretation for other high EC zones within the study area, indicated by a blue to purple colour to the south and south western areas.

Due to the large range of EC's value (Table 7.4), the colour scale used in the plots is wider and the minimum interval is 1000mS/m. Part of the red contour where the EC value is more than 100mS/m is uncontaminated which is very difficult to differentiate in the plan view EC map. Focusing into the area where the TP110 is located in the first layer, no high value of EC has been observed, indicating the ground materials are very resistive which corresponds to the presence of the plants, building materials and gravels. In a clear area at zone B where the bullet tanks are located, this shows that the ground is contaminated especially near to the back gate (Figure 7.12).

At the deeper layer 2.5m (31025Hz E/M wave), a very clear high EC zone can be seen in the zone A under the TP110 (Figure 7.13). The southwest area from the TP110 also gives a very high EC value (dark blue to purple colour) which is not seen in the upper layer. In the Zone B, the high EC values still remain in the middle near to the back gate. Looking at the EC distributions pattern, it's possible that, the high values of EC in the southwest area have a connection to the high EC in middle of the Zone B.

The deeper layers which are represented by the data obtained from E/M frequency 16075Hz (3.5m depth) and 7075Hz (5.0m depth) shows the distributions pattern are similar. However, the EC values surrounding TP110 are slightly lower compared to similar location in the second layer (Figure 7.14 and 7.15). This doesn't mean it has not been contaminated because of the overall value of the EC is still within the range of the contaminated zone (more than 100mS/m). Probably in these two layers, the contamination is slightly less compared to the second layer.

As a comparison between EC's distributions over the depth, all five of EC layers had been combined plotted as seen in Figure 7.17

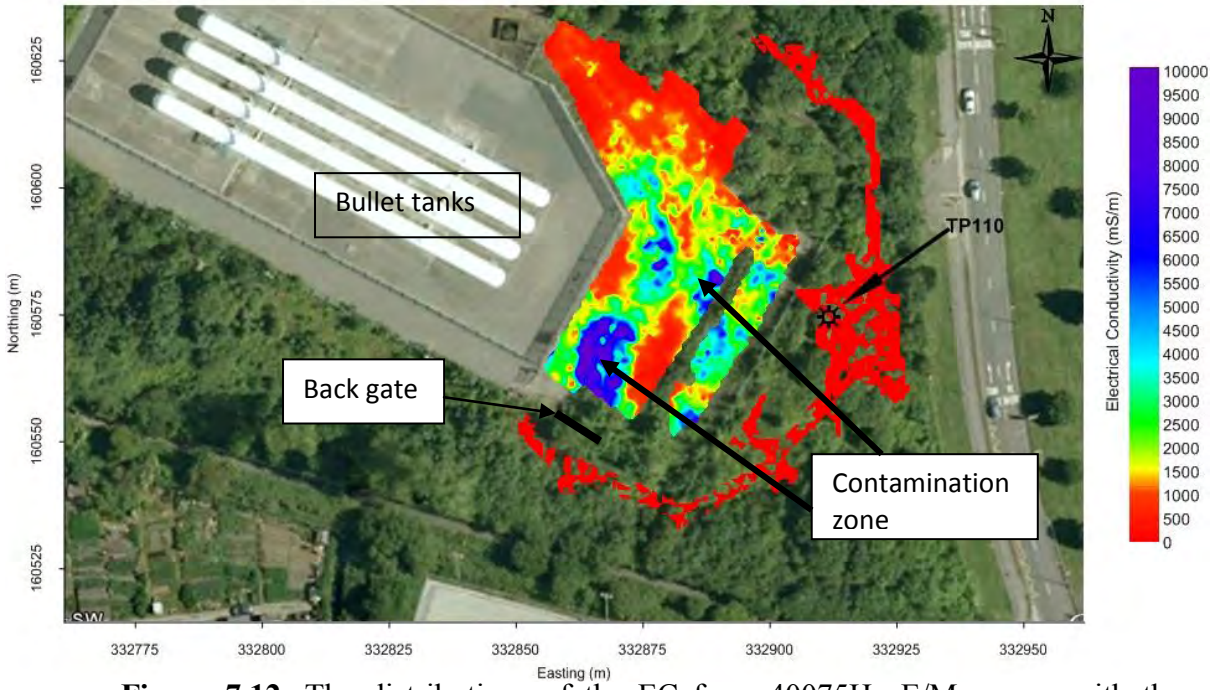

Figure 7.12: The distributions of the EC from 40075Hz E/M survey with the approximate depth 2.0m

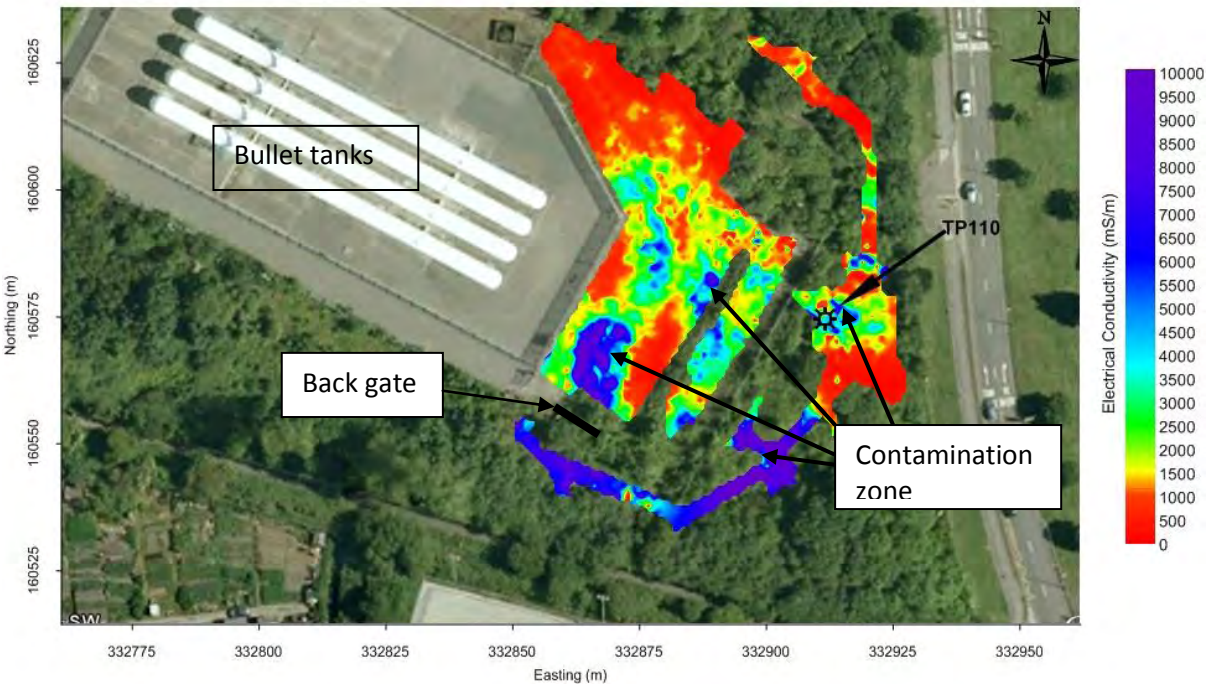

Figure 7.13: The distributions of the EC from 31025Hz E/M survey with the approximate depth 2.5m

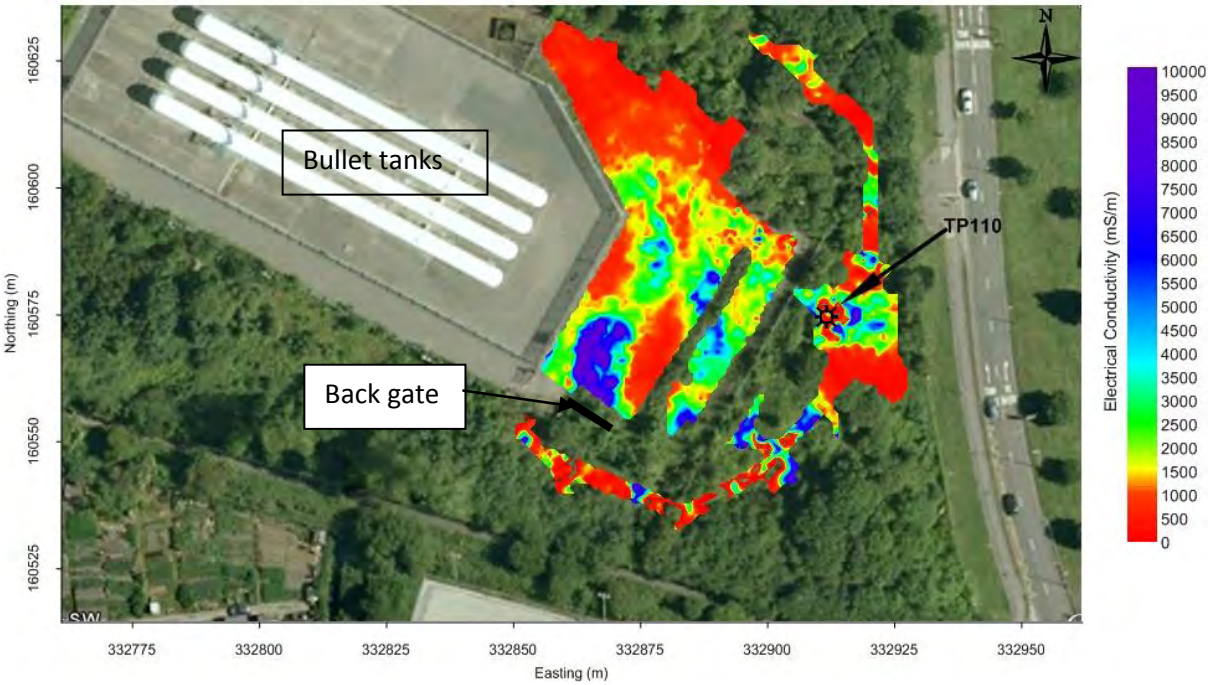

Figure 7.14: The distributions of the EC from 16075Hz E/M survey with the approximate depth 3.5m

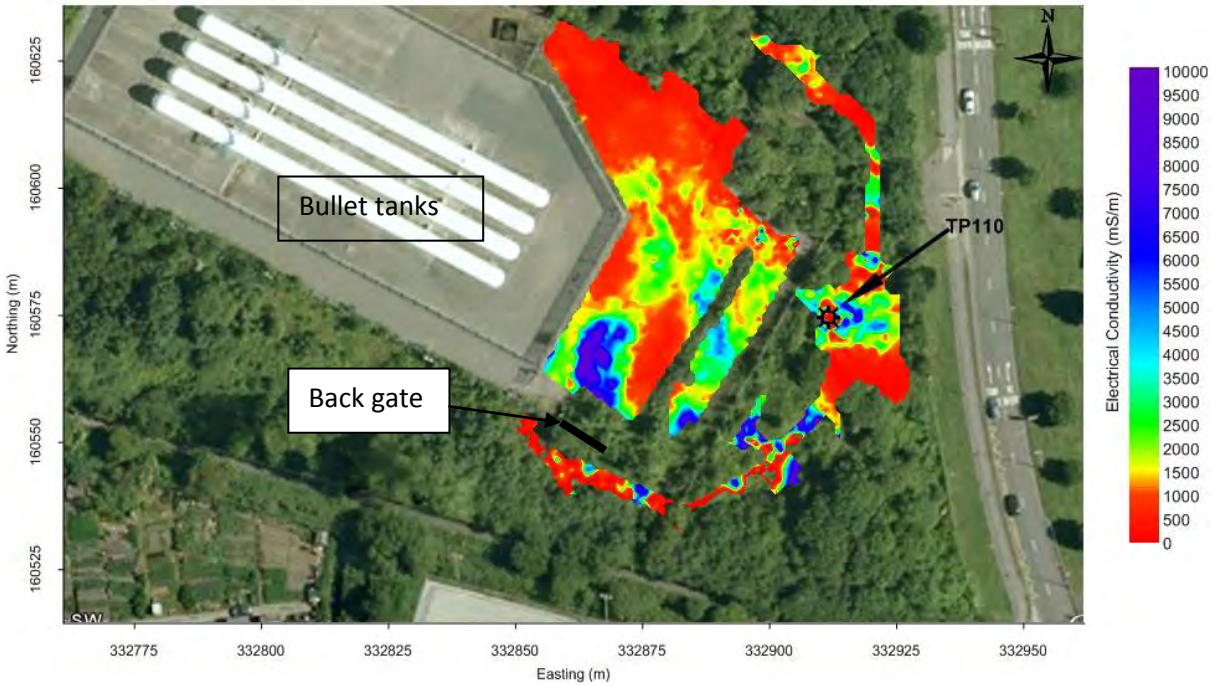

Figure 7.15: The distributions of the EC from 7075Hz E/M survey with the approximate depth 5.0m

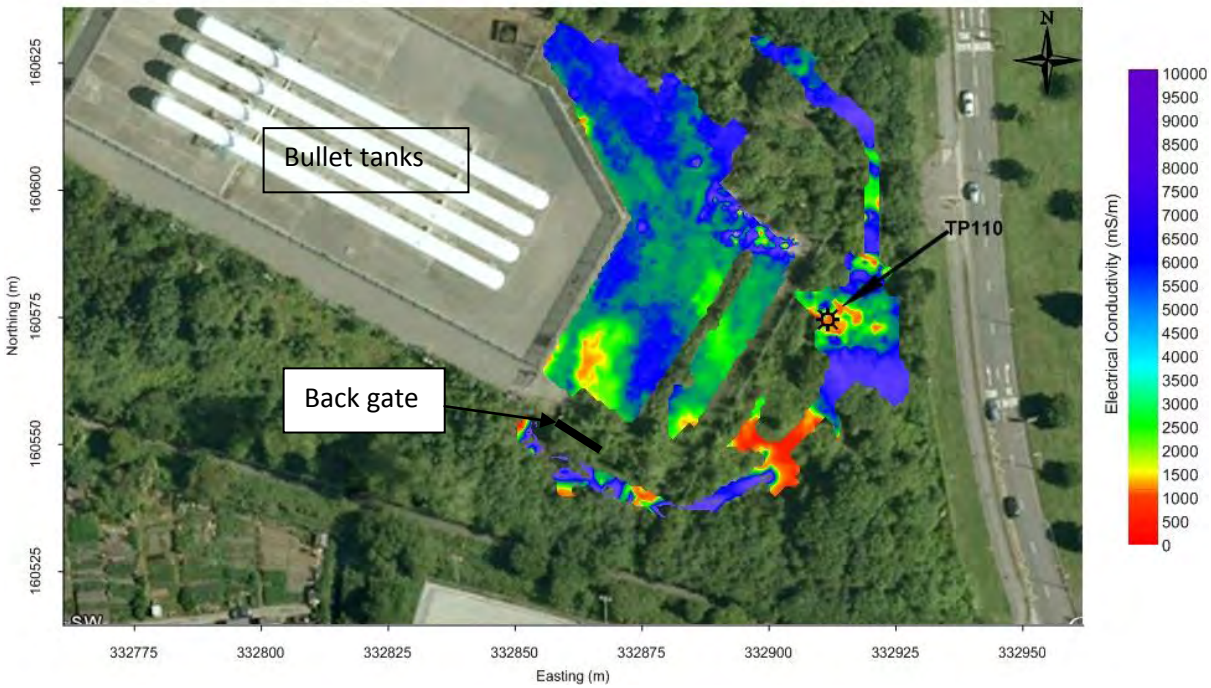

Figure 7.16: The distributions of the EC from 875Hz E/M survey with the approximate depth 15.0m

7.6 Combination of research observations

The SVS data covers only a small area of the research site and more data is collected in the Zone A compared to Zone B. In fact, the data obtained from the SVS survey probably represents the distributions of gases from the near-surface materials. By using this assumption, the EC's data from 31025Hz frequency GEM-2 E/M survey is the best to compare with the RES 1 profile for the resistivity. The interrelation between all the results is presented in Figure 7.18.

Clearly in the RES 1 profile, low resistivity values are found under the TP110 which is high EC in the GEM-2 data, also a high of the TPH (gas) and CO_2 but shows up as being low in the CH_4. This probably occurred due to the aerobic biodegradation activity that has been taking part in that area. Aerobic biodegradation will use oxygen from the surrounding materials and from surface through the water infiltration into the ground to activate the process and released the CO_2 and breakdown the tar into the simpler structures which is then more electrically conductive.

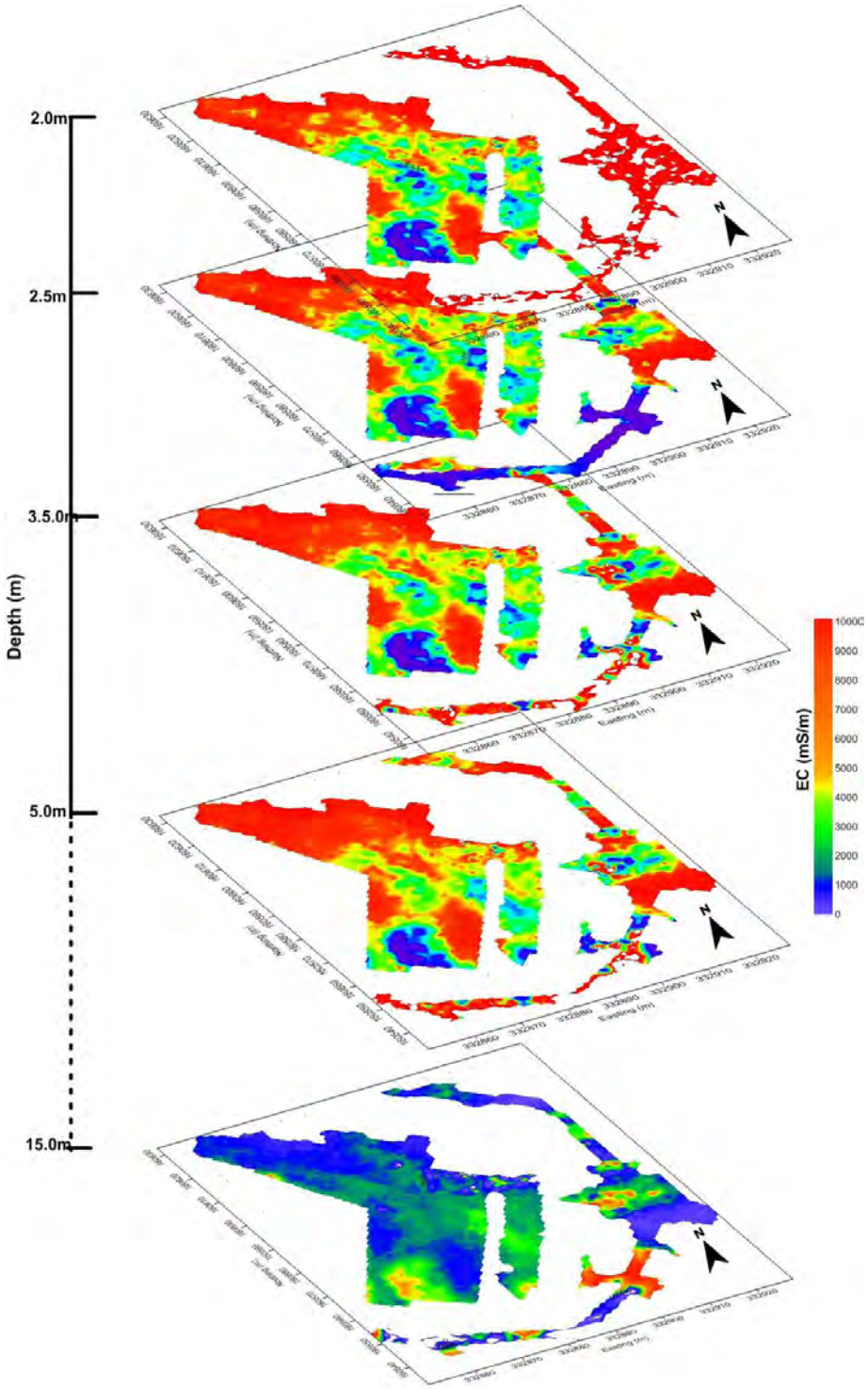

Figure 7.17: The combined plot of the EC's distributions map for the all five layers

7.7 Conclusions

Through this investigation of a former gasworks station in Western Super-Mare using the geophysical and soil vapour surveys shows the sites is contaminated by hydrocarbons. Due to the length of time that the site had been in operation, the hydrocarbons released from the past activities has had a very long time to biodegrade by the microorganisms which have changed the electrical properties of the HCs from isolator to being more conductive. This is proven by the data obtained from the GEM-2 survey (ground electrical conductivity) and Resistivity Imaging at the area previously reported has having tar contamination (TP110).

One of the major concerns in interpreting the geophysical data is the presence of both the natural tidal flood materials and hydrocarbon contamination at the site (as proven by the trial pits samples) both of which will produce low resistivity (high conductivity) values. Therefore, the background effect on the apparent resistivity measurements caused by spatial variations in the superficial geology comprising of tidal flood material cannot be totally discounted in this interpretation. However, based on 12 trial pits samples any spatial variation in the pre-industrial superficial geology cannot be mapped in any great detail. The natural superficial geology would not be expected to be highly variable over the site in this geological context. Further detailed geological investigations are recomended to differentiate between the natural tidal flood material's and hydrocarbon pollution's various contributions to the spatial variations in the resistivity measurements made at this site.

Overall, the approach that has been used here to map hydrocarbon contamination is rapid and non-invasive and much cheaper than drilling numerous boreholes and excavating numerous trial pits.

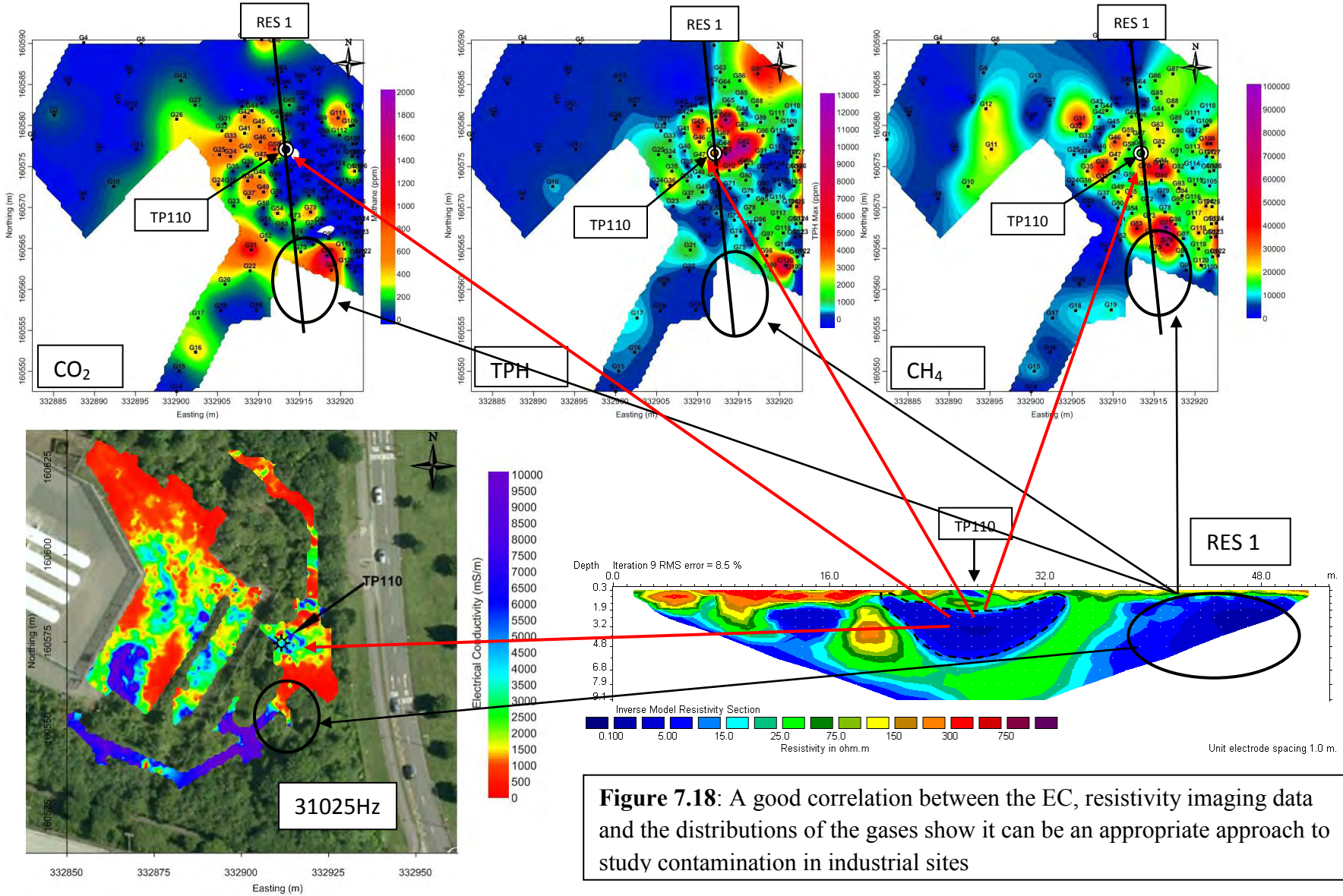

Figure 7.18: A good correlation between the EC, resistivity imaging data and the distributions of the gases show it can be an appropriate approach to study contamination in industrial sites

CHAPTER 8
RESULTS AND INTERPRETATION
CASE STUDY III: BARRY DOCK SITE

8.1 Introduction

As previously stated in Chapter Three, the Barry Dock research site is complex in terms of its ground contamination issues. This is related to the ground pollution arising from the historical dock activities, as a result of railways, landfill and numerous tank storage areas for hydrocarbons and other chemical products. The geophysical, geochemical and hydrogeological data and the investigation results obtained from this site are discussed in this chapter.

In total, this includes the heavy metal and hydrocarbon distributions in the West Pond, Central District and South Quay areas. The geophysical results from the GEM-2 survey and two long resistivity lines crossing the Tank Farm Zone and the West Pond Zone are presented and correlated with the HC and metal distribution on site. A part of the discussion also includes the geophysical results obtained at a small 3D area in the southeast, near to the Barry Island cliff line where six short parallel resistivity lines were collected.

8.2 Geochemical results

Geochemical data has been obtained from the Ove ARUP Report (2008) and has been re-analysed and re-processed using Surfer 9 software to better define its distribution across the site. The soil analysis results made by Ove ARUP represent depths between 0m and 2m including the:

a) Total heavy metals and Total Petroleum Hydrocarbons (TPHs) distribution throughout the study area
b) Total heavy metals and Total Petroleum Hydrocarbons (TPHs) distribution in the tank farm zone which are compared with the GEM-2 results at the similar area.

In this study, a total of 270 soil samples were analyzed, 214 samples obtained from trial pits and the remaining 56 samples from boreholes, this represents 135 sampling locations over the site and at every location two soil samples were collected at different depths.

For the heavy metal analysis, the total ion content has been calculated by adding both ions composition in the two soil samples taken at each location. The first sample taken is between depth 0m-1m and another sample is from 1m – 2m depth. Copper, Lead, Zinc, Chromium, Cadmium, Nickel, Antimony, Mercury, Selenium, Barium, Arsenic and Beryllium are included in the analysis. Whereas, the TPHs content is calculated by adding all the aromatic and aliphatic hydrocarbons present in the soil samples which has a number of carbon compounds from 6 to 40 (> C6 – C40).

8.2.1 Distribution of the heavy metals and TPHs at the study area

The distribution of the heavy metal over the research site is shown in Figures 8.1 and 8.2. The higher concentrations are mostly located at the middle of the study area which is between the old tank farm zone and the West Pond. This is shown in the figures by a blue colour or in a range more than 3000mg/kg (ppm). While, the lowest concentrations a found in the old landfill area and in the part of the tank farm zone.

This distribution pattern is most probably due to these factors:

a) The highest concentration of heavy metal distribution at the middle of the study area can be explained due to fact that area was formerly railway tracks and sidings. This is shown in Figure 8.2 where most of the old railway tracks are located in this area. The past railway activities are believed to contribute to the dispersion of the metal over this research site similar to what is happening at the Cathays Railway depot in Cardiff.

b) The low concentration of heavy metals found at the West Pond area is believed to be due to the ground works carried out in 1996 which skimmed the top soil and took it off site (Ove Arup & Partners, 2008). The others

reason is because this area is slightly higher topography compared to the surrounding area due to backfilling before 1998. So all the runoff will flow toward a lower topographic elevation at the middle of the study area (the higher concentration area) this will carry the heavy metals and deposit them into this area.

c) Meanwhile at the tank farm zone, the low concentration of the heavy metal can be suggested to occur because the storage tanks were built purposely to store fuel and a HC base chemical. So it is believed that the heavy metal contamination is unlikely to have occurred from the secure storage tanks. If there any heavy metal contamination in tank farm zone, the surface runoff water will carry them toward the shoreline as it is lower in elevation compared to the tank farm zone. However, the runoff flows toward the shoreline is blocked after the contractor did the backfilling works at the south of the West Pond (believed as a part of the remediation works). This is probably another reason why the tank farm zone didn't have a serious heavy metal contamination because the runoff flushed the heavy metals and carried them toward the southwest where the highest concentration of heavy metal been observed.

The TPHs dispersion plots didn’t give a really clear pattern but it can be found almost over the whole area. The TPHs distributions are similar as the heavy metal with the high concentration is mostly located at the middle of the study area but little sign of it being present in the north. However, a high concentration of the TPHs ranges between 1000 to 3000ppm is recorded at the north at the farm tank zone (Figures 8.3 and 8.4). This area is recorded as having a distribution of lower concentration of heavy metals as shown in Figure 8.1 and 8.2.

TPHs distribution patterns occur in such a way that can be described based on the similar environments where heavy metals are spread. So, the pattern formed in the middle is due to three factors as described above. However, the presence of high concentrations of TPHs at the tank farm in the northern zone may be associated with the presence of the historical hydrocarbon storage tanks. But, why is it found there and not in the entire tank

farm zone area? This question may be answered by taking into account the two factors below;

a) Demolition of the storage tank which only ended at the end of 2000 to early 2001. This means that the research is carried out 10 years after it was demolished. This period is considered short for contaminants to migrate to a more stable environment in the middle of the area. So, the TPHs have a tendency to remain in this area.

b) The second possibility is geared more to the occurrence of a leak or spills of TPHs in the area. It may occur in other areas, but more seriously there, so this will take a longer time to clean up by natural processes.

8.2.2 The distribution of metals and TPH in the tank farm zone

As a mentioned above, the tank farm zone contained old storage tanks which included seven big tanks, another seven small tanks and several bullet tanks as shown in Figure 8.5. Most of the tanks were connected by pipe-lines to each other.

The distribution of the high concentrations of heavy metals can be found in the southwest (3000 – 10000 mg/kg) which formerly had a high density of railway tracks and sidings (Figure 8.6). Slightly high concentration (1000 – 3000 mg/kg) as shown by a blue colour spot in the middle of the area between tank No 4 and No 5, south of tank No 1, and on the north of tank No 7. This area has a higher heavy metal concentration which is expected, due to the railway activities of the past. It also probably occurred due to regular spillages, when the coal was transported to the ship from the wagons. The TPH distribution for the first 2m depth of soil layer is shown in Figure 8.7. The pattern of the distribution over the tank farm zone can be explained as followed:

a) The higher TPHs values are found at base of tank No 7, No 6 (> 1000mg/kg), No 5 (~400mg/kg) and No 1 (~500mg/kg). This probably shows that the storage tanks may have beem leaking when in use. Another possibility might be the pipelines connected to the tanks leaked and the TPHs are remaining on the site since that time.

b) The soil samples were collected in 2007-2008, which is 8 years after the storage tanks were demobilised. This short period most probably is not enough to flush the TPHs naturally from the site.

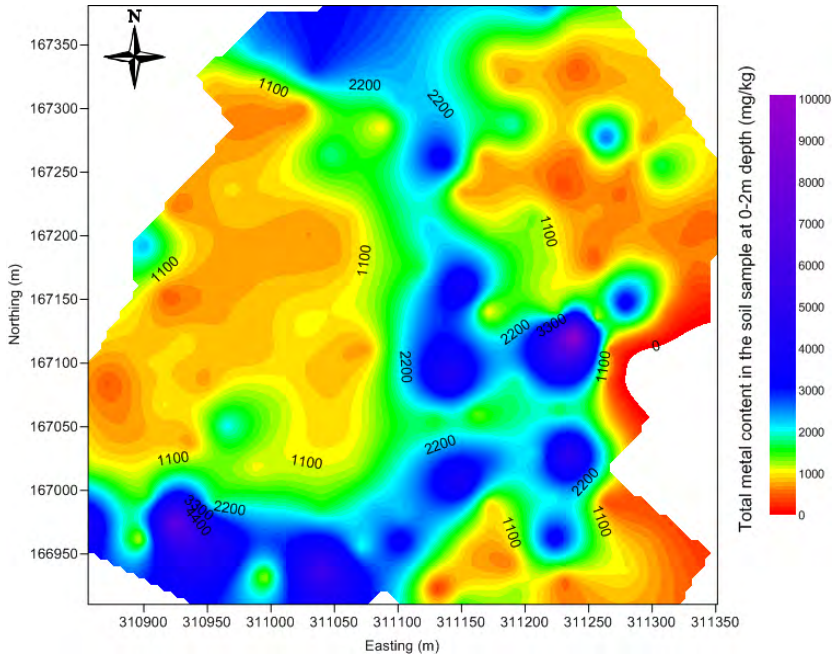

Figure 8.1: The heavy metal distribution on the site, dominated in the southwest on the lower elevation topography

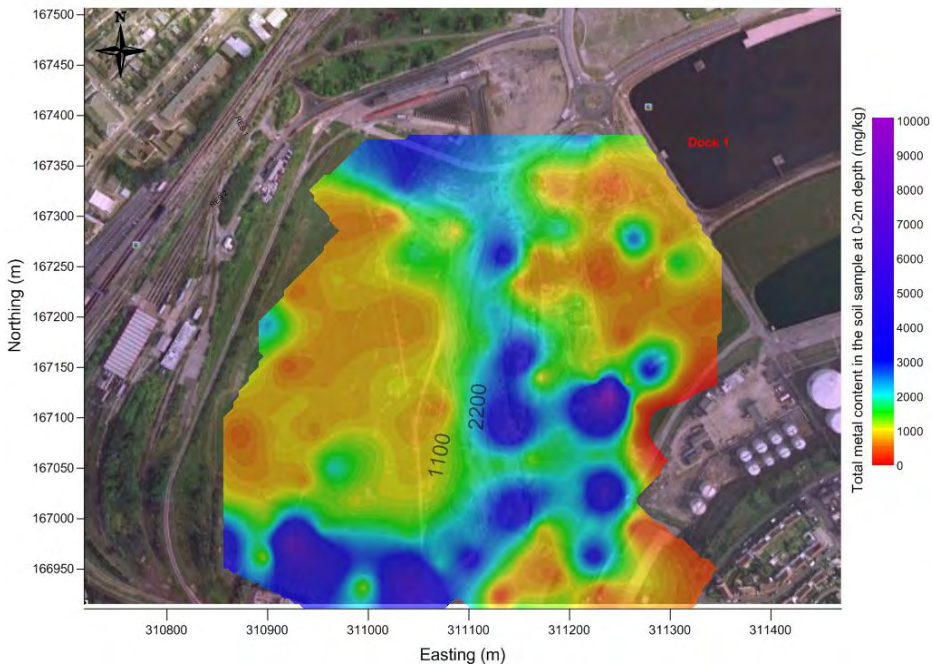

Figure 8.2: The distribution has a strong relationship with old railway tracks, sidings and the tank farm zone

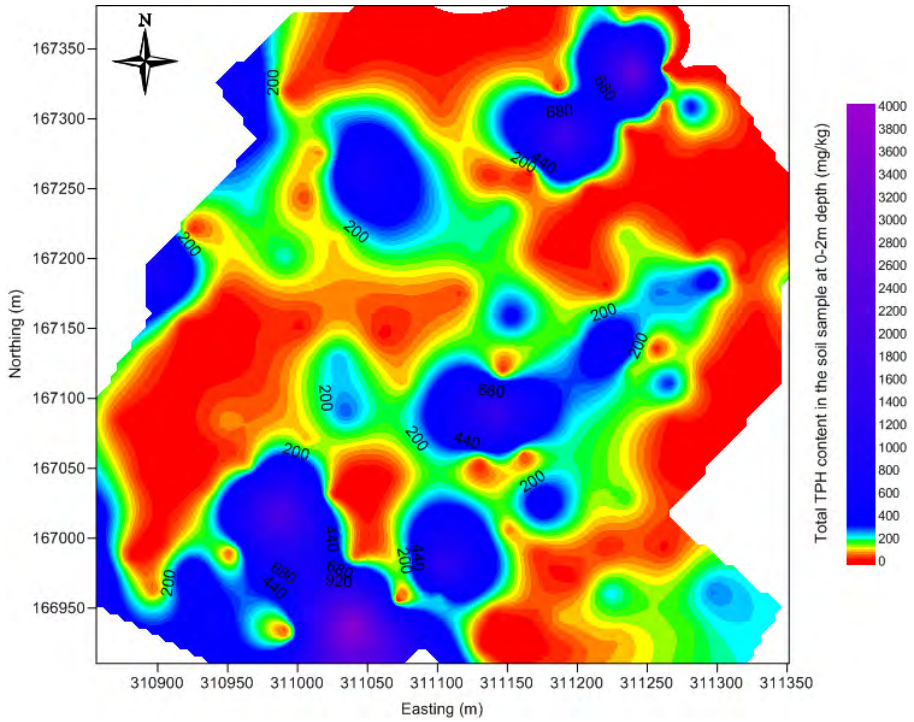

Figure 8.3: Showing the distribution of the HC slightly being random but predominantly on the southwest (lower topography), partially at the middle and at the tank farm zone

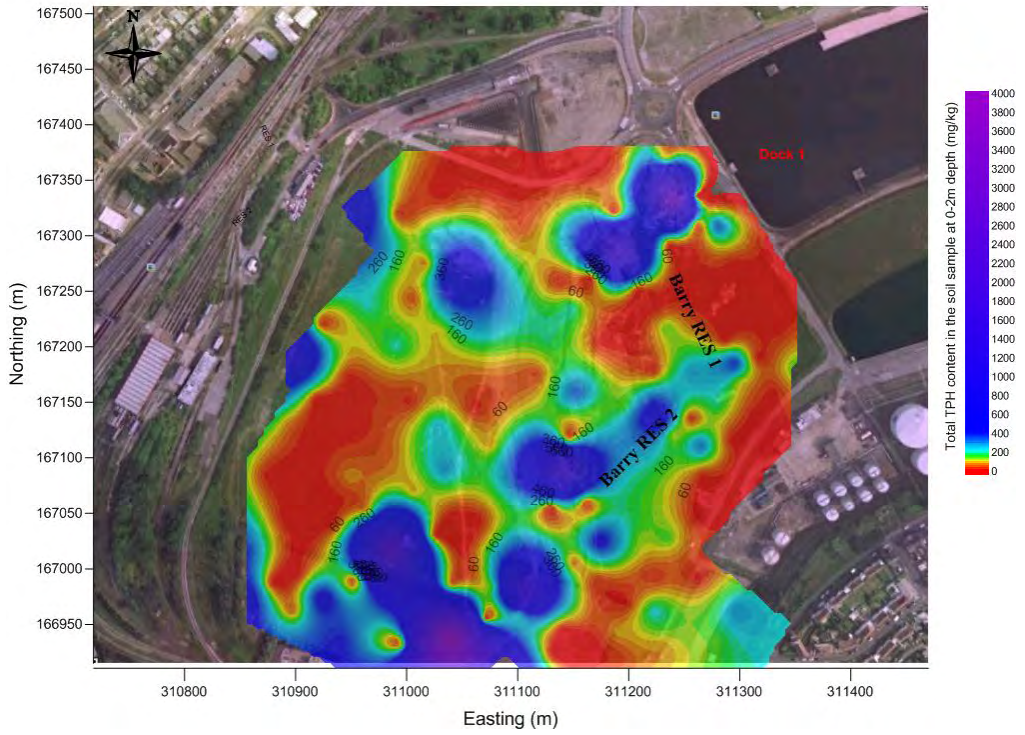

Figure 8.4: The HC distribution has a strong relationship with old railway tracks, sidings and the tank farm zone

Table 8.1: Oral and inhalation threshold toxicity values for petroleum hydrocarbon fractions for the Total Petroleum Hydrocarbon Source, Environment Agency (2011) – **Web 8.1**

Exposure route	Carbon range[b]	Toxicity value	Surrogate and basis for TPHCWG derivation
Oral	**aliphatic**	**(mg kg^{-1} bw d^{-1})**	
	EC_5 - EC_8	5	*n*-Heptane / commercial hexane(s)
	$EC_{>8}$ - EC_{16}	0.1	Dearomatised petroleum stream
	$EC_{>16}$ - EC_{35}	2	Basis of 7 highly refined mineral oil studies
	aromatic		
	$EC_{>5}$ - EC_8	0.2	Toluene (C_6 benzene evaluated separately as a carcinogen)
	$EC_{>8}$-EC_{16}	0.04	Considered USEPA derived RfDs for isopropylbenzene, acenaphthene, biphenyl, fluorene, anthracene, fluoranthene, naphthalene and pyrene. 4 of these compounds had RfDs of 0.04 mg kg^{-1} bw d^{-1}
	$EC_{>16}$- C_{35}	0.03	Pyrene
Inhalation	**aliphatic**	**(mg m^{-3})**	
	EC_5 - EC_8	18.4	Commercial hexane
	$EC_{>8}$-EC_{16}	1	Isoparaffin mixture
	$EC_{>16}$ - EC_{35}	NA[c]	Inhalation exposure may depend on inhaled particulate matter
	aromatic		
	$EC_{>5}$ - EC_8	0.4	Fraction-specific RfC (C_6 benzene separately)
	$EC_{>8}$ - EC_{16}	0.2	C_9- C_{16} aromatic mixture surrogate
	$EC_{>16}$-C_{35}	NA[c]	Inhalation exposure may depend on inhaled particulate matter

[a] this table is for information only and does not represent the UK position
[b] equivalent carbon ranges
[c] not applicable to inhalation exposures of free compounds since compounds not volatile

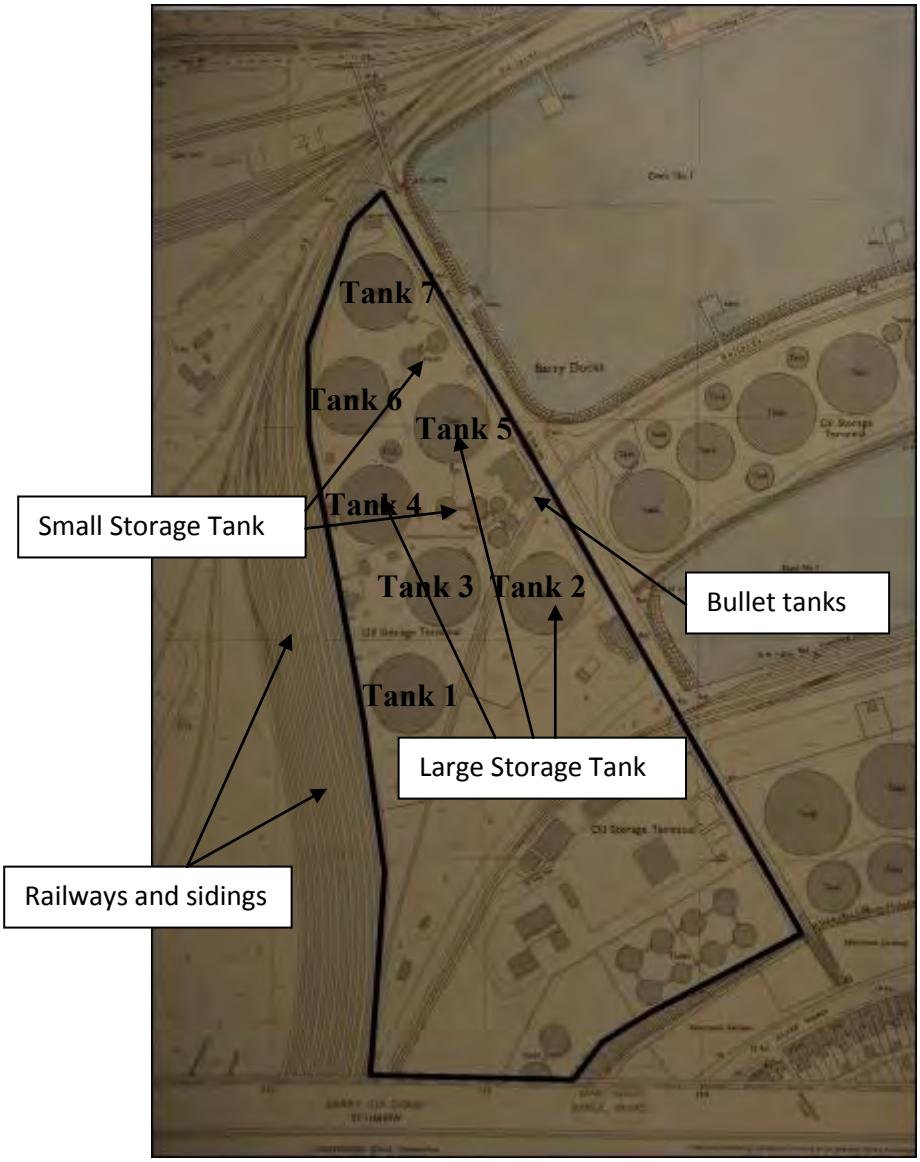

Figure 8.5: Showing a 1970s layout drawing image of the tank farm zone (source: Ordnance Survey)

8.2.3 The interaction between the Metals and TPHs distribution

The comparison between the distribution of metals and TPHs in this tank farm zone shows several observations that can be explained as followed:

a) The higher values of heavy metal and TPHs distribution have been observed at the middle to the southwest parts of this zone. This probably is caused by two reasons. Firstly is due to the fact that the site formerly had a high density of the railway

tracks and the sidings. That will potentially have the busiest industrial activities in the past and contributes to higher contamination values observed on the ground. Secondly, it can be related to the elevation of the ground, in that it is topographically lower compared to surrounding area. It therefore potentially allows the heavy metals and TPHs migrate from the higher elevation and deposited in this lower topographic area.

b) While at the north of the area, approximately located at tanks No 5, No 6 and No 7, the TPHs values are higher but the heavy metal significantly lower. This observation can relate to historical leaking of the storage tanks or due to some of the HC materials still remaining on the site. Less concentration of heavy metal in the tanks area would be expected, because before they built the storage tanks, the area was cleared and any contaminated surface soil are believed to have been removed. This area once contained many railway tracks and sidings which one would expect to give a higher value of the heavy metal but this is not shown. This may be due to the flushing activities on the surface materials by runoff water and subsequent deposition at the lower topographic elevation on the southern part of the site.

Generally from these two observations a conclusion can be made. Heavy metals are over the whole site but its concentration is higher in the deposited area at the south to southwest. Meanwhile, the TPHs which are believed to be younger are also deposited at the lower elevation at the south and southwest area together with the heavy metals and some of the area where the storage tanks foundations are located.

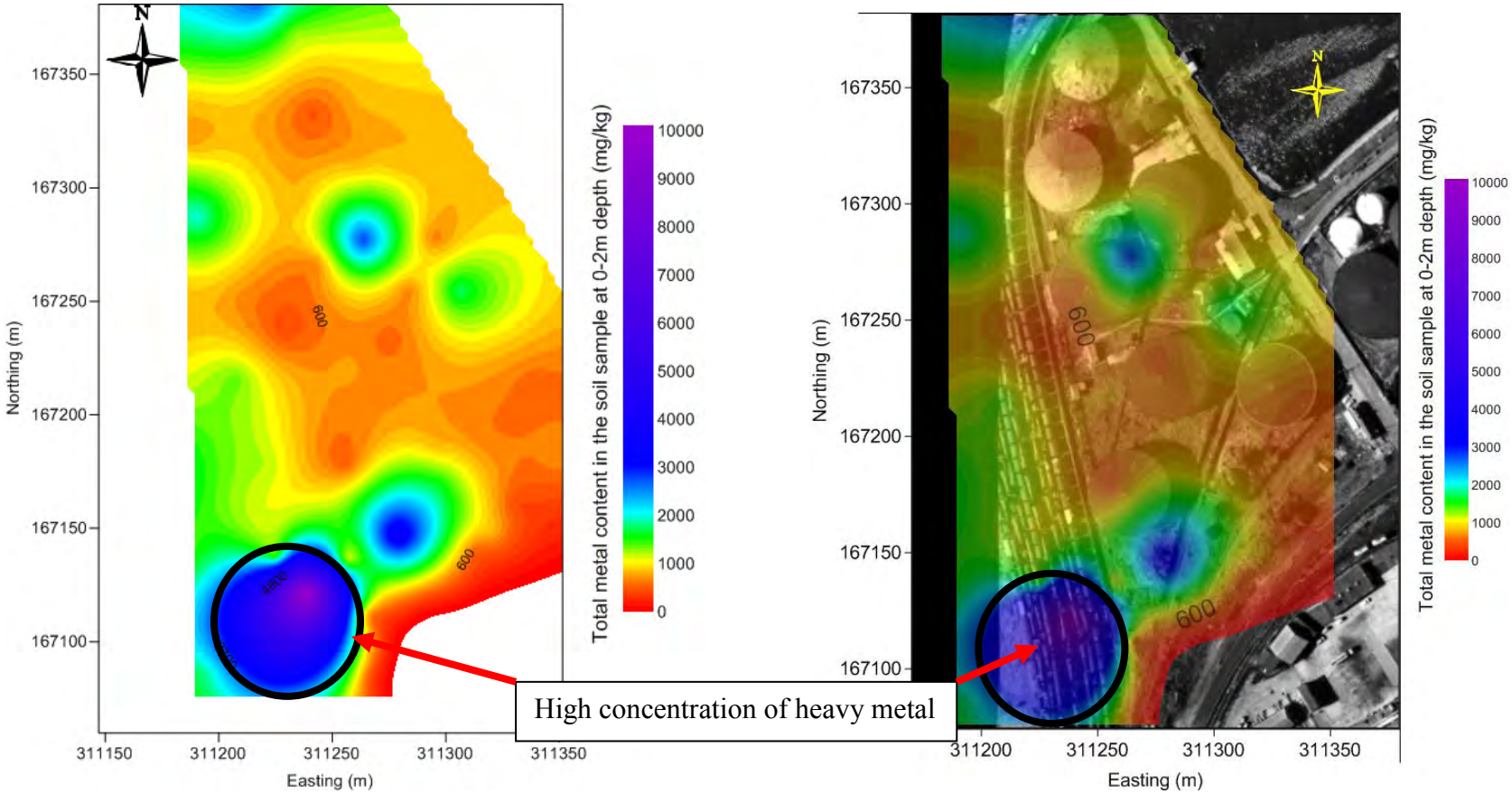

Figure 8.6: Distribution of total heavy metals on the site showing the hot spot zone at the southwest of the study area

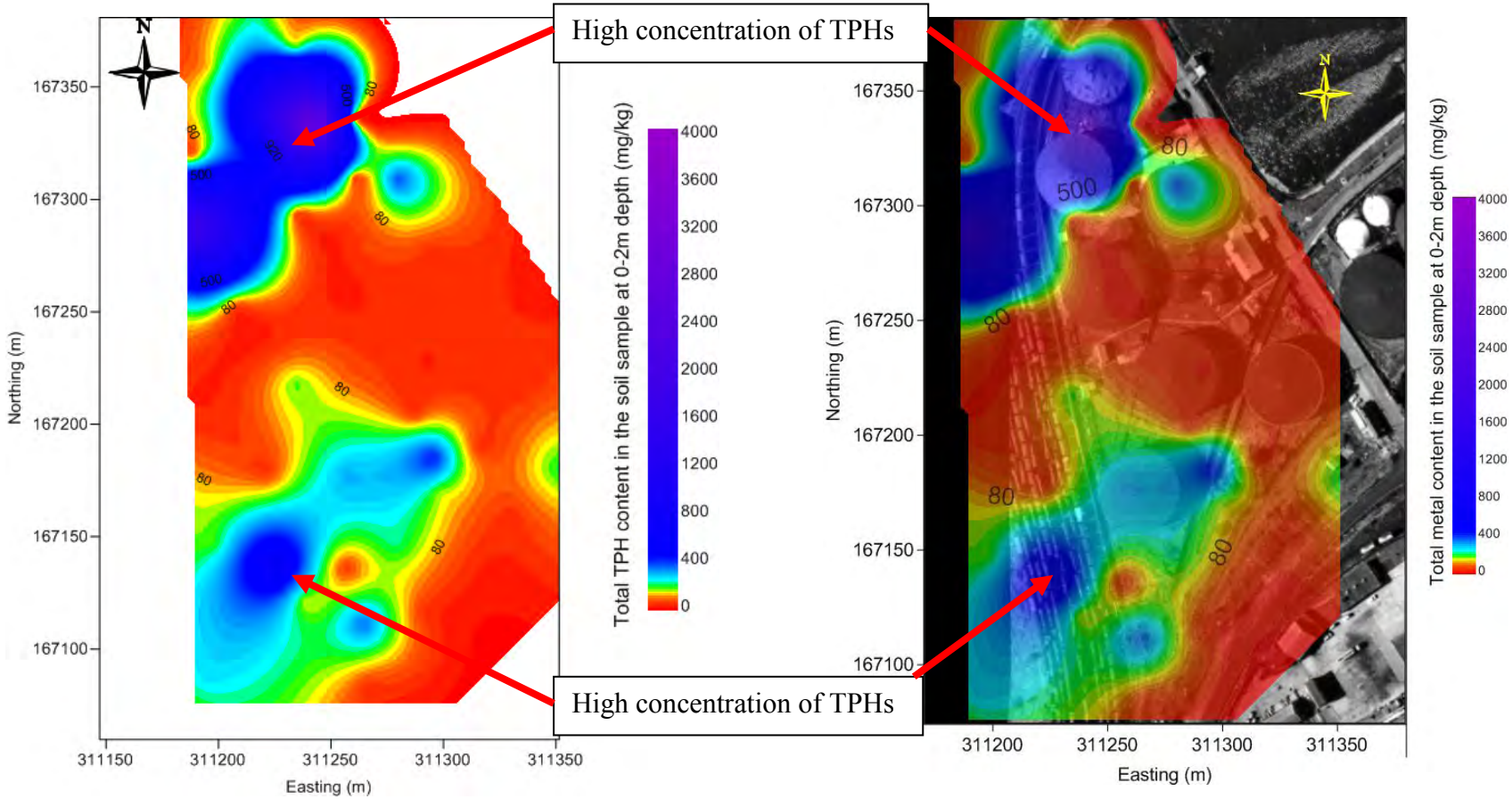

Figure 8.7: Distribution of total heavy metals on the site showing the hot spot zone at the southwest and north of the study area

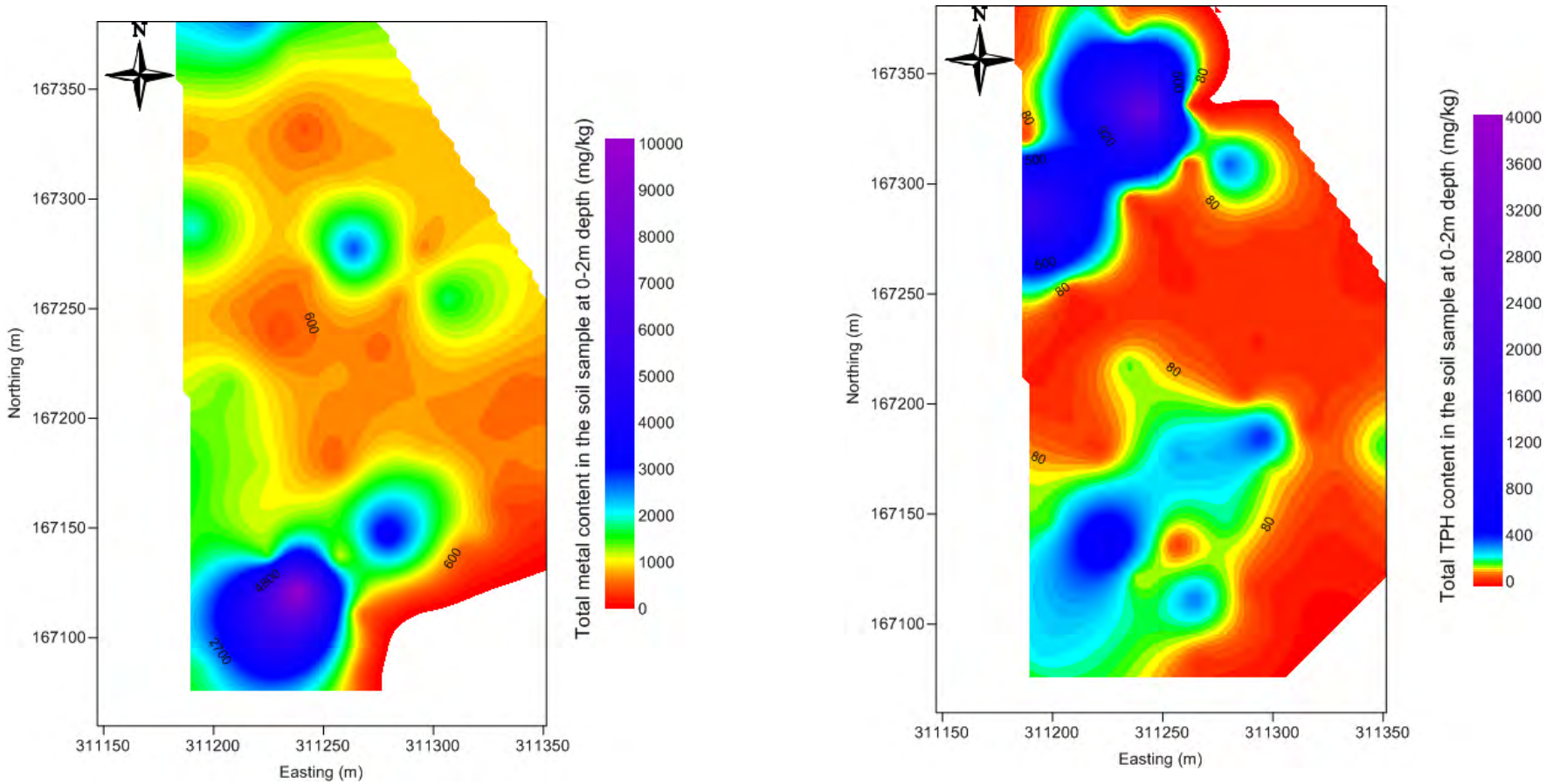

Figure 8.8: The comparison of heavy metals and TPHs distribution on the site showing both are presence at the southwest but TPHs is more dominant at the north

8.3 Resistivity and Gem-2 survey results at the tank farm zone

As mentioned previously in Chapter 5, two resistivity lines were carried out, crossing the tank farm area in a southeast-northwest and southwest-northeast direction (Figure 8.9). A ground conductivity survey also was carried out over the whole area. The data and the results of the investigation will be discussed in this subchapter. These results will provide deeper information regarding the geological and the contamination properties found on the site.

8.3.1 2D resistivity profiling

The resistivity profiles for both Barry RES 1 and Barry RES 2 line are shown in Figure 8.9. These two long lines are appropriately used to determine the geological conditions on the site. Contamination present on the site might be difficult to detect because it is expected to occur from the surface to the groundwater table which has a depth between 0 – 5m (vadose zone). Any deeper contamination is believed have an interaction with the salty or brackish groundwater as a result of the sea water intrusion at depth from the Bristol Channel.

The resistivity profile for a Barry Res1 line has an azimuth almost N-S and the Barry Res2 has an orientation SW-NE and provide a very interesting site information.

a) Geological ground model: The weathered bedrock and bedrock is detected at the south of the line which is represented by the resistivity values from 100Ωm to 300Ωm observed at the bottom of the profile. The bedrock topography is steeply dipping toward the middle of the survey line in Barry Res. This may be due to a software modelling artefact as discussed in Chapter 4, especially when the upper layer material has a very low resistivity compared to the deeper layer. While in the Barry Res2 line, the bedrock topography is flat unless at the middle of the profile which is looks like it has a large scouring structure. This structure also believed occurred because of modelling artefact from the software.

b) A shallower layer which is represented by the light green colour (50 - 100 Ωm) is interpreted as an estuarine alluvium layer consisting of mixed clay, silt, sand and gravel. The blue colour (20Ωm) at the middle is believed to be the buried

Cadoxton river channel and the higher resistivity value near to the surface is from the made ground and vadose zone.

c) These resistivity profiles also give valuable information regarding the hydrogeological condition found on the site. The groundwater table is detected just under the high resistivity layer near to the surface and its depth is in agreement with borehole measurements. The important feature in the Barry Res 1 profile is the presence of low resistivity zones in the estuarine alluvium layer which can be interpreted as the occurrence of perched water. The lower resistivity for the perched water is occurring likely due to the presence of contamination which corresponds to historical tank locations.

d) In the Barry Res2 profile, the long low resistivity zone (Blue colour) occurred due to the presence of the buried Cadoxton River channel. In the SW, the zone looks to be exposed to the ground surface which one can interpret due to this area not being capped during the previous works and is hydraulically connected to underlying historical buried river channel. Rain water has been able to infiltrate and percolate down which allows this area to be more conductive. It is corresponds geographically to the present car park area and the sewage treatment plant.

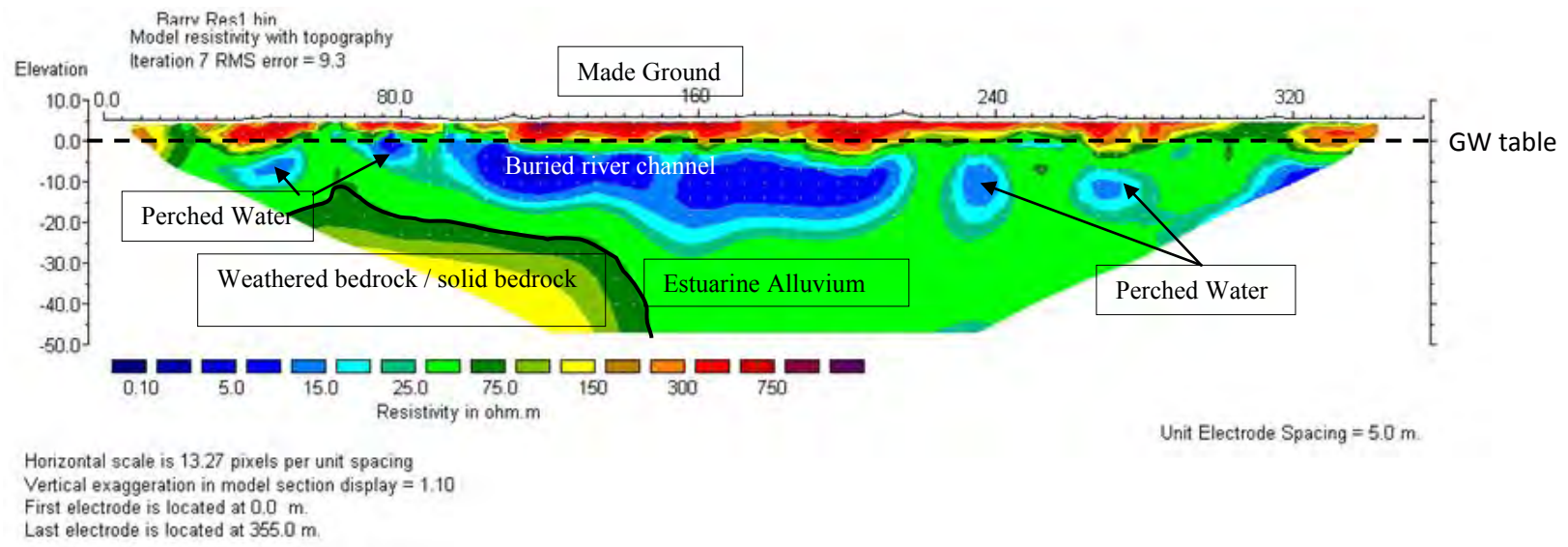

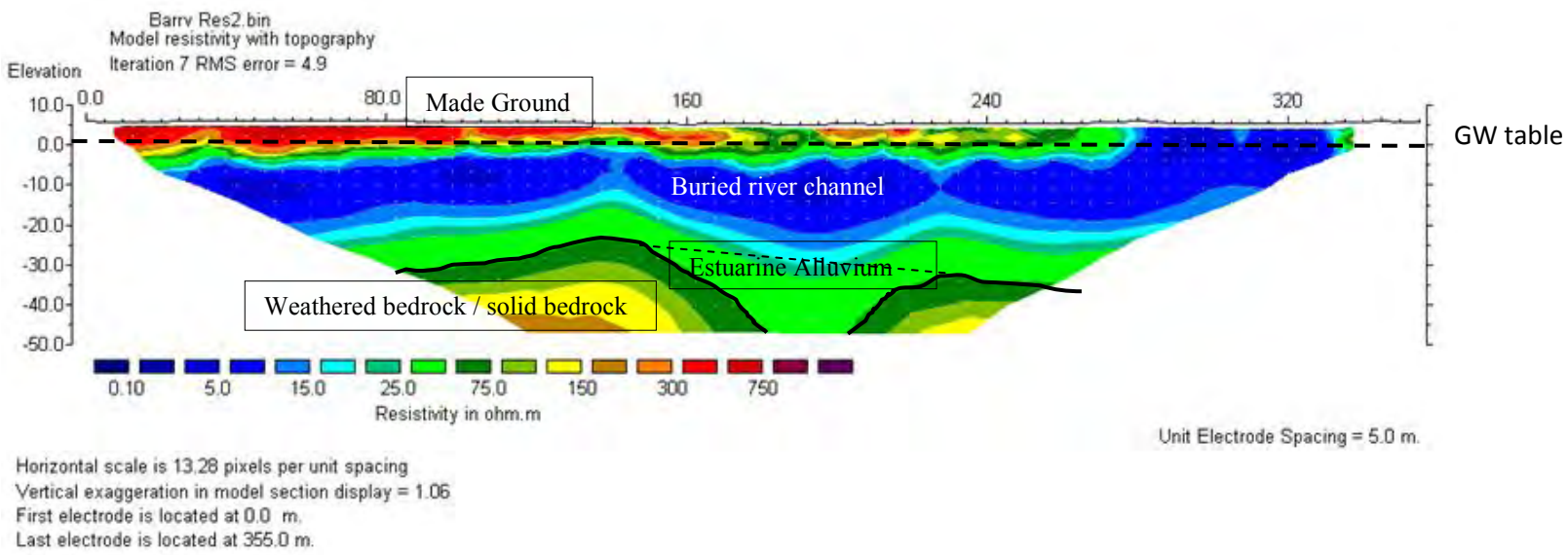

Figure 8.9: This figure shows resistivity properties of Barry RES1 and Barry RES2 line. Both show clear bedrock topography, buried river channel and the groundwater table

8.3.2 GEM-2 results

Using the Gem-2 instrument, a survey of five different depths of electrical conductivity layers has been obtained. The estimated depths of each layer are calculated using the 'Skin Depth Nomogram' established by Won (1980). According to the Figure 8.11, the depth of penetration can be calculated by using the material conductivity and the frequencies of the electromagnetic wave used in survey. Geological information of the site shows that it was originally formed of tidal flat deposits, the expected marine clays probably have electrical conductivity the ranges between 1 - 1000 mS/m (10^{-3} – 1.0 S/m). But, for this study the electrical conductivity used to define survey depth was calculated by getting an average of the conductivities from the GEM-2 survey. Around 180,000 data points have been used for the calculation and the average value obtained is 0.8362 S/m. By using this value, the depths of the layer represented by the respective frequencies are shown in the Table 8.2 below.

Table 8.2: The expected depth of the electromagnetic wave penetrated into the ground based on the electromagnetic frequency used.

EM Wave Frequency (Hz)	Expected depth (m)
40075	2.6
31025	3.2
16075	4.5
7075	6.0
875	19.0

The first two layers calculated have a close depth values which as expected do not give significant different results on the material conductivity distribution in those layers (Figure 8.11 and 8.12). However, the deeper layers represent by 4.5m (Figure 8.13) and 6.0m (Figure8.14), probably the conductivity distribution will be influenced by the groundwater effect. According to the Ove ARUP Report (2008), during the site investigation, groundwater strikes were encountered in the made ground between approximately 3m bgl and 6m bgl (4m AoD and 1m AoD) and in alluvium typically between 10mbgl and 12 mbgl (-3m OD and -5m OD). Generally, when a GEM-2 survey is carried out, the groundwater level in the selected boreholes were between 3m bgl and 6m bgl. Due to this, the conductivity of the material in these layers is increasing slightly.

In the layer number five (Figure 8.15), the conductivity looks higher and it is dispersed over the whole layer. Its presence is probably due to the layer is saturated with the seawater which drastically increases the conductivity of the ground material.

Interesting ECs distribution patterns are observed in the four top layers where almost all old tank locations surrounded by a high EC values except to tank number 3. It means that areas are potentially contaminated.

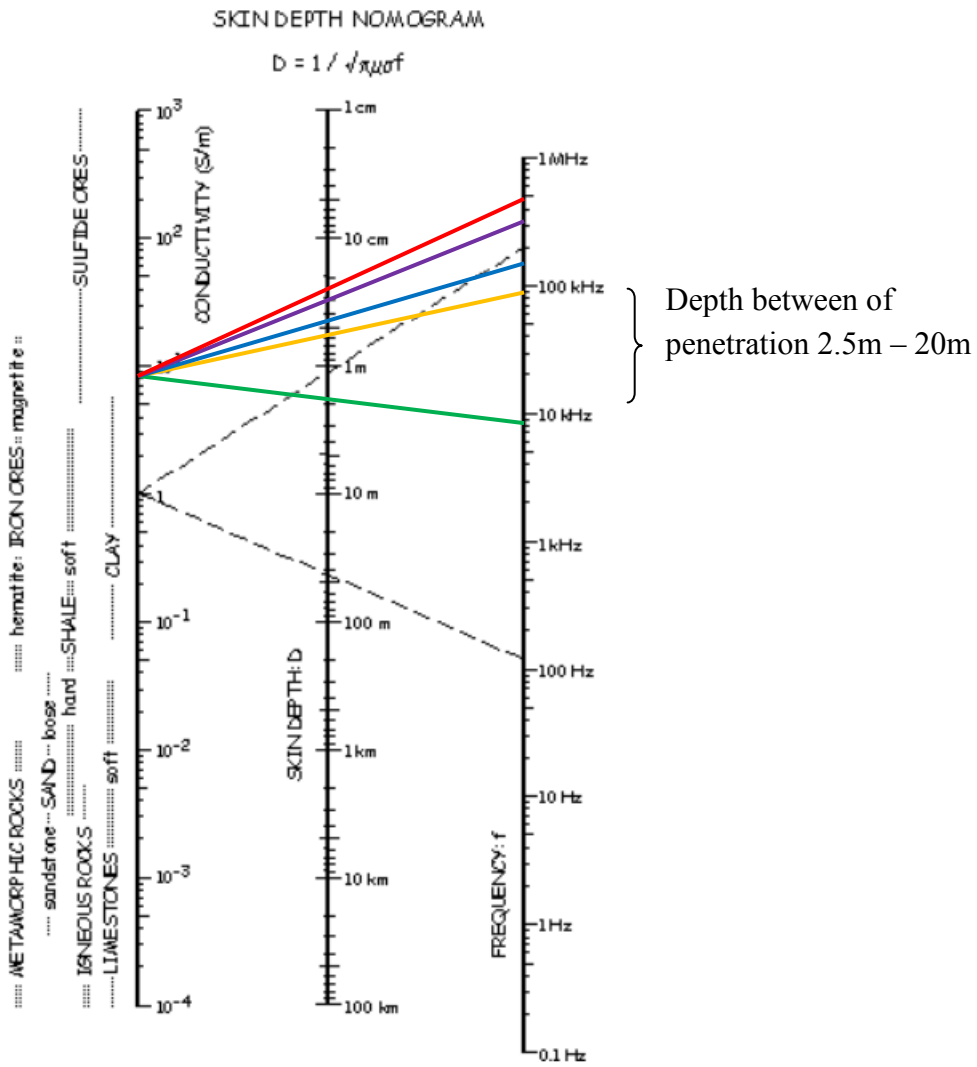

Figure 8.10: 'Skin Depth Nomogram' diagram is used to determine depth of layers

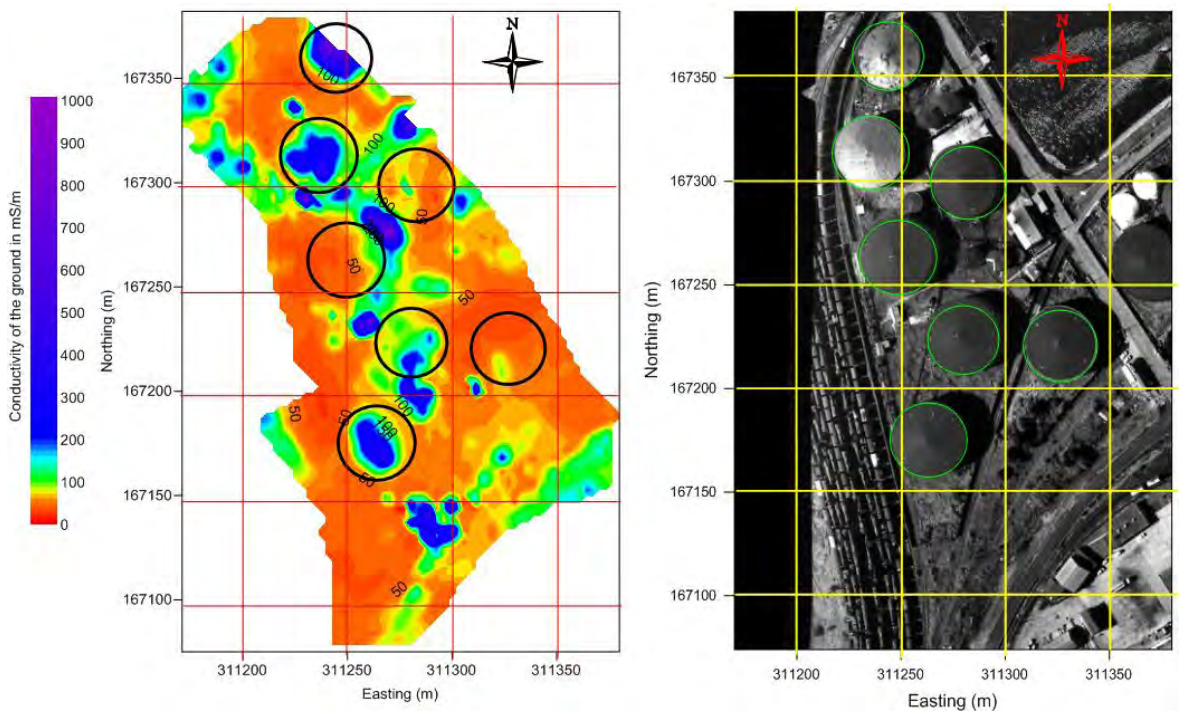

Figure 8.11: Distribution of electrical conductivity at approximately 2.6m depth

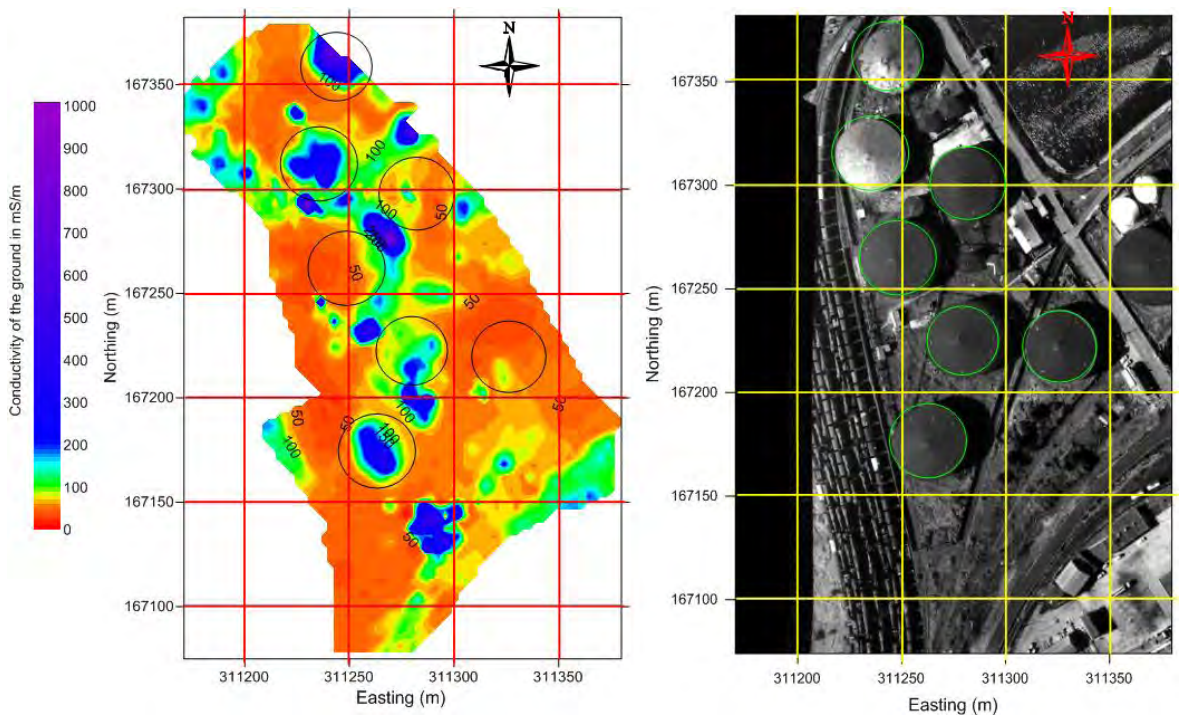

Figure 8.12: Distribution of electrical conductivity at approximately 3.2m depth

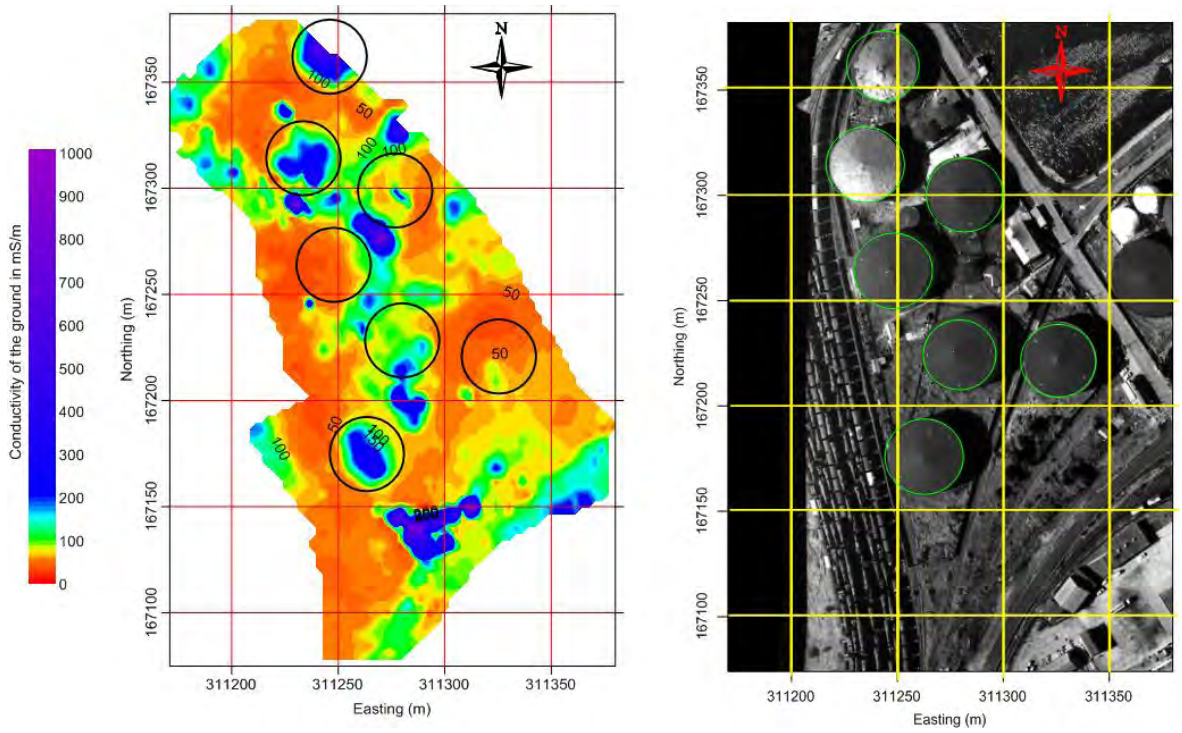

Figure 8.13: Distribution of electrical conductivity at approximately 4.5m depth

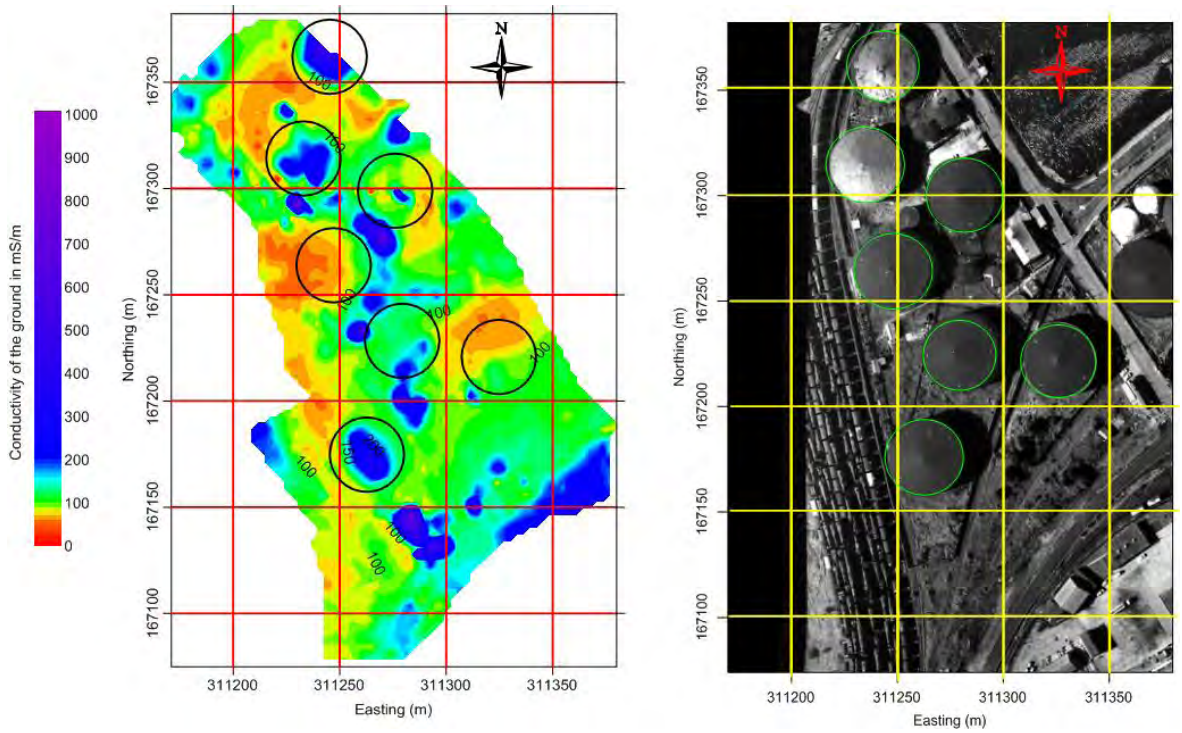

Figure 8.14: Distribution of electrical conductivity at approximately 6.0m depth

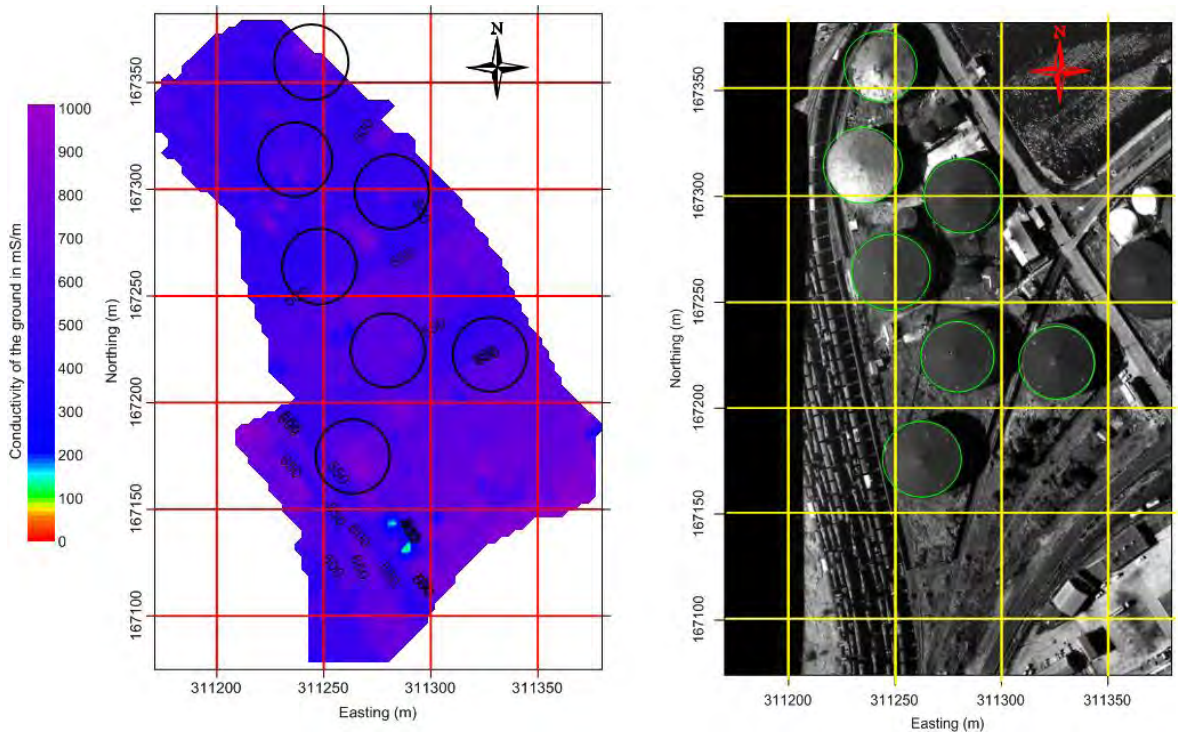

Figure 8.15: Distribution of electrical conductivity at approximately 19.0m depth

The interaction between the conductivity of the material and the distribution of heavy metal and the TPHs is shown in Figure 8.16, where the value of the conductivity is chosen from the 2.6m depth. In this figure, three major observations can be made regarding the relationship of those four pictures.

a) The high conductivity zones are located at the base of the old tanks or adjacent to the tanks except for tank No. 3, which hasn't a significantly high conductivity values. This meant the conductivity is likely has a relation with any chemical content stored in the tank. Due to all the tanks are used to store hydrocarbon based products, the high values of the conductivity at the tank farm area is significant and most likely due to the presence of this material.

b) An interesting part is at the south where both heavy metal and TPHs give a similar response by showing higher values. This then also been observed as a higher conductivity zone by the GEM-2. Qualitatively, the higher conductivity occurred due to high concentration of heavy metal and high TPHs presence in this area. It also shown as the high conductivity value observed at the tank No. 7, where both

heavy metal and TPHs distribution showing high value followed the increasing of the conductivity.

c) Meanwhile, high conductivity at the region of tank No 5, 6 and 7 can be related with the high value of TPHs because the heavy metal presence is lower in that area

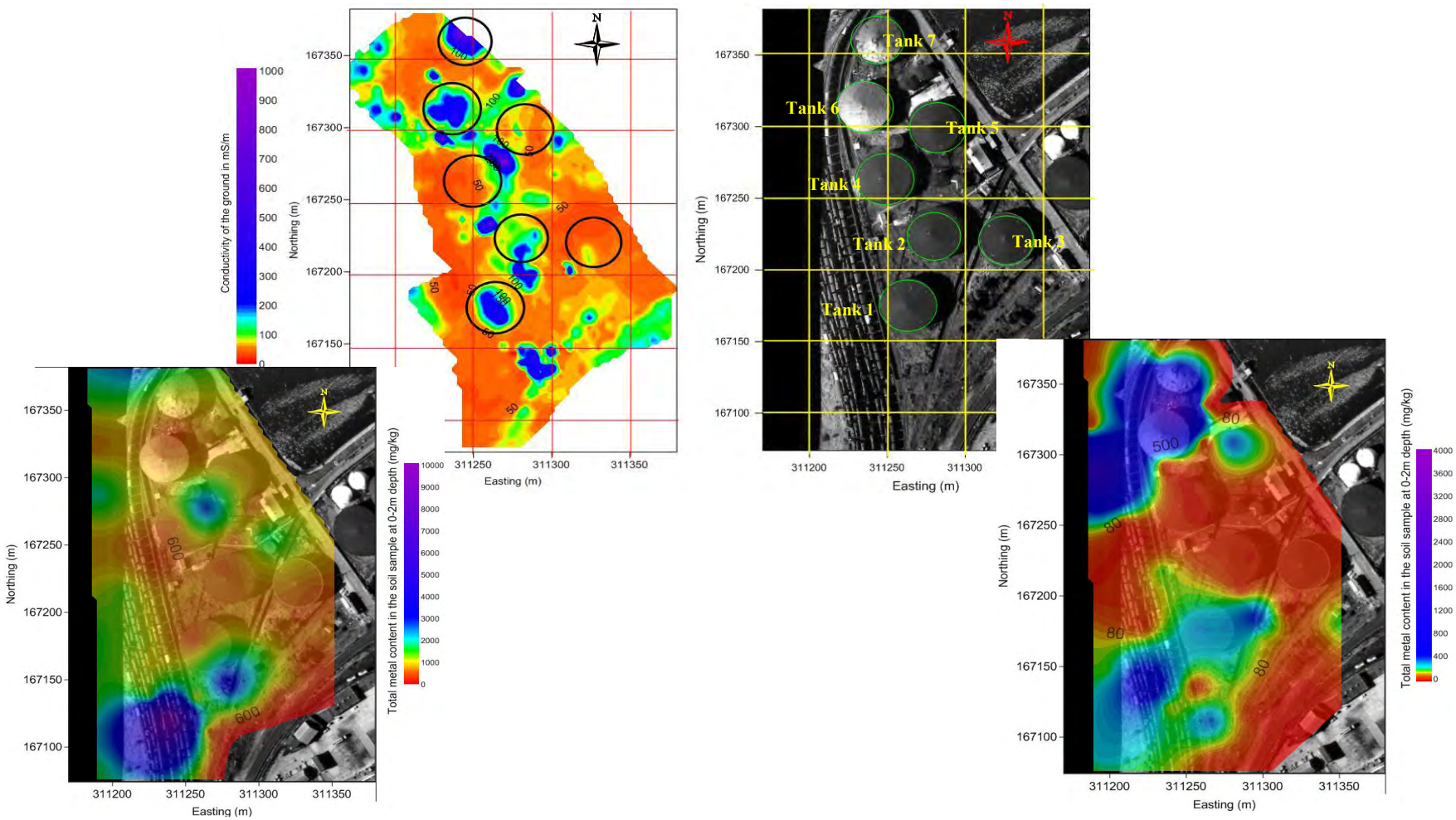

Figure 8.16: Showing interaction between the conductivity of the material and the heavy metal and TPHs distribution. High TPHs at the north, combination high heavy metal and high TPHs on the south

8.4 Resistivity and Gem-2 survey results at the small area

Electrical ground resistivity data from six short parallel resistivity survey lines was collected using a 36 electrodes and 1m electrode spacing in a small study area. A GEM-2 survey was also carried out in this same area. Results from these two surveys are discussed in the following section.

8.4.1 2D Resistivity profiling

Generally, the soil layer in this area shows similar consistent resistivity properties as previous surveys at the Barry site (Figure 8.9). The lower resistivity value zone (<20Ωm) which is shown as the light to dark blue colour is found at the middle and at the end of the profiles (24m – 32m) – Figure 8.17. For all the resistivity lines this can be interpreted as a contamination zone. This resistivity value can also be related to the presence of a clay layer, but due to the site being situated near to the rock cliff and it was formerly the storage tanks foundation it is unlikely that the clay layer is present in this area.

Higher resistivity values between 20 – 50Ωm are interpreted as brackish zone or semi contamination zone. The value 50 - 150Ωm is interpreted as a saturated un-contamination zone with fresh water. Weathered bedrock exhibits a resistivity value of more than 150Ωm and it clearly can be seen in the resistivity profiles. It is shallow near to the cliff and gradually deepens away from the cliff. The highest resistivity measured near to the surface is due to the concrete tank foundations which are still present on site.

It is surprise here that the resistivity of the TPHs appears lower at this site, in contradiction to what been found in the Cathays Railway Depot site. There are two explanations which can be used to help understand this observation.

a) The TPHs were dumped into the site longer than what is has in the Cathays Railway Depot (Chapter 6). The aggressive use of the site for the tanks storage activity is recorded by air photography back to World War II (approximately 1942 onwards) when the docks are use to supply fuel and supplies to USA ships. In Cathays, the use of DMU (Diesel Multiple Units) locomotives which is first use of diesel commences in 1958. According to Atekwana et.al 1988, the longer the petroleum products are dumped into the ground, the greater the biodegradation

processes and the lower the value of resistivity of material will be as a result of the biodegradation processes. This is probably a good reason to explain why Barry Dock has a lower measured electrical resistivity for a hydrocarbon contamination.

b) Compared to the Cathays Railway Depot site, Barry Docks has a much more complex geology with the presence of many geological features such as rock fissures, faults and dipping bedrock. The geological units are impermeable but also fissures as a pathway for surface water infiltrating into the subsurface to the groundwater. This means that potentially the ground water is more oxygenated, which is required for the biodegradation process to be more aggressive.

Table 8.3: Showing the resistivity ranges for interpretation together with a possibility type of materials

Resistivity Values (Ωm)	Probable Types of Material	References
0-20	Contamination zone (heavy metal/TPHs)	Meju.A.2000.
20 -50	Brackish zone (semi contamination zone)	Keller and Frischknecht, 1970
50 – 150	Fresh water/ un contamination water/layer	Keller and Frischknecht, 1970
150 – 500	Weathered bedrock or incompact material (alluvium, clay, sandstone, Shale and limestone)	Loke, 2000, 2006
>500	Vadose zone and hard rock or made ground material.	Atekwana et.al. 1998

Referring to the resistivity profiles in Figure 8.17, the pattern of lower resistivity zones is similar in all the profiles, except for profile 3D Res 6 which shows a disorderly pattern. This is believed to have occurred because the survey line is located near to the concrete wall at the right (Easterly) side of the line. The concrete wall is built down to the bedrock to strengthen of the storage tanks foundation. Concrete is a good impermeable barrier to stop any liquid flowing through the sub-surface and it will be a good trapping structure to collect any contamination liquid from this area. It will increase the contamination zone size as shown in this resistivity profile (3D Res 6).

Meanwhile, looking to the bedrock structures, the top layer shows a scouring pattern which is believed to be due to unequally fractures of rock and a different weathered rock grade. The weathering grade has a high density of fractures which increases the porosity of the rocks.

Another clear structure which can be seen in the resistivity profiles is a dipping of the bedrock profile at the end of each survey line. This is believed to have occurred due to presence of the normal fault at that area which separated the Penarth Group in the north with the St. Mary's Well Bay Member at the south (the outcrop is t at the cliff) – Figure 3.30 in Chapter 3. It provides a high porosity sump to deposit contaminants in that area.

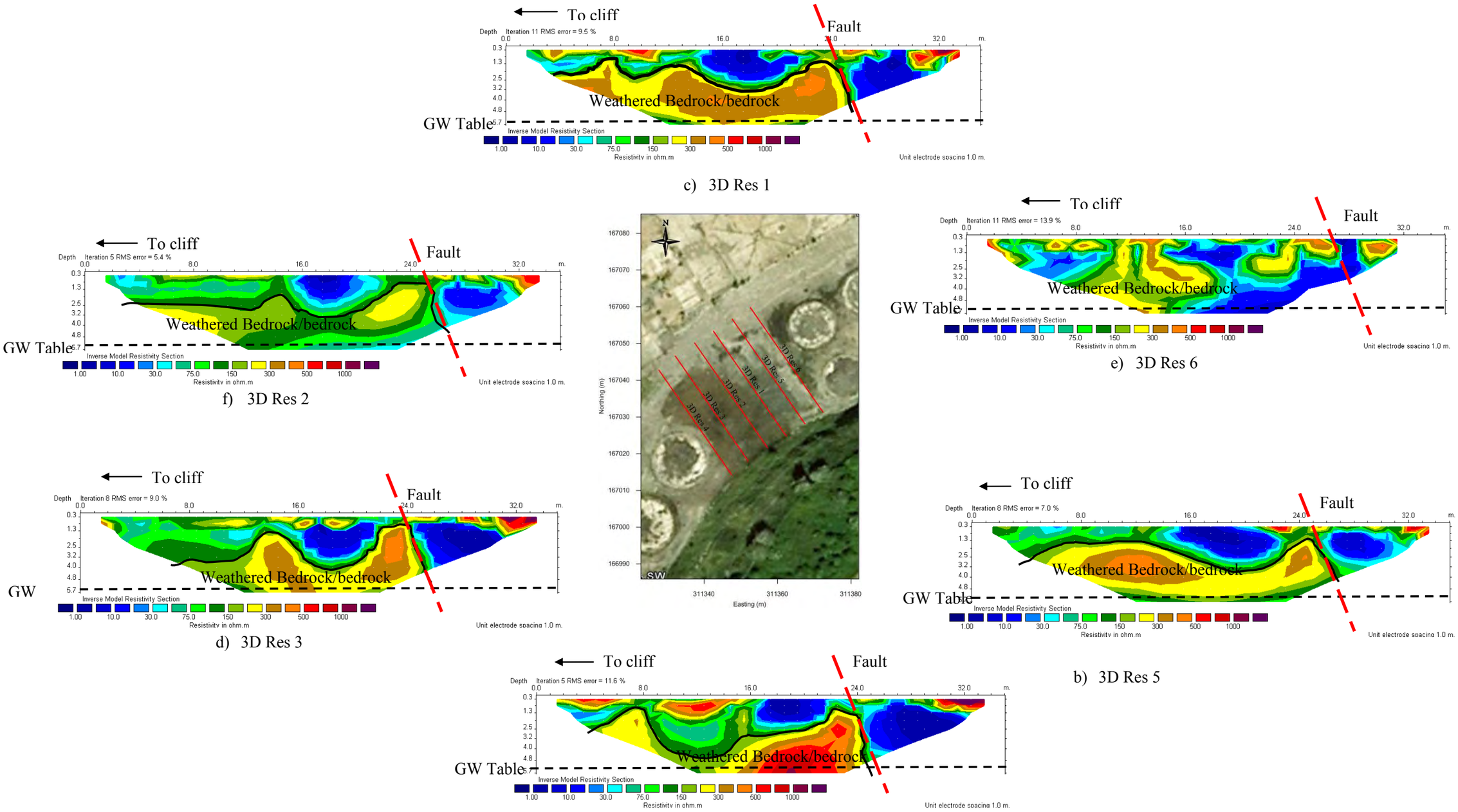

Figure 8.17: The 2D resistivity profiles showing a contamination zones representing by blue colour (<10Ωm). All the profiles has a similar pattern unless for 3D Res 6 where it's has a blue colour distribution larger than other profiles. It's believed occur due to the resistivity line was built beside the concrete wall. Normally concrete can be a good barrier and contaminant plume potentially trapped along it side

8.4.2 Resistivity 2D plan view

The 2D plan views are created by using the final resistivity inversion data from the previous resistivity profiles as shown in Figure 8.17. The ASCII format file has the resistivity values of every calculated point and as well the depth of a layer. It is also provides the X and Y location on the surface. Using this information a set of data including the X and Y location and the resistivity values of every line in a similar depth can be compiled. Finally, similar to the analysis for the 2D resistivity plan view in Cathays, the analysis has been made using Surfer-9.

In this analysis, eight different depths of data had been plotted. Each of them represent depths of 0.5m, 1.0m, 1.6m, 2.2m, 2.8m, 3.6m, 4.4m and 5.2m. For the first two shallow layers (<1m depth), the distribution of low resistivity zones shows a random pattern (Figure 8.18 and 8.19). Interactions between low and high resistivity have no clear pattern, this shows that the material near to surface are mixed. Probably the higher resistivity is produced from the rock aggregates and the concrete foundations on the ground. Meanwhile the lower resistivity can be related to the presence of the tar observed on the surface and possibly also a clay material.

For the layers at 1.6m, 2.2m and 2.8m, the distribution of the resistivity values are unchanged (Figure 8.20, 8.21 and 8.22). The resistivity distribution is creating two lower resistivity band zones in each layer. This first band of lower resistivity zone at the north is expected to be due to the presence of a normal fault at depth. Generally, the fault zone always has fractured rocks which potentially increase the rock's porosity and at the same time is likely to be rich in clay minerals. This allows this zone to exhibit a lower resistivity as shown in this lower resistivity band in the Figure 8.20 to 8.22. Another low resistivity zone is interpreted due to the presence of HC contamination. Tar marks are found on the surface of this zone in almost every line as shown in a Photo 8.1 and 8.2. This is observed as the scouring structures in the 2D resistivity profiles.

Going to the deeper layers (3.6m depth), the lower resistivity zone gradually disappears (Figure 8.23) and only having small spots at the depths of 4.4m (Figure 8.24) and 5.2m (Figure 8.25). These zones are slightly bigger in a layer number eight (5.2m depth) and this is expected due to its interaction with the groundwater.

The second layer (1.0m depth) has slightly different resistivity distribution which might be due to the presence of the hard concrete foundation material to 1.0m depth.

In layer number six (3.6m depth), the yellow colour contour is believed to represent the weathered bedrock and its distribution is dominant in the southeast (Barry Island Cliff). It means that the bedrock is shallower nearer to the cliff compared. However, the lower resistivity band in the northwest still exists, showing that the fault zone can be observed in this layer. The distribution of the higher resistivity zone is larger in the layer number 7 at 4.4m depth which means that this layer consist of bedrock material left a two small lower resistivity zones at the north and northwest of the layer. These zones are observed as a deeper scouring structure on the top of the bedrock in the 2D resistivity profiles. It probably occurs due to unequal rock strength where in these zones are expected to be weaker due to the presence of the deeper fractured rocks.

Two interesting observations can be seen in these last two layers:

a) The disappearance of the low resistivity bands. The northern band disappearance can be explained based on the structure of normal fault itself. The fault axis is dipping slightly toward northwest, so the occurrence of the fault axis in deeper layer is expected far from the cliff. It does not show in the 2D plan view as it is located outside the survey line area.

b) The two low spot zones resistivity are bigger in the eighth layer, which shows it's has an interaction with the groundwater. This allow a conclusion to be made that the groundwater in this region is potentially contaminated

Photo 8.1: Showing the HC (Bitumen) marks on the ground in the 2D small area

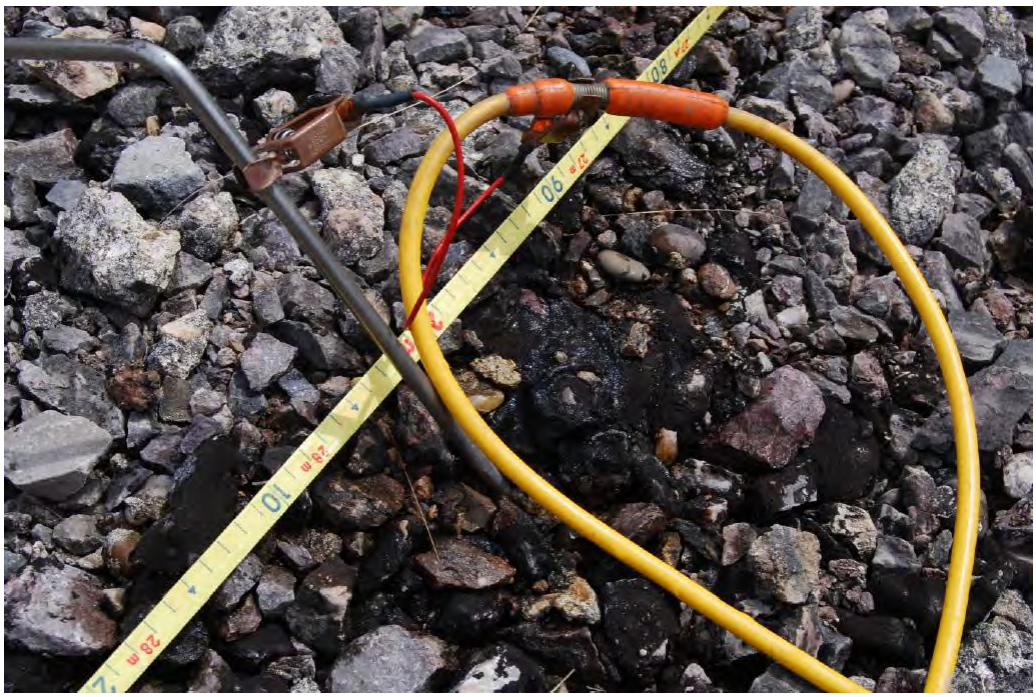

Photo 8.2: Showing tar has been found on the surface

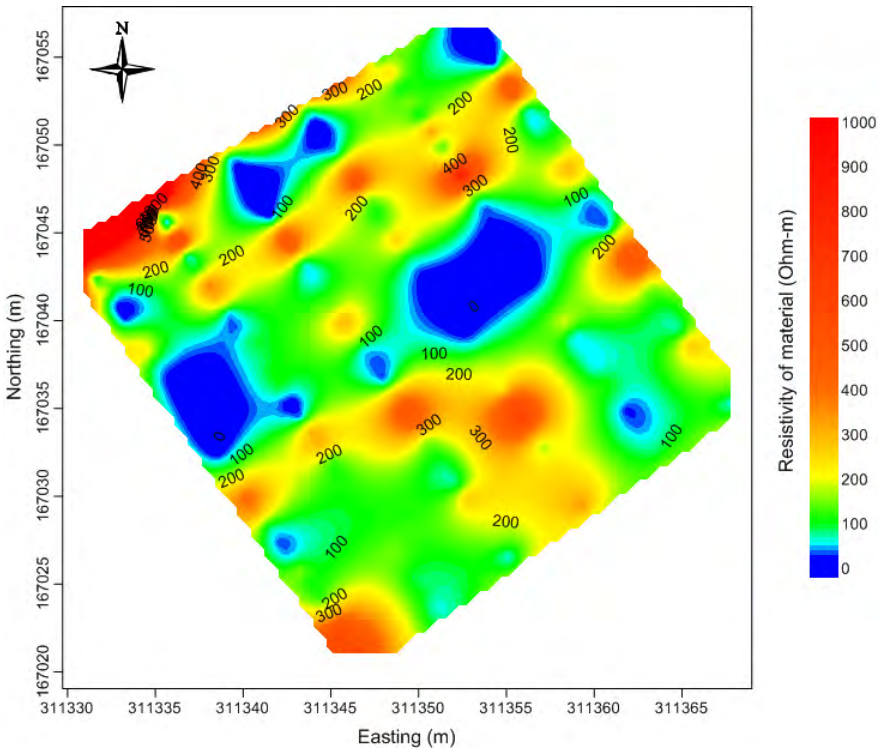

Figure 8.18: At 0.5m depth, showing two bands of lower resistivity zones

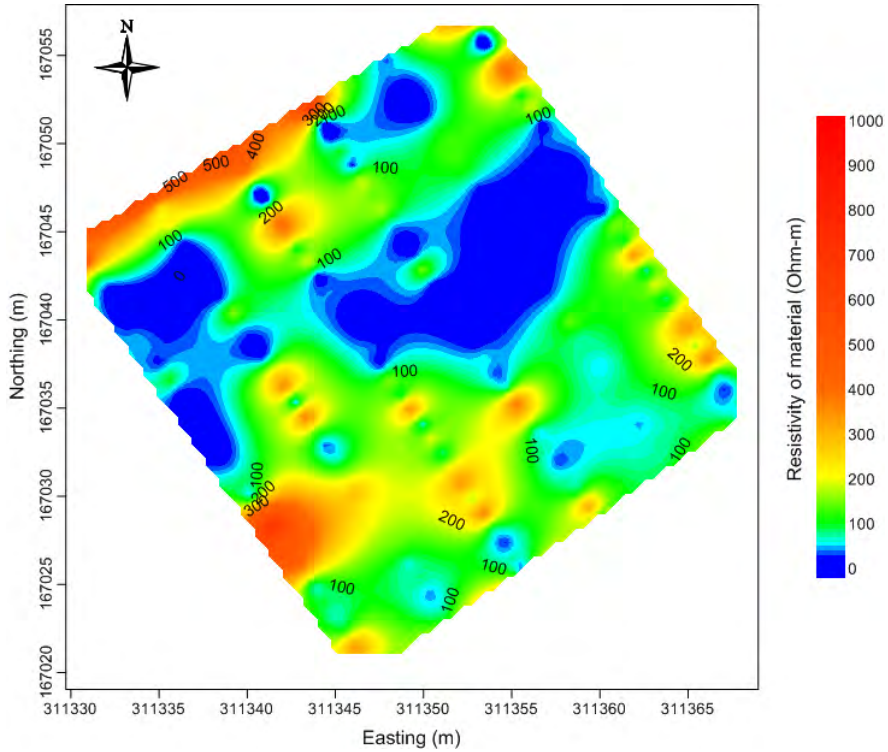

Figure 8.19: At 1.0m depth, the two bands still can be seen but not very clear

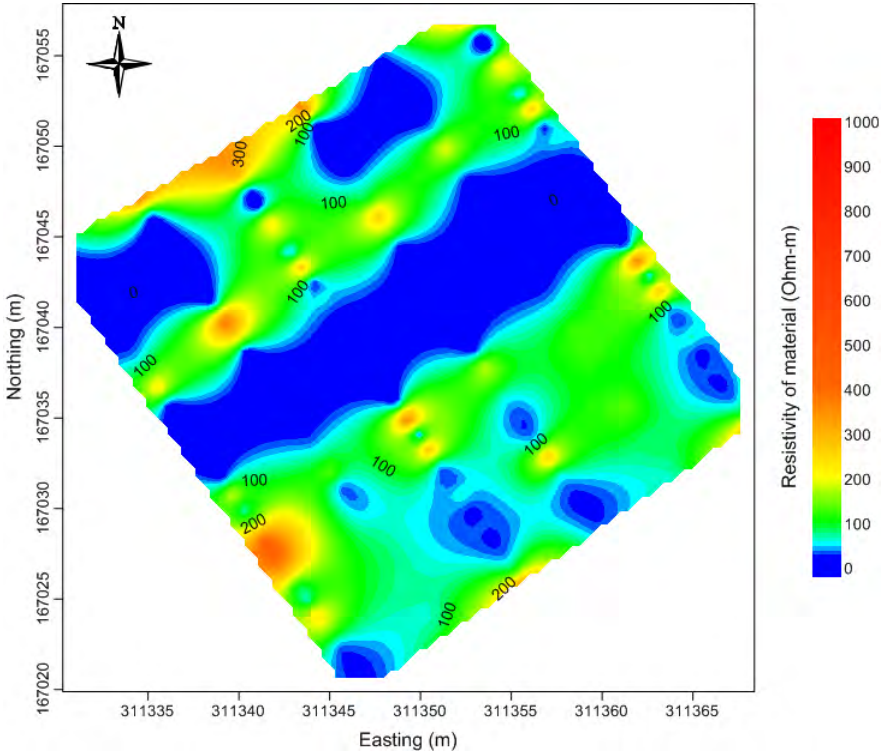

Figure 8.20: The bands are seen clearly in the1.6m depth

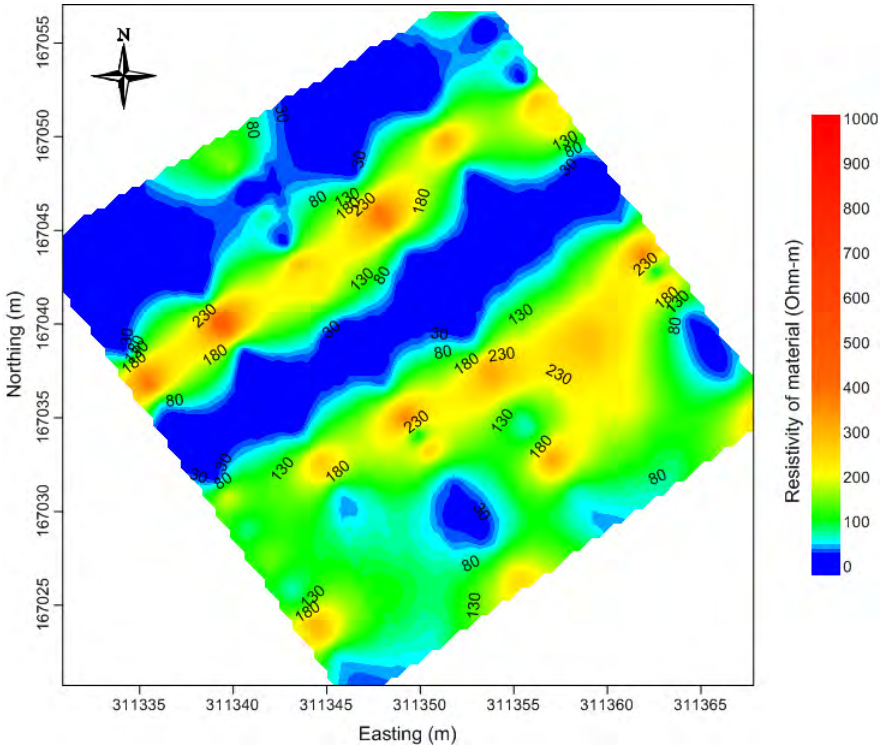

Figure 8.21: Remain clear in this layer (2.2 m depth)

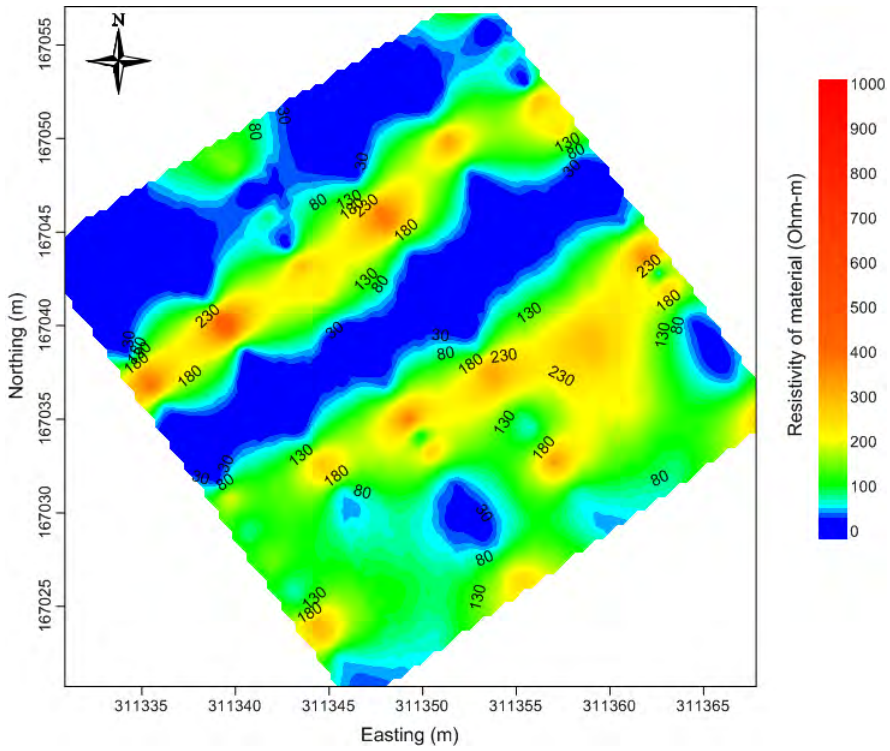

Figure 8.22: Remain in 2.8m depth

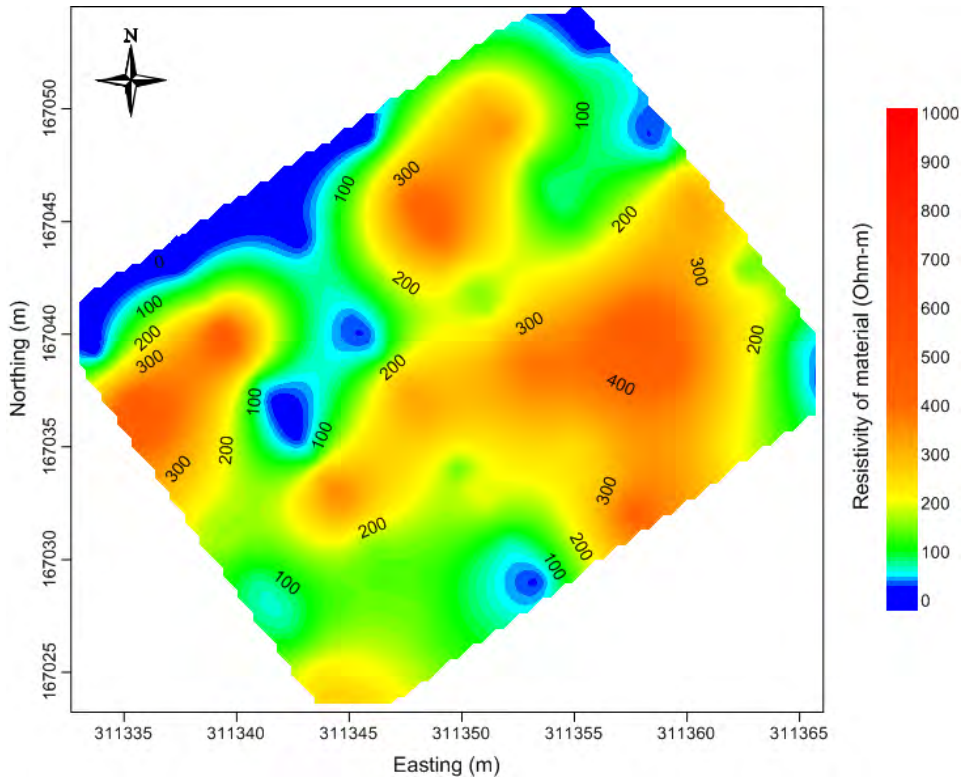

Figure 8.23: Disappear for the inside band and still can be seen for the outer band at the 3.6m depth. The bedrock slightly can be observed as shown in the yellow colour contour

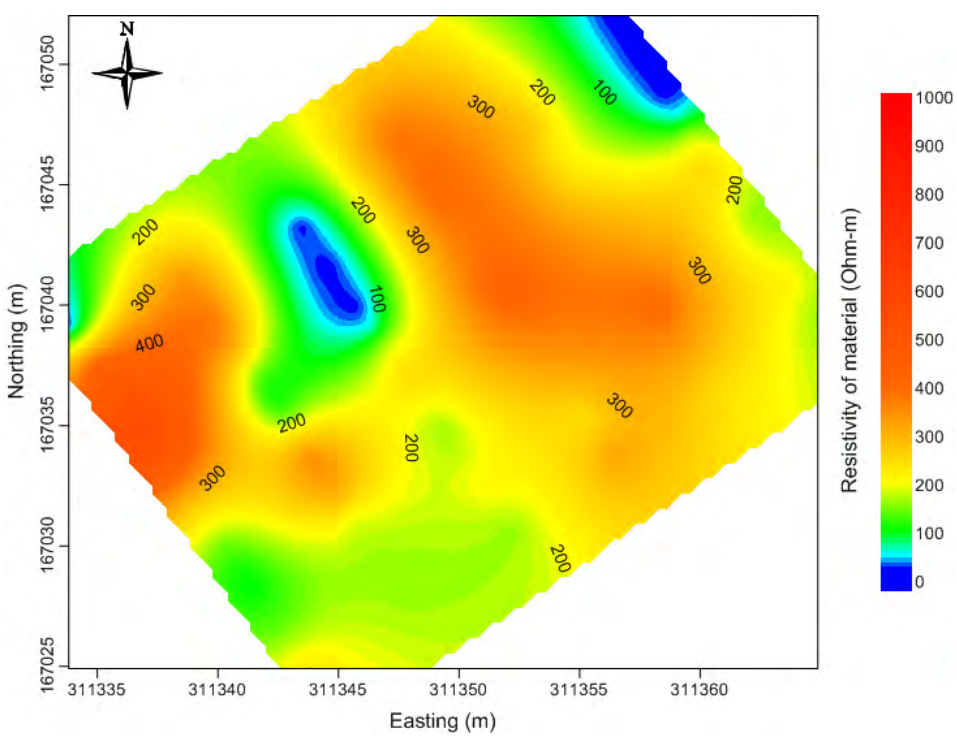

Figure 8.24: At 4.4m depth, almost all the area is cover by the bedrock but still have two lower resistivity zones which believed due to scouring structure fill by the contaminants

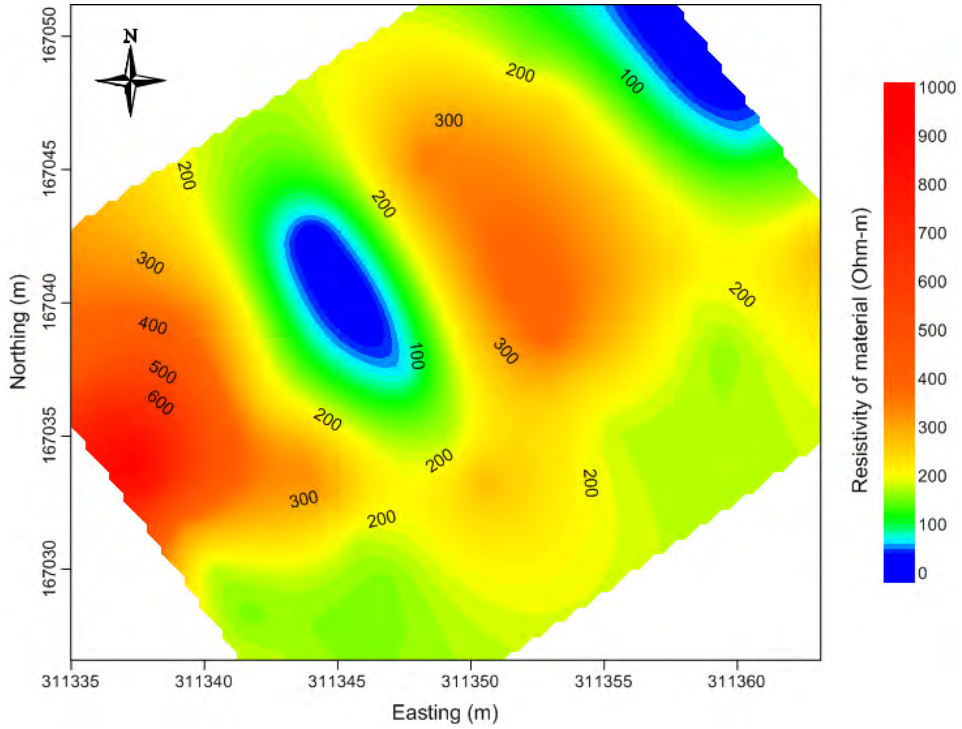

Figure 8.25: The low resistivity zones going bigger probably due to its interaction with the groundwater at the 5.2m depth

8.4.3 GEM-2 results at small area

An average conductivity for the material calculated by the GEM-2 data using 48,000 data points is 1.5092 S/m. By using a 'skin depth nomogram', (Figure 8.26) the depth of penetration given by selected electromagnetic wave frequencies is shown in Table 8.4 below.

Table 8.4: The effective depth of the electromagnetic wave which penetrates into the ground based on the frequencies employed.

EM Wave Frequency (Hz)	Expected depth (m)
40075	2.1
31025	2.5
16075	3.5
7075	5.0
825	16

The depth of the first four layers is not significantly different to the depths of the resistivity layers calculated previously. Only the fifth layer, which maps to about 16m depth is this different. The survey area for the GEM-2 is slightly larger than the resistivity 2D area, to allow more information to be obtained. The conductivity distribution for each layer is plotted as shown in Figure 8.28.

The distribution of conductivity for first 3 layers is remains similar, which the higher conductivity is present in the northwest and in the middle of the plot. It likely these two bands of high conductivity zones are connected at both ends.

There is not many different observations that can be made to this GEM-2 results because of it's similarly to the 2D resistivity plan view. Here are some observations:

a) The first three layers (up to 3.5m depth) show higher conductivity zones on the northwest (fault zone) and middle (contamination zone).

b) Lower conductivity at the southeast is expected to occur due to the presence of the bedrock and this is shallower because it is nearer to the cliff.

c) At the 5.0m depth represent by the 7075Hz electromagnetic wave, data shows the conductivity becoming slightly higher. The contour colour in the bedrock regions is changing from reddish/orange to greenish and bluish colour. This can be interpreted as being due to an interaction with the groundwater.

d) At the northeast and southwest, the four layers all display a higher conductivity zone. This area is previously where the storage tanks were situated which have potentially introduced ground contamination. So, the higher conductivity in this area is probably due to contamination soil/layers. This did not show in the resistivity profiles because these two zones are outside of the resistivity survey area.

e) The deepest layer shows the whole area has a high conductivity. However, this potentially does not represent a true conductivity because the occurrence of high conductivity in deeper layer may be due to noise or weak e/m signals from the ground.

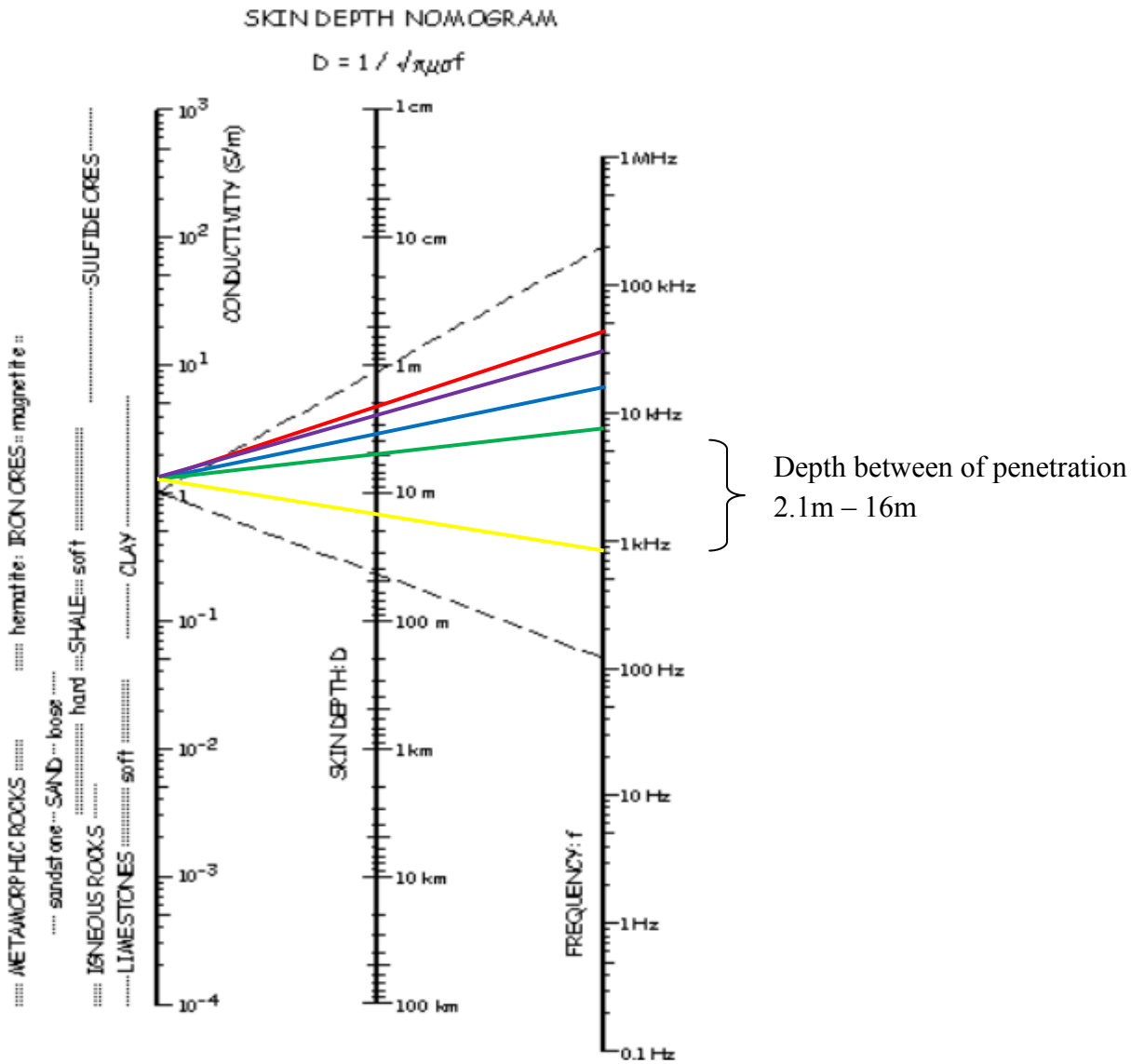

Figure 8.26: 'Skin Depth Nomogram' for the GEM-2 survey at 3D small area. The average conductivity of material is 1.509 S/m which is calculated using the GEM-2 data

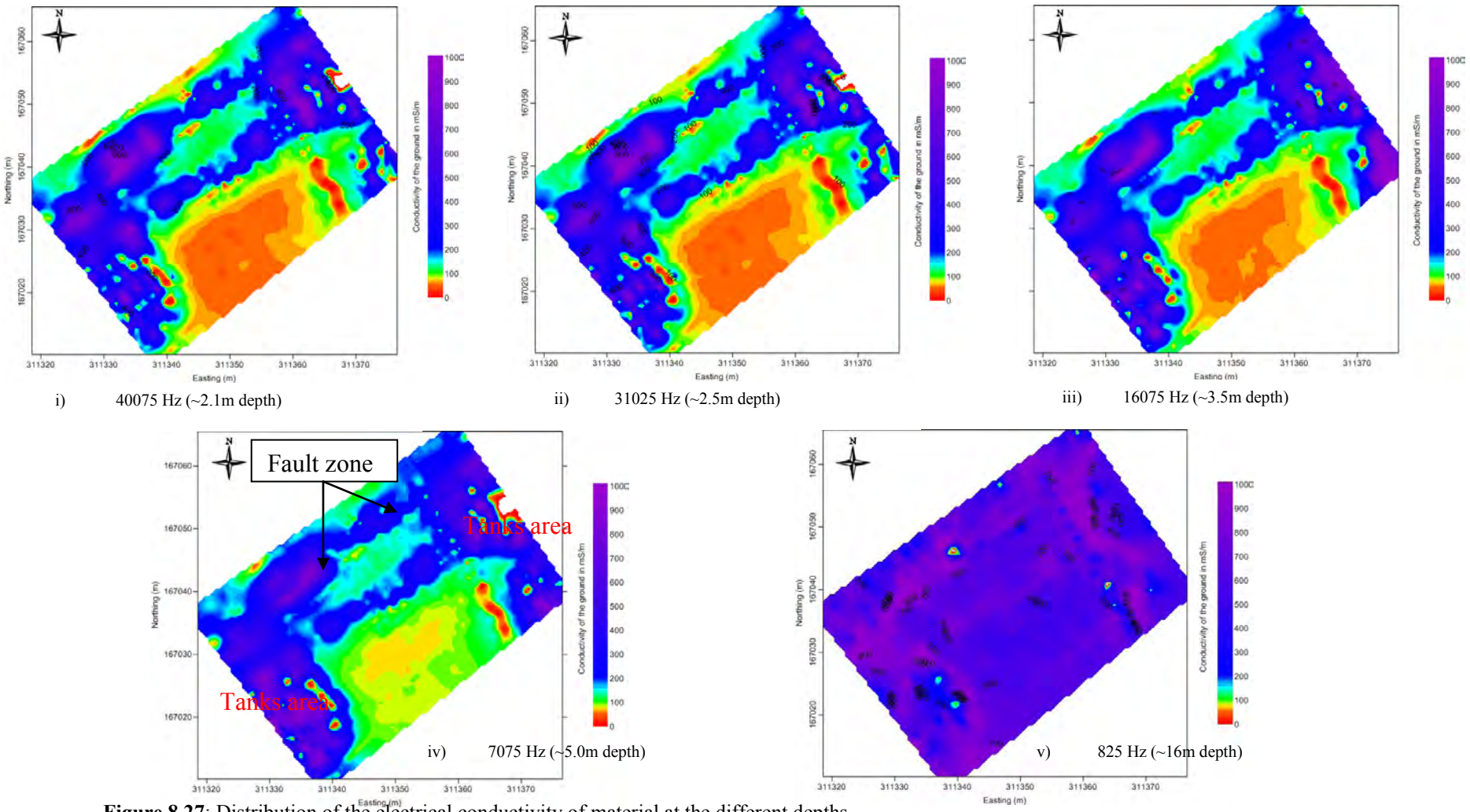

i) 40075 Hz (~2.1m depth)

ii) 31025 Hz (~2.5m depth)

iii) 16075 Hz (~3.5m depth)

iv) 7075 Hz (~5.0m depth)

v) 825 Hz (~16m depth)

Figure 8.27: Distribution of the electrical conductivity of material at the different depths.

Observations: a) First three layers show a similar pattern and values

b) Fourth layer, the pattern remained but the value is slightly higher most probably due to interaction with the groundwater.

c) Fifth layer has a higher conductivity in the whole area which believed due to the signal is very weak.

8.5 Conclusions

Generally, the Barry Dock research site is complex in terms of its geological setting, hydrogeological properties and complex industrial history due to variety of past activities on the site. The contamination on the site is complicated, with an integration of both heavy metals and hydrocarbons. The overall distribution pattern of heavy metals and HC is similar with the high concentration found dominantly in the southwest and in the middle of the study area. A high concentration of HC can also be found in the north where the historical storage tanks were once located.

In the tank farm zone, heavy metal and HC show a good correlation. Both have a high concentration zone in similar locations which is dominantly in the south (railways and sidings area) and at tanks No 1. However, the heavy metal did not present in high concentration at the tank numbers 5, 6 and 7 where the HC levels are higher. This is likely to have occurred because the storage tanks (tar and other petrochemical liquids) were probably leaking or had spills on the ground over the period of its operation

The high concentrations of heavy metals and hydrocarbons are shown as a high conductivity zone in the GEM-2 plots. The distributions are well matched with the high conductivity zones which are observed in the south and at the tank number 1 for heavy metal and HC, and at tank numbers 5, 6, 7 for HC only. These zones are detected up to layer four in the GEM-2 data as shown in Figure 8.28.

Generally, the Ground Conductivity Survey has very clear results. The high conductivity zones present are due to three possibilities:

a) The presence of high TPHs found in soil samples in the north

b) The high level of heavy metal content presence in all soil samples

c) A combination of both the above, which shows in the south of the tank farm zone

The long resistivity survey lines cannot be used to detect contaminated ground in high resolution, as it has a widely spaced data points. However, the data still can be use to determine the geological site model and also to map the groundwater table (Figure 8.29).

Six short survey lines provide individual 2D cross-sectional profiles. In this small area, all resistivity data were combined to visualize the resistivity distributions at the different depth using 2D plan view plots (Figure 8.30 and Figure 8.31). The results show that the distributions of the 2D resistivity slices correspond well with GEM-2 data (Figure 8.32).

Overall, the geophysical techniques employed have shown good correlation with the distribution of heavy metal and HC measured in the ground by totally independent methods. Using a combination of both electrical resistivity and electromagnetic GEM-2 data the electrical properties of the ground can be mapped in vertical and horizontal slices of the electrical properties of the ground material.

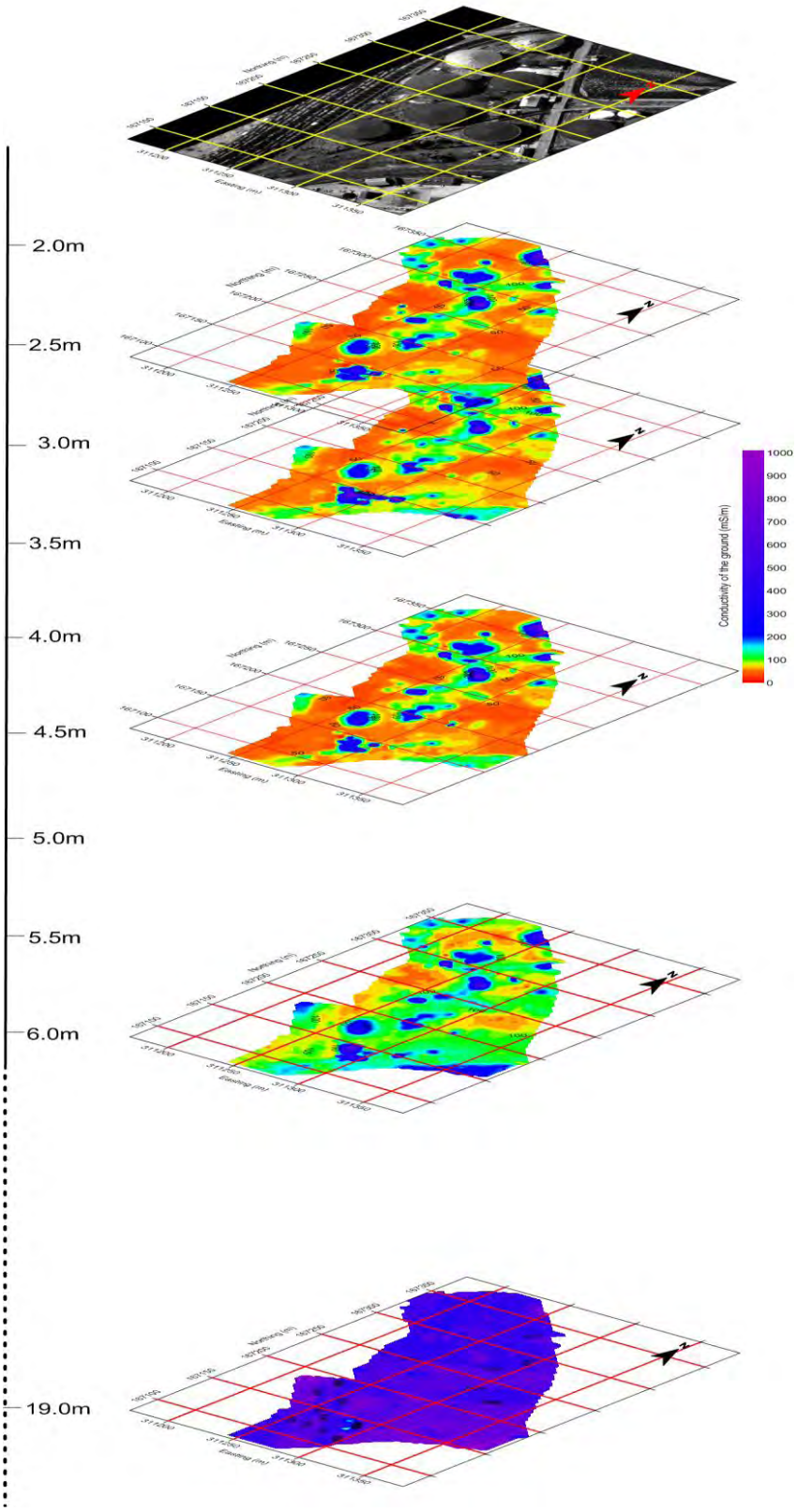

Figure 8.28: Showing the combined conductivity of the ground against depth

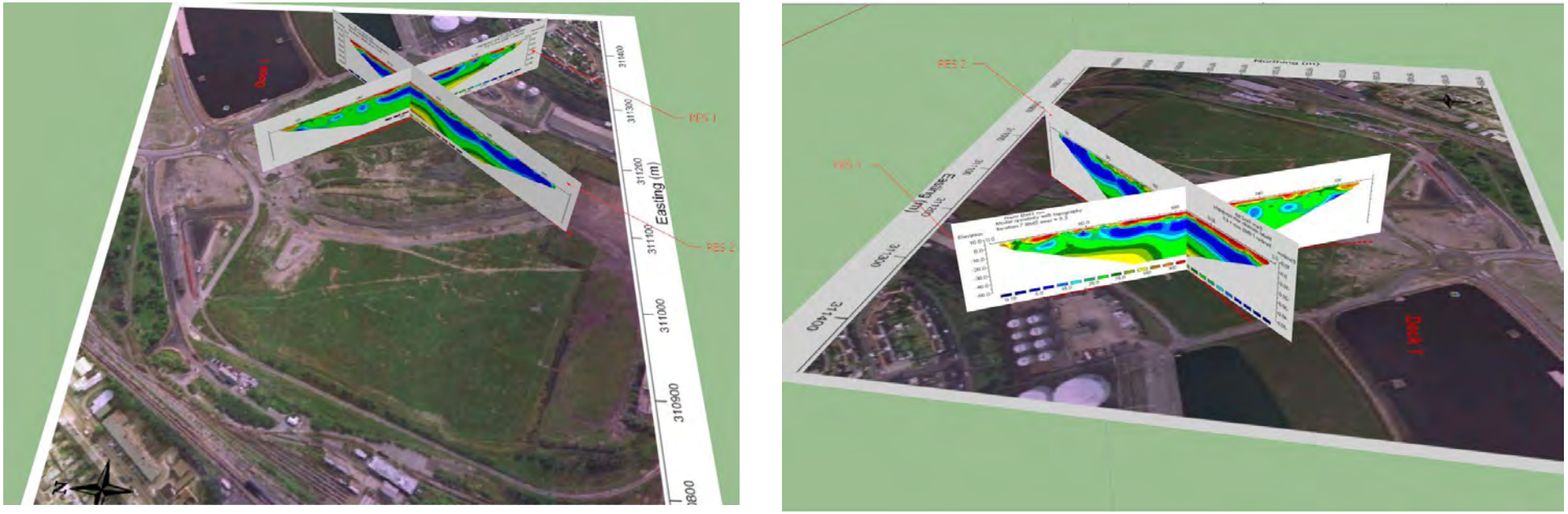

Figure 8.29: Two different 3D views of a combined resistivity profiles in the tank farm area showing a clear lower resistivity of buried river channel

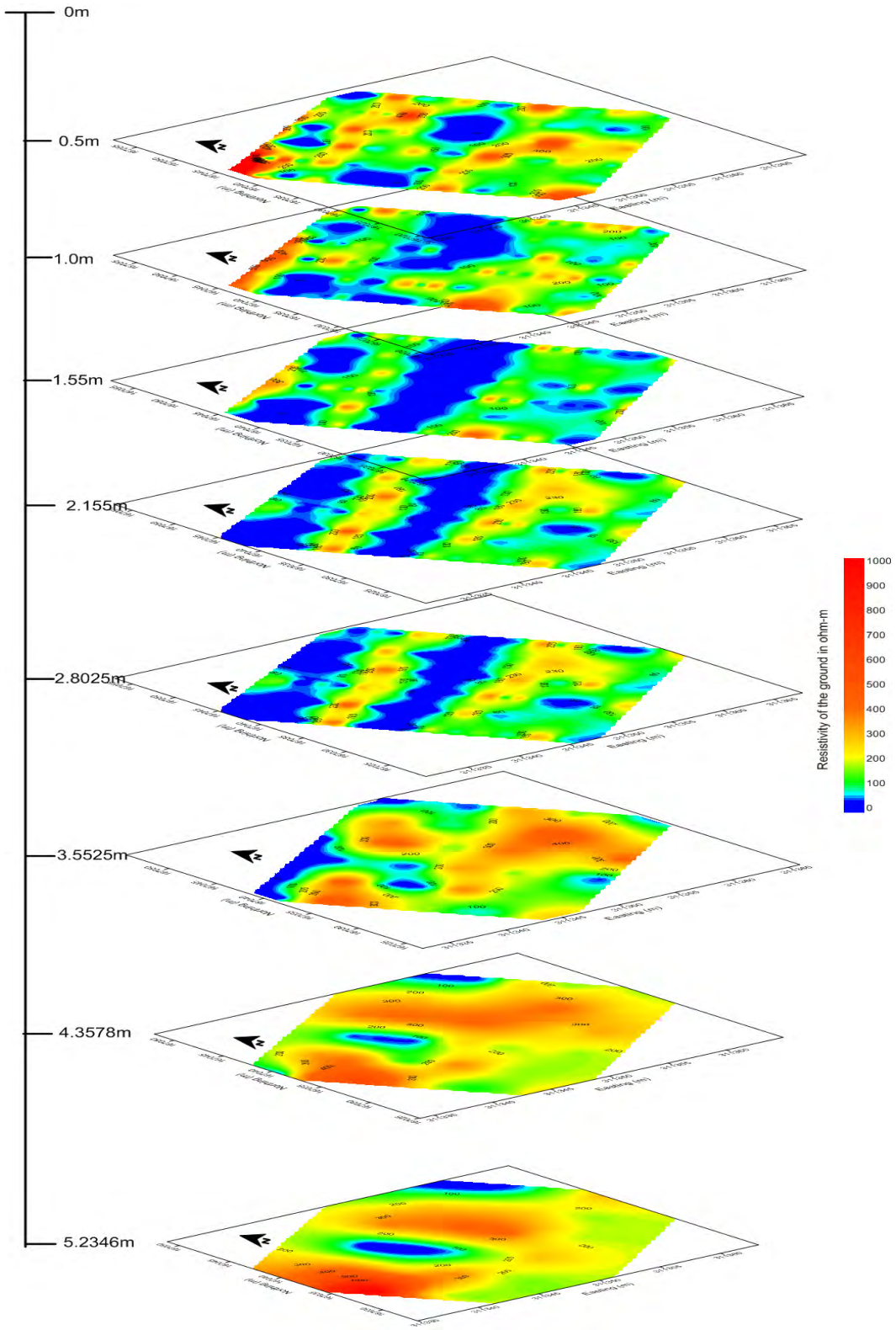

Figure 8.30: The resistivity 2D plan view against depth of the layers

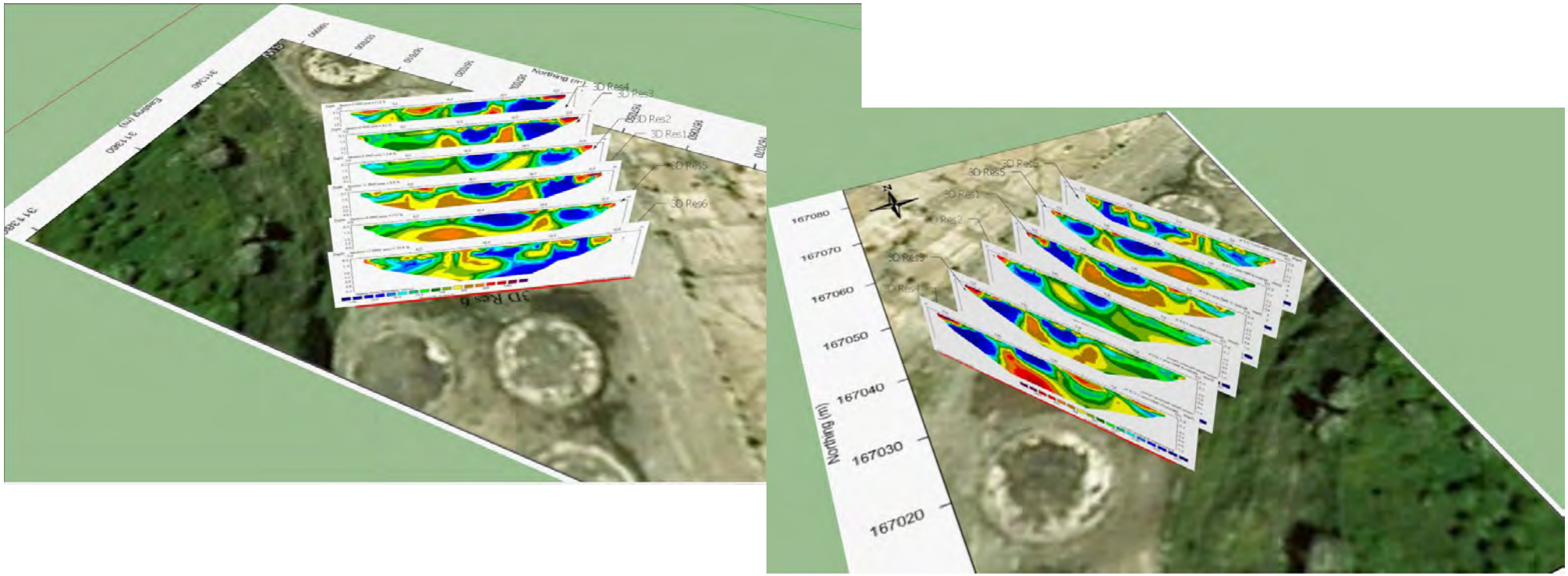

Figure 8.31: Two different 3D views of a combined resistivity profiles in the 3D small area showing a clear lower resistivity zones corresponding to the hydrocarbon contamination and fault zone

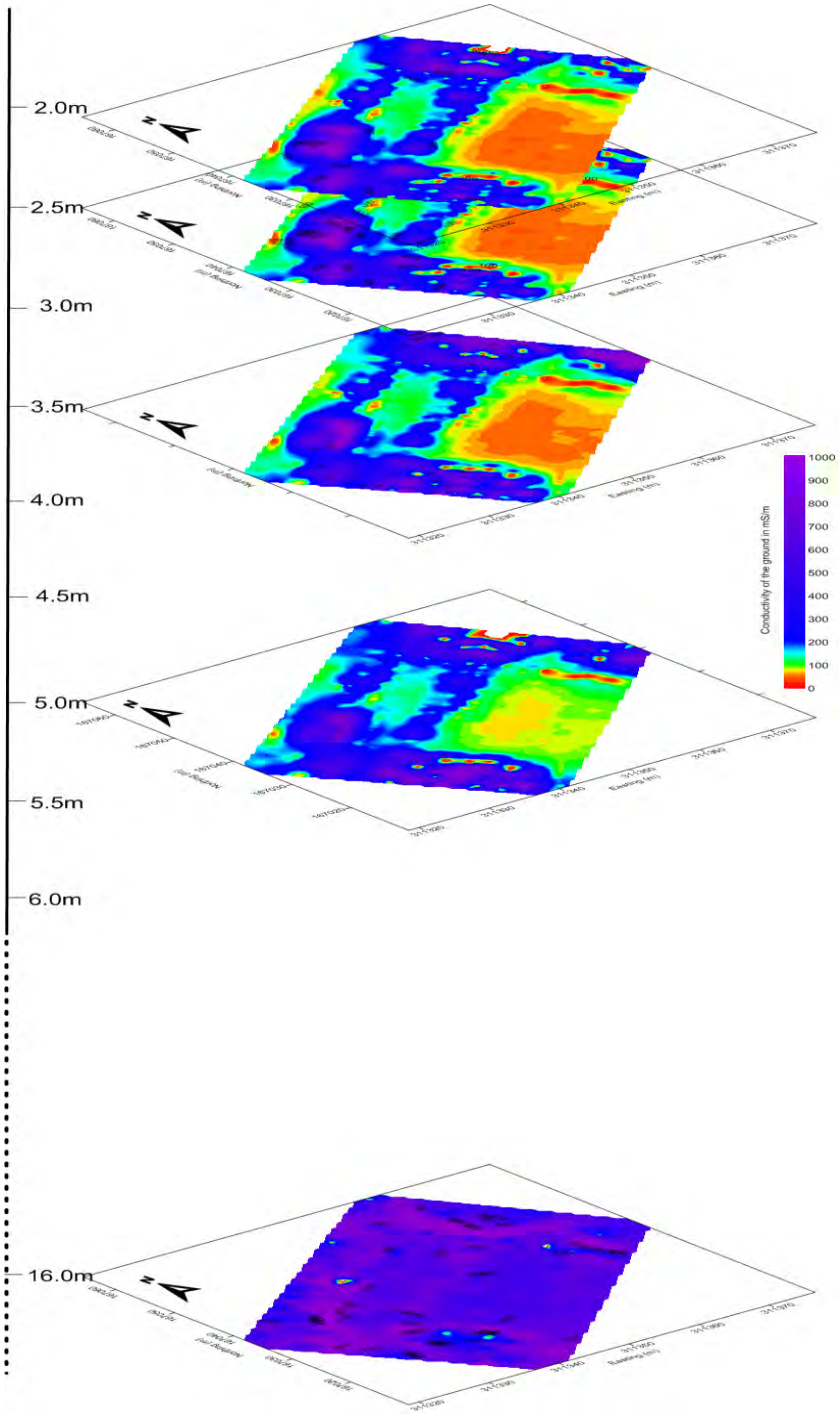

Figure 8.32: Showing a combined conductivity of ground at the 3D small area in different depths

REFERENCES

AJO-FRANKLIN, J. B., GELLER, J. T. & HARRIS, J. M. 2006. A survey of the geophysical properties of chlorinated DNAPLs. *Journal of Applied Geophysics.,* 59**,** Pg. 177- 189.

ALUMBAUGH, D., CHANG, P. Y., PAPROCKI, L., BRAINARD, I. R., GLASS, R. J. & RAUTMAN, C. A. 2002. Estimating moisture contents in the vadose zone using cross borehole ground penetration radar: A study of accuracy and repeatability. *Water Resources Res,* 38.

ANDERSON, J. G. C. 1958. *Geology around the University Towns: The Cardiff District*, Benham.

ANNAN, A. P. (ed.) 2005. *GPR methods for hydrogeological studies,* New York: Springer.

ARISTODEMOU, E. & THOMAS-BETTS, A. 2000. DC resistivity and induced polarization investigations at a waste disposal site and its environments. *Journal of Applied Geophysics.,* 44**,** Pg. 275 – 302.

ATEKWANA, E. A., SAUCK, W. A. & WERKEMA, J. D. D. 2000. Investigations of geoelectrical signatures at a hydrocarbon contaminated site. *Journal of Applied Geophysics. ,* 44.

BARKER, R. D. 1990. Improving the quality of resistivity sounding data in landfill studies. *In:* WARD, S. H. (ed.) *Geotech. Environmental Geophysics.* Society of Exploration Geophysicists.

BENSON, A. K. 1995. Applications of ground penetrating radar in assessing some geological hazards: examples of groundwater contamination, faults, cavities. *Journal of Applied Geophysics.,* 33.

BENSON, A. K. & STUBBEN, M. A. 1995. Interval resistivities and very low frequency electromagnetic induction - an aid to detecting groundwater contamination in space and time: A case study. *Journal of Environmental Geosciences,* 2**,** Pg. 74 - 84.

BERNER, E. & BERNER, R. 1987. *The Global Water Cycle,* New Jersey, Prentice Hall.

BINLEY, A. & KEMNA, A. 2005. Electrical Methods. *In:* HUBBARD, R. A. (ed.) *Hydrogeophysics.* Springer.

BINLEY, A. M., WINSHIP, L. J., WEST, M. P. & MIDDLETON, R. 2002. Seasonal variation of moisture content in unsaturated sandstone inferred from borehole radar and resistivity profiles. *Journal of Hydrology.,* 267**,** Pg.160 - 172.

BOULDING, J. R. & GINN, J. S. 2004. *Soil, Vadose Zone and Ground-water Contamination. Assessment, Prevention and Remediation,* New York, Lewis Publishers.

BRITISH STANDARDS INSTITUTION 2002. BS 12457-Part 2 . Characterisation of waste - Leaching - Compliance test for leaching of granular waste materials and sludges. . *One stage batch test at a liquid to solidratio of 10 l/kg for materials with particle size below 4 mm (without or with size reduction).* London.

BUSELLI, G., BARBER, C. & ZERILLI, A. 1988. The mapping of groundwater contaminations with TEM and DC methods. *Exploration Geophysics,* 19**,** Pg. 240-243.

BUSELLI, G., DAVIS, G. B., BARBER, C., HEIGHT, M. I. & HOWARD, S. H. D. 1992. The application of electromagnetic and electrical methods to groundwater pollution problems in urban environments. *Exploration Geophysics,* 23**,** pg. 534-556.

BUSELLI, G. & LU, K. 2001. Groundwater contamination monitoring with multichannel electrical and electromagnetic methods. *Journal of Applied Geophysics.,* 48 Pg. 11 - 23.

CASSIANI, G., STROBBIA, C. & GALLOTRI, L. 2004. Vertical radar profiles for the characterization of deep vadose zone. *Vadose Zone Journal,* 3**,** Pg. 1093 - 1115.

CASSIDY, N. J. 2007. Evaluating LNAPL contamination using GPR signal attenuation analysis and dielectric property measurement: Practical implications for hydrological studies. *Journal of Contaminant Hydrology,* 94**,** Pg. 49 - 75.

CLARKS, A. J. 1986. Archaeological geophysics in Britian. *Geophysics.,* 51**,** Pg. 1404 - 1413.

DEIANA, R., VILLA, A. B. & BRUNO, V. 2008. Calibration of a vadose zone model using water injection monitored by GPR and Electrical Resistance Tomography. *Vadose Zone Journal* 1**,** Page 215-226.

DEY A. AND MORRISON H.F. 1979. Resistivity modelling for arbitrary shaped two-dimensional structures. Geophysical Prospecting 27, 1020-1036.

DOMENICO, P. & SCHWARTZ, F. 1990. *Physical and Chemical Hydrogeology,* New Yorks, John Wiley and Son.

DUTTON, K. L. 2009. *An Investigation under Part 2A of the Environmental Protection Act 1990 into the Potential Risks Posed by a Dilute and Disperse Landfill site near Bromsgrove, Worchestershire.* MSc, Cardiff University.

ENDRES, A. L. & GREENHOUSE, J. P. 1996. Detection and monitoring of chlorinated solvents by thermal neutron logging. *Journal of Groundwater,* 34**,** Pg. 283 - 292.

ENVIROS 2009. Environment Agency, Part 2A Compliant B20C Inspection of Bromsgrove Landfill Sites: Madeley Heath and Yew Tree Farm Factual and Interpretative Report.

FANG, H. Y. 1995. Bacteria and tree root attack on landfill liners. *In:* SARSBY, R. W. (ed.) *Waste Disposal by landfill - GREEN 93.* Rotterdam: A.A. Balkema.

FETTER, C. W. 1999. *Contaminant hydrogeology,* New Jersey, Prentice Hall.

GEORGE, A. 2006. *Development of Geoelectrical Techniques for Investigation and Monitoring of Landfills.* PhD Thesis, Cardiff University.

GLEDHILL, D. 2003. Gas Works of Somerset. SIAS Survey No.17.

GOLDSCHMIDT, V. M. 1954. *Geochemistry,* Oxford, Clarendon Press.

GORDON, T., SKUSE, M. & STATHAM, I. 2004. Urban Geology of Cardiff City Centre and the Bay Region. Urban Geology in Wales. *National Museum of Wales Geological Series.*

HAUCK, C. (2001), Frozen ground monitoring using DC resistivity tomography, Geophys. Res. Lett., 29(21), 2016, doi:10.1029/2002GL014995

HEINCKE, B., GÜNTHER, T., DALSEGG, E., RONNING, J. S., GANEROD, G. V. & ELVEBAKK, H. 2010. Combined three-dimensional electric and seismic tomography study on Aknes rockslide in Weston Norway. . *Journal of Applied Geophysics.,* 70**,** Pg 292 - 306.

HESSE, A., JOLIVET, A. & TABBAGH, A. 1986. New prospects in shallow depth electrical surveying for archaeological and pedological applications. *Geophysics.,* 51**,** Pg. 585 - 594.

HOWARD, A. S., WARRINGTON, G., AMBROSE, K. & REES, J. G. 2008. A formational framework for the Mercia Mudstone Group (Triassic) of England and Wales. *British Geological Survey Research Report. RR/08/04.* BGS.

HUANG, H. 2005. Depth of investigation for small broadband electromagnetic sensors. *Geophysics.,* 70**,** Pg. G135-G142.

HUANG, H. & WON, I. J. 2000. Conductivity and susceptibility mapping using broadband electromagnetic sensors. *Journal of Environmental and Engineering Geophysics.,* 5**,** Pp. 31-41.

HUANG, H. & WON, I. J. 2003. Real-time resistivity sounding using a handheld broadband electromagnetic sensor. *Geophysics,* 68**,** Pg.1224-1231.

HUANG, H. & WON, I. J. 2004. Electromagnetic detection of buried metallic objects using quad-quad conductivity. *Geophysics.,* 69**,** Pg 1387 - 1393.

HUBBARD, S. S., PETERSON, J. J. E., MAJER, E. I., ZAWISLANSKI, P. T., WILLIAMS, K. H., ROBERTS, J. & WOBBER, F. 1997. Estimate of permeable pathways and water content using tomographic radar data. *Leading Edge,* 16**,** Pg 1623 - 1628.

JORDAN, D. 2009. How effective is geophysical survey? A regional review. *Archaeological Prospection,* 16**,** Pg. 77 - 90.

JORDAN, T. E., BAKER, G. S., HENN, K. & MESSIER, J. 2004. Using amplitude variation with offset and normalized residualpolarization analysis of ground penetrating radar data to differentiate an NAPL release from stratigraphic changes. *Journal of Applied Geophysics.,* 56**,** Pg. 41- 58.

KAMPKE, A. 1999. Focused imaging of electrical resistivity data in archaeological prospecting. *Journal of Applied Geophysics.,* 41**,** Pg. 215 - 227.

KEAREY, P., BROOKS, M. & HILL, I. 2002. *An Introduction to Geophysical Exploration*, 3rd ed. Oxford: Blackwell Science.

KEAY, S., EARL, G., HAY, S., KAY, S. O. J. & STRUTT, K. D. 2009. The Role of Integrated Geophysical Survey Methods in the Assessment of Archaeological Landscapes: the Case of Portus. . *Archaeol. Prospect,* 16**,** Pg. 154-166.

KELLER, G. V. & FRISCHKNECHT, F. C. 1970. *Electrical methods in geophysical prospecting.,* New York Pergamon Press.

KUMAR, R. C. 2008. *Research Methodology,* New Delhi, APH Publishing Corporation.

LLOYD, J. W. & HEATHCOTE, J. A. 1985. *Natural Inorganic Hydrochemistry in Relation to Groundwater,* Oxford, England, Clarendon Press.

LOKE, M. H. Tutorial : 2-D and 3-D electrical imaging surveys. Penang

LOKE, M. H. & BARKER, R. D. 1996. Rapid least-squares inversion of apparent resistivity pseudosections by a quasi-Newton method. *Geophysical Prospecting,* 44**,** Pg. 131 - 152.

LOPES DE CASTRO, D., MARIANO, R. & CASTELO, B. G. 2003. 4-D ground penetration radar monitoring of a hydrocarbon leakage site in Fortaleza (Brazil) during its remediation process: A case history. *Journal of Applied Geophysics.,* 5**,** Pg 127 - 144.

MARTINHO, E., ALMEIDA, F. & SENOS MATOAS, M. J. 2006. An experimental study of organic pollutant effects on time domain induced polarization measurements. . *Journal of Applied Geophysics.,* 60**,** pg 27 - 40.

MASON, B. H. 1966. *Principles of Geochemistry.3nd Ed.,* New York, John Wiley and Sons.

J. D. McNeill, 1980a, Applications of Transient Electromagnetic Techniques, Technical Note 7, Geonics Ltd., Mississauga, Ontario

MEJU, M. A. Geophysical mapping of polluted groundwater in a closed landfill site. 3rd International Congress, 1993 Brazil. Geophysics Society, Pg 425-428.

MEJU, M. A. 1995. Geophysics and computer models in the evaluation of a landfill site in Leicester. *In:* SARSBY, R. W. (ed.) *Waste Disposal by Landfill - GREEN 1993.* Rotterdam: A.A.Balkema.

MEJU, M. A. 2000. Geoelectrical investigation of old abandoned covered landfill sites in urban areas: Model development with a genetic diagnosis approach. *Journal of Exploration Geophysics,* 44.

OLHEOFT, G. R. Geophysical detection of hydrocarbon and organic chemical contamination. Proceedings of the Symposium on the Application of Geophysics to Engineering and Environmental Problems., 1992 Oakbrook, IL.

OLIVAR, A. D. L., SATO, H. K. & PORSANI, M. J. 1995. Imaging Industrial contaminant plumes with resistivity techniques. *Journal of Applied Geophysics.,* 34**,** Pg. 93 - 108.

OSAZUWA, I. B. & CHINEDU, A. D. 2008. Seismic refraction tomography imaging of high-permeability zones beneath an earthen dam, in Zaria area, Nigeria. *Journal of Applied Geophysics.,* 66**,** Pg. 44 - 58.

OVE ARUP & PARTNERS 2008. Waterfront Barry, South Quay and West Pond, Geo-Environmental Site Investigation Report.

PARASNIS, D. S. 1986. *Principles of Applied Geophysics. ,* London, Capman and Hall.

PARSONS BRINCKERHOFFF 2010. Supplementary Site Investigation Interpretive Report. Parsons Brinckerhoff.

PETTERSSON, J. K. & NOBES, D. C. 2003. Environmental geophysics at Scott Base: ground penetrating radar and electromagnetic induction as tools for mapping contaminated ground at Antarctic research bases. . *Cold Regions Science and Technology,* 37**,** Pg 187- 195.

PORSANI, J. L., WALTER, M. F., E., V. R., FISSEHA, S., DOURADO, J. C. & MOURA, H. P. 2004. The use of GPR and VES in delineating a contamination plume in a landfill site: a case study in SE Brazil. *Journal of Applied Geophysics.,* 55**,** pg 199-209.

RAHMAN, Y., MOHD TADZA, A. R., LAKAM, M., KAMARUDIN, S., ROSLANZAIRI, M., UMAR, H., NABSIAH, A. W. & ISMAIL, A. Pollution Distribution Study in Soil Strata Using DC-Resistivity Imaging Technique at Taiping Landfill, Perak, Malaysia. The 7th SEGJ International Symposium - Imaging Technology, 2004 Tohoku University, Sendai Japan. SEGJ, Pg. 492-496.

RAHMAN, Y., MOHD TADZA, A. R., LAKAM, M., NAZRUL HIZAM, Y., ROSLANZAIRI, M., MOHD RIFAIE, M. M., KAMARUDIN, S. & ISMAIL, A. 2004. Pollutant distribution in soil strata using the transient electromagnetic technique at Pulau Burung landfill site, Nibong Tebal, Penang. *Geophysical Conference.* Bangi Selangor, Malaysia.

ROSS, H. P., MACKELPRANG, C. E. & WRIGHT, P. M. 1990. Dipole-dipole electrical resistivity surveys at waste disposal study sites in Northern Utah. *In:* WARD, S. H. (ed.) *Geotech. Environmental Geophysics.* Society of Exploration Geophysicists.

RUCKER, D. F., LEVITT, M. T. G. & REENWOOD, W. J. 2009. Three-dimensional electrical resistivity model of a nuclear waste disposal site. *Journal of Applied Geophysics.,* 69**,** pg150 - 164.

SAUCK, W. A. 2000. A model for resistivity structure of LNAPL plumes and their environs in sandy sediments. *Journal of Applied Geophysics.,* 44**,** Pg. 151 - 165.

SAUCK, W. A., ATEKWANA, E. A. & NASH, M. S. 1998. Elevated conductivities associated with an LNAPL plume imaged by integrated geophysical techniques. *Journal of Environmental and Engineering Geophysics. ,* 2.

SCOLLAR, I., WEIDNER, B. & SEGETH, K. 1986. Display archaeological magnetic data. *Geophysics,* 51**,** Pg. 623 - 633.

SJODAHL, P., DAHLIN, T., JOHNSSON, S. & LOKE, M. H. 2008. Resistivity monitoring for leakage and internal erosion detection at Hallby embankment dam. . *Journal of Applied Geophysics.,* 65**,** pg 155 - 164.

SNEDDON, K. W., OLHOELF, G. R. & POWERS, M. H. Determining and mapping DNAPL saturation values from non-invasive GPR measurements. Proc. Of Sageep, 2000 Crystal City Hyatt, Arlington, VA.

SOCCO, L. V., JONGMANS, D., BOIERO, D., STOCCO, S., MARASCHINI, K. T. & HANTZ, D. 2010. Geophysical investigation of the Sandalp rock avalance deposits. *Journal of Applied Geophysics.*

STEWART, M. & NORTH, L. 2006. A borehole geophysical method for detection and quantification of dense non-aqueous phase liquids (DNAPL) in saturated soils. *Journal of Applied Geophysics.,* 60**,** Pg. 87 - 99.

TELFORD, W. M., GELDART, L. P. & SHERIFF, R. E. 2000. *Applied Geophysics: Second Edition. ,* Cambridge, Cambridge University Press.

TOBAGA, A. 2011. Development of high resolution geophysical monitoring of landslides in the South Wales Valleys. PhD Thesis. Cardiff University.

TODD, D. K. & MAYS, L. W. 2005. *Groundwater Hydrology (3rd edition). ,* New York., John Wiley and Son Inc. .

VOLLHARDT, K. P. C. & SCHORE, N. E. 2006. *Organic Chemistry: Structure and Function,* New York, W.H. Freeman.

WARD, A. D. & TRIMBLE, S. W. 2004. *Environmental Hydrology (2nd edition),* New York., Lewis Publishers. .

WATERS, L. 1995. *"Railways of Cardiff",* Surrey, Ian Allan Ltd.

WEIGHT, W. D. 2008. *Hydrogeology field manual.,* New York., McGraw-Hill.

WHITELEY, J. 2010. *A comparison between geophysical and soil vapour survey technique used to detect hydrocarbon contamination at former gasworks site.* MSc. Thesis, Cardiff University.

WHITELEY, R. J. & JEWELL, C. 1992. Geophysical techniques in contamination lands assessment: -do they deliver? . *Journal of Exploration Geophysics,* 23 557 - 565.

WITTEN, A. J., CALBERT, G., WITTEN, B. & LEVY, T. 2003. Magnetic and electromagnetic induction studies at archaeological sites in southwestern Jordan. *Journal of Environmental and Engineering Geophysics.,* 8**,** pp. 209-215.

WITTEN, A. J., LEVY, T. E., ADAMS, R. B. & WON, I. J. 2000. Geophysical surveys in the Jebel Hamrat Fidan, Jordan. *Geoarchaeology,* 15**,** pp. 135-150.

WON, I. J. 1980. A wideband electromagnetic exploration method - Some theoretical and experimental results. *Geophysics,* 45**,** pp. 928-940.

WON, I. J. & HUANG, H. 2004. Magnetometers and electro-magnetometers. *The Leading Edge, a trade journal published by the Society of Exploration Geophysicists***,** pp. 448-451.

WON, I. J., KEISWETTER, D. A., FIELDS, G. R. A. & SUTTON, L. C. 1996. GEM-2: A new multifrequency electromagnetic sensor. *Journal of Environmental and Engineering Geophysics.,* 1**,** pp. 129-138.

WON, I. J., MURPHY, V. J., HUBBARD, P., OREN, A. & DAVIS, K. 2004. Geophysics and weapons inspection. *The Leading Edge,* trade journal published by the Society of Exploration Geophysicists**,** pp. 658-662.

ZHENG, C. & BENNETT, G. D. 2002. *Applied Contaminant Transport Modelling*, John Wiley & Son Inc.

WEB REFERENCES

Web 1.1 – ENVIRONMENT AGENCY. 2011. *Land Contamination* [Online]. Available: http://www.environment-agency.gov.uk/research/planning/33706.aspx [Accessed 23 November 2011].

Web 1.2 – ENVIRONMENT AGENCY. 2011. *Briefing Note. FAQ about our report entitled Dealing With Contaminated Land in England and Wales* [Online]. Available: http://www.environment-agency.gov.uk/static/documents/Leisure/100209_External_FAQ_FINAL.pdf [Accessed 23 November 2011].

Web 1.3 – EUGRIS. 2011. *Portal of Soil and Water Management in Europe. In the United Kingdom Statistics and Related.* [Online]. Available: http://www.eugris.info/search/search.asp?zoom_query=Part+IIA+regulatory+Activity++England&zoom_page=2&zoom_per_page=10&zoom_cat=-1&zoom_and=0&zoom_sort=0 [Accessed 22 November 2011].

Web 1.4 – ENVIRONMENTAL PROTECTION UK. 2011. *What is contaminated land?* [Online]. Available: http://www.environmental-protection.org.uk/land-quality/contaminated-land/ [Accessed 23 November 2011].

Web 2.1 – USGS. 2010. *The Water Cycle, a Quick Summary.* [Online]. Available: http://ga.water.usgs.gov/edu/watercyclehi.html [Accessed 21 August 2010].

Web 2.2 – THE GROUNDWATER FOUNDATION. 2009. *What is groundwater?* [Online]. Available: http://www.groundwater.org/kc/whatis.html [Accessed 17 June 2009.].

Web 2.3 – FOOD AND AGRICULTURE ORGANISATION OF THE UNION NATION. 2003. *Water Reports: Review of World Water Resources by Country.* [Online]. Available: ftp://ftp.fao.org/agl/aglw/docs/wr23e.pdf [Accessed 20 July 2009].

Web 2.4 – WHO. 2009. *Water, sanitation and hygiene links to health* [Online]. Available: http://www.who.int/water_sanitation_health/publications/facts2004/en/index.html [Accessed 25 June 2009].

Web 2.5 – ORGANISATION FOR ECONOMIC CO-OPERATION AND DEVELOPMENT. 2006. *Improve Co-ordination between Environmental and Health Policies. Final Report.* [Online]. Available: http://www.oecd.org/dataoecd/10/14/38200976.pdf [Accessed 12 June 2009].

Web 2.6 – UNICEF & WHO. 2004. *Joint Monitoring programme for Water Supply and Sanitary. Meeting the MDG Drinking Water and Sanitation Target. A midterm Assessment and Progress.* [Online]. Available: http://www.who.int/water_sanitation_health/monitoring/jmp04.pdf. [Accessed 15 May 2009].

Web 2.7 – WHO. 2000. *Global Water Supply and sanitation Assessment 2000 Report.* [Online]. Available: http://www.who.int/water_sanitation_health/monitoring/jmp2000.pdf [Accessed 18 December 2008].

Web 2.8 – WHO. 2006. *Protecting Groundwater for Health: Managing the Quality of Drinking-water Sources* [Online]. Available: http://www.who.int/water_sanitation_health/publications/PGWsection1.pdf [Accessed 22 December 2008].

Web 2.9 – WHO. 2009. *Guidelines for drinking-water quality, third edition.* [Online]. Available: http://www.who.int/water_sanitation_health/dwq/gdwq3rev/en/index.html [Accessed 15 June 2009].

Web 2.10 – BUREAU OF ENVIRONMENTAL HEALTH. 2009. *BTEX, Benzene, Toluene, Ethylbenzene and Xylenes* [Online]. Available: http://www.odh.ohio.gov/ASSETS/489EA8FB630C4AB49269A95FB2975DC4/BTEX%20Fact%20Sheet.pdf [Accessed 8 September 2010].

Web 2.11 – EUROPEAN CHLORINATED SOLVENTS ASSOCIATION. 2011. *About chlorinated solvents* [Online]. Available: http://www.eurochlor.org/chlorinated-solvents-(ecsa)/about-chlorinated-solvents/facts-figures/perchloroethylene.aspx [Accessed 5 November 2011].

Web 2.12 – HALLER, L., MCCARTHY, P., O'BRIEN, T., RIEHLE, J. & STUHLDREHER, T. 2011. *Nitrate pollution of groundwater* [Online]. Available: http://www.reopure.com/nitratinfo.html [Accessed 25 November 2011].

Web 2.13 – USGS. 2008. *Light Non-Aqueous Phase Liquids (LNAPLs)* [Online]. Available: http://toxics.usgs.gov/definitions/lnapls.html [Accessed 15 March 2008].

Web 2.14 – USGS. 2008. *Dense Nonaqueous Phase Liquid (DNAPL)* [Online]. Available: http://toxics.usgs.gov/definitions/dnapl_def.html [Accessed 12 March 2008].

Web 2.15 – USGS. 2008. *Non-Aqueous Phase Liquids (NAPLs)* [Online]. Available: http://toxics.usgs.gov/definitions/napls.html) [Accessed 17 March 2008].

Web 2.16 – DREWES, M., BARRET, M., J. , CHILTON, J., APPLEYARD, S., WAUCHOPE, D. & FASTNER, J. 2006. *Chapter 4 in the WHO report. Chemicals: Health relevance, transport and attenuation.* [Online]. Available: http://www.bvsde.paho.org/bvsacd/cd59/protecting/sect1-4.pdf [Accessed 4 April 2008].

Web 2.17 – ROBERT, C. R. 2011. *A Clarifying concept of Archie's resistivity relationship, a model and discussion.* [Online]. Available: http://www.archieparameters.com/archie'srelatioa.html [Accessed 28 August 2010].

Web 2.18 – LOKE, M. H. 2000. *Electrical Imaging Surveys for Environmental Engineering Studies. A Practical Guide to 2D and 3D Surveys* [Online]. Available: http://www.geoelec.com.mx/softelectricos/lokenote.pdf [Accessed 20 February 2009].

Web 2.19 – LOKE, M. H. 2004. *Tutorial: 2-D and 3-D electrical imaging surveys* [Online]. Available: http://www.geoelectrical.com/ [Accessed 20 February 2009].

Web 2.20 – ABEM INSTRUMENT AB. 2009. *ABEM Instruction Manual. Terrameter SAS 4000/SAS 1000* [Online]. Available: http://www.abem.se/files/upload/Manual_Terrameter.pdf [Accessed 28 August 2009].

Web 2.21 – STIERMAN, D. 2005. *Geophysical Electrical Resistivity Measurements. Resistivity of rocks and Archie's Law.* [Online]. Available: http://www.eeescience.utoledo.edu/faculty/stierman/EEG/notes/RR.htm [Accessed 23 August 2010].

Web 2.22 – TERRAPLUS. 2011. *GEM 2 Multi-Frequency EM Sensor.* [Online]. Available: http://www.terraplus.ca/products/electromagnetics/gem2.htm [Accessed 8 July 2011].

Web 2.23 – GEO-SERVICE INTERNATIONAL (UK) LIMITED. 2009. *Electromagnetic Techniques* [Online]. Available: http://www.geophysics.co.uk/mets1.html#ffe [Accessed 20 April 2009].

Web 2.24 – THE AMERICAN HERITAGE® SCIENCE DICTIONARY 2005. *The American Heritage® Science Dictionary.* Boston MA: Houghton Mifflin Company.

Web 2.25 – DEPARTMENT OF ENVIRONMENT FOODS AND RURAL AFFAIRS. 2006. *Assessing Risks from Land Contamination - a Proportionate Approach. Soil Guideline Values: The Way Forward* [Online]. DEFRA. Available: http://www.doeni.gov.uk/sgvs_-_the_way_forward.pdf [Accessed 25 November 2011].

Web 2.26 – CONTAMINATED LAND UK. 2009. *ICRCL 59/83 Trigger Concentrations* [Online]. Available: http://www.contaminatedland.co.uk/std-guid/icrcl-l.htm [Accessed 06 March 2009].

Web 2.27– CONTAMINATED LAND UK. 2009. *The New Dutchlist* [Online]. Available: http://www.contaminatedland.co.uk/std-guid/dutch-l.htm [Accessed 10 March 2009].

Web 2.28 – CONTAMINATED LAND UK. 2009. *The Kelly Indices* [Online]. Available: http://www.contaminatedland.co.uk/std-guid/kelly-l.htm [Accessed 10 March 2009].

Web 2.29– CONTAMINATED LAND UK. 2009. *Standards and Guidelines* [Online]. Available: http://www.contaminatedland.co.uk/std-guid.htm [Accessed 10 March 2009].

Web 3.1 – UNITED STATE ENVIRONMENTAL PROTECTION AGENCY (EPA). 2009. *Human Health. Brief overview of lead in the environment* [Online]. Available: http://www.epa.gov/superfund/health/contaminants/lead/health.htm [Accessed 18 February 2009].

Web 3.2 – LENNTECH. 2009. *Water Treatment Solutions* [Online]. Available: http://www.lenntech.com/processes/heavy/heavy-metals/heavy-metals.htm [Accessed 24 February 2009].

Web 3.3 – LIFEEXTENSION. 2009. *Health Concern. Heavy Metals Toxicity* [Online]. Available: http://www.lef.org/protocols/prtcl-156.shtml [Accessed 28 February 2009].

Web 3.4 – ENVIRONMENT AGENCY. 2011. *Aquifer. What are the new aquifer designations?* [Online]. Available: http://www.environment-agency.gov.uk/homeandleisure/117020.aspx [Accessed 4 April 2011].

Web 3.5 – ENVIRONMENT AGENCY. 1995. *Railway Land* [Online]. Department of Environment. Industry Profile Available: http://publications.environment-agency.gov.uk/pdf/SCHO0195BJLB-e-e.pdf?lang=_e [Accessed 18 January 2009].

Web 3.6 – CHENEY, C. S. 2004. *The Hydrogeology of Leicester District (Geological Sheet 156)* [Online]. BGS. Available: http://nora.nerc.ac.uk/12613/1/IR04085.pdf [Accessed 15 March 2011].

Web 3.7 – ENVIRONMENT AGENCY. 2011. *Groundwater. Weston Super-Mare* [Online]. Available: http://maps.environment-agency.gov.uk/wiyby/wiybyController?x=350500.0&y=152500.0&topic=drinkingwater&ep=map&scale=8&location=Bristol Plain Fm, Somerset&lang=_e&layerGroups=default&textonly=off#x=334704&y=160570&lg=3,&scale=7 [Accessed 16 March 2011].

Web 3.8 – ENVIRONMENT AGENCY. 2011. *Groundwater. Barry Docks, The Vale of Glamorgan.* [Online]. Available: http://maps.environment-agency.gov.uk/wiyby/wiybyController?value=Barry+Dock%2C+The+Vale+of+Glamorgan&submit=Search%09&lang=_e&ep=map&topic=drinkingwater&layerGroups=default&scale=8&textonly=off#x=309633&y=169980&lg=4,3,&scale=6 [Accessed 16 March 2011].

Web 3.9 – ENVIRONMENT AGENCY. 2011. *Groundwater source Protection Zone. Barry Dock, The Vale of Glamorgan* [Online]. Available: http://maps.environment-agency.gov.uk/wiyby/wiybyController?value=Barry+Dock%2C+The+Vale+of+Glamorgan&submit=Search%09&lang=_e&ep=map&topic=drinkingwater&layerGroups=default&scale=8&textonly=off#x=313264&y=170496&lg=1,&scale=7 [Accessed 16 March 2011].

Web 3.10 – ENVIRONMENT AGENCY. 2011. *Groundwater source Protection Zone. Bromsgrove, Worcestershire* [Online]. Available: http://maps.environment-agency.gov.uk/wiyby/wiybyController?value=Bromsgrove%2C+Worcestershire&submit=Search%09&lang=_e&ep=map&topic=drinkingwater&layerGroups=default&scale=8&textonly=off#x=396004&y=276561&lg=1,&scale=7 [Accessed 16 March 2011].

Web 3.11 – ENVIRONMENT AGENCY. 2011. *Groundwater. Bromsgrove, Worcestershire* [Online]. Available: http://maps.environment-agency.gov.uk/wiyby/wiybyController?value=Bromsgrove%2C+Worcestershire&submit=Search%09&lang=_e&ep=map&topic=drinkingwater&layerGroups=default&scale=8&textonly=off#x=396590&y=275827&lg=3,&scale=7 [Accessed 16 March 2011].

Web 4.1 – ADVANCE INSTRUMENTS. 2010. *Why is Calibration Important?* [Online]. Available: http://www.aicompanies.com/index.cfm/ServiceAndSupport/CalibrationExplained/Why_is_Calibration_Important [Accessed 05 January 2010].

Web 4.2 – ISO 9000:2005. 2005. *Quality management systems -- Fundamentals and vocabulary* [Online]. Available: http://www.iso.org/iso/iso_catalogue/catalogue_tc/catalogue_detail.htm?csnumber=42180 2011].

Web 4.3 – NORFOLKS AND HYDROPONICS CENTRE LTD. 2010. *Hanna Digital W/Proof Combo Meter for pH/EC - HI 98129.* [Online]. Available: http://www.norfolklights.com/hanna-digital-wproof-combo-meter-for-phec-hi-98129-p-648.html?zenid=dba48d80f4ddddc93f39cd69b2aa0fd6. [Accessed 20 February 2010].

Web 4.4 – IRIS INSTRUMENTS. 2010. *Electrode II Software* [Online]. Available: http://www.iris-instruments.com/Pdf%20file/ElectreII_Gb.pdf [Accessed 20 February 2010].

Web 4.5 – IRIS INSTRUMENTS. 2010. *Support* [Online]. Available: http://www.iris-instruments.com/Support/support.html [Accessed 20 February 2010].

Web 4.6 – ZERELLI, F. 2011. *Conductivity and Resistance* [Online]. Available: http://www.physnet.org/modules/pdf_modules/m118.pdf [Accessed 25 March 2010].

Web 5.1 – WORLEY, J. & KVECH, S. 2009. *ICP-MS* [Online]. Available: http://www.cee.vt.edu/ewr/environmental/teach/smprimer/icpms/icpms.htm [Accessed 06 March 2009].

Web 5.2 – UNIVERSITY OF CALIFORNIA. 2009. *Inductively coupled plasma-mass spectrometry (ICP-MS)* [Online]. Available: http://icpms.ucdavis.edu/ [Accessed 3 March 2009].

Web 7.1 – U SGS. 2011. *Aerobic Biodegradation. Definitions.* [Online]. Available: http://toxics.usgs.gov/definitions/aerobic_biodegradation.html [Accessed 7 November 2011].

Web 7.2 – USGS. 2011. *Anaerobic Biodegradation. Definations.* [Online]. Available: http://toxics.usgs.gov/definitions/anaerobic_biodegradation.html [Accessed 7 November 2011].

Web 8.1 – ENVIRONMENT AGENCY. 2011. *The UK approach for evaluating Human Health Risks from Petroleum Hydrocarbon in Soils. Science Report P5-080/TR3.* [Online]. Available: http://www.environment-agency.gov.uk/static/documents/2-SCHO1104BIKB-e-e.pdf [Accessed 8 September 2011].

Web 10.1 – ENVIRONMENT AGENCY & BRITISH GEOLOGICAL SURVEY (BGS). 2002. *Baseline Report Series: 3 The Permo-Triassic Sandstone of South Staffordshire and North Worcestershire.* [Online]. Available: http://publications.environment-agency.gov.uk/PDF/SCHO0207BLXZ-E-E.pdf [Accessed 22 October 2011].

Web 10.2 – USGS. 2011. *Water Resources Applications Software, Summary of MODPATH* [Online]. Available: http://water.usgs.gov/cgi-bin/man_wrdapp?modpath [Accessed 20 November 2011].

Web 10.3 – USGS. 2011. *Water Resources Applications Software, Summary of ZoneBudget* [Online]. Available: http://water.usgs.gov/nrp/gwsoftware/zonebud3/zonbud.txt [Accessed 20 November 2011].

Web 10.4 – GMS. 2011. *MODFLOW Software Links. MT3D Solute Transport for Modflow* [Online]. Available: http://modflow.com/mt3d/mt3d.html [Accessed 20 November 2011].

Web 10.5 – GMS. 2011. *MODFLOW Software Links. RT3D simulates 3-D multispecies, reactive transport in groundwater* [Online]. Available: http://modflow.com/rt3d/rt3d.html [Accessed 20 November 2011].

APPENDICES

Appendix A

The cations analysis results and the percentages of the single ions in the soil samples

Appendix B

Single and Total Anions Plots

Appendix C

Single and Total Cations Plots

Appendix D

Brief Information on the Resistivity Data Processing

APPENDIX A

Table A1: The cations analysis results and the percentages of the single ion in the soil samples

Sample ID	23Na	Total	% in the	26Mg	Total	% in the	27Al	Total	% in the	29Si	Total	% in the	31P	Total	% in the	39K	Total	% in the	44Ca	Total	% in the
	ppm	amount	sample	ppm	amount	sample	ppm	amount	sample	ppm	amount	sample	ppm	amount	sample	ppm	amount	sample	ppm	amount	sample
C1	1.006	22.265	4.518	**0.878**	28.462	3.085	**0.177**	5.694	3.109	**1.214**	26.229	4.628	**0.032**	1.879	1.703	**0.642**	21.763	2.950	**12.160**	289.914	4.194
C2	1.502	22.265	6.746	**1.019**	28.462	3.580	**0.216**	5.694	3.793	**1.235**	26.229	4.709	**0.544**	1.879	28.952	**1.318**	21.763	6.056	**7.731**	289.914	2.667
C3	0.654	22.265	2.937	**2.141**	28.462	7.522	**0.280**	5.694	4.917	**0.644**	26.229	2.455	**0.051**	1.879	2.714	**0.609**	21.763	2.798	**11.350**	289.914	3.915
C4	0.703	22.265	3.157	**1.133**	28.462	3.981	**0.259**	5.694	4.549	**0.899**	26.229	3.428	**0.016**	1.879	0.852	**1.274**	21.763	5.854	**8.755**	289.914	3.020
C5	1.199	22.265	5.385	**0.505**	28.462	1.774	**0.216**	5.694	3.793	**0.608**	26.229	2.318	**0.098**	1.879	5.216	**1.042**	21.763	4.788	**16.460**	289.914	5.678
C6	0.809	22.265	3.634	**0.361**	28.462	1.268	**0.256**	5.694	4.496	**1.094**	26.229	4.171	**0.053**	1.879	2.821	**0.511**	21.763	2.348	**10.270**	289.914	3.542
C7	1.104	22.265	4.958	**0.523**	28.462	1.838	**0.396**	5.694	6.955	**0.847**	26.229	3.229	**0.043**	1.879	2.288	**0.678**	21.763	3.115	**14.010**	289.914	4.832
C8	0.766	22.265	3.440	**0.376**	28.462	1.321	**0.457**	5.694	8.026	**0.455**	26.229	1.735	**0.032**	1.879	1.703	**0.639**	21.763	2.936	**13.150**	289.914	4.536
C9	1.031	22.265	4.631	**0.946**	28.462	3.324	**0.214**	5.694	3.758	**1.015**	26.229	3.870	**0.061**	1.879	3.246	**1.058**	21.763	4.861	**15.330**	289.914	5.288
C10	0.869	22.265	3.903	**2.766**	28.462	9.718	**0.166**	5.694	2.915	**0.773**	26.229	2.947	**0.027**	1.879	1.437	**0.519**	21.763	2.385	**11.550**	289.914	3.984
C11	0.929	22.265	4.172	**0.945**	28.462	3.320	**0.082**	5.694	1.440	**1.648**	26.229	6.283	**0.031**	1.879	1.650	**0.680**	21.763	3.125	**15.900**	289.914	5.484
C12	0.732	22.265	3.288	**2.419**	28.462	8.499	**0.369**	5.694	6.481	**1.526**	26.229	5.818	**0.089**	1.879	4.737	**1.408**	21.763	6.470	**13.530**	289.914	4.667
C13	1.057	22.265	4.747	**3.032**	28.462	10.653	**0.266**	5.694	4.672	**1.607**	26.229	6.127	**0.078**	1.879	4.151	**1.092**	21.763	5.018	**8.451**	289.914	2.915
C14	1.234	22.265	5.542	**1.177**	28.462	4.135	**0.139**	5.694	2.441	**1.872**	26.229	7.137	**0.052**	1.879	2.767	**0.936**	21.763	4.301	**12.560**	289.914	4.332
C15	0.761	22.265	3.418	**1.292**	28.462	4.539	**0.235**	5.694	4.127	**0.590**	26.229	2.249	**0.056**	1.879	2.980	**0.517**	21.763	2.376	**9.056**	289.914	3.124
C16	0.942	22.265	4.231	**1.649**	28.462	5.794	**0.141**	5.694	2.476	**1.195**	26.229	4.556	**0.075**	1.879	3.991	**1.918**	21.763	8.813	**14.320**	289.914	4.939
C17	0.696	22.265	3.126	**1.507**	28.462	5.295	**0.154**	5.694	2.705	**0.779**	26.229	2.970	**0.053**	1.879	2.821	**0.608**	21.763	2.794	**10.750**	289.914	3.708
C18	0.830	22.265	3.728	**1.100**	28.462	3.865	**0.150**	5.694	2.634	**1.193**	26.229	4.548	**0.071**	1.879	3.779	**0.741**	21.763	3.405	**13.550**	289.914	4.674
C19	0.612	22.265	2.749	**0.559**	28.462	1.964	**0.140**	5.694	2.459	**0.867**	26.229	3.306	**0.059**	1.879	3.140	**0.606**	21.763	2.785	**7.231**	289.914	2.494
C20	0.885	22.265	3.975	**0.417**	28.462	1.465	**0.508**	5.694	8.922	**0.505**	26.229	1.925	**0.064**	1.879	3.406	**1.124**	21.763	5.165	**12.830**	289.914	4.425
C21	1.064	22.265	4.779	**1.928**	28.462	6.774	**0.103**	5.694	1.809	**1.060**	26.229	4.041	**0.054**	1.879	2.874	**1.048**	21.763	4.816	**11.040**	289.914	3.808
C22	0.848	22.265	3.809	**0.474**	28.462	1.665	**0.347**	5.694	6.094	**0.780**	26.229	2.974	**0.037**	1.879	1.969	**0.629**	21.763	2.890	**14.480**	289.914	4.995
C23	0.963	22.265	4.325	**0.784**	28.462	2.755	**0.113**	5.694	1.985	**0.569**	26.229	2.169	**0.063**	1.879	3.353	**0.848**	21.763	3.897	**10.510**	289.914	3.625
C24	1.069	22.265	4.801	**0.531**	28.462	1.866	**0.310**	5.694	5.444	**3.254**	26.229	12.406	**0.140**	1.879	7.451	**1.318**	21.763	6.056	**14.940**	289.914	5.153
	22.265		100.000	28.462		100.000	5.694		100.000	26.229		100.000	1.879		100.000	21.763		100.000	289.914		100.000

Table A2: The cations analysis results and the percentages of the single ion in the soil samples

Sample ID	51V	Total	% in the	52Cr	Total	% in the	55Mn	Total	% in the	57Fe	Total	% in the	59Co	Total	% in the	60Ni	Total	% in the
	ppb	amount	sample	ppb	amount	sample	ppb	amount	sample	ppm	amount	sample	ppb	amount	sample	ppb	amount	sample
C1	**0.738**	36.212	2.038	**1.110**	24.106	4.605	**18.410**	307.896	5.979	**0.548**	7.943	6.899	**0.242**	5.730	4.223	**8.686**	59.862	14.510
C2	**12.530**	36.212	34.602	**1.139**	24.106	4.725	**17.420**	307.896	5.658	**0.338**	7.943	4.255	**0.318**	5.730	5.550	**1.543**	59.862	2.578
C3	**1.007**	36.212	2.781	**1.150**	24.106	4.771	**6.171**	307.896	2.004	**0.235**	7.943	2.959	**0.104**	5.730	1.815	**0.848**	59.862	1.417
C4	**0.441**	36.212	1.218	**0.809**	24.106	3.356	**10.520**	307.896	3.417	**0.396**	7.943	4.986	**0.286**	5.730	4.991	**1.401**	59.862	2.340
C5	**0.844**	36.212	2.331	**1.162**	24.106	4.820	**8.577**	307.896	2.786	**0.374**	7.943	4.709	**0.246**	5.730	4.293	**1.223**	59.862	2.043
C6	**1.225**	36.212	3.383	**0.829**	24.106	3.439	**5.715**	307.896	1.856	**0.258**	7.943	3.248	**0.208**	5.730	3.630	**0.920**	59.862	1.537
C7	**1.244**	36.212	3.435	**0.973**	24.106	4.036	**6.090**	307.896	1.978	**0.285**	7.943	3.588	**0.185**	5.730	3.229	**1.127**	59.862	1.883
C8	**1.461**	36.212	4.035	**1.121**	24.106	4.650	**9.368**	307.896	3.043	**0.258**	7.943	3.248	**0.256**	5.730	4.468	**0.920**	59.862	1.537
C9	**0.600**	36.212	1.657	**0.782**	24.106	3.244	**10.820**	307.896	3.514	**0.324**	7.943	4.079	**0.238**	5.730	4.154	**1.265**	59.862	2.113
C10	**0.889**	36.212	2.455	**0.953**	24.106	3.953	**1.607**	307.896	0.522	**0.139**	7.943	1.750	**0.056**	5.730	0.977	**0.832**	59.862	1.390
C11	**0.277**	36.212	0.765	**1.334**	24.106	5.534	**13.840**	307.896	4.495	**0.534**	7.943	6.723	**0.400**	5.730	6.981	**1.614**	59.862	2.696
C12	**1.079**	36.212	2.980	**1.474**	24.106	6.115	**23.810**	307.896	7.733	**0.526**	7.943	6.622	**0.129**	5.730	2.251	**1.880**	59.862	3.141
C13	**1.514**	36.212	4.181	**1.673**	24.106	6.940	**67.610**	307.896	21.959	**0.916**	7.943	11.532	**0.560**	5.730	9.773	**2.459**	59.862	4.108
C14	**0.410**	36.212	1.132	**1.153**	24.106	4.783	**7.818**	307.896	2.539	**0.347**	7.943	4.369	**0.155**	5.730	2.705	**1.565**	59.862	2.614
C15	**1.167**	36.212	3.223	**0.743**	24.106	3.082	**12.880**	307.896	4.183	**0.215**	7.943	2.707	**0.226**	5.730	3.944	**1.036**	59.862	1.731
C16	**0.646**	36.212	1.784	**0.811**	24.106	3.364	**19.370**	307.896	6.291	**0.336**	7.943	4.230	**0.348**	5.730	6.073	**1.943**	59.862	3.246
C17	**1.219**	36.212	3.366	**0.650**	24.106	2.696	**2.642**	307.896	0.858	**0.166**	7.943	2.090	**0.263**	5.730	4.590	**2.328**	59.862	3.889
C18	**1.493**	36.212	4.123	**0.818**	24.106	3.393	**4.359**	307.896	1.416	**0.192**	7.943	2.417	**0.129**	5.730	2.251	**1.013**	59.862	1.692
C19	**1.350**	36.212	3.728	**0.643**	24.106	2.667	**5.225**	307.896	1.697	**0.157**	7.943	1.977	**0.189**	5.730	3.298	**0.980**	59.862	1.637
C20	**1.641**	36.212	4.532	**0.760**	24.106	3.153	**5.542**	307.896	1.800	**0.222**	7.943	2.795	**0.297**	5.730	5.183	**1.233**	59.862	2.060
C21	**0.587**	36.212	1.621	**0.766**	24.106	3.178	**19.480**	307.896	6.327	**0.372**	7.943	4.683	**0.326**	5.730	5.689	**20.940**	59.862	34.980
C22	**1.555**	36.212	4.294	**0.916**	24.106	3.800	**5.378**	307.896	1.747	**0.232**	7.943	2.921	**0.180**	5.730	3.141	**1.405**	59.862	2.347
C23	**0.360**	36.212	0.994	**1.002**	24.106	4.157	**6.814**	307.896	2.213	**0.177**	7.943	2.228	**0.165**	5.730	2.880	**0.682**	59.862	1.139
C24	**1.935**	36.212	5.344	**1.335**	24.106	5.538	**18.430**	307.896	5.986	**0.396**	7.943	4.986	**0.224**	5.730	3.909	**2.019**	59.862	3.373
	36.212		100.000	24.106		100.000	307.896		100.000	7.943		100.000	5.730		100.000	59.862		100.000

Table A3: The cations analysis results and the percentages of the single ion in the soil samples

ample ID	65Cu	Total	% in the	66Zn	Total	% in the	75As	Total	% in the	77Se	Total	% in the	85Rb	Total	% in the	88Sr	Total	% in the
	ppb	amount	sample	ppb	amount	sample	ppb	amount	sample	ppb	amount	sample	ppb	amount	sample	ppb	amount	sample
C1	**14.210**	706.407	2.012	**22.750**	963.242	2.362	**0.755**	38.271	1.973	**0.434**	11.228	3.865	**1.478**	24.262	6.092	**61.220**	2100.740	2.914
C2	**15.790**	706.407	2.235	**93.640**	963.242	9.721	**2.130**	38.271	5.566	**0.341**	11.228	3.037	**2.303**	24.262	9.492	**82.110**	2100.740	3.909
C3	**17.780**	706.407	2.517	**6.995**	963.242	0.726	**0.809**	38.271	2.114	**0.312**	11.228	2.779	**0.352**	24.262	1.451	**33.280**	2100.740	1.584
C4	**19.110**	706.407	2.705	**9.737**	963.242	1.011	**0.448**	38.271	1.171	**0.275**	11.228	2.449	**1.094**	24.262	4.509	**27.900**	2100.740	1.328
C5	**19.680**	706.407	2.786	**19.430**	963.242	2.017	**1.244**	38.271	3.251	**0.473**	11.228	4.213	**0.851**	24.262	3.508	**40.750**	2100.740	1.940
C6	**9.338**	706.407	1.322	**6.154**	963.242	0.639	**2.364**	38.271	6.177	**0.427**	11.228	3.803	**0.740**	24.262	3.050	**76.250**	2100.740	3.630
C7	**8.486**	706.407	1.201	**9.131**	963.242	0.948	**1.184**	38.271	3.094	**0.440**	11.228	3.919	**0.691**	24.262	2.848	**91.300**	2100.740	4.346
C8	**9.938**	706.407	1.407	**21.640**	963.242	2.247	**0.724**	38.271	1.892	**0.448**	11.228	3.990	**0.505**	24.262	2.081	**33.720**	2100.740	1.605
C9	**42.840**	706.407	6.064	**8.092**	963.242	0.840	**0.860**	38.271	2.247	**0.579**	11.228	5.157	**1.105**	24.262	4.554	**90.820**	2100.740	4.323
C10	**19.100**	706.407	2.704	**2.388**	963.242	0.248	**0.907**	38.271	2.370	**0.321**	11.228	2.859	**0.146**	24.262	0.602	**44.080**	2100.740	2.098
C11	**188.100**	706.407	26.628	**20.410**	963.242	2.119	**0.614**	38.271	1.604	**0.461**	11.228	4.106	**1.266**	24.262	5.218	**333.000**	2100.740	15.852
C12	**22.550**	706.407	3.192	**14.980**	963.242	1.555	**1.043**	38.271	2.725	**0.299**	11.228	2.663	**0.860**	24.262	3.545	**53.040**	2100.740	2.525
C13	**24.770**	706.407	3.506	**388.200**	963.242	40.301	**2.292**	38.271	5.989	**0.402**	11.228	3.580	**2.076**	24.262	8.557	**37.600**	2100.740	1.790
C14	**81.250**	706.407	11.502	**197.100**	963.242	20.462	**1.061**	38.271	2.772	**0.562**	11.228	5.005	**1.825**	24.262	7.522	**281.600**	2100.740	13.405
C15	**8.844**	706.407	1.252	**10.540**	963.242	1.094	**3.917**	38.271	10.235	**0.419**	11.228	3.732	**0.473**	24.262	1.950	**37.170**	2100.740	1.769
C16	**32.780**	706.407	4.640	**9.223**	963.242	0.957	**1.027**	38.271	2.683	**0.588**	11.228	5.237	**1.454**	24.262	5.993	**94.570**	2100.740	4.502
C17	**10.910**	706.407	1.544	**12.290**	963.242	1.276	**1.463**	38.271	3.823	**0.440**	11.228	3.919	**0.627**	24.262	2.584	**60.370**	2100.740	2.874
C18	**11.490**	706.407	1.627	**5.222**	963.242	0.542	**2.450**	38.271	6.402	**0.775**	11.228	6.902	**0.899**	24.262	3.705	**140.400**	2100.740	6.683
C19	**5.871**	706.407	0.831	**11.400**	963.242	1.184	**3.037**	38.271	7.936	**0.494**	11.228	4.400	**0.703**	24.262	2.898	**67.560**	2100.740	3.216
C20	**13.950**	706.407	1.975	**9.531**	963.242	0.989	**2.093**	38.271	5.469	**0.633**	11.228	5.638	**0.623**	24.262	2.568	**45.300**	2100.740	2.156
C21	**13.640**	706.407	1.931	**9.746**	963.242	1.012	**1.076**	38.271	2.812	**0.583**	11.228	5.192	**0.799**	24.262	3.293	**100.300**	2100.740	4.775
C22	**12.000**	706.407	1.699	**6.240**	963.242	0.648	**1.796**	38.271	4.693	**0.581**	11.228	5.175	**0.352**	24.262	1.451	**69.590**	2100.740	3.313
C23	**67.500**	706.407	9.555	**9.973**	963.242	1.035	**1.741**	38.271	4.549	**0.479**	11.228	4.266	**0.893**	24.262	3.681	**104.000**	2100.740	4.951
C24	**36.480**	706.407	5.164	**58.430**	963.242	6.066	**3.236**	38.271	8.455	**0.462**	11.228	4.115	**2.147**	24.262	8.849	**94.810**	2100.740	4.513
	706.407		100.000	963.242		100.000	38.271		100.000	11.228		100.000	24.262		100.000	2100.740		100.000

Table A4: The cations analysis results and the percentages of the single ion in the soil samples

Sample ID	111Cd	Total	% in the	121Sb	Total	% in the	133Cs	Total	% in the	137Ba	Total	% in the	182W	Total	% in the	202Hg	Total	% in the
	ppb	amount	sample	ppb	amount	sample	ppb	amount	sample	ppb	amount	sample	ppb	amount	sample	ppb	amount	sample
C1	**0.057**	3.216	1.772	**1.319**	26.784	4.925	**0.103**	8.694	1.185	**98.730**	3945.740	2.502	**0.284**	5.674	5.005	**0.176**	4.339	4.056
C2	**0.341**	3.216	10.603	**3.182**	26.784	11.880	**1.932**	8.694	22.222	**69.950**	3945.740	1.773	**0.418**	5.674	7.367	**0.214**	4.339	4.932
C3	**0.061**	3.216	1.897	**0.679**	26.784	2.535	**0.225**	8.694	2.588	**312.500**	3945.740	7.920	**0.140**	5.674	2.467	**0.184**	4.339	4.241
C4	**0.029**	3.216	0.902	**0.406**	26.784	1.516	**0.027**	8.694	0.311	**67.040**	3945.740	1.699	**0.102**	5.674	1.798	**0.155**	4.339	3.572
C5	**0.046**	3.216	1.430	**0.653**	26.784	2.438	**0.032**	8.694	0.368	**145.000**	3945.740	3.675	**0.244**	5.674	4.300	**0.234**	4.339	5.393
C6	**0.023**	3.216	0.715	**0.722**	26.784	2.696	**0.020**	8.694	0.230	**58.850**	3945.740	1.491	**0.229**	5.674	4.036	**0.320**	4.339	7.375
C7	**0.033**	3.216	1.026	**0.468**	26.784	1.747	**0.017**	8.694	0.196	**95.990**	3945.740	2.433	**0.162**	5.674	2.855	**0.151**	4.339	3.480
C8	**0.030**	3.216	0.933	**0.429**	26.784	1.602	**0.014**	8.694	0.161	**90.250**	3945.740	2.287	**0.174**	5.674	3.067	**0.148**	4.339	3.411
C9	**0.037**	3.216	1.150	**1.685**	26.784	6.291	**4.597**	8.694	52.876	**108.100**	3945.740	2.740	**0.284**	5.674	5.005	**0.140**	4.339	3.227
C10	**0.013**	3.216	0.404	**0.754**	26.784	2.815	**0.010**	8.694	0.115	**444.500**	3945.740	11.265	**0.143**	5.674	2.520	**0.217**	4.339	5.001
C11	**0.030**	3.216	0.933	**0.558**	26.784	2.083	**0.017**	8.694	0.196	**270.700**	3945.740	6.861	**0.067**	5.674	1.181	**0.154**	4.339	3.549
C12	**0.040**	3.216	1.244	**0.361**	26.784	1.348	**1.249**	8.694	14.366	**537.600**	3945.740	13.625	**0.206**	5.674	3.631	**0.183**	4.339	4.218
C13	**1.455**	3.216	45.243	**2.291**	26.784	8.554	**0.031**	8.694	0.357	**180.400**	3945.740	4.572	**0.313**	5.674	5.516	**0.144**	4.339	3.319
C14	**0.141**	3.216	4.384	**2.388**	26.784	8.916	**0.025**	8.694	0.288	**537.500**	3945.740	13.622	**0.178**	5.674	3.137	**0.408**	4.339	9.403
C15	**0.026**	3.216	0.808	**0.472**	26.784	1.762	**0.014**	8.694	0.161	**96.220**	3945.740	2.439	**0.115**	5.674	2.027	**0.227**	4.339	5.232
C16	**0.039**	3.216	1.213	**1.775**	26.784	6.627	**0.017**	8.694	0.196	**109.900**	3945.740	2.785	**0.274**	5.674	4.829	**0.131**	4.339	3.019
C17	**0.024**	3.216	0.746	**0.651**	26.784	2.431	**0.037**	8.694	0.426	**64.570**	3945.740	1.636	**0.158**	5.674	2.785	**0.129**	4.339	2.973
C18	**0.021**	3.216	0.653	**1.111**	26.784	4.148	**0.015**	8.694	0.173	**71.690**	3945.740	1.817	**0.770**	5.674	13.571	**0.141**	4.339	3.250
C19	**0.304**	3.216	9.453	**0.878**	26.784	3.278	**0.042**	8.694	0.483	**36.730**	3945.740	0.931	**0.146**	5.674	2.573	**0.120**	4.339	2.766
C20	**0.033**	3.216	1.026	**0.469**	26.784	1.751	**0.202**	8.694	2.323	**125.500**	3945.740	3.181	**0.138**	5.674	2.432	**0.151**	4.339	3.480
C21	**0.040**	3.216	1.244	**1.094**	26.784	4.085	**0.014**	8.694	0.161	**122.000**	3945.740	3.092	**0.307**	5.674	5.411	**0.212**	4.339	4.886
C22	**0.031**	3.216	0.964	**1.671**	26.784	6.239	**0.018**	8.694	0.207	**107.700**	3945.740	2.730	**0.203**	5.674	3.578	**0.135**	4.339	3.111
C23	**0.021**	3.216	0.653	**0.871**	26.784	3.252	**0.011**	8.694	0.127	**149.500**	3945.740	3.789	**0.222**	5.674	3.913	**0.161**	4.339	3.711
C24	**0.341**	3.216	10.603	**1.897**	26.784	7.083	**0.025**	8.694	0.288	**44.820**	3945.740	1.136	**0.397**	5.674	6.997	**0.104**	4.339	2.397
	3.216		100.000	26.784		100.000	8.694		100.000	3945.740		100.000	5.674		100.000	4.339		100.000

Table A5: The cations analysis results and the percentages of the single ion in the soil samples

Sample ID	208Pb	Total	% in the	**Total % in**	**Total % over**
	ppb	amount	sample	**24 samples**	**24 samples**
C1	**10.160**	1085.606	0.936	**102.041**	**3.925**
C2	**28.620**	1085.606	2.636	**209.244**	**8.048**
C3	**7.521**	1085.606	0.693	**76.517**	**2.943**
C4	**5.826**	1085.606	0.537	**68.654**	**2.641**
C5	**10.900**	1085.606	1.004	**86.256**	**3.318**
C6	**5.437**	1085.606	0.501	**75.037**	**2.886**
C7	**2.728**	1085.606	0.251	**73.709**	**2.835**
C8	**3.471**	1085.606	0.320	**69.679**	**2.680**
C9	**7.593**	1085.606	0.699	**142.913**	**5.497**
C10	**0.870**	1085.606	0.080	**71.419**	**2.747**
C11	**322.000**	1085.606	29.661	**152.658**	**5.871**
C12	**5.953**	1085.606	0.548	**123.984**	**4.769**
C13	**67.470**	1085.606	6.215	**234.274**	**9.011**
C14	**454.200**	1085.606	41.838	**191.056**	**7.348**
C15	**4.887**	1085.606	0.450	**74.594**	**2.869**
C16	**5.164**	1085.606	0.476	**102.947**	**3.959**
C17	**2.685**	1085.606	0.247	**68.171**	**2.622**
C18	**1.225**	1085.606	0.113	**91.510**	**3.520**
C19	**2.292**	1085.606	0.211	**74.058**	**2.848**
C20	**2.565**	1085.606	0.236	**82.030**	**3.155**
C21	**3.525**	1085.606	0.325	**123.596**	**4.754**
C22	**1.734**	1085.606	0.160	**76.611**	**2.947**
C23	**117.100**	1085.606	10.787	**89.987**	**3.461**
C24	**11.680**	1085.606	1.076	**139.054**	**5.348**
	1085.606		100.000	**2600.000**	**100.000**

Appendix B

Single and Total Anions Plots

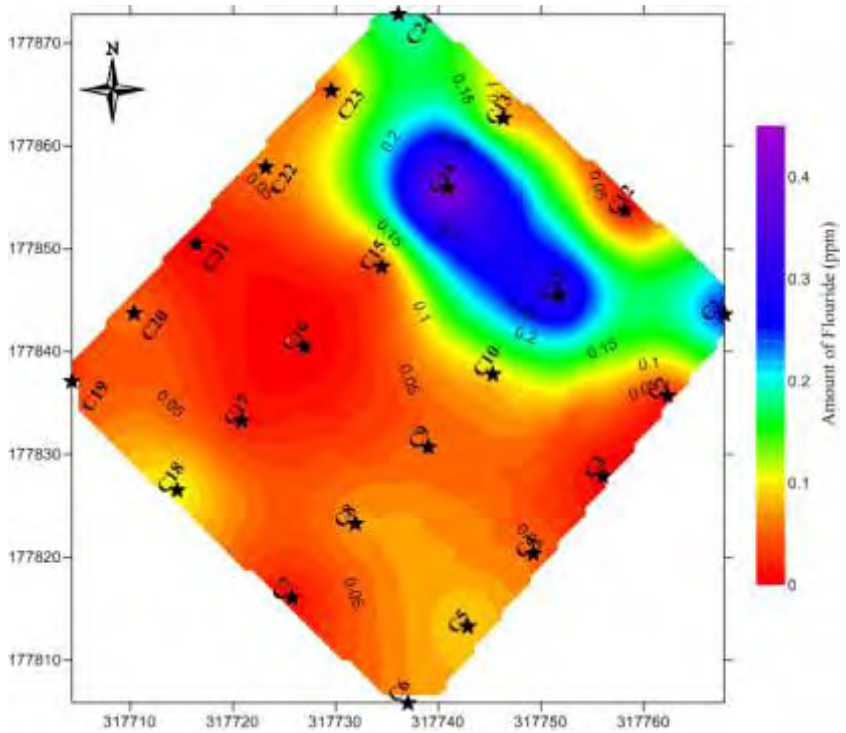

Figure B1: The distribution of Flouride in soil samples

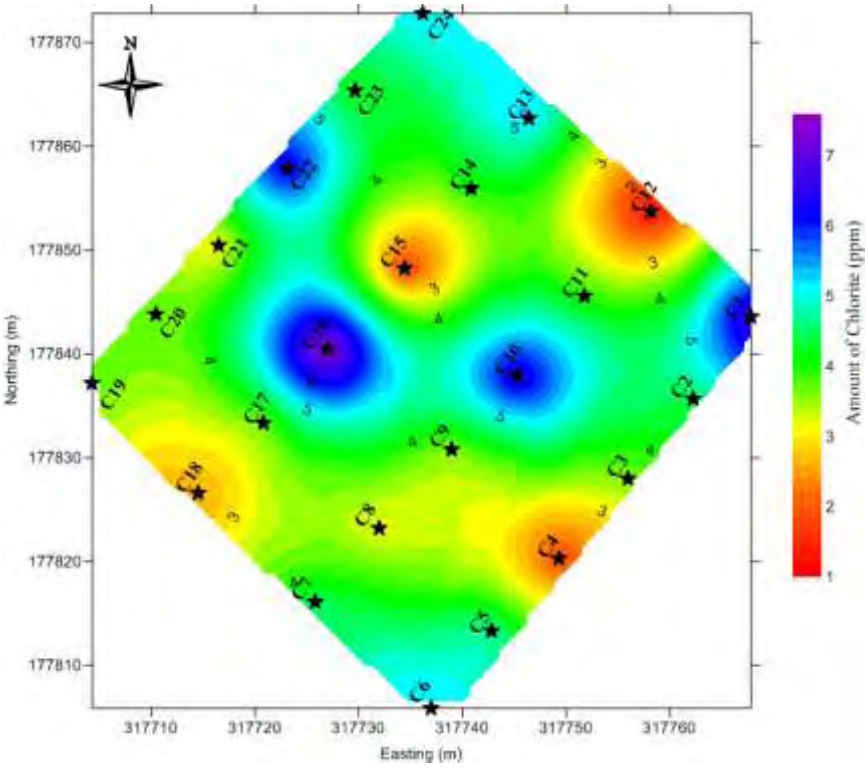

Figure B2: The distribution of Chloride in soil samples

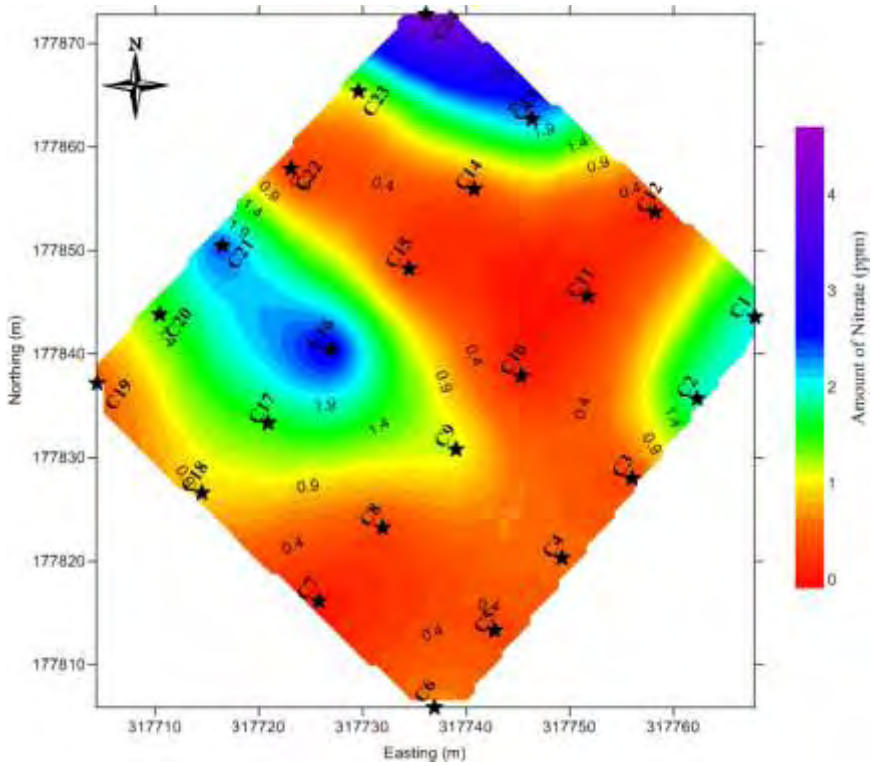

Figure B3: The distribution of Nitrate in soil samples

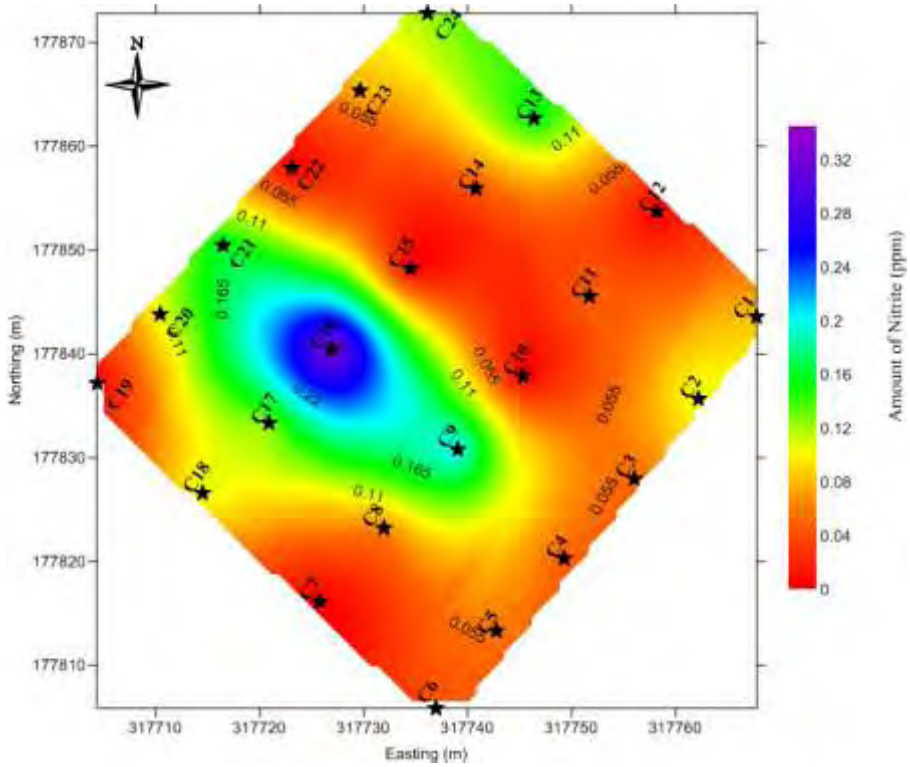

Figure B4: The distribution of Nitrite in soil samples

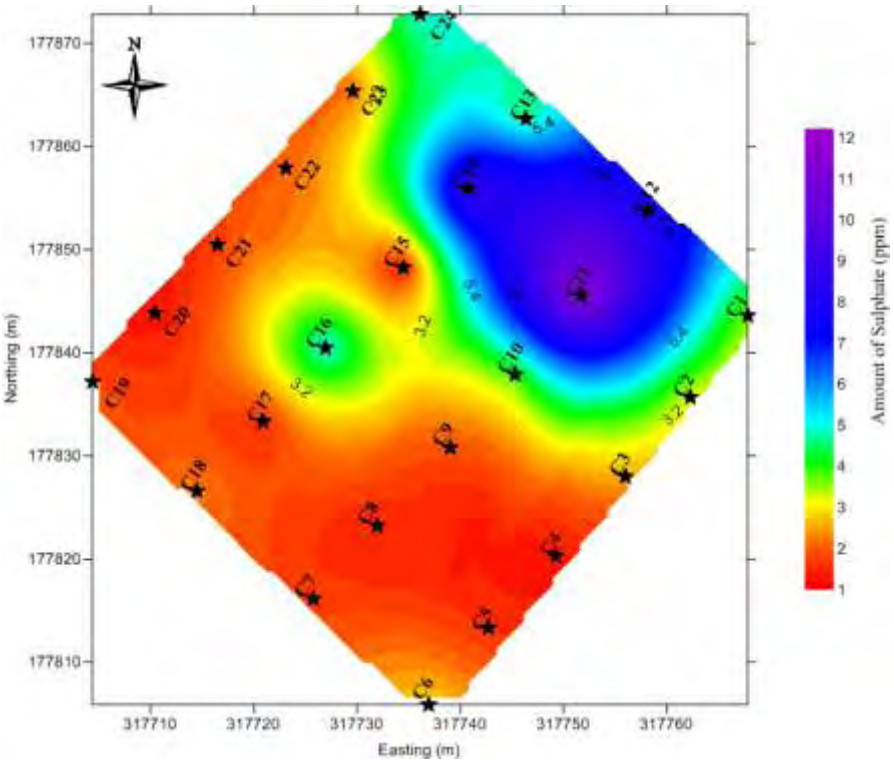

Figure B5: The distribution of Sulphate in soil samples

Appendix C

Single and Total Cations Plots

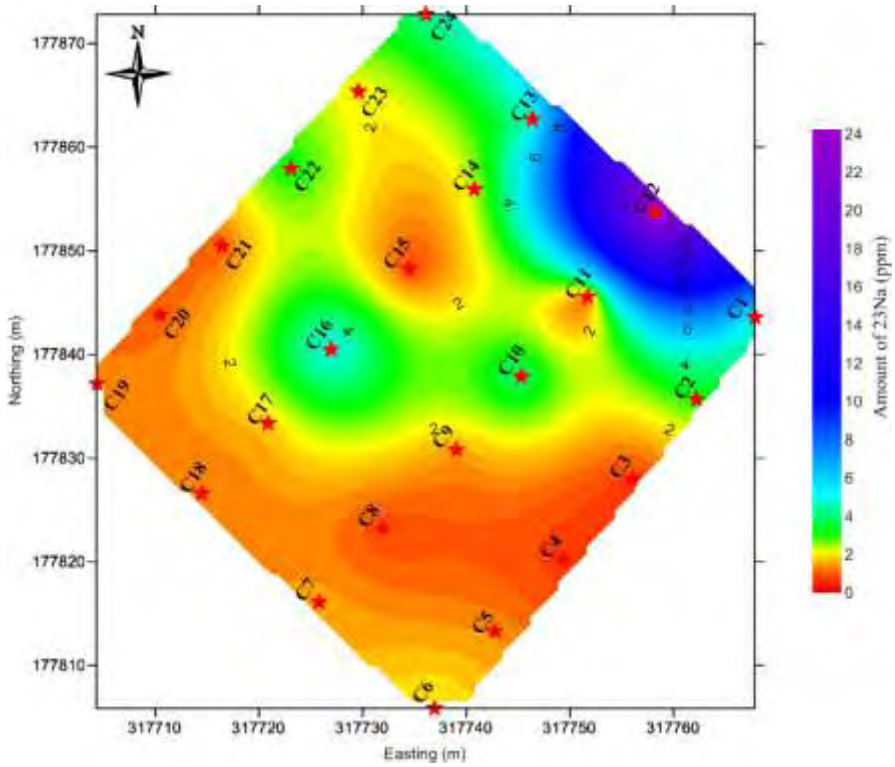

Figure C1: The distribution of 23Na (Sodium) in soil samples

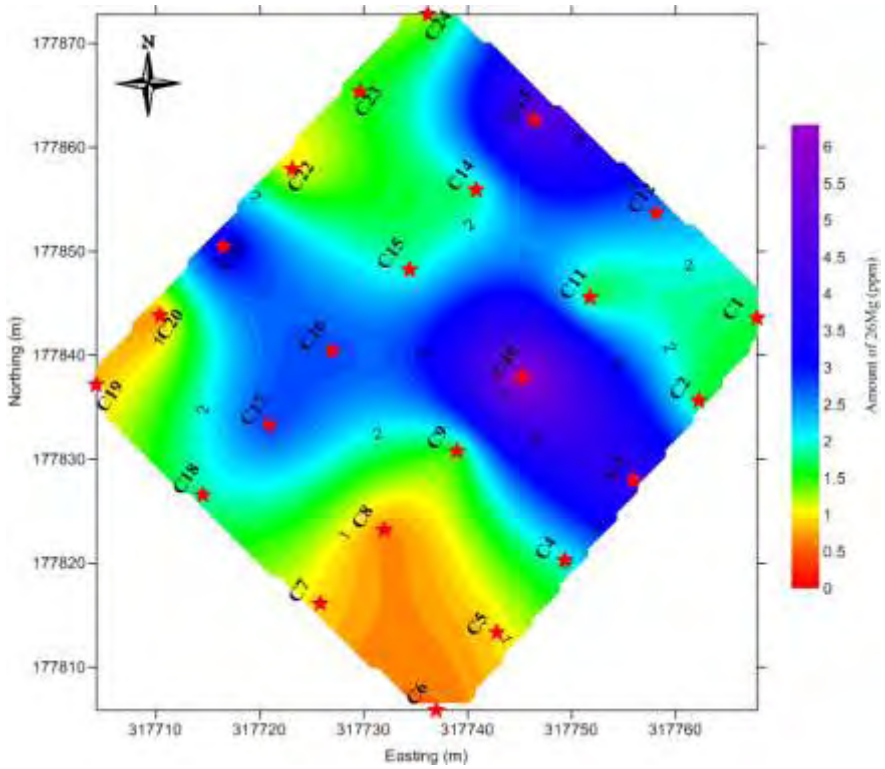

Figure C2: The distribution of 26Mg (Magnesium) in soil samples

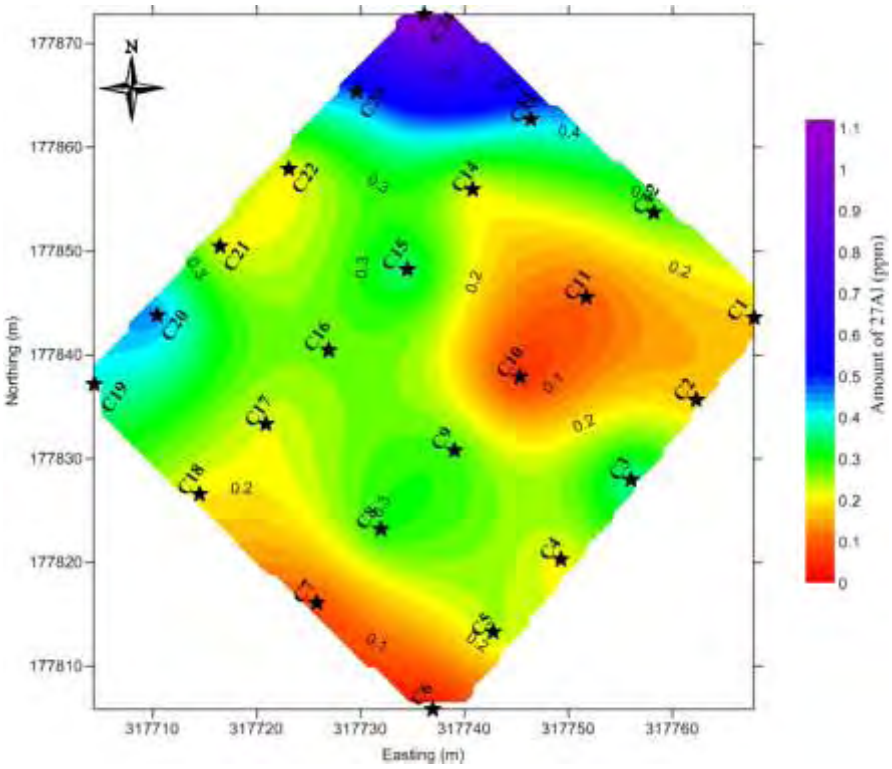

Figure C3: The distribution of 27Al (Aluminium) in soil samples

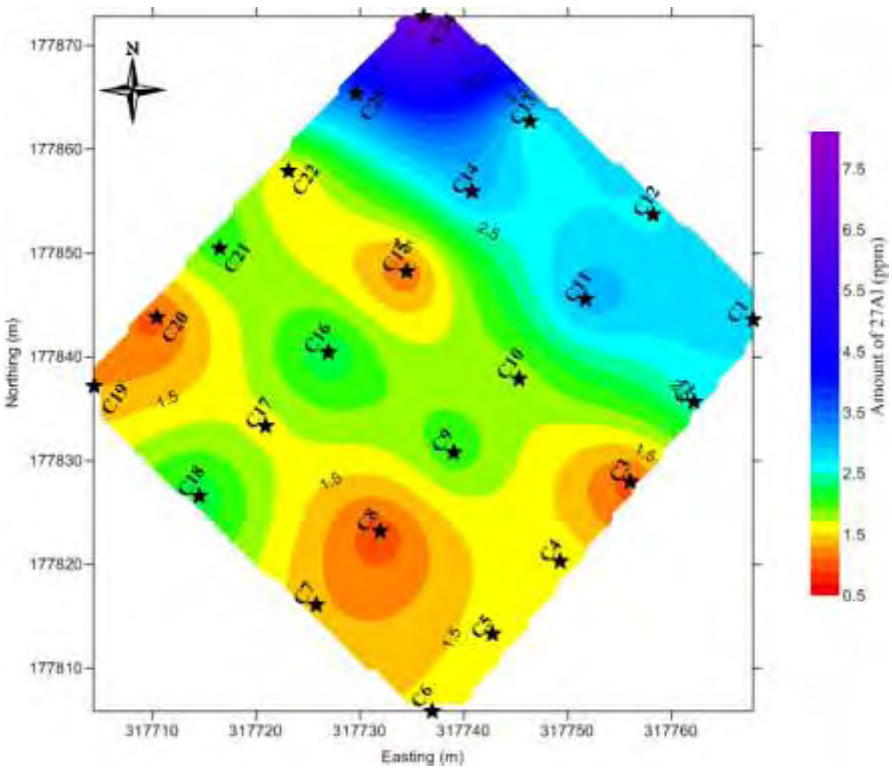

Figure C4: The distribution of 29Si (Silicon) in soil samples

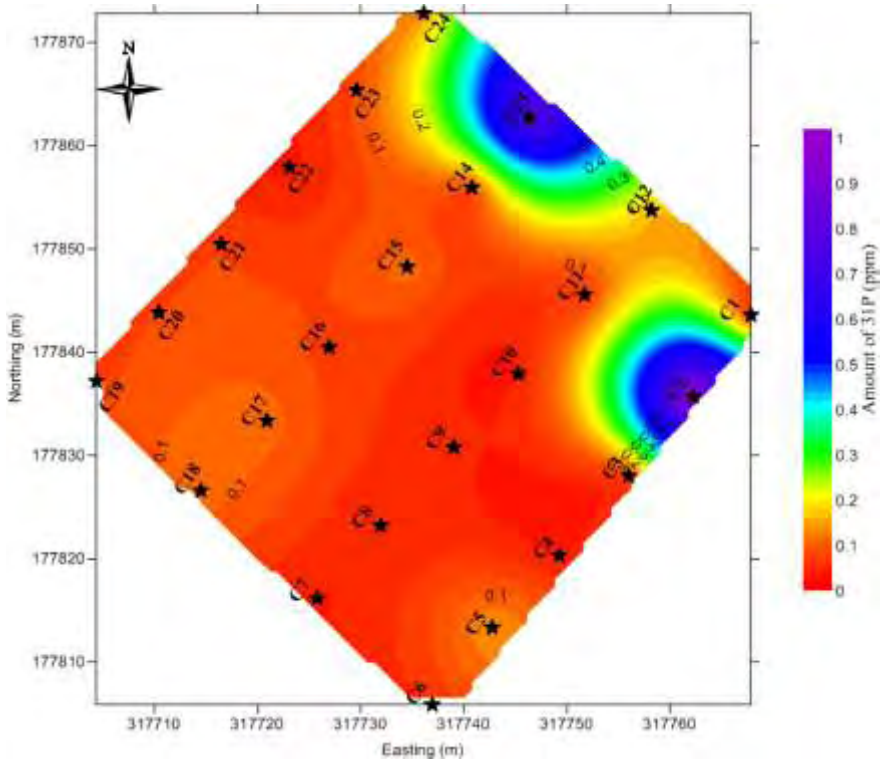

Figure C5: The distribution of 31P (phosphorous) in soil samples

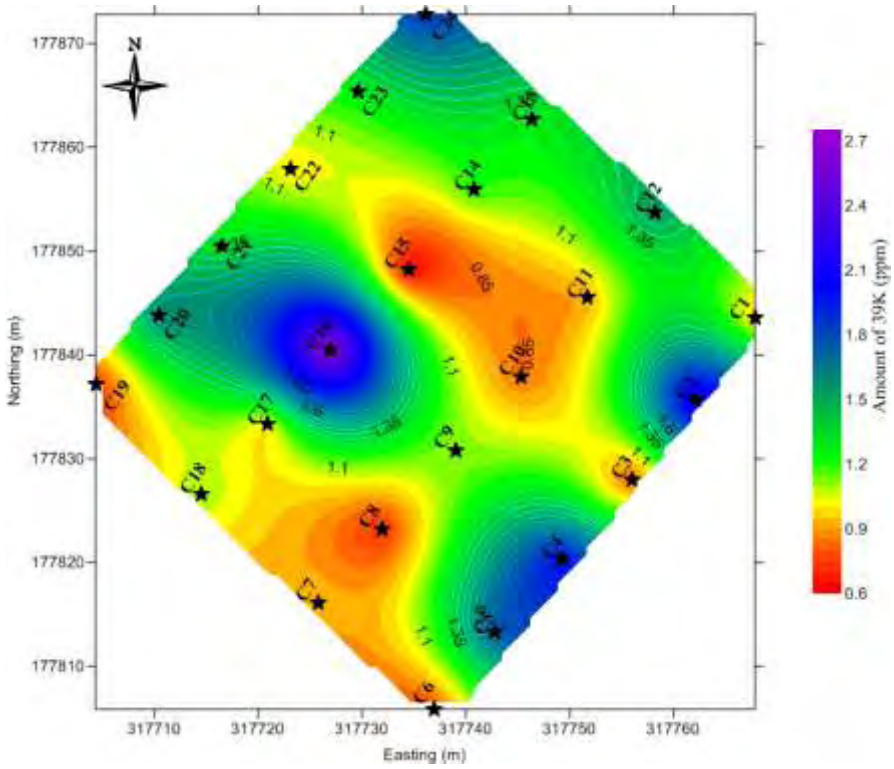

Figure C6: The distribution of 39K (Potassium) in soil samples

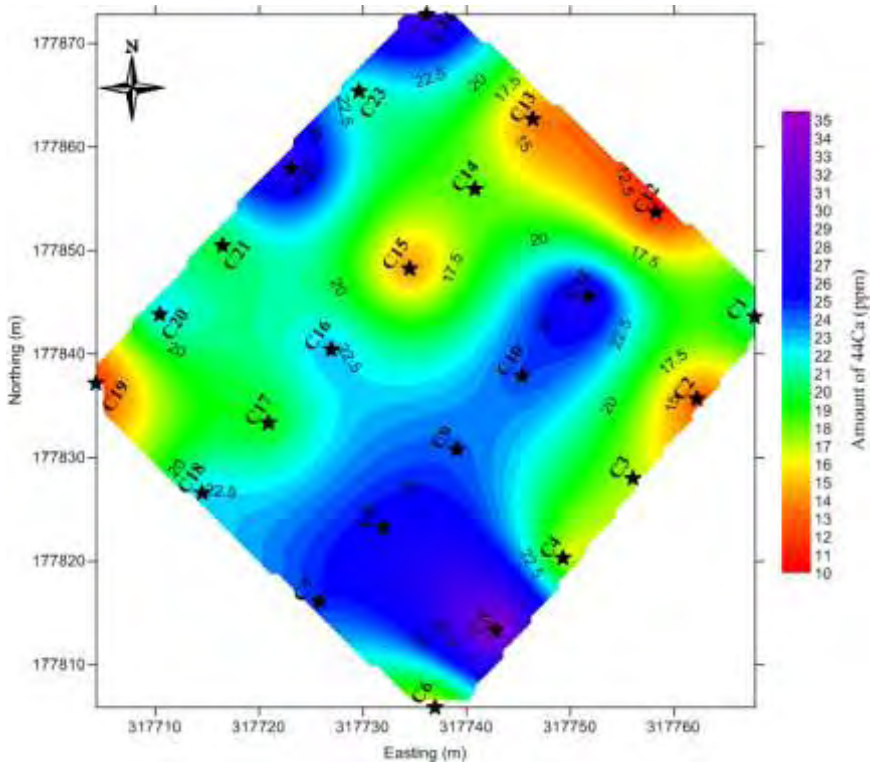

Figure C7: The distribution of 44Ca (Calcium) in soil samples

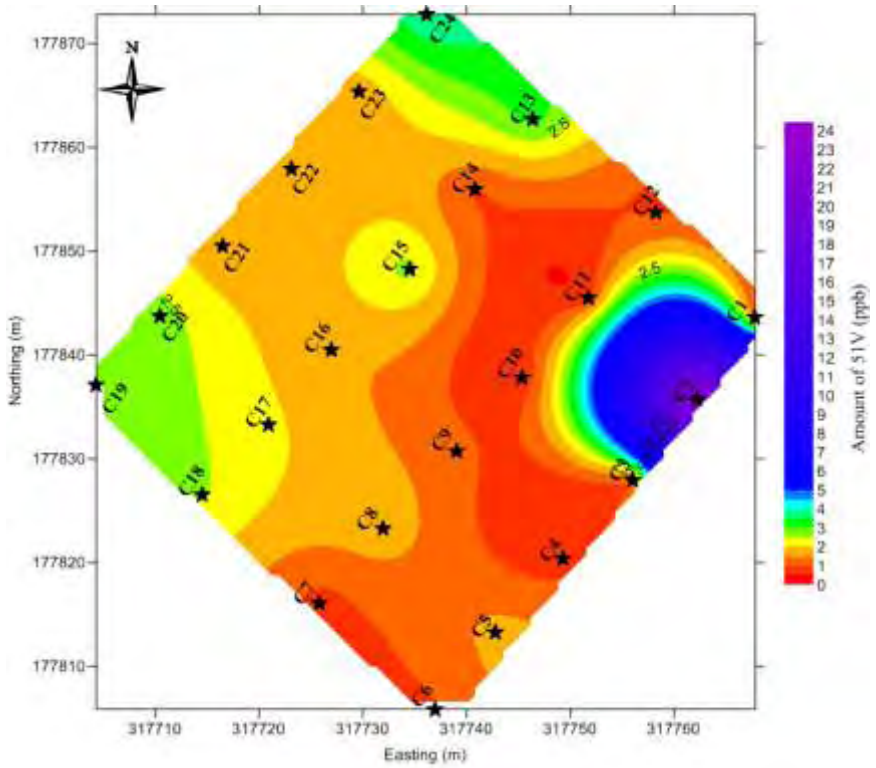

Figure C8: The distribution of 51V (Vanadium) in soil samples

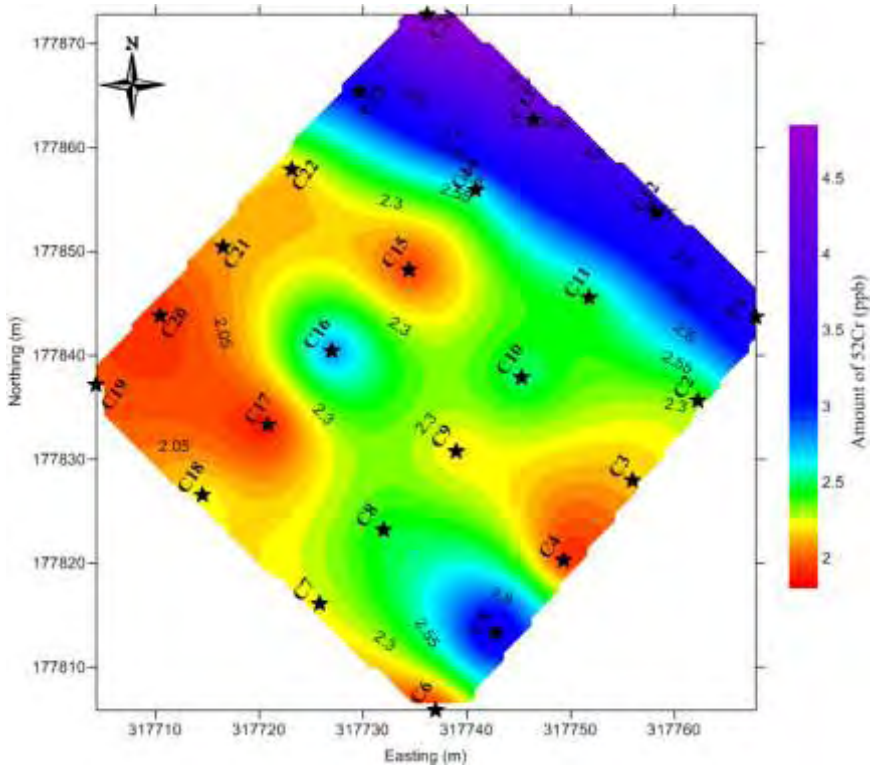

Figure C9: The distribution of 52Cr (Chromium) in soil samples

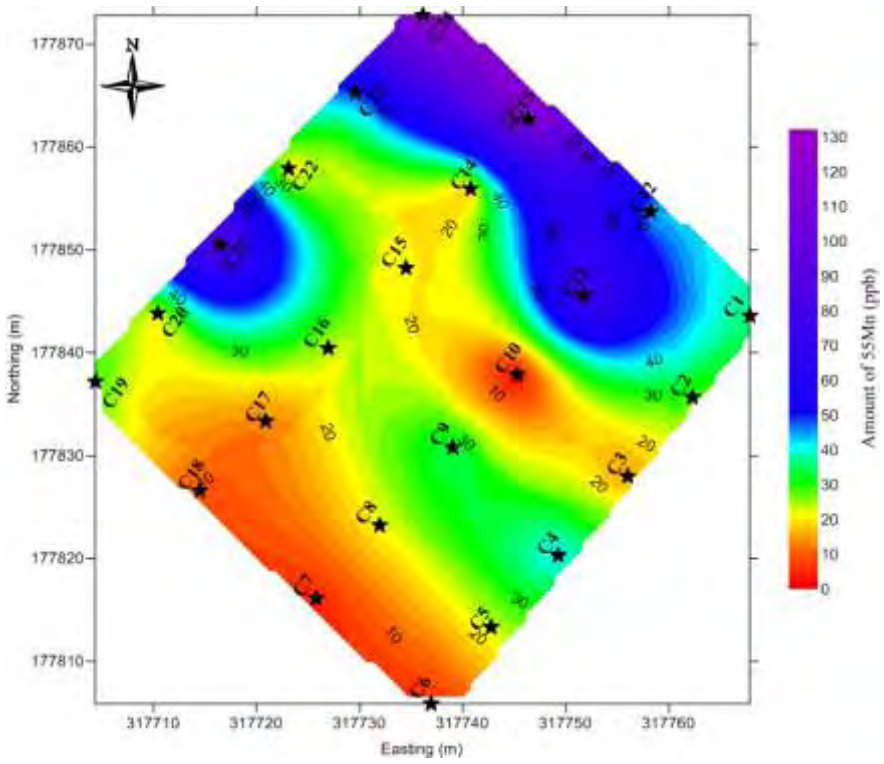

Figure C10: The distribution of 55Mn (Manganese) in soil samples

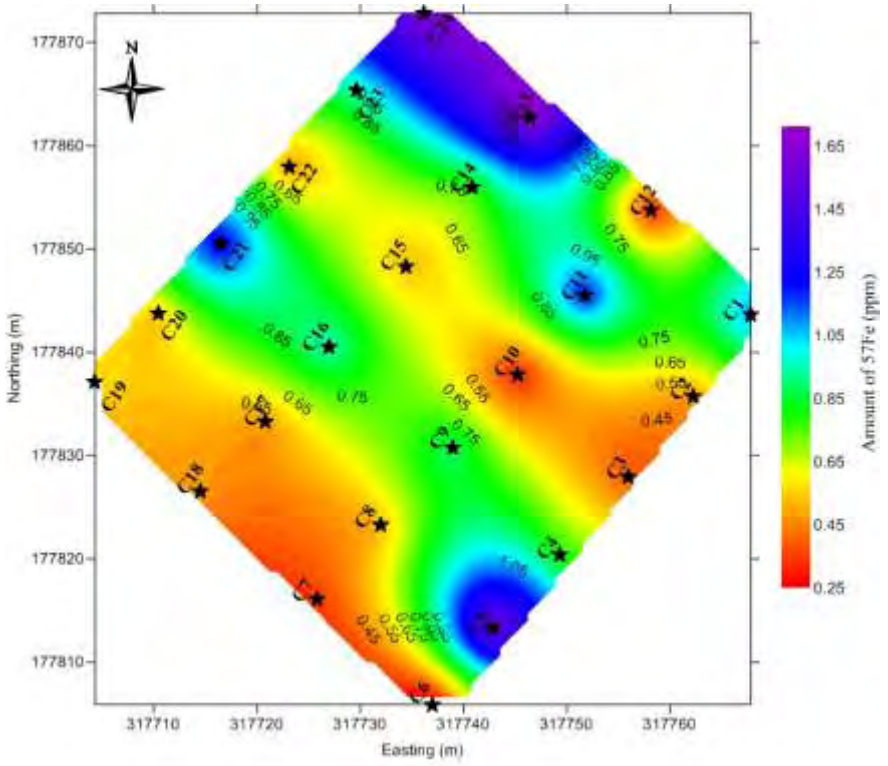

Figure C11: The distribution of 57Fe (Iron) in soil samples

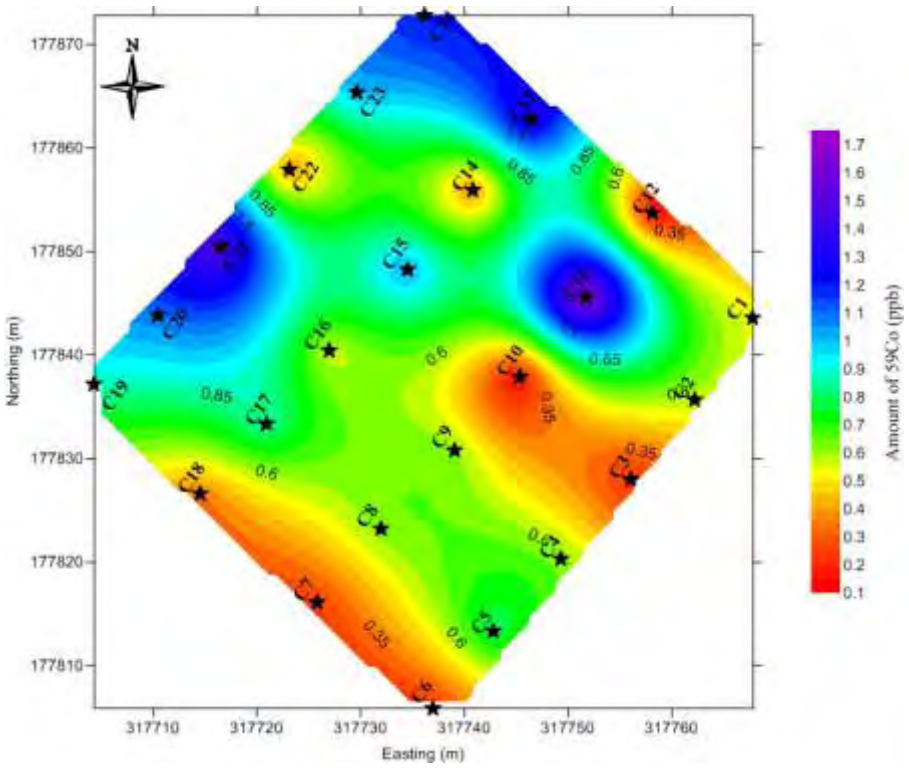

Figure C12: The distribution of 59Co (Cobalt) in soil samples

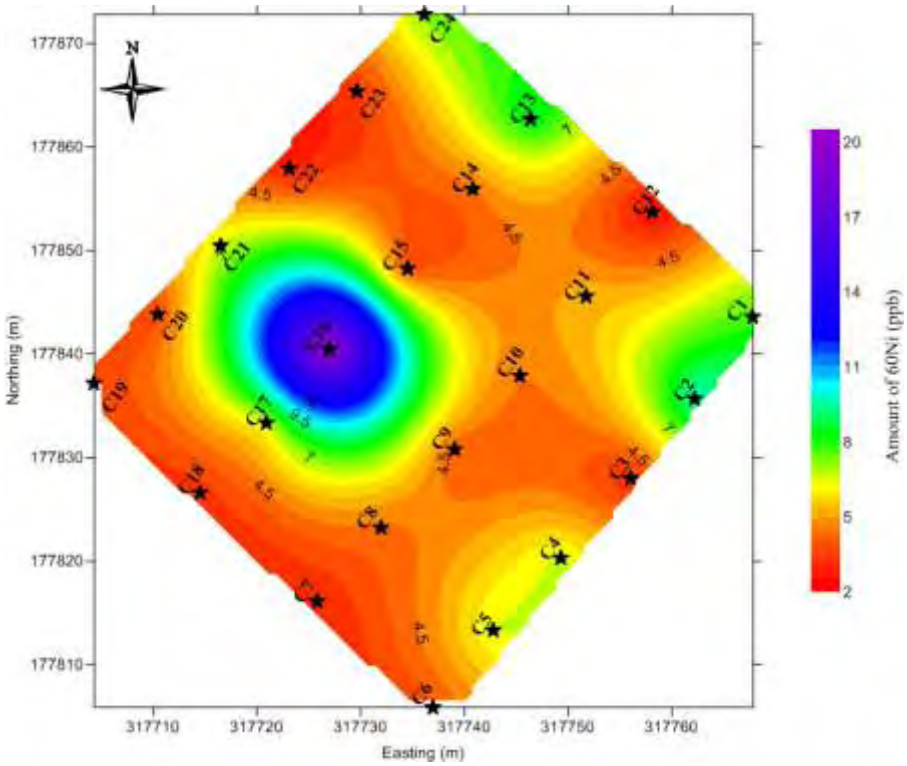

Figure C13: The distribution of 60Ni (Nickel) in soil samples

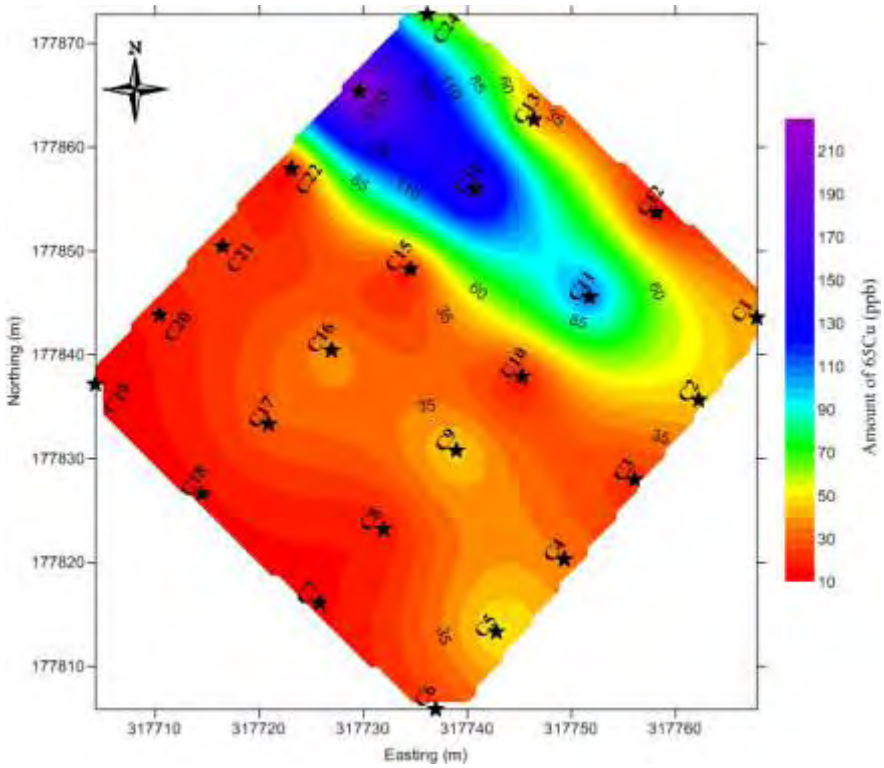

Figure C14: The distribution of 65Cu (Copper) in soil samples

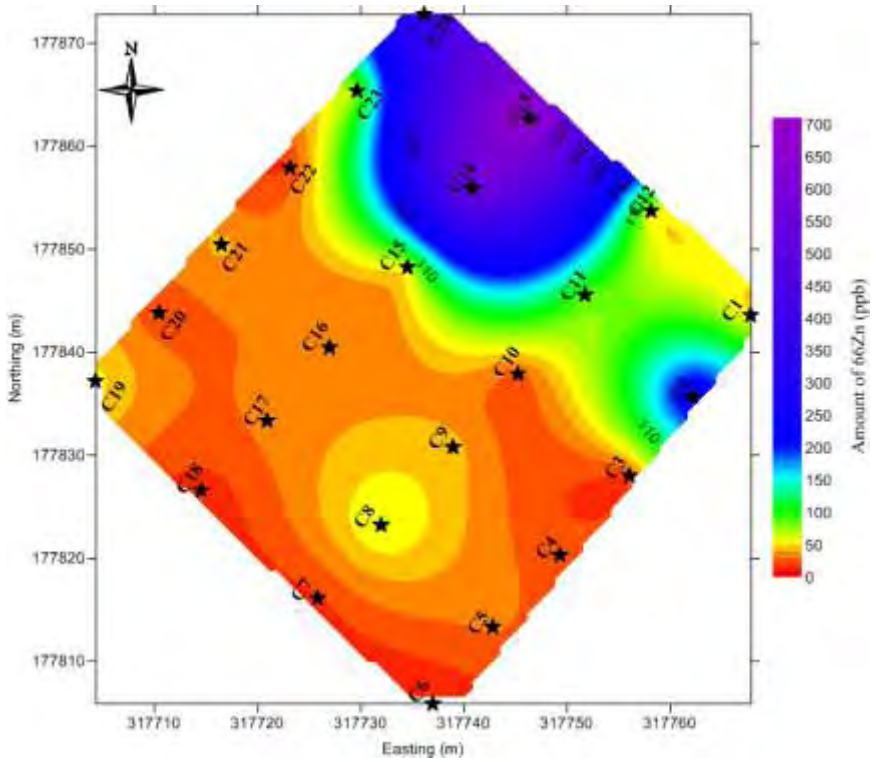

Figure C15: The distribution of 66Zn (Zinc) in soil samples

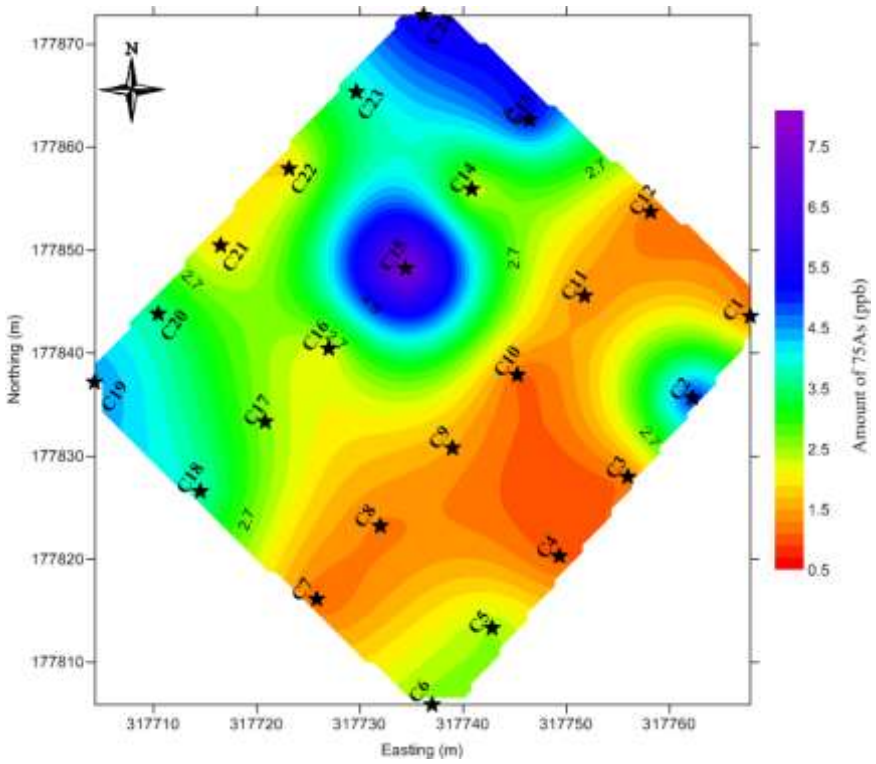

Figure C16: The distribution of 75As (Arsenic) in soil samples

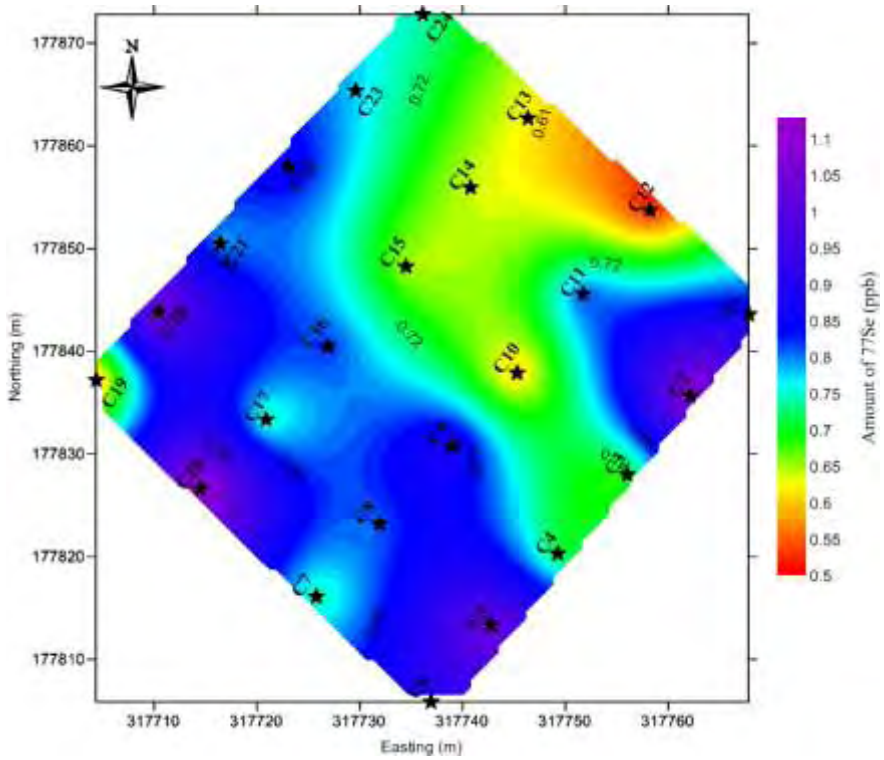

Figure C17: The distribution of 77Se (Selenium) in soil samples

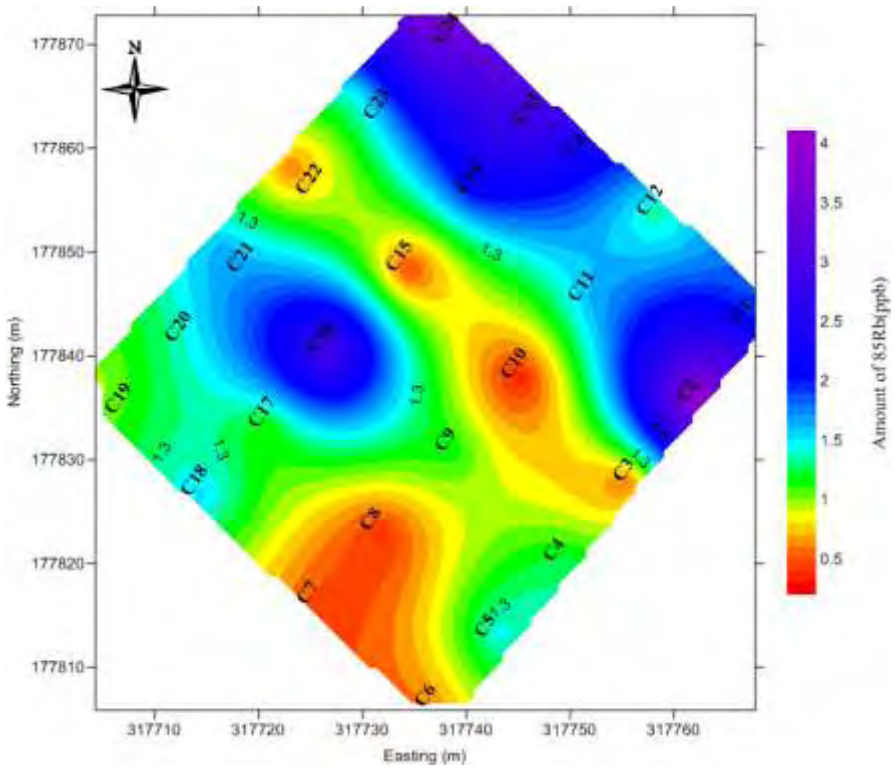

Figure C18: The distribution of 85Rb (Rubidium) in soil samples

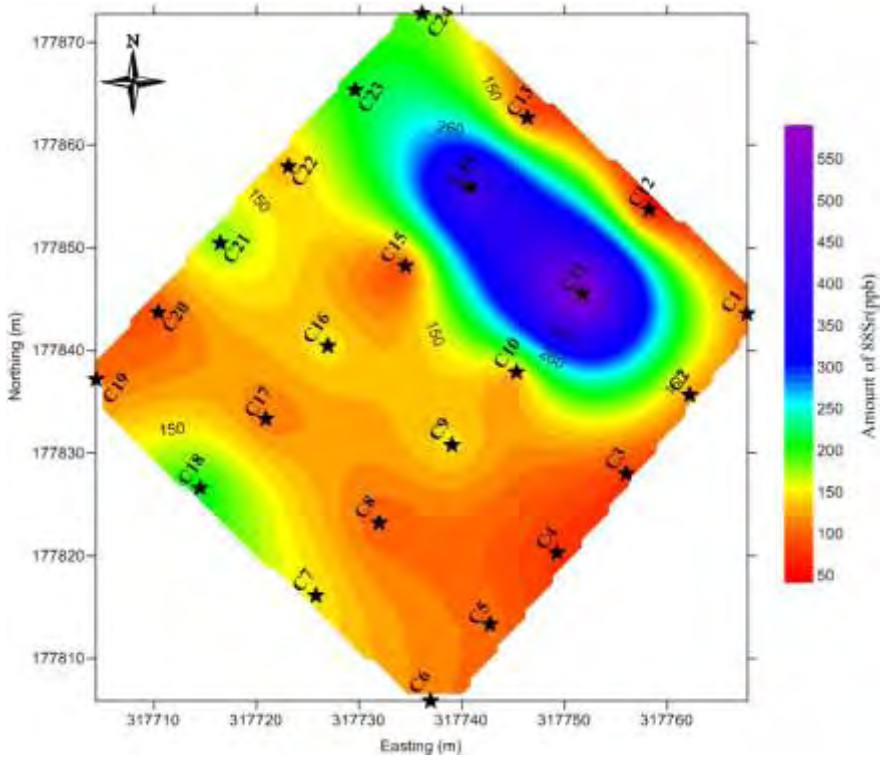

Figure C19: The distribution of 88Sr (Strontium) in soil samples

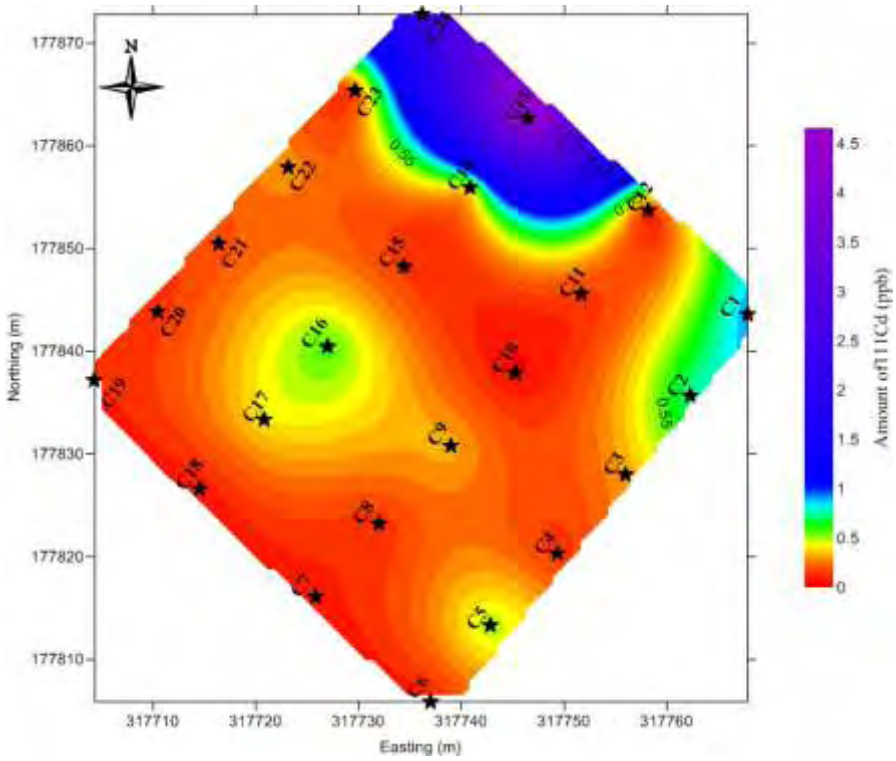

Figure C20: The distribution of 111Cd (Cadmium) in soil samples

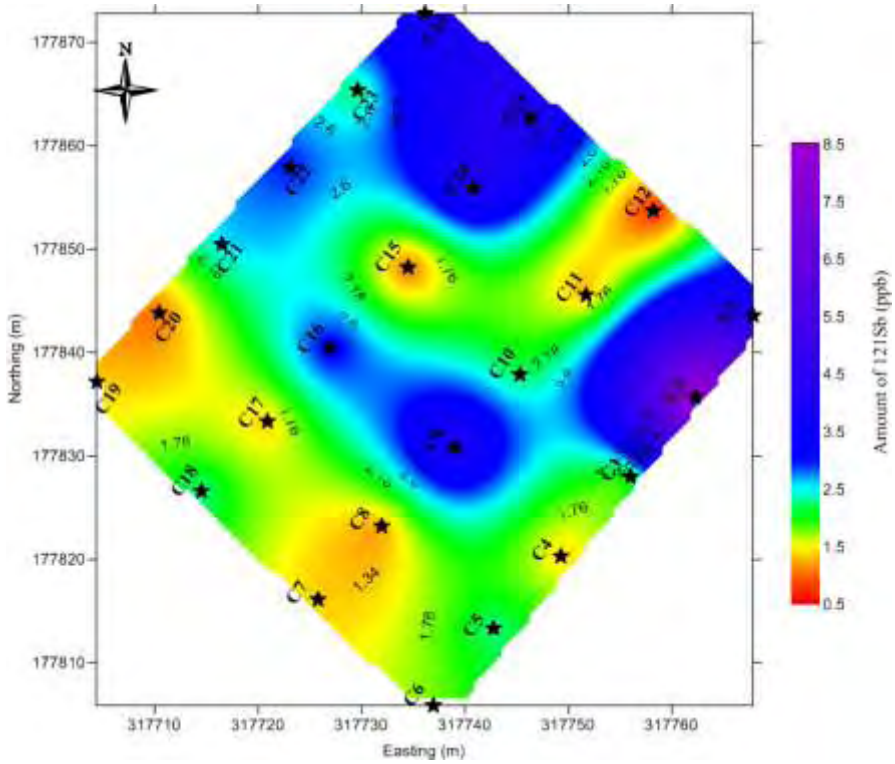

Figure C21: The distribution of 121Sb (Antimony) in soil samples

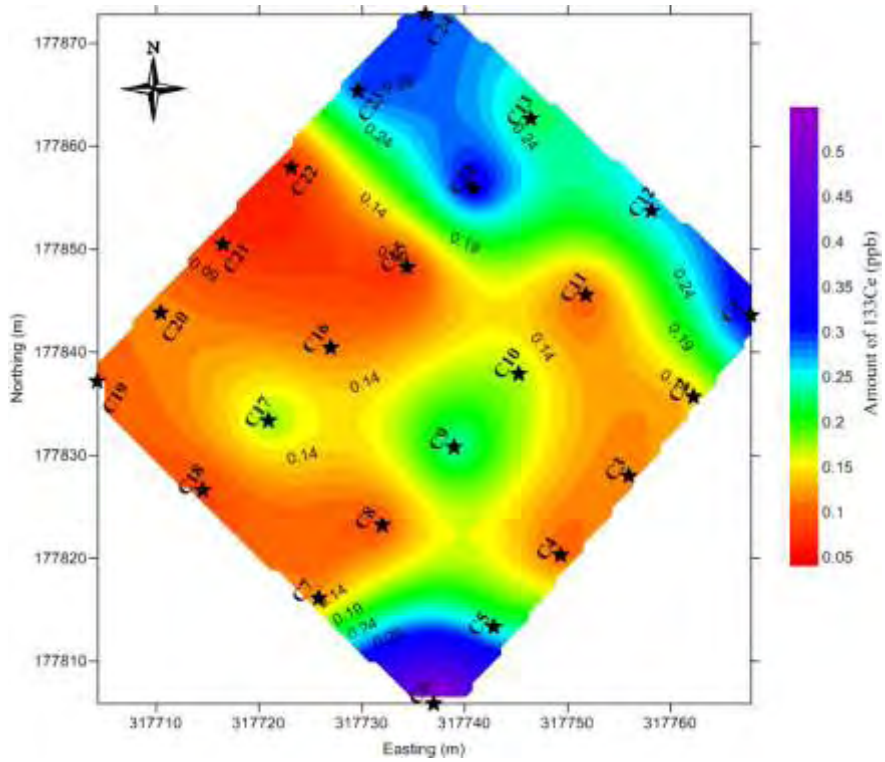

Figure C22: The distribution of 133Cs (Cesium) in soil samples

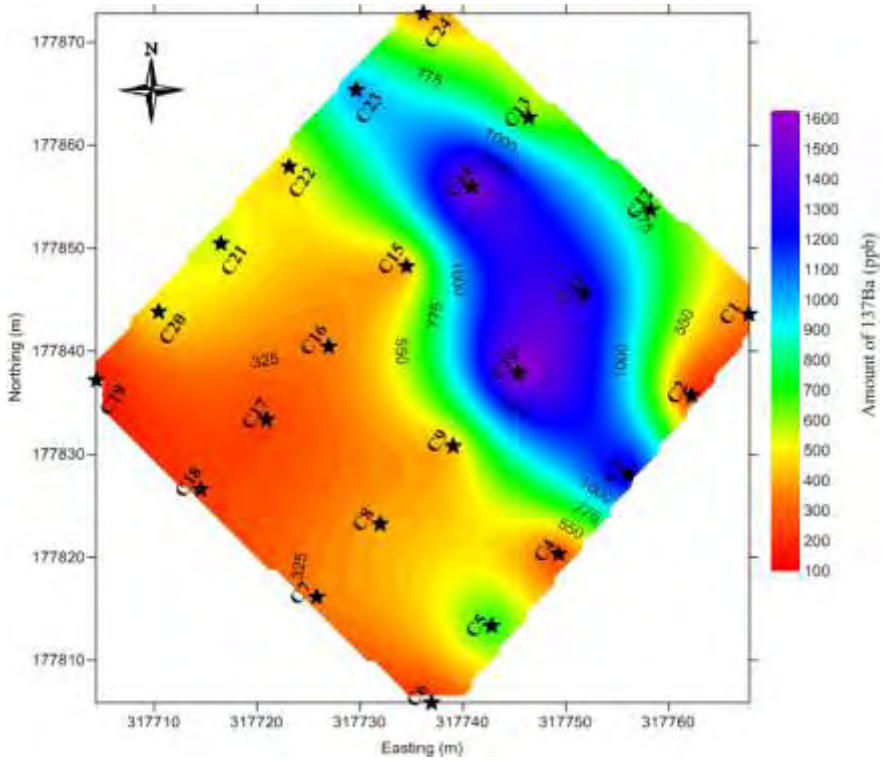

Figure C23: The distribution of 137Ba (Barium) in soil samples

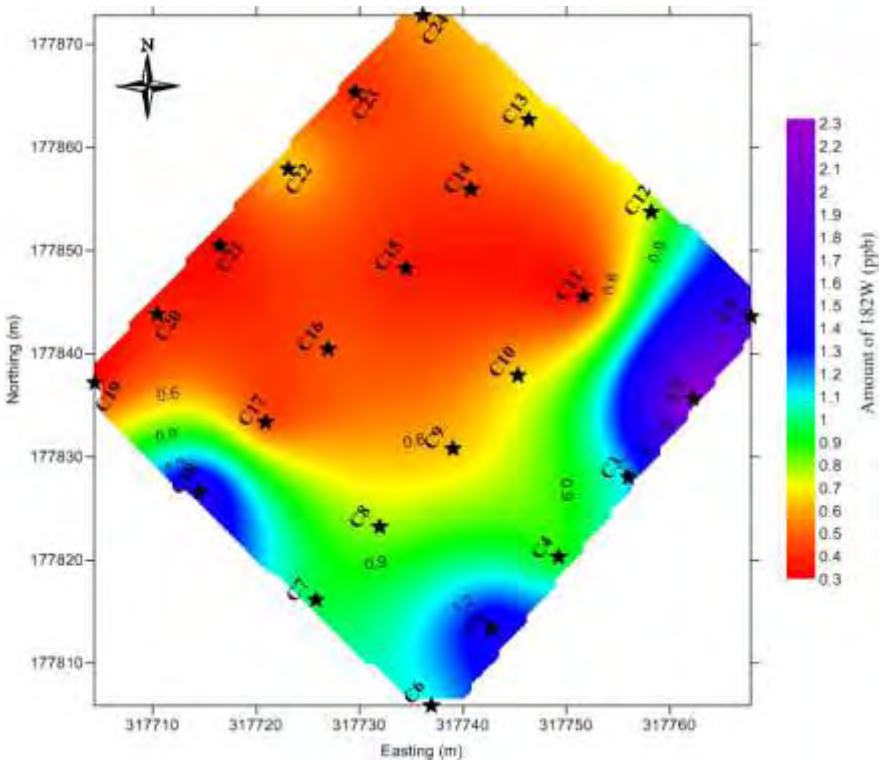

Figure C24: The distribution of 182W (Tungsten) in soil samples

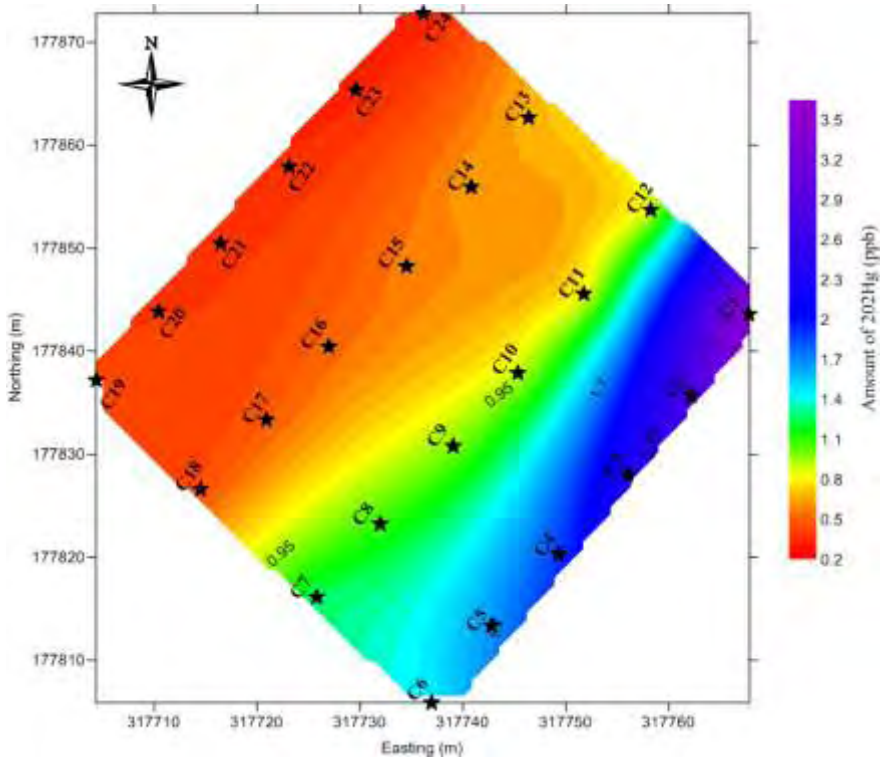

Figure C25: The distribution of 202Hg (Mercury) in soil samples

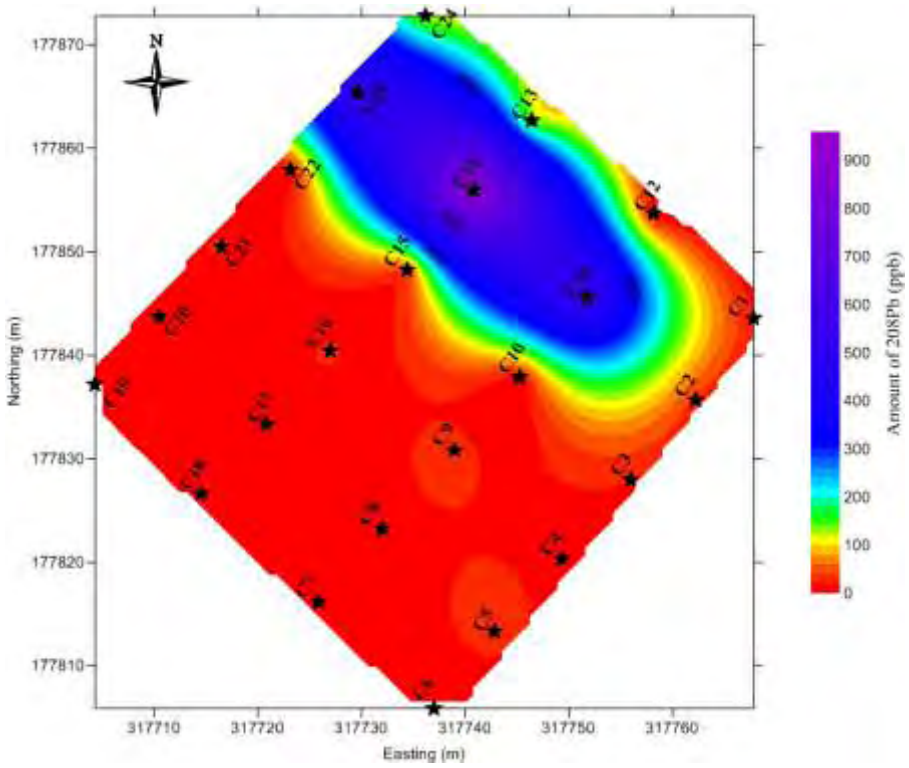

Figure C26: The distribution of 208Pb (Lead) in soil samples

APPENDIX D

Brief Information on the Resistivity Data Processing

The main objective of the resistivity data inversion using the Res2Dinv is to get the minimise RMS Error so that the rough data (from the field), calculating data (from the software) and the final inversion model should be match well (all are shown as a profile). In this study, not all the resistivity data for every line has to use the similar inversion parameters and it depend on the field data quality. Here is the brief procedure how to reduce the RMS Error in the inversion process of the resistivity data using Res2Dinv.
Before that highlight here is the brief theoretical of the inversion routine used by Res2Dinv software.

Theory

The inversion routine used by the program is based on the smoothness-constrainedleast-squares method (Loke et al. 2003). The smoothness-constrained least-squares method isbased on the following equation

$$\left(\mathbf{J}^{\mathrm{T}}\mathbf{J} + \lambda\mathbf{F}\right)\Delta\mathbf{q}_{\mathrm{k}} = \mathbf{J}^{\mathrm{T}}\mathbf{g} - \lambda\mathbf{F}\mathbf{q}_{\mathrm{k}} \quad (4.1)$$

where $\mathbf{F} = \alpha_x \mathbf{C}_x^{\mathrm{T}}\mathbf{C}_x + \alpha_z \mathbf{C}_z^{\mathrm{T}}\mathbf{C}_z$ ----------(a)

Cx= horizontal roughness filters
Cz= vertical roughness filter
J = Jacobian matrix of partial derivatives
JT = transpose of **J**
l = damping factor
q = model change vector
g = data misfit vector

One advantage of this is that the damping factor and the roughness filters can be adjusted to suit different types of data. The detail description of the different variations of smoothness-constrained least-squares method can be found in the free tutorial notes by Loke (2012).The optimization method tried to reduce the different between calculated and

apparent resistivity values by adjusting the resistivity of the model blocks subject to the smoothness-constrained used. A measure of this difference is given by root-mean-squared (RMS) error.

Field/Laboratory Data Quality Control

1. Survey line should be built in a straight line
2. The electrode spacing had to be equally similar
3. Testing the electrodes connection and the grounding condition. Normally, if has a grounding error or has a high resistivity value, salt water or normal water is use to improve the grounding condition
4. The variant coefficient percentage is set as 3% in the equipment so that the statically error in calculation can be minimised starting from the field data acquisition

PROSYS II Resistivity Data Management

The **PROSYS II**software is a program allowing to transfer, edit, process and export resistivity andchargeability data of the *IRIS Instruments* resistivity-meters (SYSCAL) and IP receivers (ELREC).

The main functions of the **PROSYS II**software are the following:

● Data download
● Numeric and graphic presentation (raw parameters, resistivity, chargeability)
● Processing (filter on threshold values, apply a sliding or median average, reject a node, reject thegapfiller quadric poles, create a batch file with a specific filtering to apply to a set of files)
● Topography insertion
● Plot of the apparent resistivity and chargeability sections
● Export to various formats (″txt″, Res2dinv) and visualization of the exported files

Originally, the field data is in BIN format will be converted into dat.files before it can be read or uploaded into Res2Dinv software and it is done in the PROSYS II software. In the conversion processes, the field data (BIN files) will be sorted or filtering to remove any bad data point and to insert any topographic data for the electrodes. In this process, any

negative data or high error in reading (Standard Deviation) will be remove data set before proceed to convert the file into DAT file (readable format for the Res2Dinv software).

Data Processing Using Res2Dinv

In the Res2Dinv software, after loading the data files from the read data file option. Normally in the processing of the resistivity data, three options have to be check before start the inversion process. It is '**Edit**', '**Change Setting**' and '**Inversion**' options.

Edit options

This section covers a few data editing options to remove bad data points, trim very long profiles and reverse the direction of a data set and to change the locationof the beginning of the line.In this option, the apparent resistivity data values are displayed in the form ofprofiles for each data level. For data quality control, the option called '**Exterminate bad datum point'** is the useful option to remove unreliable data point as shown in figure below. Such bad data points could be due to the failure of therelays at one of the electrodes, poor electrode ground contact due to dry soil, orshorting across the cables due to very wet ground conditions. These bad datapoints usually have apparent resistivity values that are obviously too large ortoo small compared to the neighboring data points. In order to get low RMS Error in the modeling, the bad datum points have to drop before start the inversion.

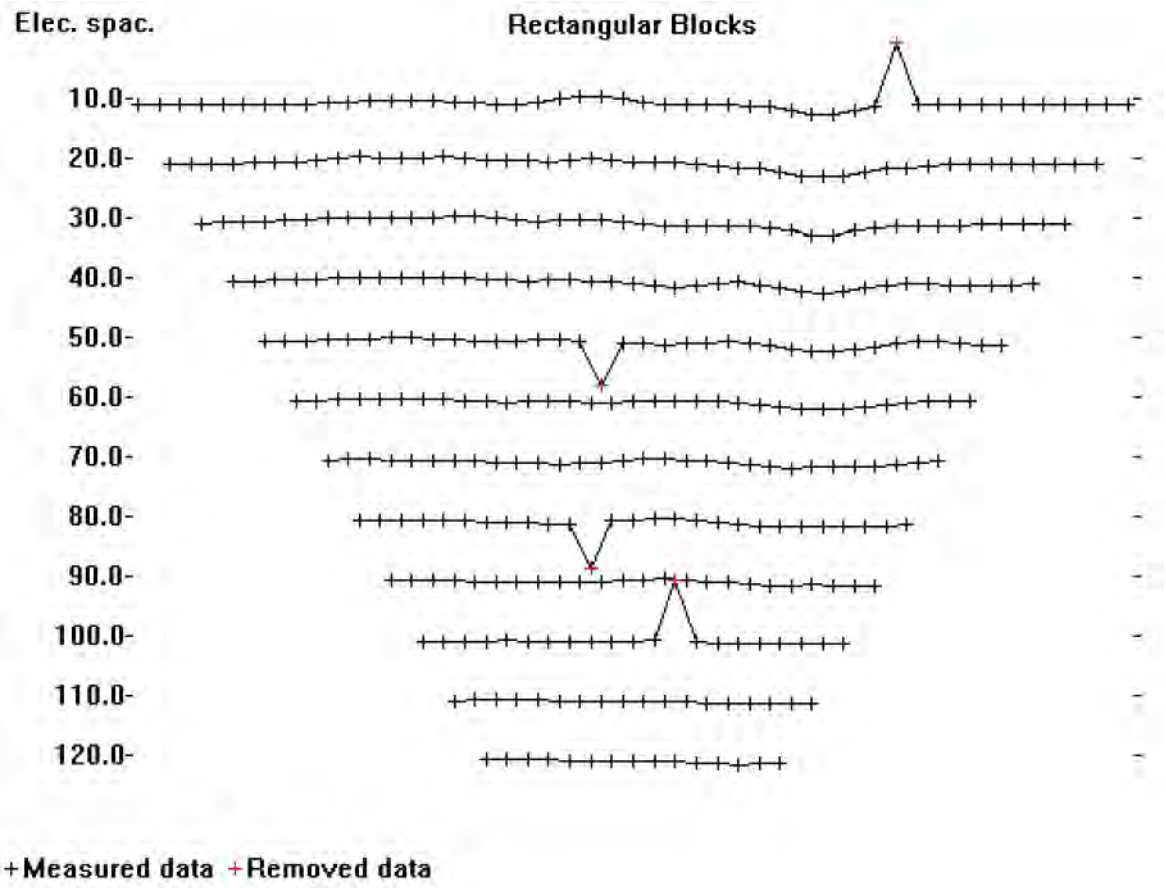

Change Settings menu options

This menu contains a number of options that control the parameters used in theinversion of the data set. This option shows the following menu.

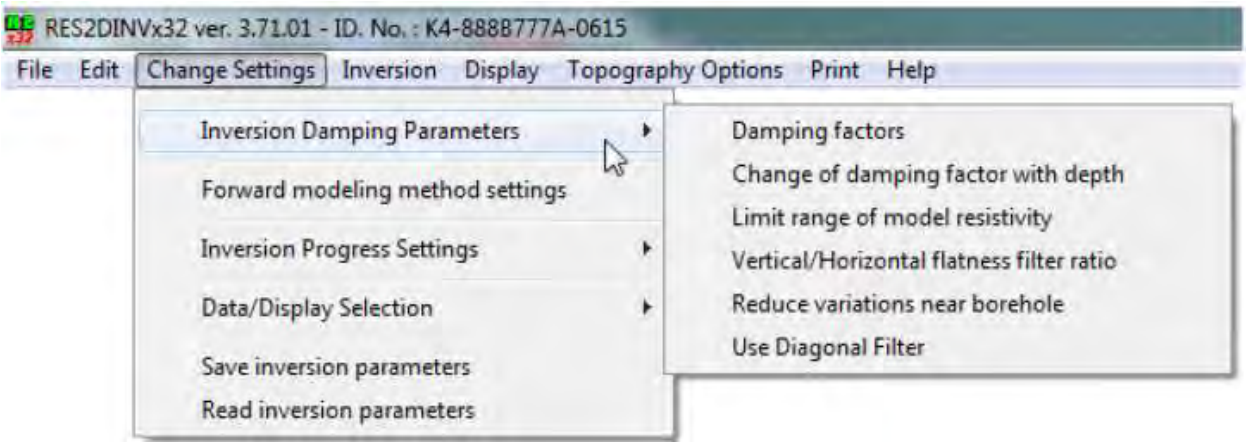

Inversion Damping Parameters

This covers a list of options that control the damping factor, l in equation (a) used in the smoothness-constrained least-squares inversion equations.The following list of sub-menu options is displayed when this option isselected.

Damping factors

In this option, you can set the damping factor l used in equation (a). Selectingthis option will bring up the following dialog box.

You can set the initial value for the damping factor in equation (a), as well asthe minimum damping factor. The inversion program automatically reduces thedamping factor by about half after each iteration until it reaches the selectedminimum value. Generally to get the low RMS Error such options have to follow in the inversion process.

a) If the data set is very noisy, you should use a relatively larger damping factor (for example 0.3).
b) If the data set is less noisy, use a smaller initial damping factor (for example 0.1).

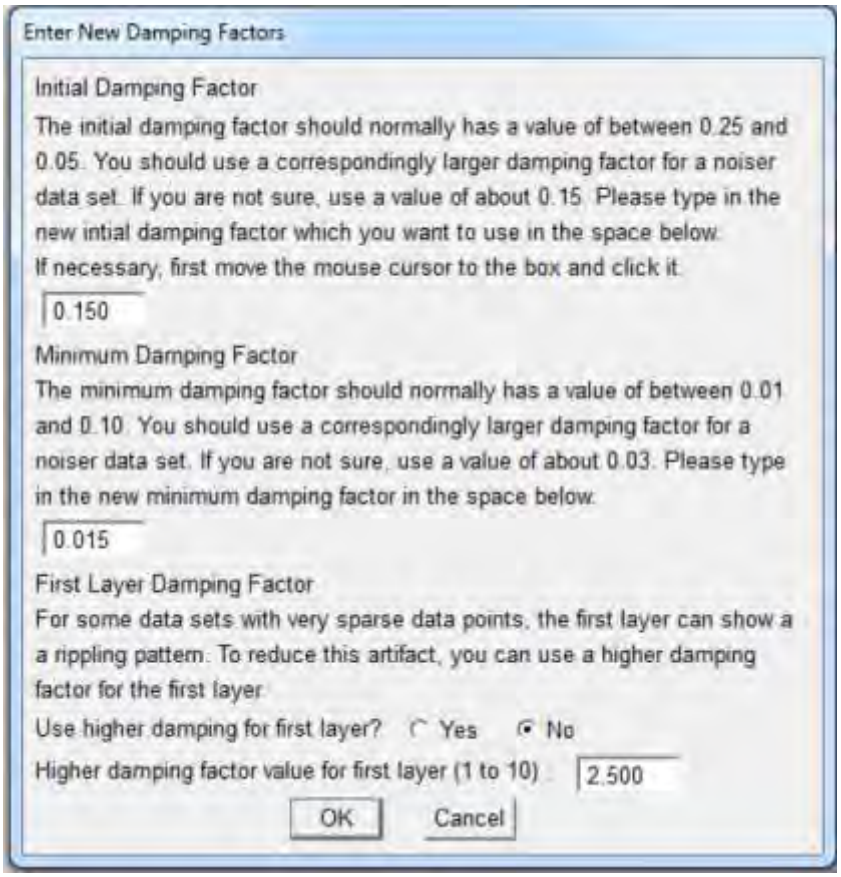

The inversion subroutine will generally reduce the damping factor but a minimum limit for the damping factor must be set to stabilize the inversion process. The minimum value should usually set to about one-tenth to one-fifth the initial damping factorvalue.

Change of damping factor with depth

This option also can reduce the RMS Error. It can be made by changing the damping factor with depth according to quality of the data. Because of the resolution of the resistivity method decreases exponentially withdepth, the damping factor used in the inversion least-squares method isnormally also increased with each deeper layer in order to stabilise theinversion process. Normally, the damping factor is increased by 1.05 timeswith each deeper layer, but you can change it. Use a larger value if the modelshows unnatural oscillations in the resistivity values in the lower sections. Thiswill help to suppress the oscillations. You can also select the choice to allowthe program to determine the value to increase the damping factor with depthautomatically. This might be a good choice if the thickness of the layers ismuch thinner than the default values, for example if you had reduced the unitelectrode spacing by half in the data file in order to produce a model withsmaller model blocks.

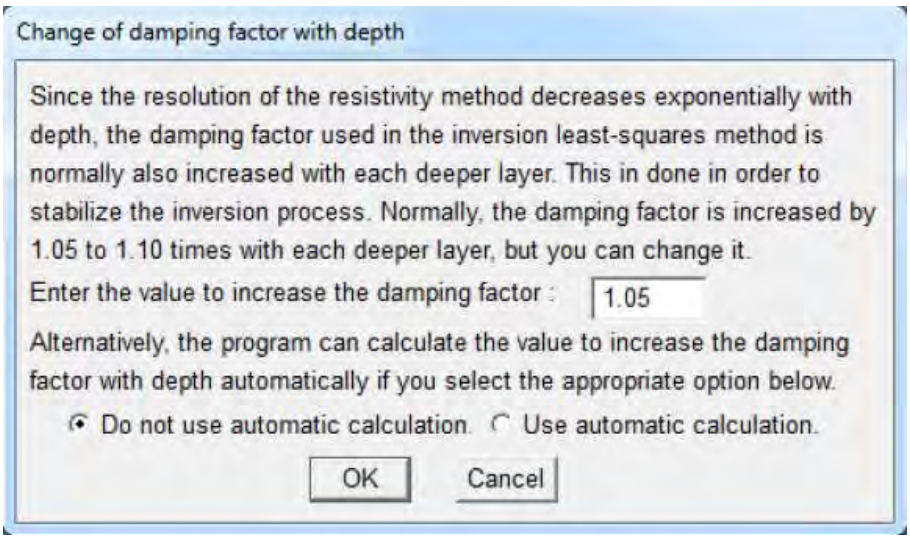

RMS Error Statistic

After finished with the inversion process, the statistic of the misfit between the measured and calculated apparent resistivity values in the form of histogram is automatically plotted by the software. This following option can be displayed by using the menu option as shown below.

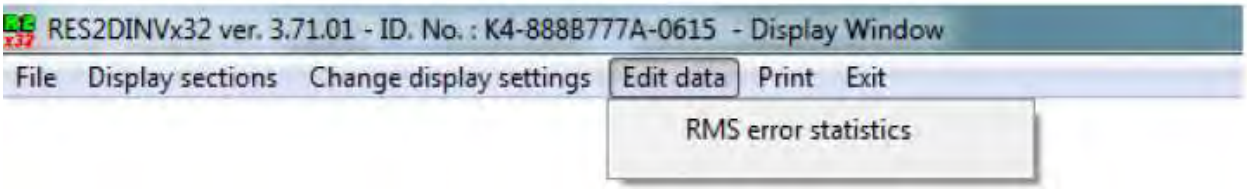

This option can be used to filter the outliers. Data with random noise will show an exponential decrease in the number of data points with increasing data misfit, as in the initial part in the figure below. Data outliers are likely have too much higher data misfit values which can be use to separate them from the other data points as shown by a few points on the right side of the figure.

From this option, the misfit cutoff value can be selected and saved as a new data files with the points higher data misfit data than the cutoff value removed from the data set. This data then will be reprocess to get a better resistivity inversion profile with less RMS Error.

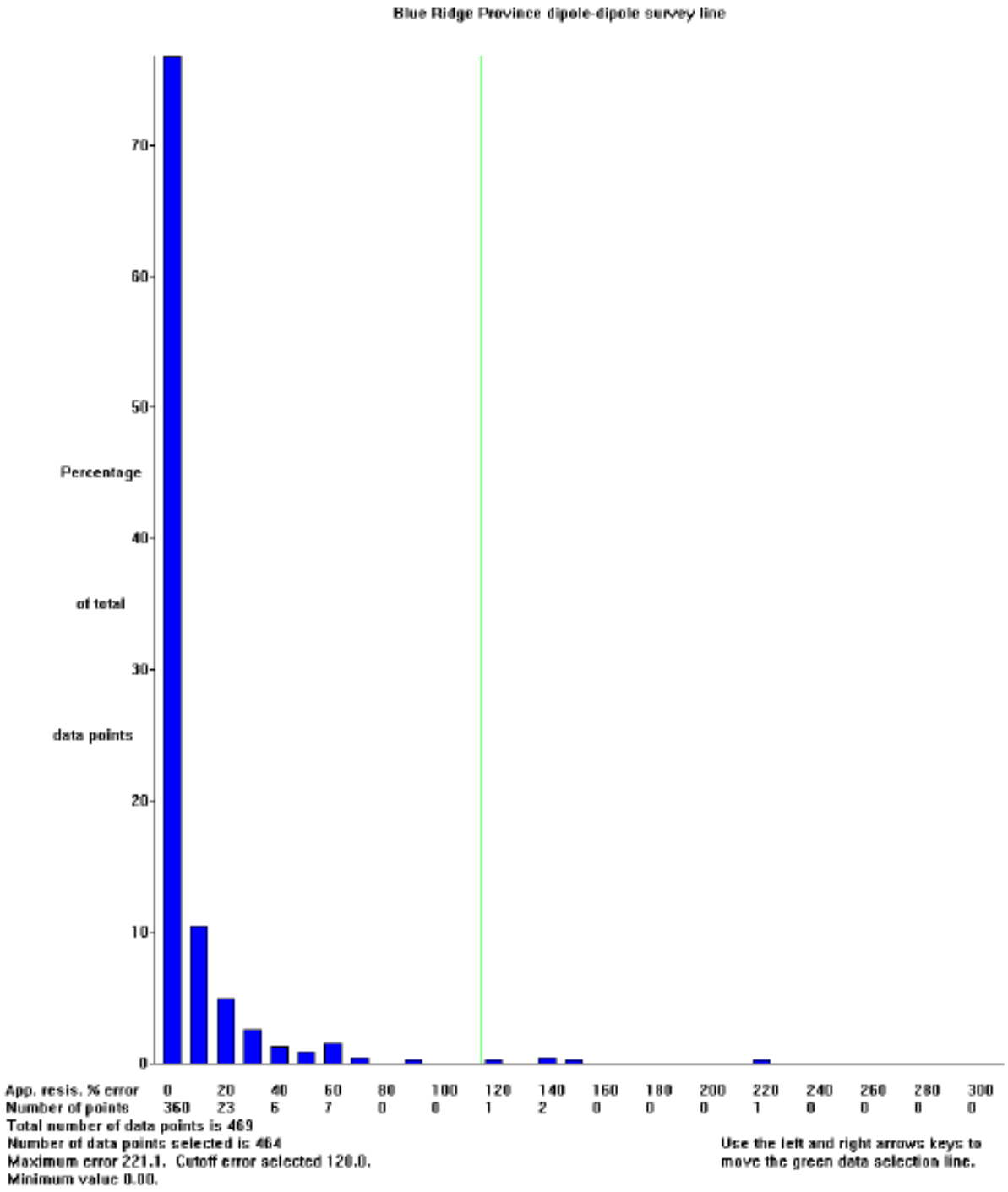
Blue Ridge Province dipole-dipole survey line
Percentage
of total
data points
70
60
50
40
30
20
10
0
App. resis. % error 0 20 40 60 80 100 120 140 160 180 200 220 240 260 280 300
Number of points 360 23 6 7 0 0 1 2 0 0 0 1 0 0 0 0
Total number of data points is 469
Number of data points selected is 464
Maximum error 221.1. Cutoff error selected 120.0.
Minimum value 0.00.
Use the left and right arrows keys to
move the green data selection line.

An Example of the Inversion Parameters used in one of the Resistivity Survey

Line Name:	YTFarm Res2-24June2010
Location:	Bromsgrove Landfill
Electrode Spacing:	5m
Electrode Array:	Wenner-Schlumberger
Weather:	Windy and Shinny

Processing the data:

Exterminate bad datum point: Remove all unreliable data points

Res2Dinv Parameters:

Damping Factor:	0.2
First Layer Damping factor:	0.02
Changing Damping Factor with Depth:	1.05

Forward modelling Parameters:

Horizontal Mesh Size:	4 nodes	
Vertical Mesh Size:	Normal Mesh	
Type of Forward Modelling Method:	Finite-Difference	
Convergence Limit:	a) Error change of Convergence Limit:	5.00%
	b) % RMS error for Convergence:	1.00%
Number of Iterations:		6
Model resistivity values check:	Check Model Resistivity for Extreme values	

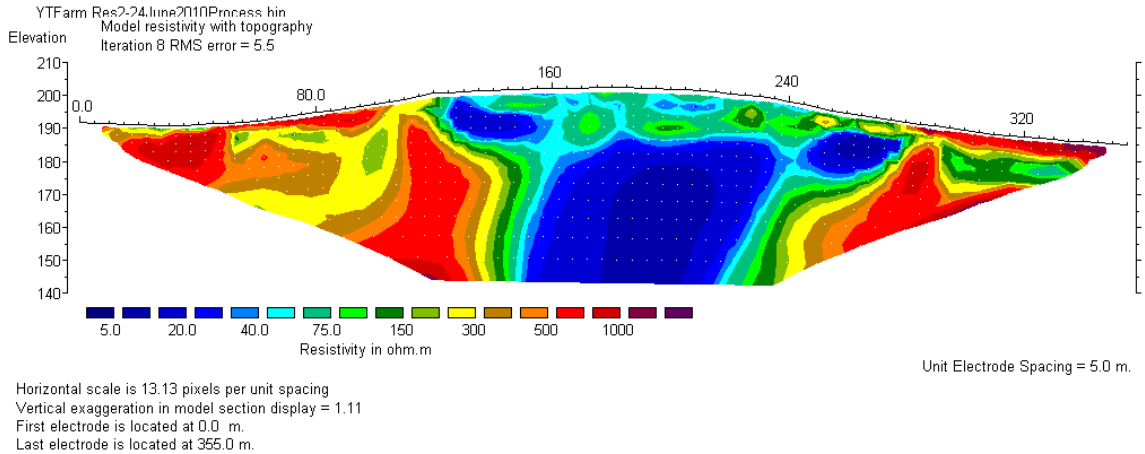

Horizontal scale is 13.13 pixels per unit spacing
Vertical exaggeration in model section display = 1.11
First electrode is located at 0.0 m.
Last electrode is located at 355.0 m.